Vol. 15 Nos 8–9 1996 ISSN 0277–3791

QUATERNARY SCIENCE REVIEWS

The International Multidisciplinary Research and Review Journal

RECORDS OF RAPID EVENTS IN LATE QUATERNARY SHORELINES

Guest Editors

D. B. SCOTT and L. ORTLIEB

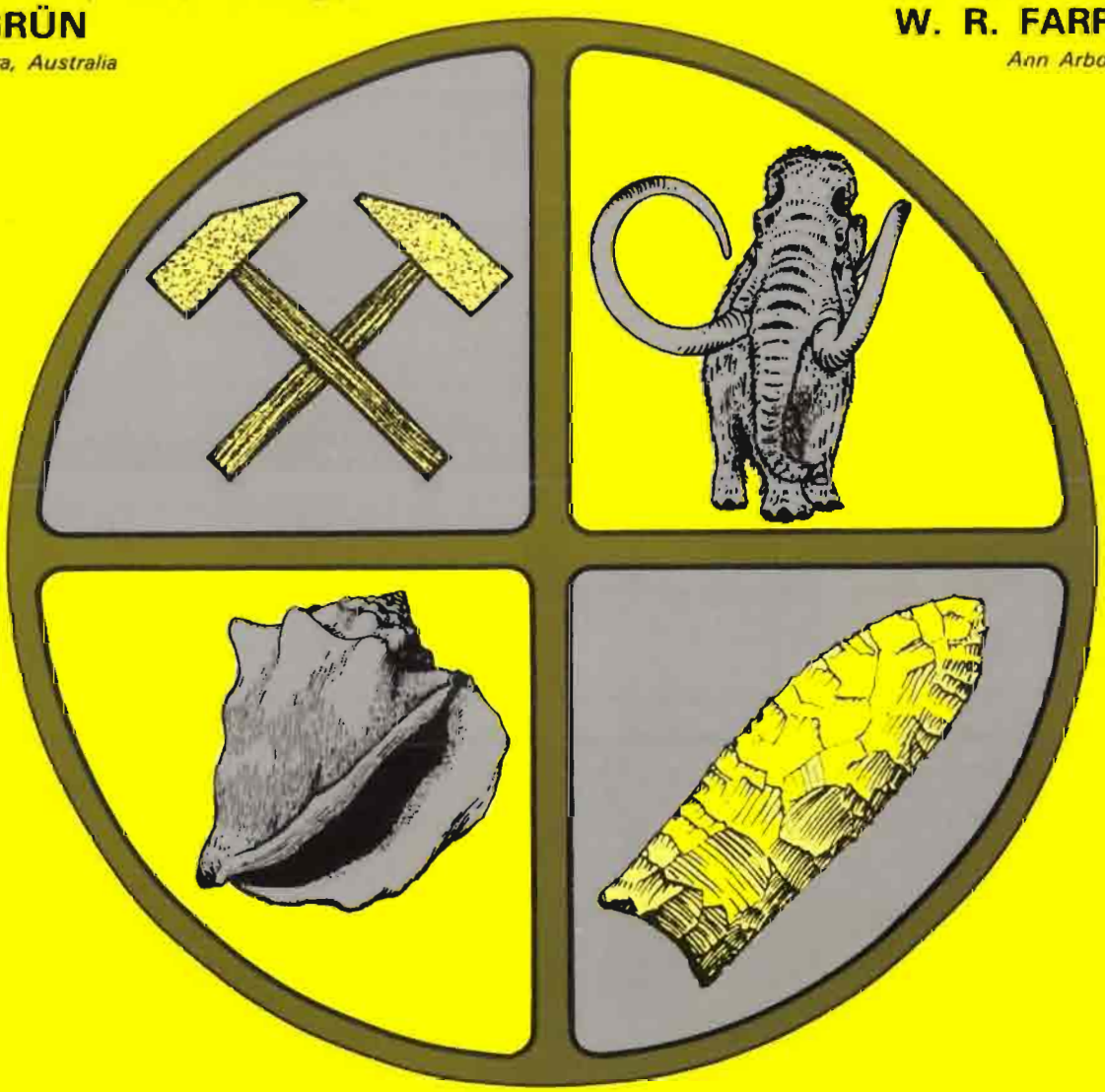

Pergamon

QUATERNARY SCIENCE REVIEWS

The International Multidisciplinary Research and Review Journal

Publishing and Advertising Offices: The Boulevard, Langford Lane, Kidlington, Oxford OX5 1GB, U.K.

Subscription Information
Annual Institutional Subscription Rates 1997: Europe, The CIS and Japan, 1292 Dutch Guilders. All other countries, U.S.$563.00. Associated Personal Subscription rates are available on request for those whose institutions are library subscribers. Dutch Guilder prices exclude VAT. Non-VAT registered customers in the European Community will be charged the appropriate VAT in addition to the price listed. Prices include postage and insurance and are subject to change without notice. Any enquiries relating to subscriptions should be sent to: **The Americas:** Elsevier Science Customer Support Department, P.O. Box 945, New York, NY 10010, U.S.A. [Tel: (+1) 212-633-3730/1-888 4ES-INFO; Fax (+1) 212-633-3680; E-mail: usinfo-f@elsevier.com]. **Japan:** Elsevier Science Customer Support Department, 9–15 Higashi-Azabu 1-chome, Minato-ku, Tokyo 106, Japan [Tel: (+3) 5561-5033; Fax: (+3) 5561-5047; E-mail: kyf04035@niftyserve.or.jp]. **Asia Pacific (*excluding Japan*):** Elsevier Science (Singapore) Pte Ltd, No. 1 Temasek Avenue, 17-01 Millenia Tower, Singapore 039192 [Tel: (+65) 434-3727; Fax: (+65) 337-2230; E-mail: asiainfo@elsevier.com.sg]. **Rest of the World:** Elsevier Science Customer Service Department, P.O. Box 211, 1001 AE Amsterdam, The Netherlands [Tel: (+31) 20-485-3757; Fax: (+31) 20-485-3432; E-mail: nlinfo-f@elsevier.nl].

For orders, claims, product enquiries (not manuscript enquiries) please contact the Customer Support Department at the Regional Sales Office nearest to you.

Periodicals postage paid at Newark, NJ. *Quaternary Science Reviews* (ISSN 0277-3791) is published as 1 volume per annum consisting of 10 issues (January, March, April, July, September, October, November, December), by Elsevier Science Ltd, The Boulevard, Langford Lane, Kidlington, Oxford OX5 1GB, U.K. The annual subscription in the U.S.A. is $563. *Quaternary Science Reviews* is distributed by Mercury Airfreight International Ltd, 10 Camptown Road, Irvington, New Jersey 07111-1105, U.S.A. Postmaster: please send address corrections to *Quaternary Science Reviews*, c/o Elsevier Science Regional Sales Office, Customer Support Department, 655 Avenue of the Americas, New York, NY 10010, U.S.A. [Tel: (+1) 212-633-3730/1-888 4ES-INFO; Fax: (+1) 212-633-3680; E-mail: usinfo-f@elsevier.com].

October/November 1996 issues

RECORDS OF RAPID EVENTS IN LATE QUATERNARY SHORELINES

Guest Editors

D. B. SCOTT* and L. ORTLIEB†

**Marine Science Institute, University of California, Santa Barbara, CA 93106-6150, U.S.A.*

†ORSTOM (Institut Français de Recherche Scientifique pour le Développement en Coopération), Depart de Geología, Universidad de Antofagasta, Casilla 1190, Antofagasta, Chile

PERGAMON

AIMS AND SCOPE

Quaternary Science Reviews caters for all aspects of Quaternary Science, and includes, for example, geology, geomorphology, geography, archaeology, soil science, palaeobotany, palaeontology, palaeoclimatology and the full range of applicable dating methods.

The dividing line between what constitutes the review paper and one which contains new original data is not easy to establish, so QSR also publishes papers with new data especially if these perform a review function, or can be so adapted for a wider perspective, for example, as in methods of dating.

All the Quaternary Sciences are changing rapidly and subject to re-evaluation as the pace of discovery quickens; thus the eclectic and comprehensive role of *Quaternary Science Reviews* keeps readers abreast of the wider issues relating to new developments in the field.

The Item-Fee Code for this publication is: 0277–3791/96 $32.00

Cover design: symbolizes the interdependent nature of the Quaternary sciences: crossed hammers for the vast range of geological sciences; *Strombus bubonius*, the tropical gastropod for the biological sciences; a Clovis projectile point from the New World for the archaeological sciences; and the inevitable woolly mammoth representing the traditional 'ice-age' connection.

Contents

Pergamon

Quaternary Science Reviews, Vol 15, pp. 761–762, 1996.

0277–3791/96 $32.00

PREFACE

DAVID B. SCOTT* and LUC ORTLIEB†
**IGCP 367 Project Leader, Halifax, Canada*
†Conference Organizer, ORSTOM, Antofagasta, Chile

This double issue represents a cross-section of papers presented at the Second Annual Meeting of the IGCP (International Geological Correlation Program) Project 367-Late Quaternary coastal records of rapid change: application to present and future conditions, held in the spectacular setting of northern Chile in the city of Antofagasta. Besides the symposium, there were field trips to many of the places discussed in the lectures showing incredible exposures of coseismic uplift, tsunami deposits, and mudslides, to name a few. Just to emphasize that this area is one of rapid change, there was a 7.1 magnitude earthquake 3 months before the meeting that caused only a few casualties, relative to its magnitude (Hs 7.3, Mw 8.1). As a major earthquake was expected in the seismic gap of Northern Chile, a series of geophysical and geological studies have been carried out in recent years and were, of course, intensified immediately after the Antofagasta earthquake. Among the visible effects of the earthquake was a limited uplift of parts of Antofagasta Bay, that was evidenced by the apparition of a bright fringe of dead corraline algae in the intertidal area of the rocky shores. The biological evidence was useful to constrain the deformation models proposed by the seismologists and researchers that had monitored the area with GPS techniques.

The field trips were led by both local scientists (L. Ortlieb, S. Barrientos, G. Chong, D. Lazo, J. E. Novoa, G. Vargas and N. Guzman) and foreign scientists (R. Paskoff, J. Goy, C. Zazo, C. Hillaire-Marcel, U. Radtke, E. M. Leonard and J. Wehmiller). The Atacama Desert is the driest place on Earth and the Quaternary exposures were preserved in pristine condition.

Of course, IGCP Project 367 deals with other aspects of coastal change in addition to tectonic, and this double issue tries to capture sense of all of them. We have divided the volume into four sections: (1) rapid shoreline change and geomorphological responses, with eight papers mostly concerning European coastal responses to factors such as Holocene relative sea-level rise, tectonics and changes in sediment supply, and also Pleistocene coastal evolution along the Pacific and Atlantic sides of South America; (2) climate and sea level, with three papers discussing carbon storage on former continental land masses, palaeontological evidence for warmer climatic conditions during Oxygen Isotope Stage 11, and a climatic link with a later Holocene climatic oscillation; (3) tides and human influences, with two papers, one on tidal models around the U.K. and the other discussing human impacts on the coast of Taiwan; and (4) seismic events recorded in coastlines, with four papers including one on Northern Chile, one on a recent tsunami deposit in Java, one on marsh stratigraphy from the west coast of Canada, and one on a 10,000-year-old tsunami in Sweden. The number of papers presented at the conference amounted to 59 and can be consulted in the abstract volume edited for the meeting.

We would like to take this opportunity to thank all the participants from over 20 countries, and particularly all the Chilean colleagues and students who were instrumental in making this a successful conference. Also we

thank IGCP (sponsored by International Union of Geosciences and UNESCO) and all the IGCP National Committees who helped defray some of the travel costs for many participants. Other academic institutions that took an important part in organisation of the meeting were ORSTOM (Institute Français de Recherche Scientifique pour le Development en Cooperation), Universidad de Antofagasta, Universidad de Chile, Universidad Arturo Piat (Iquique), Universidad Catlica del Norte, Universidad La Serena, CONICYT (Consejo Nacional de Ciencia y Technologa, Chile) and Dalhousie University. Finally it must be mentioned that the Quaternary shorelines and Neotectonics Commissions of INQUA provided their auspices. Also we wish to thank the many reviewers we enlisted to review the manuscripts; reviewers are included in the list at the end of this year's volume.

RAPID SHORELINE CHANGES AND GEMORPHOLOGICAL RESPONSES

Pergamon

Quaternary Science Reviews, Vol. 15, pp. 763–771, 1996

0277–3791/96 $32.00

PII: S0277–3791(96)00072–8

EVIDENCE FOR SHORT TERM RETREAT OF THE BARRIER SHORELINES

J. PAUL BARUSSEAU,* ÉMILE AKOUANGO,* MARILINE BÂ,† CYR DESCAMPS* and ANTOINE GOLF‡

**L.S.G.M., URA 715, Université de Perpignan, 66860 Perpignan, France*
†Département de Géologie, Université Cheikh Anta Diop, Dakar-Fann, Sénégal
‡20, rue de la Liberté, 34340 Marseillan, France

Abstract — In many places on the present shoreface, offshore bar or beach sands with a sharp-basal contact overlie thin-bedded fine sands and muds. Ancient analogues are commonly interpreted as lowstand shoreface deposits lying on an erosional surface cut into the shelf during a relative sea-level fall. New observations may challenge this interpretation by providing evidence that such sequences develop during a recent shoreline retreat under highstand conditions without any significant change in sea level.

Two examples of such a superimposition are provided by wave-dominated clastic shorefaces in the microtidal environment from the Senegal coast (Saloum delta, Sangomar spit) and in a non-tidal environment on the French Mediterranean coast in the Gulf of Lions.

In the Saloum, a littoral cross-section across the Sangomar beach barrier shows a dune sand deposit overlying a man-made shell accumulation, dated 600 BP, and a layer of green muds formed in a lagoon at the back of an ancient beach barrier whose remnants are dated 3150 BP. The retreat of this ancient beach barrier is demonstrated by mapping the former offshore extension of a littoral sand unit which is defined clearly in the region by a grain-size signature. Other observations in the region of the Saloum delta give evidence of the widespread occurrence of coastal recession along the whole Sangomar sedimentary spit.

In the Gulf of Lions, vibrocores were used to sample the beach and the shoreface of the Thau lagoon lido. The geological record of recent and present sedimentation exhibits varied littoral sands overlying ancient deposits of fine muddy sand and, at the very bottom of the sections, shoreface sands including fragments of beachrock. Radiocarbon datings give ages of 2050–6700 BP for the underlying muddy fine sand which has been interpreted as a lagoonal deposit enriched in organic matter, typical of lagoon environments in the region. An evolution similar to that proposed for the Sangomar region is supported by additional evidences of a very recent (some centuries) landward displacement of the beach barrier. Lines of wrecks of different ages are observed along this part of the Gulf of Lions, showing that the shoal determined by the offshore bars has migrated successively landwards as the littoral sedimentary prism has receded. Copyright © 1996 Elsevier Science Ltd

INTRODUCTION

The direct superimposition of a modern beach barrier–shoreface sand sequence on an older fine-grained deposit is frequently observed in microtidal or non-tidal environments as a consequence of widely spread erosion in present times (Köster, 1995).

In the geological record, such superimpositions have been considered to result from either lowstand shoreface deposits lying on an erosional surface, cut into the inner shelf fine sediments during a relative sea level fall, or progradational beach barrier sequences during a highstand phase. Plint (1988) described an offshore bar sequence in the Cardium Formation of Alberta (Turonian) in terms of the first model. Here the sharp-based shoreface sequence, made of a relatively thin sand body with swaley cross-stratification, breaker bar cross-bedding and beach lamination, lies upon bioturbated mudstone and sandstone. Plint demonstrates that after an episode of stable relative sea level forming a normal gradational-based shoreface sequence, a fall of relative sea level caused: (1) a scouring of inner shelf fine sediments by fair-weather waves; and (2) deposition of a coarse upper shoreface sand sequence superimposed on the older fine shelf sequence. The second scenario was employed by Gagan *et al.* (1994) who described a mid- to late Holocene highstand formation of a series of beach ridges in an embayment located landward of the central Great Barrier Reef. The basal contact of the beach barrier is sharp and overlies thinly bedded and laminated, micaceous muddy sand fining downward to sandy mud, interpreted as upper and lower shoreface deposits respectively. According to Gagan *et al.* (1994), beach ridge progradation occurred when sea level was at (or very close to) its present position.

Observations reported here, made in two other modern environments, provide an alternative explanation of such superimpositions. Our model corresponds to the development of a shoreface sequence, under conditions of a coastal retreat, during a highstand phase without any significant change in sea level.

PRESENTATION OF THE STUDIED AREAS

The results presented here come from two regions (Fig. 1). The Senegal coastline, south of Dakar, is a tectonically stable area. This sandy coast ends with a long sand spit (Sangomar spit) which deflects the lower reach of the Saloum river. The Saloum delta formation was studied previously (Ausseil-Badie *et al.*, 1991). The sensitivity of spit formation and location changes was interpreted as a response to small climatic and sedimentological variations. A recent major change in the spit morphology (Barusseau and Radakovitch, 1996), in February 1987 resulted from the exceptional conjunction of a gale and a short-lived period of high sea level in the tropical Atlantic Ocean (Verstraete, 1986) within the general context of sediment starvation of the coastline in recent times (Barusseau, 1980). The beach and shoreface morphology includes a steep and monotonous slope down to 3–4 m below sea level. The tidal regime on this part of the Senegal coast is microtidal.

The second region studied is the beach barrier (lido) of a lagoon on the north coast of the Gulf of Lions (Northwestern Mediterranean). The area is considered to be tectonically stable in the upper Quaternary; the argument of epirogenic activity is not convincing since the Thau lagoon is largely out of the possible subsiding area of the Rhône delta (L'Homer *et al.*, 1981). In this region, the oceanographic regime is mainly dominated by the wave action since the tidal range is very small (lower than 0.15 m, Barusseau *et al.*, 1994). High frequency sea level fluctuations are only determined by the meteorological situation (pressure and wind stress) characterized by two patterns: one created by winds having a net offshore component (from the north and the northwest) and the other one by winds having a net onshore component (from the east and the southeast). In the first case, the wind driven surface transport in the cross-shore direction produces a set-down of the mean surface level over the entire shoreface (Niedoroda *et al.*, 1985), the reverse occurring with opposite wind directions. The longshore sediment transport is low (Anonymous, 1984). The normal profile is more irregular than on the Senegal coast with one or two well-developed offshore bars parallel to the coast line. The crest of the outermost one is between 2.5 and 4 m deep. In fact, the offshore bars constitute a distinctive element of a very well defined sedimentary prism (Ausseil-Badie, 1978) comprising, from the coastal environment to the inner shelf region (Fig. 2): a lagoonal sequence (as far as a lagoon exists), a beach barrier (dune and beach), an offshore bar system (Barusseau and Saint-Guily, 1981), and a thin veneer of nearshore sands grading to midshelf muds (Jago and Barusseau, 1981). As is the case in the Rhône delta (Aloïsi, 1986), a similar complex of units was laid down in the Gulf of Lions each time the sea level was stabilized. Early Holocene sedimentary prisms, at 50–60 m and 30–

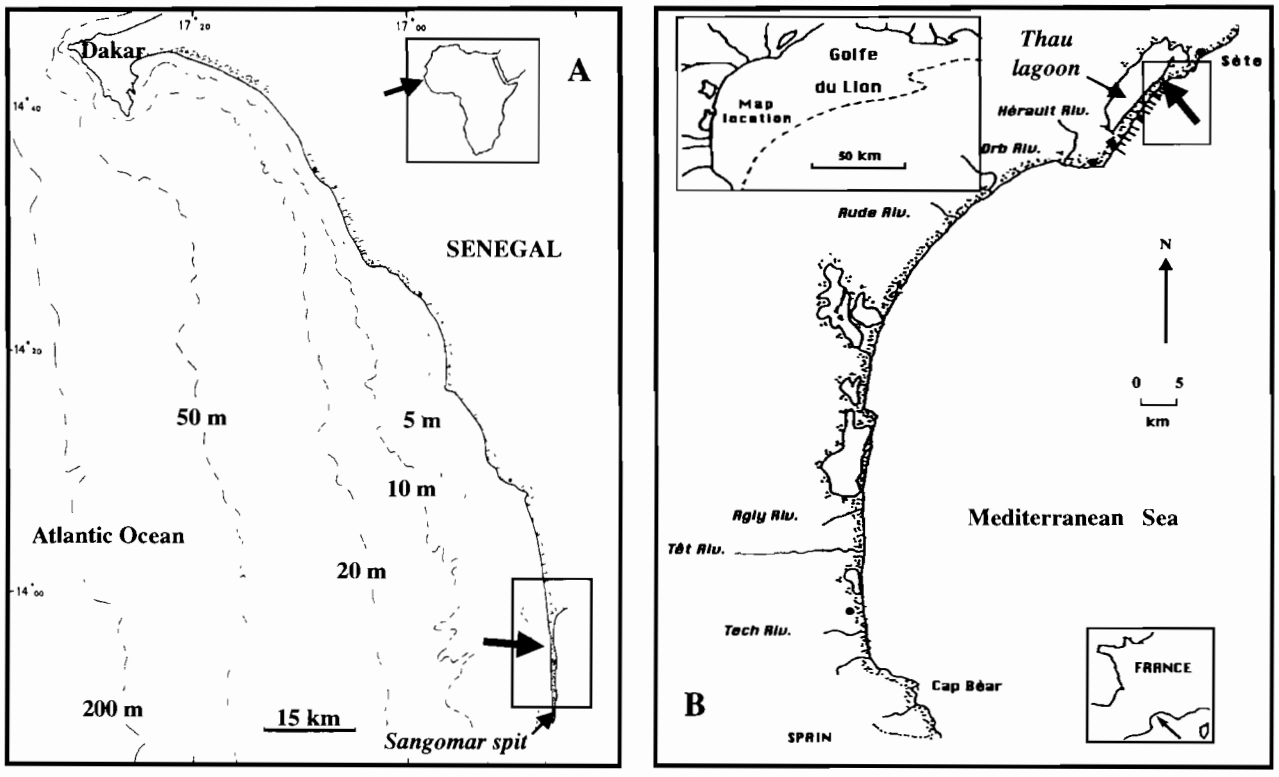

FIG 1. Location of the studied areas (A) Senegal coast; the heavy arrow shows the position of the cross-section in the study area (B) Gulf of lions coast; the heavy arrow shows the position of cores in the study area.

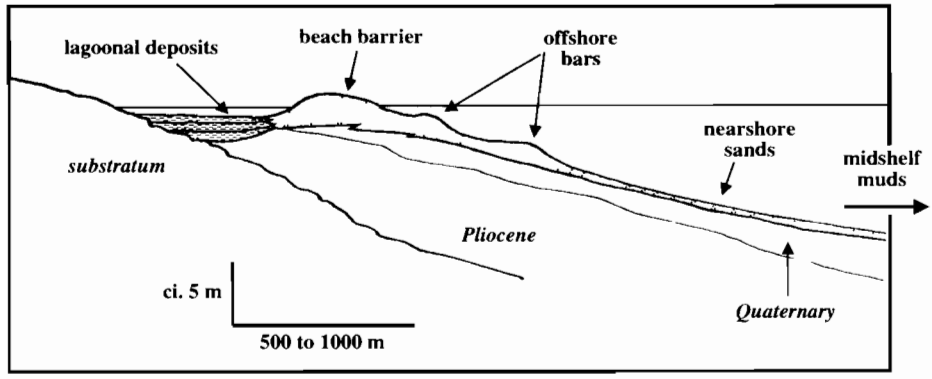

FIG. 2. Idealized sketch of the sedimentary prism in the gulf of Lions.

35 m below the present sea level, formed around 10,000 and 8000 BP, respectively. Since a complete sedimentary unit is built when sea level remains fixed at a given level, it follows that the sedimentary prism as a whole, may be considered as an indicator of the relative sea level position.

Both of the regions studied are presently experiencing coastal erosion requiring, in the urban zones, an extensive use of protective structures and dynamic protections (groynes, breakwaters and beach nourishment).

METHODS

A general description of the distribution of surface sediment in both regions was based on usual sedimentological techniques. Material recovery was made by dredging in the Senegal region and coring in both the Mediteranean and the Senegal coastal zone. In the Thau lagoon region, the shoreface sediments were vibrocored using a small vibrocorer designed by Amaury de Resseguier at the University of Bordeaux. Grain-size analysis of the sediments were performed by dry sieving. Data after sieve mesh correction were obtained by a modal grain-size analysis (Barusseau, 1973) including: inventory of the modal values of all the unimodal and polymodal sediments, frequency analysis of the modal values, and definition of the modal populations. Each modal population is considered as a sedimentary type, the mapping of which may be made taking into account the proportion of each type in the sediment when mixed with other sedimentary type(s). Description of cores and vibrocores was made visually. Radiocarbon datings were obtained through Beta Analytic Inc. and reported as conventional radiocarbon ages with no local reservoir correction for the shell samples.

In the Gulf of Lions, archaeological archives were exploited and the information interpreted from a morphological and bathymetric point of view. All morphological operations were carried out according to the procedure described in Barusseau *et al.* (1994): shorter baselines (500 m) were established and marked on the coast for 11 profiles regularly spaced out (50 m). They were usually monitored using a Geodimeter-140 electronic tachymeter fitted with an electro-optical range finder for both the subaerial beach and the nearshore zone. Depth measurements were taken by using a Fuso fathometer aboard a Zodiac boat with an accuracy of ± 15 cm.

RESULTS

The Senegal Region

On the coastal zone south of Dakar, the modal grain-size analysis showed the existence of 5 sedimentary types (Barusseau *et al.*, 1983). The nearshore sediments belong to the fine sand population (type II with modal values M between 105 and 175 microns). It is a well-sorted sediment (Fig. 3) extensively distributed in the whole inner shelf (Barusseau *et al.*, 1988) as a palaeo-shoreline marker (Fig. 4). Near the long Sangomar spit, it is worth noting that the type II sand extends beyond the 5 m depth contour. The type III (175<M>500 microns) is closely associated to the type II and represents the sand facies of the beach environment.

A typical cross-section of the beach and shoreface sequence, from the marine flank of the Sangomar beach barrier, gives a lithological succession showing the occurrence of a fine green mud flat deposit below the beach barrier sand (Fig. 5). The sharp contact between both facies exhibits no erosional marks (for instance mud pebbles reworked into the lower part of the sand layer). The muddy deposit which has been observed in many parts of the coastal zone in the Saloum delta (Djiffère, Niodior) is 0.4–1 m thick, contains small plant debris and rests on a type III medium sand containing *Anadara senilis* (-310/-320 cm) and finely broken shell fragments below (-320/-410 cm). The clay mineral association within the fine layer is characterized by a rather high micaceous clay–kaolinite ratio. Smectite, present in confined environments, is not registered here. The microfaunal assemblage is dominated by *Ammonia tepida*, *Ammonia parkinsoniana* and *Elphidium poeyanum*. *Ammonia beccarii* and *Trochammina inflata*, frequently present in the fine sediments of the delta area, are completely absent here. The section is topped by a small shell-midden layer overlain by a recent dune sand. This part of the section was formerly studied (Ausseil-Badie *et al.*, 1991) showing a recent human settlement (600 BP) interrupted by a more recent climatic change (Barusseau, 1986). Dates for the lower part of the section

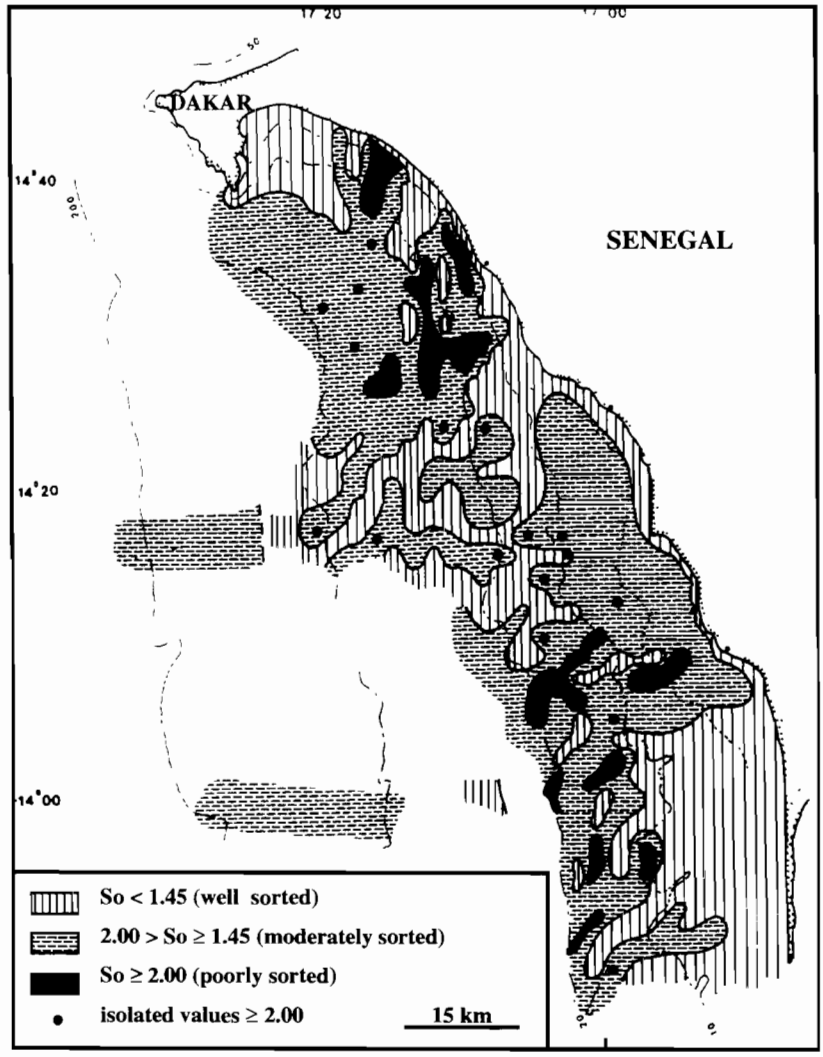

FIG. 3. Distribution of the sorting index (So Trask) of the sediment on the Senegal shelf, nearshore and beach, south of Dakar.

give an age of 1180 BP for the fine sediment layer and 3150 BP for the *Anadara* layer.

The Gulf of Lions

Six vibrocores were located on the upper foreshore (beachface) of the lagoon lido, the bar crests (Crxe and Crxi) and in the intermediate troughs (Crte and Crti). Two of them are presented in Fig. 6 but all exhibit the same superimposition of beach sand over a fine sediment layer, 5–35 cm thick, itself overlying a basal sand with littoral sandstone debris or cementations. This sequence is very common in most of the lagoons of the Gulf of Lions and generally corresponds to a back barrier sequence (Martin *et al.*, 1981). For instance, in the Canet lagoon, a small lagoonal body in the southern part of the Gulf, silt and mud infilling formed during the time interval of the final Atlantic, the Subboreal and the Subatlantic phases. The corresponding silt and mud layers are clearly interfingered on the seaward face of the lagoon with the lido sands. ^{14}C datings obtained on the fine sediment of the Thau lido, ranging from 2050±60 BP to 6700±70 BP, are consistant with these results. The pollen assemblage recovered in this layer, although poor in taxa (*Chenopodiaceae* and *Composaceae*), gives a coastal Mediterranean signature (G. Cambon, *in litteris*). As for the Senegal coast, altimetric measurements give the same values for the fossil fine sediments just outside the beach barrier and the present ones inside.

DISCUSSION

In the Saloum area two sedimentological observations provide useful indications of recent changes in the region: the continuous extension of the sand layer made of the grain-size types II and III from the 7–6 m depth to the present shoreline (Fig. 4) and the evidence of rapid environmental changes (Fig. 5).

The clay association in the mud layer gives a good indication of the palaeoenvironmental conditions. According to Kalk (1978), clay minerals have two origins in this part of the West African coast. Kaolinite derived from the so-called 'Continental Terminal', a deeply altered post Eocene formation. Erosion of other sedimentary formations, of Mesozoic and Cenozoic age, gave smectite and illite; the latter might have increased due to

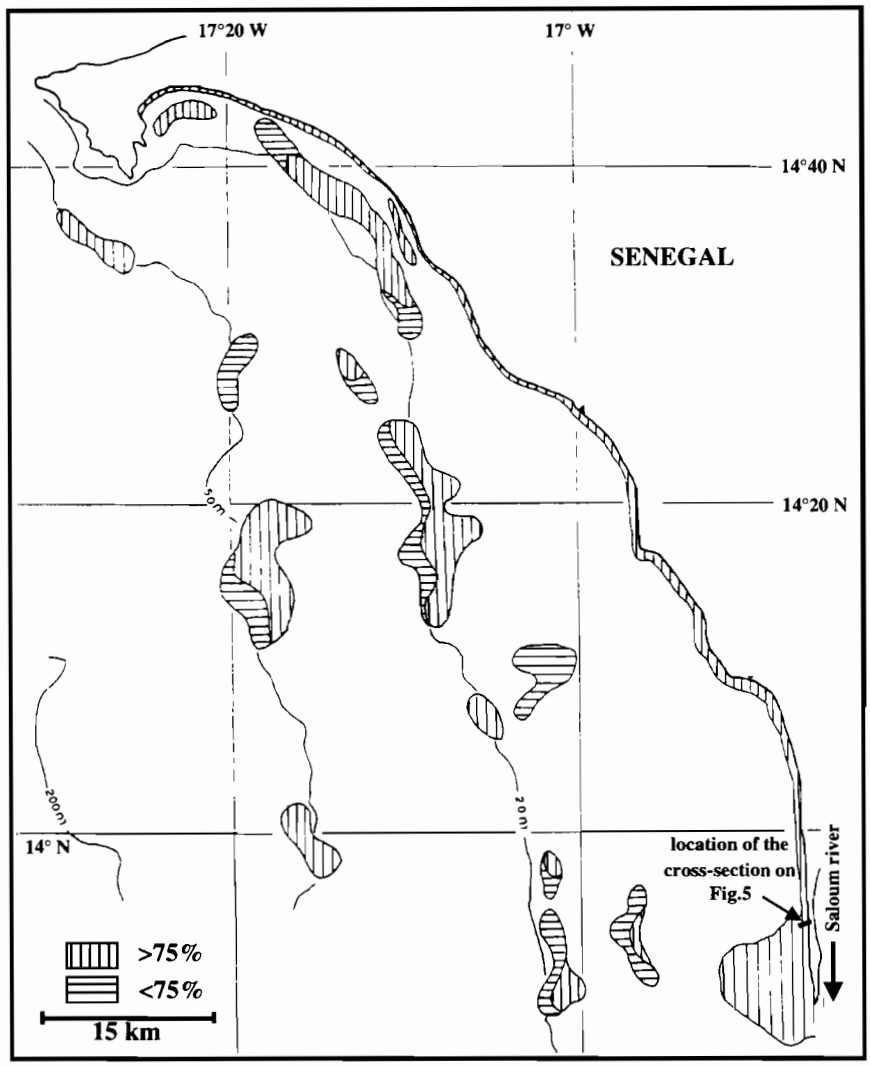

FIG. 4. The type II fine and well-sorted sand as a characteristic of different fossil shorelines and of the modern one on the Senegalese southern shelf (vertical and horizontal hatching gives the percentage of the type II population in the whole sediment).

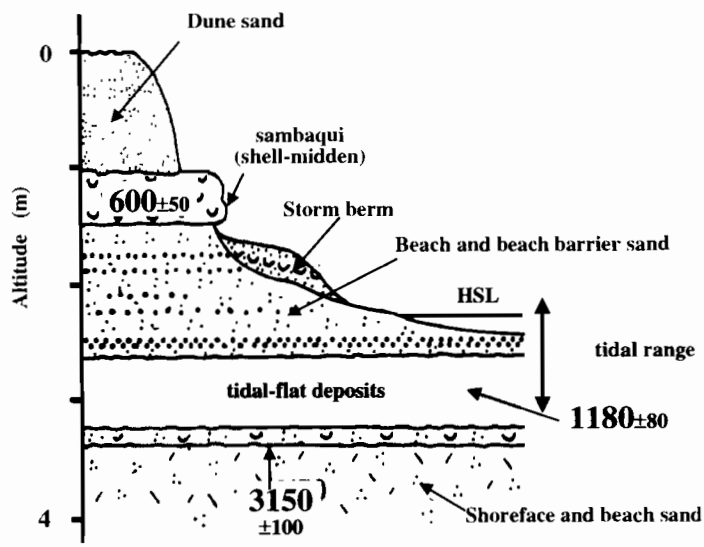

FIG. 5. The Sangomar spit cross-section (the location of the section is given on Fig. 4; values are radiocarbon conventional ages; HSL: instantaneous high tide level; the contact between the tidal-flat deposit and the overlying sand is sharp, non-erosional).

pedological effects such as those explaining the illite enrichment recorded in the numerous shell-middens (Leprun *et al.*, 1976; Thilmans and Descamps, 1982). Here smectite is absent in the silt and mud layer which implies a mechanical sorting effect corresponding to an environment well-connected to marine waters. According to Ausseil-Badie (1988) who studied the Foraminifera assemblage at a regional scale, a few suborders (*Textulariinae, Miliolina* and *Rotaliina*) have representatives in the sediments of estuarine and deltaic environments of the Senegal coast. The assemblage recorded in the section shown in Fig. 5, dominated by *Rotaliina*, shows an estuarine influence that reflects a lowering of the salinity corresponding to a regular fluvial input in the biotope. It may be concluded that the fine silt and mud layer was deposited in a tidal-flat environment in the vicinity of a major fluvial or interdistributary channel, a position very close to what is commonly observed *behind* the beach barrier. The former location of a beach barrier in a more external position might explain such a pattern, an hypothesis which is supported by the displacement signature of the type II sand offshore Sangomar spit (Fig. 4). This situation is schematically depicted in Fig. 7A. An important fact to be noted is that the upper level of the fine green level is located at the same height as in other present mud-flats (for instance those located on the river side of the present beach barrier). Therefore, no change in the sea level location would be involved in

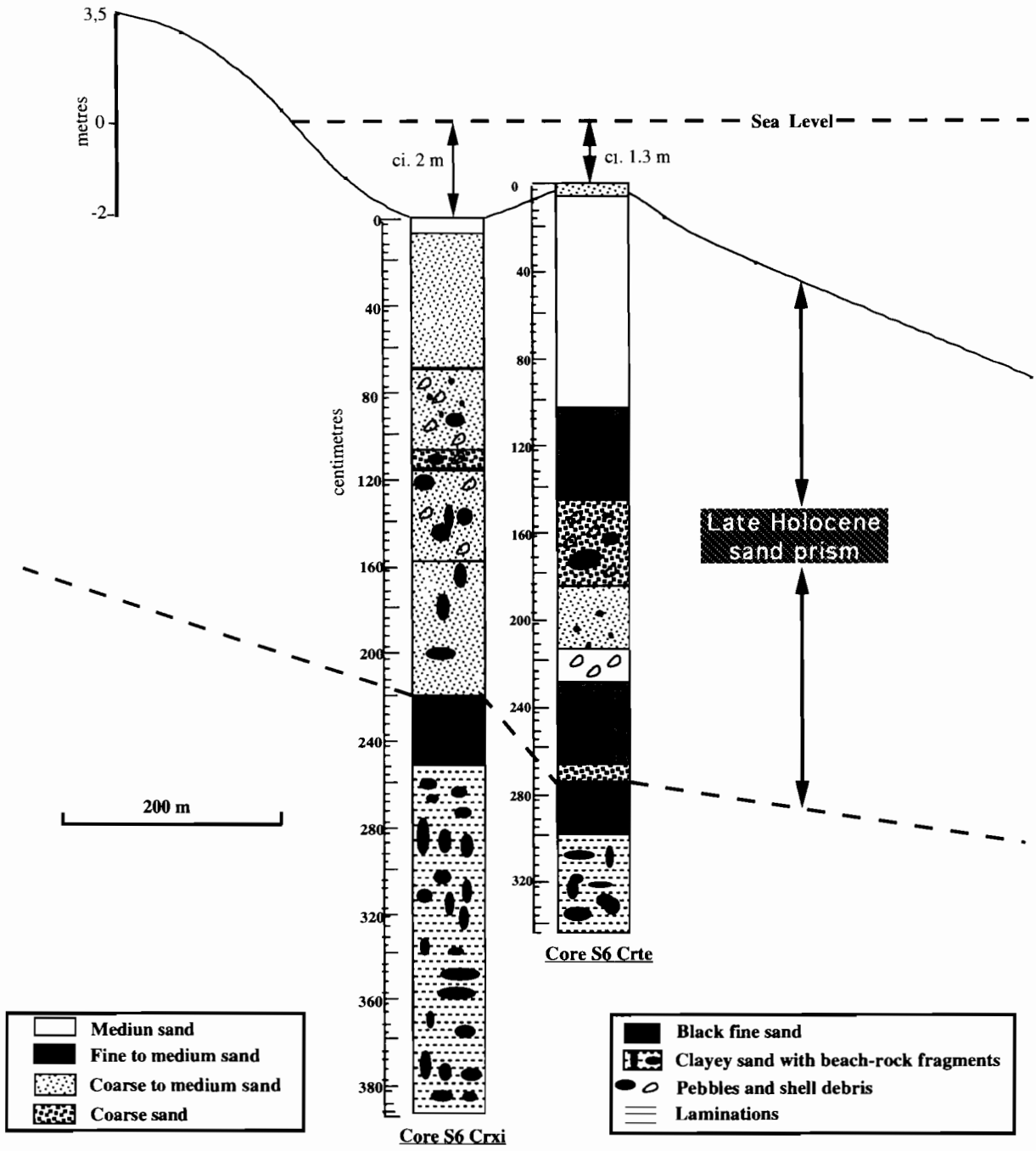

FIG. 6. Sedimentary columns of vibrocores taken in the offshore bar system in the gulf of Lions.

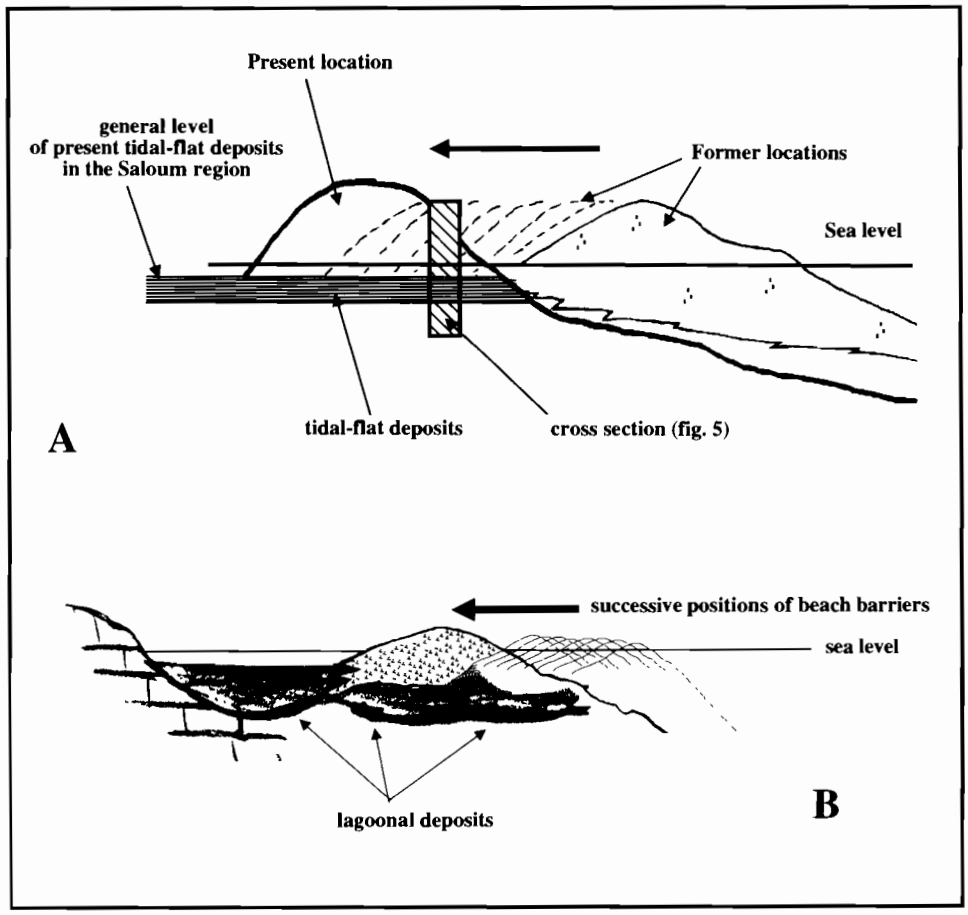

FIG. 7. Regressive trends on the Senegal (A) and the Mediterranean (B) coast. The contact between the beach barrier sands rolling over the tidal-flat or lagoonal deposits is non-erosional. The fine sediments are finally truncated on the shoreface.

the recession trend of the beach barrier during the interval encompassed by the time of deposition of the fine sediments and the layers above.

In the Gulf of Lions, according to the sedimentary prism model described above, it is likely that the fine sediment sharply separated from the overlying beach barrier sand, corresponds to the lagoonal sedimentary unit. Thus the location of a back barrier lagoonal sequence below the present beach-shoreface sediment also implies the landward migration of a former beach barrier (Fig. 7B). The age and the duration of that displacement remain to be documented.

Some indications of coastal recession are provided by shipwreck remnants like the column shafts and a grinding stone disclosed during the sounding operations at a 6 m-depth. A circular depression, 0.5–1 m in depth, has been scoured around the protruding cylinder blocks and indicates their tendency to sink *in situ* into the sand. Archaeologists believe they could be the cargo of a Roman wrecked ship but, unfortunately, no precise age may be given. Similar pieces are recorded in the neighbourhood and dated between the 1st and the 3rd century A.D. In fact, wrecks in the vicinity of the 6 m-line were recorded since the beginning of diving exploration of the coast suggesting it was the location of a particular barrier in the past. A modern wreck, the French vessel 'Rhône', recently explored (Degage *et al.*, 1991) was stranded in 1836 not far from the shore as demonstrated by paintings. Recent observations clearly relate the location of this wreck to the position of the present-day outer offshore bar.

Then, we have assumed that most of the wrecks were the consequence of grounding on the outer offshore bar the position of which should have been around the present 6 m bathymetric line. If this assumption is true the location of wrecks like the one with the shafts mentioned above implies a 400 m shift of the littoral system. About 17 wrecks have been recorded by the Archaeological Service (DRASM in Marseilles) for the marine region being facing the Thau lido. Among them two only are out of the nearshore zone (ca. 8 and 11 m) and the possibility of a grounding may be discarded for them. If the age of the wreck is plotted against the depth of recovery (each of them with a variable accuracy due to the varying quality of diving reports), it may be noticed a lack of information about wrecks between the 1st century A.D. and the 17th/18th century (Fig. 8). Therefore, two scenarios may explain the retrogradational trend of the coastline. One with a very rapid and perhaps recent change in the coastal regime between both time limits and another one with a more regular variation.

DISCUSSION AND CONCLUSION

Whatever the cause of the retrogradational migration

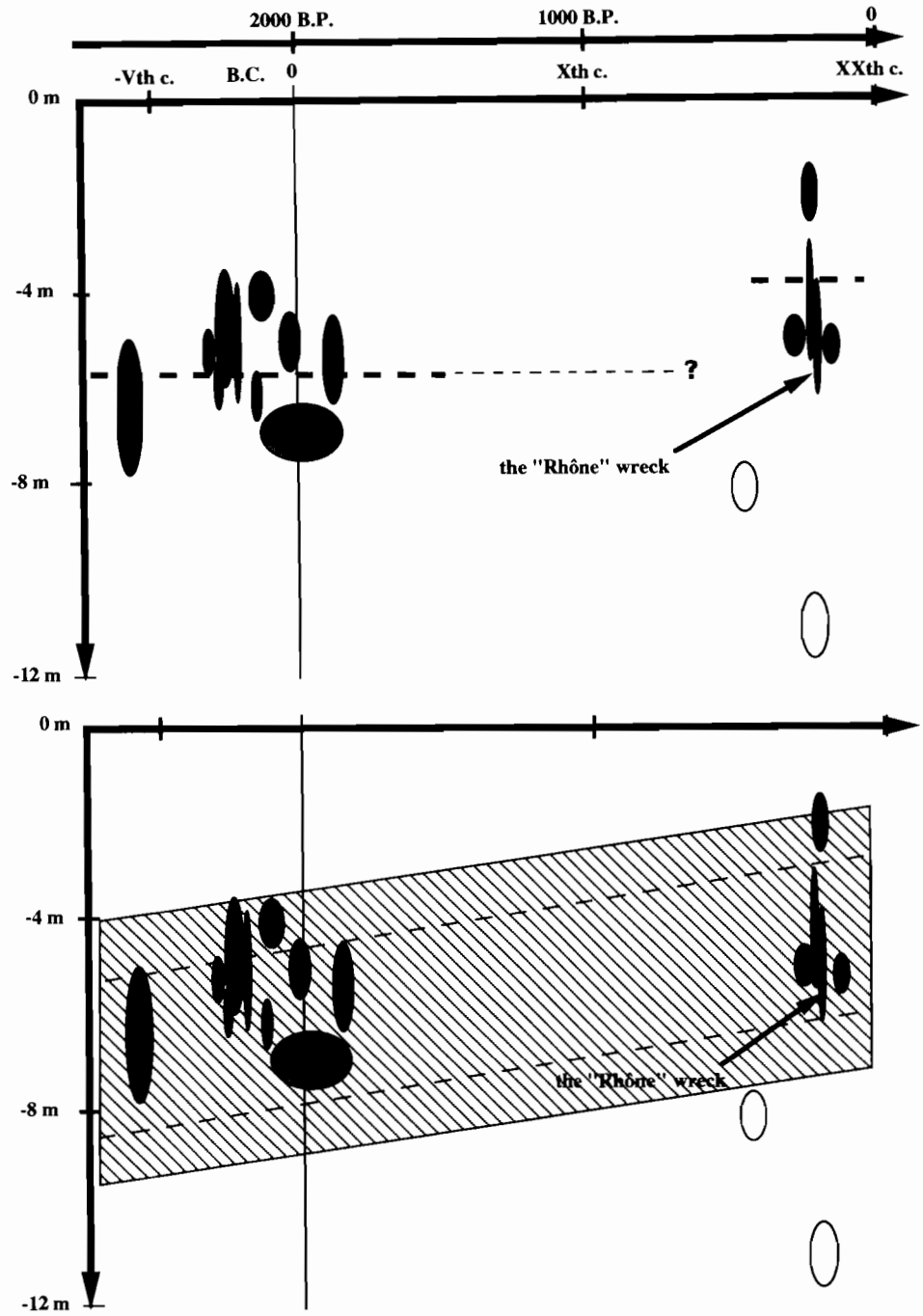

FIG. 8. Age vs. depth plot for wrecks recorded on the Thau lido shoreface.

of the beach and shoreface system in both examples described above, the following characters emerge: (1) the beach barrier rolled over the lagoonal or mud flat deposits when migrating landward, (2) sea level did not undergo any significant change during a time interval encompassing the more recent dates of the sedimentary record for the formation of the fine deposits, around 1180 BP (Senegal coast) or 2050 BP (Gulf of Lions coast).

Various models that account the first characteristic usually assume that there has been a sea level change (Bruun, 1954; Plint, 1988; Gagan *et al.*, 1994). According to the Bruun model, a regressive trend of the shoreline is the consequence of a sea level rise according the relation $R/S = 1/\tan\theta$ (with R the horizontal retreat, S the rise in mean water level and $\tan\theta$ the mean slope of the coastal zone). In the case study of the Thau lido shoreface (R = 400 m; $\tan\theta$ = 1%), this relationship would signify an unrealistic 4 m sea level rise in the last 2 millenia. Roy and Cowell (1995) recently have shown that a slow rate (<0.3 m/century) of relative sea level change gives an important role to external factors such as the sediment supply (or loss) rate, a position supported also by Barusseau and Radakovitch (1996). In such a case, Gagan *et al.* (1994), observed a progradational trend of the littoral system. The reverse is observed here illustrating the extreme sensitivity of the balance between active factors: sediment input and morphodynamic agents, as suggested by Gagan *et al.* (1994), Roy *et al.* (1994) and Cowell *et al.* (1995). The starvation context,

in both cases studied here, might be the main factor of the observed retrogradational trend.

ACKNOWLEDGEMENTS

We are greatly indebted to Dr R.J. Devoy for a thorough revision of the first Frenglish text and to Dr Peter Roy for discussing and greatly improving this first version and for his constructive recommendations.

The authors wish to thank: the French Ministry of Cooperation, whose series of subsidies granted in the framework of a CAMPUS program and of an inter-university Convention between the Universities of Perpignan and Dakar, allowed the work on the Flèche de Sangomar to be carried out, the ORSTOM for its assistance, mainly logistic, during the field work, the Languedoc-Roussillon region for a contract on the subject of coastal erosion.

REFERENCES

Aloïsi, J.C. (1986). Sur un modèle de sédimentation deltaïque. Contribution à la connaissance des marges passives. Unpublished Thesis, Perpignan, 162 pp.

Anonymous (1984). *Catalogue sédimentologique des côtes de France, Côtes de la Méditerranée*. Collection de la Direction des Etudes et Recherches d'Electricité de france, 52, Editions Eyrolles, Paris.

Ausseil-Badie, J. (1978). Contribution à l'étude paléoécologique des foraminifères du Quaternaire terminal sur le plateau continental languedocien. Unpublished Thesis, Toulouse, 164 pp.

Ausseil-Badie, J. (1988). Influence des environnements intertropicaux sur le morphologie et la composition géochimique de tests de Foraminifères (genre *Ammonia*) du Sénégal. *Compte-rendus de l'Académie des Sciences, Paris*, **306**, 565–568.

Ausseil-Badie, J., Barusseau, J.P., Descamps, C., Diop, E.S., Giresse, P. and Pazdur, M. (1991). The Holocene deltaic sequence in the Saloum estuary (Senegal). *Quaternary Research*, **36,** 178–194.

Barusseau, J.P. (1980). Essai d'évaluation des transports sableux sous l'action des houles entre Saint-Louis et Joal (Sénégal). *Bulletin de l'Association Sénégalaise d'Etude du Quaternaire, Dakar*, **58-59,** 31–39.

Barusseau, J.P. and Radakovitch, O. (1996). Geological record of littoral sedimentary processes at short time-scales. *Journal of Coastal Research*, **12,** 3.

Barusseau, J.P. (1986). Conséquences sédimentologiques de l'évolution climatique récente dans le delta du Saloum. *Océanographie Tropicale*, **21,** 89–98.

Barusseau, J.P., Descamps, C., Radulescu, M., Akouango, E. and Gerbe, A. (1994). Morphosedimentary multiyear changes on a barred coast (Gulf of Lions, Mediterranean Sea, France). *Marine Geology*, **122,** 47–62.

Barusseau, J.P. (1973). Evolution du plateau continental rochelais (golfe de Gascogne) au cours du Pléistocène terminal et de l'Holocène. Les processus actuels de la sédimentation. Unpublished thesis, Bordeaux, 366 pp.

Barusseau, J.P., Diop, E.H.S., Giresse, P., Monteillet, J. and Saos, J.L. (1983). Etude de l'environnement côtier au Sud-Est du Cap-Vert (Sénégal). Analyse sédimentologique. *Rapports Scientifiques du Centre de Recherches Océanographiques de Dakar-Thiaroye*, pp. 65–83.

Barusseau, J.P., Giresse, P., Faure, H., Lezine, A.M. and Masse, J.P. (1988). Marine sedimentary environments on some parts of the tropical and equatorial margins of Africa during the late Quaternary. *Continental Shelf Research*, **8,** 1–21.

Barusseau, J.P. and Saint-Guily, B. (1981). Disposition, caractères et mode de formation des barres d'avant-côte festonnées du littoral Languedoc-Roussillon. *Oceanologica Acta*, **4,** 297–304.

Bruun, P.M. (1954) Coast erosion and the development on beach profile. *Technical report, Beach Erosion board*, **54,** 22.

Cowell, P.J., Roy, P.S. and Thom, B.G. (1995). Effect of barrier and offshore slope on rates of coastal change due to sea level rise and littoral sand loss. *International Geological Correlation Program Project 367: Late Quaternary coastal records of rapid change: Application to present and future conditions. IInd Annual Meeting (Antofogasta, Chile)*. Abstract volume, pp. 23–24.

Degage, A., Golf, A. and Sagnes, J. (1991). *Le Rhône. Histoire d'une corvette de charge et de ses commandants*. CLERSMAR, Marseillan, 173 pp.

Gagan, M.K., Johnson, D.P. and Crowley, G.M. (1994). Sea level control of stacked late Quaternary coastal sequences, central Great Barrier Reef. *Sedimentology*, **41,** 329–351.

Jago, C.F. and Barusseau, J.P. (1981). Sediment entrainment on a wave-graded shelf, Roussillon, France. *Marine Geology*, **42,** 279–299.

Kalk, Y. (1978). Evolution des zones à mangrove du Sénégal au Quaternaire récent. Etudes géologiques et géochimiques. Unpublished Thesis, University Louis Pasteur, Strasbourg, 117 pp.

Köster, R. (1995). Shoreline erosion, climatic change and sea level oscillations on islands of the North Sea and the Baltic Sea. *International Geological Correlation Program Project 367: Late Quaternary coastal records of rapid change: Application to present and future conditions. IInd Annual Meeting (Antofogasta, Chile)*. Abstract volume, pp. 67–68.

L'Homer, A., Bazile, F., Thommeret, J. and Thommeret, Y. (1981). Principales étapes de l'édification du delta du Rhône de 7000 ans BP à nos jours: variations du niveau marin. *Océanis, Variations in sea-level, Special Issue*, **7,** 389–408.

Leprun, J.C., Marius, C. and Perraud, E. (1976). Caractérisation de la pédogenèse durant le dernier millénaire sur les amas coquilliers des îles du Saloum (Sénégal). *Bulletin de l'Association Sénégalaise d'Etude du Quaternaire, Dakar*, **49,** 13–25.

Martin, R., Gadel, F.Y. and Barusseau, J.P. (1981). Evolution of Canet-St-Nazaire Lagoon (golfe du Lion, France) during the last stages of the Holocene. *Sedimentology*, **28,** 823–836.

Niedoroda, A.W., Swift, D.J.P. and Hopkins, T.S. (1985). The shoreface. *In*: Davis, R.A., Jr (ed.). *Coastal Sedimentary Environments*, **8**, 533–624.

Plint, A.G. (1988). Sharp-based shoreface sequences and 'offshore bars' in the Cardium formation of Alberta: their relationship to relative changes in sea level. *In*: Wilgus, C.K., Hastings, B.S., Posamentier, H. Van Wagoner, J., Ross, C.A. and Kendall, C.G. St C. (eds), *Sea-level changes - An integrated approach. Tulsa: SEPM Special Publication*, **42**, 357–370.

Roy, P.S., Cowell, P.J., Ferland, M.A. and Thom, B.G. (1994) Wave dominated coast. *In*: Carter, R.W.G. and Woodroffe, C.D. (eds), *Coastal Evolution*, pp. 121–186. Cambridge University Press.

Roy, P.S., and Cowell, P.J. (1995). Chaotic coastal behaviour under conditions of slowly rising sea level. *International Geological Correlation Program Project 367: Late Quaternary coastal records of rapid change: Application to present and future conditions. IInd Annual Meeting (Antofogasta, Chile)*. Abstract volume, pp. 101–102.

Thilmans, G. and Descamps, C. (1982). Amas et tumulus coquilliers du delta du Saloum. *Mémoires de l'Institut Fondamental d'Afrique Noire*, **92,** 31–50.

Verstraete, J.M. (1986). Variations saisonnières et interannuelles du niveau moyen dans l'Atlantique équatorial et tropical en 1983-84. *Changements globaux en Afrique durant le Quaternaire Paris: ORSTOM, Travaux et Documents*, **197,** 481–482.

Pergamon

Quaternary Science Reviews, Vol 15, pp 773–780, 1996.

PII: S0277-3791(96)00071-6
0277-3791/96 $32.00

GLOBAL AND REGIONAL FACTORS CONTROLLING CHANGES OF COASTLINES IN SOUTHERN IBERIA (SPAIN) DURING THE HOLOCENE

JOSÉ LUIS GOY,* CARI ZAZO,† CRISTINO J. DABRIO,‡ JAVIER LARIO,† FRANCISCO BORJA,§ FRANCISCO J. SIERRO* and JOSÉ ABEL FLORES*

**Departamento de Geología (Geodinámica), Facultad de Ciencias, Universidad de Salamanca, 37008-Salamanca, Spain*

†Departamento de Geología, Museo Nacional Ciencias Naturales, C.S.I.C., Jose Gutiérrez Abascal 2, 28006-Madrid, Spain

‡Departamento de Estratigrafía (Facultad de Ciencias Geológicas) and Instituto de Geología Económica, C.S.I.C., Universidad Complutense, 28040-Madrid, Spain

§Area de Geografía Física, Facultad de Humanidades, Universidad de Huelva, 21007-Huelva, Spain

Abstract — The interaction between global (glacio-eustatic sea-level rise) and regional factors (oceanographic and tectonic) has controlled the evolution of coastline during the Holocene in Southern Iberia.

At ca. 10,000 ^{14}C years BP a deceleration of relative sea-level rise took place both in the Atlantic and Mediterranean littorals, with a maximum transgression at 6450 ^{14}C years BP. In subsiding areas (present tidal flats) estuaries illustrate a clear marine influence recorded both in sediments and the fauna while in uplifting areas prograding spit–bar systems developed. Two phases of major progradation are distinguished in these systems: the first one between 6450 and 3000 ^{14}C years BP, with a sedimentary gap at ca. 4000 ^{14}C years BP; and the second one from 2750 ^{14}C years BP up to present, with an intervening gap between 1200 and 1050 ^{14}C years BP. These progradation phases develop during stillstands followed by relative sea-level fall, while the sedimentary gaps represent relative high sea level. In the Mediterranean areas, with a higher uplift rate, marine terraces almost coeval to those gaps occur.

The most pronounced modifications in littoral dynamics occurred at between 3000 and 2750 ^{14}C years BP represented by changes in the direction of longshore drift and prevailing winds and in the predominance of progradation over aggradation processes.

At ca. 1000 ^{14}C years BP the estuaries record a greater fluvial than marine influence, and at 500 years ago an extraordinary increase in coastal progradation took place in all littoral zones. The European Medieval Warm period is characterized, at least during its initial phase, by low pressure climate conditions, while during the Little Ice Age anticyclonic conditions gave rise to a strong coastal progradation. Copyright © 1996 Elsevier Science Ltd

INTRODUCTION

Global factors, such as the general glacio-eustatic sea-level rise that took place from the Last Glacial Maximum until 6450^{14}C years BP, together with regional factors, such as tectonic or oceanographic ones, control the Holocene evolution of the coastline in the Iberian coast (Zazo *et al.*, 1996a). Here, the coasts of the Southern Iberian Peninsula, the main regional factors are: the tectonic framework (boundary between the European and African plates) with numerous active faults (Fig. 1) during the Late Pleistocene and Holocene that affected the coastline that produced areas of either uplifting or subsiding trends (Zazo *et al.*, 1994). Moreover, the area suffers the effects of the interchange of Atlantic and Mediterranean waters through the Gibraltar Strait, the present input of which bears seasonal variations, being greater in summer under anticyclonic conditions.

Detailed mapping, sedimentological analysis, archaeological and historical studies, and radiocarbon datings (Tables 1 and 2) carried out mainly in spit–bar systems, suggested the existence of two major phases of coastal progradation: the older one lasted from 6450–3000 ^{14}C years BP with a sedimentary gap or period of reduced sedimentation around ca. 4000 ^{14}C years BP; the younger one extends from 2750 ^{14}C years BP to Present, with an intervening gap in sedimentation between 1200 and 1050 ^{14}C years BP. Zazo *et al.* (1994) and Lario *et al.* (1995) have interpreted that the phases of progradation occur during periods of stillstand to gentle sea-level fall (minor lowstands), and are also related to increased entrance of 'Superficial Atlantic Waters' in the Mediterranean under anticyclonic conditions.

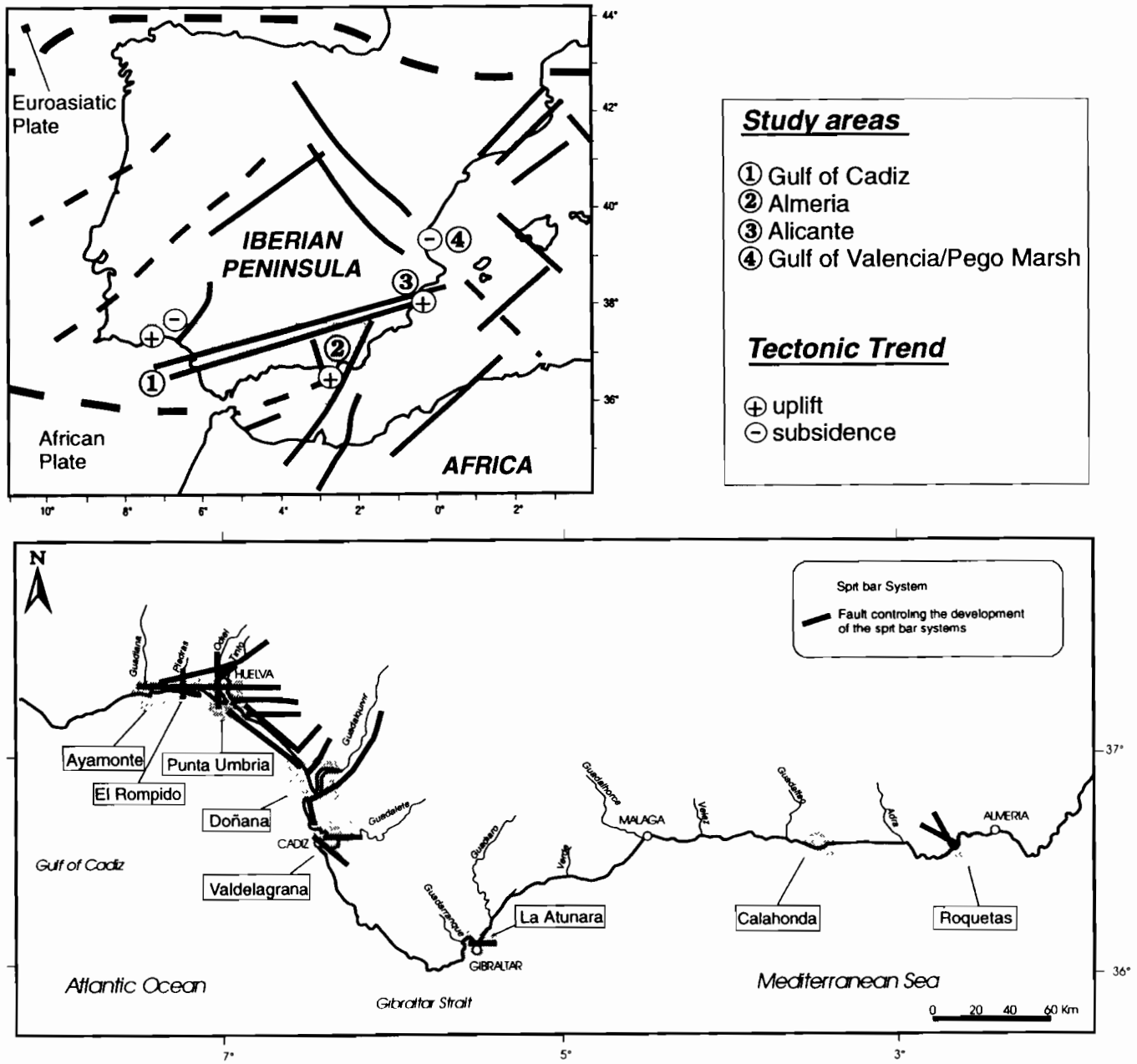

FIG. 1. Location of the study area and main fault systems affecting Late Pleistocene and Holocene coastal deposits.

More ^{14}C analysis and archaeological data, and increased availability of drill cores in the estuaries of Guadalete (Dabrio *et al.*, 1995) and Guadalquivir (Goy *et al.*, 1995) show evidence of rapid modifications to coastlines in Southern Iberia because of changes in littoral dynamics (changes in direction of prevailing winds and littoral drift) both before and after the two phases of coastal progradation (Tables 1 and 2).

The aims of this paper are: (1) to analyze the changes produced in the surveyed coastline and the main factors responsible for these changes during the Holocene, based on the analysis of the exposed morphosedimentary units (spit bars, tidal flats, deltas, alluvial plains) and drill cores from Gulf of Cadiz (Atlantic) and Gulf of Valencia (Viñals, 1991; Viñals and Fumanal, 1995); (2) to place these changes in a chronological sequence based upon radiocarbon dating (using uncorrected radiocarbon ages), archaeological, and historical data; and (3) to compare the changes with the classic climate changes described in Northern Europe.

CHANGES OF COASTLINES CA. 10,000 ^{14}C YEARS BP

Figure 2 shows the main changes observed in coastal morphology of Southern Iberian Peninsula taking into account the variable geodynamic behaviour both in tidal range (mesotidal in Atlantic and microtidal in Mediterranean) and the tectonic trend (uplift/subsidence). Data from morphosedimentary units exposed on land or drowned (estuaries, tidal flats, alluvial plains, peat

TABLE 1. ^{14}C Ages of coastal deposits from south and southeast Spain

Sample	Locality	Laboratory	^{14}C years BP	Material	Unit	Reference
PG-12	La Atunara	UQM	2675±110	shell	beach	Lario *et al.*, 1995
PG-13	La Atunara	UQM	3200±110	shell	beach	Lario *et al.*, 1995
PG-14	La Atunara	UQM	3140±120	shell	beach	Lario *et al.*, 1995
PEGO	Alicante	R-2013	6130±100	shell	beach	Viñals and Fumanal, 1995
CH-1	Calahonda	LGQ-1025	1520±170	shell	spit bar	Lario *et al.*, 1995
CH-2	Calahonda	LGQ-1026	2720±180	shell	spit bar	Lario *et al.*, 1995
CH-3	Calahonda	LGQ-1027	800±190	shell	spit bar	Lario *et al.*, 1995
CH-4	Calahonda	LGQ-1028	720±190	shell	spit bar	Lario *et al.*, 1995
R-8	Roquetas	UQM	6450±100	shell	spit bar	Goy *et al.*, 1986
R-7	Roquetas	UQM	3600±100	shell	spit bar	Goy *et al.*, 1986
R-10	Roquetas	UQM	2150±400	shell	spit bar	Goy *et al.*, 1986
R-2	Roquetas	UQM	1870±35	shell	spit bar	Goy *et al.*, 1986
F-24	La Atunara	IRPA-1159	1210±35	shell	spit bar	
H-2	El Rompido	R-2179	1460±50	shell	spit bar	Zazo *et al.*, 1994
H-3	El Rompido	R-2180	1875±50	shell	spit bar	Zazo *et al.*, 1994
H-4	El Rompido	R-2207	1440±50	shell	spit bar	Zazo *et al.*, 1994
H-5	El Rompido	R-2203	2605±50	shell	spit bar	Zazo *et al.*, 1994
D-2	Doñana	R-2187	1790±50	shell	spit bar	Zazo *et al.*, 1994
D-7	Doñana	R-2206	2185±50	shell	spit bar	Zazo *et al.*, 1994
D-9	Doñana	R-2185	1860±50	shell	spit bar	Zazo *et al.*, 1994
D-11	Doñana	R-2210	2010±50	shell	spit bar	Zazo *et al.*, 1994
D-14	Doñana	R-2204	1490±50	shell	spit bar	Zazo *et al.*, 1994
D-15	Doñana	UtC-4185	2340±60	shell	spit bar	
D-16	Doñana	UtC-4188	1650±50	shell	spit bar	
D-17	Doñana	R-2188	1850±50	shell	spit bar	Zazo *et al.*, 1994
D-18	Doñana	UtC-4192	1370±60	shell	spit bar	
C-3	Valdelagrana	R-2182	2320±50	shell	spit bar	Zazo *et al.*, 1994
C-4	Valdelagrana	R-2208	3145±50	shell	spit bar	Zazo *et al.*, 1994
C-5	Valdelagrana	R-2181	2270±50	shell	spit bar	Zazo *et al.*, 1994
C-6	Valdelagrana	R-2186	2120±50	shell	spit bar	Zazo *et al.*, 1994

deposits, spit bars, marine terraces, and aeolian dunes) have been incorporated because they are useful for dating (Tables 1 and 2) and because their variable development allows interpretation of many major changes of coastal processes, climate and sea level.

Letters and symbols, in Fig. 2, indicate some processes of coastal dynamics (changes in littoral drift, or wind directions, fauna, and trends of relative sea level) that have been recorded and dated with a certain degree of confidence in the morphosedimentary units. Approximate present elevations of some morphosedimentary units (datum: Present Mean Sea Level, MSL) are indicated.

Drill cores from the Mediterranean area, particularly in the alluvial plain of Valencia Gulf (Viñals, 1991; Viñals and Fumanal, 1995), and in tidal flats of the Gulf of Cadiz (Dabrio *et al.*, 1995; Goy *et al.*, 1995; Zazo *et al.*, 1996b) indicate that the 'global' glacio-eustatic relative rise of sea level prior to ca. 10,000 ^{14}C years BP experienced a deceleration that favoured the start of development of peat layers that occur interbedded in lagoonal deposits (Mediterranean coast) or on intertidal flat sediments (Atlantic coast) (Fig. 3). A series of prograding bodies occurring in the shelf at about 50–60 m water depth are interpreted as stillstand deposits (Hernández-Molina *et al.*, 1994).

EVOLUTION OF THE COASTLINE BETWEEN CA. 10,000 AND 6450 ^{14}C YEARS BP

Atlantic Littoral

Wind patterns recorded in the systems of coastal dunes forming the present Asperillo cliff (northwest of the Guadalquivir estuary, Huelva coast), an area with an uplift trend, show a change in the direction of prevailing winds (Borja and Díaz del Olmo, 1995) between two dune deposits separated by a layer rich in organic matter dated (Tables 1 and 2) as ca. 10,000 ^{14}C years BP (Zazo *et al.*, 1996a). Wind directions changed from SW to W (palaeocurrents pointing towards the NE and E respectively).

Cores drilled in tidal flats of the Gulf of Cadiz (Fig. 3) record the rise of sea level as estuarine clay that directly overlay peat layers. Upward increase in sand content and faunal content indicate partial filling of the estuary and development of tidal flats.

Analysis of microfauna (Fig. 4) reveals a noticeable increase of Miliolids and fragments of Echinoderms and a decrease of *Haynesina germanica* and *Elphidium excavatum* in sediments deposited between 8000 and 7000 ^{14}C years BP. We think that the change is related to more-open marine conditions in the estuaries during this time.

TABLE 1. *cont'd*

Sample	Locality	Laboratory	^{14}C yearsBP	Material	Unit	Reference
PU95-1	Punta Umbría	GX-20907	3315±70	shell	spit bar	
PU95-2	Punta Umbría	GX-20908	3555±75	shell	spit bar	
PU95-3	Punta Umbría	GX-20909	1900±70	shell	spit bar	
IC95-1	Ayamonte (I.Canela)	GX-20899	835±65	shell	spit bar	
IC95-3	Ayamonte (I.Canela)	GX-20900	3130±70	shell	spit bar	
AG-1	Alicante	SAN-CEDEX	5190±300	shell	marine terrace	Gozalvez, 1985
AG-2	Alicante	SAN-CEDEX	3640±330	shell	marine terrace	Gozalvez, 1985
AG-4	Alicante	SAN-CEDEX	5540±170	shell	marine terrace	Gozalvez, 1985
F-17	S.Roque-La Atunara	UtC-4189[1]	2760±50	shell	marine terrace	
PEGO-1	Alicante	UBAR-77	10,120±460	organic mud	marsh	Viñals and Fumanal, 1995
PEGO-3	Alicante	UBAR-78	8300±90	organic mud	marsh[2]	Viñals, 1991
PEGO-5	Alicante	UBAR-43	7120±90	organic mud	marsh[2]	Viñals, 1991
LP-13	Guadalquivir	UtC-4026[1]	2490±60	twigs	estuary[2]	
LP-13	Guadalquivir	UtC-4031[1]	2930±60	shell	estuary[2]	
PSM104/C0	Guadalete	GX-20913[1]	3505±55	organic muds	estuary[2]	
PSM104/C3	Guadalete	GX-20914[1]	5885±60	shell	estuary[2]	
PSM104/C5	Guadalete	GX-20925[1]	6420±45	shell	estuary[2]	
PSM104/C9	Guadalete	GX-20916[1]	7620±55	shell	estuary[2]	
PSM104/C11	Guadalete	GX-20917[1]	7840±45	shell	estuary[2]	
PSM104/C15	Guadalete	GX-20918[1]	8040±55	shell	estuary[2]	
PSM104/C20	Guadalete	GX-20919	8915±100	peat	estuary[2]	Dabrio *et al.*, 1995
PSM104/C21	Guadalete	GX-20920	9495±340	peat	estuary[2]	Dabrio *et al.*, 1995
A-7	El Asperillo	LGQ-759	10,500±50	peaty sand	dune slack	Zazo *et al.*, 1996a
A-7B	El Asperillo	LGQ-897	11,240±220	peaty sand	dune slack	Zazo *et al.*, 1996a

(1) AMS; (2) core Laboratories: UQM - GEOTOP, Université du Québèc à Montreal, H3C 3P8 Montréal, Canada; R - Dip. Fisica, Centro di Studio per la Geochimica Aplicata, Universitá 'La Sapienza', Roma, Italy; LGQ - Lab. de Géologie du Quaternaire, CNRS, Luminy, 13288 Marseille, France; IRPA - Institute Royal du Patrimonie Artistique, 1040 Bruxelles, Belgium; UtC - R.J. Van de Graaf Lab. 35080 TA Utrecht, The Netherlands; GX - Geochron Laboratory, Cambridge, Massachusetts, 02138 USA; SAN CEDEX - Serv. Aplic.Nucleares, Centro de Est. y Experiment. de O.P., Madrid, Sapin UBAR - Dept. Química Analítica, Universidad de Barcelona, CETA - CEDEX, Barcelona, Spain.

Mediterranean Littoral

A layer of basal peat found in cores drilled in the Pego marsh (Viñals, 1991; Viñals and Fumanal, 1995) provides ages ranging from 10,120±460 to 7120±90 ^{14}C years BP as it was deposited progressively landwards and peat layers were drowned and covered by retreating-beach deposits. This arrangement suggests coastal onlap and the corresponding relative rise of sea level.

The Holocene maximum (Flandrian transgression) has been dated in Southern Spain at 6450 ^{14}C years BP. This is when the progradation of spit bars began (Goy *et al.*, 1986; Zazo *et al.*, 1994).

EVOLUTION OF THE COASTLINE BETWEEN CA. 6450 AND 3000 ^{14}C YEARS BP

The first spit–bar system began to grow in areas with an uplift trend, particularly on the Mediterranean coast. There, in the most complete case study (Roquetas, Almería), the first phase of progradation includes two spit bars called H1 and H2 (Zazo *et al.*, 1994; Goy *et al.*, 1995; Lario *et al.*, 1995) separated from each other by a sedimentary gap at ca. 4000 ^{14}C years BP (Fig. 2).

In places where the geomorphological context does not favour the development of spit bars and there is a higher uplift trend, there is deposition of two raised marine terraces approximately at +1 m above present mean sea level. These have been dated at 5190±300 and 5540±170, the most ancient one; and 3640±330 ^{14}C years BP, the youngest one, in the Alicante coast (Gozalvez, 1985).

In subsiding areas (Gulf of Valencia) drill cores record marine beach deposits dated as 6130±100 ^{14}C years BP, overlaying lagoon deposits (Viñals and Fumanal, 1995). These are placed below present MSL.

In the Atlantic area, filling of open estuaries began at this time and aggradation clearly surpassed coastal progradation (Figs 2 and 3). Palaeontological (Fig. 4) and sedimentological data indicate that the marine influence in all the surveyed estuaries was less.

Regarding the relative changes of sea level, we interpret that spit–bar systems began to grow immediately after the maximum glacio-eustatic rise of sea level (ca. 6450 ^{14}C years BP). Progradation of spits was favoured by stillstand or gentle lowstand conditions, whereas the gap separating spit bars H1 and H2 (ca. 4000 ^{14}C years BP) should indicate a positive oscillation (rise) of sea level with gentle transgression inside the general regressive trend of the first phase of progradation.

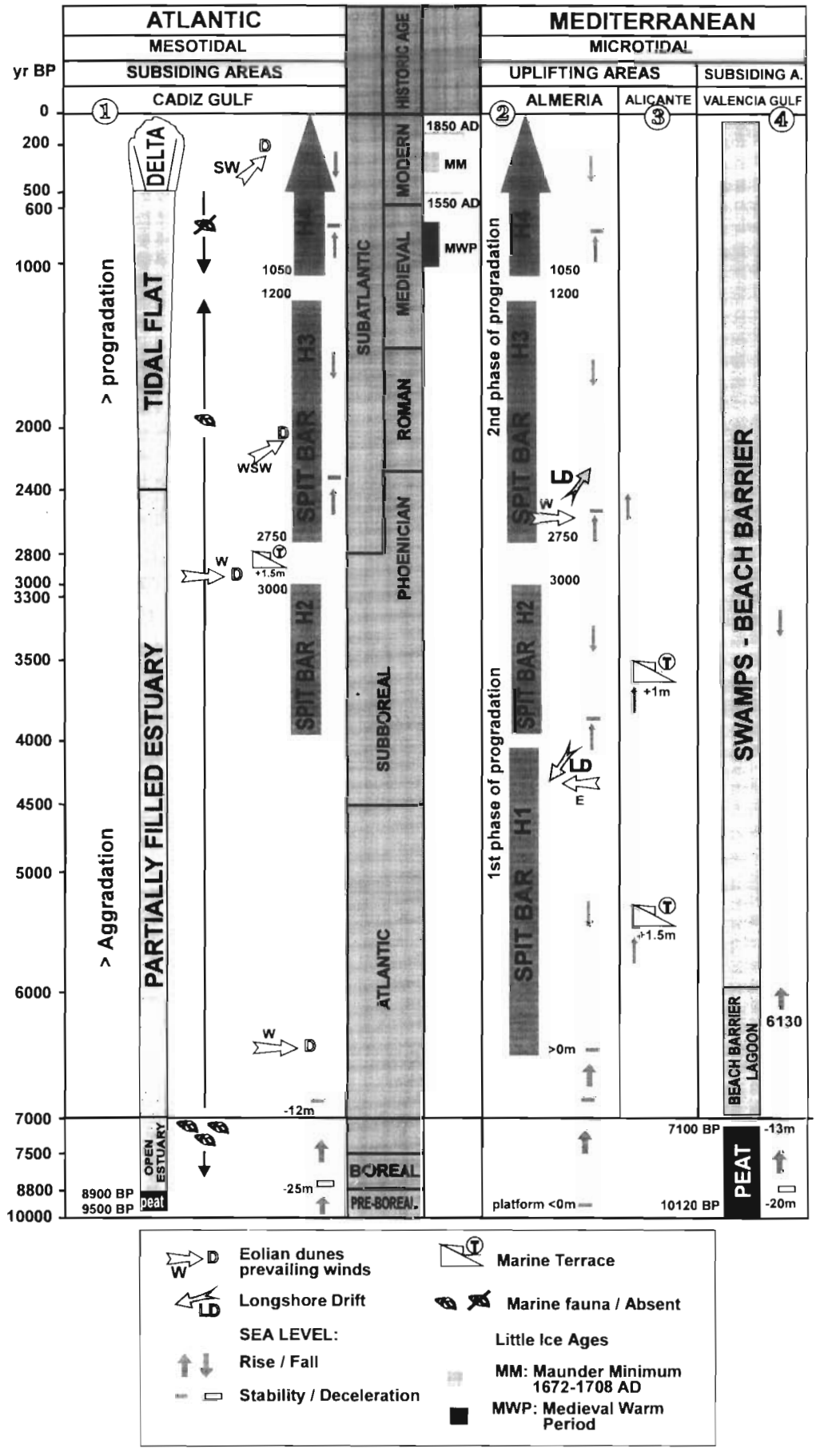

FIG. 2. Evolution of the shoreline during the Holocene in the Atlantic and Mediterranean littorals of Southern Spain in variable tectonic and tidal range settings (modified after Zazo *et al.*, 1996b).

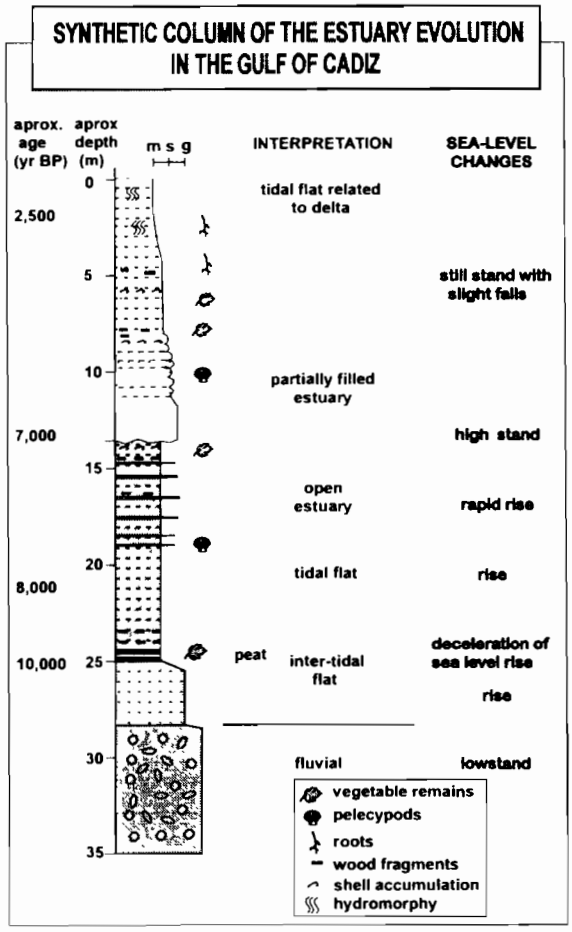

FIG. 3. Synthetic section of the evolution of the estuaries of the Gulf of Cadiz (Atlantic littoral) deduced from drill-core data (modified after Dabrio *et al.*, 1995).

Between 3000 and 2750 ^{14}C years BP a larger positive oscillation (rise) of sea level formed the gap that separates the two major phases of progradation (Fig. 2).

A seismic progradational unit made up by two minor subunits found in the Spanish Mediterranean continental shelf off Almeria (Hernández-Molina *et al.*, 1995) is interpreted as the record of two minor sea-level falls in the last 6500 years and correlated with the two prograding phases of the coast.

EVOLUTION OF THE COASTLINE BETWEEN CA. 2750 ^{14}C YEARS BP AND PRESENT

In the second, younger phase, processes of coastal progradation prevailed over aggradation in this region, independently of the tectonically-induced rate, and of subsidence of the area. As a result, the deposition of large systems of emerged spit bars in both the Mediterranean and Atlantic (Ayamonte, El Rompido, Punta Umbria, Doñana, Valdelagrana) coastlines reduced the connection of the Guadiana, Tinto-Odiel, Guadalquivir, and Guadalete (Gulf of Cadiz) estuaries with the open sea and they turned progressively into lagoons until they reached their present-day stage dominated by tidal flats and marsh.

Between 3000 and 2750 BP, a major change in the direction of prevailing winds in Almería (from Westerly to Easterly, palaeocurrents N90°E and 270°E respectively) caused reversing of littoral drift (Goy *et al.*, 1986) that is recorded in the systems of spit bars (H3 and H4) deposited during the second phase of progradation.

A change in prevailing winds is also recorded in the Atlantic coast along the Asperillo cliff outcrop (located between Huelva and Doñana). Aeolian-dune deposits yielding Roman remains were deposited under prevailing winds blowing from WSW. These overlay deposits of former aeolian-dune systems, accumulated by winds blowing from the west, which are covered by a palaeosoil incorporating neolithic–calcolithic artefacts (Borja and Díaz del Olmo, 1995). The younger systems of dunes step over the beach barrier deposits of spit bars accumulated during the second phase of progradation in Doñana (Huelva). There is evidence of a sudden marine fauna impoverishment and diversity drop ca 1000 ^{14}C years BP in cores drilled in the Guadalquivir marshland. Grain size

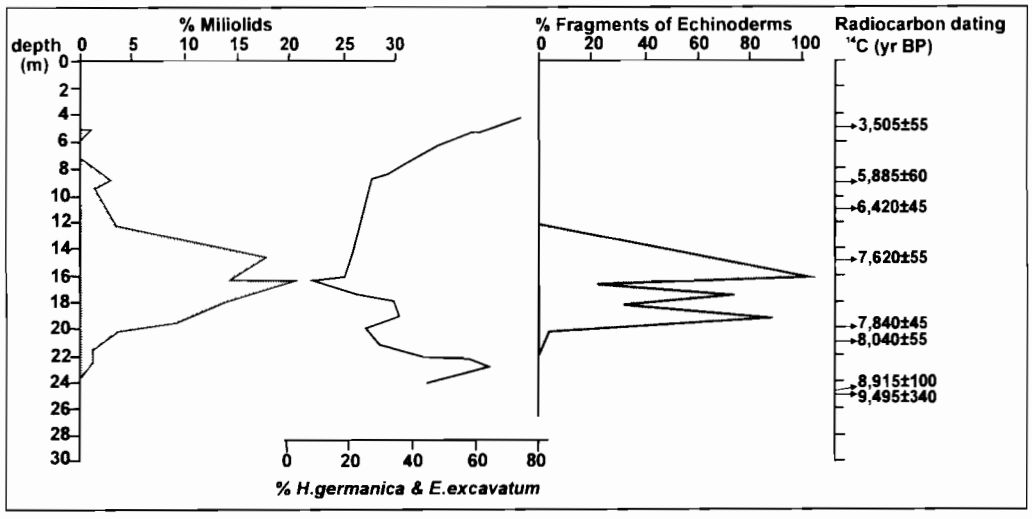

FIG. 4. Drill core PSM-104 (Guadalete marshlands, Gulf of Cadız) with indication of percent content of some faunal taxa with paleoenvironmental significance (Miliolids, *Haynesina germanica, Elphidium excavatum*, and fragments of Echinoderms), and radiocarbon data in the core.

analysis, particularly the mean and standard deviation, in the same cores indicate that the main phase of sedimentation with strong fluvial influence occurred after 2750 ^{14}C years BP.

An extraordinary increase in progradation is detected in both the Atlantic and Mediterranean littorals ca. 500 years ago and, particularly, after the 17th century as demonstrated by the present location of watch towers built up in that time (some of them are 200 m inland in Doñana spit bar) and also by other historical data like histroical maps and flood records (Lario *et al.*, 1995).

DISCUSSION AND CONCLUSIONS

The present arrangement of Holocene morphosedimentary units (emerged or drowned marine terraces, spit bars, peat layers) found in the littoral areas of Southern Iberian Peninsula results from the control of: (a) tectonic factors that imposed the rate, sign, and magnitude of subsidence; (b) the distance to sources of sediment supply for the coastal budget (river mouths), and (c) the variable input of superficial Atlantic Waters into the Mediterranean. This is particularly evident from ca. 6500 ^{14}C years BP up to Present.

The analysis of the morphosedimentary units allowed recontruction of the sea-level history as follows:

(1) The peat layer accumulation at ca. 10,000 ^{14}C years BP suggests a deceleration of the general sea-level rise.

(2) Spit–bar systems began to accumulate immediately after the Holocene highstand (at 6450 ^{14}C years BP) during stillstands followed by gentle relative sea-level falls.

(3) The gaps of sedimentation/progradation in the spit–bar systems record relative high sea level. Nevertheless there is a light diachronism with the ages obtained in the Mediterranean raised marine terraces which also developed during relative high sea-level, moreover in the Atlantic littoral the marine terrace exposed at +1.5 m in San Roque (La Atunara) is coeval with the gap that separates the two progradation phases (Fig. 2).

(4) Regarding the climate, the input of sediment in our lattitudes increased during floods (short period, strong rain under drought conditions) with anticyclonic conditions; under these conditions (presently in summer) the input of superficial Atlantic Waters in the Mediterranean increases as well.

The initial phase of the European Medieval Warm Period coincides with an epoch of reduced progradation probably under dominantly low-pressure conditions, while the 'Little Ice Age' corresponds to epochs of anticyclonic conditions, that is warm and with strong rain in short periods that results in a high sediment supply to the coast.

Until now, we have recognized several major changes of climatic parameters, recorded in the area as changes of littoral dynamics:

(1) Between 3000 and 2750 ^{14}C years BP the direction of prevailing winds both in Atlantic and Mediterranean coasts; littoral drift in the Mediterranean coasts changed; and there was an increase of progradation processes, that prevailed upon aggradation.

(2) At ca. 1000 ^{14}C years BP the coastal palaeogeography of the Atlantic area changed: as connections of estuaries with open sea were drastically reduced, faunas experienced a sudden impoverishment recorded in drill cores as lower diversity and absence of marine faunas in estuarine deposits.

(3) At ca. 500 years ago there was an extraordinary increase of coastal progradation in all the surveyed littorals. The direction of prevailing winds changed in the Atlantic and became the same as present.

ACKNOWLEDGEMENTS

Research supported by European Union Project EV5V-CT94-0445, Spanish DGICYT Projects PB92-0023 and PB92-282, Estación Biológica de Doñana C.S.I.C Project 143/90 and Research Fellowship EV5V-CT94-5243. It is a part of INQUA Shorelines Commission and IGCP Project 367.

REFERENCES

Borja, F. and Díaz del Olmo, F. (1995). Manto eólico litoral del Abalario (Huelva: Episodios morfogenéticos posteriores al 22.000 BP. Resum. Comunicación. *Congreso Paleoambientales cuaternarios de la Península Ibérica*, Santiago de Compostela, Octubre 1995. Abstract. Vol. **2**.

Dabrio, C.J., Goy, J.L., Lario, J., Zazo, C., González, A. and Borja, F. (1995). The Guadalete estuary during the Holocene times (Bay of Cadiz, Spain). *INQUA MBSS Subc, Newsletter,* **17,** 19–22.

Goy, J.L., Zazo, C., Dabrio, C.J. and Hillaire-Marcel, C.L. (1986). Evolution des systèmes de lagons-îles barrière du Tyrrhénien a l'actualité à Campo de Dalías (Almería, Espagne). *Edit. de l'Orstom, Coll. Travaux et Docments,* **197,** 169–171.

Goy, J.L., Zazo, C., Dabrio, C.J., Lario, J., Borja, F., Sierro, F.J. and Flores, J.A. (1995). Global and Regional factors controlling changes of coastlines in southern Iberia during the Holocene. *IGCP Project 367: Late Quaternary coastal records of rapid change; Application to present and future conditions.IInd Annual Meeting* (Antofagasta, Chile, Nov, 1995), *Abst. vol.,* pp. 37–38.

Gozalvez, V. (1985). Precisiones sobre los depósitos cuaternarios en la antigua albufera del Saladar de Alicante. *In*: Servicio de Publicaciones Universidad de Valencia (Ed.). *Pleistoceno y Geomorfología litoral.* Libro Homenaje a Juan Cuerda, pp. 35–52.

Hernández-Molina, F.J., Somoza, L., Rey, J. and Pomar, L. (1994). Late Pleistocene–Holocene sediments on the spanish continental shelves: Model for very high resolution sequence stratigraphy. *Marine Geology,* **120,** 129–174.

Hernández-Molina, F.J., Somoza, L., Vázquez, J.T. and Rey, J. (1995). Estructuración de los prismas litorales del Cabo de Gata: respuesta a los cambios climáticos-eustáticos holocenos. *Geogaceta,* **18,** 79–82.

Lario, J., Zazo, C., Dabrio, C.J., Somoza, L., Goy, J.L., Bardaji, T. and Silva, P.G. (1995). Record of recent Holocene sediment input on spit bars and deltas of south Spain. *In*: Core, B. (ed.), Holocene cyclic pulses and sedimentation. *Journal of Coastal Research, Special Issue*, **17**, 241–245.

Viñals, M.J. (1991). Evolución geomorfológica de la Marjal de Oliva-Pego (Valencia). Ph.D. Thesis, Universidad de Valencia, 466 pp.

Viñals, M.J. and Fumanal, M.P. (1995). Quaternary development and evolution of sedimentary environments in the Central Spanish Coast. *Quaternary International*, **29/30**, 119–128.

Zazo, C., Goy, J.L., Somoza, L., Dabrio, C.J., Belluomini, G., Improta, S., Lario, J., Bardají, Bardají and Silva, P.G. (1994). Holocene sequence of sea level fluctuations in relation to climatic trends in the Atlantic–Mediterranean linkage coast. *Journal of Coastal Research,* **10,** 933–945.

Zazo, C., Goy, J.L., Lario, J. and Silva, P.G. (1996). Littoral zone and rapid climatic changes during the last 20,000 years. The Iberia study case. *Zeitschrift fur Geomorphology,* **102,** 119–134.

Zazo, C., Dabrio, C.J., Goy, J.L., Bardaji, T., Ghaleb, B., Lario, J., Hoyos, M., Hillaire-Marcel, Cl., Sierro, F., Flores, J.A., Silva, P. and Borja, F. (1996b). Cambios en la dinámica litoral y nivel del mar durante el Holoceno en el Sur de Iberia y Canarias. *Geogaceta*, **20**, 1679–1682.

Pergamon

Quaternary Science Reviews, Vol. 15, pp. 781–787, 1996.

PII: S0277-3791(96)00070-4
0277-3791/96 $32.00

HOLOCENE SEA-LEVEL VARIATIONS AND GEOMORPHOLOGICAL RESPONSE: AN EXAMPLE FROM NORTHERN BRITTANY (FRANCE)

H. REGNAULD,* S. JENNINGS,† C. DELANEY‡ and L. LEMASSON*

**Université de Rennes 2, URA 141 and 1687 CNRS, 6 Avenue G. Berger 35043 Rennes, France*
†School of Geography, University of North London, 62–66 Highbury Grove, London N5 2AD, U.K.
‡Department of Geography, University College Cork, Cork, Ireland

Abstract — In northern Brittany an important geomorphological response to Holocene sea-level rise has been the development of coastal dunes with associated lagoons and marshes. At Anse du Verger, a marsh has formed behind a dune system which has been developing *in situ* for the last 4000 years. The lithostratigraphy of the marsh comprises extensive peat formation, with sands, silts and occasional sand lenses, the latter probably associated with storm surges. The sequence dates from 10,320±120 BP. After 3000 BP, flood episodes on the marsh are more common, while the upper marsh deposits can be correlated with the recent period of dune building. Prehistoric artifacts (remains of cooking implements) have been found on a cliff to the east of the marsh and are buried by washover deposits, which indicates a sudden abandonment of a settlement possibly due to a storm surge soon after 2460±80 BP. Surge levels are proposed as a controlling factor on dune crest elevation. Copyright © 1996 Elsevier Science Ltd

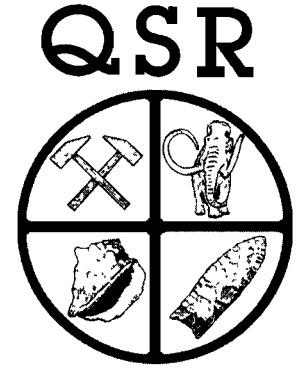

INTRODUCTION

Holocene relative sea-level (RSL) change along the Channel coast of Brittany is characterised by an almost continuous rise from −110 m NGF (Pinot, 1974) to its present position, with three short periods of negative tendency at around 10,000 BP, 4000 BP and 3000 BP (Guilcher and Hallegouet, 1991; Meur, 1993). This paper aims to examine the geomorphological response of this coastline to long-term (Holocene) and to short-term (storm surge) RSL movements.

The study area is located between Saint Malo and the Mont Saint Michel (Fig. 1). This area is composed of several bays, about 1 km across, separated from each other by the rocky (migmatite) capes of Anse du Guesclin, Anse du Petit Port, Anse du Verger, Anse de la Touesse, Anse de la Moulière and Anse de la Saussaye. The submarine topography comprises a large sand flat locally interrupted by rocky islands. The beaches are reflective and consist of medium to coarse sand, behind which are dunes six to twelve metres high that enclose freshwater marshes. The slopes of the capes are covered by periglacial drift, mainly head with intercalated aeolian sand layers.

TECHNIQUES

Field investigations from 1991 to 1995 established a series of topographic profiles across the beaches shown on Fig. 1, down to the 10 m isobath. This has included a survey every month for the last year (1994–1995). Cross-sections of the slope deposits were examined, and grain size and shape analysis was undertaken. Over 20 cores, mostly in the marsh at Anse du Verger, examined the lithostratigraphy of backbarrier/lagoonal sediments, with a small number of cores taken on the foreshore. A total of 12 radiocarbon dates were obtained from the marsh, foreshore and slope deposits (Tables 1 and 2). Air photographic data were used to measure changes in the position of dunes since 1948.

RESULTS AND INTERPRETATIONS

Dune and Beach Profiles

An example of recent changes to dune and beach profiles is given by the results from the Anse de la Saussaye. Since the Second World War the dune has receded by more than 50 m at an average rate of 1 ma^{-1} (Ministère de l'Equipement Data Base). This represents a loss of 250,000 m^3 of sand. However, the dune has not been receding over the last five years and has gained 600 m^3 of sand, suggesting that there are short-term cycles of growth within the longer-term trend of dune erosion. Short-term dune building can be correlated with periods of reduced storm surge activity, whereas erosion follows major surge events, for example in 1987, 1991 (Regnauld and Kuzucuoglu, 1992) and 1995, suggesting

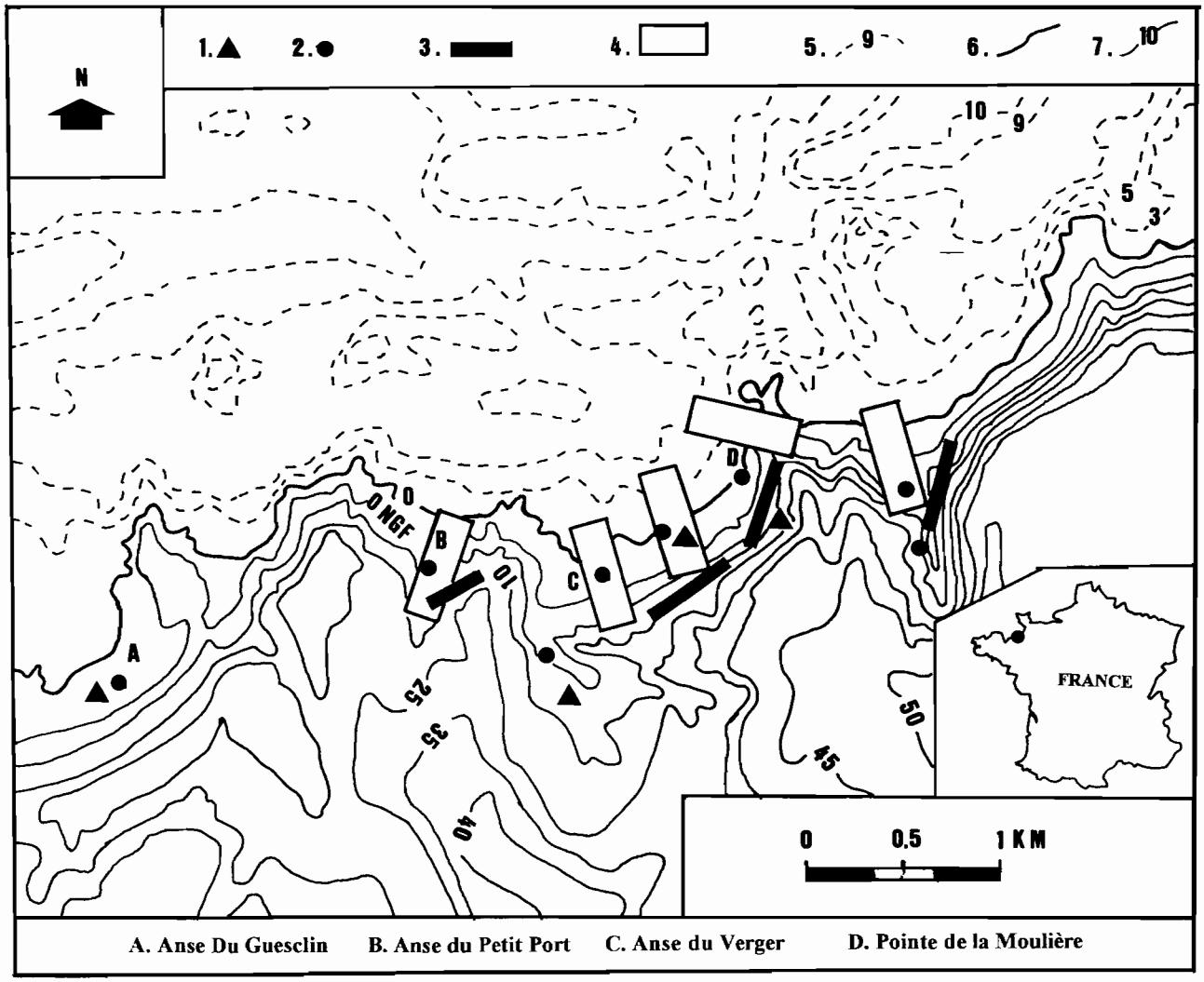

FIG. 1. Location of sites mentioned in the text. Tidal range in this area is 14 m during spring tides. Key: (1) location of ^{14}C samples; (2) area of coring; (3) area of trenches and cross-sections; (4) location of topographic profiles; (5) marine chart datum; (6) N.G.F. sea level datum, 7.45 m above marine chart sea level datum; (7) land surface datum (NGF).

that dune development is closely controlled by climatic forcing.

The eroded dune profile comprises a low ridge with an elevation of 1 to 1.5 m above MHWST level, before accumulation begins again. Transfer of sand between the dune and the beach face takes place, so that beach profiles also undergo considerable change. One example is illustrated in Fig. 2, showing profile changes over a single year, 10 years and 47 years.

At Anse de la Moulière, a transect from the foreshore, through a dune and onto the adjoining hill slope illustrates a succession of deposits that is typical of the other bays in this area (Fig. 3). Beneath the lower foreshore, at −7 to −8 m NGF (and therefore below the LW mark), is a thin layer of silty peat dated to 7580 BP (Bourcart and Boillot, 1960) and to 7310±80 BP (this paper, Tables 1 and 2) which rests upon a coarse sand with angular blocks and fragments of migmatite. This basal layer is probably equivalent to the head deposits on the exposed cliff section. Above the peat are the sands of the present beach, 1 to 1.5 m thick. In places a wave-cut platform rises above the beach sand to a maximum height of 3 m, which in turn is covered by head capped by bioturbated, aeolian deposits at the foot of the hill slope (Fig. 3). The origin of

TABLE 1. The results of radiocarbon dating from the Anse du Verger marsh and dune areaMarsh

Depth (m)	BH no.	Age BP	Calibrated age	Sediment
1.7	13 (beach)	7310±80	6145 BC	silty peat
1.0	5 (marsh)	113±10	1660 AD	peat
1.45	5 (marsh)	240±60	60 AD	peat
4.9	2 (marsh)	2630±130	805 BC	sandy peat
4.91	4 (marsh)	4020±170	2555 BC	silty peat
7.22	9 (marsh)	6980±140	5805 BC	sandy peat
7.5	9 (marsh)	9900±180		peat
8.09	9 (marsh)	10320±120		peat+grit

TABLE 2. Kitchen middens in dunes

Dune top (m)	Age BP	Calibrated age	Sediment	Dated artifacts
1.0	2560±80	770 BC	sand	shells
1.5	3640±80	2140 BC	sand	shells
0.98	2460±80	810 BC	sand	shells
1.2	3135±80	1515 BC	sand	shells

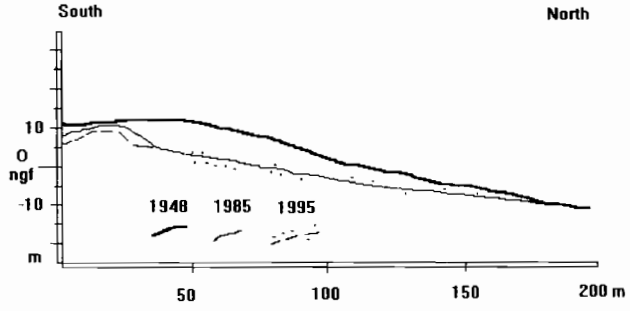

FIG. 2. Beach profile changes in Anse de la Touesse for 1995 (storm and constructional profiles); 1985; 1948.

the wave-cut platform is probably polycyclic, being reworked during successive interglacial sea-level maxima (Loyer *et al.*, 1995). A discontinuous pebble layer at the base of the head is considered to be the *in situ* remains of an Eemian beach, with the head and aeolian sand cover representing Weichselian deposits (Clet, 1983; Guilcher and Hallegouet, 1991). A dune which covers these Weichselian deposits contains 'kjökkenmödings' dating from 3640±80 BP (uncalibrated) to 2460±80 BP (uncalibrated; Regnauld *et al.*, 1995; this paper, Tables 1 and 2), which are covered by a storm surge deposit (Jelgersma *et al.*, 1995) of post-2460±80 BP age.

Anse du Verger Marsh Stratigraphy

Eighteen boreholes were cored in the marsh behind the dunes (Fig. 4). Most of the boreholes reached the migmatite basement, and therefore record the entire sequence of sediments. Depth to the basement is variable, ranging from 2 to 8 m, and this variability allows the basement topography to be reconstructed. The marsh sediments infill a depression, possibly a solution basin in the migmatite, enlarged by frost action during the cold stages of the Quaternary. Such features are common in Brittany. Typically, the basal layer of the infill is a grit

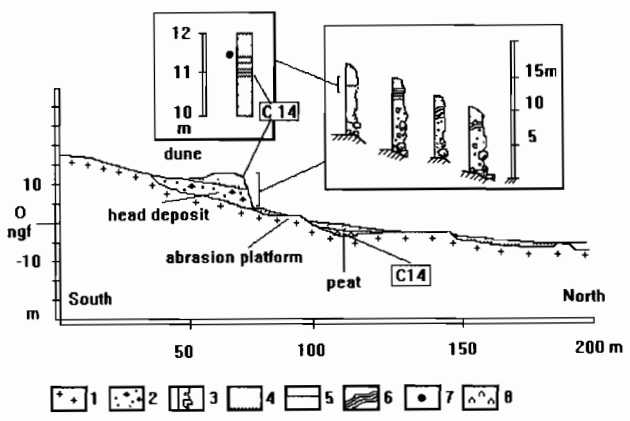

FIG. 3. Profile at Anse de la Moulière from below the LWST mark to a sequence of slope deposits above the HWST level. Inset shows details of east to west profile parallel to the beach. Key: (1) basement; (2) undifferentiated head; (3) head with underlying layer of raised beach gravels; (4) undifferentiated sand; (5) archaeological artifacts (cooking implements); (6) palaeosols within the head; (7) storm surge deposit; (8) peat dated to 7310±80 BP (Table 1).

with angular rock fragments in a silty matrix, which is similar to the coarse sand layer found under the foreshore peat (e.g. BH 13 in Fig. 4). This basal layer is interpreted as a periglacial slope deposit.

Overlying the basal layer is a freshwater peat which has a maximum recorded thickness of approximately 7 m, and dates from 10,320±120 BP (BH 9). Occasionally, terrestrial sand (with migmatite gravel) is incorporated into the base of the peat, and shell layers (broken *Mytilus* mainly) and marine sand lenses are found within the main body of the peat, which were probably deposited by extreme events, such as storm surges. The initiation of peat growth was diachronous within the marsh area, which is illustrated by the different dates obtained from the base of the peat in boreholes 2 and 4, even though they are at approximately the same depth (Fig. 4). This diachronous nature to peat formation may be explained by the palaeogeography of the marsh, as discussed below. BH 2 is located at the head of a thalweg which would have been the focus of a drainage system, and possibly later used as a tidal channel, delaying peat growth relative to surrounding areas (e.g. the location of BH 4).

The upper layers of the peat contain an increasing amount of sand and silt, which passes up into a surface sand deposit. This sand contains a mixture of aeolian dune sand and material derived from adjacent slopes. In BH 3 and 4 sand and peat intercalate, the latter providing radiocarbon dates of 113±10 BP and 240±60 BP. It is probable that the sand layers recorded in BH 3 and 4 are associated with slope wash resulting from agricultural activity, while the peat layers represent phases of slope stability. However, testing of this hypothesis must await the results of pollen analysis.

Palaeogeographical Reconstruction (Anse du Verger)

The results of the coring allow the palaeoenvironments of the Anse du Verger to be reconstructed (Fig. 5 in plan and Fig. 6 in section). At the opening of the Holocene (Fig. 5A), the Anse du Verger formed part of a broad drainage system which extended to a shoreline over 300 km to the west (Le Ricollais *et al.*, 1995). Within this drainage system, organic material accumulated in poorly drained areas (BH 9) on a gently inclined slope that culminates in a planation surface at an altitude of ±30 m NGF. The planation surface is polygenetic dating either to the Eocene (Guilcher and Hallegouet, 1991) or to the early Miocene (Le Ricollais *et al.*, 1995). A small abrasion platform was cut into the slope during the Eemian sea-level maximum (shown in Fig. 3).

By 7000 BP (Fig. 6a) peat growth had continued in the area of the present-day marsh, and organic material had also begun to accumulate on the slope below the abrasion platform (also illustrated in Fig. 3). By 4000 BP (Fig. 5b and Fig. 6b) RSL had risen sufficiently to deposit marine sediments over the organic deposits below the abrasion platform, while peat growth in the marsh area was probably assisted by increasingly impeded drainage due to RSL elevation and dune development. At this time in

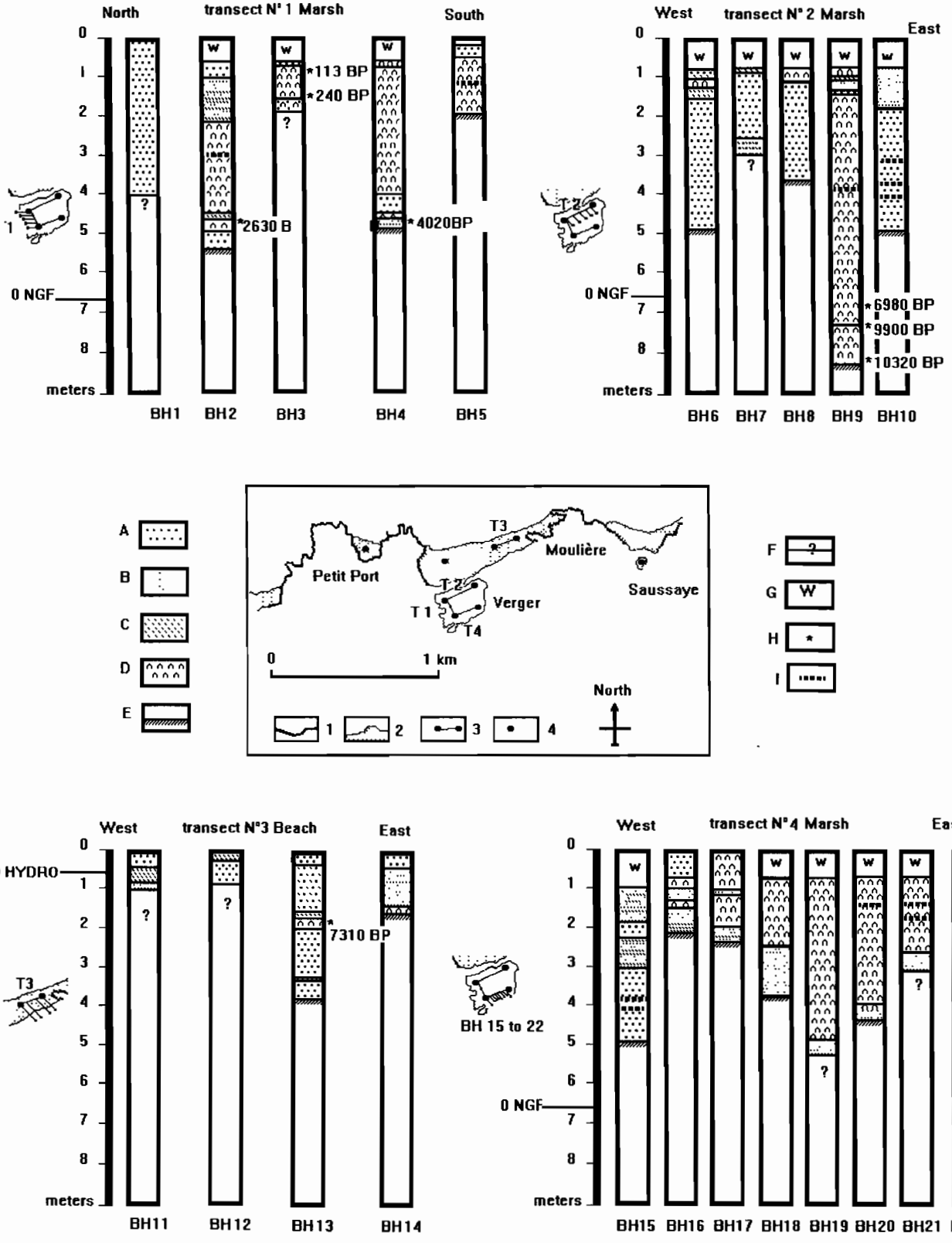

FIG. 4. Lithostratigraphic detail of the cores from the marsh in Anse du Verger. Key: (A) sand (terrestrial except in BHs 11, 13 and 14 in which it is marine); (B) silt; (C) clay; (D) freshwater peat; (E) basement with associated grit; (F) end of core, not reaching the basement; (G) water; (H) ^{14}C date; (I) storm surge deposit. Location of the cores is shown on the inset: (1) rocky outcrop; (2) beaches; (3) transects of cores; (4) isolated core.

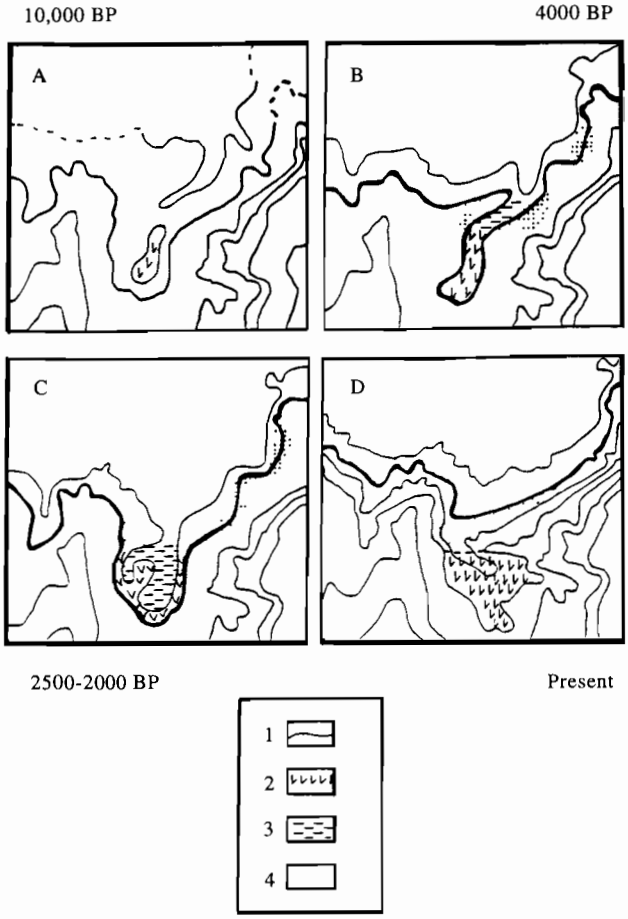

FIG. 5. Palaeoenvironmental reconstruction for the Anse du Verger area. Plan view. Stages of development at 10,000 BP, 4000 BP, 2600 BP and the present are shown. Key: (1) symbolises position of thalweg on 'A', but shows the approximate position of mean sea-level on 'B' and 'C'; (2) freshwater marsh; (3) tidal flats and channels; (4) dunes.

the neighbouring Anse de la Moulière, dunes had also developed and attained an elevation of at least 0.5 m above their contemporary HAT level (Regnauld *et al.*, 1995). The marsh at Anse du Verger was occasionally inundated by marine water, probably as a result of storm surges.

Between 2500 and 2000 BP (Fig. 5C and Fig. 6C) RSL rose more quickly (Fig. 7), attaining a position close to the present level. The marsh was again occasionally flooded by seawater (surge events?) during this period. It is likely that the sea had access to the marsh via two tidal channels, although there was probably a progressive withdrawal of the sea from the marsh due to continued dune development.

RSL Change and Storm Surge Events

A detailed assessment on RSL change and storm surge events from this work must await the outcome of a comprehensive biostratigraphic examination of the sediments below the marsh at Anse du Verger. However, the lithostratigraphic results presented here allow a preliminary reconstruction of RSL movements to be made, and suggest a general agreement between our data and the

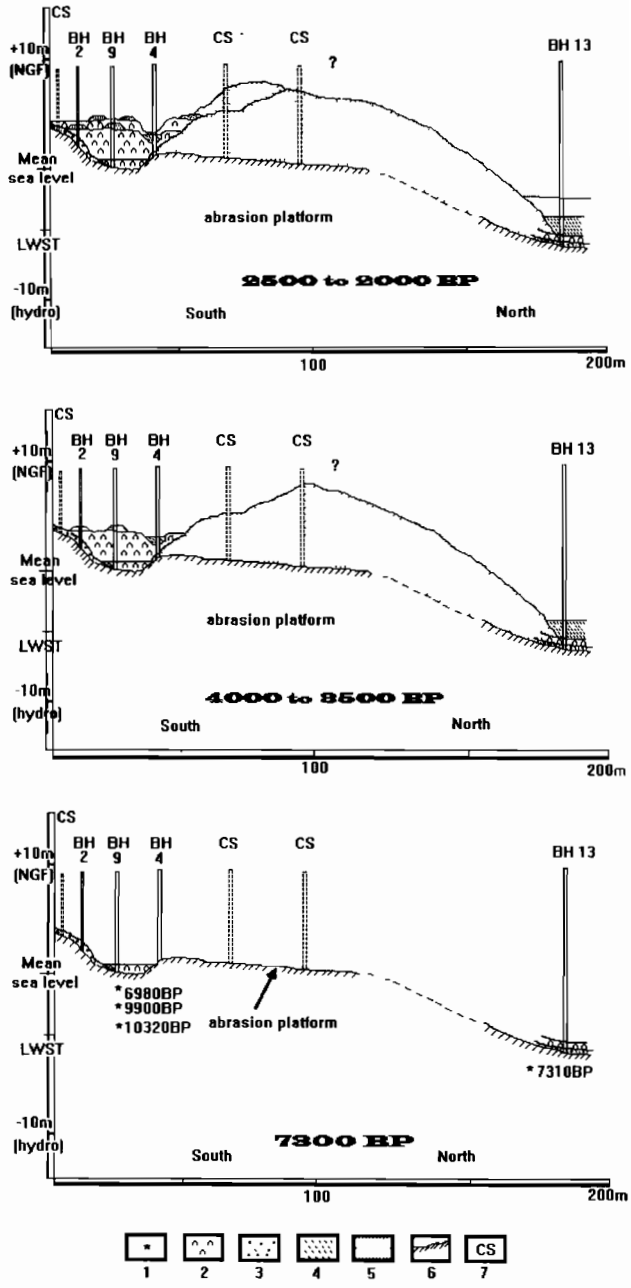

FIG. 6. Palaeoenvironmental reconstruction for the Anse du Verger marsh and dunes. Cross-section. Stages of development at 7000–10,000 BP, 3500–4000 BP and 2000–2500 BP are shown. Key: (1) ^{14}C date (see Table 1); (2) peat; (3) terrestrial sand; (4) marine silty clay; (5) marine and aeolian sand; (6) basement; (7) cross-section or borehole location.

RSL curve of Guilcher and Hallegouet (1991) (Fig. 7), which Pirazzoli (1991) considers to be the most reliable curve for this region. The degree to which the RSL trend has been affected by land movements is debatable. A slow uplift (1 mm/century) is suspected in the western part of Brittany, with a slower subsidence rate in the Mont Saint Michel area (Lenotre, 1994).

Within the sediments of the marsh are sand layers with shells which we interpret as storm surge deposits. Most of these have not been dated directly, and their approximate age has been inferred from the radiocarbon dating of the peat deposits within which the storm surge layers are embedded. These storm surge layers with their inferred

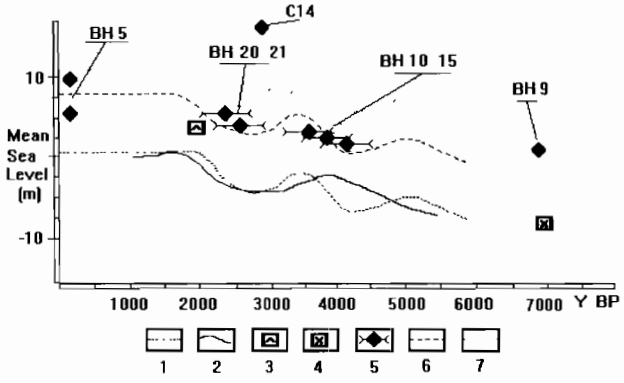

FIG. 7. Altitude of (palaeo)storm surge deposits (Anse du Verger) in relation to RSL elevation during the Holocene. Key: (1) RSL curve from Guilcher and Hallegouet (1991); (2) RSL curve from Morzadec-Kerfourn 1974; (3) high tide level index point; (4) tidal channel index point taken from the dated contact between the marine clay and organic sandy clay in BH 13; (5) storm surge level with time error range; (6) curve of dune crest elevation. Present value extrapolated back to the mid-Holocene; (7) 10^2 and 10^3 extreme wave height based on present values (data from the Navy, STNMTE, 1994) extrapolated back to the mid-Holocene.

age range are illustrated in Fig. 7. Their altitudinal relationship to their contemporary RSL, as extrapolated from the RSL curves of Guilcher and Hallegouet (1991), Morzadec-Kerfourn (1974) and Morzadec-Kerfourn and Monnier (1982) is shown. The elevation of each surge layer in Fig. 7 is drawn at a height just above its contemporary HWST level, and assumes no significant change in the tidal range during the mid- to late-Holocene. Despite the poor dating resolution for the storm surge events there is a correspondence between the timing of these events with periods of RSL rise on the Guilcher and Hallegouet (1991) RSL curve. This correspondence may be a consequence of the preservation potential of surge layers within the marsh, and is not a reflection of storm surge frequency. Preservation of storm surge deposits is enhanced during RSL rise periods due to faster accumulation rates of peat during these periods, as a result of a rising water-table.

DISCUSSION AND CONCLUSION

The recognition of climatic variability from stratigraphic and other data is central to our understanding of environmental change (Hugget, 1991; Dubreuil, 1992; Cortijo *et al.*, 1995). Storm frequency and intensity is one aspect to climatic variability, and one which is likely to have impacts on coastal areas, and therefore is likely to be, at least partially, recorded in coastal depositionary sequences, for example in dune morphology.

The storm surge deposits recorded in the Anse du Verger marsh and surrounding area would appear to represent surge magnitudes similar to modern day surges, although for reasons of preservation potential, it is unclear whether the frequency of surges has changed during the late-Holocene. Present accretion rates on dunes appear to be higher than the mean for the late-Holocene (0.5 m/1000 years), which may reflect an increase in wind speed, as recorded in the mid-1970s and 1980s and which was believed to be responsible for extreme surge events (Costa, 1995). However, this increase in surge magnitude may be a short-term cycle comparable with similar events during the Holocene recorded stratigraphically in the Anse du Verger area by the extreme surge levels dated to approximately 2460 BP and 7310 BP, shown on Fig. 7 as the two surge deposit 'outliers' recorded in the cross-section and BH 9, respectively.

A relationship between surge magnitude and dune development may exist through the control that surge levels have on dune height. As an initial step in testing this hypothesis using the Anse du Verger data, the height of the present dune relative to HWST has been extrapolated back to the mid-Holocene, using the RSL curve of Guilcher and Hallegouet (1991), and is based on the assumption of a constant sediment volume being available for dune building as RSL changed over this period. This extrapolated dune height 'curve' is shown by symbol 6 in Fig. 7. There is a close alignment between the dune height 'curve' and surge elevations, suggesting that dune crest elevation in the Anse du Verger has been controlled by surge levels.

REFERENCES

Bourcart, J. and Boillot, G. (1960). Etude des dépots flandriens de l'Anse du Guesclin, près de Cancale (Ille et Vilaine). *Bulletin de la Société Géologique de France*, **7,** 45–49.

Clet, M. (1983). *Le Plio Pléistocène en Normandie*. Apport de la palynologie. Thesis, University of Caen, 1–135.

Cortijo, E., Reynaud, J.Y., Labeyrie, L., Paillard, D., Lehman, B., Cremer, M. and Grousset, F. (1995). Etude de la variabilité climatique à haute résolution dans les sédiments de l'Atlantique Nord. *Comptes Rendus de l'Académie des Sciences*, **321,** 321–328.

Costa, S. (1995). Vulnérabilité des villes côtières de haute Normandie et de Picardie face à l'élévation du niveau marin. *Hommes et Terres du Nord*, **1/2,** 48–57.

Dubreuil, V. (1992). La variabilité spatiale de l'évapotranspiration potentielle journalière. *Norois*, **39,** 145–162.

Guilcher, A. and Hallegouet, B. (1991). Coastal dunes in Brittany and their management. *Journal of Coastal Research*, **7/2,** 517–533.

Hugget, R.J. (1991). *Climate, Earth Processes and Earth History*. Springer Verlag.

Jelgersma, S., Stive, M.J.F. and van der Valk, L. (1995). Holocene storm surges in the coastal dunes of the western Netherlands. *Marine Geology*, **125,** 95–110.

Lenotre, N. (1994). Niveau de la mer et tectonique actuelle: carte de France des mouvements verticaux. *Séminaire Eaux, Environnement, Ministère de l'Environnement*, **4,** 99–101.

Le Ricollais, G., Auffret, J.P., Dourillet, J.F., Berné, S., Guennoc, P., Le Drezen, E., Normand, A. and Guillocheau, F. (1995). L'énigmatique fosse de la Manche: une approche de sa morphologie et de son remplissage par géophysique haute résolution. *Comptes Rendus de l'Académie des Sciences*, **321,** 39–46.

Loyer, S., Van Vliet Lanoë, B., Monnier, J.L., Hallegouet, B. and Mercier, N. (1995). La coupe de Nantois (baie de St Brieuc, France): datations par thermoluminescence et données paléo environementales nouvelles pour le Pléistocène de Bretagne. *Quaternaire*, **6,** 21–34.

Meur, C (1993). *Géomorphologie, protection et gestion des Dunes de Bretagne septentrionale*. These, Université de Brest, 1-353.

Morzadec-Kerfourn, M.T. (1974). Variations de la ligne de rivage Armoricaine au Quaternaire. *Mem. Soc. Geol. Miner. Bretagne*, **17**, 1–208.

Morzadec-Kerfourn, M.T. and Monnier, J.L. (1982). Chronologie relative des cordons littoraux Pleistocènes de Bretagne. *Bulletin de l' Association Française d'Etude du Quaternaire*, **19**, 195–203.

Pinot, J.P. (1974). *Le précontinent breton*. Lannion Impram, 1–256.

Pirazzoli, P.A. (1991). *World Atlas of Holocene Sea Level Changes*. Elsevier.

Regnauld, H., Cocaign, J.Y., Salièges, J.F. and Fournier, J. (1995). Mise en évidence d'une continuité temporelle dans la constitution de massif dunaires du Sub Boréal (3600 BP) à l'Actuel sur le littoral septentrional de la Bretagne. Un exemple dans l'Anse du Verger (Ille et Vilaine). *Comptes Rendus à l'Académie des Sciences*, **321**, 303–310.

Regnauld, H. and Kuzucuoglu, C. (1992). Rebuilding of a dune field landscape after a catastrophic storm: beaches of Ille et Vilaine, Brittany, France. In Carter R W.G., Curtis T.G S. and Sheehy-Skeffington M.J (eds), *Coastal Dunes, Geomorphology, Ecology and Management for Conservation*, pp 379–387. Balkema, Rotterdam.

Pergamon

Quaternary Science Reviews, Vol. 15, pp 789–802, 1996

PII: S0277-3791(96)00069-8
0277-3791/96 $32.00

THE VALENCIAN COAST (WESTERN MEDITERRANEAN): NEOTECTONICS AND GEOMORPHOLOGY

JORGE REY* and M. PILAR FUMANAL†

**Estudios Geológicos Marinos. Espacio 4, 29006 Málaga, Spain*

†Departamento de Geografía. University of Valencia, 46080 Valencia, Spain

Abstract — An analysis of terrestrial and marine data has shown the coastal fringe of the emerged continent to be naturally divided into five distinct morphosedimentary sectors, whereas three clearly different large domains are visible in the submarine shelf. This geographic coastal space corresponds to an area of wide tectonic activity where the internal and external units of Betic Ranges meet, showing a morphological expression of the substratum structure. On the contrary, the continental shelf located to the North, in the Gulf of Valencia, is subsiding and has important accumulations of sediments as a consequence of the influence of units linked to the Iberic orogeny. The detailed analysis of the tectonic and geomorphic elements illustrated a correlation between the morphosedimentary sectors of the emerged coastal area and the corresponding ones in the inner and middle continental shelf. This reveals that the littoral is affected by a general increase in structural and morphological complexity from North to South. Copyright © 1996 Published by Elsevier Science Ltd

INTRODUCTION

The cooperative interdisciplinary project 'La Nao', carried out along the Valencian littoral (Western Mediterranean) under the initiative of the Department of Geography, University of Valencia (Martínez-Gallego *et al.*, 1992; Fumanal *et al.*, 1993a, 1993b; Rey *et al.*, 1993; Viñals *et al.*, 1993; Martínez-Gallego *et al.*, 1994; Blázquez, 1995), has studied a coastal fringe from Valencia to Alicante (Fig. 1). The methodology employed has consisted of combining the geomorphological and sedimentological studies of the emerged continental area with that of the inner and outer continental shelf. For this purpose, three campaigns of coastal and oceanographical surveys have been carried out. Mechanical and electric cores in the emerged zone were combined with marine seismic reflection profiles on the continental shelf (Fig. 1). The particular results obtained in each area have been published in previous works (Goy *et al.*, 1987; Fumanal *et al.*, 1993a, 1993b, 1995; Rey *et al.*, 1993; Martínez-Gallego *et al.*, 1994; Rosselló *et al.*, 1995).

The complexity of the continental margin studied increases from north to south, because of the following factors: (a) the gradual variations which take place in the transect from a progradational shelf to another one of erosional type in a reduced distance; (b) the influence of the Betic system on the materials forming the shelf; and (c) the presence of the Neogene-Quaternary basins and the effect of the neotectonics linked to the episodes of the sea level oscillation. (Rey and Díaz del Río, 1983; ITGE, 1994).

The factors considered above have established geological relationships among the different morphostratigraphical transversal units forming the coastal fringe, thus relating the emerged sectors to the submerged ones through formations (belonging to both domains) which are synchronous during the phases of landward or seaward migration of the littoral depositional systems at the Quaternary (Goy *et al.*, 1987; Fumanal *et al.*, 1993a).

THE TERRESTRIAL RESEARCH

The area studied in this work includes the southern coast of Valencia and corresponds structurally to the outer units of the Betic Ranges. Its geomorphological and sedimentary characteristics and the tectonic behavior of the geomorphic and structural units in the emerged coastal areas establish a natural division into five sectors which are described as follows.

Cullera-Denia Segment (Fig. 2)

It represents the Southern end of the Gulf of Valencia, where the Betic and Iberic structural domains meet (Fig. 1). It features an uninterrupted extension of low coast modelled with the characteristic elements of beach-barrier and lagoonal sedimentary units. This system was closed during the Late Holocene by a wide, long sandy body resting on the continental bulges.

The area generally shows a subsidence lasting from the Plio-Pleistocene to the present (approximately, a ratio of 0.45 m per 1 ka) suggesting structural control both in the depositional behaviour and in the coastal morphology

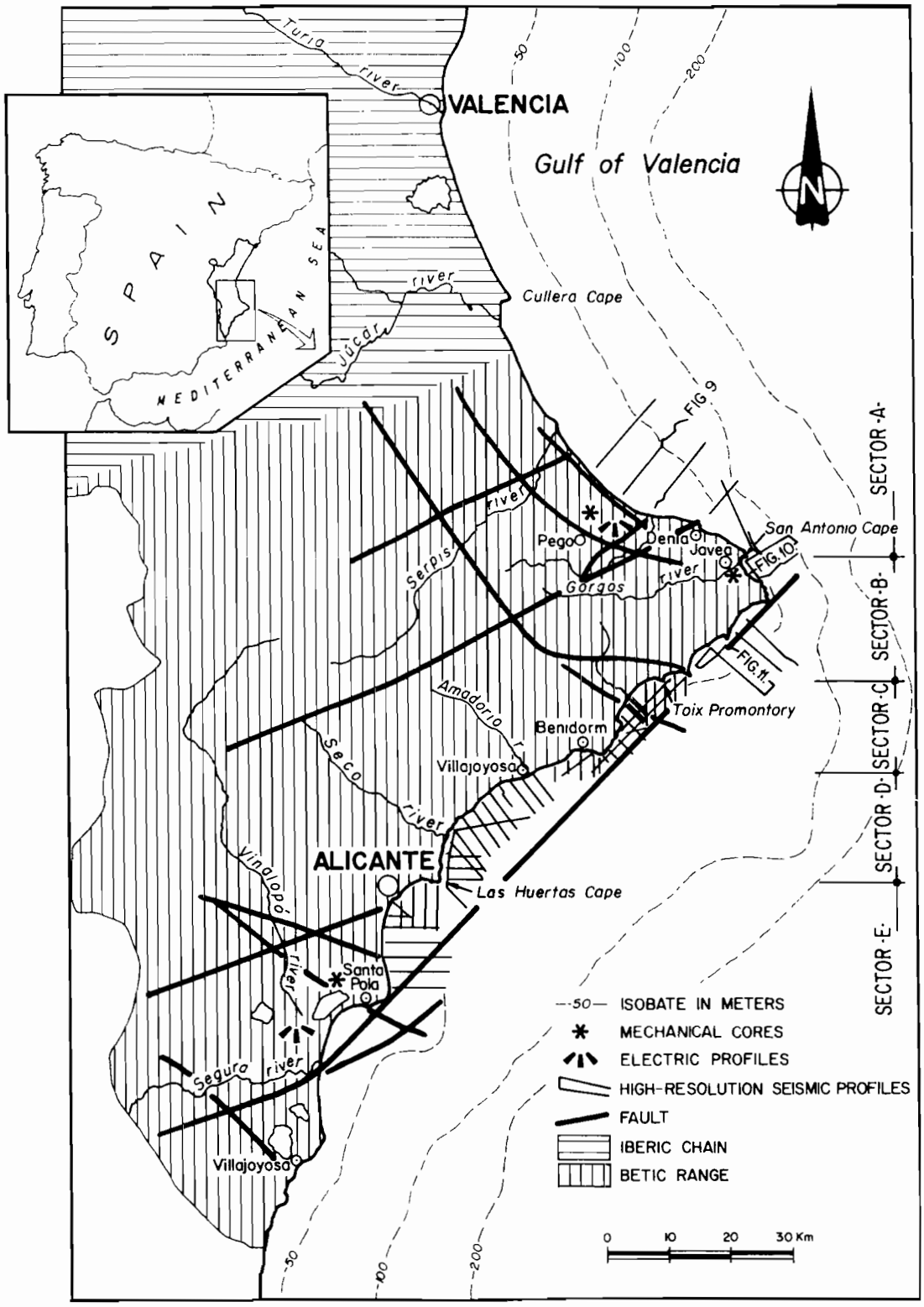

FIG. 1. Location map showing the study area and methodologies type employed (mechanical cores, electric profiles and high-resolution seismic lines along the Valencia-Alicante shelf).

typical at the area. The continental sedimentary sequence of the Upper Quaternary has been reconstructed in this sector basically from the chrono-stratigraphic study of the subsurface deposits of the Pego lagoon (Fig. 2), where a series of mechanical and electric cores were collected (Dupré *et al.*, 1988; Viñals, 1991).

^{14}C and TL isotopic measurement analysis for samples of the record obtained from a mechanical core that starts at −50 m in a sandy body (beach-barrier) built during the last phases of isotopic stage 5, show an age of 112,000±17,000 BP, and units made up of lagoon bottom sediments and alluvial fans formed during the last cold period (Alpine Würm, isotopic stages 4 (72,000±11,000 BP), 3 (55,000±8000 BP) and 2

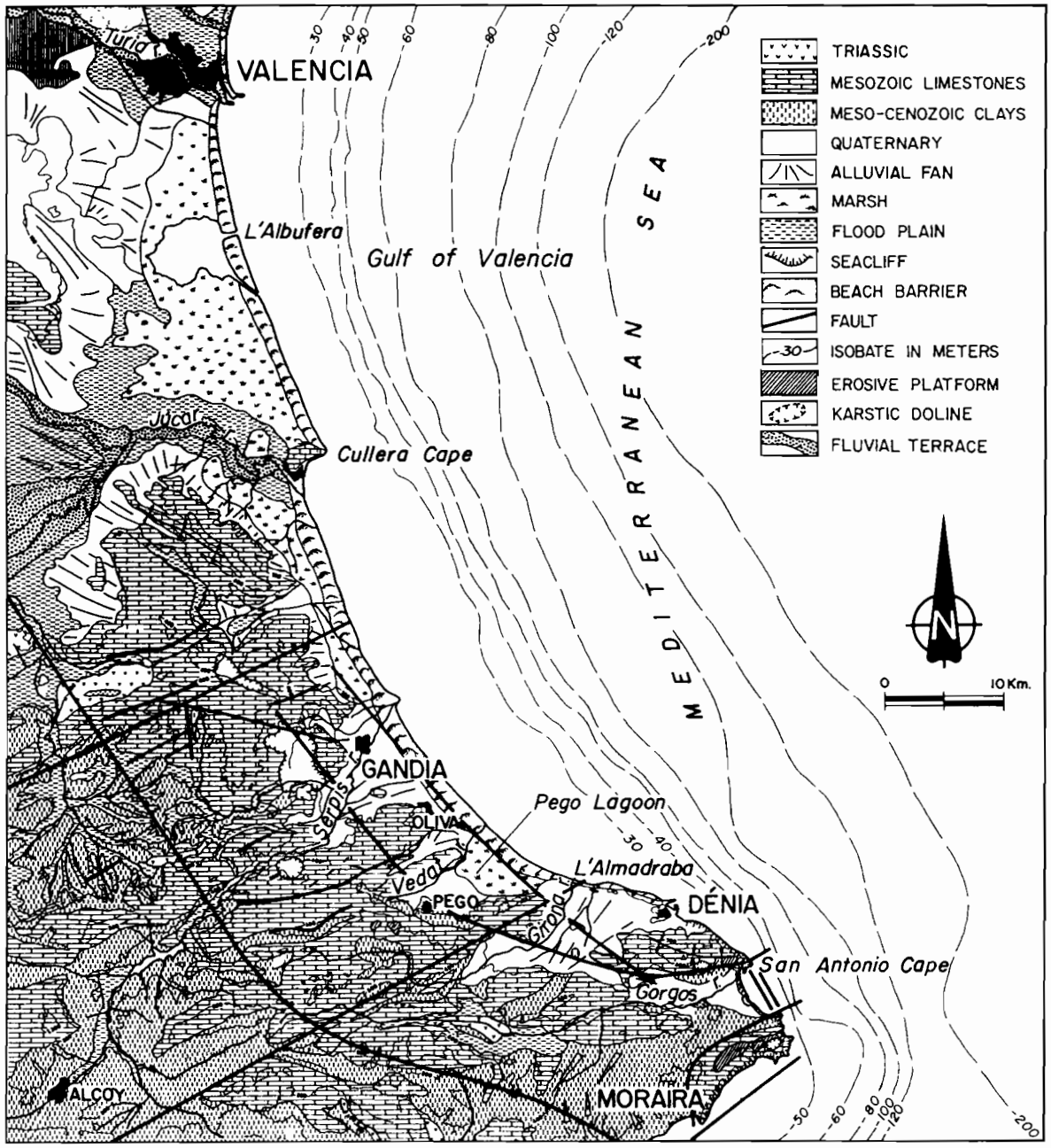

FIG. 2. Cullera-Dénia segment.

(19,000±3000 BP)) deposited on this formed barrier. The active deposit is covered in turn by a 15 m thick layer of Holocene sediments made up of littoral and lagoon deposits (Viñals, 1991).

San Antonio Cape-Moraira Cape Segment (Fig. 3)

This corresponds to a relatively long segment (17 km) of which, opposite to the previous one (A), is made up of 100–170 m high sea cliffs on Mesozoic and Tertiary materials (Fig. 3). This marine front is sporadically interrupted by a low coast segments where sandy beaches and coves are to be found.

The orthogonal pattern of the fault net in this area is clearly revealed by the layout of the relief blocks, in the inner area as well as on the coast. The rough morphology of cliffs is due to fractures and tearings which follow headings parallel to the coast, whereas the lower areas found between are the result of faults perpendicular to the coastal profile which have created small grabens.

Pleistocene deposits (consisting of interbedded colluvium, calcretes and aeolianites) preserved on cliff walls (Fig. 4) as well as in coves and bays (Fig. 5), and also chronostratigraphic data (Tl and Th/U isotopic measurements) related with the cores collected in Jávea Bay, tell us about the tectonic behaviour (distensive movements, normal faults and differencial subsidence of blocks) of the area (Fumanal, 1995a). Cliff segments (San Antonio Cape, La Nao Cape, Ifach Promontory and Toix Promontory (Figs 3 and 4)) correspond to more stable blocks within the active Quaternary neotectonics, opposite to the acute subsidence of lower sectors. In Jávea Bay (Fig. 5), mechanical drilling reaching the

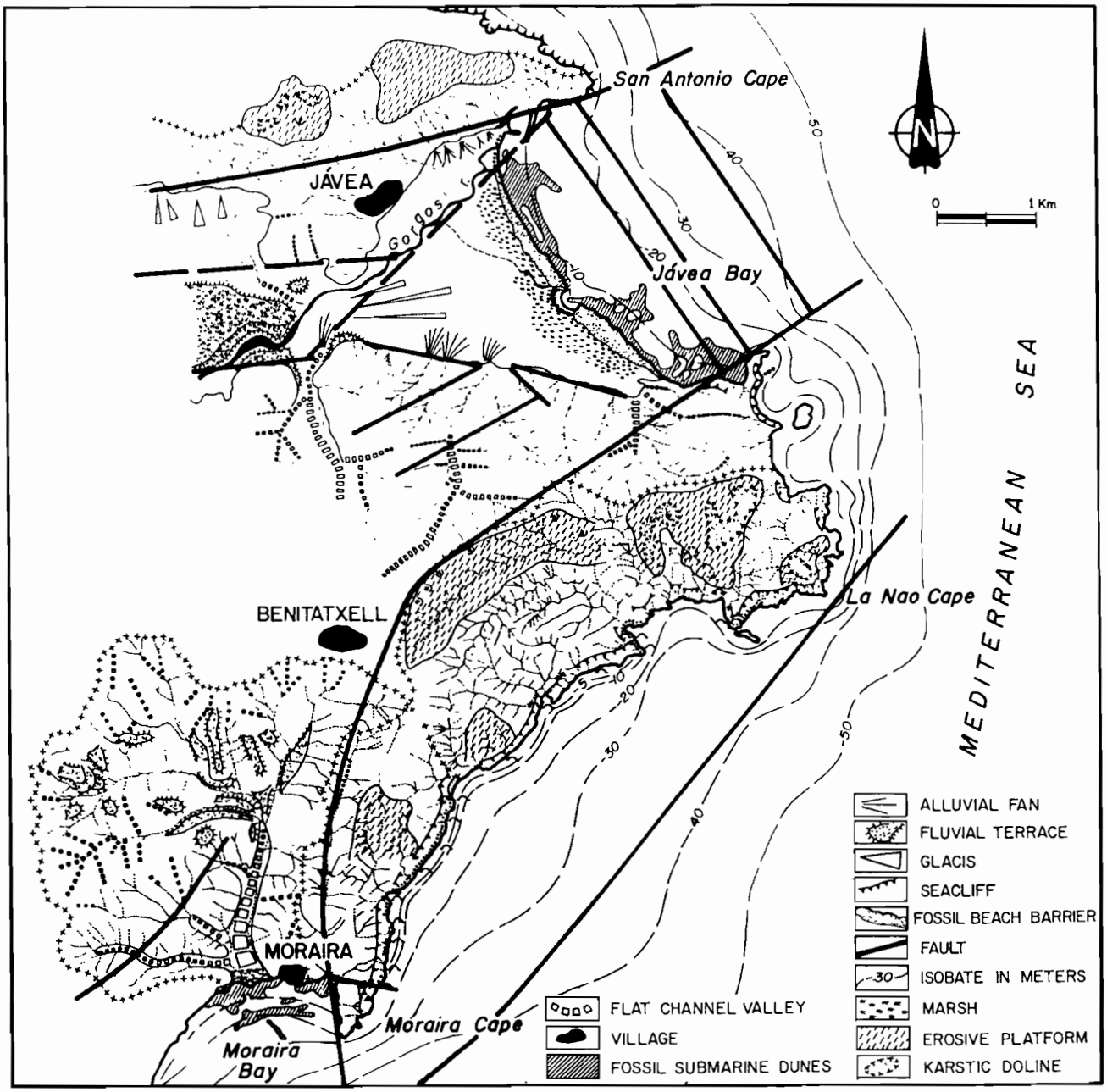

FIG. 3. San Antonio Cape-Moraira Cape segment.

substratum (Mesozoic limestones and clays) at −32 m, allowed us to verify the fracturing and subsidence of the distal area of a detritic deposit belonging to Gorgos river and formed in phases of Lower-Middle Pleistocene (Martínez-Gallego *et al.*, 1992; Fumanal, 1995b). Presently, a record remains of a terrace some 3 km up from the river mouth on the Mediterranean, 20 m over the talweg, whereas we can observe this same deposit at −30 m below the coast. In this area, the Tyrrhenian beach-barrier which created an inland marsh had its central sector fractured as early as Upper Quaternary, favouring the settling of the river channel. This block has been subsiding since the Holocene, as we can deduce from chronostratigraphical record of Jávea Bay (Fig. 5). Further South, in the Moraira-Toix Promontory segment (Figs 3 and 6), the entire littoral fringe is undergoing subsidence during Middle Pleistocene, thus causing disorder in the primitive Quaternary river net (which, with opposite direction, was a tributary to the middle basin from the Gorgos river).

Altea-Benidorm Segment (Fig. 6)

From this point low coast and moderate high cliffs (20–30 m) begin to prevail. This area includes the broad Altea Bay, which lies between two calcareous spurs that are still high: Toix Promontory to the North and Sierra Helada to the South (Fig. 6). Further, we find Benidorm Bay spreading out until the landscape of the Paleogene folded belt of Villajoyosa. The clays and evaporites of the Keuper facies of Upper Triassic are responsible for diapirical phenomena and obvious uplifts and translocations of the Quaternary deposits in this zone.

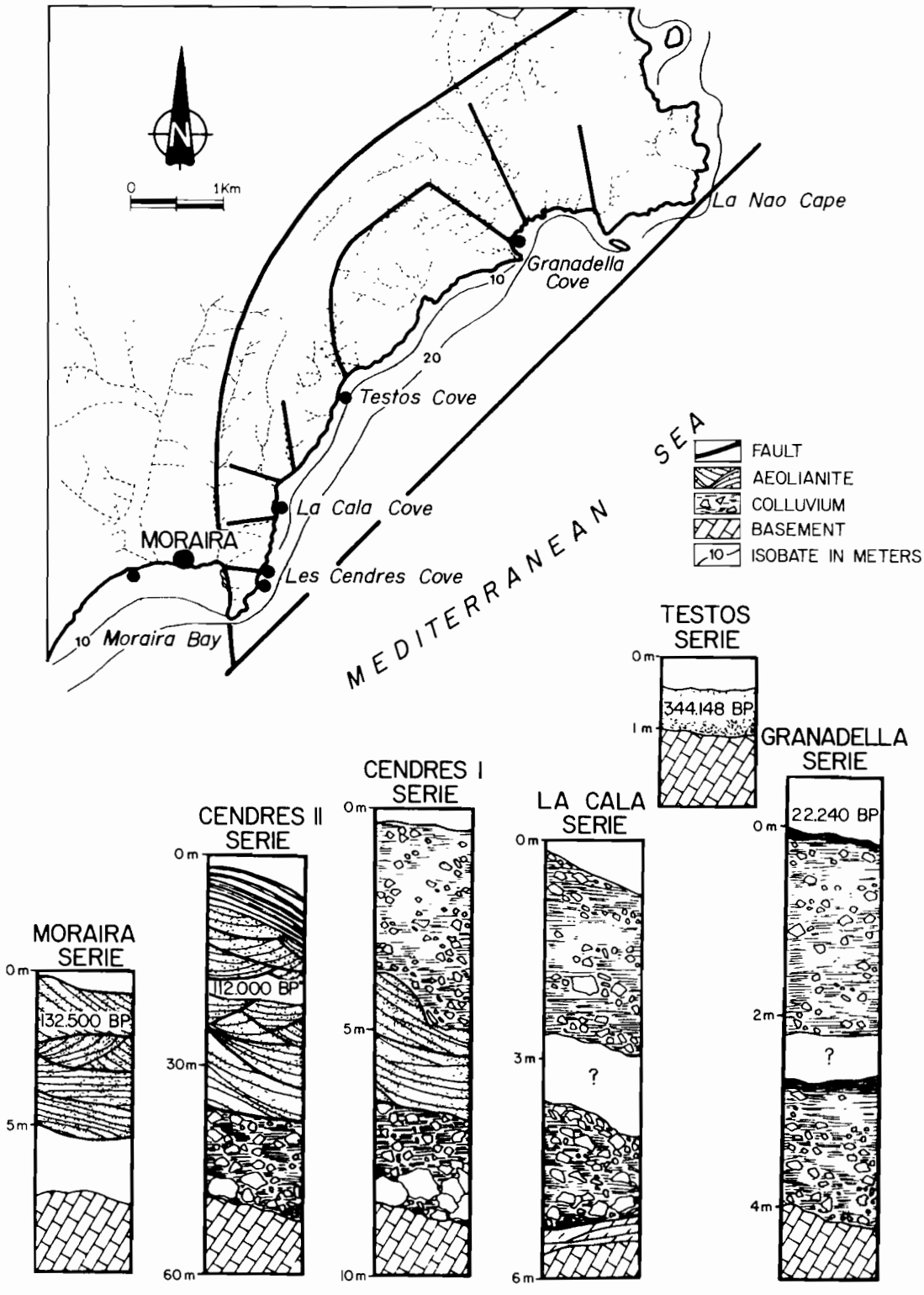

FIG. 4. Cliff segment between La Nao Cape and Moraira Bay. Stratigraphic profiles of Pleistocene deposits.

As in the Northern cliffs described before, the geomorphologic study (Rosselló *et al.*, 1995) allowed us to detect in Sierra Helada some remains of a Quaternary drainage paleonet trenched in an eastward projecting relief. This area, disrupted and subsided into the sea bottom (2 ma ky; Hernández-Molina *et al.*, 1994a, b), consists today of a rough cliff in whose higher parts there are still witnesses of the old drainage net. After the new profile of Sierra Helada (which is today the marine front) got its new configuration, colluvial deposits began to develop during the last phases of Lower Pleistocene. Younger colluvial and aeolic deposits, whose Tl chronology assigns them to Upper Pleistocene, are found among the gullies carved in the older colluvial one.

Benidorm-Las Huertas Cape Segment (Figs 6 and 7)

The coastal profile in this sector is a result of both the incompetent lithologies of the flysch facies and to the

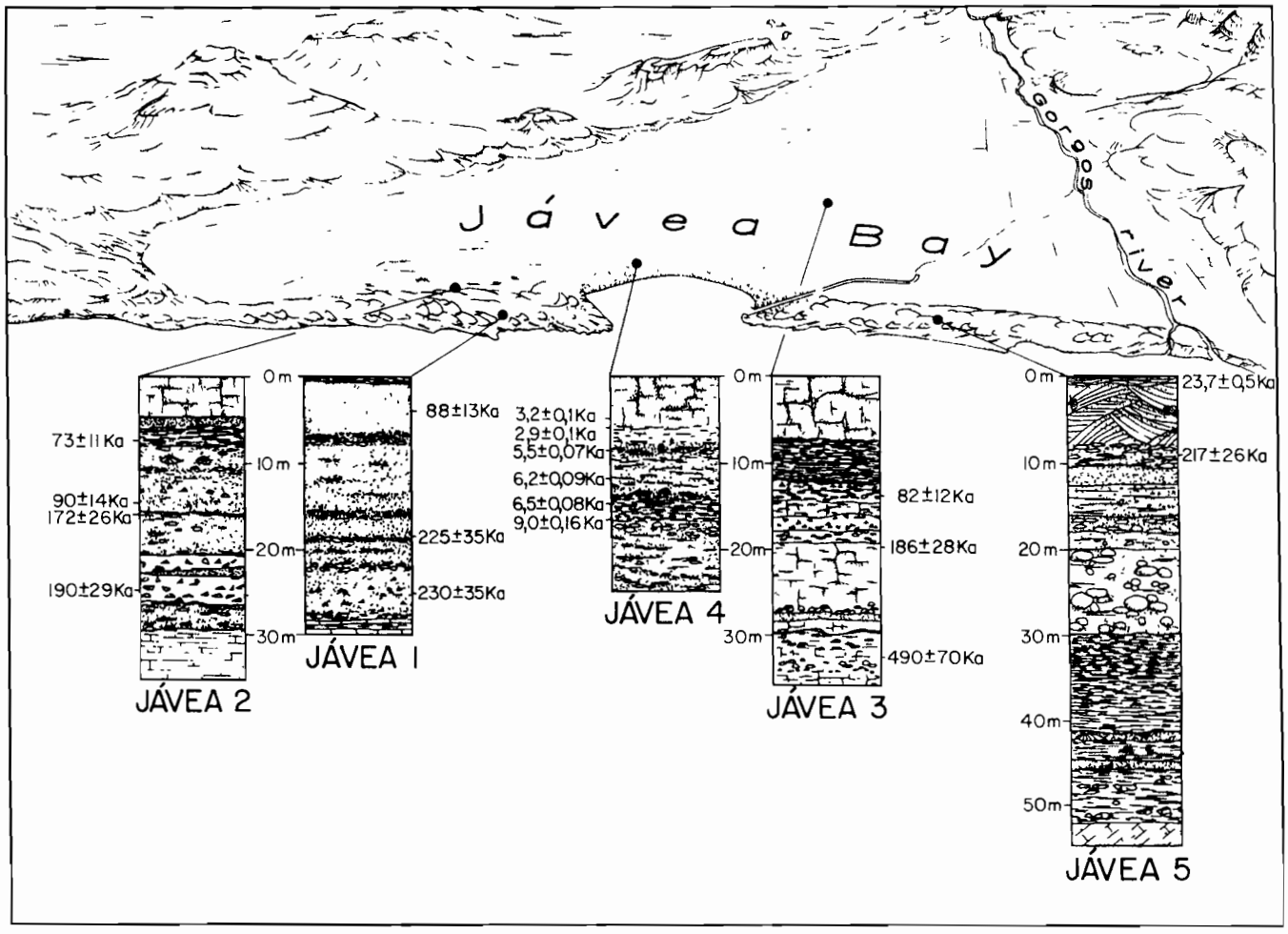

FIG. 5. Stratigraphic records of Javea Bay. Chronologic data in ka BP.

tectonic style which deforms them. Middle-sized cliffs can be found aligned in the Northern sector, from Villajoyosa to Campello (Fig. 7).

The drainage net commanded by the Amadorio river (Figs 1 and 7) consists of short ephemeral streams. The channels have been carved out in Keuper and Tertiary clays, that occassionally brings about regressive erosion. The bed of Seco river (Fig. 7) in Campello, is the starting point for the influence of a set of faults (perpendicular to the coastal profile) which subside the San Juan depression (Fig. 7). Successive phases of this neotectonics affect not only the old Quaternary deposits but also the Tyrrhenian sediments, preserved at South of Las Huertas Cape and Isleta of Campello (Fig. 7).

Chronostratigraphic data of littoral bodies (after Stearns and Thurber, 1965) illustrate that there are two sets of Quaternary marine terraces. The oldest belongs to the Middle Pleistocene (Dumas, 1977), and its remains appear tilted and broken at different heights (15, 20 and 30 m) at Las Huertas Cape. The earliest is Tyrrhenian and it is located irregularly between −2 and +3 m. In Las Huertas Cape (Fig. 7) marine terraces between 1.5 and 3 m can be found. In the Isleta of Campello (Fig. 7) the remains of a beach, also considered Tyrrhenian, are located between 3 and 4 m above the modern sea-level.

Alicante-Torrevieja Segment (Fig. 8)

After the straight fault scarp which outlines the Southern sector of Las Huertas Cape, two smooth arches make up the Valencian Southern coastline (whose central sector leans on the dome of Santa Pola) up to Torrevieja. This sector belongs to the geological domain of Alicante Prebetic complex formed by calcareous Mesozoic materials (Fig. 8). The following traits of this unit must be pointed out:

This sector is directly influenced by the Cádiz-Alicante fault system reaching the Mediterranean Santa Pola North (Cuenca, 1988). This fact brings about a distinctive behaviour which is reflected in the development of a generalizated subsiding axis along which littoral reliefs are uplifted (Santa Pola, Sierra of Colmenar and Tabarca Island).

The Elche Pleistocene trough (Fig. 8) offers a remarkable subsidence stressed by Pleistocene and Holocene tectonics. This depression is presently closed by a double beach-barrier; on one hand the present one, and an older one of Tyrrhenian age. All levels are affected by neotectonical processes, in such a way that Tyrrhenian terraces reach their maximum heights in heaving areas like horsts and anticlines whereas their remains have already disappeared in those areas

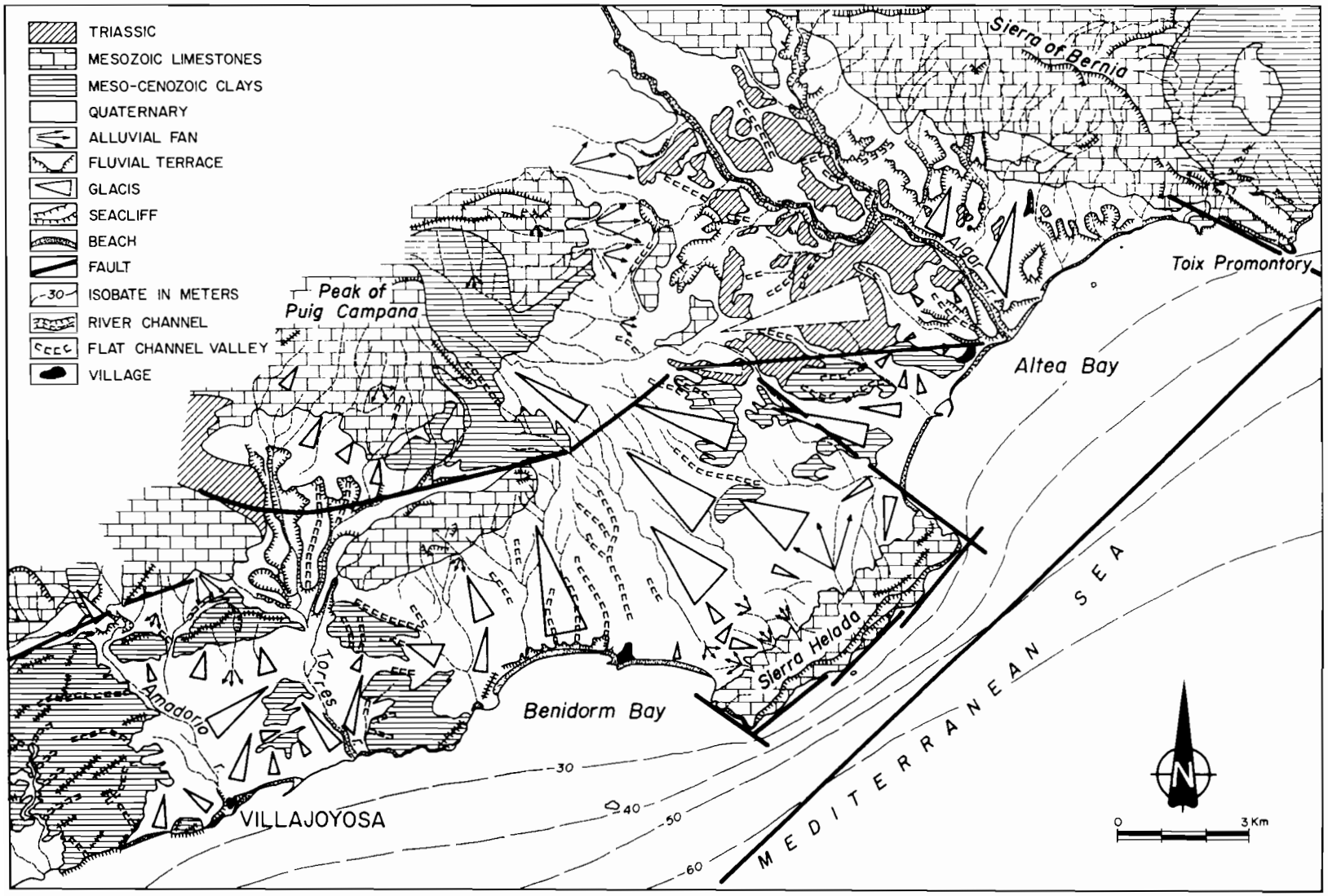

FIG. 6. Altea-Benidorm segment.

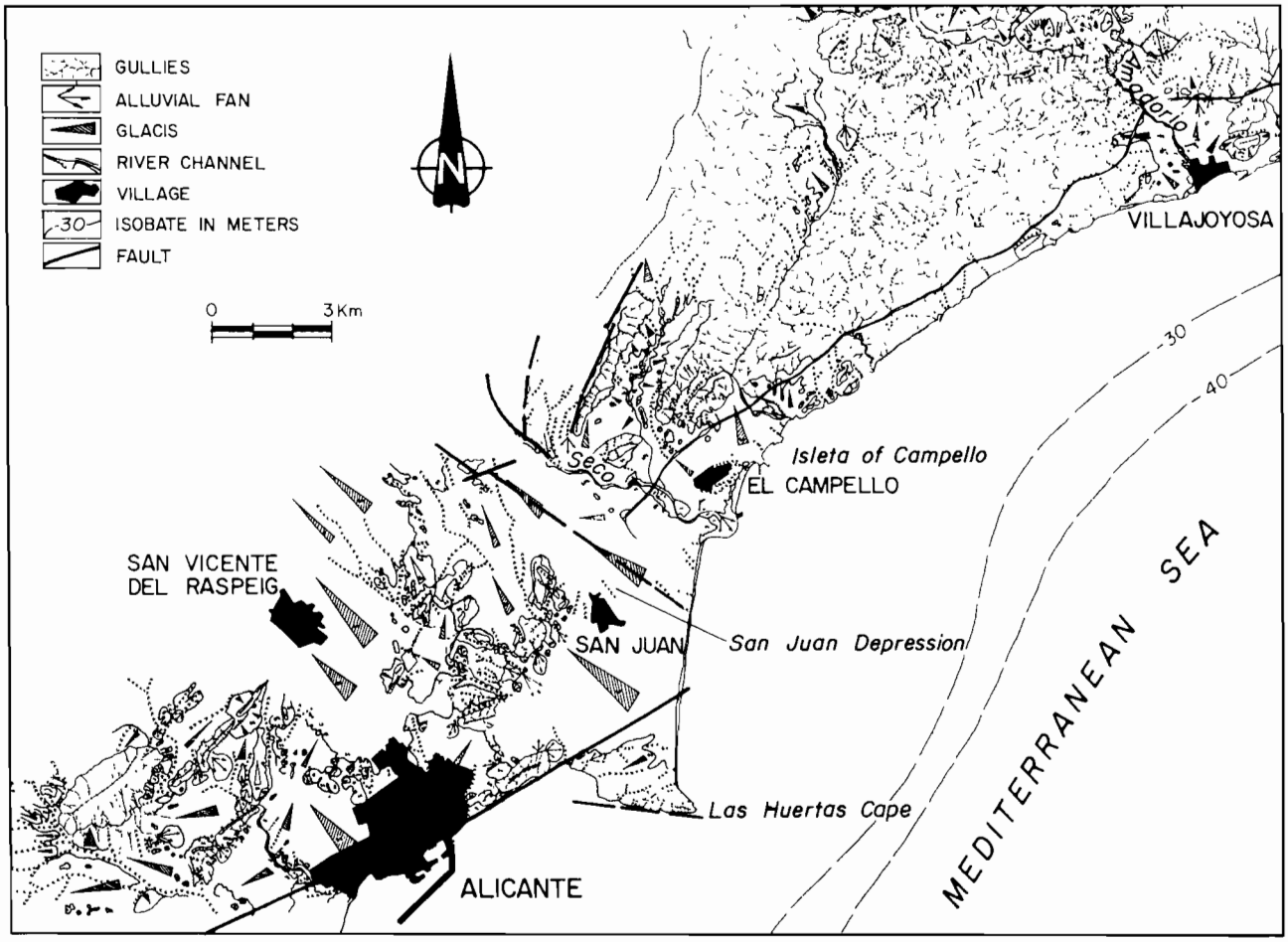

FIG. 7. Benidorm-Las Huertas Cape segment.

affected by subsidence. All this creates staircased sedimentary sequences (as in Santa Pola), or superimposed ones (as in La Marina). Dumas (1977) and Goy *et al.* (1993) both suggest two superimposed Tyrrhenian levels in the Albufereta (Fig. 8) and another two by Sierra of Colmenar hills. Goy and Zazo (1987, 1988) have mapped in Elche Depression three Tyrrhenian levels at 8.7, 4.5 and 1.5 m over the present sea-level under a Pretyrrhenian episode located at +36 m (Dumas, 1977). Last, the existence of at least two Tyrrhenian levels with oolithic and siliceous facies has been suggested East of Sierra of Molar promontory (Fig. 8), where a system of Tyrrhenian shoals isolating the Santa Pola marshes developed.

In addition to this information, it is worth saying that our present research (Ferrer and Fumanal, in press) near a Roman site (Picola, a fish salting factory at the time of the Late Roman Empire) located South of Santa Pola rise and 500 m from the present coast, shows that the site placed at that time near an open beach; this has been illustrated by carrying out surveys in the immediate vicinity. This reinforces the idea that the littoral sandy bar closing the bay has been formed recently.

THE MARINE RESEARCH

Sequence stratigraphy analysis of single-channel high resolution seismic profiles (Geopulse 300 Joules) of late Pleistocene-Holocene sediments has been carried out on three marine research campaigns on the submarine shelf from Gandía to Santa Pola Cape. The very high vertical resolution of this system (0.5 to 1.0 m) allows the definition of geometrical features of sedimentary bodies. The seismic lines (Fig. 1) are representative of the geometry of the stratal architecture of areas with different subsidence and sediment rates depending on local factors. The length of these seismic lines has permited the reconstruction of the sequences in detail with great lateral continuity. Five sectors are distinguished according to the morphostructural and stratigraphic complexity of the units making up the inner areas of the shelf.

Morphostratigraphic Scheme

The research has been conducted in the provinces of the inner and a part of the outer shelf. The former spreads out up to approximately 30 or 70 m deep and is characterized by a great variety of sedimentary morphologies and environments, which are greatly influenced by continental factors. However, the middle shelf, which covers from a depth of 40 m up to 60–80 m, presents a slightly sloped subhorizontal surface standing out among the erosive forms because of its great morphological complexity.

As to the morphostructural scheme of the inner shelf, it generally coincides with the division established for the

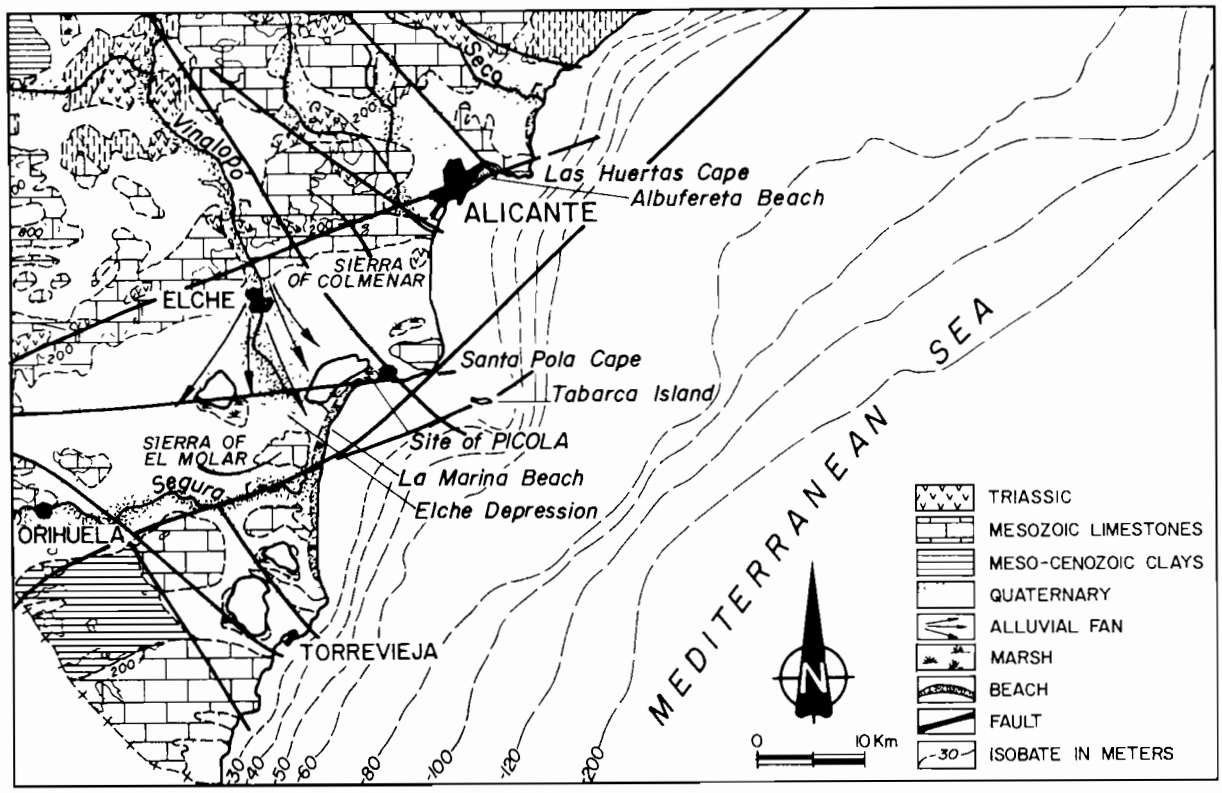

FIG. 8. Alicante-Torrevieja segment.

emerged continental area. This scheme is made up of three well defined tectonic domains limited by the following (from North to South) structural horsts: San Antonio Cape; Las Huertas Cape; and Santa Pola Cape. The Northern domain leans on a progradant platform formed as the elongation of the Neogene-Quaternary basin of the Gulf of Valencia, to which shallow depositional environments affected by the subsidence of epirogenic bending movements have been associated. The sedimentary cover on the shelf, which corresponds to a thick series of Plio-Quaternary deposits, becomes progressively thinner southward to Betic system. Foldings and non-deposition surfaces made up of Pleistocene outcrops related with beach-rocks prevail in the intermediate sector. Last, tensional faults and a great morphological variety of erosional surfaces prevail in the Southern sector, where we find the structural rise of Santa Pola Dome and Tabarca Island (Rey and Díaz del Río, 1983).

The last two domains described above belong to a mixed platform stratigraphically and structurally controlled by the Betic Ranges. A differential tectonic subsidence of normal fractures which generates little parcelled basins is added. The reason for this is that it is an area of great tectonic activity where the two Betic domains meet. This fact makes some morphological expression of the basal structure to appear on the shelf, opposite to the Northern sector in the Gulf of Valencia, where the platform is subsiding and shows important sediment accumulations (Díaz del Río *et al.*, 1986). Also, near Alicante, normal component faults have controlled the genesis of a thick Neogene-Quaternary sedimentary basin affected by halokinetic phenomena associated to Triassic plastic materials and a high subsidence (2 ma ky).

Morphology Types

A total of four different morphology types can be defined along the studied shelf.

Depositional morphologies

They constitute sedimentary bodies represented by large-scale bedforms in the inner and middle shelf, prodeltae, Quaternary alluvial fans, sand waves, dorsals and littoral prisms. They are the most common for their development and extension as well as for their number. These kinds of formations are strongly determined by the characteristics of feeding systems and the littoral hydrodynamic scheme of coastal currents. They are representative of the northen part of the study area.

Erosive morphologies

They correspond to inherited deposits partially modified by present erosion and sediment conditions. They include morphological rises and slope breaks, erosive terraces and cliffs, abrasion and undulating surfaces, wavy surfaces, depressions and talweg and channel morphologies. They appear generally truncated or cut into old formations. This kind of morphology is very well represented in depositional interstratified units, as well as in the southtern part of the study area.

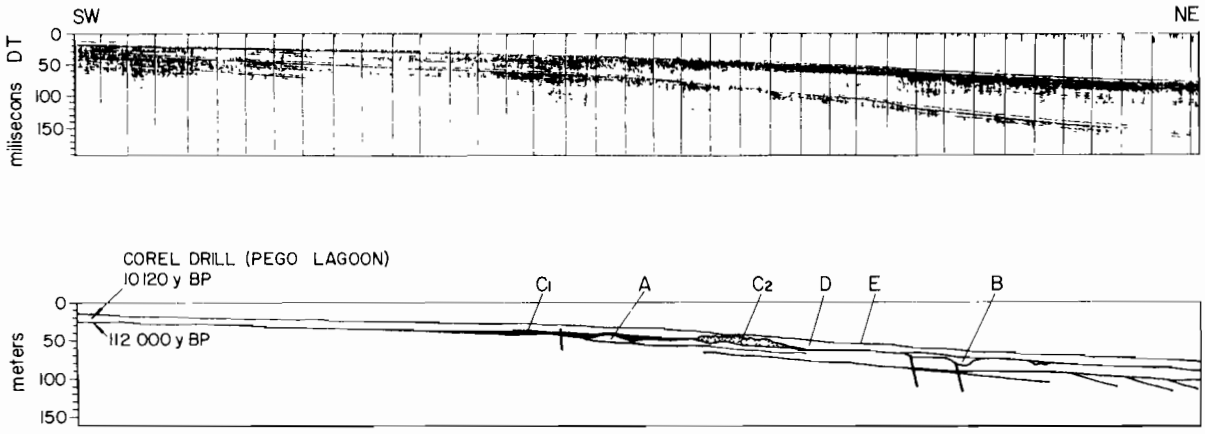

FIG. 9. Seismic profile (Geopulse 300 Joules) across the continental shelf in front of Pego Lagoon, revelating: upper Pleistocene seismic depositional unit (A); channel fill unit (B); beach-rock (C1) and back-barrier associated (C2); transgressive deposits (D) and actual shelf deposits; Fault (F). See Fig. 1 for location.

Relict morphologies

They are found all over the inner and middle shelf and are related to relict bodies. These morphologies are lithified and incrusted accumulations associated to former coastlines (beach-rocks) or, in other cases, as the top surface of relict sedimentary bodies later modified by mechanisms linked to present day dynamics. They appear as hardened or partially lithified bottoms showing much relief and irregular elongated surfaces subparallel to the coast.

Structural morphologies

Though scarce, they are well represented all over the studied shelf by scarps and small submarine cliffs generally showing a seaward slope change. Another kind of such morphologies are hard bottoms corresponding to the surfaces making up the top of structural rises. This last type of morphology is very characteristic of the Southern part of the submarine shelf between Alicante and Torrevieja.

Submarine Shelf Sectors

On a regional scale five local sectors can be established. According to morphostratigraphic characteristics, and from a genetic point of view, the offshore features would largely coincide with the equivalent areas located in the same sectors of the emerged coastal area.

Northern sector

This spreads from Cullera to Denia (Fig. 2) and represents the Southern part of the Gulf of Valencia, where we get closer to the Betic substratum as we move on Southwards. This causes a gradual decrease of the subsidence gradient starting in the center of the basin and continuing towards its edges (Gulf of Valencia; Rey and Díaz del Río, 1983; Díaz del Río *et al.*, 1986). For that reason, the Pleistocene littoral deposits (beach-rocks) located in the South of this sector (La Almadraba) subside progressively as we move Northwards, as the Holocene sequence develops more strongly until covering and burying them completely. The geometry of seismic sequences in this sector (belonging to Holocene and Pleistocene beach-barrier sedimentary bodies) are correlated to the sedimentary units defined by sedimentological and paleontological criteria and absolute dates obtained from cores collected in the Pego marshes (Viñals, 1991; Fig. 9). This sector contains characteristic thick layers, because of the high rate of sediment supply from an upland environment into the submarine domain and also the suspended fine sediment moving sothward along the shelf from the Ebro River in the North of the study area (Maldonado *et al.*, 1983).

San Antonio Cape-Moraira Cape sector (Fig. 3)

As in the emerged area, this sector presents a poorly developed inner shelf due to the lack of an uniform depth gradient. This is an irregular coast with many cliff areas, where the beaches are rare and located in small bays between rocky relief.

Quaternary deposits are determined by tectonic processes of continuous differential subsidence associated to block stepping, related to the structural features of the Valencia Trough and the Betic ranges (Fumanal *et al.*, 1991). This fact brings about a piled depositional system detected in seismic profiles where we find, nearest to the inner shelf, a stack of beach-rocks of different ages parallel to the coast and frequent depositional hiatus caused by the differential subsided-uplifted blocks as a consequence of tectonics (Fig. 10). The high degree of differential subsidence in this submarine sector, showed in the seismic profile, has modified the coastal environment from Middle Pleistocene until Holocene. This area has evolved from a coast dominated by shoals and littoral bars formed on a small gradient platform into a cliffed coast featuring a strong water depth gradient in the infralittoral area (Fumanal *et al.*, 1993a, b). Tectonic control and differential subsidence are characteristics of this sector.

Moraira Cape-Villajoyosa sector (Figs 3 and 6)

This sector shows an almost planar inner and middle

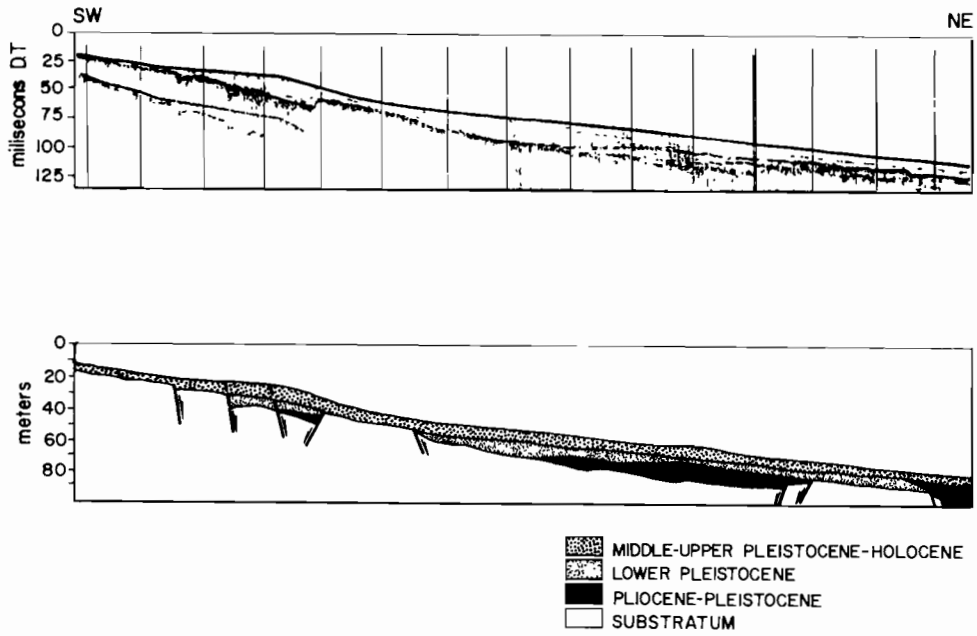

FIG. 10. Seismic profile (Geopulse 300 Joules) across the continental shelf in front of Jávea Bay, showing the tectonic control and high degree of differential subsided-uplifted blocks. F, fault. See Fig. 1 for location.

shelf; continuity is only broken by some thick sedimentary prisms. The littoral area is strongly related to a non-depositional continuous platform made up of an outcrop of undefined age. Thick Holocene depositional sedimentary bodies, more than 20 m thick, occupying nearly all the inner and middle shelf develop from this littoral area (Fig. 11). The process of formation for this sector is closely related to the changes of the sea-level and to neotectonics, in which normal fractures affect Mesozoic as well as Neogene materials (Díaz del Río *et al.*, 1986). The presence of a fossilized beach system (at the base of the Sierra Helada cliff) continues in the emerged area as aeolic and marine deposits located in the cliff slopes.

Other normal tectonic features oriented E–W affecting the Post Holocene–Neogene depositional units as well as the older Mesozoic and Tertiary materials related to Triassic stresses begin to appear in the South of this sector. Holocene depositional sequences are affected by tectonic reactivation and diapirism.

In brief, the main features of this sector are strongly determined by tectonic control, relative sea-level changes, the supply characteristics of the shelf (Martínez-Gallego *et al.*, 1992) and the southward-increasing halokinetic effects of Triassic plastic materials.

Villajoyosa-Las Huertas Cape sector (Fig. 7)

It contains a thick sedimentary wedge (20–40 m) and this sector is divided into three areas controlled by a fault

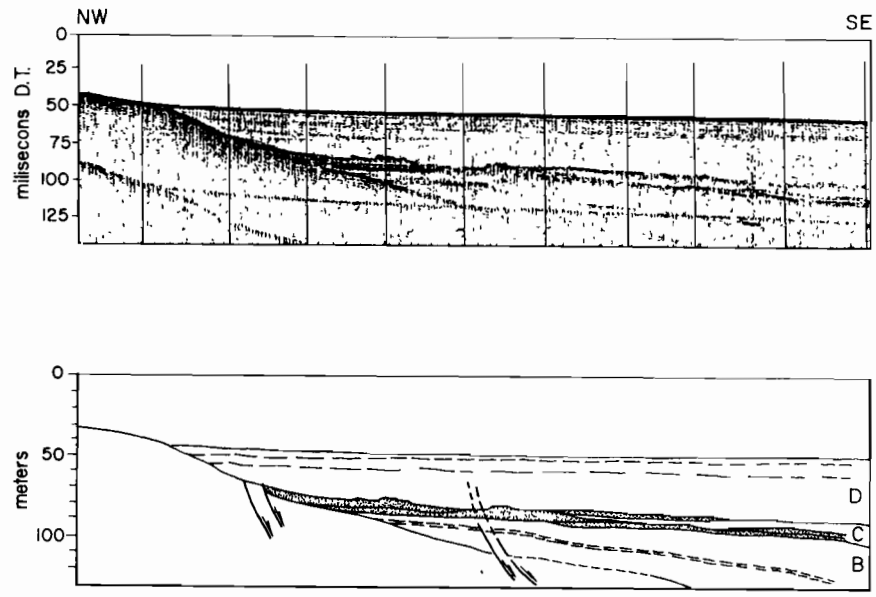

FIG. 11. Seismic profile (Geopulse 300 Joules) showing the depositional sedimentary bodies-architecture related to the changes of the sea-level and to neotectonics. Note that the normal faults affect Neogene materials. See Fig. 1 for location.

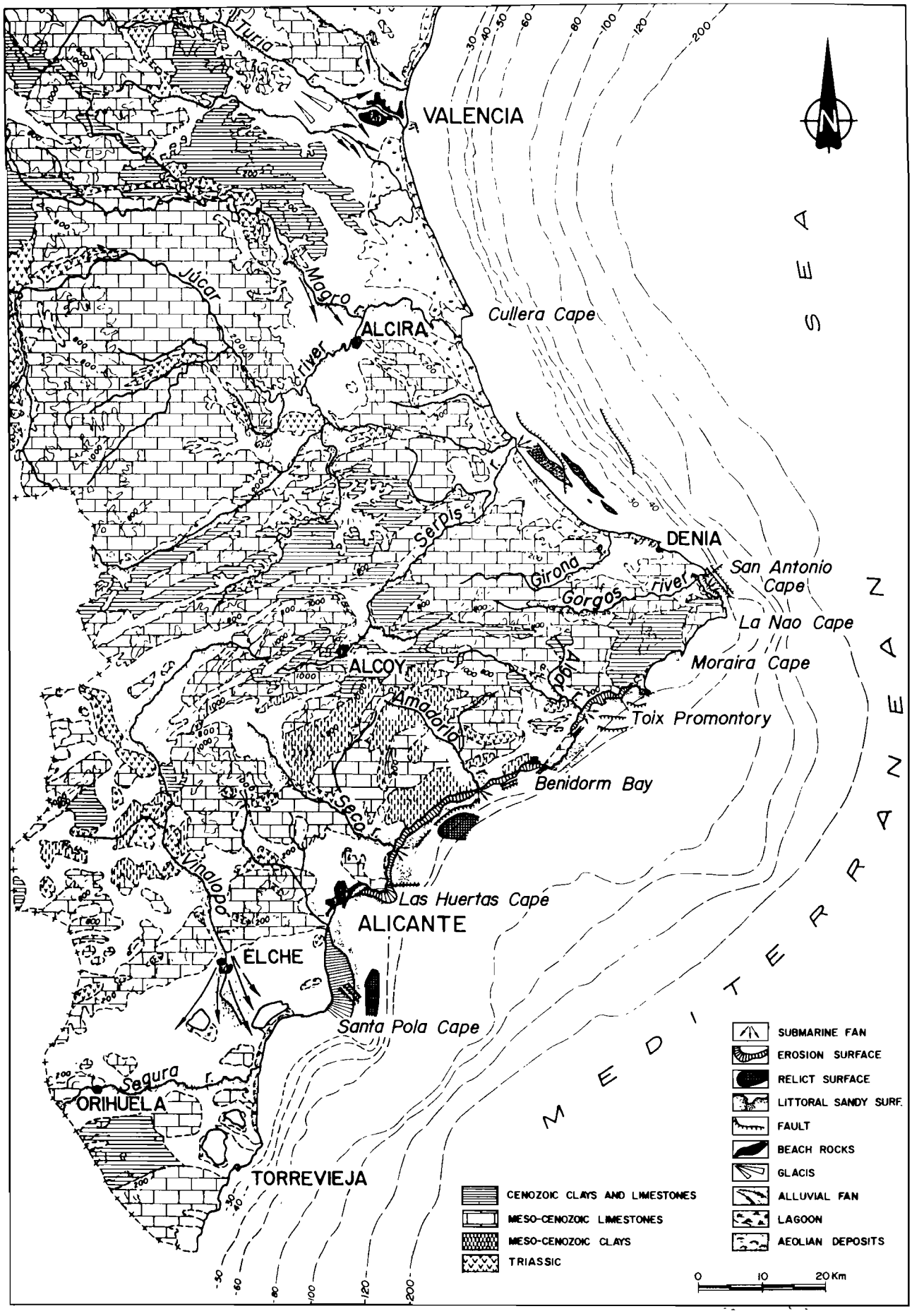

FIG. 12. Schematic summary of morphoestratigraphical continental and submarine areas.

system oriented NE–SW and NW–SE; this fact is related to halokinetic processes of Triassic plastic materials and high subsidence areas (Mauffret, 1976; Sanz de Galdeano, 1983):

Eastern area, South of Villajoyosa, featuring a gradual increase in sediment thickness from infralittoral domains up to the middle shelf; a thickness value of 80 m is reached at a depth of 60 m.

Central area, located between the South of Villajoyosa and the Northern part of Las Huertas Cape. This is a strongly subsiding area linked with San Juan Depression, which is controlled by the fault system NW–SE and NE–SW and shows an important deposition up to 80 m thick in the inner shelf. Sedimentary filling material obtains its structure from small depocentres and horsts revealing the existence of differential subsidence.

Western area, in front of Las Huertas Cape. Characterized by a structural high (actually the submarine prolongation of Santa Pola Dome) limited to the North by a NW–SE fracture which strongly determines the distribution of the sedimentary filling materials. South of the rise we find a sedimentary wedge which reaches a thickness of 60 m as soon as we move seaward only 500 m. In this place there are structural submarine cliffs fossilized by Plio-Quaternary deposits.

Las Huertas Cape-Torrevieja (Santa Pola Cape) sector (Fig. 8)

It shows a widespread thin sedimentary deposit and a strong control by the Cádiz-Alicante fault system. As far as morphosedimentary characteristics are concerned, this sector is divided into two separate areas by a NW–SE axis passing through the city of Alicante.

Northern area, showing an important sedimentary wedge spreading from the infralittoral environment up to a depth of 50 m in the middle shelf.

Southern area, associated to a structural elevation on which lies a sedimentary cover no more than 20 m thick. This is the prolongation towards shallow waters of Santa Pola (Betic horsts), located on the shelf (ITGE, 1994) and generated by an emersion brought about by the reactivation of deep accidents.

CONCLUSIONS AND SUMMARY

In short, the previous work states that there has been a progressive modification of the coastal profile all over the studied area through the Quaternary.

About the emerged area our research has pointed out the following.

To the North (Valencian Gulf), the continental geomorphic landscape mainly consists of a narrow corridor limited to the East by the Mediterranean Sea and to the West by a high calcareous relief. Along that territory, with a continuous tendency to subside, flood plains and lagoonal sedimentary environments of Holocene age develop. Cores of the thick sedimentary record reveal that the deposits corresponding to the high sea-level of isotopic stage 5 are found deeper than 50 m (as in the case of Pego lagoon).

To the South, from San Antonio Cape, this configuration changes. An abrupt sea-cliff relief extends towards Alicante City. The drainage basin geometry shows a frequent reshift into a new base level or, in other cases, is frequently captured as a consequence of the evolution of younger fluvial systems. This behaviour is generated by the fact that the coastline has experienced important changes during Pleistocene and Holocene times, because of the partial collapse of a fringe bordering the sea. The reconstruction of this space is difficult.

Segments A to E are differentially affected by neotectonics and so we have interglacial deposits at a very wide range of different positions. Also along Holocene times the subsidence of some spaces has formed depressions where marshes and small lagoons have developed.

In the submarine shelf, in turn, a generalized evolution has taken place from Upper Pleistocene up to Holocene, thus causing the transformation of a coastline made up of low sandy beaches, shoals and uniform slope littoral bars towards strongly sloped coasts including abundant cliff areas. This fact has caused a large proportion of old littoral systems to appear submerged and fossilized on the submarine shelf nowadays. The form this evolution has taken in each sector depends on the most relevant depositional factor present there.

These studies allow us to know in more or less in detail the variations in time of morphologies and sedimentary bodies. Nevertheless, few studies deal with continent-platform Quaternary depositional dynamics as a whole, and no one faces the questions of transference processes, suspended particle matter, and interactions among the different factors and distribution mechanisms of the continent-platform depositional environments. In this sense, this work can be considered as a contribution to the evolutionary knowledge of the geomorphological link established between the emerged and submerged littoral domains.

Figure 12 is a schematic summary of morphourestratigraphical units on the Valencia and Alicante continental and submarine areas based on examination of the data.

ACKNOWLEDGEMENTS

The authors would like thank to Dr David B. Scott of Dalhousie University and Dr Paolo Pirazzoli of Laboratoire de Géographie Physique, CNRS, for their critical review and helpful suggestions. The scientific contents of this work is a part of the projects 'Quaternary Evolution from Villajoyosa to Huertas Cape and Littoral Quaternary on the Alicante Coast', funded, respectively, by the Institució Valenciana d'Estudis i Investigació (Project 061-007) and Conselleria de Cultura de la Generalitat Valenciana (Project 101-90 'La Nao'). This paper is a contribution of IGCP Project 367.

REFERENCES

Blázquez, A.M. (1995). Facies sedimentarias y asociaciones de foraminíferos bentónicos actuales en la plataforma submarina interna situada entre la Marjal de Oliva-Pego y la Vila Joiosa. Tesis. Universitat de Valencia, 144 pp.

Cuenca, A. (1988). Terminación oriental del Accidente Cádiz-Alicante. *Investigaciones Geográficas*, **6**, 95–102. Instituto Universitario de Geografía, Universitat de Alicante.

Díaz del Río, V., Rey, J. and Vegas, R. (1986). The Gulf of Valencia continental shelf: extensional tectonics in Neogene and Quaternary sediments. *Marine Geology*, **73,** 169–179.

Dumas, B. (1977). Le Levant Espagnol. La génèse du relief. Thesis. Université Paris Val de Marne.

Dupré, M., Fumanal, M.P., Sanjaume, E., Santisteban, C., Usera, J. and Viñals, M.J. (1988). Quaternary Evolution of Pego coastal lagoon (Southern Valencia, Spain). *Palaeogeography, Palaeoclimatology, Palaeoecology*, **68,** 291–299.

Ferrer, C. and Fumanal, M.P. (in press). Evolución holocena de las costas bajas en el sector bético valenciano.

Fumanal, M.P., Viñals, M.J., Belluomini, G., Usera, J., Mateu, G. and Dupré, M. (1991). Evolución cuaternaria de la bahía de Xábia: Registro sedimentario, rasgos biológicos y cronoestratigráficos. VIII *Reunión Nacional sobre Cuaternario*. Libro de excursiones, Valencia, Septiembre, 1991, pp 58–63.

Fumanal, M.P., Mateu, G., Rey., J., Somoza., L. and Viñals, M.J. (1993a). Las unidades morfosedimentarias cuaternarias del litoral del Cap de la Nau (Valencia-Alicante) y su correlación con la plataforma continental. *In*: Fumanal, M.P. and Bernaeu, J. (eds), *Estudios sobre el Cuaternario. Medios Sedimentarios. Cambios Ambientales. Hábitat Humano*, pp. 53–64.

Fumanal, M.P., Usera, J., Viñals, M.J., Mateu, G., Belluomini, G., Manfra, L. and Proszynska-Bordás, H. (1993b). Evolución cuaternaria de la bahía de Xàbia (Alicante). *In*: Fumanal, M.P. and Bernabeu, J. (eds), *Estudios sobre Cuaternario*, pp. 17–26. Valencia.

Fumanal, M.P., Hernández Molina, F.J., Rey, J., Blázquez, A.M. y Somoza, L. (1995). Evolución morfosedimentaria de la plataforma continental y el dominio costero entre Villajoyosa y el Cabo de Santa Pola (Alicante) durante el Cuaternario terminal. *In*: Aleixandre, T. and Pérez-González (eds), *Reconstrucción de paleoambientes y cambios climáticos durante el Cuaternario*, pp. 27–42. Madrid.

Fumanal, M.P. (1995a). Los acantilados béticos valencianos. *En El Cuaternario del País Valenciano*. AEQUA y Universitat de València, pp. 177–186. Valencia.

Fumanal, M.P. (1995b). El valle del Gorgos. Litoral de Xàbia: Un transecto en el dominio bético del País Valenciano. *En El Cuaternario del País Valenciano*. AEQUA y Universitat de València, pp. 169–185. Valencia.

Goy, J.L. and Zazo, C. (1987). Quaternary shorelines: their dispositions related to the continental deposits and neotectonics in the Elche Depression (Alicante, Spain). *Absts. 12th INQUA, Congress*, Ottawa, Canada, pp. 176.

Goy, J.L., Rey, J., Díaz del Río, V. and Zazo, C. (1987). Relación entre las unidades geomorfológicas cuaternarias del litoral y de la plataforma interna de Valencia (España): implicaciones paleográficas. *Geología Ambiental y Ordenación del Territorio*, 1369–1380. Valencia.

Goy, J.L. and Zazo, C. (1988). Sequences of Quaternary marine levels in Elche Basin (Eastern Betic Cordillera, Spain). *Palaeogeography, Palaeoclimatology, Palaeoecology*, **68,** 301–310.

Goy, J.L., Zazo, C., Bardají, T., Somoza, L., Causse, C. and Hillaire-Marcel, C. (1993). Élements d'une chronostratigraphie du Tyrrhénien des régions d'Alicante-Murcie, Sud-Est de l'Espagne. *Geodinamica Acta*, **6**, 104–119.

Hernández-Molina, F.J., Somoza, L., Rey, J. and Pomar, L. (1994). Late Pleistocene-Holocene sediments on the Spanish continental shelves: Model for very high resolution sequence stratigraphy. *Marine Geology*, **120,** 1–15.

Hernández-Molina, F.J., Somoza, L., Rey, J. and Pomar, L. (1994b). Very high resolution sequence stratigraphy model for the Late Pleistocene-Holocene on the spanish continental shelf. Abstract Volume. *Liverpool Sequence Stratigraphy Conference*, March 1994, 382–386.

ITGE (1994). *Mapa Geológico de la Plataforma Continental Española y Zonas Adyacentes*. Scale 1:200 000. Elche-Alicante. Instituto Tecnológico y Geominero de España. Ministerio de Industria y Energía.

Maldonado, A., Swift, D.J.P., Robert, A.Y., Han, G., Nittrouer, C.A., DeMaster, D.J., Rey, J., Palomo, C., Acosta, J., Ballester, A. and Castellvi, J. (1983). Sedimentation on the Valencia Continental Shell: preliminary results. *Continental Shelf Research*, **2,** 195–211.

Martínez-Gallego, J., Fumanal, M.P., Viñals, M.J., Rey, J. and Somoza, L. (1992). Geomorfología y Neotectónica en la bahía de Xàbia (Alicante). *In*: López Bermúdez, F., Conesa, C. and Romero, M.A. (eds), *Estudios de Geomorfología en España, Murcia*.

Martínez-Gallego, J., Rey, J., Fumanal, M.P. and Somoza, L. (1994). Evolución Cuaternaria del dominio marinocontinental situado entre el Puntal de Moraira y la Sierra de Bèrnia (Alicante, España) (in press).

Mauffret, A. (1976). Étude Geodynamique de la Marge des Iles Baleares. Thèse D'État. Université Pierre et Marie Curie, París, 137 pp.

Rey, J. and Díaz del Río, V. (1983). Aspectos geológicos sobre la estructura poco profunda de la plataforma continental del Levante español. *In*: Castellví, J. (ed.), *Estudio Oceanográfico de la Plataforma Continental. Seminario Interdisciplinar*, pp 53–74. Cadiz.

Rey, J., Fumanal, M P., Ferrer, C., Viñals, M.J. and Yébenes, A. (1993). Correlación de las unidades morfológicas cuaternarias (Dominio Continental y plataforma submarina) del sector Altea-La Vila Joiosa, País Valenciano (España). *Cuad. de Geogr.*, **54,** 249–267.

Rossello, V.M., Esteban, V., Yebenes, A. y Fumanal, M.P. (1995). Les Penyes de l'Albir: geomorfología litoral cuaternaria. *In*: Aleixandre, T. and Pérez-González (eds), *Reconstrucción de paleoambientes y cambios climáticos durante el Cuaternario*, pp. 3–14. Madrid.

Sanz de Galdeano, C. (1983). Los accidentes y fracturas principales de las Cordilleras Béticas. *Estudios Geol*, **39,** 157–165.

Stearns, C.E. and Thurber, D.L. (1965). Th^{230}–U^{234} dates of late Pleistocene marine fossils from the Mediterranean and Morrocan littorals. *Quaternaria*, **7,** 29–42.

Viñals, M.J. (1991). Evolución de la marjal de Oliva-Pego. Tesis Doctoral, Departamento de Geografía, Universidad de Valencia (unpublished).

Viñals, M.J., Belluomini, G., Fumanal, M.P., Dupré, M., Usera, J., Mestres, J. and Manfra, L. (1993). Rasgos paleoambientales holocenos en la bahía de Xàbia (Alicante). *In*: Fumanal, M.P. and Beranbeu, J. (eds), *Estudios sobre Cuaternario, Valencia*, 107–114.

Pergamon

Quaternary Science Reviews, Vol. 15, pp. 803–809, 1996

0277–3791/96 $32.00

PII: S0277–3791(96)00068–6

RECENT COASTAL EVOLUTION OF THE DOÑANA NATIONAL PARK (SW SPAIN)

ANTONIO RODRÍGUEZ-RAMÍREZ,* JOAQUÍN RODRÍGUEZ-VIDAL,* LUIS CÁCERES,* LUIS CLEMENTE,† GIORGIO BELLUOMINI,‡ LUIGIA MANFRA,§ SALVATORE IMPROTA‖ and JOSÉ RAMÓN DE ANDRÉS**

**Departamento de Geología, Universidad de Huelva, Campus de La Rábida, 21819 Palos de la Frontera, Huelva, Spain*

†Instituto de Recursos Naturales y Agrobiología (CSIC), Apartado 1052, 41080 Sevilla, Spain

‡Centro di Studio per il Quaternario e l'Evoluzione Ambientale del CNR, Dipartimento di Scienze della Terra, Università 'La Sapienza', 00185 Roma, Italy

§Dipartimento di Scienze della Terra, Università 'La Sapienza', 00185 Roma, Italy

‖Dipartimento di Fisica, Università 'La Sapienza', 00185 Roma, Italy

***Instituto Tecnológico y Geominero de España, Ríos Rosas, 23, 28003 Madrid, Spain*

Abstract — Since the last Holocene sea level rise, about 6900 BP, a series of depositional littoral landforms has been generated at the outlet of the Guadalquivir River, with progradation along the predominant longshore drift (towards the east).

The first coastal progradation occurred between 6900 and 4500 BP. The Doñana and (perhaps) La Algaida spits, both associated with the oldest and highest marshland in the Doñana National Park, are assumed to have been developed at an early stage. Originally, the Guadalquivir estuary was wider and deeper than now, and its environment was mainly marine.

The oldest littoral formations have been dated as ca. 4735 BP. They show erosional events, and indicate the breaking-up of earlier spit-barriers to form inlets. The marine environment became increasingly dominant, with heavy erosion of cliffs and a retreating coastline.

This period was followed by another sedimentary cycle (4200–2600 BP) that surrounded the earlier eroded barriers. The size of the estuary decreased due to the increasing marsh deposits, and a fluvial environment was born.

About 2600 years ago, progradation gave way to a new period of intense erosion. The resulting morphology of littoral strands and erosional surfaces permitted the return to a marine environment. The shoreline again retreated.

From 2300 BP, coastal progradation has prevailed, with an erosional interruption at 1000 BP. The present-day outlet of the Guadalquivir is an estuarine delta of inactive marshland (the Doñana National Park), the dominant environment is fluvial.

INTRODUCTION

The present-day Iberian south-Atlantic littoral is characterized by a series of broad zones under tidal influence associated with the mouths of the main rivers. These outlets have tended to be sealed by the growth of littoral spits and barrier-islands. In this way, extensive wetlands of great ecological interest have been formed. The most important — for its size and variety — is the Doñana National Park.

Such a coast is the result of various circumstances. Firstly is the rise in sea level following the Last Glacial Age (the Flandrian transgression), which reached a maximum in this sector around 6500 BP (Zazo *et al.*, 1994). The domination by the marine environment meant the invasion of the low part — the river valleys — to form estuaries and bays, and the configuration of the interfluvial areas as coastal projections (promontories and capes) on which cliffs were formed. Secondly, after the transgression maximum the agents modelling this coastal sector were dynamic ones such as longshore drift, tide, and wind. They were aided by the labile, Neogene and Quaternary sandy substratum. The prevailing longshore drift has been towards the E and SE, so that the sandy barriers have been formed in that direction. Drift intensity increases in the Gibraltar Strait region, because of the greater entrance of Atlantic water into the Mediterranean in anticyclonic periods (the Azores anticyclone). The modelling and filling of the zones protected from the open sea, such as estuaries, is determined by the tide, with additional contribution from fluvial sediments. Lastly, the prevailing SW winds

TABLE 1. Samples and ages in the Guadalquivir outlet area (Atlantic coast, SW Spain)

Location	Sample	^{14}C Conventional age (BP)	^{14}C Calibrated age (95%)	Age (BP)
Doñana	R-2205[1]	2185±50	80 A.D.–270 A.D.	1775
	R-2185[1]	1860±50	440 A.D.–655 A.D.	1402
	R-2210[1]	2010±50	270 A D.–470 A.D.	1580
	R-2204[1]	1490±50	830 A.D.–1020 A.D.	1025
	R-2187[1]	1790±50	530 A.D.–700 A.D.	1335
	R-2188[1]	1850±50	440 A.D.–660 A.D.	1400
	R-2271	2641±47	392 B.C. –339 B.C.	2315
	R-2282	1620±34	736 A.D.–815 A.D.	1175
	R-2286	1353±31	1,028 A.D.–1,069 A.D.	902
	R-2287	1518±36	859 A.D.– 948 A.D.	1047
La Algaida	R-2262	1865±35	530 A.D.–608 A.D.	1380
	R-2263	1800±40	591 A.D.–662 A.D.	1325
	R-2272	1972±40	400 A.D.–475 A.D.	1515
	R-2284	2233±29	93 A.D.–158 A.D.	1825
	B-88018[2]	1600±60	1222 BP–1071BP	1146
	B-88019[2]	1340±60	931 BP–804 BP	867
	B-88020[2]	1450±70	1055 BP–918 BP	986
	B-88021[2]	1530±70	1153 BP–978 BP	1065
	B-88022[2]	2487±70	2487 BP–2322 BP	2404
Carrizosa-V. la Arena	R-2273	4548±59	2870 B.C.–2697 B.C.	4735
Vetalengua	R-2283	2171±36	147 A.D.–248 A.D.	1753
	B-88016[2]	2230±60	1879 BP–1738 BP	1808
Marsh strand	R-2278	2284±39	28 A.D.–119 A.D.	1877
	R-2279	3679±48	1680 B.C.–1553 B.C.	3567
	R-2280	3694±61	1716 B.C.–1562 B.C.	3589
	B-88017[2]	3460±90	3421 BP–3219 BP	3320

Laboratories Centro di Studio per il Quaternario e l'Evoluzione Ambientale del CNR–Dipartimento Scienze della Terra, Università 'La Sapienza' (Roma, Italy)
Zazo *et al.* (1994) Beta Analytic Inc, Miami, FL, USA

have helped (and continue to help) the development of dune fields systems.

Study of the different, most recent (Holocene) sedimentary bodies of the south-Iberian littoral has distinguished four main cycles of coastal progradation (Zazo *et al.*, 1994): H_1 from 6900 to 4000 BP; H_2 from 4000 to 2500 BP; H_3 from 2500 to 1000 BP; and H_4 from 1000 BP to the present. These periods are separated by shorter ones of no progradation or erosion.

This work aims to establish the space–time evolution of the Doñana National Park and its surroundings during the last millennia, and to determine the possible modifications of the different factors affecting it, such as climate, marine dynamics, and variations in sea level. To these must be added anthropogenic activity of some hundreds of years. Detailed geomorphological mapping has been used to make morphosedimentary analysis and both calibrated (amino acids and ^{14}C, see Table 1) and archaeological datings.

Geomorphologically, the present-day Doñana National Park and its surroundings comprise three morphogenic systems: littoral, estuarine, and aeolian (Fig. 1). The littoral system is formed by the various spits and sandy strands that tend to seal off the Guadalquivir estuary. On the right bank is the Doñana spit. This comprises the most extensive system of spits, which has grown towards the E and SE. They are partly covered today by active dunes. On the left bank is La Algaida spit, which has grown towards the NNE.

The estuarine system comprises the marshes filling the extensive area behind the littoral spits. This filling has taken place gradually as the littoral formations have sealed the estuary. Thus there is a direct relationship between the littoral formations and the estuarine ones. The marshes include various morphologies, as a result of the intense fluvial action.

The aeolian system comprises the dune fields, extensive both continentally and littorally. Geomorphological mapping reveals five sequences of dunes: the three oldest are stable and inland, occupying a considerable area, while the two more recent ones are coastal, of smaller area, and frequently overlapping. They are the most distinctive dune complexes, and include the active dune systems, covering the most recent littoral formations.

The three oldest dune fields (phases I–III, Fig. 1) have a light grey to yellowish colour, 10YR7/2 to 10YR7/8, and the two recent ones have a pale brown colour, 10YR7/4 (after Siljeström, 1985).

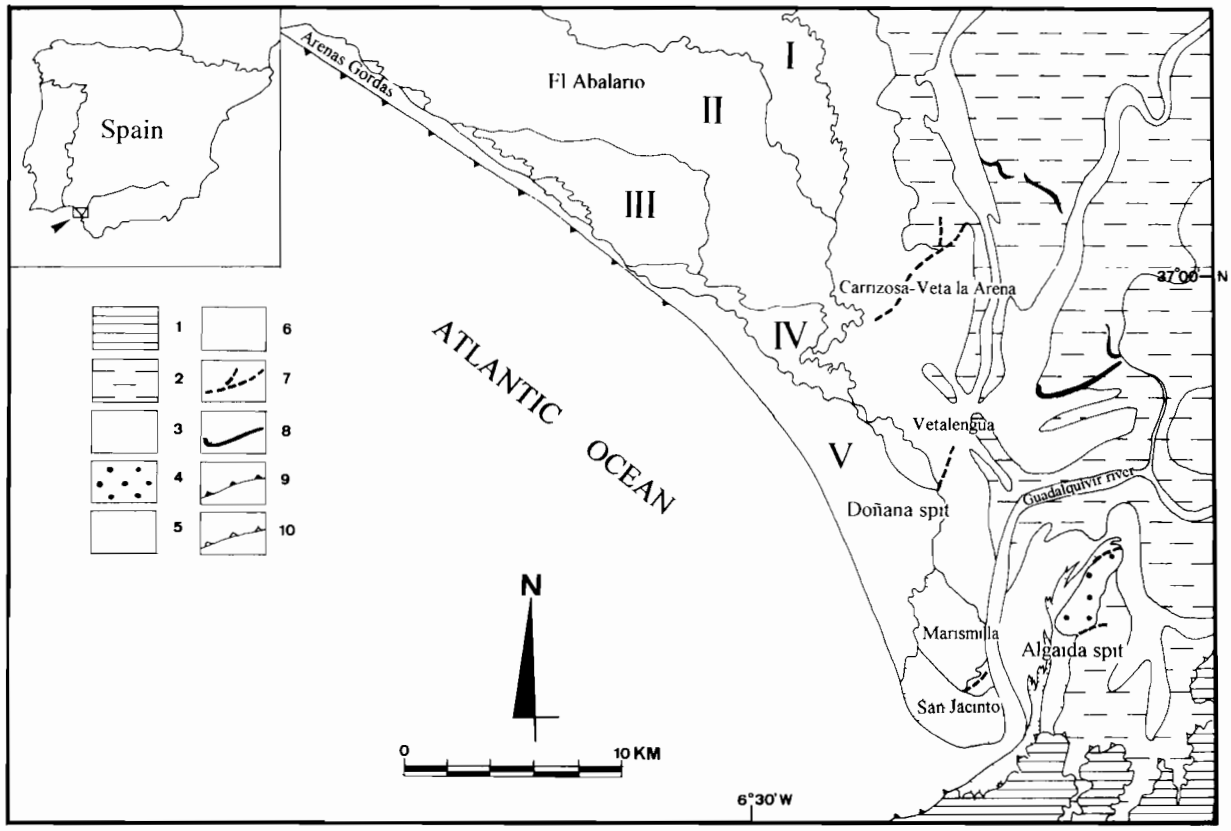

FIG. 1. Geographical location and geomorphological synthesis of the Guadalquivir outlet area. I–V: Sequences of Holocene dunes. 1. Neogene substratum, 2. Marshland, 3. Saltmarsh, 4. Second progradation phase, 5. Third progradation phase, 6. Fourth progradation phase, 7. Erosional strands, 8. Marsh strands, 9. Active cliffs, 10. Inactive cliffs.

COASTAL MORPHOLOGY AT THE TRANSGRESSION MAXIMUM

The rapid rise in sea level following the final phase of the Last Glacial Maximum caused a rapid and marked coastal retreat along the whole of this sector of the Iberian South-Atlantic coast. Lower rates of rise during this period generated deposits of peat (such as that found at a depth of 25 m in Cádiz Bay), between 9495±340 and 8915±100 BP (Dabrio *et al.*, 1995).

The lower valley of the Guadalquivir — the most important river of the region — was transformed into a wide estuary, and the coastal promontories and flanking headlands were eroded into cliffs (Fig. 2A).

Coastline retreat was helped by a topography of gentle slopes and a bare shore formed basically of weakly-cemented Neogene and Quaternary sands. Detritus became highly available, and was transported along the whole coast, to be deposited mainly in estuaries, dunes and submerged parts of the continental platform.

The high rates of coastal erosion and the intense supply of fluvial detritus helped to continentalize the Guadalquivir estuary. The present-day estuary is filled with sediments and the river flows sluggishly. The extensive tidal flats of the Doñana National Park are the result of gradual accretion and withdrawal of the marsh during the last 6900 years, with the consequent reduction in the estuary area.

To the west of the present-day mouth of the Guadalquivir (Fig. 1), complex systems of transgressive dunes have formed along almost 60 km of coastline, migrating inland as the coastline retreats. Geomorphological cartography at regional level has enabled three ancient stable aeolian systems to be distinguished. Their direction of displacement indicates a prevailing WSW wind.

FIRST PROGRADATION PHASE

The activity following the transgression maximum, helped by the relative stability of the sea level, gave rise to a series of progradation phases, tending to make the coastal profile uniform, followed by erosion. Thus the estuarine inlets were filled or sealed and the promontories were eroded.

The oldest evidence of the beginning of coastal progradation in this Iberian South-Atlantic sector comes from the first peat deposits that accumulated in the main lagoons (such as the lagoon of Las Madres) from 5536 BP (Menéndez and Florschütz, 1964). These show that the coastal profile was already becoming uniform, with littoral barriers closing off the inlets. This was particularly so in the rivulet valleys, which were converted into littoral lagoons. Many of these first deposits of peat have been eroded by coastal retreat.

Pollen analysis of these peat levels (Freijeiro and Rothemberg, 1981; Stevenson, 1984) reveals temperate-

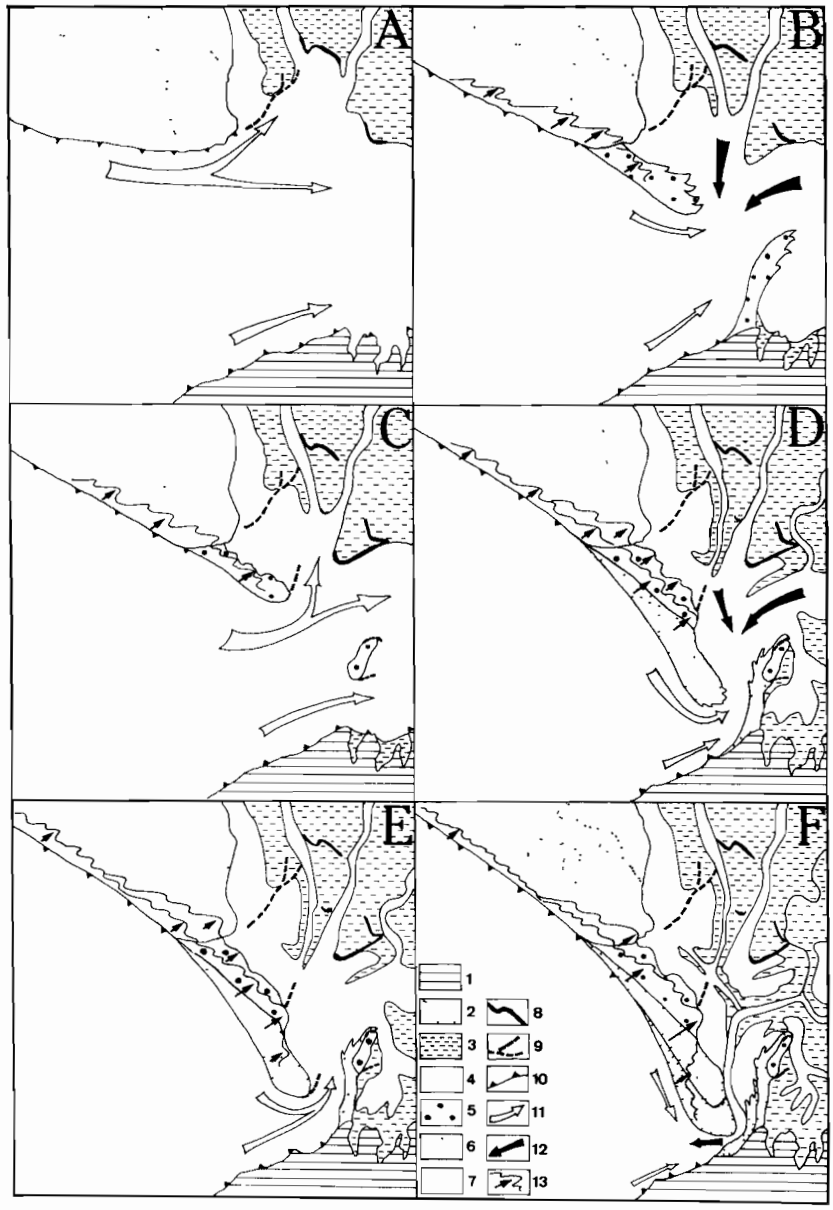

FIG. 2. Evolutive sequence of the Guadalquivir outlet area (Doñana National Park): A. First erosional event, B. Second progradation phase, C. Second erosional event, D. Third progradation phase, E. Third erosional event, F. Fourth progradation phase. Legend: 1. Neogene substratum, 2. Ancient aeolian system (phases I–III), 3. Saltmarsh, 4. Mudflat, 5. Second progradation phase, 6. Third progradation phase, 7. Fourth progradation phase, 8. Marsh strands, 9. Erosional strands, 10. Cliffs, 11. Marine streams, 12. Fluvial streams, 13. Recent aeolian system (phases IV–V).

wet palaeoclimatic conditions, between Atlantic and Subboreal episodes.

In the area occupied by the present-day mouth of the Guadalquivir, the oldest littoral formations (detectable by geomorphological mapping) are the Carrizosa-Veta la Arena strands (Figs 1 and 2A). Aminoacid and ^{14}C dating of shells gives a calibrated age of 4735 BP. The real age may be somewhat lower (because of possible removing of the sample), which would place it within the first erosional event (4000 BP) defined by Zazo *et al.* (1994) for southern Spain.

The geomorphological arrangement of these littoral formations (perpendicular to the direction of the main barriers) and their small size are evidence of a short-lived but highly intense erosional event that destroyed an earlier sandy barrier.

The main direction of progradation was towards the NE — that is, into the estuary. The formations are supported laterally on earlier marshland deposits, at a height of +2 m, showing the palaeocoastline and giving a slight increase in above-sea-level height.

At a regional level, the first phase of progradation deposits was between 6900 and 4000 BP (phase H_1 of Zazo *et al.*, 1994). In the Guadalquivir mouth, this episode has been eroded; its remains can be found below the transgressive aeolian formations in the zone of El Abalario. The root zone of this first littoral spit was located on the west side of the outlet, on a coastal headland, today eroded. The direction of advance was towards the ESE.

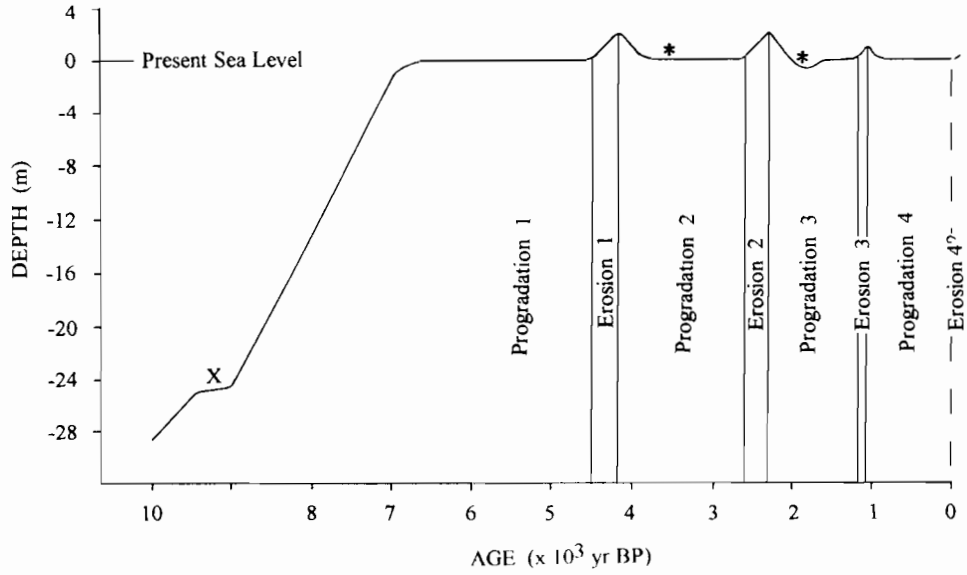

FIG. 3. Regional curve of relative sea-level changes during the last 10,000 years, derived from the positions and morphologies of the associated sedimentary bodies. (*) Biological crises, (X) Sea-level position about Dabrio *et al.* (1995).

SECOND PROGRADATION PHASE

This phase, which isolated the Guadalquivir estuary from the sea, led to a decreased marine influence in its interior, and a dominant continental environment (Fig. 2B). Filling of the estuary was helped by small, fingered delta bodies (like a birds-foot) in the main affluents.

The fluvial dominance provoked a marked biological crisis in the marine fauna (Fig. 3), with considerable accumulations of organic remains at the sides of the palaeoestuary. Such shell deposit remains have been dated as from ca. 3567–3589 BP. This marks the moment of the environmental crisis and the progradation of the littoral barriers, so reducing the openings communicating the sea with the estuary.

On the right side of the Guadalquivir mouth (Doñana littoral spit), the remains of this progradation phase are very eroded by fluvial action, and are hidden below the sheets of active dunes that advance towards the NE. These active dunes (fourth aeolian system) are associated with this second progradation phase.

On the left side, the first vestiges of deposits that could be determined cartographically are located on La Algaida spit. On them have been found pre-Roman settlements and archaeological remains of the VIIth to IInd centuries B.C. (Menanteau, 1979).

The morphological features of this littoral spit indicate that there was progradation towards the NE, but it is not possible to determine whether there was union with the continent at that time or not; that is, we are not sure whether morphologically it was a spit or an island.

The headlands situated on either flank of the Guadalquivir outlet must originally have been more prominent, and their erosion and consequent retreat were linked to this second progradation phase.

In the sandy formations of both the right and left banks, this progradation phase is interrupted by an erosional event, with a height above sea level of around +2 m. This event resulted in a greater estuarine domination within the marsh, with a new coastline being defined in the marine inlet and the development of characteristic fauna, especially of the genus *Cerastoderma.*

In the area of the Doñana National Park, this rupture is seen in the Vetalengua strands (Figs 1 and 2C), which advanced towards the NNE. A similar phenomenon was produced on La Algaida spit, with the erosion of the earlier sandy formation leaving an island of oval shape surrounded by two arms of sea — one very wide (some 6 km) between Doñana and La Algaida, and the other, smaller, between the latter and the continent.

Estrabón in his work *Geographica*, written between 29 and 7 B.C., speaks of this estuary as an inland lagoon, which he called *Lacus Ligustinus*, with a double outlet to the sea. Between the two channels was an island where, according to oral tradition, there was a city with the same name as the river — *Tartessos*. Despite these historical references, the data do not enable a sure estimate of the beginning of this erosional event. The only dating made on the Vetalengua strands gives a date of ca. 1753 BP, which is probably of a later point in its evolution. At regional level, Rodríguez-Vidal (1987) and Zazo *et al.* (1994) date this event around 2500–2000 BP and 2500 BP respectively.

THIRD PROGRADATION PHASE

This new progradation phase resulted in a considerable growth of the littoral and aeolian formations, a retreat of the cliffs, and the gradual sealing of the Guadalquivir estuary (Fig. 2D). The decrease in size of the mouth of the old Roman estuary (*Lacus Ligustinus*) helped to increase the fluvial influence. The Guadalquivir delta extended within the estuary by surface fingers of the delta system, causing a new crisis of the fauna adapted to the salt-water

medium (Fig. 3). Accumulations of organic remains — mainly of the genus *Cerastoderma* — can be found at the sides of the palaeoestuary. The calibrated age of these is ca. 1877 BP, marking the littoral progradation.

In Doñana, this phase gave rise to the strands of La Marismilla, with a direction of progradation towards the SSE. This sedimentary episode shows a marked alternation between ridges and runnels, with a greatest age of ca. 1870 BP and an estimated periodicity in the growth of each ridge of 100 years (Zazo *et al.*, 1994).

In La Algaida, this phase is shown by a series of ridges and runnels oriented towards the NE, engulfing the older sedimentary body. Its calibrated age is 2404 BP. Its morphological configuration changed from that of an island to that of a spit joined to the continent.

At the same time, the littoral strands of La Marismilla, on the other side of the mouth, grew rapidly, causing a decrease of sedimentation on La Algaida. This spit thus became isolated from marine action, completely losing its functionality within the estuary. Since then, it has been surrounded by deposits from the marsh.

It must be remembered that the dating of the sandy formations of La Algaida and Doñana was not made from the oldest beach ridges. Thus it can be assumed that the beginning of progradation is earlier than the dates given. At regional level, Zazo *et al.* (1994) estimate this to be from 2500 BP.

A little further to the west of this coastal sector, the present-day beach situated in front of Las Madres lagoon contains levels of peat (Cáceres, 1995) at −0.5 m in depth, aged between 1900±180 and 1790±180 BP. Thus the coastline was more advanced and the sea level lower than at present (from −0.5 m to −1.0 m, Fig. 3).

This third progradation phase is also characterized by very important dune systems, whose activity continued until the later phase This resulted in the beginning of the genesis of the fifth aeolian system (Fig. 1), which has lasted until the present. It comprises sandy constructions of great morphological importance, extending geographically from Arenas Gordas to Doñana. In Arenas Gordas, the dunes overlap, with breadths of up to 100 m, showing the maximum cliff retreat in this sector. Four main aeolian episodes of parabolic dunes have been differentiated cartographically. Their axes of symmetry indicate the prevailing wind direction at the time. Statistical analysis of these directions (Rodríguez-Vidal *et al.*, 1993) reveals a gradual change — from WSW to SW — showing the variations in regional atmospheric circulation.

The sandy formations of this episode were curtailed by a new erosional event (Fig. 2E), shown in Doñana by strands which advanced towards the NE and separated the progradation units of La Marismilla and San Jacinto (Fig. 1). Their calibrated age is 1175 BP. On La Algaida spit this event is less obvious, as its deposits are protected inside the estuary, and suffer less from marine action. At regional level, this erosional event took place some 1000 BP.

FOURTH PROGRADATION PHASE

The fourth progradation phase in this coastal sector is related with that established by Zazo *et al.* (1994) for southern Spain (phase H_4), from 1000 BP to the present. In Doñana it is shown in the littoral strands of San Jacinto (Figs 1 and 2F), accompanied by a considerable aeolian sheet. It seems to have reactivated with greater force from the XVIth century, as shown by the last phases of littoral accretion. On La Algaida spit, the most western hooks are related to this last progradation phase.

The marked coastal retreat of Arenas Gordas continued in this phase, shown by the more recent aeolian accumulations and by the destruction of coastal buildings of the XVIth century (watch-towers). The retreat at Matalascañas can thus be estimated as 170 m in the last 240 years.

The smoothing of this promontory or coastal headland, situated to the west of Doñana, has moved the erosional-sedimentary point of inflexion towards the east. The erosional processes have extended towards the root of the ancient littoral spit of Doñana (first progradation phase). The rate of retreat has been estimated as 200 m in the last 220 years. The sediments resulting from this erosion have accumulated at the extreme SE, on the San Jacinto strands, which have prograded 180 m.

Today, the longshore drift is becoming stronger, and erosion is increasing at the end of the San Jacinto strands. Hooks are being formed with NE orientation, encroaching into the Guadalquivir channel. This process is similar to that which took place in preceding erosional events, and could be the result of the present-day increase in sea level. Dabrio *et al.* (1993) estimate, from chronostratigraphic and sedimentological data, a slight rise until 2050 A.D.

CONCLUSIONS

Changes in coastal relief following the last postglacial increase in sea level have brought about marked environmental changes in all the natural systems of the Iberian south-Atlantic coast. Geomorphological mapping has enabled time relations to be established between the different sedimentary formations and erosional processes. Archaeological evidence and calibrated dating of ^{14}C and aminoacids of fossil shells (Table 1) has helped to establish an absolute chronology.

The littoral spit systems mapped constitute four progradation phases (Fig. 3). The first is dated between the Flandrian maximum (6900 BP) and 4500 BP; the second between 4200 and 3900 BP and 2700 and 2600 BP; the third between 2300 and 1100 BP; and the fourth between 1000 BP and the present. There were separations of successive erosional phases between 4500 and 4200 BP, 2600 and 2300 BP, and 1100 and 1000 BP.

Thus, cycles of higher sedimentation are established, with a slight fall and then stability of sea level. Littoral barrier constructions dominate, with the genesis of extensive tidal flats that decrease the size of the estuaries. These sedimentary phases are interrupted by rapid rises in

sea level lasting from 100 to 300 years, when the previously constructed littoral barriers are eroded. The cliffs retreat, causing migration inland of dunar constructions, with frequent overlapping layers. Marine influence within the estuaries increases.

The Holocene environmental changes that we have been able to show have thus been generated by global changes in atmospheric circulation and sea currents. Today, we are in a dominant anticyclone situation, controlled by the semi-permanent rotation at the Azores. This leads to increased longshore drift, progradation of the sandy barriers, and high rates of sedimentation.

The progradation phases studied developed immediately following a period of relatively high sea level, when stability was lost and there was a slight fall — that is, in the climatic transition from cyclonic to anticyclonic conditions, and above all, under the latter. That time was especially tragic for the salt-water fauna of the estuaries. In the Guadalquivir, biological crises can be dated around 3550 and 1870 BP.

In periods of low atmospheric pressure, the energy of the marine medium was higher, causing slight rises in sea level and a dominant coastal erosion.

ACKNOWLEDGEMENTS

The authors would like to thank C. Zazo, D. Gorsline and J. Murillo for critical revisions which have led up to this paper. Financial support was provided by Spanish DGICYT Projects PB91-0622-C03-01 and PB94-1090-C03-01. It is a contribution to IGCP Project 367.

REFERENCES

Cáceres, L. M. (1995). Geomorfología del sector occidental de la Depresión del Guadalquivir. Unpublished Ph.D. Thesis, University of Huelva.

Dabrio, C.J., Zazo, C. and Goy, J.L. (1993). Litoral y riesgos geológicos. *V Reunión Nacional de Geología Ambiental y Ord. Territ.*, Murcia.

Dabrio, C.J., Goy, J.L., Lario, J., Zazo, C., Borja, F. and González, A. (1995). The Guadalete Estuary during the Holocene times (Bay of Cádiz, Spain). *Mediterranean and Black Sea Shorelines (INQUA) Newsletter*, **17,** 19–22.

Freijeiro, A. and Rothemberg, B. (1981). *Exploración Arqueometalúrgica de Huelva*. Ed. Labor. Huelva.

Menanteau, L. (1979). Les Marismas du Guadalquivir. Exemple de transformation d'un paysage alluvial au cours du Quaternaire récent. These 3e cycle, University of Paris-Sorbonne.

Menéndez, J. and Florschütz, F. (1964). Resultados del análisis paleobotánico de una capa de turba en las cercanías de Huelva (Andalucía). *Estudios Geológicos*, **20,** 183–186.

Rodríguez-Vidal, J. (1987). Modelo de evolución geomorfológica de la Flecha Litoral de Punta Umbría, Huelva, España *Cuaternario y Geomorfología*, **1,** 247–256.

Rodríguez-Vidal, J., Cáceres, L., Rodríguez-Ramírez, A. and Clemente, L. (1993). Coastal dunes and postflandrian shoreline changes. Gulf of Cadiz (SW Spain). *Mediterranean and Black Sea Shorelines (INQUA) Newsletter*, **15,** 12–15.

Siljeström, P. (1985). Geomorfología y edafogénesis de las arenas del Parque Nacional de Doñana. Unpublished Ph.D. Thesis, University of Sevilla.

Stevenson, A.C. (1984). Studies in the vegetational history of SW Spain. III Palynological investigations at El Asperillo, Huelva. *Journal of Biogeography*, **11,** 527–551.

Zazo, C., Goy, J.L., Somoza, L., Dabrio, C.J., Belluomini, G., Improta, S., Lario, J., Bardají, T. and Silva, P.G. (1994). Holocene secuence of sea-level fluctuations in relation to climatic trends in the Atlantic–Mediterranean linkage coast. *Journal of Coastal Research*, **10,** 933–945.

Pergamon

Quaternary Science Reviews, Vol 15, pp. 811–818, 1996.

0277–3791/96 $32.00

PII: S0277–3791(96)00067–4

MORPHOSEDIMENTARY BEHAVIOUR OF THE DELTAIC FRINGE IN COMPARISON TO THE RELATIVE SEA-LEVEL RISE ON THE RHONE DELTA

SERGE SUANEZ and MIREILLE PROVANSAL

Universite de Provence, Institut de Géographie, Laboratoire de Géographie Physique (URA-903), 29 Av. Robert Schuman, 13621 Aix-en-Provence, France

Abstract — For the first time, mareographic data obtained by the 'Compagnie du Salin du Midi' have been used to estimate the relative sea-level rise (RSLR) in the Rhone delta. The results were compared with the data obtained in the Marseille region which is known to be a tectonically stable zone, at least, on the secular time scale. The magnitude of relative sea-level rise is equal to 2.1 mm/year, from which 1 mm/year could be attributed to subsidence. The morphosedimentary behaviour of the deltaic fringe has been analyzed in order to see if the amount of sediment input is sufficient to allow the wetlands to continue to exist with RSLR. The horizontal variations (erosion and progradation) have been quantified from land surface changes obtained by shoreline variation analysis. The vertical accretion is measured using isotopic dating (^{137}Cs). It appears that the eastern part of the mouth of the Rhone is characterized by high sediment input, sufficient enough to offset the recent rise of sea level. The western part remains vulnerable due to the lack of sediment in this area. Copyright © 1996 Elsevier Science Ltd

INTRODUCTION

The vulnerability of the Mediterranean coast to sea-level rise has already been studied using different approaches (Jeftic *et al.*, 1992). The scenario based on the Global Vulnerability Analysis (GVA) showed that the southern Mediterranean coast is more vulnerable than the northern Mediterranean coast (Nicholls and Hoozemans, 1995). Nevertheless, the absolute protection costs are higher for the northern Mediterranean coast; it is equivalent to 0.02% of the GNP. The deltaic zones have been described as the most vulnerable sectors, therefore the Rhone delta is concerned with this scenario. Even if there is not a large population affected in this area compared to other Mediterranean deltas such as the Nile delta, vulnerability to sea-level rise will mainly concern industrial and tourism activities. For the salt industry 'Compagnie du Salin du Midi' located on the western part of the mouth of the Rhone, the total expenditure for coastal protection for the last decade is equal to 0.4% of the global input of the company. For the industrial complex of Fos (Port Autonome de Marseille) located on the eastern part of the mouth, the figure is unknown but the total expenditure has been important for the last few years mainly due to the program of dune management (Table 1).

However, any rise in sea level will have different impacts depending on the sectors. Those impacts being a function of several parameters such as magnitude of the rise, subsidence, human response, sediment supply, etc. For the deltaic zones, subsidence is an important factor. It is mainly due to the compaction of thick sediments or the pumping of water For the Rhone delta, previous work based on the study of archeological sites has shown that subsidence ranges from 0.5 to 4.5 mm/year (L'Homer, 1992). Nevertheless, it is admitted that the sediment deficit will become more important with an acceleration in sea-level rise caused by global warming (Day *et al.*, 1995).

Following this approach, our aim was (a) to estimate the extent of the rise of sea level in the Rhone delta and (b) to evaluate the sediment input in terms of vertical accretion and horizontal surface changes. The first part of this study will focus on the estimation of the secular trend in relative sea-level rise in the Rhone delta by using mareographic data. The second part will look at the evolution of the

TABLE 1. Total expenditure for coastal protection for the last decade concerning the littoral located on each side of the mouth of the Rhone (information given by the 'Compagnie du Salin du Midi' and the 'Port Autonome de Marseille')

Global input/year (Fr.)	C.S.M. 1×10^9	P.A.M unknown
Protection costs/year (Fr. 10^3)		
1986–1989	14,000	unknown
1990–1995	15,500	6350
% global input/year	0.4	unknown

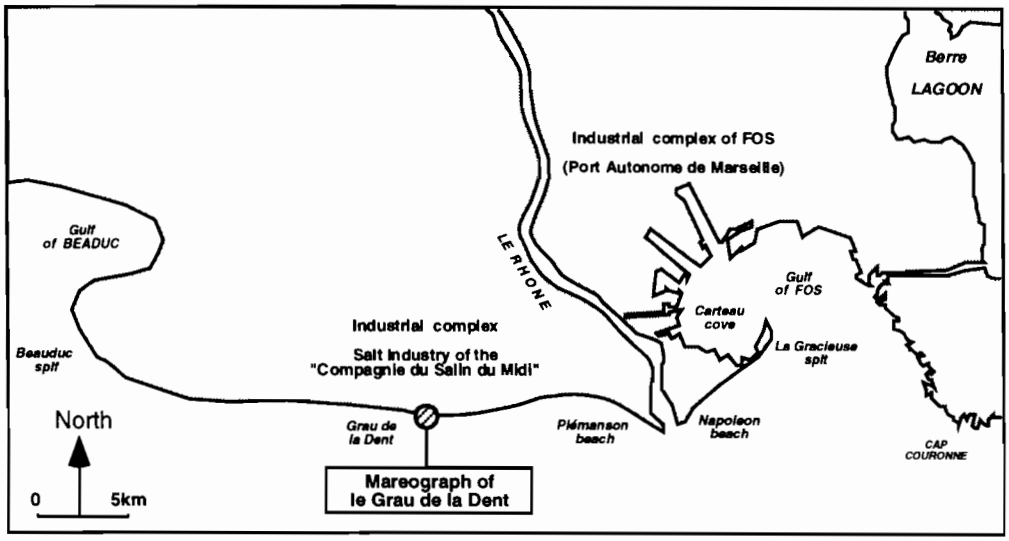

FIG. 1. Location map of the mareograph of Le Grau de la Dent (Compagnie du Salin du Midi, Rhone delta).

global sediment budget over the last fifty years by using shoreline changes and isotopic dating (^{137}Cs) analysis.

ESTIMATION OF RELATIVE SEA-LEVEL RISE IN THE RHONE DELTA

The acquisition of mareographic measurements has been used to estimate the relative sea-level rise in the Rhone delta. The comparison was made with data obtained in the Marseille area.

Data Acquisition and Method

Since the begining of the century (1905), mean sea level measurement has been undertaken by the 'Compagnie du Salin du Midi' (C.S.M) in the Rhone delta using the mareograph of 'Le Grau de la Dent' (Fig. 1). A daily recording of the sea level was made at 07.00 h by the technical services of the C.S.M. Due to the loss of an archive document, there is an 11-year hiatus (from 1963–1973) in the data.

The secular trend of sea-level rise was estimated by calculating the linear regression function. The gap caused by the 11-years of missing values was not taken into account by the linear regression.

Results

The result shows that the secular change in sea level was equal to 2.1 mm/year. A comparison was made with the data obtained from the mareograph of Marseille (Endoume) and already analysed by different authors (Pirazzoli, 1986; Blanc and Faure, 1990). It appears that the rise in sea level is less extensive in the Marseille area of 1 mm/year than in the Rhone delta (Fig. 2). There is a difference of 1 mm/year between the two sites.

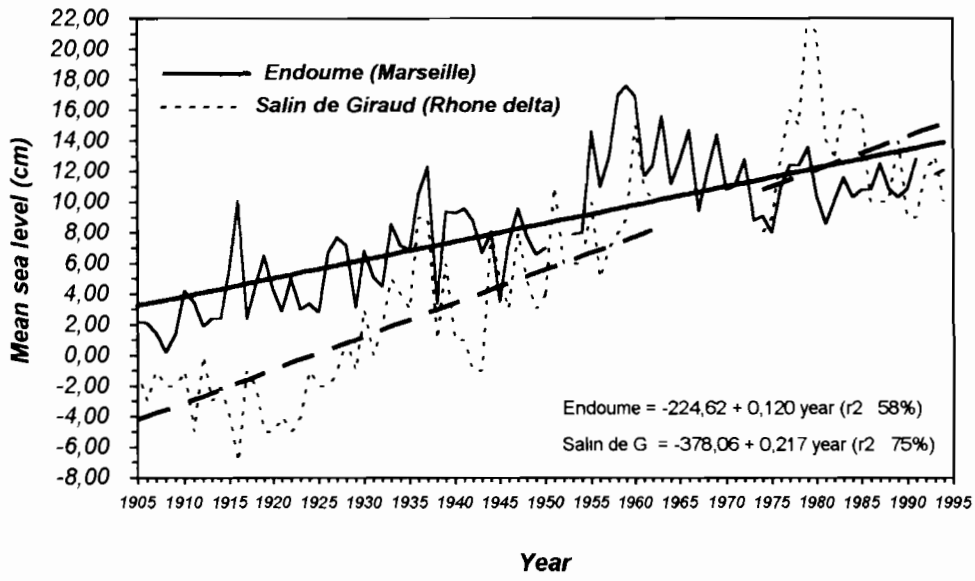

FIG. 2. Secular trend of the RSLR on the Rhone delta and Marseille area.

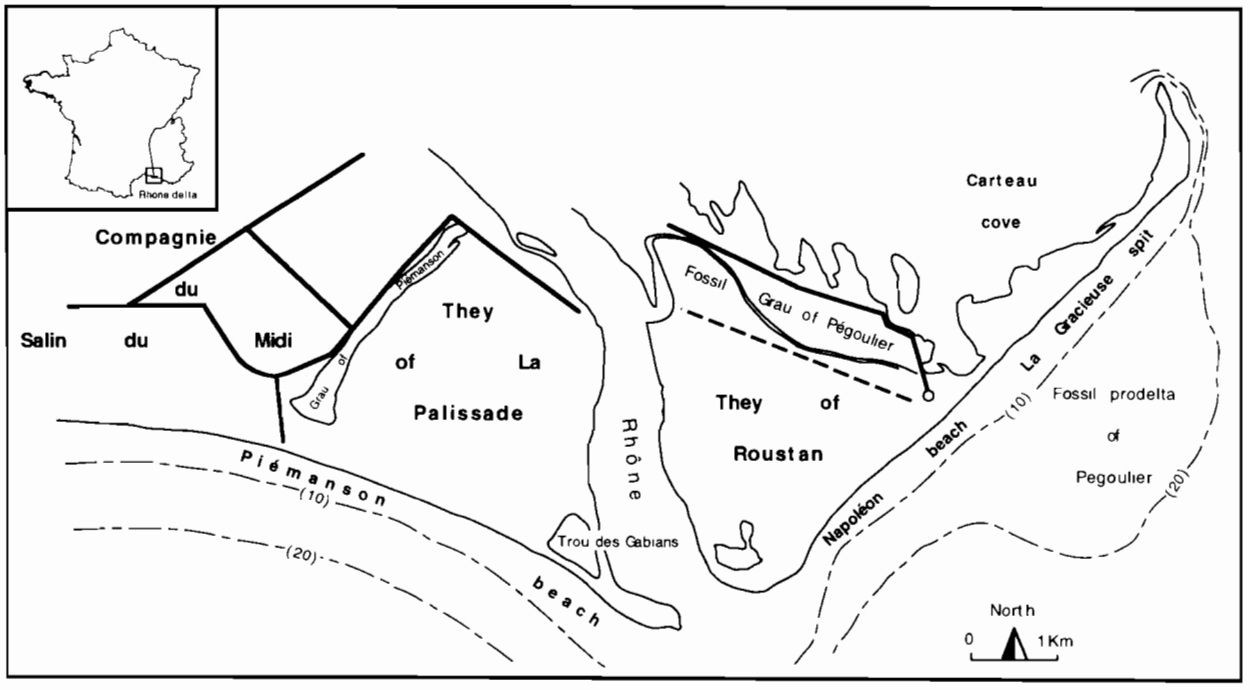

FIG. 3. Location map of the studied area.

Conclusion

Calculation of the secular trend of the rise in sea level in the Rhone delta (2.1 mm/year) gives higher values than those described in the literature (Gornitz *et al.*, 1982; Pirazzoli, 1986; Gornitz and Lebedeff, 1987; Blanc and Faure, 1990; Wigley and Raper, 1992). Marseille is located in a Mediterranean zone where tectonism is insignificant, at least over the last century (Flemming and Webb, 1986; Emery *et al.*, 1988; Morhange, 1994). Therefore, the difference of 1 mm/year could be attributed to the subsidence movements that affect the Rhone delta. These vertical ground movements are mainly localized along the littoral fringe. They can be explained, in some part, by human intervention in morphosedimentary processes of the deltaic system. Damming of the Rhone since the 19th century has eliminated flooding of the deltaic plain, which resulted in the accumulation of Rhone sediments on the littoral margin. The magnitude of the sedimentary mass in the submerged zone might explain the origin of this subsidence. However, the processes linked to such recent human intervention may play a secondary role. In fact, the value of subsidence (1 mm/year) corresponds to that measured on a pluri-millenium time scale obtained from the study of the archeological sites (Flemming and Webb, 1986; L'Homer, 1992). Therefore the subsidence may not be limited to the margin, but will concern the whole deltaic plain.

EVOLUTION OF THE GLOBAL SEDIMENT BUDGET

The sediment budget analysis has been calculated using the horizontal variation of the shoreline and the vertical accretion. The first approach gives an estimation of the land surface changes, the second one estimates the accretion rate.

The study area is located on either side of the mouth of the Rhone (Fig. 3). It is formed by La Gracieuse spit and Napoléon beach to the east and Piémanson beach to the west. The driving agents are defined by:

The river discharge, characterized by sediment input from the river to the sea, principally during floods. The suspended matter has been estimated to 8.5×10^6 t/year (Pont, 1993; Roditis and Pont, 1993). The bottom load, mainly sandy (Carrio, 1988) plays a major role in the sediment supply to beaches.

The wave climate, represented by swells coming from three main directions: SW (30% of the total regime and which are the most frequent during the year); SSE (16%); and SE (11%) related to episodic events such as storms.

The currents, represented by the dominant one called the Liguro-Provençal current flowing from east to west. It does not influence the morphogenesis of the littoral very much because it is located in the open sea (Duboul-Razavet, 1956). The most important for the littoral area is represented by drift currents flowing near to the coast from west to east.

The wind climate, represented by continental winds (Mistral oriented N–NW, 31% of total regime) and sea winds, mostly oriented from E to SE (27% of the total regime). The latter is principally related to storms.

Horizontal variation: Land Surface Changes (Fig. 4(a–b))

Land surface changes have been calculated from shoreline variations using image processing analysis.

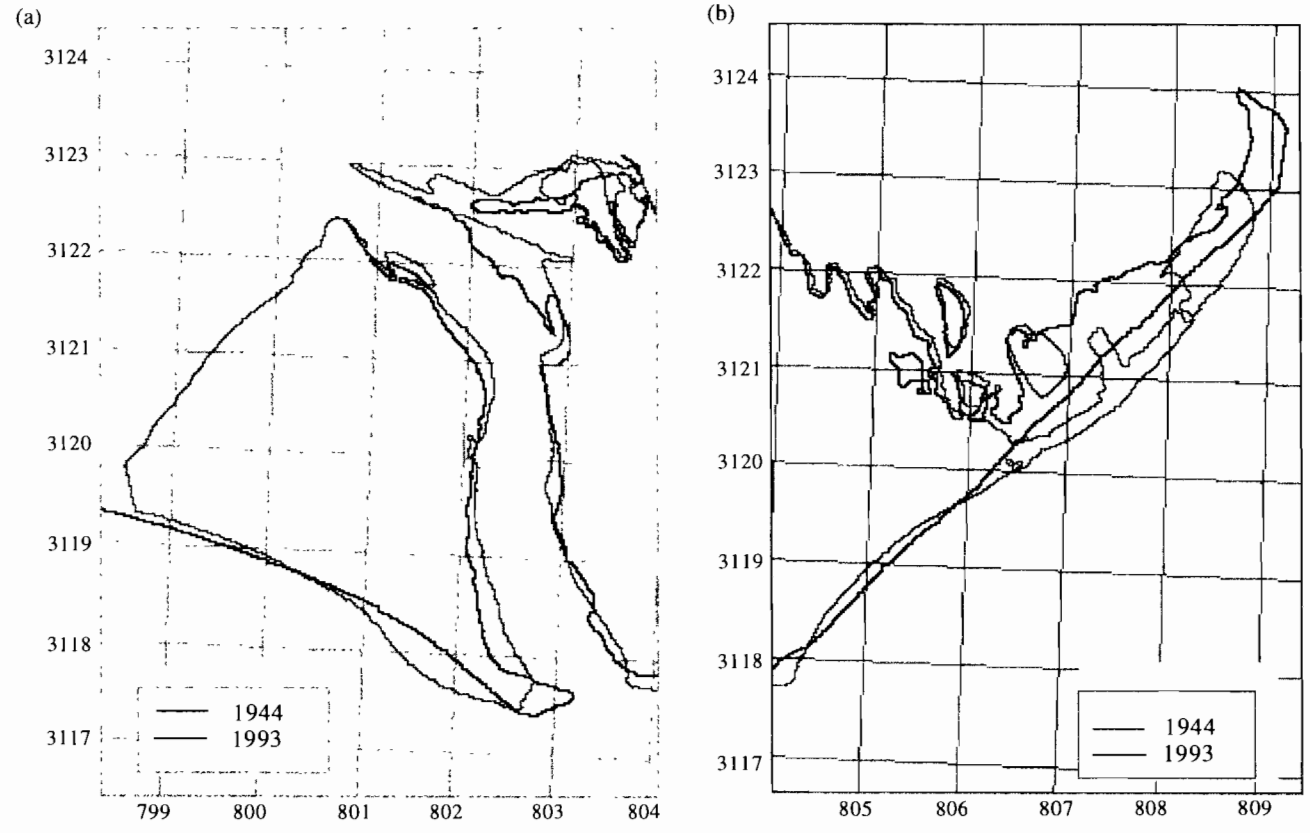

FIG. 4. (a) Shoreline changes from 1944 to 1993 for the western part of the Rhone delta coast (the LAMBERT III geographic coordinate system is used as a reference). (b) Shoreline changes from 1944 to 1993 for the eastern part of the Rhone delta coast (the LAMBERT III geographic coordinate system is used as a reference).

The diachronic analysis, based on the study of aerial photographs and satellite images, shows the change in coastline over the last fifty years. The method consists of superposing the layers of information date by date.

Data acquisition and methodology[1]

Height difference dates were chosen corresponding to aerial photograph campaigns[2]: 1944–1955; 1960–1971; 1979–1989, and satellite images[3]: 1984 and 1993. The methodology was based on those used in previous works on changes of the littoral using image processing analysis (Grenier and Bubois, 1990; Crowell *et al.*, 1991, 1993; Dolan *et al.*, 1991; Shoshany and Degani, 1992). Photo-interpretative zoning of the shoreline was used for the aerial photographs. The information was then captured by video camera and digitalized from the screen. Geometrical corrections were made using a landmark system taken on the topographic map as a reference grid document. Analysis of satellite data was done using the traditional methods of classification. Discrimination of the emerged part of the littoral was obtained by classifying wet zones, using the infrared TM5 channel. Skeletization of the coastline was extracted using contours.

Diachronic analysis

To make possible the comparison, the evolution of the global sediment budget has been reduced to three periods characterized by the same interval of time 1944–1960, 1960–1979, 1979–1993. The whole zone has been divided into four homogeneous sectors defined according to their dominant morphodynamic factors (Fig. 5): (a) Piémanson beach, oriented NW–SE, is a sector that is very vulnerable to SW swells, which are the most frequent type during the year; (b) the zone situated at the mouth of the Rhone is directly related to the sediment supplied by the river; (c) Napoléon beach is vulnerable to SE swells and is also supplied by Rhone sediments transported by littoral beach drift currents, flowing west to east; and (d) La Gracieuse spit is characterized by a double evolution. From the end of the 19th century to the 1970s, it has evolved naturally. Due to the rehabilitation program at La Gracieuse spit, started by the Port Autonome de Marseille in 1988, all of the morphosedimentary processes have become entirely artificial.

Results (Fig. 6)

The first period (1944–1960) is characterized by very

[1]Acquistion and analysis of the image data were made at the Computer Resource Centre of St Jerome University (Marseille), using software called PERICOLOR (MATRA), and IAX software installed on the IBM 3090 system.

[2]Aerial photographs from 1944 were taken during the last world war by allied forces. These data are actually managed by the Archeological Department of the University of Provence *'Centre Camille Jullian, Université de Provence'* Aerial photographs from 1944–1955; 1960–1971, 1979–1989 were taken later on by IGN *(Institut Géographique National)* and a private compagny (Aerial).

[3]The satellite images used for 1984 and 1993 correspond to Landsat TM

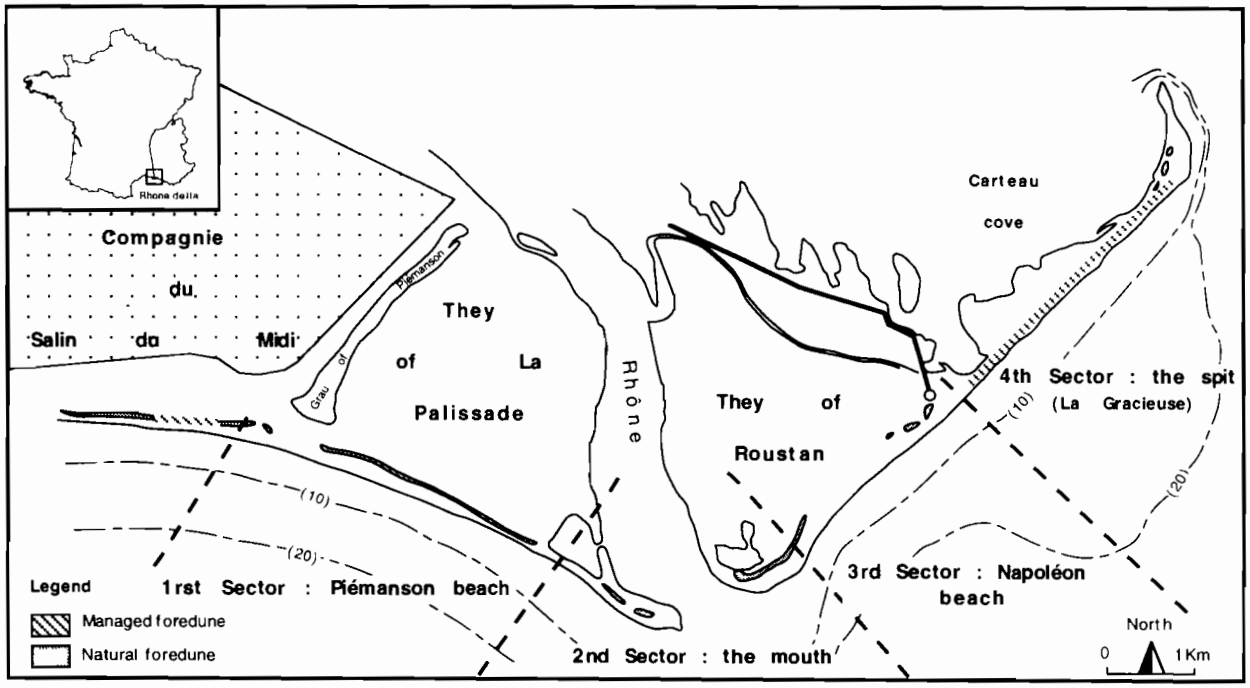

FIG. 5. Location of the division of the coast into four sectors.

low changes. The whole coast has not recorded significant variations. Important changes appear for the second period (1960–1979). The Piémanson beach is characterized by a loss of sediment while the other sectors were prograded. The last period (1979–1993) shows the same situation except for the mouth sector which has eroded, the Piémanson beach is still characterized by a loss of sediment while La Gracieuse spit has strongly prograded.

The global sediment budget shows that the western part of the mouth of the Rhone formed by the Piémanson has eroded while the eastern part formed by La Gracieuse spit and Napoléon beach has prograded.

Conclusion

The evolution of this part of the littoral over the last fifty years is characterized by a general displacement of the whole system to the east. This evolution is the result of the combination of natural processes and human management (Suanez, 1995).

The evolution of the river mouth is complex. It is marked by alternating periods of accretion and erosion, which correspond to flood periods of the Rhone. There is a continuous displacement of the river mouth towards the east, indicated by the accumulation of sediments related to drift currents. Piémanson beach is characterized by a slow but continuous evolution over time which corresponds: (a) to a 'natural regularization' of its profile in the ESE direction; and (b) to the fact that it is partially isolated or disconnected from the Rhone river, inducing a nil or negative sedimentary balance. The retreat of the littoral is particularly extensive during the second period (1960–1979) and tends to be reduced

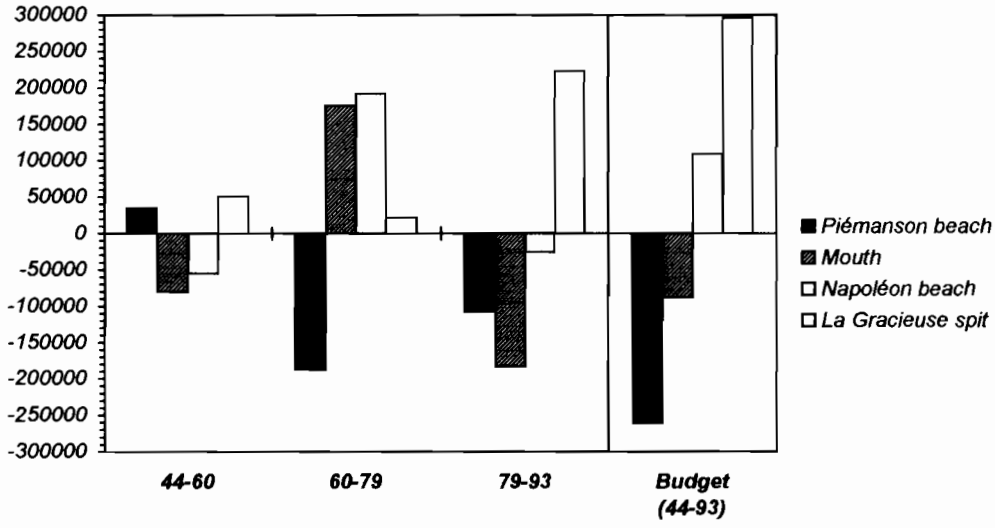

FIG. 6. Evolution of the global sediment budget since 1944.

for the recent period when the profile has reached its stability. The sedimentary material lost in the eastern part of the beach is transported and deposited to the east, forming the bar that partially closes the outlet of the Rhone. This sediment transfer is facilitated by drift currents. It appears that the coast located to the east of the mouth of the Rhone is directly influenced by the river, and is therefore characterized by a surplus sedimentary balance. For Napoléon beach, the periods of progradation coincide with those occurring when the river mouth records a loss of material. Napoléon beach is considered as a transit zone where sedimentary transfers indicate a time lag between the flood sediments of the Rhone and their redistribution to La Gracieuse spit located further east. The evolution of La Gracieuse spit between 1944 and 1984 is a prolongation of the morphological and sedimentary history of this sector since the end of the 19th century (Vernier, 1976). The present-day equilibrium profile was made in the mid-1980s. Since this period, the build-up as a whole seems to have stabilized, and since the beginning of the 1990s the progradation of the littoral is greater due to the coastal management carried out by the Port Autonome de Marseille. The rehabilitation of coastal dunes and the immersion of barges has stopped the loss of sediments inducing the enlargement of the beach from the reconstituted dunes and drift currents.

The results obtained from land surface changes show that the eastern part of the mouth of the Rhone is characterized by sediment supply sufficient enough to allow the continuing existence of wetlands with relative sea-level rise. By contrast, the lack of sediment input in the western part of the littoral makes this zone more fragile and vulnerable to the rise of sea level.

Vertical Variation: Accretion Rates

In order to confirm the result obtained by the shoreline variation analysis, the vertical accretion has been measured using isotopic dating (^{137}Cs) on samples collected on each side of the mouth of the Rhone river[4]. The aim was to find the depth associated with the limit of ^{137}Cs concentration which corresponds to the beginning of nuclear activities in the drainage basin of the Rhone river (1950s).

Sampling and methodology

Cores were taken on each side of the mouth of the Rhone river in Piémanson and Napoléon beaches (Fig. 7). They were collected from the back beach, a few meters from the bottom of the dune. Isotopic dating (^{137}Cs) was carried out on silty-clay samples located at a depth of 40 cm for Piémanson beach and 43 cm for Napoléon beach. The existence of silty-clay layers interstratified with sandy layers is related to the fluvial dynamics which have already been studied in a previous work (Suanez and Provansal, 1993). The accumulation of fine sediment in the back beach occurs during floods of the Rhone, which cause the inundation of the emerged beach. This is mainly due to the connections through the foredune existing between the lagoons and the beach. Therefore, the silty-clay deposits appear to be a useful chronological parameter directly connected with pulsing events.

Results

The results show that the end of the signal was not reached for either of the measurements. The concentra-

[4]Isotopic analysis have been done by C.E.A. IFREMER (Toulon).

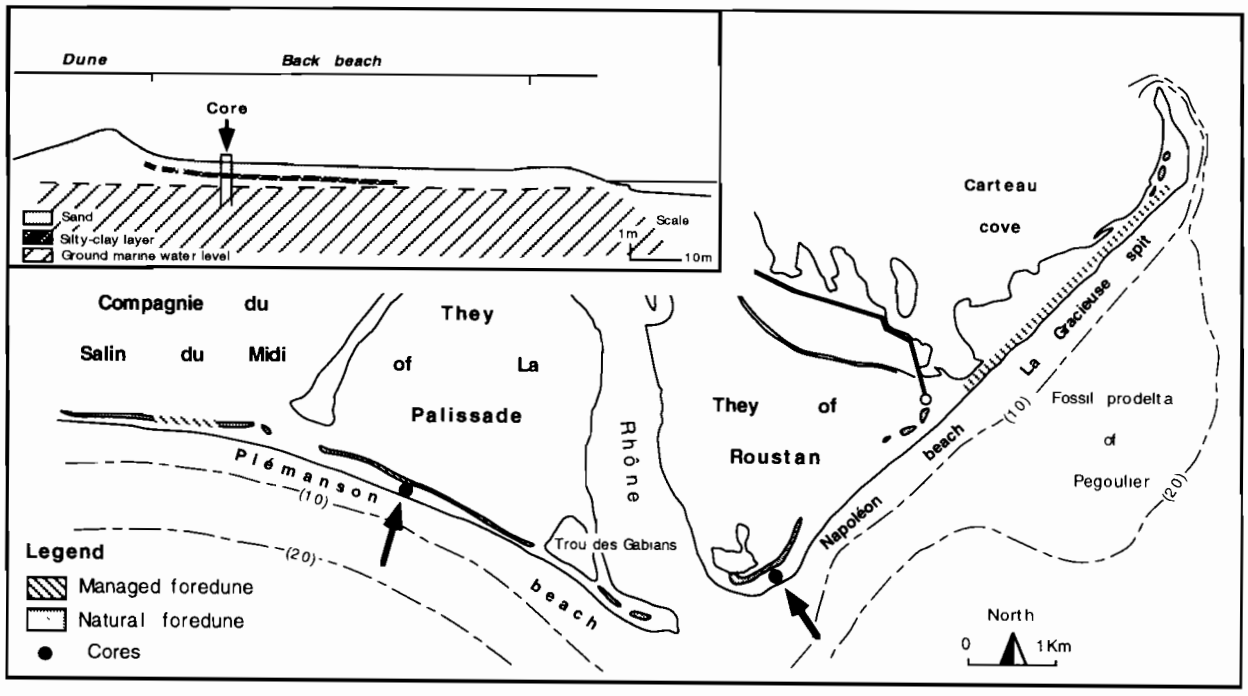

FIG. 7. Location map of the cores.

TABLE 2. Results obtained from isotopic measurement analysis

Sediment	Quantity	PF/PS	Duration (sec)	Am-241	±	^{134}Cs ±	^{137}Cs	±	K-40	±
Piémanson	131 g	1.01	84719		—	—	7.90	0.50	630	30
Napoléon	125.20 g	1.01	82285	10.1	0.7	—	199	8.00	780	40

tion of ^{137}Cs was still present in the samples collected on each side of the mouth of the Rhone (Table 2). Nevertheless, the concentration rate obtained at Napoléon beach was much higher than at Piémanson beach.

Conclusion

The presence of ^{137}Cs concentration for both samples means that the deposits are quite recent, at least, later than 1950. The lack of measurements beneath and above these levels to fill the whole profile does not allow us to estimate a more accurate date in accordance with the reference curve obtained for the Rhone river (P.N.O.C., 1994). Therefore, a minimum value of sedimentation rate equal to +1 cm/year is suggested. The higher concentration of ^{137}Cs obtained on Napoléon beach could be explained by the fact that the deposit is more recent than at Piémanson beach, inducing a sedimentation rate more important in the eastern part of the mouth of the Rhone. This hypothesis will confirm the result obtained by the shoreline variation analysis with a loss of sediment for the western part since the 1960s and an increase of global sediment budget for the estern part until the present-day.

DISCUSSION

For the first time, analysis of tide-gauge records in the Rhone delta is produced. The comparison with the magnitude of RSLR obtained from several other north Mediterranean stations (1.2 mm/year) shows the extent of subsidence (1 mm/year). This value is less important than those obtained from other Mediterranean deltas such as the Pô delta: in Venezia, analysis of tide-gauge records of the recent period indicated an accelerated sinking of 7.3 mm/year (Emery *et al.*, 1988); the Nile delta with subsidence of 4.8 mm/year (Stanley and Warne, 1993). This is mainly due to human activities, notably groundwater withdrawal. The lower human pressure on the Rhone delta may explain the lower subsidence rate obtained in this area.

In regards to the morphosedimentary behaviour, it appears that in the western part of the mouth of the Rhone the vulnerability to RSLR seems to be more critical than the eastern part of the littoral. These observations confirm the previous works carried out on this zone characterized by a retreat of the coast for the last several decades (Blanc, 1975, 1977; Blanc and Jeudy De Grissac, 1982; Blanc and Poydenot, 1993). The results obtained for the eastern part of the Rhone confirm the importance of river input despite the recent managements (dams, dykes, etc.). Input of sandy material seems to be sufficient to supply this part of the Rhone delta. The position of this sector in relation to the mouth is a determinant factor. Nevertheless, driving agents play an important role; the importance of western swells and drift currents in the evolution of the littoral as a supplier of sediment which cause unequal redistribution of this material between the littoral situated to the east and to the west of the river mouth (Suanez and Provansal, 1995). Therefore, the outer coast influenced by the Rhone river supply is not threatened by relative sea-level rise. On the contrary, when no sediment is being added to the coast, it becomes lower each year, as sea level rises. This pattern confirms observations made in the deltaic plain (Pont *et al.*, 1995).

ACKNOWLEDGEMENTS

This work was carried out as a part of the *MEDDELT* project. It was supported by the EC Environment Research Programme, Directorate General for Science, Research and Development under Contracts N° EV5V-CT94-0465

REFERENCES

Blanc, J.J. (1975). Evolution du profil des plages et phénomènes d'érosion littorale. *TETHYS*, **7,** 299–306.

Blanc, J.J. (1977). Recherches de sédimentologie appliquée au littoral du delta du Rhône, de Fos au Grau du Roi, Contrat C.N.E.X.O. 75/1193, 69 pp.

Blanc, J.J. and Jeudy De Grissac, A. (1982). Dangers d'érosion littorale en Petite Camargue (aire occidentale du delta du Rhône, France). *TETHYS*, **10,** 349–354.

Blanc, J.J. and Faure, H. (1990). La remontée récente du niveau de la mer. Exemples de Marseille, Gênes et Venise (Méditerranée). *Géologie Méditerranèenne*, **XVII,** 109–122.

Blanc, J.J. and Poydenot, F. (1993). Le rivage de Faraman en Camargue (SE France): un géosystème côtier en déséquilibre; méthodes d'étude — conséquences pratiques. *Géologie Méditerranéenne*, **XX,** 75–87.

Carrio, C. (1988). Contributions à l'étude dynamo-sédimentaire du delta rhodanien et du processus d'émersion de la plaine deltaïque associée. Exemple du domaine de la Palissade, Camargue, France. Thèse de 3ème cycle soutenue le 1er Juillet 1988, Université de Provence Aix-Marseille I.

Crowell, M., Leatherman, S.P. and Buckley, M.K. (1991). Historical shoreline change: error analysis and mapping accuracy. *Journal of Coastal Research*, **7,** 839–852.

Crowell, M., Leatherman, S.P. and Buckley, M.K. (1993). Shoreline change rate analysis: long term versus short term data. *Shore and Beach*, **61,** 13–20.

Day, J.W., Pont, D., Hensel, P.F. and Ibanez, C. (1995). Pulsing events and sustainability of Mediterranean deltas, *Medcoast* 95, October 24–27, 1995, Tarragona, Spain, E. Özhan (Ed.), pp. 781–791.

Dolan, R., Fenster, M.S. and Holme, S.J. (1991). Temporal analysis of shoreline recession and accretion. *Journal of Coastal Research*, **7,** 723–744.

Duboul-Razavet, C. (1956). Contribution à l'étude géologique et sédimentologique du delta du Rhône. *Mém. Soc. Géol. de France*, **76,** 234.

Emery, K.O., Aubrey, D.G. and Goldsmith, V. (1988). Coastal neo-tectonics of the Mediterranean from tide-gauge records. *Marine Geology*, **81,** 41–52.

Flemming, N.C. and Webb, C.O. (1986). Tectonic and eustatic coastal changes during the last 10,000 years derived from archeological data. *Z. Geomorph. N.F., Suppl.*, **62,** 1–29.

Gornitz, V., Lebedeff, S and Hansen, J. (1982). Global sea level trend in the past century *Science*, **215,** 287–289.

Gornitz, V. and Lebedeff, S. (1987). Global sea-level changes during the past century. *The Society of Economic Paleontologist and Mineralogist, Speciale Publication*, **41,** 3–16.

Grenier, A. and Bubois, J.J.M. (1990). Evolution littorale récente par télédétection: synthèse méthodologique. *Photo Interprétation*, **90-6,** 3–7.

Jeftic, L., Millıman, J.D. and Sestini, G. (1992). *Climatic Change and the Mediterranean*. Edward Arnold, London, 673 pp.

L'Homer, A. (1992). Sea level changes and impacts on the Rhone delta coastal lowlands. *In*: Tooley, M.J. and Jelgersma, S. (eds) *Impact of Sea-level Rise on European Coastal Lowlands*, pp. 136–152. Blackwell, UK.

Morhange, C. (1994). La mobilité récente des littoraux provençaux: éléments d'analyse géomorphologique, Thèse de 3ème cycle, Aix-en-Provence, Université de Provence.

Nicholls, R.J. and Hoozemans, F.M.J. (1995). Vulnerability to sea-level rise with reference to the Mediterranean region. *Medcoast 95*, October 24–27, 1995, Tarragona, Spain. Özhan, E. (ed.), pp. 1199–1213.

Pirazzoli, P.A. (1986). Secular trends of relative sea-level (RSL) changes indicated by tide gauge records. *Journal of Coastal Research, SI,* **1,** 1–26.

P.N.O.C. (1994). Rapport d'activité, Perpignan, 16 pp.

Pont, D. (1993). Vers une meilleure connaissance des apports du Rhône à la Méditerranée, 4es Rencontres de l'Agence Régionale Pour l'Environnement, PACA, pp. 16–24.

Pont, D., Day, J.W., Hensel, P.F. and Ibanez, C. (1995). Sediment dynamics in the Rhone deltaïc plain. Impacts of management practices, MEDDELT (EV5V-CT94-0465), Mid-term workshop, Arles, March 1995.

Roditis, J.-C and Pont, D. (1993). Dynamiques fluviales et milieux de sédimentation du Rhône à l'amont immédiat de son delta. *Méditerranée*, **3–4,** 5–18.

Shoshany, M. and Degani, A. (1992). Shoreline detection by digital image processing of aerial photography. *Journal of Coastal Research*, **8,** 29–34.

Stanley, D.J. and Warne, A.G. (1993). Nile delta: recent geological evolution and human impact. *Nature,* **250,** 628–634.

Suanez, S. and Provansal, M. (1993). Etude des modifications morphosédimentaires du littoral à l'embouchure du Rhône: plages de Piémanson et Napoléon. *Méditerrannée*, **3–4,** 43–56.

Suanez, S. (1995). Quelques données nouvelles sur l'évolution mi-séculaire du littoral camarguais à l'embouchure du Rhône (France, Sud-est). *B.A.G.F.*, **5,** 440–454.

Suanez, S. and Provansal, M. (1995). Dynamics of beach/dune systems of the Rhone delta (France), *submitted*.

Vernier, E. (1976). Edification et évolution de la flèche de la Gracieuse, Ouest du golfe de Fos. *Bull. B.R.G.M. (2ème Série)*, **IV,** 103–115.

Wigley, T.M.L. and Raper, S.C.B. (1992). Implications for climate and sea level of revised IPCC emissions scenarios. *Nature*, **357,** 293–300.

Pergamon

PII: S0277-3791(96)00066-2

Quaternary Science Reviews, Vol. 15, pp. 819–831, 1996.

0277-3791/96 $32.00

COASTAL DEFORMATION AND SEA-LEVEL CHANGES IN THE NORTHERN CHILE SUBDUCTION AREA (23°S) DURING THE LAST 330 KY

LUC ORTLIEB,* CARI ZAZO,† JOSÉ LUIS GOY,‡ CLAUDE HILLAIRE-MARCEL,§ BASSAM GHALEB§ and LOUISE COURNOYER§

**ORSTOM (Institut Français de Recherche Scientifique pour le Développement en Coopération), Depart de Geología, Universidad de Chile & Facultad de Recursos del Mar, Universidad de Antofagasta, Casilla 1190, Antofagasta, Chile*

†Departamento de Geología, Museo Nacional de Ciencias Naturales, C.S.I.C., J.Gutierrez Abascal 2, Madrid, Spain

‡Departamento de Geología (Area de Geodinámica), Facultad de Ciencias, Universidad de Salamanca, 37008-Salamanca, Spain

§GEOTOP, Université du Québec à Montréal, Case 8888 (Centre ville), Montréal, Québec, H3C 3PB Canada

Abstract — The Nazca–South American plate boundary is a subduction zone where a relatively complex pattern of vertical deformation can be inferred from the study of emerged marine terraces. Along the coasts of southern Peru and northern Chile, the vertical distribution of remnants of Pleistocene terraces suggests that a crustal, large scale uplift motion is combined with more regional/local tectonic processes. In northern Chile, the area of Hornitos (23°S) offers a remarkable sequence of well-defined marine terraces that may be dated through U-series and amino-stratigraphic studies on mollusc shells. The unusual preservation of the landforms and of the shell material, which enabled the age determination of the deposits, is largely due to the lengthy history of extreme aridity in this area. The exceptional record of late Middle Pleistocene to Late Pleistocene high seastands is also favoured by the slight warping of two distinct fault blocks that have enhanced the morphostratigraphic relationships between the distinct coastal units.

Detailed geomorphological, sedimentological and chronostratigraphic studies of the Hornitos area led to the identification, with reasonable confidence, of the depositional remnants of sea-level maxima coeval with the Oxygen Isotope Substages 5c, 5e, 7 (probably two episodes) and the isotope stage 9 (series of beach ridges). The coastal plain, at the foot of the major Coastal Escarpment of northern Chile, appears to have been uplifted at a mean rate of 240 mm/ky in the course of the last 330 ky. From the elevation of the older terraces and late Pliocene shorelines, it can be inferred that these steady vertical motions were much more rapid than during the Early Pleistocene. Copyright © 1996 Elsevier Science Ltd

INTRODUCTION

Over the last 150 years, several famous studies on coastal deformations and neotectonic uplift have been reported in Chile. After D'Orbigny (1842) and Darwin (1846), other naturalists (e.g. Domeyko, 1848, 1860; Pissis, 1856; Vidal Gormaz, 1901; Courty, 1907) have discussed, at length, the significance of the Quaternary marine terraces preserved along the coast of northern Chile, particularly in the areas of La Serena-Coquimbo (30°S) and also between Antofagasta and Iquique (24–22°S). For more than a century, the evidence of coastal uplift in Chile was tentatively related with the Andean Cordillera orogenesis and/or with the historically active seismicity of the country. It was only in the 1970s that the plate tectonic model offered a geodynamic framework that integrated the marine terraces, the seismic activity, the plate boundary and the subduction of the Nazca plate below the South-American plate (Barazangi and Isacks, 1976). However, until recently, much uncertainty has remained concerning the age of the Quaternary terraces, and thus the rate of uplift recorded along the Chilean coast. The age of the conspicuous terraces at La Serena and Coquimbo, on which had been based the chronostratigraphy of the Quaternary marine units in Chile (Herm and Paskoff, 1967; Herm, 1969; Paskoff, 1970, 1977) could not be established precisely. Furthermore, it was commonly assumed that the terraces had been formed during episodes of significantly higher sea level stands than the present datum.

Subduction Plate-Boundaries and Quaternary Uplift Motions

At subduction plate boundaries the margin of the overlying plate generally registers strong uplift motions

during Quaternary times (Ota, 1986). In the western Pacific, the identification of Late Pleistocene and late Middle Pleistocene emerged reef tracts at elevations of hundreds of metres above present sea level indicates uplift rates in the order of several millimetres per year over timescales of several hundred thousand years (Chappell, 1974; Bloom *et al.*, 1974; Ota, 1986). Therefore, it has been commonly considered that such high values of uplift rate were representative of any subduction zones. Actually, uplift values of over 0.5 mm/year, in the long range, may prove to be quite exceptional. In Peru and Chile, for instance, the vertical deformation of the coastal area appears to be much weaker: uplift rates are about an order of magnitude lower than those calculated across the Pacific Ocean. Along the coast of southern Peru, Pleistocene marine terraces are seldom observed at more than +200 m above present sea level, and regional uplift rates are of the order of 150–100 mm/ky for the entire Quaternary (Ortlieb *et al.*, 1995a). In some localities affected by local tectonic activity, though, uplift rates of up to 300 to 460 mm/ky were determined (Goy *et al.*, 1992; Ortlieb *et al.*, 1994a, *in press*). Besides, a several hundred kilometre long coastal segment in north-central Peru (7–14°S) does not show any evidence of Quaternary uplift (Macharé, 1987; Ortlieb and Macharé, 1990a). In contrast, the area in front of the termination of the aseismic Nazca Ridge (14–15°S) was uplifted, during the last million years, at a maximum rate of 740 mm/ky (Macharé and Ortlieb, 1992). Thus, it is clear that the deep-seated processes directly associated with the subduction of the Nazca plate, which should present some regional homogeneity, do account for only a part of the vertical deformation registered along the Peru plate boundary. Before a general pattern of regional deformation can be determined along this subduction plate boundary, we still need to decipher the detailed history of local uplift motions in distinct coastal sectors.

Geochronological Problems

Quantifying positive vertical motions along coastal regions requires that the emerged Pleistocene marine terraces be dated and correlated with interglacial high seastands. But dating marine terraces is a difficult task. The lack of corals along the Pacific coast of South America, south of 4°S, implies that radiometric measurements need to be done on mollusc shells, although U-series dating of molluscan material is often considered as unreliable (Kaufman *et al.*, 1971). Other geochronological methods were used, but did not always yield clear-cut and definitive results. The electron spin resonance (ESR) method was attempted in a series of localities from southern Peru and northern Chile (Radtke, 1985, 1989; Ratusny and Radtke, 1988; Hsu *et al.*, 1989), and amino acid epimerisation (allo/isoleucine) and racemisation measurements were performed on shells from numerous marine terraces of the same area (Hsu, 1988; Hsu *et al.*, 1989; Ortlieb *et al.*, 1992, *in press*; Leonard and Wehmiller, 1992). These geochronological methods all have their inherent limitations, and none are straightforward for the dating of fossiliferous deposits associated with former high seastands. The radiometric methods (U-series and ESR) are limited by the migrations of radionuclides within mollusc shell carbonate during diagenesis. Amino acid racemisation (or epimerisation) in contrast is primarily a relative dating method, which needs to be calibrated by an independent geochronological method in every region. One of the chronological problems that arose in the last decade was a regional aminostratigraphic framework, 'calibrated' on ESR data and largely based on a kinetic model of epimerisation developed in California and adapted to Chile (Hsu, 1988; Hsu *et al.*, 1989) that yielded dates for deposits at variance with some morphostratigraphic evidence (cf. Ortlieb and Macharé, 1990b; Ortlieb *et al.*, *in press*). The discrepancy is not resolved yet, although some new data from central Chile may lead to the elaboration of a revised aminostratigraphic scale (Leonard and Wehmiller, 1992; Leonard, *pers. commun.*, 1995). While one can count only on the geochronological tools presently available, no age determination of marine terraces in Peru and Chile should be proposed without, at least strong supporting morphostratigraphical criteria.

The major purpose of the present work is to provide new morphostratigraphic and geochronological data from an area considered representative of a several hundred kilometre long sector of the coast of northern Chile. The chronostratigraphic interpretation of the sequence of terraces and neotectonic observations strongly suggest that, beside some local warping and faulting activity, the study area has experienced neotectonic uplift of regional significance. The apparent steadiness of the vertical deformation during at least the last 330 ka is taken as an indication of the crustal nature of the involved motions. We interpret that they constitute a passive response of the edge of the continental margin to the process of subduction of the Nazca plate. It will also be shown, from the distribution of the older marine terraces, that some modification occurred, during the early Middle Pleistocene, in the regional uplift rate and, possibly, in the subduction regime. Vertical deformation was much slower in the Early Pleistocene along the studied sector of the plate boundary.

THE NORTHERN CHILE COAST: GEOLOGICAL SETTING

Pleistocene Marine Terraces at the Foot of the Coastal Escarpment

The landscape of northern Chile is dominated by the Coastal Cordillera, a narrow range that reaches 2000 m in elevation and is limited to the west by a major escarpment. The Coastal Escarpment runs along the coast for more than 1000 km and suddenly vanishes at Arica, at the international boundary with Peru, where the coastline changes its general trend from N–S to NW–SE. Between Arica (18°S) and Iquique (20°S), the Coastal Escarpment is very steep, measures more than 1000 m (and locally up

to 2000 m) and plunges directly into the sea; no marine terraces are preserved along this coastal sector (Paskoff, 1978). But, from Iquique southwards, a narrow coastal plain develops at the foot of the escarpment; this coastal fringe cut into the basement of the Coastal Cordillera (mainly thick Jurassic volcanics) exhibits remnants of Pleistocene marine deposits. In some places, several marine abrasion surfaces are preserved in staircase disposition, between the coastline and up to +200 m (all elevations hereby are given above present mean sea level). In many cases, a thin sheet of coastal and marine sediments blankets the wave-cut abraded platforms (Ratusny and Radtke, 1988; Radtke, 1989).

In the coastal stretch between Iquique and Antofagasta (23°30′S), the width of the coastal plain is uneven (typically between 1 and 3 km). Immediately north of Antofagasta the coastal plain broadens towards the west to constitute the core of Mejillones Peninsula (see inset of Fig. 1). This peninsula is a large, anomalous, structural block cut by some large crustal faults, which disrupts the N–S trending coastline of northern Chile. In Mejillones Peninsula, numerous emerged coastal and marine features of Plio-Pleistocene age, like staircased marine platforms and wide strand plains covered with long sequences of beach-ridges, indicate that, during the late Cenozoic, strong vertical motions have been occurring (Okada, 1971; Ferraris and Di Biase, 1978; Armijo and Thiele, 1990). The highest-lying Early Pleistocene marine sediments are found at an elevation of +440 m, on the edge of a faulted block (Ortlieb *et al.*, 1995b). However, in the major part of the peninsula and along the adjacent coastal plain, the latest Pliocene and earliest Pleistocene marine deposits are commonly lying at elevations of the order of +200 to +220 m (Ortlieb, 1993). Thus, the peninsula may be viewed as a large, composite, crustal block which was uplifted by a mean amount of about 200 m in approximately the last 2 My, and some faulted compartments were differentially uplifted by an additional amount of up to 240 m. More rapid uplift motions had been previously suggested by authors who actually did not study the chronology or stratigraphy of the emerged terraces and associated deposits (Okada, 1971; Armijo and Thiele, 1990). Some of the highest (above +400 m) wide marine platforms visible in the peninsula that were interpreted as Pleistocene landforms, were actually cut by Pliocene seas, as revealed by the faunal content of the associated deposits.

At Antofagasta, where the coastal plain is narrow again, the Quaternary marine terraces are largely eroded and degraded. The highest-lying shore-platform (the 'Antofagasta Terrace'), at the foot of the Coastal Escarpment, is located at a mean +100 m elevation, and was assigned to the Pliocene on palaeontological grounds (Martínez de los Ríos and Niemeyer, 1982). Recent re-examination of the sedimentary cover of this conspicuous terrace revealed that coastal deposits bearing Pleistocene faunal elements locally overlie the Pliocene beds associated with the platform (Ortlieb *et al.*, 1995b). 15 km south of Antofagasta, at Coloso, the coastal plain narrows and disappears, so that the Coastal Escarpment reaches the coastline. At Coloso, the Antofagasta Terrace is +80 m high, while the last interglacial shoreline is preserved at about +6 m (Ortlieb *et al.*, 1993, 1995b). Thus, at the southern extremity of the 400 km-long Iquique-Antofagasta coastal plain, it is inferred that the net vertical motions were limited. For the whole Quaternary period (=last 1.8 My), a mean uplift rate of the order of 50 mm/ky is calculated. But, assuming that the last interglacial sea level was a few metres above the present datum, it is also interpreted that the vertical deformation was almost nil during the late Quaternary (Ortlieb *et al.*, 1993).

Study Area

At 100 km north of Antofagasta, one sector of the coastal plain exhibits a particularly well preserved sequence of three marine terraces, with fossiliferous deposits protected by a thin layer of alluvial cover. It is located at Hornitos, immediately to the NE of the Mejillones peninsula, where the width of the coastal plain is less than 4 km. The study area extends from Punta Yayes (22°48′S) to Punta Chacaya (22°59′S; Fig. 1). The narrow coastal sector can be subdivided from north to south into two embayments (Caleta Hornitos and Caleta Chacaya) that are limited by three rocky promontories (Punta Yayes, Punta Hornos and Punta Chacaya; Fig. 1). The most conspicuous sequence of marine terraces is located in the southern half of the Hornitos embayment. A more complete series of terrace remnants (numbered I to IV in Fig. 1) is preserved in the Chacaya embayment, but these are partially covered with eolian sand sheets and alluvial fan deposits (Ortlieb *et al.*, 1995c). On the rocky headlands of Punta Hornos and Punta Chacaya the remnants of Pleistocene marine transgressions consist of shore-platforms that are generally devoid of marine sediments. At least six platforms are recognised in the three morphological ridges of Punta Yayes, Punta Hornos and Punta Chacaya (and identified by correlative numbers 1–6 in Fig. 1). To the east of Punta Chacaya, the terrace identified by number "4" is preserved at +130 to +140 m elevation; morphostratigraphically it seems to predate terrace IV of the Chacaya embayment.

In the embayments the substrate of the terraces is formed by Pliocene marine sandstones (Herm, 1969; Ferraris and Di Biase, 1978) that were easily eroded by the succeeding transgressions. The sediment covering the marine platforms are typically coarse-grained sands and gravels, with a varying amount of marine pebbles and larger blocks. The faunal content of the marine terrace deposits do not vary significantly from the present day nearshore fauna (Ortlieb *et al.*, 1994c; Ortlieb and Guzmán, 1994). The major difference lies in a somewhat greater diversity of the fossil assemblages with respect to the modern fauna. No particular change in the nearshore oceanographic conditions seems to have occurred from one interglacial stage to the other, at least in the last three interglaciations. This means also, that no paleontological

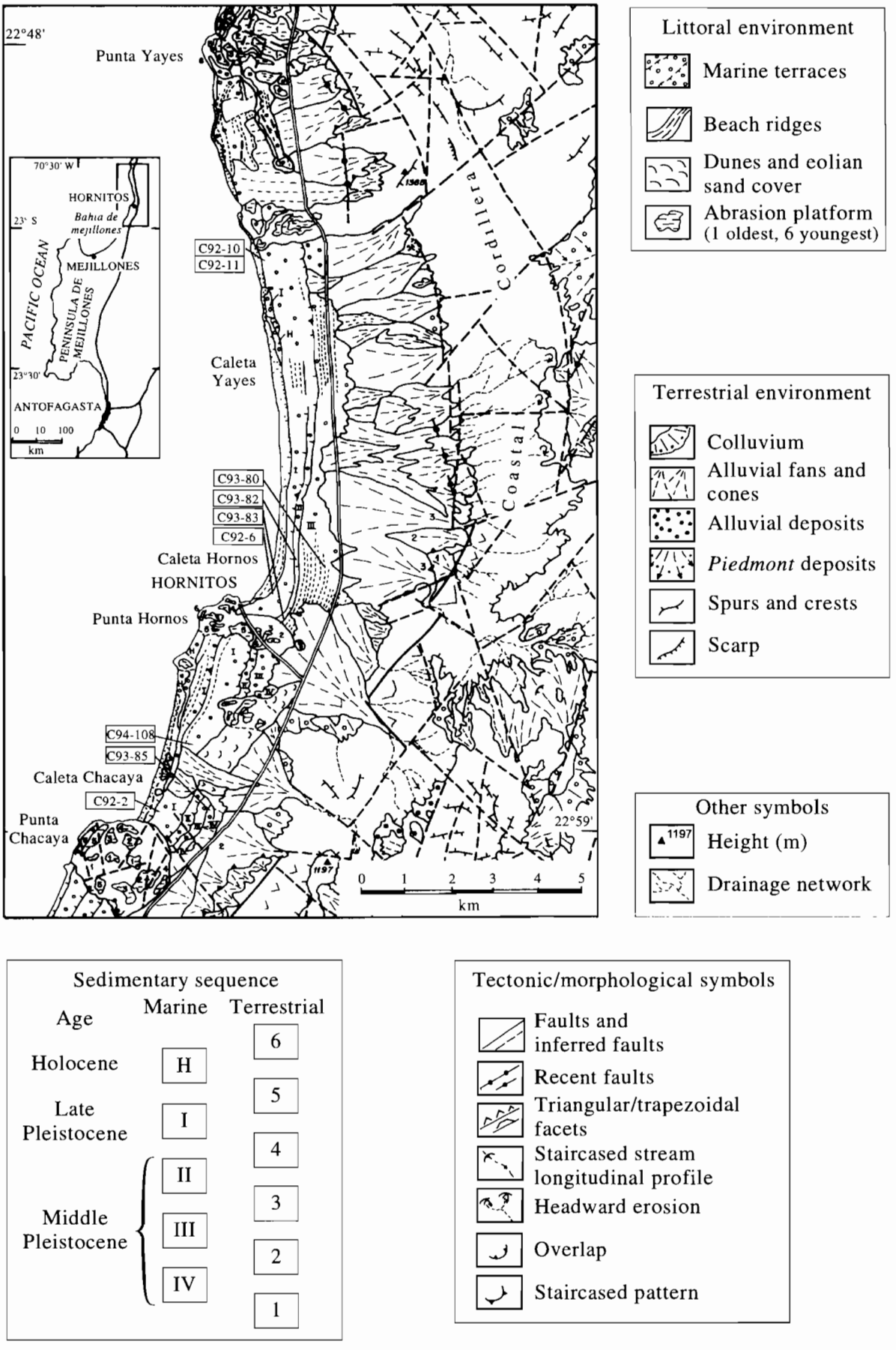

FIG. 1. Geomorphological sketch map of the study area between Punta Yayes and Punta Chacaya, to the northwest of Mejillones Peninsula, northern Chile, showing the geological and morphotectonic context in which are preserved the three major marine terraces I, II and III. These staircased terraces are correlated with the isotopic stages 5, 7 and 9.

argument may be used to identify any particular marine terrace at Hornitos.

The Coastal Escarpment is almost 1000 m high in the eastern part of the study area. The alluvial fans that piled up at the foot of the escarpment obscure any evidence for marine terraces higher than those cropping out at +80 to +100 m. Nevertheless, in the northernmost part of the study area, due east of Punta Yayes, is preserved a small remnant of Early Pleistocene deposits, at an elevation of ca. +170 m (Ortlieb *et al.*, 1995b). This isolated outcrop is tentatively correlated with other occurrences of a similar unit (identified by an overlying ash layer) to the north (Michilla, at +160 m) and south (Antofagasta, at +100 m) of the study area. Its faunal content indicates a Pleistocene age, and its morphostratigraphic position (as highest-lying terrace) lead to consider it as the oldest Pleistocene marine remnant of the area.

Holocene Coastal Evolution

The major Holocene coastal feature in the Hornitos embayment is a several hundred metre wide eroded platform covered by littoral drift sand. The elevation of the inner edge of the modern terrace at the base of the sea cliff locally reaches about +5 m. The coastal cliff was abandoned several thousand years ago, after sea level fell by some 2 m (?). Radiocarbon and U-series (TIMS) dating of a recent emerged shore deposit at Michilla (20 km north of Hornitos) suggests that the highest sea level stand during the Holocene occurred at 7000 BP (Leonard and Wehmiller, 1991; Ortlieb *et al.*, 1995b). A few metre high small morphological terrace (that includes an alluvial component) is preserved at the foot of the coastal cliff in the middle of the Hornitos embayment. The lack of emerged Holocene coastal sediments in the south of the Hornitos embayment is attributed to the effect of recurrent tsunami events. The last strong seismic events that struck the northern Chile coast (in 1868 and 1877) were accompanied by tsunami waves whose runup reached a height of, respectively, 6 and 9 m in the Cobija-Hornitos area (Lockridge, 1985). In the Chacaya embayment, as in the north-easternmost Bay of Mejillones, the backshore is formed by a 3 to 4 m high, sandy terrace which was probably formed during one (or several) late Holocene former tsunami event(s). A feature characteristic of the back shore of the southern Chacaya embayment is the accumulation of recent mud flow deposits atop the marine sandy sediment.

The Holocene strand plain is particularly wide at Hornitos. This coastal landform is more developed than along other sectors of the northern Chile coast, and constitutes a modern equivalent of the Pleistocene emerged terraces that were preserved in the study area. The exceptional development of the modern and older terraces is attributed to geological (favourable Pliocene substrate), geographical (embayment morphology and semi-protected topography) and oceanographic (long-shore transport) conditions, and also to a slightly more rapid uplift regime than in nearby localities.

THE HORNITOS SEQUENCE OF MARINE TERRACES

Morphostratigraphy of the Terraces

In the Hornitos embayment, three marine terraces can be distinguished between the Holocene seacliff and the foot of the Coastal Escarpment (Figs 1 and 2). These terraces present various morphological differences.

The lowest (youngest) Pleistocene terrace, numbered 'I' in Figs 1 and 2, is well preserved all along the Hornitos embayment. Its distal edge, atop the 12 km long coastal cliff that was formed in the mid-Holocene, lies at +18 to +25 m (a.s.l.). Its inner margin, at the foot of the palaeo-seacliff formed during the maximum of the transgression, is found at about +30 m, with a maximum elevation of +36 m east of the village of Hornitos. This terrace is morphologically well defined and was considered up to now as having been cut during a single episode of high sea-level (Herm, 1969; Radtke, 1985, 1989; Ortlieb *et al.*, 1994b). However, the flat morphology of that terrace

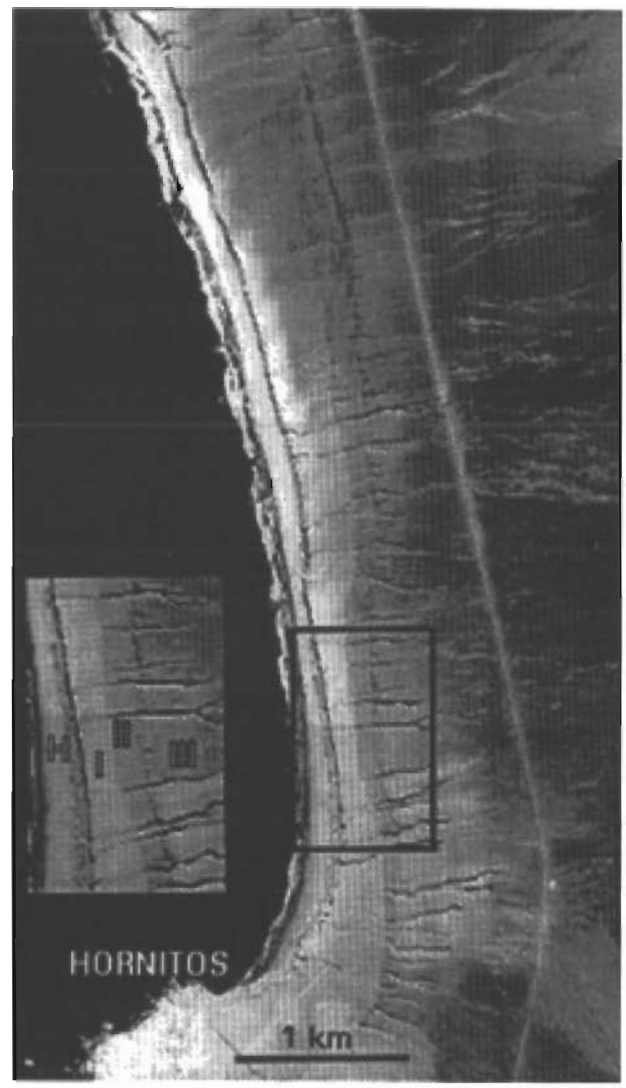

FIG. 2. Aerial photograph of the Hornitos embayment, with enlargement of a sector where the three Pleistocene terraces and the Holocene terrace are well preserved, and in staircased disposition. (Document Servicio Aerofotogramétrico SAF- 81, CH60-S.5-3, 018962, Fuerza Aerea de Chile).

FIG. 3. Photograph taken from the first Pleistocene marine terrace (I) showing that below the alluvial component of the coastal terrace, there is a two-step marine abraded platform with two separate nearshore units. Each step was formed during distinct episodes of high sea level: isotopic substages 5c and 5e.

surface mainly reflects the attitude of a sheet of alluvium, which actually hides a composite marine terrace; below the alluvial cover the coastal sediments of the terrace form two distinct stratigraphic units (Ortlieb *et al.*, 1995b, 1995c). Each unit is associated with a distinct wave-cut platform, and a vertical offset of up to 2 m was measured between the inner edge of the lower platform and the outer edge of the higher one (Fig. 3). The limit between the two platforms is located at about +25 m, and can only be observed in some of the 'quebrada' (arroyo) entrenchments that cut the terrace I and its Pliocene substratum. This morphostratigraphic disposition suggests that the two wave-cut platforms were formed one after the other, probably during two interstadial high seastands, within the same interglacial episode. As this is the lowest lying Pleistocene marine terrace, it is inferred that both platforms were cut during two substages of the isotopic stage 5 (probably substages, 5e and 5c).

The second higher marine terrace at Hornitos is the least developed of the three. It is narrower than the other two and disappears in the northern half of the embayment (Figs 1 and 2). The maximum elevation of its inner edge varies between +50 m and +55 m to the east of Hornitos; however, at the southern extremity of the Hornitos embayment, a slight upwarp of the terrace brings it up to a maximum elevation of +63 m. On the structural ridge formed by Punta Hornos, to the south of Hornitos village, remnants of this terrace were found at up to +75 m. Locally, two distinct platforms with their associated marine sediments were distinguished; they are interpreted as the remnants of two episodes of high seastand, probably during a single interglaciation. As the terrace was formed prior to the lower terrace, it is confidently assigned to the penultimate interglacial period (i.e. isotopic stage 7). Both subunits might correspond to Oxygen Isotope Substages 7a and 7c.

The third higher terrace is very wide, particularly east of Hornitos. Its inner edge, hidden by the large alluvial fans formed at the foot of the Coastal Cordillera, is located at an elevation slightly higher than +80 m. Numerous 'quebrada' cut perpendicular to the coast show that the thin sedimentary cover (typically less than 2 m) of this remarkably flat terrace consists of a series of prograding units of coarse beach deposits set in off-lap disposition. Four sedimentary units were clearly recognised in the field, but up to eight parallel lineaments are visible in aerial photographs (see Figs 1 and 2). These lineaments are remnants of beach ridges that were probably formed coevally with some of the much wider and larger beach-ridges of the northern Mejillones peninsula (Ortlieb *et al.*, 1995b).

In Chacaya embayment, the equivalent of Terrace I is represented by two terraces, one well-developed with an abundant sedimentary cover and an abrasion platform on which no sediments are preserved. The best developed marine terrace (with sediments) is cut by N–S trending small normal faults which produced small vertical scarps (a metre, or two, high). As mentioned above, the three lower terraces equivalent to those of Hornitos are extensively covered by sand dunes and alluvium (Fig. 1). In spite of the thick alluvial fans accumulated at the foot of the major escarpment, several remnants of a fourth terrace (IV), are observed at a +90 m elevation (Fig. 1). This terrace predates Terrace III but as the latter is much

narrower than in Hornitos embayment, it is not clear whether Terrace IV should be assigned to a previous interstadial within the same interglaciation or to a previous isotopic stage.

Previous Chronostratigraphic Interpretations

Herm (1969) was the first author to describe the three conspicuous terraces at Hornitos and to study their faunal content. He proposed to correlate them with the Serena I, Serena II, and Herradura I terraces identified in the Coquimbo-La Serena region (30°S), but the lateral correlation was essentially based on altimetric criteria. According to the chronostratigraphic scale elaborated at that time by Herm and Paskoff (1967), the Herradura I terrace would correspond to the penultimate interglaciation while the Serena I and II units were tentatively assigned to the Early Pleistocene. Later, Radtke (1985, 1989) obtained the first geochronological results through ESR and U-series dating from mollusc shells of the three Hornitos terraces. He determined that the most recent Pleistocene terrace at Hornitos was of last interglacial age (i.e. younger than previously considered), while the two older terraces, which did not yield quite reliable radiometric results, were assigned to some previous transgressions of the Middle and/or the Early Pleistocene (Radtke, 1989). Amino acid epimerisation and racemisation studies were also performed in the area by Leonard *et al.* (1987) and Hsu *et al.* (1989) who, however, did not give any detail on the sampling localities. Later, Leonard and Wehmiller (1991) described the most recent Pleistocene marine terrace (equivalent to Terrace I at Hornitos) at Michilla. These authors also suggested that the low terrace should be assigned an isotopic stage 5 age, but without more refinement regarding substages of the last interglaciation.

New Geochronological Analyses

In this investigation, more than 70 amino acid epimerisation analyses and 10 U-series measurements were performed. The internal consistency of the chronometric results, together with the general coherency between these results and the morphostratigraphic and sedimentological interpretations provide a strong basis for establishing a chronostratigraphic scale for the northern Chile coast (Table 1). The shell species used for the geochronological analyses are all pelecypods, mostly veneridae (*Protothaca thaca*, *Eurhomalea rufa* and *Venus antiqua*) but also *Mulinia* cf. *edulis* and *Mesodesma donacium*. They are nearshore molluscs, commonly found in the marine terrace deposits and sometimes in growing position (paired valves). Material for amino acid analyses was sytematically collected at a depth of several decimetres, whenever possible at 1 m depth, below the surface, to limit the effect of thermal variations within the

TABLE 1. U-series and aminostratigraphic results from shells of the four marine terraces in the embayments of Hornitos and Chacaya, northern Chile. The four staircased terraces (I, II, III, IV) are assigned to the isotopic stages 5, 7, 9 and 9 or 11 (?). Allo/isoleucine and U-series data support the morphostratigraphical observation of a double sea stand record in the more recent terrace (1): substages 5c and 5e

Samplelocality	Elevation (m a.s.l.)	Shell species	Allo/Isoleucine value	*n*	std	mean	U/Th apparent age TIMS	alpha count	Assumed age (I.S.)
HORNITOS									
C92-6	+25	*Protothaca thaca*	0.36	3	0.02	0.39	105.3±1.0		
"		*Mulinia edulis*	0.42	2	0.01		108.3±0.8		5c
"		*Eurhomalea rufa*	0.38	1			108.8±1.0		
C92-10	+18	*Protothaca thaca*	0.49	2	0.07	0.50	106.1±0.8	124±7.0	
"		*Eurhomalea rufa*	0.51	2	0.02		109.2±0.9	116±6.0	
"		*Eurhomalea rufa*						106±5.0	5e
"		*Eurhomalea rufa*						119±5.0	
C92-11	+18	*Mulinia edulis*	0.51	4	0.07				
C93-83	+60	*Mulinia edulis*	0.63	3	0.04	0.62			
"		*Mesodesma donacium*	0.61	3	0.04				7
C93-82	+55	*Eurhomalea rufa*	0.62	3	0.08	0.62			
C93-80	+75	*Mulinia edulis*	0.71	3	0.06				
"		*Protothaca thaca*	0.73	3	0.05	0.71			9
"		*Mesodesma donacium*	0.69	3	0.05				
"		*Venus antiqua*	0.70	1					
CHACAYA									
C92-2	+23	*Mulinia edulis*	0.47	3	0.05	0.47			
"		*Mesodesma donacium*	0.46	3	0.03				
C94-108	+30	*Mulinia edulis*	0.45	3	0.05				5e
"		*Mesodesma donacium*	0.47	3	0.05	0.48			
"		*Venus antiqua*	0.53	3	0.02				
C93-85	+90	*Protothaca thaca*	0.79	2	0.10	?	(217.2±9.4)		9 or 11?
"		*Eurhomalea rufa*	1.10	3	0.02				

soil. In most cases a set of valves from three distinct individuals were analysed. All the mentioned species epimerise at an identical rate (Hsu *et al.*, 1989; Leonard and Wehmiller, 1992; Ortlieb *et al.*, 1990b, 1996). The species *Eurhomalea lenticularis* undergoes epimerisation at faster rates, and did not yield consistent results when compared with the other species, so that results obtained on this material were not taken into consideration. Besides, two localities at Chacaya provided anomalously spread results, with high allo/isoleucine ratios: these data were attributed to a local overheating of the samples (within the soil) and were discarded. All the allo/isoleucine and U-series analyses were performed at GEOTOP, Université du Québec à Montréal. Details about analytical procedures can be found in Hillaire-Marcel *et al.* (1995).

U-series data

U-series data ($^{230}Th/^{234}U$, $^{234}U/^{238}U$) include alpha-spectrometry and TIMS (thermal ionisation mass spectrometry) measurements. The first method was used for samples from a single locality in the northern extremity of the study area (C92-10/11, Table 1). There, three out of four measurements yielded apparent ages of ca. 120 ka and a fourth sample gave a result of 106 ka (±5 ky). In the same locality, two additional samples analysed through TIMS yielded results of 106 ka (±0.8 ky) and 109 ky (±0.9 ky). At the present stage, two interpretations may be forwarded. Either, this unit was deposited during Oxygen Isotope Substage 5c and incorporated some fossil shells reworked from substage 5e deposits, or it correlates to substage 5e. Then, the somewhat younger apparent U-series ages would indicate late diagenetic incorporation of uranium into the shells (during Oxygen Isotope Substage 5c?), resulting in lower $^{230}Th/^{234}U$ ratios (i.e. lower ages). As will be seen below, allo/isoleucine (A/I ~ 0.5; Table 1) data from this site would support an assignment of the unit to the highest sea-level episode of the last interglacial (isotopic substage 5e).

In another locality (C92-6), which also corresponds to the edge of the coastal cliff but in the southern extremity of the Hornitos embayment, three TIMS results were obtained; they range from 105 to 109 ka (±1 ky; Table 1). In this case, we surmise that the shells are coeval with the substage 5c because their allo/isoleucine ratios (A/I ~ 0.4; Table 1) are significantly lower than in the former case.

Finally, an articulated sample of bivalve *Eurhomalea rufa* from the +90 m terrace (IV) at Chacaya yielded a 'finite' age of ~217±9 ka (C93-85, Table 1). The embedding unit can be assigned to either an early isotopic substage 9, or to stage 11 (see below). We thus conclude that some discrete late diagenetic U-uptake occurred in the corresponding sample, resulting in a 'young' apparent age.

Aminostratigraphy

The results of the amino acid epimerisation analyses are generally coherent within the study area. Five aminozones could be distinguished among the four Pleistocene morphostratigraphic units (Table 1). Within the youngest terrace deposits, two aminozones with mean values around 0.4 and 0.5, respectively, were defined. The most recent samples (C92-6), according to the aminostratigraphic analyses (Table 1), come from the same locality which provided apparent U-series ages in the range 105–108 ka; they are thought to represent substage 5c. In the locality at the south of Hornitos embayment (C92-10), samples from the same three species of pelecypods yielded higher allo/isoleucine ratios, and thus are assigned to an older high sea stand, most probably substage 5e. In Chacaya embayment, two localities of the lowest marine terrace (C92-2 and C94-108) yielded A/I ratios of 0.47 and 0.48 (means of several species), that correlate with the 0.5 aminozone of Hornitos. We interpret that the A/I ratios of 0.47 to 0.50 correspond to the isotopic substage 5e.

The deposits of the second higher terrace (II) were sampled in two localities one to the east of the village of Hornitos (C93-82) and another one close to the Punta Hornos ridge where the fossils were better preserved in a finer, sandy sediment (C93-83), and at a slightly more elevated (+60 m) altitude than the typical +50 m elevation of the inner edge of terrace II. The third terrace was sampled in the middle part of the wide platform, to the east of Hornitos village (C93-80); the shelly bed is located between a coarse basal conglomerate and a finer grained unit which was capped by alluvial silt. Finally, the shells from the fourth terrace were sampled, in the Chacaya embayment, in a nearshore *in situ* deposit (C93-85) that had been covered by a thick mudflow unit; all the analyses were made on paired shells in the last locality.

The mean A/I ratios obtained on shells from the three older terraces (II, III and IV) were 0.62, 0.71 and either 0.79 (*Protothaca* mean) or 0.95 (*Protothaca* and *Eurhomalea* interspecific mean), respectively (Table 1). The difference in the ratios is of the same order of magnitude as the range between the two distinct aminozones of the younger terrace. Nevertheless, as the samples were collected in staircased terraces, it is inferred that these aminozones correspond to two, or three, interglacial high seastands prior to the last interglacial (Oxygen Isotope Stages 7, 9 and possibly 11). The difference observed in the A/I ratios provided by *Protothaca thaca* and *Eurhomalea rufa* samples of the +100 m terrace precludes any age determination for now.

The reliability of the aminostratigraphic results for the three younger terraces is assessed by the cluster of values obtained from every locality, among, as well as within, the species of pelecypods that were analysed. The correlation observed between the increasing values of A/I ratios and the morphostratigraphic position of the samples (i.e. elevation of terrace/relative age of the deposits) strongly suggests that in the Hornitos area, the thermal history of the buried samples was rather homogeneous from one locality to the other, except for a few localities at Chacaya already mentioned. The consistency of the morphostratigraphy and the aminostratigraphy does not validate the latter by itself, but at

least provides some confidence into the proposed interpretation.

An additional element of chronostratigraphic correlation, and of calibration of the regional aminostratigraphy, is provided by geochronological results from a locality some 90 km south of Hornitos, in the northern part of the bay of Antofagasta. At that locality (called La Portada), U-series dating and aminostratigraphic analyses were performed on *Mulinia* cf. *M. edulis* and *Mesodesma donacium* (Ortlieb *et al.*, 1996). Three concordant U-series apparent ages of ca. 282 ka (275±11 ky, 282±9 ky and 288±12 ky) were obtained, while a double series of 14 shells of *Mulinia* cf. *edulis* and 14 shells of *Mesodesma donacium* yielded mean A/I ratios of 0.66 and 0.67, respectively (unpublished results obtained at GEOTOP, Montréal). We assume that this marine terrace was formed during the isotopic stage 9 (at 300–330 ka). The mean A/I ratio of 0.67 that was obtained from the analysis of 28 shells would be representative of the isotopic stage 9 in the Antofagasta Bay area (Ortlieb *et al.*, 1996). A chronological correlation between this value of A/I ratio of 0.67 and the 0.71 aminozone at Hornitos is quite acceptable, and supports the chronostratigraphy elaborated at Hornitos.

From previous ESR and U-series dating (Radtke, 1985, 1989) as well as from the amino acid racemisation and epimerisation studies performed in this sector of the northern Chile coast (Hsu *et al.*, 1989: Leonard and Wehmiller, 1991), it had been concluded that the most recent Pleistocene terrace could be assigned to the last interglacial episode. The new set of results provides more specific interpretations for the youngest terrace and proposes a more precise chronostratigraphical framework for the older ones. We conclude that, in the Hornitos-Chacaya area, the lower terrace was formed during two successive transgressions within the last interglaciation, most probably the substages 5e and 5c. The second terrace also shows morphostratigraphic evidence that it was formed in a two-step process. The second and third older terraces were not properly dated by the radiometric method, but amino acid epimerisation data is sound enough to enable a chronological correlation between terraces II and III with the Oxygen Isotope Stages 7 and 9.

TECTONIC DEFORMATION

Faulting and Warping Activity

Field observation and aerial photograph analysis of the study area indicate that some tectonic deformation did occur since the end of the Middle Pleistocene in the coastal region. Relatively recent fault scarps are visible along the Coastal Escarpment, across the alluvial fans and in the coastal plain itself. The most recent faults are observed near the head of some alluvial fans, close to the front of the escarpment (Fig. 1). Two fault systems oriented N120–140° and N20–30° and a few N–S trending faults are identified. These fault systems were mildly activated, or reactivated, both north and south of Hornitos (Punta Yayes and Punta Chacaya).

The marine terraces are seldom cut by fault traces, but they show warping and deformations that could be related to the reactivation of previous fractures. Besides, the attitude of the marine terraces and their geometrical disposition clearly point to a block deformation (Ortlieb *et al.*, 1995c). Two tectonic blocks can be distinguished: one in the Yayes-Hornitos embayment, and another one in Chacaya embayment. The variation of altitude of the Pleistocene shorelines, at the inner edge of the terraces, indicates that a small-amplitude tilt occurred in both blocks (Fig. 4). As every terrace reaches a higher elevation in the north of the embayments, it is inferred that the southward tilt of each block has been active (but not necessarily continuous) for a relatively long time span. The spatial disposition of the terraces suggests that the registered motions concern the whole blocks, and not small compartments within the blocks. The tilt motions of the two faulted blocks are interpreted as minor, and repeated, readjustments linked to the active deformation occurring in the half-graben of northern Mejillones Peninsula for the last several hundred thousand years (Ortlieb, 1993).

Regional Uplift Rates

In neotectonic studies dealing with vertical deformation of the coastal zone, two problems must be addressed; the age determination of emerged shorelines and the original position of the sea level (with respect to present sea level, for instance) at the time the terraces were formed. For the first problem, morphostratigraphical arguments and available geochronologic data were presented. For the second problem, some discussion is needed as there is no general consensus regarding the reconstruction of the palaeo-sea level coeval with every high seastand (e.g. Bloom *et al.*, 1974; Shackleton, 1987; Radtke, 1989).

The late Quaternary uplift motions

From the study of a large number of localities worldwide of the last interglacial shoreline, it could be inferred that the 'eustatic' sea level corresponding to the maximum of the last major transgression (at ca. 124 ka) was a few (about 6?) metres above its present-day position. These data which have a global value, and do not necessarily apply in every region (e.g. Murray-Wallace and Belperio, 1991), are classically used to evaluate the amplitude of the uplift motions in coastal areas where the trace of the 124 ka sea level is well identified. In the study area, the trace of the shoreline coeval with the peak of the last interglaciation is best identified to the east of the village of Hornitos, at the foot of the palaeo-seacliff that cuts the second higher terrace. The inner edge of Terrace I, east of Hornitos, is located at a +36 m maximum elevation. This altitude of the substage 5e highest stand of sea level thus suggests a net amount of uplift of 30 m during the last 120 ky or so, and provides a mean uplift rate estimate of 240 mm/ky.

As the shoreline remnants assigned to the isotopic

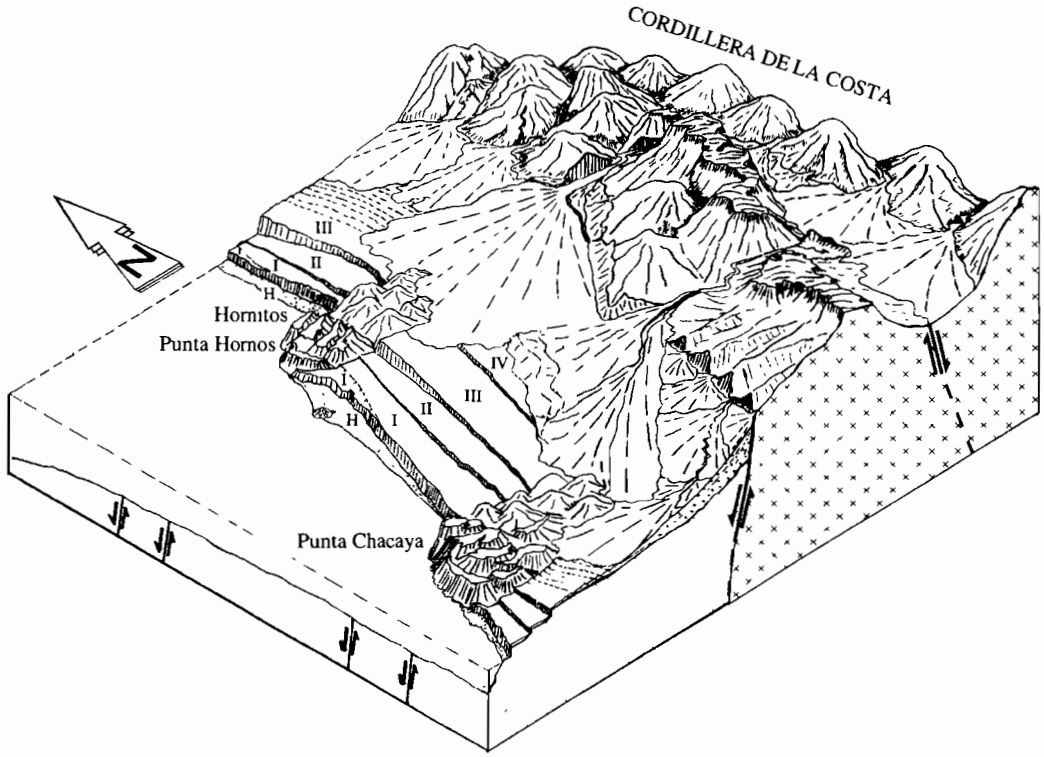

FIG. 4. Block diagram of the southern half of the Hornitos embayment and of Chacaya embayment showing the major active faults during the late Middle and Late Pleistocene and the southward tilt of the two faulted blocks separated by the Punta Hornos ridge. Numbers I to IV correspond to the four staircased terraces correlated with the isotopic stages 5, 7, 9 and possibly 11 (?).

substage 5c are found at an elevation of ca. +25 m on the same transect to the east of the village of Hornitos, some inferences can be made regarding the palaeo-sea level position during this interstadial episode. If it is assumed that a regional uplift rate of 240 mm/ky remained constant since the substage 5e, a former shoreline preserved at +25 m, and dated at 105 ka, would imply that, at that time, the palaeo-sea level was very close to the present datum. The hypothesis that the substage 5c sea level was not lower than the present sea level was previously proposed in a detailed study on the Ilo region (18°S) in southern Peru (Ortlieb *et al.*, *in press*). This palaeo-sea level reconstruction does not agree with the traditional 'eustatic' model of sea level fluctuations during the last interglacial period which was proposed by Bloom *et al.* (1974) and Chappell and Shackleton (1987), but is supported by reports and studies from distinct regions of the world (Bloom and Yonekura, 1985; Li *et al.*, 1989; Toscano and York, 1992).

The late Middle Pleistocene uplift motions.

A reconstruction of palaeo-sea level during the previous interglacial periods cannot be attempted in the same way as for the substage 5c, unless it can be established that the uplift rate has been constant through time. On the reverse, if it could be assessed that the reconstructed sea level coeval with the isotopic stages 7 and 9, respectively, are in a vertical position compatible with a given uplift rate, this would bring some support to the hypothesis that the uplift rate was constant through time. Following this reasoning, and considering that the stage 9 interglaciation was almost as warm as stage 5 (Shackleton, 1987), we suppose that at the transgression maximum the sea level was very close to its present-day position. With this assumption, the +80 m elevation of the inner age of Terrace III at Hornitos, which is assigned to the stage 9 (peak at ca. 330 ka), would indicate a net uplift rate of 240 mm/ky. This coincidence is significant. We consider it as a strong argument in favour of the permanency, for at least 330 ka, of an uninterrupted uplift motion of the southern half of the Hornitos embayment.

With an assumed continuous uplift rate of 240 mm/ky, the highest shoreline corresponding to Terrace II, found at +50 to +55 m, would be about 220 ky old. The younger of the two abrasion platforms of this terrace, with its shore platform cut some 5 m below the transgressive maximum, might well have been formed at ca. 200 ka (Oxygen Isotope Substage 7a). From this calculation, based on the assumption of a continuous uplift rate, we conclude that the sea level coeval with the substages 7a and 7c was probably also close to the present datum. The reconstruction of the sea level position during isotopic stage 7 has been controversial; several field indications from various parts of the world (e.g. Radtke, 1987; Murray-Wallace *et al.*, 1987) are not consistent with the estimate of a low high stand proposed by Shackleton (1987) through an interpretation of deep sea core data.

The geometrical disposition and the absolute altitude of the inner edge of the terraces I, II and III suggest a continuous uplift motion of the area to the east of Hornitos. The calculated net rate of 240 mm/ky is

compatible with sea level reconstructions during the Oxygen Isotope Stages 5, 7 and 9.

The whole Pleistocene uplift motions.

Remnants of early Middle Pleistocene and of Early Pleistocene are scarce and difficult to identify. Several abrasion platforms, with scanty associated deposits, are preserved on the ridges of Punta Chacaya and Punta Hornitos. The most elevated ones may be of early Middle Pleistocene age. The highest elevated deposit in the area, which was assigned a tentative Early Pleistocene age, was observed at a +170 m elevation east of Punta Yayes. Considering that the isotopic stage 25, at ca. 950 ka, might have been as warm as the Holocene, according to Shackleton (1987), and might have been characterised by the highest sea level position during the early Pleistocene, it may be envisaged that the +170 m terrace corresponds to that interglacial. Anyway, if the age of this deposit is comprised in the range 1.6 to 0.8 Ma (i.e. the assumed range of the Early Pleistocene) and if an assumption of palaeo-sea level close to the present datum is made, an approximate estimate of net uplift rate of 100 to 200 mm/ky can be calculated. These values might represent underestimates if the palaeo-sea level was eustatically lower than the present one. In any case, these approximate estimates calculated for the whole Quaternary period, suggest that prior to the last 330 ky the regional uplift rates were significantly lower than subsequent uplift rates. We thus conclude that the evolution of the vertical deformation would be twofold: a slow, or very slow, uplift regime during the Early Pleistocene and, later on, a more rapid uplift in the last 400 ky or so. Such increase in the uplift rate is observed at a regional scale and may imply that some acceleration of the subduction motion occurred in the second half of the Quaternary.

CONCLUSION

Precise chronostratigraphy of emerged marine terraces is essential for neotectonic studies that aim to determine vertical deformation of coastal regions, and the variation in uplift rates throughout the Quaternary. In the areas of the world where no coral reefs are present, the dating of Pleistocene shorelines has been a problem. In general, it is recommended to confront two, or more, geochronological methods. Nowadays the U-series measurement through the TIMS technique allows to put constraints on the behaviour of the U-Th system and therefore to better assess age differences between Late and Middle Pleistocene age deposits. In any case, the geochronological attempts should be accompanied by careful morphostratigraphic analyses which involve field studies, aerial photograph interpretation and neotectonic mapping. Until recently, this combination of approaches could not be performed in northern Chile. This largely explains that the evaluation of vertical motions recorded along the northern Chilean sector of the south-eastern Pacific plate boundary remained a matter of vivid discussions (Armijo and Thiele, 1990; Flint *et al.*, 1991; Leonard and Wehmiller, 1991, 1992; Ortlieb, 1993; Hartley and Jolley, 1995; Ortlieb *et al.*, 1995a, b).

In this paper, we selected the coastal sector of the northern coast of Chile where the three more recent Pleistocene terraces are well developed, with a wide extension, and where they are neatly separated by clearly exposed palaeo-seacliffs. The morphological evidence of the chronology of the successive encroachments of the sea is particularly clear. It is no coincidence that this was also the first area where marine terraces were studied in northern Chile (Herm, 1969). Through our morphostratigraphic study and with the support of some U-series measurements and a relatively large number of amino acid epimerisation analyses, we propose a new interpretation of the record of late Middle Pleistocene and Late Pleistocene sea level fluctuations in the region, and an evaluation of the regional uplift rate during the last three interglacial cycles.

The chronostratigraphic study of the remnants of marine terraces in the Hornitos area suggests a relatively continuous uplift motion during the last 330,000 years, with a mean value of 240 mm/ky. This uplift rate was calculated on the basis of the elevation of the inner edge of the last three terraces along an E–W transect that cuts the village of Hornitos. A transect in Chacaya embayment, or in the northern end of the Hornitos embayment, would have yielded slightly distinct values (by a few cm/ky) because local tilting did occur in both embayments. But the important point is that the tilt motions were sufficiently regular through time, and of such an amplitude, that the geometrical relationships between the last three terraces and the present coastal zone were maintained. In fact, it should be added that these tilting motions played a role in the preservation of the distinct marine sedimentary units and coastal landforms, and made possible the recognition of the substages within the two lower terraces.

The particular development of the lower marine terrace (Terrace I) at Hornitos in a context of regular uplift motion of the coastal area enabled the record of two sea level fluctuations within the Oxygen Isotope Stage 5. Thus, contrary to what had been interpreted up to now (Herm, 1969; Radtke, 1989; and ourselves in a preliminary report (Ortlieb *et al.*, 1993)), it is established that the substages 5e and 5c are registered in this coastal sector. The altimetric position of the 5c deposit and its geometric disposition with respect to the 5e deposit imply that the 5c sea level was very close to the present datum. This conclusion confirms a similar interpretation made elsewhere and in southernmost Peru, close to the Chilean border (Ortlieb *et al.*, *in press*). It also explains many problems of interpretation of aminostratigraphic analyses recently performed on material from the last interglacial terrace in southern Peru and northern Chile.

The uplift rate determined for the Hornitos area, for the period 330 ky–Present, is higher than those calculated in the Mejillones Peninsula or in the Antofagasta area. But, considering the altitude of the last interglacial terrace, it should be representative of the coastal sector extending to the north for more than 100 km, and probably 300 km

(Iquique). The regional character of this vertical deformation, that is prevalent upon the small amplitude faulting activity and/or small tilt or warping that affected the coastal region from Chacaya northward, and its steadiness during hundreds of thousand years strongly suggest that relatively deep, crustal, phenomena are involved. We surmise that the processes that have been driving the calculated 240 mm/ky uplift rate are directly linked to the subduction of the oceanic Nazca plate below the South American continental plate.

A precise evaluation of the uplift motions in a longer span of time is hindered by the scarcity of remnants of older marine terraces, and by the difficulty to establish any chronostratigraphy of the deposits. However, available data on the position of a late Pliocene marine platform and of a supposedly Early Pleistocene terrace suggest that the region has not been uplifted at a rate of the order of 240 mm/ky during the whole Quaternary. They would rather indicate a much slower uplift during the Early Pleistocene, and possibly, during the first half of the Middle Pleistocene. Some (deep-seated?) phenomena may have occurred during the early Middle Pleistocene and might be responsible for a sudden acceleration of the vertical motions along this sector of the plate boundary.

ACKNOWLEDGEMENTS

Scientific agreements between ORSTOM (UR14, programme DESIRS) and the Universidad de Chile, Departamento de Geología, and between ORSTOM (UR 12, programme AIMPACT) and the Universidad de Antofagasta. Awards from the Fonds FCAR of Québec and the Natural Science and Engineering Research Council of Canada to C. Hillaire-Marcel supported the analytical costs. Scientific agreement between the CSIC (Madrid) and the Universidad de Chile (1993–94) We benefitted from useful remarks from two reviewers on a previous version of the paper C Murray-Wallace and J Wehmiller are sincerely thanked for their help This work is a contribution to the IGCP Project 367, and to both Neotectonics and Shorelines Commissions of INQUA.

REFERENCES

Armijo, R. and Thiele, R. (1990). Active faulting in northern Chile: ramp stacking and lateral decoupling along a subduction plate boundary? *Earth and Planetary Science Letters,* **98,** 40–61.

Barazangi, M. and Isacks, B.L. (1976). Spatial distribution of earthquakes and subduction of the Nazca plate beneath South America. *Geology,* **4,** 686–692.

Bloom, A.L., Broecker, W.S., Chappell, J.M.A., Matthews, R.K. and Mesolella, K.J. (1974). Quaternary sea level fluctuations on a tectonic coast: new $^{230}Th/^{234}U$ dates from the Huon Peninsula, New Guinea. *Quaternary Research,* **4,** 185–205.

Bloom, A.L. and Yonekura, N. (1985). Coastal terraces generated by sea level change and tectonic uplift. *In*: Woldenberg, M.J. (ed.), *Models in Geomorphology*, pp. 139–154. Allen and Unwin, Winchester (MA).

Chappell, J. (1974). Geology of coral reef terraces, Huon Peninsula, New Guinea: a study of Quaternary tectonic movements and sea-level changes. *Geological Society of America Bulletin,* **85,** 553–570.

Chappell, J. and Shackleton, N.J. (1987). Oxygen isotopes and sea level. *Nature,* **324,** 137–140.

Courty, G. (1907). *Explorations Géologiques dans l'Amérique du Sud, Suivi de Tableaux Météorologiques.* Imprimerie Nationale, Paris, 208 pp.

D'Orbigny, A.-D. (1842). *Voyages dans l'Amérique méridionale exécuté pendant les années 1826, 1827, 1828, 1829, 1830, 1831, 1832 et 1833 III: Partie Géologique*. Paris.

Darwin, C. (1846). *Geological Observations on South America.* Smith, Elder and Co., London.

Domeyko, I. (1848). Sur le terrain et les lignes d'ancien niveau de l'Océan du Sud, aux environs de Coquimbo (Chili). *Annales des Mines*, Paris, 4, série **14,** 153–162.

Domeyko, I. (1860). Solevantamiento de la costa de Chile. *Anales de la Universidad de Chile*, **17,** 573–599.

Ferraris, F. and Di Biase, F. (1978). Hoja Antofagasta, región de Antofagasta. *Carta Geológica de Chile* n°30, Instituto de Investigaciones Geológicas, Chile. 48 p., 1 map 1:250.000.

Flint, S., Turner, P. and Jolley, E.J. (1991). Depositional architecture of Quaternary fan-delta deposits of the Andean fore-arc: relative sea-level changes as a response to aseismic ridge subduction. *Special Publications of the International Association of Sedimentologists*, **12**, 91–103.

Goy, J.L., Macharé, J., Ortlieb, L. and Zazo, C. (1992). Quaternary shorelines and neotectonics in southern Peru: the Chala embayment. *Quaternary International,* **15–16,** 99–112.

Hartley, A.J. and Jolley, E.J. (1995). Tectonic implications of Late Cenozoic sedimentation from the Coastal Cordillera of northern Chile (22–24°S). *Journal of the Geological Society*, **152**, 51–63.

Herm, D. (1969). Marines Pliozän und Pleistozän in Nord und Mittel-Chile unter besonderer Berücksichtigung der Enwicklung der Mollusken-Faunen. *Zitteliana* (München), **2**, 1–159.

Herm, D. and Paskoff, R. (1967) Vorschlag zur Gliederung des marinen Quartärs in Nord- und Mittel Chile. *Neues Jahrbuch für Geologie und Paläontologie, Monatshefte,* **10,** 577–588.

Hillaire-Marcel, C., Ghaleb, B., Gariépy, C., Zazo, C., Hoyos, M. and Goy, J.-L. (1995). U-Series dating by the TIMS technique of land snails from paleosols in the Canary Islands. *Quaternary Research*, **44,** 276–282.

Hsu, J. (1988). Emerged Quaternary marine terraces in southern Peru: sea level changes and continental margin tectonics over the subducting Nazca Ridge. (Unpublished) PhD dissertation, Cornell University.

Hsu, J.T., Leonard, E.M. and Wehmiller, J.F. (1989). Aminostratigraphy of Peruvian and Chilean Quaternary marine terraces. *Quaternary Science Reviews,* **8,** 255–262.

Kaufman, A., Broecker, W.S., Ku, T.L. and Thurber, D.L. (1971) The status of U-series methods of mollusk dating. *Geochimica et Cosmochimica Acta,* **35,** 1155–1183.

Leonard, E., Mirecki, J.R. and Wehmiller, J.F. (1987). Amino-acid age estimates for late Pleistocene marine terraces in northern Chile: implications for uplift rates. *Geological Society of America, Abstracts with Programs,* **19,** 744 pp.

Leonard, E. and Wehmiller, J.F. (1991). Geochronology of marine terraces at Caleta Michilla, northern Chile; Implications for late Pleistocene and Holocene uplift. *Revista Geologica de Chile,* **18,** 81–86.

Leonard, E. and Wehmiller, J.F. (1992). Low uplift rates and terrace reoccupation inferred from mollusk aminostratigraphy, Coquimbo Bay area, Chile. *Quaternary Research,* **38,** 246–259.

Li, W.-X., Lundberg, J., Dickin, A.P., Ford, D.C., Schwarcz, H.P., McNutt, R. and Williams, D. (1989). High-precision mass spectrometric uranium-series dating of cave deposits and implications for paleoclimate studies. *Nature*, **339,** 534–536.

Lockridge, P.A. (1985). Tsunamis in Peru-Chile. Data Center and World Data Center A for solid Earth geophysics, NOAA, Boulder, Co., Report SE-39. 97 pp.

Macharé, J. (1987). La marge continentale du Pérou: Régimes tectoniques et sédmentaires cénozoiques de l'avant-arc des Andes centrales. Thèse Docteur en Sciences, Université Paris XI-Orsay, 391 pp.

Macharé, J. and Ortlieb, L. (1992). Plio-Quaternary vertical motions and the subduction of the Nazca Ridge, central coast of Peru. *Tectonophysics*, **205,** 97–108.

Martínez de los Ríos, E. and Niemeyer, H. (1982). Depósitos marinos aterrazados del Plioceno superior en la ciudad de Antofagasta, su relación con la Falla Atacama. *Actas del III Congreso Geológico Chileno*, **1,** A176–A188.

Murray-Wallace, C.V., Kimber, R.W.L., Belperio, A.P. and Gostin, V.A. (1988). Aminostratigraphy of the Last Interglacial in Southern Australia. *Search*, **19,** 33–36.

Murray-Wallace, C.V. and Belperio, A.P. (1991). The last interglacial shoreline in Australia — a review. *Quaternary Science Reviews*, **10,** 441–461.

Okada, A. (1971). On the neotectonics of the Atacama fault zone region. Preliminary notes on late Cenozoic faulting and geomorphic development of the Coast Range of northern Chile. *Bulletin of the Department of Geography Kyoto University*, **3,** 47–65.

Ortlieb, L.. (1993). Vertical motions inferred from Pleistocene shoreline elevations in Mejillones Peninsula, northern Chile: some reassessments. II International Symposium on Andean Geodynamics (Oxford, 1993), extended abstract volume, 125–128.

Ortlieb, L. and Macharé, J. (1990a) Quaternary marine terraces on the Peruvian coast and recent vertical motions. International Symposium on Andean Geodynamics (Grenoble, 1990), Abstract volume, 95–98

Ortlieb, L. and Macharé, J. (1990b). Geocronología y morfoestratigrafía de terrazas marinas del Pleistoceno superior: El caso de San Juan-Marcona, Perú. *Boletín de la Sociedad Geológica del Perú*, **81,** 87–106.

Ortlieb, L., Ghaleb, B., Hillaire-Marcel, C., Macharé, J. and Pichet, P. (1992). Déséquilibres U/Th, rapports allo-isoleucine et teneurs en ^{18}O des mollusques littoraux pléistocènes du sud du Pérou: une base d'appréciation chronostratigraphique. *Comptes Rendus de l'Académie des Sciences*, Paris, 314, série **II,** 101–107.

Ortlieb, L., Ghaleb, B., Hillaire-Marcel, Cl. and Pichet, P. (1993). Deformación de la línea de costa del último interglacial en la región de Antofagasta, N de Chile. *International workshop on The Quaternary of Chile* (Santiago, 1993), abstract volume, 25.

Ortlieb, L. and Guzmán, N. (1994). La malacofauna pleistocena de la région de Antofagasta: variaciones en la distribución biogeográfica y potencial paleoceanográfico. *Actas VII Congreso Geológico Chileno* (Concepción, 1994), 1, 498–502.

Ortlieb, L., Macharé, J., Goy, J.L. and Zazo, C. (1994a). Secuencias de terrazas marinas cuaternarias en la región de Chala, Perú central: interpretación morfoestratigráfica y neotectónica. *VIII Congreso Peruano de Geología* (Lima), Abstract volume, 242–246.

Ortlieb, L., Ghaleb, B., Goy, J.L., Zazo, C. and Thiele, R. (1994b). Terrazas marinas pleistocenas del área de Hornitos (Ilda región): Nuevos estudios morfoestratigráficos y neotectónicos en el Norte Grande de Chile. *Actas VII Congreso Geológico Chileno* (Concepción, 1994), extended abstracts volume 1, 356–360.

Ortlieb, L., Guzmán, N. and Candia, M. (1994c). Moluscos litorales del Pleistoceno superior en el area de Antofagasta, Chile: Primeras determinaciones e indicaciones paleoceanográficas. *Estudios Oceanológicos*, **13,** 51–57.

Ortlieb, L., Ghaleb, B. Hillaire-Marcel, Cl., Goy, J.L., Macharé, J., Zazo, C. and Thiele, R. (1995a). Quaternary vertical deformation along the southern Peru-northern Chile coast: Marine terrace data. XIV INQUA Congress (Berlin, 1995), Abstract volume, *Terra Nostra*, **2/95,** 205.

Ortlieb, L., in coll. with Goy, J.L. Zazo, C., Hillaire-Marcel, C. and Vargas, G. (1995b). *Late Quaternary coastal changes in northern Chile*. Guidebook for a fieldtrip, II annual meeting of the International Geological Correlation Program, Project 367 (Antofagasta, 19–28 Nov 1995), ORSTOM, Antofagasta, Chile. 175 pp.

Ortlieb, L., Zazo, C., Goy., J.L., Hillaire-Marcel, C. and Ghaleb, B. (1995c). Quaternary coastal evolution of the Hornitos area (Northern Chile) in the last 300,000 years: Neotectonic interpretations. International Geological Correlation Programme 367, II annual meeting (Antofagasta, 1995), Abstract volume, 85–86.

Ortlieb, L., Zazo, C., Goy, J., Dabrio, C. and Macharé, J. (*in press*). Pampa del Palo: An anomalous composite marine terrace in the uprising coast of southern Peru. *Journal of South-American Earth Sciences*, **9**.

Ortlieb, L., Díaz, A. and Guzmán, N. (1996). A warm interglacial episode during Oxygen Isotope Stage 21 in northern Chile. *Quaternary Science Reviews*, **15**, 857–871.

Ota, Y. (1986). Marine terraces as reference surfaces in Late Quaternary tectonic studies: examples from the Pacific rim. *Royal Society of New Zealand Bulletin*, **74,** 357–375.

Paskoff, R. (1970). *Recherches géomorphologiques dans le Chili semi-aride*. Biscaye Frères, Bordeaux. 420 pp.

Paskoff, R. (1977). Quaternary of Chile: the state of research. *Quaternary Research*, **8,** 2–31.

Paskoff, R. (1978). Sur l'évolution géomorphologique du grand escarpement côtier du désert chilien. *Géographie physique et Quaternaire*, **32,** 351–360.

Pissis, A. (1856). Recherches sur les systèmes de soulèvement de l'Amérique du Sud. *Annales des Mines*, Paris, 5e série, **IX**.

Radtke, U. (1985). Chronostratigraphie und Neotektonik mariner Terrassen in Nord — und Mittelchile Erste Ergebnisse. *Actas IV Congreso Geológico Chileno (Antofagasta, 1985)*, **4**, 436–457.

Radtke, U. (1987). Paleo sea levels and discrimination of the last and the penultimate interglacial fossiliferous deposits by absolute dating methods and geomorphological investigations, illustrated from marine terraces in Chile. *Berliner Geographische Studien*, **25,** 313–342.

Radtke, U. (1989). Marine Terrassen und Korallenriffe. Das Probleem der Quartären Meeresspiegeischwankungen erläntert an Fallstudien aus Chile, Argentinien und Barbados. *Düsseldorfer Geographische Schriften*, **27,** 245 pp.

Ratusny, A. and Radtke, U. (1988). Jungere ergebnisse Küstenmorphologischer untersuchungen im grossen Norden Chiles. *Hamburger geographische Studien*, **44,** 31–46.

Shackleton, N.J. (1987). Oxygen isotopes, ice volume and sea level. *Quaternary Science Reviews*, **6,** 183–190.

Toscano, M.A. and York, L.L. (1992). Quaternary stratigraphy and sea-level history of the U.S, Middle Atlantic coastal plain. *Quaternary Science Reviews*, **11,** 301–328.

Vidal Gormaz, F. (1901). Hundimientos y solevantamientos verificados en las costas chilenas. *Revista Chilena de Historia Natural*, 213–224.

Pergamon

PII: S0277-3791(96)00065-0

Quaternary Science Reviews, Vol 15, pp 833–841, 1996

0277–3791/96 $32.00

PLEISTOCENE AND HOLOCENE BEACHES AND ESTUARIES ALONG THE SOUTHERN BARRIER OF BUENOS AIRES, ARGENTINA

FEDERICO I. ISLA,* LUIS C. CORTIZO* and ENRIQUE J. SCHNACK†

**Centro de Geología de Costas y del Cuaternario, c.c. 722, 7600 Mar del Plata, Argentina*

†Laboratorio de Oceanografía Costera, c.c. 45, 1900 La Plata, Argentina

Abstract — The Buenos Aires aggradation plain has a good record of Quaternary sea-level fluctuations. To the east of the Tandilia Range, the elevations of the Pleistocene beaches respond to the tectonic behaviour of the Salado Basin. Holocene beaches indicate a maximum transgression higher than 2 m. The low relief permitted an extended horizontal record of beach/chenier plains interfingered with estuarine environments (coastal lagoons, marshes) covered by a sandy (Eastern) barrier.

Between the Tandilia and Ventania ranges, the location of Pleistocene and Holocene beaches are related to a former higher relief; i.e. they are attached to low-altitude cliffs and underneath cliff-top dunes composing the Southern Barrier. At Claromecó, Pleistocene gravel beaches, mostly composed of caliche pebbles, occur at heights between 4 and 7 m, and are overlying estuarine Pleistocene environments. Beaches of the same age are at a level of 10 m at Mar del Plata Harbour and Arroyo Sotelo (west of Mar Chiquita Lagoon).

Holocene beaches found at Punta Mogotes and Costa Bonita are at higher altitudes than on the Eastern Barrier (ca. 2–4 m). The Holocene estuarine sequences are related laterally to present operating inlets (Las Brusquitas, La Ballenera, Quequén Grande, Claromecó, Quequén Salado). They are seldom thicker than 2.4 m, and comprise basal layers of black muds; towards the top, the layers are thinner, of coarser grain size and white colours.

Grain-size analyses were performed comparatively on Pleistocene, mid-Holocene and present beaches. Sangamonian beaches are gravelly or coarser than medium sand (mean). Holocene beaches are usually coarser than medium sand, but dominantly shelly to the north of Mar del Plata, and composed of volcanic clasts to the south of this city. Modern beaches are dominated by fine sand, except at some erosive beaches between the Mar del Plata capes. They have a lesser content of shells than those of mid-Holocene. Copyright © 1996 Elsevier Science Ltd

INTRODUCTION

Within the Salado Basin, Eastern Buenos Aires Province (Fig. 1), Upper Pleistocene beaches are located in relation to coastal progradation rates: attached to former cliffs at Punta Piedras, more than 28 km inland, in the centre of Samborombón Bay (Pascua Bridge; Colado *et al.*, 1990), and less than 1 km from the Holocene beach of Mar Chiquita (only 13 km from the coast; Isla *et al.*, 1986). This setting is caused by the tectonic behaviour of the basin between the Monte Veloz Block and the Tandilia Range. In the middle of the basin, the Holocene transgression produced beach/chenier plains, that are not closely related to the younger Eastern Barrier.

In the Southern Barrier, Upper Pleistocene coastal deposits are recognized as eroded cliff-top beaches or aeolian fine sands composed of well rounded grains rich in volcanic fragments. The Holocene estuarine sequences are composed of massive muds overlain by laminated sandy muds (Isla *et al.*, 1986). The estuarine sandy muds were called 'querandinense' (in the sense of Frenguelli, 1928) while the regressive sands and shelly sands (ridges) were called 'platense'. The Holocene beaches can be also found attached to former palaeocliffs.

In the present paper, the Pleistocene and Holocene littoral deposits of this Southern Barrier are described and analyzed. Some of the Holocene estuarine sequences (Las Brusquitas, Punta Hermengo, Quequén) have been analyzed sedimentologically or micropalaeontologically (Isla *et al.*, 1986; Isla and Espinosa, 1995); new sequences are included in this analysis. Special consideration is given to the comparative evolution of the Eastern and Southern barriers during the Holocene sea-level fluctuation.

SETTING

The Buenos Aires coastline was assumed to be a stable coast and hence subject only to glacioeustatic fluctuations. However, new studies based on different evidences are suggesting minor tectonic phenomena (Isla *et al.*,

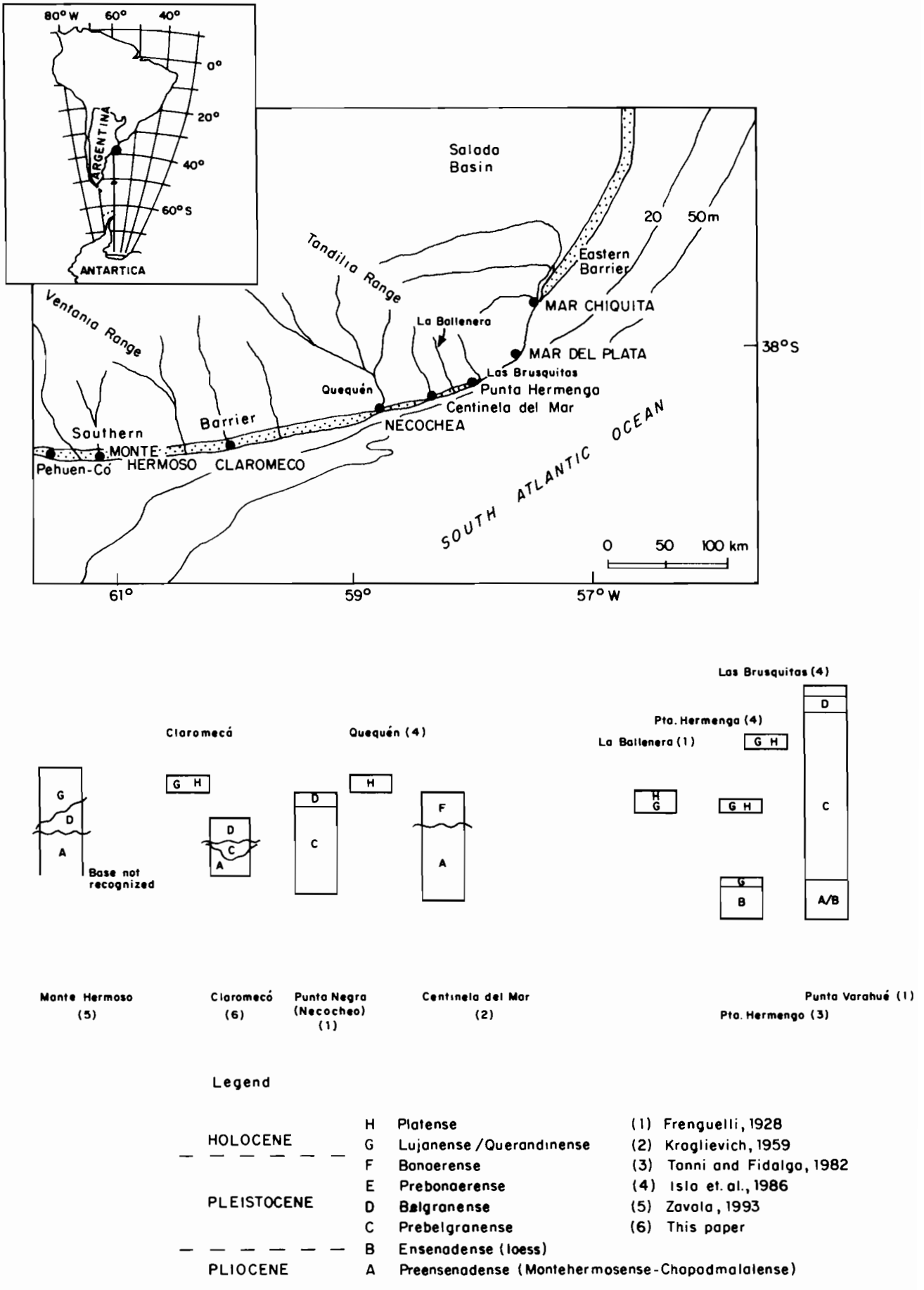

FIG. 1. Location map and stratigraphical relationships between Quaternary coastal profiles of the Southern Barrier.

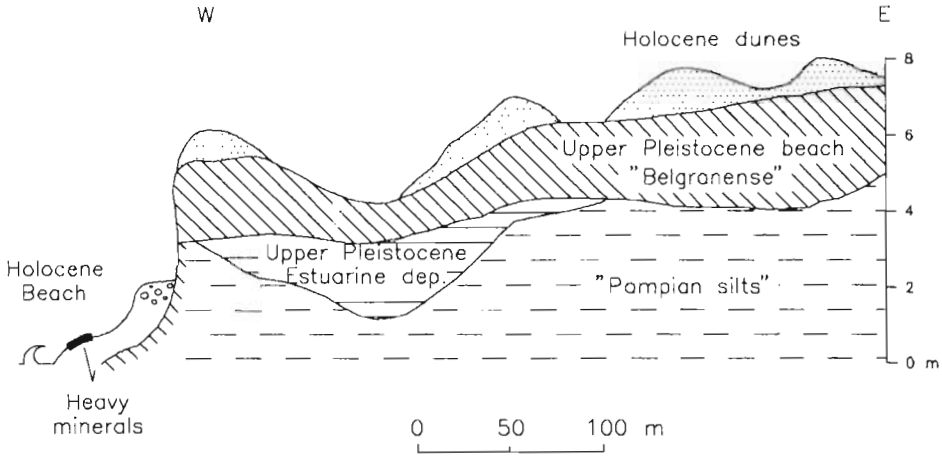

FIG. 2. Schematic profile of the Claromecó (Lighthouse) Pleistocene sequence. The Belgranense beach is overlying the estuarine deposit belonging to a marsh (*sensu* Frenguelli, 1928).

1986). Two ranges, Tandilia and Ventania, oriented NW–SE determine the regional slope. The La Plata–Salado Basin extends north of Tandilia; the Eastern Barrier extends from the southern border to the center of this basin. The Colorado Basin extends south of Ventania. The Southern Barrier extends along the coastline of the undulated landscape between Tandilia and Ventania Ranges (Fig. 1). It extends from Punta Hermengo (Miramar) at the east, to Pehuen Co at the west, reaching a maximum width of 3.5 km. Several creeks cross this barrier. At some of these inlets it is possible to recognize infill estuarine sequences of Holocene age and this is the subject of this paper.

Tides are less than 2 m although increasing towards the south. North of Mar del Plata, littoral drift is to the north and usually of the order of 1,000,000 m^3/year. South of Mar del Plata, the drift is significantly lower towards the east. From a certain point close to Pehuén Co, the littoral drift is towards the west of the Bahía Blanca estuarine environments.

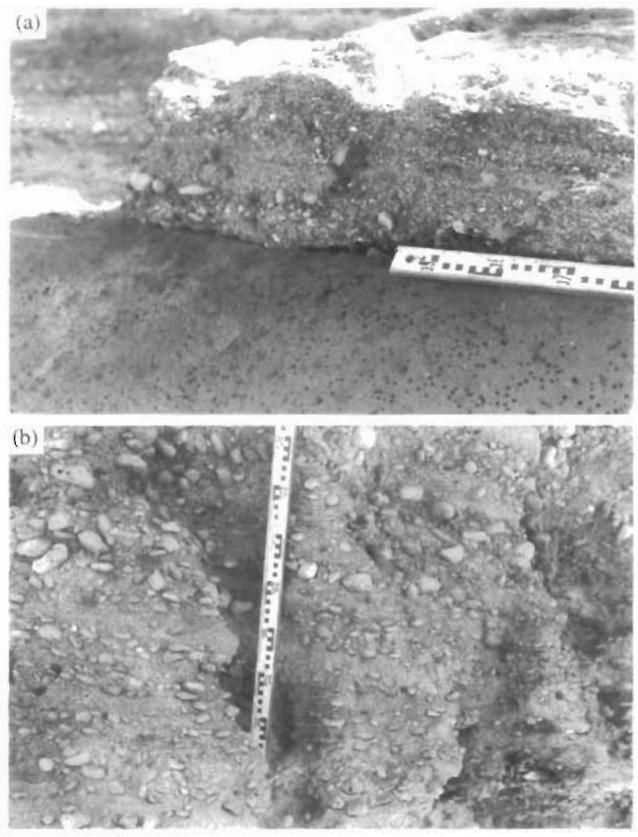

FIG. 3. (a) Erosional uncomformity between the estuarine silts ('prebelgranense') and the overlying gravel beach deposit ('belgranense'). (b) Imbricated gravels at the 'belgranense' (Sangamonian) beach of Claromecó.

QUATERNARY STRATIGRAPHY

To recognize the inherited tectonic behaviour along this Southern Barrier, the agradational and erosional history of the pampian silts (Plio-Pleistocene) is analyzed here. The relationships of different chronostratigraphical units and facies are outlined in Fig. 1.

The pampian sandy silts comprise a group of deposits formed in different environments (Frenguelli, 1928; Risso Dominguez, 1949; Kraglievich, 1959; Tonni and Fidalgo, 1982; Zarate and Fasano, 1989; Zavala, 1993).

Preensenadense deposits correspond to a continental environment dominated by silt with different kind of transport by water (fluvial to debris flow). Different post-depositional characteristics such as reddish colours and caliche-horizon abundance, help to distinguish it from the overlying Ensenandense deposits.

The **Ensenadense** should have higher loess contents in the sense of Frenguelli (1928), but this is not true for this area. Usually, it is recognized from the Preensenadense because it contains less reddish colors and a higher abundance of caliche horizons (Zárate, *pers. commun.*).

The **Prebelgranense** is composed of sandy silts with shell fragments underlying the Belgranense transgression. They were interpreted as a salt marsh deposit based on diatoms content (Frenguelli, 1928).

Belgranense are littoral (Claromecó), shallow marine (Puerto Mar del Plata) or aeolian (Punta Negra, Punta Mogotes) deposits belonging to the Sangamonian transgression. Each deposit has a different composition: gravels (Claromecó), coarse sand with pebbles (Puerto

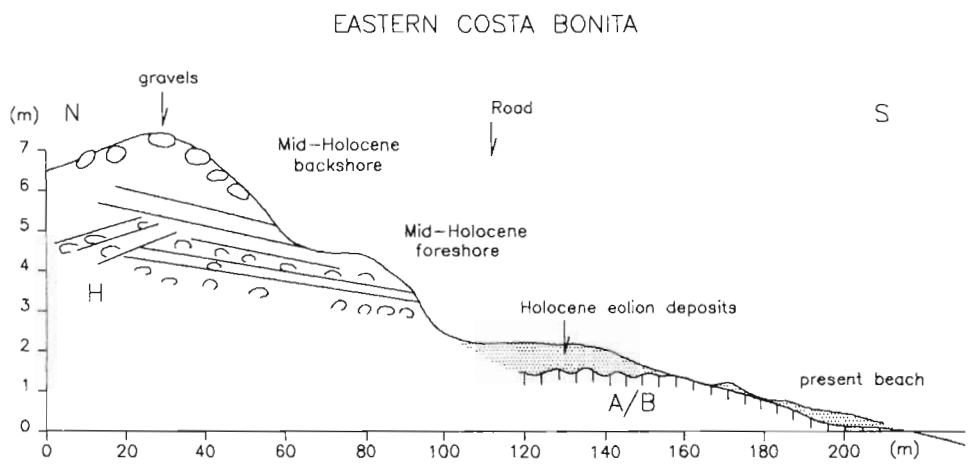

FIG. 4. Schematic profile of the Costa Bonita Holocene beach deposit higher than the present beach. Radiocarbon dates performed on *T. patafonica* shells for ages of 6000±70 (LP 720).

Mar del Plata) and fine sand (Punta Negra, Punta Mogotes). These deposits were also found further west at Monte Hermoso (Zavala, 1993).

In the Southern Barrier, above the Belgranense transgression, it is not easy to recognize the Bonaerense loessic silts. This relation is clear north of Mar del Plata (Eastern Barrier, Fasano, 1989). In Centinela del Mar (Southern Barrier), the Bonaerense (Lobería Formation), composed of loessic tuffs, is overlying Belgranense sandstones with shell fragments (Santa Isabel Formation *sensu* Kraglievich, 1959; Fig. 1).

Lujanense deposits represent the infill of fluvial valleys. These greenish or yellowish silts are restricted to present rivers and creeks. Above this, the coastal valleys become completely infilled by sandy muds (Querandinense and Platense) belonging to the Late Holocene sea-level fluctuation and subject of this paper.

The Platense is finally covered by the aeolian fine sands composing the present dune barriers.

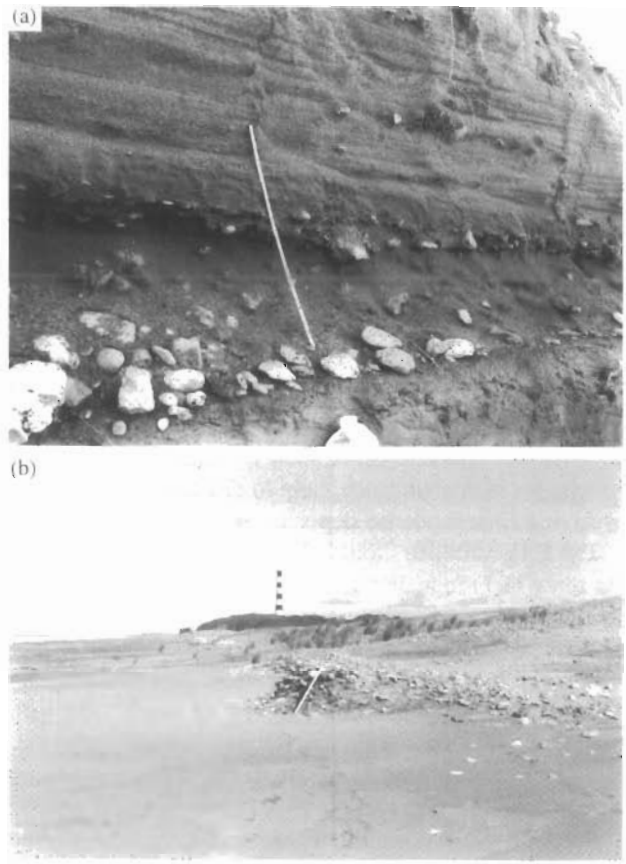

FIG. 5. (a) Holocene beach deposit at Costa Bonita. Lag gravels on the bottom grade to mediumn sands to the top. (b) At the present beach of Claromecó, there are remnants of Holocene gravelly beaches, today eroded by ocasional storms.

CLAROMECO PLEISTOCENE BEACH

As there has been some agreement about the position of the sea level during the Sangamonian transgression, it has been used to estimate the tectonic behaviour during the last 120,000 years (Cronin *et al.*, 1981).

Upper Pleistocene (Sangamonian) shoreline features are present along the Buenos Aires Atlantic coast. They occur either as beaches of very coarse sediments (Punta Piedras, Sotelo, Mar del Plata harbour) or as rounded aeolian sands (Punta Mogotes, Punta Negra, Monte Hermoso). Usually these deposits are at approximately 10 m height and close to the coast (Punta Piedras, Mar del Plata harbour), except towards the centre of the Salado Basin, where they occur several kilometres inland (Sotelo, Puente de Pascua; Fidalgo *et al.*, 1972).

In Claromecó, Frenguelli (1928) recognized two facies: the 'Belgranense' consisting of coarse beach deposits and, underneath, the 'Prebelgranense' estuarine facies, composed of sandy silts with small pieces of shells (Fig. 2). There is a sharp and horizontal contact betweem these two facies (Fig. 3a).

The overlying beach is composed of coarse gravels (larger than 4 cm) of caliche clasts dipping gently to the east (Fig. 3b), and bearing shells of *Tegula patagonica*. Within these deposits, the transition between inshore, foreshore and backshore facies were recognized towards the top. Humocky crossbeddings indicate storm effects.

Grain-size analysis of the Sangamonian shoreline indicates a high-energy coast (Table 1), higher than during

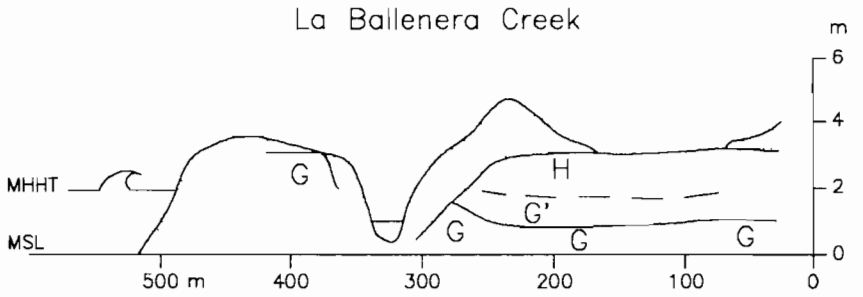

FIG. 6. Schematic profile of La Ballenera Holocene estuarine sequence. G: Lujanense; G': Querandinense, H: Platense (see Fig. 1 for chronostratigraphical relationships).

the Holocene sea-level fluctuation. The high-energy conditions and the composition (caliche clasts) of this Sangamonian beach indicate different sources compared to the Holocene and present beaches (volcanic clasts).

CLAROMECO PLEISTOCENE ESTUARINE DEPOSIT

Below this beach, the Prebelgranense estuarine facies is composed of a silty fine sand (Mz=2.4 phi), moderatedly sorted (S=0.95 phi; Table 1) with a 20.6% of carbonate fragments. Scarce diatom frustules (*Synedra platensis, Campylodiscus clypeus, Surirella ovata*) indicate brackish conditions (Espinosa, *pers. commun.*) and confirm the salt-marsh facies proposed by Frenguelli (1928).

The sharp contact between these two Upper Pleistocene facies suggests a rapid pulse during the Sangamonian transgression before the settlement of the beach.

HOLOCENE SHORELINES

The capes of Mar del Plata were a boundary for the longshore sediment transport of Holocene beaches. North of these capes, the beaches are composed dominantly of shells with less content of lithoclasts (Isla and Espinosa, 1995). However, this is a rule that needs to be tested: in the Mar Chiquita municipal quarry close to the coastal lagoon, a sand layer of heavy minerals was found below the shelly layers (Table 1).

To the south of Mar del Plata, these beaches are composed of fine sand with lithoclasts, few shells (*Glycimeris longior* and *Tegula patagonica*), and caliche clasts. At Punta Mogotes, a palaeobeach is elevated to at 6 m height. Two ^{14}C dates of the *Glycimeris longior* shells provide ages of 35,000±3000 (Ac-1071; Isla *et al.*, 1986) and 27,350±1450 (WP-123; Isla and Selivanov, 1993). However, as these shells were not in living position, we assume that they were transported after their death, retaining a Holocene age for this deposit.

At Costa Bonita, two ridges close to the present coastline are covered by boulders larger than 0.15 m (Fig. 4). Observation in a pit permitted to distinguish fine sand layers (and laminae of heavy minerals) with a lag carpet of large boulders at the bottom, containing *T. patagonica* remains, dipping towards the present shore (Fig. 5a). The higher ridge is interpreted as a storm berm with boulders on top; the lower ridge indicate foreshore facies with storm effects. The lag carpet of boulders is suggesting rapid transgressive effects over an abrasion plattform.

At Claromecó, east of the lighthouse, non-operating storm berms composed of sandy gravels are the remnants of Holocene beaches (backshore facies) with pebble segregation (Fig. 5b). The scarps of these deposits and the textural differences (boulder content) to present beaches,

TABLE 1. Grain-size analysis of Pleistocene, Holocene and Present beaches (Mz: mean grain size; S: standard deviation)

	Claromeco	Punta Negra Costa Bonita	P. Mogotes Mar Del Plata Harbour	Mar Chiquita	
Present	Foreshore Mz=2.12ϕ S=0.241ϕ	Backshore Mz=0.4ϕ S=1.49ϕ Foreshore Mz=1.8ϕ S=0.63ϕ	Backshore Mz=2.58ϕ S=0.29ϕ Foreshore Mz=2.51ϕ S=0.37ϕ	Dune Backbarrier Foreshore	Mz=2.05ϕ S=0.53ϕ Mz=2.97ϕ S=0.77ϕ Mz=2.30ϕ S=0.36ϕ
Holocene	Backshore Mz=2.07ϕ S=0.937ϕ	Foreshore Mz=1ϕ S=1.73ϕ	Foreshore Mz=0.9ϕ S=1.73ϕ	Cheniers Foreshore Heavy minerals	Mz=0.4ϕ S=0.56ϕ Mz=0ϕ S=2.21ϕ Mz=2.48ϕ S=0.56ϕ
Upper Pleistocene	Foreshore Mz=0.73ϕ S=1.74ϕ Estuary Mz=2.4ϕ S=0.35ϕ	Dune Mz=0.3ϕ S=2.99ϕ	Foreshore Mz=1.66ϕ S=1.43ϕ	Foreshore	Mz=0.6ϕ S=1.21ϕ

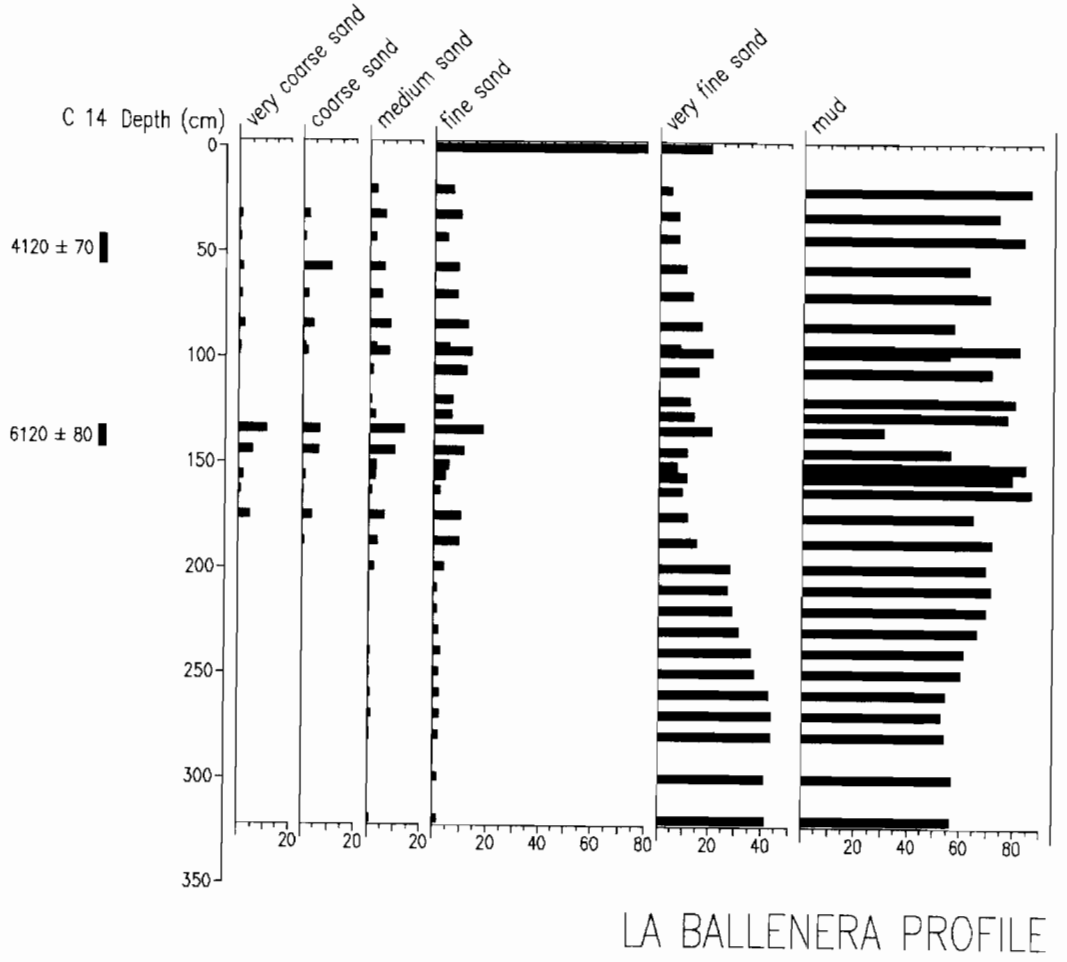

FIG. 7. Grain-size evolution of the La Ballenera Holocene estuarine sequence. The layers with very coarse sand are shell concentrations.

made us to conclude that they are eroded berms of Holocene age.

Grain-size analysis (Table 1) showed that they are usually well-sorted fine sands with gravels.

HOLOCENE ESTUARIES

Conditioned by the tectonic framework, the NE flank of the Tandilia Range is gentle (with a non-integrated drainage) while the SW flank has a steeper regional slope. This asymetry was already recognized by seismic surveys (Ewing *et al.*, 1963) and regional studies (Teruggi and Kilmurray, 1980).

On the northern gentle slope, the Holocene sea-level fluctuation (HSLF) caused a lateral succession of transitional environments (beaches, coastal lagoons, marshes, barriers), already described (Schnack *et al.*, 1982; Violante and Parker, 1992). On the southern slope, the HSLF filled small estuaries (Frenguelli, 1928) attached to ancient palaeocliffs.

La Ballenera estuarine profile (Fig. 6) is very similar to that of Arroyo Las Brusquitas (Espinosa *et al.*, 1984; Isla *et al.*, 1986). Massive muds, rich in organic matter, at the base, and in a fining-upwards sequence, were interpreted to be deposited by the turbidity maximum (Fig. 7). Towards the top, the laminated units were thinner and brighter suggesting bedload transport as the estuary was becoming infilled (fossiliferous layers containing *Litoridina* sp. were dated to 6120±80 and 4120±70; LP 720 and LP 743). Finally, the sequence was buried by a fine-sand dune.

In the Claromecó estuarine sequence (La Isla), a similar sediment successsion is recognized (Frenguelli, 1928). However, as this estuary is larger, there are several erosion surfaces produced by variations of the flow area. Organic black muds characterize the basal portions while bright laminated muds dominate to the top. However, interfingered in the laminated portion, there are several white ash layers, or layers with ash clasts. This evidence indicates that pyroclastic processes coming from the Andes dominated the Buenos Aires Plain sedimentation during the Holocene.

THE 'QUERANDINENSE' CONTROVERSY

In the original descriptions of the Quaternary stratigraphy of Buenos Aires, Frenguelli (1928) stated the Querandinense were muds enriched in organic matter belonging to a Pleistocene–Holocene marine transgres-

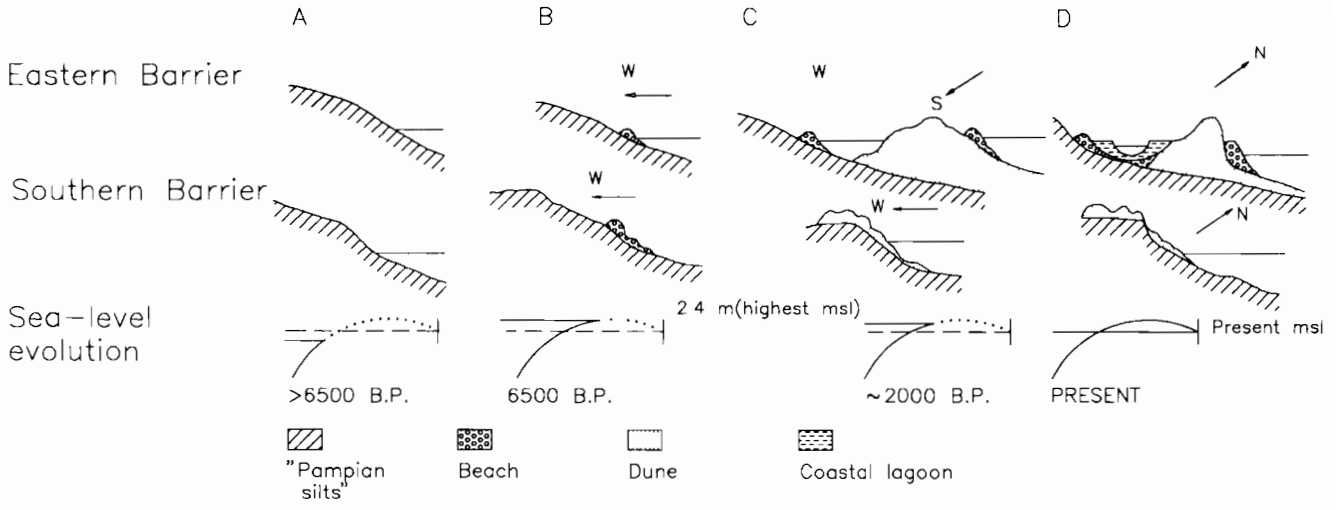

FIG. 8. Comparative evolution of the Southern and Eastern barriers of Buenos Aires.

sion. As a result of an extended erosional uncomformity, shelly littoral ridges belonging to the Platense are deposited over and compose another transgression of mid-Holocene age. This model was based on the extended character of the erosive uncomformity and topographical criteria: the greyish muds form a flat plain while the shelly deposits are positive ridges several meters thick above of the muds. This two-transgressions model continues to the presents, assigning ages older than 10,000 BP to the Querandinense deposits and younger ages for the Platense (Aguirre and Whatley, 1995; Politis *et al.*, 1995).

Within the estuarine sequences of the Southern Barrier, the black muds always grade to the top to sandy layers. These changes led Frenguelli to propose the same two-transgression model recognized in the north (1928).

The two-transgression model was based on apparent stratigraphical evidence, but some facies were misinterpreted. Black muds and bright sands belong to the same transgressive–regressive cycle of Holocene age: the grey muds were deposited in coastal lagoons or estuaries, some transgressive but many regressive. On the other hand, shelly or sandy ridges are regressive beaches or cheniers, and laminated and oxygenated muds (tidal flats, marshes) represent regressive phases ('platense') of that cycle.

It is difficult to accept a sea level higher than present 10,000 years ago on the relatively stable coast of Buenos Aires, when global data indicate that during those days the sea level was far below present level (cf. Pirazzoli, 1991's atlas of sea-level curves; Isla, 1989). Most of the problem is the lack of datable material (mollusk shells in living position) within the 'querandinense' muds. These deposits do represent estuaries or coastal lagoons rapidly filled during the mid-Holocene transgression. At these estuaries, there should have been a significant supply of mud (provided from the silty loessic pampean plains) that became hydrodynamically blocked by the sea-level rise. The massive 'querandinense' muds of Samborombón Bay, Arroyo Las Brusquitas, Punta Hermengo, Arroyo La Ballenera and Claromecó represent environments of rapid sedimentation rate, suggesting the turbidity maxima cited for estuarine depositional models (Wells, 1995). This process is not recorded in low-gradient areas (coastal lagoons) or where there is no preservation of the transgressive 'querandinense' beds. In Mar Chiquita, a rapid transgression over a flat surface (erosion platform) preserved beaches without any estuarine deposition resulting from the transgressive phase (Schnack *et al.*, 1982).

COMPARATIVE BARRIER EVOLUTION

The Southern and Eastern barriers evolved in relation to the Holocene sea-level fluctuation. During the end of the transgression (ca. 6500 BP), there was an abundance of sand at the coast. Wave energy was large enough and with winds blowing landwards, sand ramps climbed to the top of old cliffs constructing the Southern Barrier (Fig. 8). In the estuaries, there was rapid sedimentation of muds rich in organic matter. This did not occur at the low-lying coast north of Mar del Plata; shelly beach ridges were attached low cliffs (or benches), and the creeks discharged to coastal lagoons with tidal flats.

After some thousands of years of a relatively stable sea level, sand was depleted at the Southern Barrier. Sand ramps did not operate any more and the barrier became misfitted or undernourished (Fig. 8; Short, 1988). To the north, the Eastern Barrier was being constructed, dominantly by longshore currents over the flat regressive plain composed of beaches, cheniers, tidal flats and marshes. Supratidal peats underlying it were dated at 540±100 BP (Ac-0342), and indicate a very modern age for this barrier.

As the sea level had been stable for 5000 years, sand became depleted. In the Southern Barrier, beaches began to erode and old cliffs were exhumed, with sand remaining as cliff-top dunes. In the Eastern Barrier, foredunes became eroded as scarps or undernourished

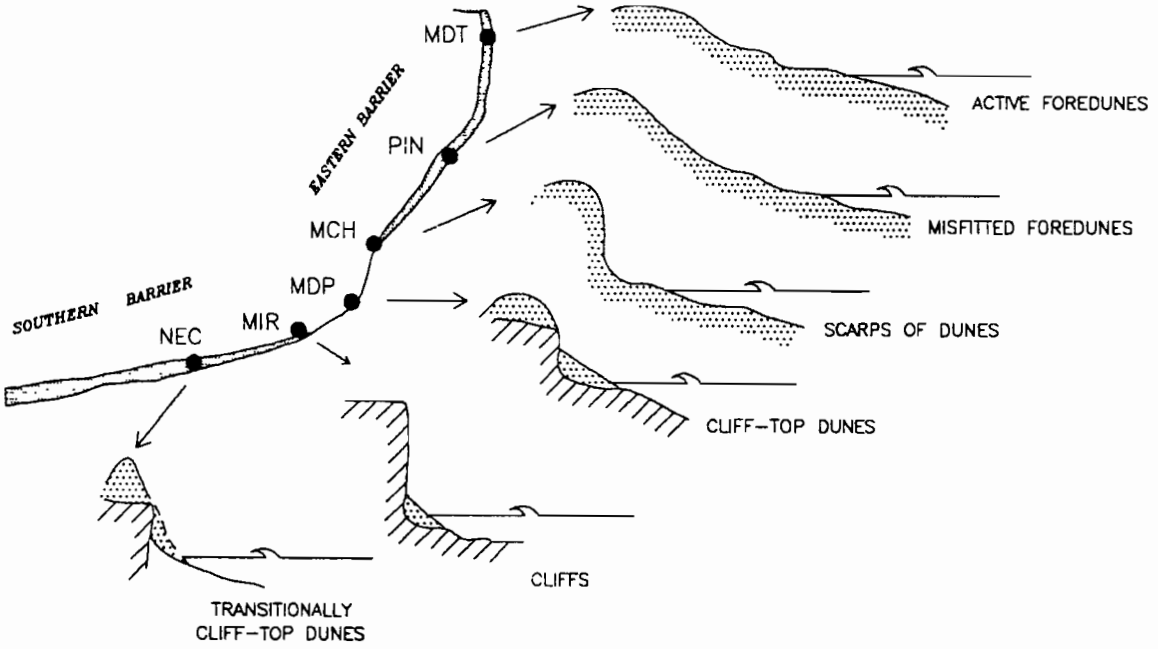

FIG. 9. Beach–dune relationship along the Southern and Eastern barriers.

dunes. Present beach–dune relationships recognize these processes along the Buenos Aires coastline (Fig. 9).

The reworking of Pleistocene and Holocene beaches at Claromecó seems responsible for the heavy-mineral concentrations reported in the literature (Angelelli and Chaar, 1969).

CONCLUSIONS

(1) Upper Pleistocene littoral deposits (Sangamon=Belgranense) from Claromecó are between 4 and 7 m above m.s.l., and in agreement with similar deposits of some other places in the world.

(2) Claromecó Pleistocene estuarine environments are below this Pleistocene beach (between +1.4 and +4.8 m). The erosional surface between these environments suggests rapid changes during the transgression.

(3) Holocene beaches at Costa Bonita are also above present m.s.l.: foreshore facies between 3 and 5.5 m, while backshore facies occur up to +7.5 m. The Holocene beaches outcropping at Punta Mogotes and Costa Bonita have similar altitudes.

(4) The Holocene estuarine sequences (Las Brusquitas, Punta Hermengo, La Ballenera, Quequén, Claromecó) are usually less than 2.4 m thick, although some of them extend higher than +4 m and several kilometers inland.

(5) These estuarine sequences, up to 4 m over present M.S.I, and backshore facies at +7.5 m, suggest a higher rate of relative sea-level rise in relation to the deposits related to the Eastern Barrier.

(6) For a same locality, there are sharp contrasts in the grain size and composition of beaches of different age.

(7) Averaged heavy-mineral concentrations along the Southern Barrier seem to be the response of progressive reworking of former beach deposits.

ACKNOWLEDGEMENTS

Finnancial support was provided by the Universidad Nacional de Mar del Plata, and Comisión de Investigaciones Científicas de Buenos Aires. S. Stutz helped during the field works. S. Serra did the grain-size analysis. M. Farenga made the drawings. M. Zárate discussed the stratigraphical terms for the Pleistocene deposits. C. Baeteman and D. Scott made many useful comments to the original manuscript. This is a contribution to IGCP-367 Quaternary sea-level records of rapid change.

REFERENCES

Aguirre, M.L. and Whatley, R.C. (1995). Late Quaternary marginal marine deposits and palaeoenvironments from northeastern Buenos Aires Province, Argentina: a review *Quaternary Science Reviews,* **14,** 223–254.

Angelelli, V. and Chaar, E. (1969). *Los médanos del área de Claromecó.* Su investigación por zircón. *Actas, IV Jornadas Geológicas Argentinas I,* 35–46.

Colado, U.R., Isla, F.I. and Farenga, M.O. (1990). Field guide: La Plata-Samborombón Bay, Province of Buenos Aires, Argentina. *IGCP 274 CIC, Nov.,* **18,** 8 pp.

Cronin, T.M., Szabo, B.J., Ager, T.A. and Owens, J.P. (1981). Quaternary climates and sea levels of the US Atlantic coastal plain. *Science,* **211,** 233–240.

Espinosa, M.A., Fasano, J.L., Ferrero, L., Isla, F.I., Mujica, A. and Schnack, E.J. (1984). *Micropaleontología y microestratigrafía de los sedimentos holocenos aflorantes en la desembocadura Arroyo Las Brusquitas (Partido de General Pueyrredón) y en Punta Hermengo (Partido de General Alvarado), Provincia de Buenos Aires,* pp. 520–537. IX Congreso Geológico Argentino, Bariloche, Actas III.

Ewing, M., Ludwig, W.J. and Ewin-g, J.I. (1963). Geophysical investigations in the submerged Argentine coastal plain. Part I. Buenos Aires to Península Valdés. *Bulletin Geological Society of America,* **74,** 275–292.

Fasano, J.L. (1989). *Geología y geomorfología.* Región III. Faro Querandí-Mar de Cobo, Provincia de Buenos Aires. Informe final convenio CFI-UNMDP, 118 pp.

Fasano, J.L., Isla, F.I., Mook, W.G. and van de Plassche, O (1987). *Máximo transgresivo postglacial de 7.000 años en*

Quequén, Provincia de Buenos Aires, pp. 475–477. Revista Asociación Geológica Argentina, XLII, 3–4.

Fidalgo, F., Colado, U.R. and de Francesco, F.O. (1972). *Sobre ingresiones marinas cuaternarias en los partidos de Castelli, Chascomús y Magdalena (Provincia de Buenos Aires)*, pp. 227–240. Actas V Congreso Geológico Argentino, Buenos Aires, III.

Frenguelli, J. (1928). *Observaciones geológicas en la región costanera Sur de la Provincia de Buenos Aires*. Anales Facultad de Cincias de la Educación, Paraná, II, 145

Isla, F.I. (1989). The Southern Hemisphere sea level fluctuation. *Quaternary Science Reviews*, **8,** 359–368.

Isla, F.I. and Espinosa, M.A. (1995). Environmental changes associated to the Holocene sea-level fluctuation: Southeastern Buenos Aires, Argentina. *Quaternary International*, **26,** 55–60.

Isla, F.I., Ferrero, L., Fasano, J.L., Espinosa, M.A. and Schnack, E.J. (1986). Late Quaternary marine-estuarine sequences of the Southeastern coast of the Buenos Aires Province, Argentina. Intnal. Symp. Sea Level Changes and Quaternary Shorelines. IGCP 200-IGCP 201, Inqua-Abequa, Sao Paulo, Brasil. *Quaternary of South America and Antarctic Peninsula*, **4,** 137–157.

Isla, F.I. and Selivanov, A. (1993). *Radiocarbon contributions to the Quaternary eustatism of Buenos Aires, Chubut and Tierra del Fuego*. Taller internacional 'El Cuaternario de Chile', Resúmenes, Santiago, 1–9 Nov. 1993, 47 pp.

Isla, F.I. and Villar, M. del C. (1992). *Ambiente costero*. Pacto Ecológico. Unpublished report, Convenio UNMDP-Cámara de Diputados de la Prov. de Bs. As., Mar del Plata, 23 pp.

Kraglievich, J.L. (1959). Contribuciones al conocimiento de la geología cuartaria en la Argentina. IV. Nota acerca de la geología costera en la desembocadura del Arroyo Malacara (Provincia de Buenos Aires). *Comunicaciones Museo Argentino de Ciencias Naturales B Rivadavia, Geología, I*, **17,** 9 pp.

Pirazzoli, P.A. (1991). World atlas of Holocene sea-level curves. *Elsevier Oceanographic Series*, **58,** 300 pp.

Politis, G.G., Prado, J.L. and Beukens, R.P. (1995). The human impact in Pleistocene-Holocene extinctions in South America: The pampean case. *In*: Johnson, E. (ed.), *Ancient Peoples and Landscapes*, pp. 187–205. Museum of Texas Technical University, Lubbock.

Risso Domínguez, C.J. (1949). *Estratigrafía de las barrancas de Chapadmalal y Vorohue*. Estudios, **81**, 440, 353–372.

Schnack, E.J., Fasano, J.L. and Isla, F.I. (1982). The evolution of Mar Chiquita lagoon, Province of Buenos Aires, Argentina *In*: Colquhoun, D.J. (ed.), *Holocene Sea-Level Fluctuations: Magnitudes and Causes*, pp. 143–155. IGCP 61, University of South Carolina, Columbia, SC.

Short, A.D. (1988). Holocene coastal dune formation in Southern Australia: a case study. *Sedimentary Geology*, **55,** 121–142.

Teruggi, M.E. and Kilmurray, J.O. (1980). *Sierras Septentrionales de la Provincia de Buenos Aires*, pp. 919–965. Geología Regional Argentina, Academia Nacional de Ciencias, Córdoba, II.

Tonni, E.P. and Fidalgo, F. (1982). *Geología y paleontología de los sedimentos del Pleistoceno en el área de Punta Hermengo (Miramar, Prov. de Buenos Aires, Rep. Argentina): Aspectos paleoclimáticos. Ameghiniana*, **19** (1–2), 79–108.

Violante, R.A. and Parker, G. (1992). *Estratigrafía y rasgos evolutivos del Pleistoceno medio a superior-Holoceno en la llanura costera de la región de Faro Querandí (Provincia de Buenos Aires). Revista Asociación Geológica Argentina*, **47** (2), 215–227.

Wells, J.T. (1995). Tide-dominated estuaries and tidal rivers. *In*:Perillo, G.M.E. (ed.), Geomorphology and Sedimentology of estuaries. *Developments in Sedimentology*, **53**, 179–205.

Zarate, M.A. and Fasano, J.L. (1989). The Plio-Pleistocene record of the Central Eastern Pampas: the Chapadmalal case study. *Palaeogeography, Palaeoclimatology and Palaeoecology*, **72,** 27–52.

Zavala, C. (1993). Estratigrafía de la localidad de Farola Monte Hermoso (Plioceno-Reciente), Provincia de Buenos Aires. *XII Congreso Geológico Argentino, Actas*, **II,** 228–235.

CLIMATE AND SEA LEVEL

Pergamon

Quaternary Science Reviews, Vol 15, pp. 843–849, 1996.

0277–3791/96 $32 00

PII: S0277–3791(96)00064–9

CARBON STORAGE AND CONTINENTAL LAND SURFACE CHANGE SINCE THE LAST GLACIAL MAXIMUM

H. FAURE,* J.M. ADAMS,*† J.P. DEBENAY,‡ L. FAURE-DENARD,* D.R. GRANT,§ P.A. PIRAZZOLI,¶ B. THOMASSIN,‖ A.A. VELICHKO and C. ZAZO††**

**Laboratoire de Géologie du Quaternaire du CNRS, Case 907, Faculté des Sciences de Luminy, 13288 Marseille Cédex 9, France, and CEREGE, BP80, 13545 Aix-en-Provence Cedex 4, France*

†Geography Department, University of Oxford, 1a Mansfield Road, Oxford, U.K.

‡Laboratoire de Géologie, Faculté des Sciences, Université d'Angers, Bd Lavoisier Belle-Beille, 49045 Angers Cédex, France

§Geological Survey of Canada, Ottawa Ontario, Canada

¶CNRS-LGP, 1 Place A. Briand, 92190 Meudon-Bellevue, France

‖Centre d'Océanologie de Marseille, CNRS-URA 41, Université de la Méditerranée, Station Marine d'Endoume, 13007 Marseille, France

***Institute of Geography, Russian Academy of Sciences, Staromonetny 29, Moscow, Russia*

††Museo Nacional de Ciencias Naturales, José Gutierrez Abascal, Madrid, Spain

Abstract — Estimates of the storage and flux of shelf carbon in vegetation, soils, carbonates, and organic matter during the period of the marine transgression since the Last Glacial Maximum (LGM) 18 ka are presented. Whereas at present each square metre of land on the planet carries about 10.65 kg of carbon in vegetation and soils, during the LGM most areas of exposed continental shelf carried relatively little carbon, probably about 5.86 kg C m^{-2}, but this increased to a maximum density of 15.49 kg C m^{-2} after 10 ka when conditions generally favoured peat deposition and forest development. In the ensuing sea level rise up until mid-Holocene time this large store of carbon was displaced. Assuming an average value of 10.65 kg m^{-2} carbon (combining the land lost to sea-level rise before and after 13 ka), a transgression covering 15–23×10^{12} m^2 would mean that 160 to 245 Gigatons of Carbon (1 Gt=10^{12} kg) were lost from the terrestrial system at the same time that the remainder of the terrestrial biosphere was still taking up organic carbon. This additional and opposite flux from the land system must be taken into account when considering changes in the global carbon cycle and CO_2 fluxes. Moreover, it complicates the interpretation of the ocean carbon isotope record.

INTRODUCTION

The melting of ice sheets which took place 17–7 ka liberated an estimated 40×10^6 km^3 of water, which is equivalent to a uniform global sea-level rise of 115 m. This rise resulted in the loss of about 20×10^6 km^2 from the global area of terrestrial ecosystems. Such a change in the global land area would have had significant consequences for the planetary environment as a whole, affecting a range of ecological, climatic, oceanographic, biogeochemical, archaeological, and pedological processes (Fig. 1).

However, this average 115 m of global eustatic sea-level rise was not uniform; the actual sea-level rise varied locally between about 75 and 155 m (115m±40 m) and perhaps more in some places. This large local variation is a hydro-isostatic effect, depending mainly on whether the shelf is sinking with the ocean floor or rising with the uplifted continents. Published estimates indicate that 10 to 25 million km^2 of land surface was lost by sea-level recovery since 18 ka, the Last Glacial Maximum (LGM). If the sea level had dropped more than expected liberating more land, this would have had little consequence on vegetation, because it would have occurred during the LGM when climatic conditions were not favourable for vegetation growth.

FACTORS

The uncertainty about the change of land area is a potentially serious problem in understanding how global processes may have changed between glacial and interglacial conditions. For example, in estimating changes in the total mass of carbon on land between glacial and interglacial conditions, Prentice and Fung

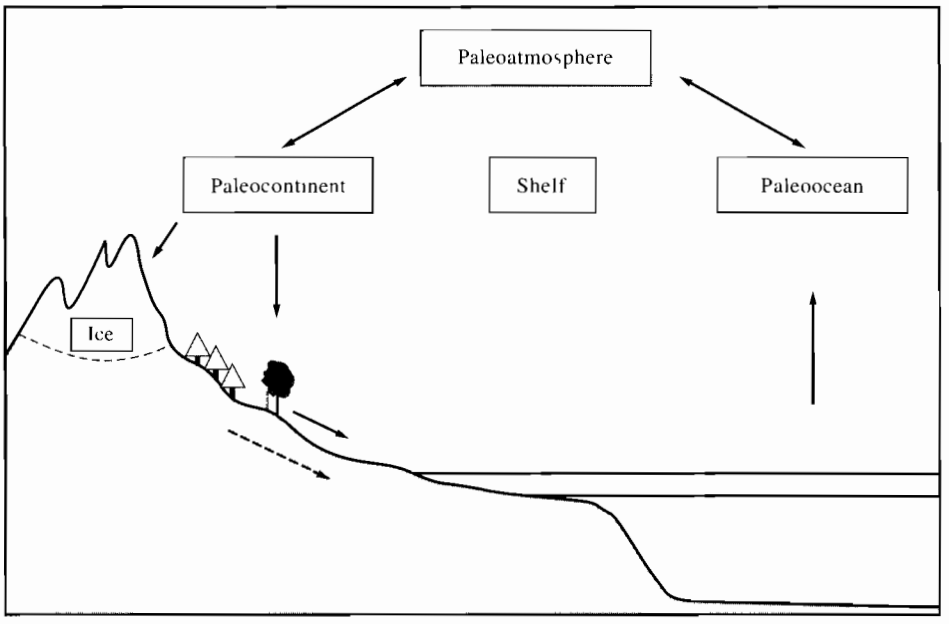

FIG. 1. Simplified model of sea-level rise changing global areas of ocean and of continents.

(1990) and Esser and Lautenschlager (1994) suggest a large additional carbon reservoir in the vegetation and soils which occupied exposed continental shelves during glacially lowered sea levels. Depending on the shelf area that is assumed during glacial conditions, a different carbon storage figure will be obtained.

To obtain more confident estimates of the change in land surface area, it will be necessary to try to take account of the complexity of processes which can affect sea level around the world. Previous attempts to model the changes in land inundation since the Last Glacial have tended to assume that the global land and ocean basin topography remained static between glacial and interglacial conditions. This obviously was not the case. Local-scale tectonic or isostatic changes, such as those resulting from changes in ice sheet loading on land, are already fairly well documented and must be properly taken into account. Erosional and depositional changes in topography must also be given due consideration. There may also have been broad-scale hydro-isostatic and tectonic changes in the shape of the deep ocean basins, or conversely in the topography of the continents, which would have affected the observed sea level rise by altering the distribution of ocean water.

Given the importance of obtaining precise and reliable estimates of the changing global distribution of land, and given also the complexity of the task, it will be necessary to bring together specialists from a wide range of fields working in different parts of the world. This paper is an initial attempt to estimate the amount of carbon in the terrestrial ecosystems destroyed by sea level rise.

RATES OF LAND SUBMERGENCE

The area of land submerged by sea level rise during global glacial melting depends mainly on the topographic slope and the rate of rise. A lesser factor is the amount of mobile sediment that can locally modify the morphology and create barriers. Biological construction such as mangrove and coral reefs can also have an important role in coastal morphology, especially during times of changing rate of sea-level rise (Bloom, 1970; Fairbanks, 1989; Thomassin, 1993).

Sea-level rise itself depends on many factors. In terms of their global effect, the two most important are ice melt rates and hydro-isostatic depression of the ocean floor due to the increased water load (Clark, 1979). This latter was delayed by several hundred or thousand years after the sea-level rise and thus had the effect of driving more water toward the ocean center. This had the effect of decreasing the apparent sea-level rise close to continents that are rising (due to the conservation of the volume of the solid Earth mantle at short time scale). Mantle volume changes due to temperature and phase changes can be neglected on the time scale of several thousand years considered here.

If the ocean floor is depressed globally by 30 m, one can calculate because of their relative areas, density contrasts and the incompressibility of the asthenosphere, that the continents should be uplifted about 40 m on average. The propagation of the asthenosphere toward the uplifted continents should be progressive on a time scale of about 5000 years. It could result in a possibly stronger uplift at continental edges and could reach the central part of the large continents much later. For this reason, the uplift of the coastal zone could theoretically be much more than the mean 40 m of the continents and contrast strongly with the deepening on the ocean side. Excluding faulted coasts, the result should be a very strong flexure following the sea-level rise. This is perhaps borne out by global crustal and sea-level models, such as that by Clark (1979) among others, which show a 5–10 m difference in the elevation of the 5 ka shoreline over distances of a few hundred kilometres.

However, the lack of observations of any such flexure of Holocene shoreline deposits along large estuaries for example (Faure *et al.*, 1980) requires explanation. Perhaps the flexure is very gentle and extends more than 1000 km or is located more seaward in the direction of thinner oceanic crust. Or perhaps it has been absorbed by fault movement. In this case, many continental shelves of wide continents could be acting in unison with the uplifting continent and thus be uplifted about 40 m or more while others are moving with the adjacent ocean floor and thus be lowered by about 30 m. Such differently acting continental shelves are perhaps indicated by their different sea-level curves (Pirazzoli, 1991). This possibility requires further field testing by greater amounts of paleobathymetric data.

RATES OF ICE MELTING

Fairbanks (1989) calculated from the Barbados sea-level curve apparent peaks in glacial meltwater discharge of 14×10^3 km^3 year^{-1} and 9×10^3 km^3 year^{-1} at 12 ka and 9.3 ka, respectively. The rate was only 3.5×10^3 km^3 year^{-1} at 11 ka during the Younger Dryas temperature minimum. These apparent discharge rates would correspond approximately to rates of sea-level rise of about 40 mm year^{-1}, 26 mm year^{-1} and 10 mm year^{-1}, respectively. These variable rates of apparent sea-level rise have to be compared to the overall rate implied by a rise of 115 m over a period of about 11.5 ka, which corresponds to a mean rate 10 mm year^{-1} between 18 ka and about 6.5 ka. If achieved over 15 ka, then the mean rate would be 7.7 mm year^{-1}.

Of course this apparent discharge rate integrates the melted ice volume as well as the changes in the level of the ocean floor due to hydro-isostatic load. This reaction to changes of water loading over the world ocean is responsible for an apparent drop (decrease in rate rise) of the relative water level around deepened areas.

The hydro-isostatic sea-level change was delayed by several thousand years after the beginning of the loading. Bloom (1970) has noted that oceanic islands in the center of a wide ocean, having the same vertical movement as the ocean bottom, records the true sea-level curve. In fact even this record is modified by volumes of water transferred from peripheral uplifted ocean margins.

To get a better idea of the relative contribution of ice-volume melt and of ocean floor effect, we have to compare two sets of data. One set is taken from islands in the central part of ocean basins where both effects are more likely to be additive. The other set of data should be taken from shelves of large continents.

SEDIMENT FLUXES DURING MARINE TRANSGRESSION

Marine transgression reworks soils and superficial deposits and the characteristics of this additional reworked material are:

(1) Its grain size heterogeneity which includes large components from the regolith (at the origin of the so called basal conglomerate). This contrasts with the usually fine grain suspended material furnished by the world rivers.

(2) Its terrestrial origin, possibly including continental fauna (as for instance Mammoth teeth found on the northwest Atlantic shelf and biomarkers of terrestrial vegetation and soil organic matter).

(3) The sudden increase in dissolved and particulate organic carbon derived from destroyed soils. This may strongly reflect the rate of the transgression because the global average soil has a high organic carbon content. But we must consider that LGM soils were poor in carbon content compared to present and Holocene soils.

(4) However in some cases the reworking of soils after submergence on the shelf may be limited (Yim and Tovey, 1995), and some terrestrial carbon may be preserved on the shelf.

PEAT BURIED ON THE CONTINENTAL SHELF

As the transgression slowed, peat and mangrove swamps on some areas of the shelf may have expanded and then have been locally buried in muddy sediments. Such sediments with 10–25% organic carbon and generally less than 1 m thick occur for example in several areas of East and West Africa and are dated around 12, 10, 8 ka (Martin, 1977). However, these sediments are commonly eroded and peat fragments are thrown onto the beaches during storms (as in Baie de Hann, South of Dakar, for example). In Mayotte (Indian Ocean) such organic sediments are poor in $CaCO_3$ (<20%) and covered by 3 m of $CaCO_3$ rich sediment (85%; Thomassin, 1993).

Because of the rarity of conditions favorable to preservation, the quantity of organic matter in the continental shelf surface sediments is quite small (certainly less than 10 Gt C), compared to the weight of Holocene terrestrial peat (around 450 Gt), or the carbon in carbonates deposited in all oceans during the same period.

INDICATORS OF LAND SUBMERGENCE

To evaluate more precisely the carbon fluxes from the shelf it is necessary to know the total area which was submerged. Ideally this should be established continuously or at least for every 500–1000 years.

Indicators of land submergence must be radiocarbon dated markers of the transition from the last terrestrial remnant to the first overlying marine deposits. Indicators are numerous and have been listed (NIVMER Group, 1979–1980). They comprise aerial karstification peat (terrestrial and mangrove), soils, sedimentary sequences and all indicators of marine transgression. As an example we summarize two simple approaches for estimating tropical land submergence areas based on benthic

foraminifera (Debenay *et al.*, 1993; Debenay and Redois, in press).

USE OF BENTHIC FORAMINIFERA INDICATORS OF LAND SUBMERGENCE

Benthic foraminiferal assemblages can be used as indicators of bathymetric variations or of ecological changes in relation with land submergence. Attempts have been made, on the coast of West Africa, to use: (1) the benthic foraminiferal assemblages from the shelf as indicators of paleobathymetry (there at best 1±20 m); and (2) the benthic foraminiferal assemblages from the paralic environments as indicators of ecological characteristics correlated with sea level.

BENTHIC FORAMINIFERA INDICATORS OF PALAEOBATHYMETRY

Benthic foraminiferal assemblages are frequently used as qualitative bathymetric indicators (e.g. review in Murray, 1991). According to Scott and Medioli (1986), species from tidal marshes can be used to estimate ancient marine levels with an accuracy of ±10 cm. However, this method is limited to tidal marshes.

On the shelf, the distribution of benthic foraminiferal assemblages may sometimes be correlated with the bathymetry. This distribution, generally used as a qualitative indicator, has been studied worldwide (locally on the African shelf in Blanc-Vernet (1988)). A depth index (Di), calculated on the basis of the benthic foraminifera of the continental shelf off Senegal (between 10 and 200 m) is proposed (Debenay and Redois, *in press*).

This index is calculated on the basis of three assemblages.

(1) Assemblage A: *Cassidulina laevigata, Trifarina fornasini* and *Uvigerina peregrina.*
(2) Assemblage B: *Textularia foliacea, Textularia mexicana, Ammobaculites pseudospirale, Pseudoeponides falsobeccarii* and *Bulimina elegans.*
(3) Assemblage C: *Pararotalia armata, Cribrolinoides curtus, Ammonia beccarii* and *Tetragonostomina rhombiformis.*

Di = 100 (A/(A+B) − C/(B+C) + 1)/2, where A, B and C are the relative percentages of the assemblages 1, 2 and 3. Calculated from about 100 samples, Di is positively correlated with the depth ($R = 0.89$; Fig. 2). These preliminary results show that it is possible to consider the use of the bathymetric index for paleobathymetric studies in Quaternary sediments. However, despite the good correlation of Di with depth, the precision cannot reach more than about ±20 m, particularly for depth of more than 100 m. Thus, as it stands, Di can only be used to determine an approximate depth and, possibly, to indicate the direction of the variation of the sea level. Work is currently in progress to improve the accuracy of this index.

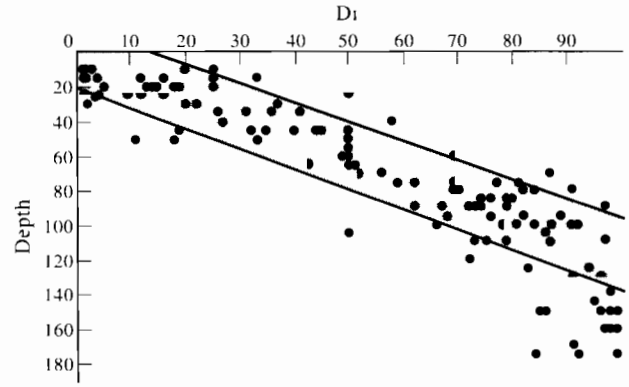

FIG. 2. Depth index (Di) correlated with depth. Di can be used to indicate sea level variations.

BENTHIC FORAMINIFERA INDICATORS OF ECOLOGICAL CHARACTERISTICS IN PARALIC ENVIRONMENTS

Paralic environments are at the transition between marine and nonmarine waters, the properties of the paralic waters depending on the intensity of marine influence (Guelorget and Perthuisot, 1983, 1992). These complex environments are very sensitive to coastline variations and can provide good indications for paleogeographic reconstructions, especially in case of submergence of land.

The Confinement Index (Ic), calculated on the basis of foraminiferal assemblages, may be one of the indicators used for the paleoecological reconstruction of these environments (Debenay, 1990, Debenay *et al.*, 1993).

Ic = (C/(B + C) − A/(A + B) +1)/2 where A, B and C are relative percentages for the assemblage 1, 2 and 3. Ic = 1 if the assemblage 3 is the only one represented (A + B = O) and Ic = O if the assemblage 1 is the only one represented (B + C = O).

(1) Assemblage 1: *Elphidium fichtelianum, E. gunteri, Pararotalia* sp., *Bolivina striatula* and *Rosalina* spp.
(2) Assemblage 2: *Eggerelloides scabrum, Quinqueloculina poeyana, Q. seminula, Haynesina germanica, Elphidium gunteri, E. limosum, Bolivina variabilis* and *Ammonia* spp.
(3) Assemblage 3: *Ammobaculites exigus, Ammotium salsum, Arenoparella mexicana, Gaudryina exilis, Haplophragmoides wilberti, Miliammina* spp., *Trochammina* spp. and *Siphotrochammina lobata.*

This index is easy to calculate and requires only a small amount of sediment (50 cm^3). It can be calculated in the field with a simple stereomicroscope. The index varies from 0 in marine waters to 1 in the most confined environments. It appears to be a valuable indicator of marine influence and the change of its numerical value indicates a tendency toward more restricted (Ic increases) or less restricted (Ic decreases) conditions. We can look for its possible use as an indicator of the sea-level change, considering that several causes can interfere with the variation of its value. A decrease of Ic, for example, may result from (1) a local or general sea-level rise with land submergence; (2) the destruction of a sand spit allowing

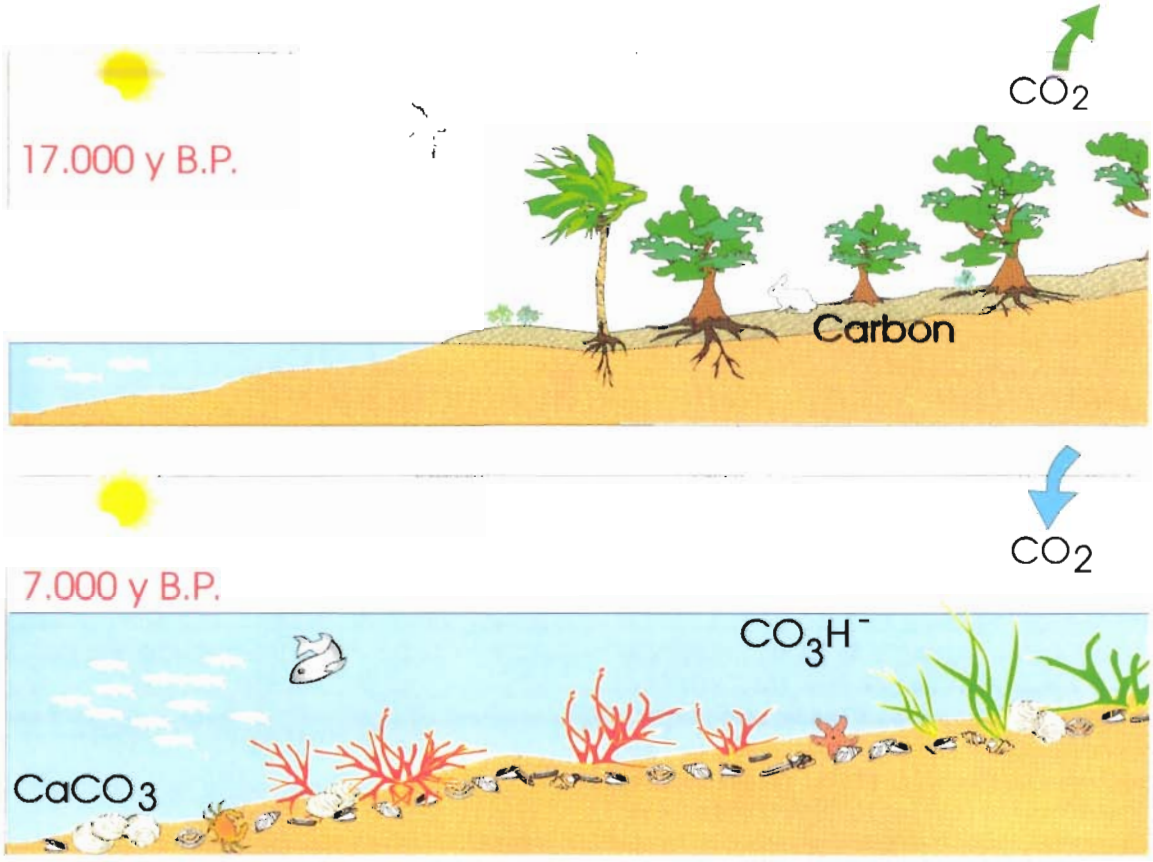

FIG. 3. Marine ecosystem taking place of terrestrial ecosystem on the continental shelf during postglacial sea-level rise.

an increased marine influence; or (3) a climatic change toward arid conditions leading to strong evaporation and penetration of marine water in the lagoons or estuaries (inverse functioning; Pritchard, 1967).

Of course, several of these causes can combine and the Casamance estuary, for example, undergoes simultaneously a drastic aridification and a slow sea-level rise (Debenay *et al.*, 1994).

It is evidence that the variation of Ic, considered alone, gives no argument to determine which of the possible causes of environmental change was responsible. Ic must be considered as one of the complementary indicators to be used for quantification of ecosystems, as recommended by Faure *et al.* (1993a, b).

SOIL CARBON IN THE SEA

Soils have a mean carbon content of 10 kg m^{-2} (1500 Gt C for the world land superficy of 150×10^{12} m^2). Thus, a 1000 km^2 area covered by the sea every year during the postglacial sea-level rise would be responsible for a carbon flux of 0.010 Gt $year^{-1}$. This is added to the input of organic carbon from the world rivers (Probst, 1992). Today this carbon flux is about 0.2 Gt $year^{-1}$.

Present day sediments brought from the continents to the ocean are estimated at 18.38 Gt C $year^{-1}$ (Probst, 1992). If these sediments contain 2% carbon, this corresponds to a flux of 0.368 Gt C $year^{-1}$. Today, carbon flux to the ocean is about 0.7 Gt C $year^{-1}$ of which about 0.4 Gt of particulate organic carbon (POC) and 0.3 Gt of dissolved organic carbon (DOC; Probst, 1992).

A FIRST APPROXIMATION OF THE CARBON FLUX FROM THE SHELF DURING SEA-LEVEL RISE.

During the sea-level rise which accompanied the melting of ice sheets, terrestrial ecosystems on the exposed shelves were replaced by the marine and littoral ecosystems which exist today (Fig. 3). The global sea-level rise occurred as a continuous process, punctuated by at least three periods of faster rise which are variously recorded in local and regional undersea structures and are dated to about 13, 10.5 and 8 ka.

For each climatic or ecological zone, the exchange between continental and marine ecosystems had particular effects which require a detailed case by case study. However, here we give a preliminary global overview of the storage of carbon by ecosystems in order to underline the necessity of local studies. Our calculations concern the uptake and release of the carbon in vegetation, soils, carbonates and organic material, during the transgression which took place between 18 ka and the present-day. On average, each square metre of continental land surface of

TABLE 1. Estimate of mean density of global terrestrial carbon during the Glacial Maximum and during the Holocene. The calculations include the biomass and soil carbon lost through the submergence of 15×10^6 km^2 and 23×10^6 km^2 of land

	Glacial	Holocene	Glacial/Holocene difference
Vegetation (GtC)	343	924	+581
Soil (and peat) (GtC)	625	1395	+770
Total (GtC)	968	2319	+1351
Area of continent (10^6 km^2) (10^{12} m^2)	165.3	150.1	−15.20
Mean carbon density (kg m^{-2})	5.86	15.45	
Mean carbon density(progressive change)over 12 000 years			10.65
Lost carbon of the continental shelf	$10.65\times15.2\times10^{12}$ m^2 = 162 Gt C		
The same calculation for higher value	$10.65\times23\times10^{12}$ m^2 = 245 Gt C		

Values for Glacial Maximum and Holocene are after Adams, Faure *et al.*, 1990.
Prentice and Fung (1990) for a sea level lowering of 130 m calculated a supplementary shelf carbon storage of 200 Gt C
The stock is in Gt C = gigatons (10^{15} g or 10^{12} kg) of carbon.
The land surface is in 10^6 km^2 (10^{12} m^2) = millions of km^2
The mean density of carbon is in kg C m^{-2} = kilograms of carbon per square meter.

the world carries **10.65 kg m^{-2}** of carbon in the vegetation and soil, as against **5.86 kg m^{-2}** (968 Gt of carbon on a continental superficy of 165.3×10^{12} m^2) during the Glacial Maximum and **15.45 kg m^{-2}** (2319 Gt of carbon on a continental superficy of 150.1×10^{12} m^2) during the Holocene Optimum (Table 1). We estimate that $15–23\times10^{12}$ m^2 of land surface were lost during the postglacial transgression. This represents the erosion and oxidation of 160 to 245 Gt of continental carbon (Table 1), because the transgression destroyed most of the soils and vegetation, and preserved very little of the organic carbon. This flux of about 200 Gt C into the atmosphere was in opposition to the much greater flux of around 1350 Gt C necessary to form the interglacial soils and vegetation following the amelioration of glacial cold and aridity (Adams *et al.*, 1990).

CONCLUSION

As the rising sea encroached over the land, marine and littoral ecosystems would have taken the place of the terrestrial ones which previously existed. This would have resulted in a greater production of marine organic matter and also inorganic carbonates (from algal coccoliths, reef corals, etc.). If the sediment has a mean depth of about 45 mm of carbonate, or 10.8 kg C m^{-2}, the transgression would store the same amount of carbon as that released by the destruction of the terrestrial vegetation. But for each carbon atom deposited as carbonate, another was liberated as CO_2, through the process of precipitation from the bicarbonate dissolved in ocean water. However, a significant difference in the isotopic composition between these two sources ($\delta^{13}C$ of about −25‰ to −12‰ vs $\delta^{13}C$ about 0‰) should have caused a considerable enrichment in light isotopes of oceanic and atmospheric CO_2. Consideration of this exchange mechanism suggests that assessments of variations in global carbon reservoir exchange from the land system will be mistaken if they are based only on evaluations of isotopic composition of oceanic and atmospheric carbon ($\Delta\ \delta^{13}C$ = 0.3 glacial-interglacial difference.)

ACKNOWLEDGEMENTS

This project was discussed at the IGCP 274 meeting in DAKAR in 1993. Preliminary investigation was led with the help of the French National Committee of IGCP, projects 253 and 274, and Laboratoire de Geologie du Quaternaire of CNRS. We thank D.B. Scott, R. Cranston and W.W.-S. Yim for useful comments and careful reviews. This publication is a contribution to IGCP 367, 349, 396 and 404, to GLOCOPH and to the INQUA Commission on Carbon Cycle.

REFERENCES

Adams, J.M., Faure, H., Faure-Denard, L., McGlade, J.M. and Woodward, F.I. (1990). Increases in terrestrial carbon storage from the Last Glacial Maximum to the present. *Nature*, **348,** 711–714.

Blanc-Vernet, L. (1988). Répartition bathymétrique des foraminifères benthiques sur la plate-forme continentale. *Géologie Méditerranéenne*, **15,** 5–12.

Bloom, A.L. (1970). Holocene submergence in Micronesia as the standard for eustatic sea-level changes. In: Symposium on the evolution of shorelines and continental shelves in their mutual relations during the Quaternary. *Quaternaria*, **12,** 145–154.

Clark, J.A. (1979). A numerical model of worldwide sea level changes on a visco elastic earth. *In*: Morner, N.A. (ed.), *Earth Rheology, Isostasy and Eustasy*. Wiley, New York.

Debenay, J.-P. (1990). Recent foraminiferal assemblages and their distribution relative to environmental stress in paralic environments of West Africa (Cape Timiris to Ebrie Lagoon). *Journal of Foraminiferal Research*, **20,** 267–282.

Debenay, J.-P., Perthuisot, J.-P. and Colleuil, B. (1993). Expression numérique du confinement par les peuplements de foraminifères. Applications aux domaines paraliques actuels d'Afrique de l'Ouest. *C.R. Acad. Sci.*, Paris, **316,** serie II, 1823–1830.

Debenay, J.-P., Pages, J. and Guillou, J.J. (1994). Transformation of a subtropical river into a hyperhaline estuary: the Casamance river (Senegal). Paleogeographical implications. *Palaeoecology, Palaeoclimatology, Palaeogeography*, **107,** 103–119.

Debenay, J.-P. and Redois F., in press. Distribution of the twenty seven dominant species of shelf benthic foraminifers on the continental shelf, north of Dakar (Senegal). *Marine Micropaleontology*.

Esser, G. and Lautenschlager, M. (1994). Estimating the change of carbon in the terrestrial biosphere from 18,000 BP to present using a carbon cycle model. *Environmental Pollution*, **83,** 45–53.

Fairbanks, R.G. (1989). A 17,000 year glacio-eustatic sea level record: influence of glacial melting rates on the Younger Dryas event and deep-ocean circulation. *Nature*, **342,** 637–642.

Faure, H., Faure-Denard, L., Hantoro, W.S., Lezine, A.M., Velichko, A., Zazo, C. and Adams, J.M. (1993a). Importance des variations des écosystèmes terrestres et marins pour la modélisation biogéochimique et climatique globale entre 18.000 et 8.000 ans B.P. *Réunion internationale PICG 274; Evolution côtière au Quaternaire*. Abstract Volume, 19–20.

Faure, H., Debenay, J.P., Faure-Denard, L., Pirazzoli P.A., Thomassin, B.A., Velichko, A.A., Zazo, C. and Adams, J.M. (1993b). Shelf carbon flux during sea level changes, *IGCP 274 meeting*, Oostduinkerke, Sept. 1993.

Faure, H., Fontes, J.C., Hebrard, L., Monteillet, J. and Pirazzoli, P.A. (1980). Geoidal change and shore-level tilt along Holocene estuaries: Sénégal river area, West Africa. *Science*, **210,** 421–423.

Guelorget, O. and Perthuisot, J.P. (1983). Le domaine paralique. Expressions géologiques, biologiques et économiques du confinement. Travaux du Laboratoire de Géologie de l'Ecole Normale Supérieure. *Paris*, **16,** 1–136.

Guelorget, O. and Perthuisot, J.P. (1992). The Paralic Realm. Biological organization and functioning. *Vie Milieu*, **42,** 215–251.

Martin, L. (1977). Morphologie, sédimentologie et paléogéographie au Quaternaire récent du plateau continental ivoirien. *Travaux et Documents de l'ORSTOM*, **61,** 265. (Doctoral Thesis, Paris, University Pierre et Marie Curie).

Murray, J. (1991). *Ecology and Paleoecology of Benthic Foraminifera*. Longman Scientific and Technical, Harlow.

NIVMER Group (1979–1980). Les Indicateurs de Niveaux Marins. *In*: *Oceanis*. Vol.**5,** Fascicule Hors-Série. pp. 145–360. Publication Institut Océanographique, Paris.

Pirazzoli, P.A. (1991). *World Atlas of Holocene Sea Level Changes*. Oceanography Series, **58.** Elsevier, Amsterdam.

Prentice, K.C. and Fung, I. (1990). The sensitivity of terrestrial carbon storage to climate change. *Nature*, **346,** 48–50.

Pritchard, D.W. (1967). What is an estuary: physical point of view. *In*: Lauff, G. H. (ed.), *Estuaries*. American Association for the Advancement of Science, Publication **83**, 3–5.

Probst, J.L. (1992). Géochimie et Hydrologie de l'Erosion Continentale. Mécanismes, bilan global actuel et fluctuations au cours des 500 derniers millions d'années. *Sciences Géologiques*. Mémoire No. 94. (Doctorat thesis; University of Strasbourg, 1992).

Scott, D.B. and Medioli, F.S. (1986). Foraminifera as sea level indicators. *In*: O. Van de Plassche (ed.), *Sea-level Research. A manual for the Collection and Evaluation of Data*, pp. 435–456. Geo Books, Norwich, U.K.

Thomassin, B.A. (1993). Construction récifale et sedimentation dans le lagon de Mayotte (S.W. Océan Indien) depuis 18.000 ans B.P. *Réunion spécialisée de la Société Géologique de France*, 97–99.

Yim, W.W.S. and Tovey, K. (1995). Dessication of inner continental shelf sediments during Quaternary low sea-level stands. *Geoscientist*, **5,** 34–35.

Pergamon

Quaternary Science Reviews, Vol. 15, pp 851–856, 1996

PII: S0277–3791(96)00063–7
0277–3791/96 $32.00

LATE MID-HOLOCENE SEA-LEVEL OSCILLATION: A POSSIBLE CAUSE

D.B. SCOTT and E.S. COLLINS
Centre for Marine Geology, Dalhousie University, Halifax, Nova Scotia B3H 3J5, Canada

Abstract — Sea level oscillated between 5500 and 3500 years ago at Murrells Inlet, South Carolina, Chezzetcook and Baie Verte, Nova Scotia and Montmagny, Quebec. The oscillation is well constrained by foraminiferal marsh zonations in three locations and by diatoms in the fourth one. The implications are: (1) there was a eustatic sea-level oscillation of about 2–10 m in the late mid-Holocene on the southeast coast of North America (South Carolina to Quebec) that is not predicted by present geophysical models of relative sea-level change; (2) this oscillation coincides with oceanographic cooling on the east coast of Canada that we associate with melting ice; and (3) this sea- level oscillation/climatic event coincides exactly with the end of pyramid building in Egypt which is suggested to have resulted from a climate change (i.e. drought, cooling).

This sea-level/climatic change is a prime example of feedback where climatic warming in the mid-Holocene promoted ice melt in the Arctic which subseqently caused climatic cooling by opening up Arctic channels releasing cold water into the Inner Labrador Current that continued to intensify until 4000 years ago. This sea-level event may also be the best way of measuring when the final ice melted since most estimates of the ages of the last melting are based on end moraine dates in the Arctic which may not coincide with when the last ice actually melted out, since there is no way of dating the final ice positions. Copyright © 1996 Elsevier Science Ltd

INTRODUCTION

In geology, it is often said that the present is the key to the past, but in the study of global climate/sea-level change, the reverse may also be true. There are many predictions in the literature (e.g. Barth and Titus, 1984; Houghton *et al.*, 1990) regarding how sea level may respond to global warming. However, many appear to neglect the most recent global warming that occurred in mid-Holocene (1–4°C, Houghton *et al.*, 1990). This event may be an analogue to the predicted 'greenhouse' warming, since a 4°C rise in temperature (at higher latitudes) is projected if present trends continue (Houghton *et al.*, 1990). During the late mid-Holocene, sea levels in some parts of the world were indeed higher than present (e.g. Dominquez *et al.*, 1987; Giresse, 1989) which are predicted by the most comprehensive geophysical model of sea level, ICE-2 (Peltier, 1988).

The ICE-3G model (Tushingham and Peltier, 1991) provides an updated model but does not include the detail reported in 1988. In the North Atlantic basin (above the equator), no higher-than-present relative sea levels had been reported until recently for the Holocene (except for areas with active isostatic rebound). However, rapid (less than 1000 years) mid-Holocene sea-level oscillations have been suggested by earlier workers for the southeastern United States (Colquhoun and Brooks, 1986; De Pratter and Howard, 1981; Gayes *et al.*, 1992; Scott *et al.*, 1995a, b) and for the Estuary of the St. Lawrence (Dionne, 1988). There are many reports of fluctuating sea levels in Scandinavia (Pirazzoli, 1991), however these appear to be local isostatic adjustments. Much earlier, Fairbridge (1961) had suggested a highly fluctuating sea level throughout the Holocene. Peltier's (Peltier, 1988) models do not predict any important Holocene oscillations in the mid-Holocene for the North Atlantic although this same model does predict the South Atlantic highstand. Most relative sea-level records from the east coast of North America supported the 1988 model predictions, apparently suggesting the eustatic sea-level event that occurred in much of the South Atlantic and many locations in the Indian and Pacific Oceans had no detectable impact in the North Atlantic Basin. By inference, the suggested global warming and rising sea levels caused by anthropogenically induced global warming might also be unevenly distributed and not have much impact in the North Atlantic. However, even the newer, more high resolution models of former sea levels need more fine tuning to predict a rapid, relatively small scale (~2 m) oscillation in sea level.

This paper will focus some of the more newly acquired data from the east coast of North America (Dionne, 1988; Gayes *et al.*, 1992; Scott *et al.*, 1995a, b, Fig. 1) and will attempt to explain the nature and cause of a late mid-Holocene sea-level event.

FIG. 1. Location map of North America showing the positions of the four sea-level sites discussed in this paper.

BACKGROUND OF LONG-TERM SEA-LEVEL CHANGE

In areas such as eastern South America, West Africa and Australia where sea-level changes are largely caused by water volume changes rather than land movement, sea-level rise essentially stopped 4000–6000 years ago and has actually fallen in many places (e.g. Brazil, Dominquez *et al.*, 1987). It has been suggested that the subsequent fall of sea level after the mid-Holocene in Australia (and by comparison in South America) was a result of hydro-isostasy (Chappell *et al.*, 1982) where water loading caused a small emergence along coastlines after the sea-level maximum. Most of the North Atlantic margin is in a tectonically inactive zone but many areas are still experiencing relatively rapid submergence which must be the result of some factor other than eustatic sea-level rise. Many models (e.g. Peltier, 1988; Tushingham and Peltier, 1991) suggest that isostatic adjustment of the Earth's surface following deglaciation plays the major role in relative sea-level change, especially in the North Atlantic, with a smaller contribution from water volume change. These models and many sea-level records from the east coast of North America suggest that this isostatic adjustment affected most, if not all, of the eastern North American coastline over the last several thousand years even though the ice margin ended in New York. Peltier (1988) suggests that all the tide gauge data from the N.E. coast of the U.S. can be explained by isostatic adjustment which conforms with most long-term sea-level records from the eastern seaboard; however Douglas (1991), using the ICE-3G model (Tushingham and Peltier, 1991) suggests a 1.8 mm/year rise globally which is presumably water level rise in addition to isostatic adjustment. Scott *et al.* (1987a) calibrated Quinlan and Beaumont's (1981) model (a small scale derivation of one of Peltier's early models) for a former ice margin in Maritime Canada but calibration to the south has been lacking. However, a direct comparison between an area just at the former ice margin (Nova Scotia) and South Carolina (several hundreds of kilometers south of an ice margin) shows a large differential: about 20 cm/100 years of submergence in the last 2500 years in Nova Scotia (Scott *et al.*, 1995a, b) vs. less than 10 cm/100 years in South Carolina (Murrells Inlet, Gayes *et al.*, 1992). Curves between these areas show varying rates of relative sea-level rise but rates tend to decrease from north to south falling between the extremes of Nova Scotia and South Carolina (e.g. Kraft, 1971). If, as Douglas (1991) suggests, the global average is 1.8 mm/year. (=18 cm/100 years), it has started relatively recently in places like South Carolina where we have dates on salt marsh peat that indicate rates of no more than 10 cm/100 years over the last 500 years.

EVIDENCE OF A RAPID LATE MID-HOLOCENE OSCILLATION IN THE EASTERN NORTH ATLANTIC

The background and evidence for the points shown in Fig. 1 have already been published and discussed thoroughly (De Pratter and Howard, 1981; Dionne, 1988; Colquhoun and Brooks, 1986; Gayes *et al.*, 1992; Scott *et al.*, 1995a, b) but we reproduce the curves of Gayes *et al.* (1992) and Scott *et al.* (1995a, b) here for discussion sake. All points on the curves shown here were determined using marsh foraminiferal zones; the least accurate points (South Carolina) are still accurate to ±30

cm and the most accurate points are accurate to ±5 cm (Nova Scotia). This has to do with regional variations of the vertical range of high marsh foraminiferal faunas (Scott and Medioli, 1980; Collins *et al.*, 1995).

The data in Fig. 2 show that there is a late mid-Holocene sea-level acceleration in the northern hemisphere. Some records from the British Isles suggest a confused signal in the 4000–5000 year interval but it is difficult to say if it is caused by the oscillation observed in North America.

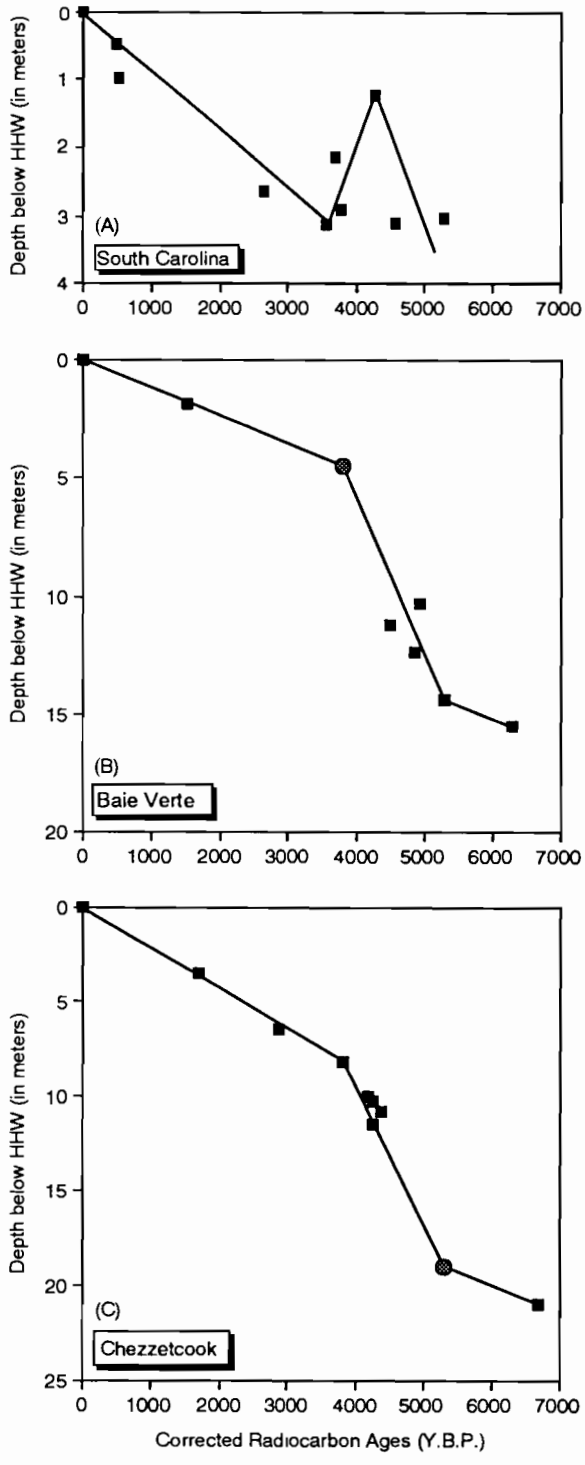

FIG. 2. (A) Sea-level curves from South Carolina from Scott *et al.* (1995a), Baie Verte, Nova Scotia; (B) and Chezzetcook, Nova Scotia; (C) from Scott *et al.* (1995b).

POSSIBLE CAUSATIVE FACTORS

Many climatic records suggest a warming trend in the mid-Holocene followed by a cooling to the 20th Century (see Houghton *et al.*, 1990) that might account for both the rapid rise and fall in sea level (as ice accumulated again after the mid-Holocene). Others suggest ice surging in the Antarctic caused by a steadily rising sea level may cause rapid rises in eustatic sea level (Anderson and Thomas, 1991). Domack *et al.* (1991) suggest increased glacial advances in Antarctica during the mid-Holocene warming which may have enhanced the rapid rise in sea level between 5000 and 4000 BP but fails to explain the subsequent rapid fall that occurs in the mid-Holocene as a result of climatic cooling and probably ice accumulation. In fact, the ice surging in Antarctica could have been a result of eustatic rise, not the cause. It was suggested that the subsequent fall of sea level in Australia might have been the result of hydro-isostatic adjustment, not a eustatic fall in sea level (Chappell *et al.*, 1982). However the time frame appears to be over 5000 years in Australia which clearly does not explain the rapid oscillation we see in South Carolina. Hence we would suggest that the mid-Holocene sea-level oscillation (including the fall of sea level in South Carolina) is a climatic effect rather than a result of ice surging in the Antarctic or hydro-isostasy. If we take this one step further we can actually correlate the mid-Holocene temperature rise (about +4°C globally, Houghton *et al.*, 1990) with various reported values of mid-Holocene eustatic sea level rise varying from 2 m to a high of 5 m (in South America). Some climate models suggest a much lower water volume increase and subsequent rise in sea level (including both thermal expansion and ice melt, 8–12 cm) with an equivalent amount of global warming (about 4°C, Kuhn, 1989) which, based on data here, appears excessively low.

A recent paper (O'Brien *et al.*, 1995) suggests several periods of warming and cooling within the Holocene which could explain the oscillation we see.

MECHANISM PREFERRED FOR THE OSCILLATION

The problem we address is how to explain sufficiently late melting of ice that would have fed the sea-level acceleration shown in Fig. 2A–C, as well as the sea-level highstand observed by Dionne (1988) that occurs simultaneously with the high stand in South Carolina. However, reviewing some earlier paleoceanographic work done on the eastern Canadian margin (Scott *et al.*, 1984, 1989) may provide some insight. Most ideas of when all melting of ice stopped would suggest there was no melting after 6000 BP (e.g. England, 1992; Stravers *et al.*, 1991) but the sea-level oscillation we show here ends at around 4000 BP (sidereal years — Stuiver and Reimer, 1986, 1987). From the ice retreat records of England (1992) and Stravers *et al.* (1991), it would be difficult to suggest ice melting in the Arctic as the cause of the oscillation we see here. But the dates of final ice retreat

are based on dates of terminal moraines, most of which are in contact with the ocean at the time of their formation; once the ice retreated from the coastline there is no record because there are no dates of the absolute last ice due to lack of organic deposition in upland lakes that is used to supply last ice dates farther south (i.e. the Maritimes, Mott, 1975). However, the paleoceanographic records on the eastern Canadian margin might indicate a different story. Scott *et al.* (1984, 1989) show an intensive cooling of shelf currents between 6000 BP and about 3000–4000 BP (dating of the transition is imprecise because of varying sedimentation rates and imprecise palynological records at that interval). The pollen records combined with trends in benthic foraminifera in two Scotian Shelf cores show clearly that cooling of the shelf currents continued long after the climatic optimum (both warmest water and warmest conditions on land) at around 6000 BP (Scott *et al.*, 1984, 1989). The critical question is why the cooling of the eastern Canadian shelf currents began during a seemingly warm period. A second critical question is how much ice would be required to melt to produce a 2 m rise in eustatic sea level (the 10 m rise in Nova Scotia is not realistic as a global response; it almost certainly is a combination of increased isostatic adjustment as well as eustatic sea level so we use the figure from South Carolina as the most realistic amount of water volume). The present day Greenland Icecap holds the equivalent of 6–8 m of sea-level rise if it all melted (Reeh, 1985). That means if only the equivalent of 1/3 of the present Greenland Icecap were in the Canadian Arctic after 5000 BP (on Baffin Island and other Arctic Islands), its melting could produce 2 m of water level rise. Given the size of Baffin Island and the other Arctic islands it is not particularly unreasonable to have had that much residual ice that may not have left a dateable trace if the margins were not on the coastline.

Prior to 5000 BP, the Labrador Current which comprises the shelf water on the eastern margin of Canada was a mixture of the Canada Current coming out of Baffin Bay, and the Irminger Current branching off the North Atlantic Drift around the southern tip of Greenland, a relatively high temperature (4°C) at high salinity (34.5‰) water mass. At about 5000–6000 years ago, this current begins to cool and divides into two components — the Inner Labrador Current (0–2°C, 31–33‰) and the Outer Labrador Current (same charactistics as the old Labrador Current). This roughly coincides with a cooling trend observed in SW Baffin Bay (Osterman, 1982), and attributed to Arctic water inflow through Nares Strait. The transition of cooling to present conditions ends at about 4000–3500 BP (^{14}C years, 4000–4500 BP sidereal years BP) with the complete separation of the Outer Labrador Current (300–800 m water depth offshore) and the Inner Labrador Current (0–300 m). The Inner Labrador Current extends along the entire eastern Canadian margin with its southern limit on the northern half of the Scotian Shelf where the position of its contact with Gulf Stream derivative water (Houghton *et al.*, 1978) does not appear to have changed since 3000–4000 years ago (Scott *et al.*, 1984). Along the rest of the eastern Canadian margin, there is a dynamic division between cold, low salinity Inner Labrador Current and warmer high salinity Outer Labrador Current at water depth greater than 300 m (Scott *et al.*, 1984; Williamson *et al.*, 1984).

Off eastern Canada, it appears that an increased input of meltwater intensified the Inner Labrador Current and drove the temperature down on land. How long did this melting continue? We would say that melting continued at least until the Inner Labrador Current reached its maximum strength about 4000 years ago, much later than most ice models would suggest, and this melting could account for the late mid-Holocene sea-level oscillation. In the Nova Scotia sea-level curves, it appears that the rate of sea-level rise actually accelerated at 5000 years ago (Fig. 3, Baie Verte) which is when cooling started in the offshore currents.

Hence the mechanisms of melting and cooling are working against each other here — increased warming promotes more ice melting but more ice melting intensifies the Arctic currents which result in colder currents to the south. This, as we see from the climate (i.e. pollen) record, has caused a sharp cooling in eastern Canada (e.g. McCarthy *et al.*, 1995), but farther south the mid-Holocene warming to cooling is not detectable (Wright, 1976, 1977) possibly because of the limited influence of the Inner Labrador Current.

This is a classic example of feedback mechanisms acting in opposition. How will this continue in the future if there really is global warming — conceivably it could cause more warming in the north, more melting of, for example, the Greenland Ice Cap, and more intensification of the Inner Labrador Current, causing this cold current to extend its range farther south causing cooling of coastal climates farther south.

This relationship shows the strong link between oceanic and terrestrial cooling together with sea level. Here we believe the local intensification of the Inner Labrador Current is an indicator of melting (i.e. sea-level rise) that had a global effect on sea level and ended when the intensification of the Inner Labrador Current caused sufficient cooling farther south to end the melting by 4000 BP and end the late mid-Holocene sea-level rise.

A well-dated historical event, the ending of pyramid building in Egypt, also happened at almost exactly the same time as the sea-level high in South Carolina (4200 BP, 2200 B.C., Roberts, 1995). It is suggested by Roberts (1995) that at 2200 B.C. the climate cooled, causing drought and pyramid building stopped. This is so close to the sidereal date of the highstand in South Carolina (4214 BP) to be almost unbelievable but clearly the two dates were obtained totally independently in complete isolation from each other. Not being familiar with all the archeological literature, we do not know of other instances like the pyramid building that may have ended at the same time but certainly this does appear to show a direct link between climate deterioration and changes in human activities that should be explored further. Is this an example of a climate/sea level having an historical impact on a large civilization? If so, maybe the Egyptian

experience should be examined more carefully to see exactly what affects caused their demise — was it sea-level change or climate change or both?

IMPLICATIONS FOR THE FUTURE

Although the former mid-Holocene high stand of sea level is lower than present day in the North Atlantic, it does indicate that rapid climatic fluctuations can cause a sharp variation in the rate of sea-level change in a short term event. Also we can see variance of response to this change from South America, where the amount of sea-level rise was over 5 m, to only 2 m in South Carolina. It was perhaps less in the northeast United States and Canada with no detectable fall in sea level (at this point at least) north of South Carolina. The variance in response might be two-fold: unequal distribution of meltwater that maintains an equipotential sea surface (Tushingham and Peltier, 1991) and/or isostatic adjustment which appears to mute the subsequent fall to just a decrease in the rate of RSL rise as you approach the former ice center. In Quebec only the acceleration that overtakes the rebound can be observed and it is impossible to measure the rate of water volume decrease over the emergence caused by isostatic rebound.

If there is a 'greenhouse' induced global sea-level rise, will it rise to a maximum and then fall (as in the mid-Holocene event)? From the mid-Holocene experience, this is a real possibility — increased warmth in the North producing more transfer of cold water to the South. But, for records covering the last 2000 years along the eastern seaboard of North America, there is no evidence of an accelerated sea-level rise in the last 100 years and hence no suggestion that the 'greenhouse' effect is causing a rise in sea level yet (Peltier, 1988); this could be a result of non-detection (as tide gauges would suggest, Douglas, 1991). Most of the mid-Holocene warming appears to have taken place prior to 6000 BP (Houghton *et al.*, 1990) while most of the higher sea levels occurred at least 1000 years later. However, one possible explanation for the delay overall is that ice melt was initiated at the climatic maximum and continued for some time after the maximum temperatures, causing the lag in sea-level response. If the same climatic phenomenon occurs again, a global warming occurring in the near future (i.e. over the next 100 years) might register a sea-level response that lags behind the global warming trend, and be in the order of a few metres of eustatic sea level rise, not a few centimetres as some climate models predict (e.g. Kuhn, 1989). A very recent paper (O'Brien *et al.*, 1995) indicates an extremely complex Holocene climate from the Summit Ice Core in Greenland. This ice record shows several coolings during the Holocene. One occurs at 2400–3100 years ago which is after the mid-Holocene highstand, but might account for the drop in sea level that is observed in South Carolina, South America and Africa.

ACKNOWLEDGEMENTS

We would like to thank our many colleagues at the Chile Meeting of IGCP Project 367 who provided us with vigorous discussion which led to some of the ideas in this paper. Partial funding was provided by the Natural Sciences and Engineering Research Council of Canada Operating Grants to Scott. This is a contribution to IGCP Project 367.

REFERENCES

Anderson, J.B. and Thomas, M.A. (1991). Marine ice-sheet decoupling as a mechanism for rapid, episodic sea-level change: the record of such events and their influence on sedimentation. *Sedimentary Geology,* **70,** 87–104.

Barth, M.C. and Titus, J.G. (eds). (1984). *Greenhouse Effect and Sea Level Rise.* New York: Van Nostrand Reinhold Company, 325 p.

Chappell, J., Rhodes, E.G., Thom, B.G. and Wallensky, E. (1982). Hydro-isostasy and the sea-level isobase of 5500 B. *P. on North Queensland, Australia. Marine Geology,* **49,** 81–90.

Collins, E.S., Scott, D.B., Gayes, P.T. and Medioli, F.S. (1995). Foraminifera in Winyah Bay and North Inlet marshes, South Carolina: Relationship to local pollution sources. *Journal of Foraminiferal Research,* **25,** 212–223.

Colquhoun, D.J. and Brooks, M.J. (1986). New evidence from the southeastern United States for eustatic components in the late Holocene sea levels. *Geoarcheology,* **1,** 275–291.

De Pratter, C. and Howard, J.D. (1981). Evidence for a sea-level lowstand between 4500 and 2400 years b.p. on the southeast coast of the United States. *Journal of Sedimentary Petrology,* **51,** 1287–1296.

Dionne, J.C. (1988). Holocene relative sea-level fluctuations in the St. *Lawrence Estuary, Quebec, Canada. Quaternary Research,* **29,** 233–244.

Dominquez, J.M.L., Martin, C. and Bittencourt, A.C.S.P. (1987). Sea-level history and Quaternary evolution of river mouth-associated beach-ridge plains along the east-southeast Brazilian coast — a summary. *In*: Nummendahl, D., Pilkey, O.H. and Howard, J.D. (eds), *Sea-Level Fluctuations and Coastal Evolution. SEPM Special Publ.*, **41**, 115–128.

Domack, E.W., Jull, A.J.T. and Nakao, S. (1991). Advance of east Antarctic outlet glaciers during the hypsithermal: implications for the volume state of the Antarctic ice sheet under global warming. *Geology,* **19,** 1059–1062.

Douglas, B.C. (1991). Global sea level rise. *Journal of Geophysical Research,* **96,** 6981–6992.

England, J. (1992). Postglacial emergence in the Canadian High Arctic: integrating glacioisostacy, eustasy, and late deglaciation. *Canadian Journal of Earth Sciences,* **29,** 984–999.

Fairbanks, R.G. (1989). A 17,000-year glacio-eustatic sea level record: Influence of glacial melting rates in the Younger Dryas event and deep ocean circulation. *Nature,* **342,** 637–642.

Fairbridge, R.W. (1961). Eustatic changes in sea level. *In*: Ahrens, L.H., Press, F., Rankama, K. and Runcorn, S.K. (eds), *Physics and Chemistry of the Earth.* **4**, 99–185.

Gayes, P.T., Scott, D.B., Collins, E.S. and Nelson, D.D. (1992). A late Holocene sea-level irregularity in South Carolina. *In*: Fletcher, C. and Wehmiller, J. (eds.), *Quaternary Coasts of the United States: Marine and Lacustrine Systems. SEPM Special Publication*, **49**, 155–160.

Giresse, P. (1989). Geodynamique des lignes de rivage Quaternaires du continent Africain et applications. *In*: Scott, D.B., Pirazzoli, P.A. and Honig, C.A. (eds), *Late Quaternary Sea- Level Correlation and Applications. Kluwer Publishing, NATO ASI Series C*, **256**, 131–152.

Houghton, R.W., Smith, P.C. and Fournier, R.O. (1978). A simple model for cross-shelf mixing on the Scotian Shelf. *Journal of the Fisheries Research Board, Canada,* **35,** 414–421.

Houghton, J.T., Jenkins, G.J. and Ephraums, J.J. (eds) (1990). *Climate Change, The IPCC Scientific Assessment.* Cambridge University Press, 365p.

Kraft, J.C. (1971). Sedimentary facies patterns and geologic history of a Holocene marine transgression. *Geological Society of America, Bulletin,* **82,** 2131–2158.

Kuhn, M.A. (1989). The role of land ice and snow in climate. *In*: Berger, A., Dickinson, R.E. and Kidson, J.W. (eds), *Understanding Climate Change*. Geophysical Monograph 52, IUGG 7, American Geophysical Union, 17–28.

McCarthy, F.M.G., Collins, E.S., McAndrews, J.H., Kerr, H.A., Scott, D.B. and Medioli, F.S. (1995). A comparison of postglacial arcellacean ('thecamoebian') and pollen succession in Atlantic Canada, illustrating the potential of Arcellaceans for paleoclimatic reconstruction. *Journal of Paleontology,* **69,** 980–993.

Mott, R.M. (1975). Palynological studies of lake sediment profiles from southwestern New Brunswick. *Canadian Journal of Earth Sciences,* **12,** 273–288.

O'Brien, S.R., Mayenski, P.A., Meeker, L.D., Messe, D.A., Twickler, M.S. and Whitlaw, S.I. (1995). Complexity of Holocene climate as reconstructed from a Greenland Ice Core. *Science,* **270,** 1962–1964.

Osterman, L.E. (1982). Late Quaternary history of southern Baffin Island, Canada: a study of foraminifera and sediments from Frobisher Bay. Ph.D. thesis, University of Colorado, 380 pp.

Peltier, W.R. (1988). Lithospheric thickness, Antarctic deglaciation history and ocean basin descretization effects in a global model of post-glacial sea-level change: A summary of some sources of nonuniqueness. *Quaternary Research,* **29,** 93–112.

Pirazzoli, P.A. (1991). *World Atlas of Holocene Sea-level Changes.* Amsterdam: Elsevier Oceanography Series 58, Elsevier Publishing, 300 pp.

Quinlan, G. and Beaumont, C. (1981). A comparison of observed and theoretical postglacial relative sea level in Atlantic Canada. *Canadian Journal of Earth Sciences,* **18,** 1146–1163.

Reeh, N. (1985). Attachment 8, Greenland ice-sheet mass balance and sea-level change. *In*: Meier, M.F. *et al.* (eds), *Glaciers, Ice Sheets, and Sea Level. Effect of a CO_2-Induced Climatic Change*, Report of Workshop held in Seattle, Wash., Sept. 1984, U.S. Department of Energy, Contract DE-FG01-84ER60235, 155-171.

Roberts, D. (1995). Egypt's Old Kingdom. (Washington DC). *National Geographic,* **187,** 2–44.

Scott, D.B., and Medioli, F.S. (1980). Quantitative studies of marsh foraminiferal distributions in Nova Scotia and comparison with those in other parts of the world: implications for sea level studies. *Cushman Foundation for Foraminiferal Research*, Special Publication No. 17, 58 p.

Scott, D.B., Mudie, P.J., Vilks, G. and Younger, D.C. (1984). Latest Pleistocene-Holocene paleoceanographic trends on the continental margin of Eastern Canada: Foraminiferal, Dinoflagellate, and Pollen evidence. *Marine Micropaleontology,* **9,** 181–218.

Scott, D.B., Boyd, R. and Medioli, F.S. (1987). Relative sea-level changes in Atlantic Canada: observed level and sedimentological changes vs. theoretical models. *In*: Nummendahl, D., Pilkey, O.H. and Howard, J.D. (eds), *Sea-level Fluctuations and Coastal Evolution. SEPM Special Publ.*, **41**, 87–96.

Scott, D.B., Baki, V. and Younger, D.C. (1989). Latest Pleistocene-Holocene paleoceanographic changes on the eastern Canadian Margin: stable isotopic evidence. *Palaeogeography, Palaeoclimatology, Palaeoecology,* **74,** 279–295.

Scott, D.B., Gayes, P.T. and Collins, E.S. (1995). Mid-Holocene precedent for a future rise in sea level along the Atlantic Coast of North America. *Journal of Coastal Research,* **11,** 615–622.

Scott, D.B., Brown, K., Collins, E.S. and Medioli, F.S. (1995). A new sea-level curve from Nova Scotia: evidence for a rapid acceleration of sea-level rise in the late mid-Holocene. *Canadian Journal of Earth Sciences,* **32,** 12 pp.

Stravers, J.A., Miller, G.H. and Kaufman, D.S. (1991). Late glacial ice margins and deglacial chronology for southeastern Baffin Island and Hudson Strait, eastern Canadian Arctic. *Canadian Journal of Earth Sciences,* **29,** 1000–1017.

Stuiver, M. and Reimer, P.J. (1986). A computer program for Radiocarbon age calibration. *Radiocarbon,* **28,** 1022–1030.

Stuiver, M. and Reimer, P.J. (1987). *User's Guide To The Programs CALIB and DISPLAY 2.1.* Quaternary Isotope Lab, University of Washington, Seattle.

Tushingham, A.M. and Peltier, W.R. (1991). ICE-3G: A new global model of Late Pleistocene deglaciation based upon geophysical predictions of post-glacial relative sea level change. *Journal of Geophysical Research,* **96,**B3 4497–4523.

Williamson, M.A., Keen, C.E. and Mudie, P.J. (1984). Foraminiferal distribution on the continental margin off Nova Scotia. *Marine Micropaleontology,* **9,** 219–239.

Wright, H.E., Jr (1976). The dynamic nature of Holocene vegetation, a problem in paleoclimatology, biogeography, and stratigraphic nomenclature. *Quaternary Research,* **6,** 581–596.

Wright, H.E., Jr (1977). Quaternary vegetation history - some comparisons between Europe and America. *Annual Review of Earth and Planetary Science,* **5,** 123–158.

Pergamon

Quaternary Science Reviews, Vol 15, pp 857–871, 1996

PII: S0277-3791(96)00062-5
0277-3791/96 $32.00

A WARM INTERGLACIAL EPISODE DURING OXYGEN ISOTOPE STAGE 11 IN NORTHERN CHILE

LUC ORTLIEB,*‡ AMANDA DIAZ*† and NURY GUZMAN‡

**ORSTOM (Institut Français de Recherche Scientifique pour le Développement en Coopération), Casilla 1190, Antofagasta, Chile*

Marine Invertebrate Museum, Division of Marine Biology and Fisheries, Rosenstiel School of Marine and Atmospheric Sciences, University of Miami, 4600 Rickenbacker Cswy, Miami, FL 33149, U.S.A.

‡Facultad de Recursos del Mar, Universidad de Antofagasta, Casilla 170, Antofagasta, Chile

Abstract — Combined palaeontological, morphostratigraphic and geochronologic data from emerged Middle Pleistocene coastal deposits in Mejillones Peninsula (23°S), northern Chile, strongly suggest that climatic conditions were particularly warm during the Oxygen Isotope Stage 11 high seastand episode. An anomalous warm-water molluscan assemblage from localities assigned to that interglaciation included several extralimital species, presently living only north of 6°S (or 14°S), that were not present in the area during subsequent Middle and Late Pleistocene, or Holocene, interglacial episodes. Only two of these extralimital species may be found nowadays at the 23°S latitude, in a protected locality, immediately after the occurrence of strong El Niño events. Many of the species of the thermally anomalous molluscan assemblage (TAMA) are the same as those which lived in a closed shallow lagoon near Santa, north-central Peru (9°S) during a brief mid-Holocene episode. The new findings thus indicate that lagoonal and protected embayments were significantly warmer than the open marine environment ca. 400 ka. Actually, the co-occurrence of cool water fauna in exposed sectors of the coastline at that time suggests that the coastal upwelling activity and the Humboldt Current effects were not strongly reduced. The warm-water conditions prevailing in lagoons and protected bays during the Mid-Brunhes episode may reflect particularly warm air temperatures and distinct ocean–atmosphere relationships than those prevalent nowadays. These data support the hypothesis that the Oxygen Isotope Stage 11 was the warmest interglaciation, at least in the southern hemisphere. Copyright © 1996 Elsevier Science Ltd

INTRODUCTION

Sea Level and Climatic Variations During the Last Million Years

During the last million years, the inter-related climatic and sea level fluctuations were strongly controlled by astronomical forcing (Milankovitch cycles of 23–19, 40 and 100 ky), with a predominance of the 100 ky cycle on the glaciations/interglaciations rhythm (e.g. Shackleton and Opdyke, 1973; Hays *et al.*, 1976; Imbrie and Imbrie, 1980; Imbrie *et al.*, 1992; Liu, 1992, 1995). It is commonly admitted that the interglacial episodes have been characterised by a sea level position close (within a few meters) to the present datum, and by global climatic conditions that compared with those experienced in the Holocene. The oxygen-isotope composition of plankton foraminifers from the world oceans indicates that, from one interglacial stage to the other, the sea surface temperature (SST) was in the same range, at least during the last half-million years (Shackleton and Opdyke, 1973; Hays *et al.*, 1976).

Oxygen Isotope Stage 7 is generally considered as having been a little colder than stages 1 (Holocene), 5, 9 and 11 (Shackleton, 1987), but no consensus was met as to which of the latter was the warmest isotopic stage. Discrepancies are observed between deep-sea core data from the various oceans and at distinct latitudes. According to many deep-sea records, the only, or major, episode warmer than the Holocene would have occurred at the beginning of the last interglacial, during Oxygen Isotope Substage 5e (Shackleton and Opdyke, 1973; Kellogg, 1977; Shackleton, 1987). An indirect confirmation of a relatively higher global temperature during the early stage of the last interglaciation is provided by widely scattered evidence for a higher sea level than nowadays at ca. 120 ka. A slightly more elevated "eustatic" sea level stand at that time (some 5–7 m above present datum?) is classically interpreted as a consequence of major global sea water volume than nowadays, a minor size of the polar ice sheets, warmer air temperature and SST. The paleo-position of "eustatic" sea level during former interglaciations is difficult to

assess for Middle Pleistocene times (700–140 ka): it can be established with some precision for Oxygen Isotope Substage 5e, but it is increasingly less precise for Oxygen Isotope Stages 7, 9 and 11. In numerous coastal areas of the world, regional and local tectonic instability as well as glacio-isostatic effects hamper a precise reconstruction of paleo-sea level position from emerged terraces and reef tracts.

A Warmer Interglacial Episode During Oxygen Isotope Stage 11?

In a recent review on multiple evidence for warmer than usual Pleistocene interglacial stages, Burckle (1993) concluded that Oxygen Isotope Stage 11 probably had been warmer than the present and the last three previous interglacial episodes. The most convincing evidence for such interpretation comes from the southern hemisphere, and includes: carbonate-rich layers in the southern Pacific Ocean at ca. 400–500 ka (Kennett, 1970), particularly high rate of opal accumulation during Oxygen Isotope Stage 11 in the southern Atlantic Ocean (Charles *et al.*, 1991), greater fluxes of North Atlantic Deep Water (NADW) into the Southern and Indian oceans during Oxygen Isotope Stage 11 (Oppo *et al.*, 1990; Hodell, 1993). On the basis of radiolarian and other data from the southern Indian Ocean, Morley (1989) and Howard and Prell (1992) also determined that Stage 11 had been the warmest, and longest, interglacial stage in the last half-million years.

As in the northern hemisphere deep sea record, the indications for a particularly warm Stage 11 are scarce (e.g. Ruddiman and McIntyre, 1976; Ruddiman *et al.*, 1986, 1989; Aksu *et al.*, 1992) or lacking. It may be hypothesised that during that particular interglaciation, anomalous warm climatic conditions were restricted to the southern hemisphere, and were not a global feature. From an orbital point of view, the Oxygen Isotope Stage 11 interglaciation actually corresponds to an eccentricity low (413 ky component) that, according to the Milankovitch theory, should have been rather colder than observed. It is the '400 ka problem' of Imbrie and Imbrie (1980), and the 'Isotopic Stage 11 problem' of Imbric *et al.* (1993) which pointed that the $\delta^{18}O$ response in the deep oceans was, for some reason, not proportional to the postulated forcing.

Paleoceanographic records of this particular interglaciation from nearshore environments may be of great value, since they may provide some interesting clues to solve the paradox of the Mid-Brunhes climate (Jansen *et al.*, 1986). In apparent contradiction with some of the deep sea record from the northern hemisphere, it may be mentioned that some indication for exceptionally warm conditions were provided by coastal faunas from northwestern Alaska. There, the Anvilian emerged coastal deposits contain a series of molluscan species that are either extinct and/or of warmer water than the present fauna (MacNeil *et al*., 1943; Hopkins, 1967); this unit had been assigned to the Early Pleistocene (Hopkins *et al.*, 1974) until a radiometric age determination and aminostratigraphic analyses strongly suggested that it was of Middle Pleistocene age, and probably coeval with Oxygen Isotope Stage 11 (Kaufman *et al.*, 1991; Kaufman and Brigham-Grette, 1993).

In this note we present paleontological data from the northern coast of Chile that supports the hypothesis of a warm interglacial period assigned to Oxygen Isotope Stage 11. The faunal assemblage, characterised by the predominance of extralimital species from the Panamic Province (Fig. 1), strongly suggests much warmer conditions than during any other Quaternary high seastand episode, including the present one.

QUATERNARY MARINE DEPOSITS OF MEJILLONES PENINSULA

Regional Geological Setting

The subduction of the Nazca Plate below the South American continent is responsible for uplift motions along the coast of northern Chile and southern Peru. The neotectonic behaviour of the northern Chile coast is documented by marine terraces formed during Pliocene and Pleistocene high seastands on the narrow coastal plain lying at the foot of the Coastal Cordillera. Thick accumulations of alluvium generally hide the highest lying emerged wave-cut platforms (Ortlieb *et al.*, 1996a). Plio-Pleistocene marine-abraded surfaces and Quaternary beach-ridge series are well preserved in Mejillones Peninsula, a 60 × 40 km large crustal block located immediately north of Antofagasta (23°S; Figs 1 and 2). The peninsula is crossed by major fracture zones which are partly active, and several faulted blocks show differential uplift motions (Okada, 1971; Ferraris and Di Biase, 1978; Armijo and Thiele, 1990). The peninsula exhibits three exceptional sequences of regressive beach ridges formed on gentle slopes that extend on hundreds of km^2 from an elevation of the order of 200 m and the present coastline (Ortlieb, 1993; Ortlieb *et al.*, 1995). The two major series of beach ridges are found on the north (Pampa Mejillones) and south (Pampa del Aeropuerto) sides of the wide isthmus linking the coastal plain to the peninsula. As a result of the extreme aridity of the area, the sediments and faunal remains of the beach ridges are generally very well preserved. The abrasion terraces and beach ridges document the Quaternary uplift of distinct sectors of the peninsula (Ortlieb, 1993; Ortlieb *et al.*, 1995, 1996b), and also provide an unusual insight into palaeoceanographic conditions during succeeding episodes of interglacial high sea-stands.

The age of the emerged Pleistocene coastal deposits in the area is still actively debated. We shall mention briefly the previous morphostratigraphic interpretations and present some results of on-going morphostratigraphic and geochronologic studies. For this purpose, three key areas will be considered: the coastal region along the northern half of Antofagasta Bay; Pampa del Aeropuerto; and Pampa Mejillones.

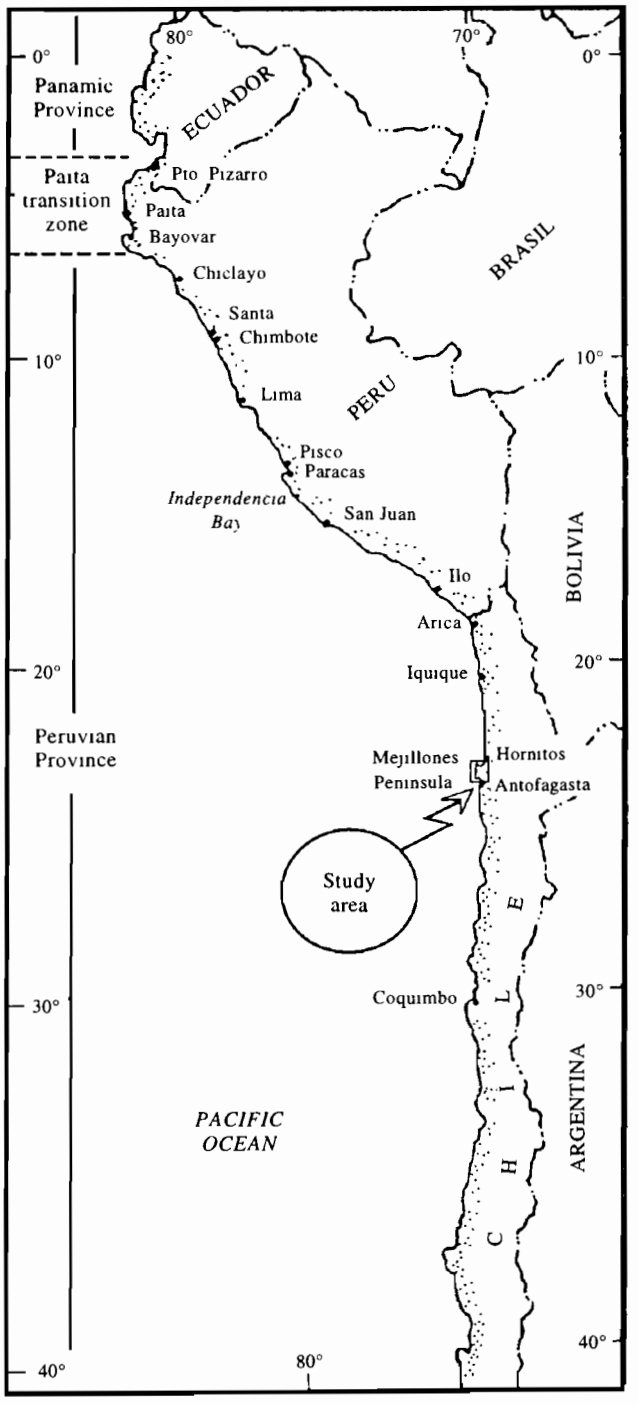

FIG. 1. Locality map of the Peru–northern Chile coasts, with indication of the boundaries of marine faunal provinces.

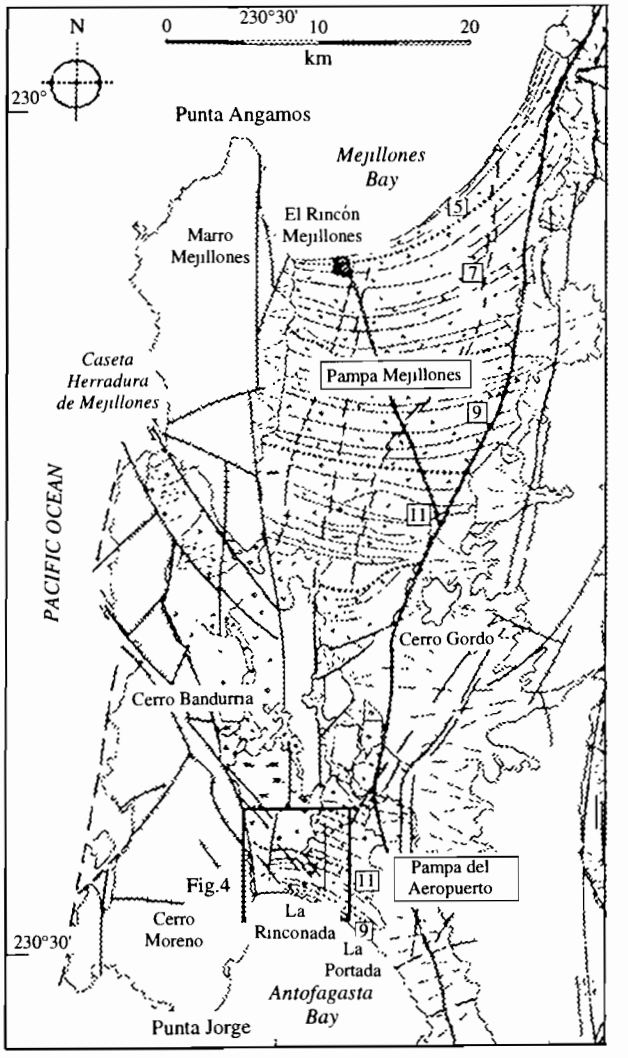

FIG. 2. Sketch map of Mejillones Peninsula, and location of the study area, near La Rinconada, north of Antofagasta Bay. The sets of Pleistocene beach ridges that form Pampa Mejillones and Pampa del Aeropuerto are assigned to successive interglacial episodes identified by the respective number of Oxygen Isotope Stage (5, 7, 9, 11), according the interpretation proposed by Ortlieb *et al.* (1996b).

Quaternary Marine Deposits along Antofagasta Bay

Antofagasta Bay is bordered to the northeast by a vertical seacliff that cuts an ~40 m thick sequence of Pliocene marine calcarenites, coquina and sandstones (La Portada Formation; Ferraris and Di Biase, 1978) covered by Pleistocene unit that is a few meters thick and composed of marine deposits and alluvium. The Pleistocene coastal sediments are loosely consolidated sands with interlayered coquina beds. They correspond to a single marine terrace unit.

New geochronological data recently obtained on mollusk shells from this last unit, at the locality called La Portada (Fig. 3), strongly suggest an Oxygen Isotope Stage 9 age (Ortlieb *et al.*, 1995). Two sets of 14 valves of each of the two dominant species (*Mulinia* cf. *edulis* and *Mesodesma donacium)* yielded mean allo/isoleucine ratios of 0.66±0.10 and 0.67±0.12, respectively. These values compare with the mean A/I ratio of 0.71 yielded by samples (from the same bivalve species) on the third emerged terrace at Hornitos (22°55′S; Ortlieb *et al.*, 1996a) and can be assigned regionally to the Stage 9 interglacial episode. Furthermore, three U/Th age determinations (obtained at GEOTOP, Université du Québec à Montréal) on shells from the same locality yielded the following results: 282±9 ka for one measurement through the TIMS (thermal ionisation mass spectrometry) technique, and 275±11 ka and 288±12 ka (mean = 282 ka) for two measurements by alpha-spectrometry. These concordant results, and additional morphostratigraphic arguments (Ortlieb *et al.*, 1995), thus strongly suggest that the Quaternary marine terrace that cuts and overlies the

Pliocene La Portada Formation was formed during Stage 9, ca. 300–330 ka.

To the west of La Portada, the seacliff height diminishes progressively as a result of a recent westward tilting of the Plio-Quaternary beds. This attitude is related to a half-graben structure limited westwards by an active major crustal fault. The N–S trending La Rinconada fault separates the uplifted Cerro Moreno block to the west and the Pampa del Aeropuerto plain (Fig. 2). The tilt of the Plio-Quaternary sequence in the northern Antofagasta Bay is accompanied by a series of recent normal faults (which systematically downthrow the western compartments) that belong to a complex *en échelon* system (NNW–SSW and N–S trends; Armijo and Thiele, 1990; Ortlieb *et al.*, 1995).

At the southwestern extremity of the Mejillones Peninsula, several marine abraded platforms were cut at elevations reaching up to about +150 m. Electron Spin Resonance (ESR), U/Th and allo/isoleucine analyses were performed on molluscs from the three lower terraces at Juan Lopez but provided only preliminary results which did not lead yet to a well established chronostratigraphy (Ratusny and Radtke, 1988; Radtke, 1989; Ortlieb *et al.*, 1995). Nevertheless, the faunal content of the deposits associated to two terraces tentatively assigned to the Oxygen Isotope Stages 7 and 9, was studied.

Along the southeastern shore of Antofagasta Bay, the last interglacial high seastand was recorded at elevations varying between +6 (Punta Coloso, Fig. 3) and +15 m (north of Antofagasta; Ortlieb *et al.*, 1994, 1995). Other terrace deposits were tentatively assigned to Oxygen Isotope Stages 7, 9 and 'older than 11' (Ortlieb and Guzmán, 1994; Ortlieb *et al.*, 1994, 1995; Fig. 3). The oldest Pleistocene terrace identified in the surroundings of Antofagasta lies at ca. +100 m elevation (Ortlieb *et al.*, 1995). These Early Pleistocene deposits, as well as some lateral equivalents in the northwestern Pampa del Aeropuerto plain, at ca. +200 m (Fig. 3), are the oldest Quaternary marine units, with characteristic Quaternary fauna (Herm, 1969), that crop out in the Antofagasta Bay area.

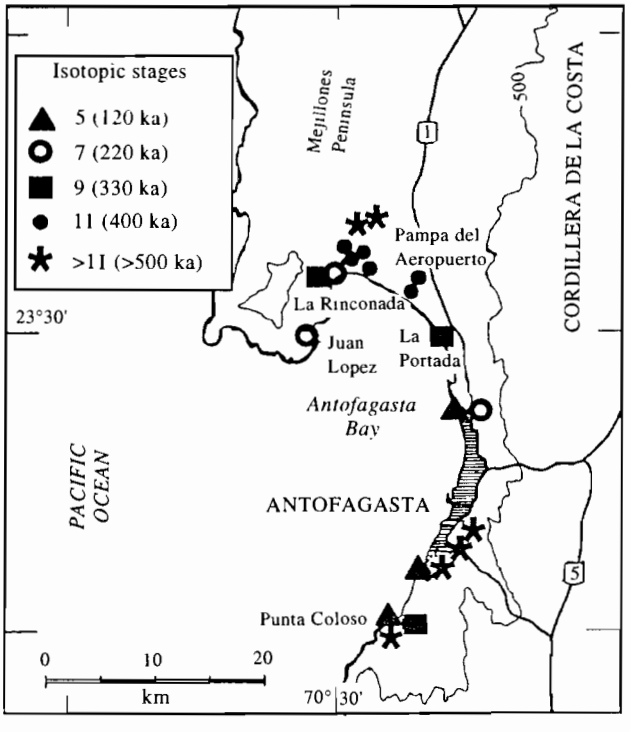

FIG. 3. Sampled localities of Pleistocene marine terraces and associated deposits, around Antofagasta Bay. The faunal content of these deposits is indicated in Table 1.

The Pleistocene Beach Ridges at Pampa del Aeropuerto

Pampa del Aeropuerto is a wide, slightly deformed, elevated coastal plain that slopes southward from the centre of the isthmus, at ca. +200 m elevation, toward the Antofagasta embayment. It is covered by a series of beach ridges disposed in a concentric way and grossly parallel to the present coastline. The beach ridges are well preserved and display beach cusp structures (visible on aerial photographs), that compare with those formed on the present beach at La Rinconada (Fig. 4). The sequence of regressive shorelines may be split into several sets that were most probably formed during succeeding episodes of interglacial high sea stands.

The age of the sets of beach ridges is still a matter of discussion. A Pliocene age was suggested on the geological map (Ferraris and Di Biase, 1978), while several authors had envisaged, without any precise study of the emerged marine deposits, that the whole beach ridge sequence might be as young as Late Pleistocene (Okada, 1971; Armijo and Thiele, 1990). However, the assignation of the Quaternary unit at the top of the seacliff at the locality of La Portada (see above) to the Oxygen Isotope Stage 9 implies that the Pampa del Aeropuerto beach ridges sets are necessarily older than 330 ka. In the northern part of Pampa del Aeropuerto, the oldest beach ridges of the sequence are observed either at the foot of a major (50 m high) paleo-seacliff (Pleistocene marine limit) or in offlap disposition upon Pliocene marine units. It is thus inferred that the older part of the beach–ridge sequence is of Early Pleistocene (or early Middle Pleistocene?) age, and that the whole beach–ridge sequence was formed in the lapse of several hundred thousand years.

The geometry of the coastal features of the area indicates that the Pampa del Aeropuerto plain was steadily uplifted until a strong deformation phase which occurred at the end of the Middle Pleistocene. This deformation included the faulting of the Plio-Pleistocene units by the NNW–SSE en *échelon* system, the dipping of recent Quaternary units (last three interglacial coastal deposits) below sea level at La Rinconada, and the upwarp of a small faulted block northwest of La Rinconada. It is on top of this southward tilted fault block and in the vicinity of a major NNW–SSE trending fault trace which cuts the western part of Pampa del Aeropuerto, that were found the outcrops of the anomalously warm faunal assemblage studied here. The lateral correlation between individual beach ridges across the large NW-trending fracture zone indicates clearly that

FIG. 4. Aerial photograph of Pampa del Aeropuerto, in the southern part of the isthmus of Mejillones peninsula (Instituto geogiáfico Militar, Hycoon 10089). The La Rinconada tilted fault block is visible to the left. Note the continuity of the beach ridges across the large NNW–SSE trending fault zone that separates the La Rinconada block from the rest of Pampa del Aeropuerto. Sample localities are indicated by black dots.

the block faulting and the tilting occurred recently, well after the deposition of the sedimentary units. The set of beach ridges studied here actually predates the marine terrace unit which caps the seacliff at La Portada and which is correlated with Oxygen Isotope Stage 9. Consequently, the former unit is tentatively assigned to the previous interglacial cycle, i.e. Oxygen Isotope Stage 11 (ca. 400 ka).

Quaternary Marine Deposits of Pampa Mejillones

The northern part of the isthmus of Mejillones Peninsula is another large (400 km^2) plain slowly dipping northward, toward Mejillones Bay (Fig. 2). It is bounded to the west by the N–S trending Mejillones fault and extends eastward to the foot of the Coastal Cordillera. Pampa Mejillones plain reaches a maximum elevation of +220 m and is almost totally covered with beach ridges sub-parallel to the present coastline of Mejillones Bay. This series of regressive shorelines have a major extension than its counterpart on the southern side of the Mejillones Peninsula. The ridges, also very well preserved and disposed in successive sets, are several tens of metres wide, some 2 to 5 m high and may be more than 20 km long. They consist of coarse, fossiliferous, loosely consolidated sediment. The ridges are separated by wide shallow troughs, now generally covered by a sheet of eolian sand. Like in Pampa del Aeropuerto, the geometric disposition of the ridge sequence shows that after a relatively long period of steady uplift, the plain suffered a strong tectonic deformation with major N–S trending normal faulting. The vertical displacement produced by these faults are of several meters, and may locally reach 20 m (Armijo and Thiele, 1990; Ortlieb *et al.*, 1995).

The precise chronostratigraphy of the series of beach ridges is yet unresolved. Herm (1969) showed that the ridges were post-Pliocene, and interpreted that a major discontinuity in the geometry of the beach ridge sets marked a limit between 'Middle Pleistocene' Serena II and 'Early Pleistocene' Serena I deposits. Alternatively, Ferraris and Di Biase (1978) mapped the northern half of

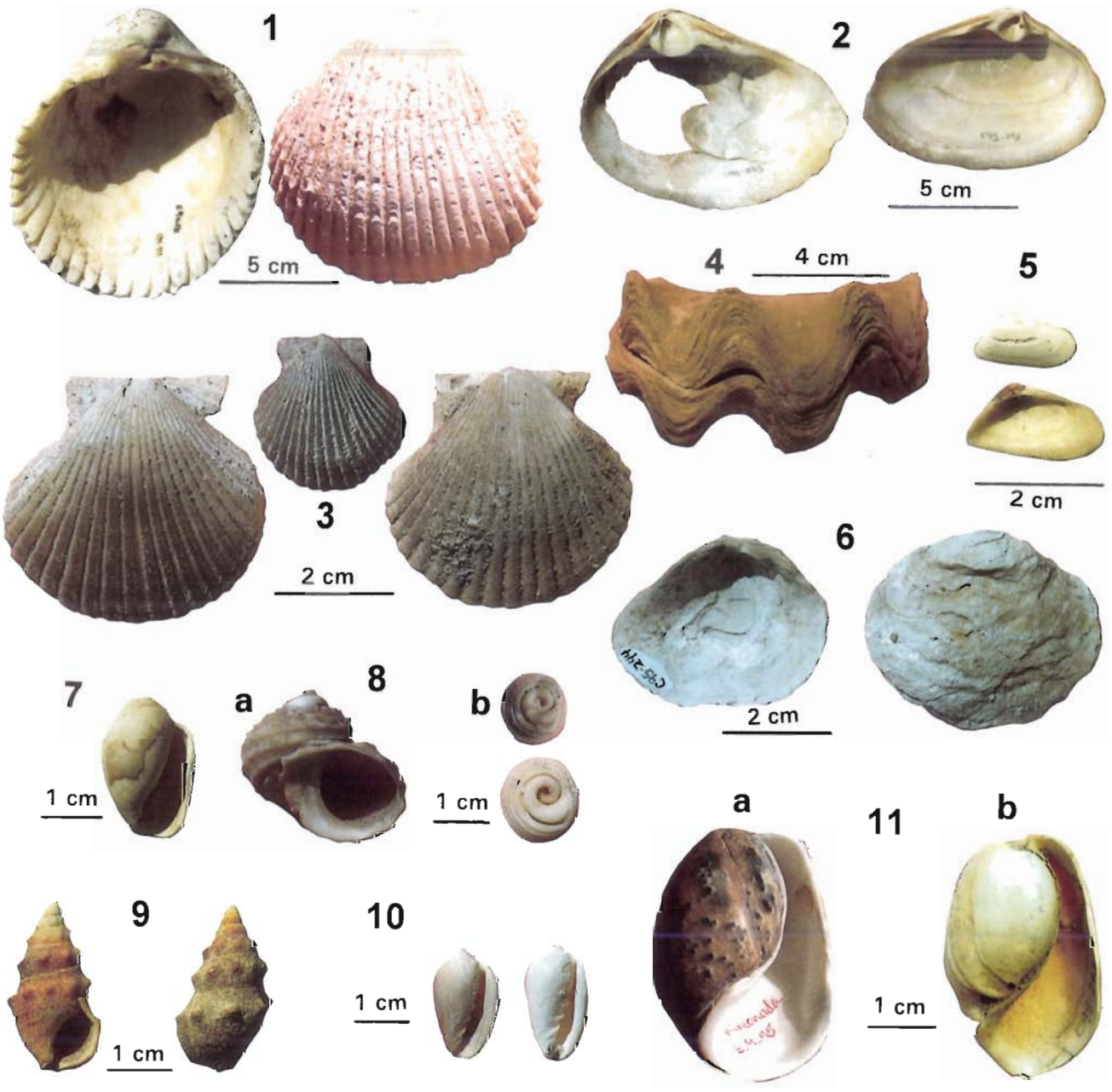

FIG. 5. Some of the most abundant extralimital species of the TAMA (thermally anomalous molluscan assemblage) of the 400 ka deposits at La Rinconada locality. All these species have been found living today in the Panamic province and/or in the Paita Transition Zone (see Fig. 1). (1) *Trachycardium* cf. *procerum* (Sowerby, 1833), right valves, interior and exterior views; (2) *Mactra velata* (Philippi, 1849), right (large, fragmented) and left (medium size) valves, interior views; (3) *Argopecten circularis* (Sowerby, 1835), two right valves, medium size, and a juvenile left valve, exterior views; (4) *Ostrea megodon* (Hanley, 1846), whole individual with articulated valves; (5) *Donax peruvianus* (Deshayes, 1855), small left valve (exterior) and right valve (interior); (6) *Anomia peruviana* (d'Orbigny, 1846), upper valves of medium size individuals (interior and exterior); (7) cf. *Melampus* sp., undetermined individual (out of three, not well preserved shells); (8) *Turbo* cf. *fluctuosus* (Wood, 1828): (a) apertural view of medium size individual; (b) two calcareous operculums; (9) *Cerithium stercusmuscarum* (Valenciennes, 1833), apertural and abapertural views; (10) *Prunum curtum* (Sowerby, 1832), apertural view of two individuals; (11) *Bulla punctulata* (A. Adams *in* Sowerby, 1850): (a) apertural view of a recent individual (from La Rinconada locality, collected in Sept. 1995); (b) apertural view of a fossil sample from the ca. 400 ka deposit near La Rinconada.

the beach–ridge sequence as Pleistocene (a so-called 'Mejillones Formation') and the southern half of the plain as Pliocene (La Portada Formation). This interpretation has been accepted by some recent workers (e.g. Flint *et al.*, 1991). According to another interpretation (Okada, 1971; Armijo and Thiele, 1990), the whole series of beach ridges might have been formed during the regression subsequent to the last high seastand (Oxygen Isotope Stage 5). In 1993, Ortlieb proposed to divide the sequence of beach ridges in a series of sets which might be coeval with as many successive interglacial (and/or interstadial) episodes. This hypothesis was based upon a preliminary air-photo interpretation of discontinuities between the successive sets of beach ridges, and on a few previously

available geochronological results (Radtke, 1987, 1989) on the youngest deposits of the Pampa Mejillones sequence (at El Rincón). This interpretation was subsequently slightly modified when we discovered that the deposits cropping out between +150 and up to +200 m in the southern part of Pampa Mejillones were characterised by a warm-water faunal composition similar to that of the youngest set of beach ridges at Pampa del Aeropuerto, near La Rinconada (Ortlieb *et al.*, 1995, 1996b).

U-series and aminostratigraphic analyses performed on shells collected across the Pampa Mejillones sequence did not yet allow precise and conclusive age determinations (Hillaire-Marcel *et al.*, 1995; Ortlieb *et al.*, 1995). High $^{234}U/^{238}Th$ ratios (>1.2), indicators of a non-marine origin of the uranium, and evidence for late diagenetic uptake of this element seriously limit the possibility to calculate the age of the Pampa Mejillones ridges. On the other hand, aminostratigraphic studies did not prove to be entirely reliable. A shallow burial of the molluscan material apparently produced differences in the thermal history of the samples, even if the samples generally yielded increasing allo/isoleucine ratios with the elevation of the ridge sets across the plain. Several measurements in localities with the anomalous warm-water fauna (above +150 m), thus produced allo/isoleucine ratios of the order of 0.9, value compatible with an Oxygen Isotope Stage 11 age in this region (Ortlieb *et al.*, 1995; *in preparation*). Immediately to the northeast of Mejillones Bay, in the area of Chacaya-Hornitos (see Ortlieb *et al.*, 1996a), the three lowermost conspicuous staircased marine terraces were tentatively correlated with Oxygen Isotope Stages 5, 7 and 9.

Thus, difficulties were met in the establishment of a solid chronostratigraphy of the exceptional series of beach ridges at Pampa Mejillones, but the available data suggest that the major part of the sequence was formed during the Middle Pleistocene. A lateral correlation based on paleontological grounds is proposed between two sets of warm-water mollusc bearing deposits from the northern and southern isthmus of Mejillones Peninsula. At Pampa del Aeropuerto, the chronological constraint is better assessed than at Pampa Mejillones and leads us to infer that both anomalous molluscan assemblages are coeval with Oxygen Isotope Stage 11.

THE WARM-WATER MOLLUSCAN ASSEMBLAGE AT LA RINCONADA

The surface of the strongly tilted fault block found 3 km north of La Rinconada is covered by a series of coastal sediments deposited previously to the tectonic deformation, which now lie at increasing elevations, between below +10 m and +80 m, from south to north. On the La Rinconada block, and across the faulted zone that separates the block from the Pampa del Aeropuerto plain, the Pleistocene coastal sediments are one to several meters thick, and lie upon Pliocene beds. They vary between fine sands to pebbly coarse sands, and also include irregularly cemented biocalciruditic coquina beds. In places, a superposition of distinct units points to a depositional regressive sequence, with lagoonal or beach deposits overlying subtidal sediments with *in situ* fauna (articulated shells of pelecypods in living position).

The varied sedimentary units contain distinct faunal assemblages that are either typically warm-water forms (open or closed lagoons, shallow marine environments), or a mix of warm and cold-water forms (nearshore environments and exposed beach). Some beds corresponding to subtidal environments are the only ones that include rather cold-water forms identical to the Holocene fauna of the area (*Argopecten purpuratus* [Lamarck, 1819], *Choromytilus chorus* [Molina, 1782], *Transennella pannosa* [Sowerby, 1835], *Petricola rugosa* [Sowerby, 1834], *Thais chocolata* [Duclos, 1832]). The variety of sedimentary facies and of associated faunal assemblages suggest multiple changes in the palaeogeography of the area, and in the nearshore conditions, within a single episode of interglacial high seastand.

From west to east of Pampa del Aeropuerto plain, a major lateral change is observed in the faunal composition of the same beach ridge set. In sharp contrast to the 'warm' fauna found upon and near the La Rinconada block, the beach deposits of the eastern and central area of the coastal plain bear a cool-water fauna (*Mulinia* cf. *edulis* [King, 1831], *Mesodesma donacium* [Lamarck, 1818], *Glycymeris ovatus* [Broderip, 1832], *Calyptraea trochiformis* [Born, 1778], *Crepipatella dilatata* [Lamarck, 1822], and *Oliva peruviana* [Lamarck, 1811]). This fauna is similar to that found in the older (higher elevated) beach–ridge sets and in the younger marine terrace deposit (Oxygen Isotope Stage 9) at La Portada. As there is no doubt that the deposits bearing cool-water fossils are coeval with those from the La Rinconada area (see Fig. 4), the variation in the faunal composition must be attributed to paleogeographic factors. Cool nearshore conditions were prevalent in the non-protected part of the Antofagasta embayment. It was only in the northwesternmost part of Antofagasta Bay, near La Rinconada, protected from the cool waters of the Humboldt current, that lagoons with restricted circulation could form.

A 'Thermally Anomalous Molluscan Assemblage' (TAMA)

Table 1 compares the composition of molluscan faunas sampled on the La Rinconada block (and adjacent areas; Fig. 4), on the modern beach and in the older and younger Pleistocene deposits (from other interglacial episodes) around Antofagasta Bay (Fig. 3). The fauna upon the 'La Rinconada block' differs significantly from altogether the modern assemblage and the fossil content of the other Late and Middle Pleistocene emerged marine deposits. Because of the predominance of warm-water elements, it constitutes a 'thermally anomalous molluscan assemblage' (= TAMA) as referred to by Valentine (1955), Zinsmeister (1974), DeVries and Wells (1990), Ortlieb *et al.* (1990) and Roy *et al.* (1995).

A number of extralimital species of this TAMA had not

TABLE 1. Comparison of the molluscan fauna around Antofagasta Bay, between deposits assigned to the major high seastands of Oxygen Isotope Stages 5 (ca. 120 ka), 7 (ca. 220 ka), 9 (ca. 330 ka) and 11 (ca. 400 ka), as well as with older (early Middle Pleistocene or Early Pleistocene?) units and with the present day living fauna (Holocene). In bold are indicated the warmer water species only found in the deposits assigned here to the 400 ka high seastand episode. Identification of the species is based on Morris (1966), Keen (1971) and Marincovich (1973). Author and date of the species designation were omitted for the sake of conciseness

Chronostratigraphic units	Hol.	5e	7	9	**11**	>11
GASTROPODS:						
Aeneator fontainei	X	P	P		P	P
Bulla punctulata	(X)				**P**	
Calyptraea (T.) trochiformis	X	V	A	V	V	V
Cancellaria (S.) buccinoides	X	P		P		P
Cerithium stercusmuscarum	—				**A**	
Collisella spp.	X	P	P	P		P
Concholepas concholepas	X	V	A	A	A	V
Crassilabrum crassilabrum	X	V	P	P	P	V
Crepidula spp.	X	A			P	P
Crepipatella dilatata	X	V	P	V	V	A
Crepipatella dorsata	X	V	P	V	V	V
Crucibulum quiriquinae	X	P	P	V	A	P
Diodora saturnalis	—				P	P
Fisurella costata	X	A	P	?		A
Fissurella crassa	X	P				A
Fissurella latimarginata	X	P	P			?
Fissurella maxima	X	P	P	P		P
Fissurella peruviana	X	P			P	P
Fissurella spp.	X	P	P	P	P	A
Liotia cancellata	X	?	?	?	P	?
Littorina (A.) peruviana	X	V				P
cf. *Melampus* sp.	—				P	
Mitra orientalis	X			P		A
Mitrella unifasciata	X				P	P
Nassarius dentifer	?	P				
Nassarius gayi	X	A	P	P	A	V
Nucella (A.) crassilabrum	?		P		P	P
Oliva (O.) peruviana	X	V	A	V	V	V
Olivella sp.	—				**V**	
Polinices (P.) uber	X		P	P	A	
Priene rude	X	V		P	P	P
Priene scabrum	X	A	P	P	V	A
Prisogaster niger	X	V	P	V	V	A
Prunum curtum	—				**A**	
Rissoina inca	X	?	P	?	P	P
Scurria spp.	X	A	P	P		P
Sinum cymba	X	?	P	P	P	
Siphonaria (T.) lessoni	X	P			P	P
Tegula (C.) atra	X	V	A	A		V
Tegula (C.) euryomphala	X	?	P	A	V	V
Tegula (C.) luctuosa	X	P	P		V	
Tegula (C.) tridentata	X	V	P	P	A	V
Thais (S.) chocolata	X	P		V	V	V
Thais haemastoma	X					
Trigonostoma tuberculosum	X		P			
Trimusculus peruvianus	X	P		P		
Turbo* cf. *fluctuosus	—				**P**	
Turritella cingulata	X	A	P	V	V	V
Xanthochorus buxea	X	P			P	P
Xanthochorus cassidiformis	X	P	P	A	P	P

V = Very abundant, A = Abundant, P = Present, X = extant, (X) = exceptionally present, — = not present in the area, ? = probably present, but not collected. Hol. = Holocene (Present), 5e, 7, 9, 11, >11 = Oxygen Isotope Stages

TABLE 1. Continued

PELECYPODS:						
Anomia peruviana					**A**	
Arcopsis solida	—				**P**	
Argopecten circularis	—				**P**	
Argopecten purpuratus	X	V	V	V	V	A
Aulacomya ater	X	P	P	P		P
Barbatia pusilla	X	P			P	P
Brachidontes granulata	X	P	P		P	P
Cyclocardia* cf. *spurca beebei	—				**P**	
Carditella tegulata	X	P	A	P	A	P
Chama pellucida	X	V	P	P	A	V
Chione (L.) peruviana	—	P				
Choromytilus chorus	?	V	A	P	A	V
Cumingia mutica	?				P	
Cyclinella subquadrata	—			P		
Diplodonta inconspicua	X				P	?
Donax peruvianus	(X)				**P**	
Ensis macha	X	P				
Eurhomalea lenticularis	?	A			P	
Eurhomalea rufa	X	V	P	A	A	P
Gari solida	X	P		P		P
Glycymeris ovatus	X	V	A	A	V	A
Mactra velata	—				**A**	
Mesodesma donacium	X	V	P	V	A	P
Mulinia cf. *edulis*	—	P	P	V	V	V
Mysella spp.	X	P			?	
Nucula cf. *exigua*	X		P			
Ostrea cf. *columbiensis*	—		V			
Ostrea megodon	—				**V**	
Perumytilus purpuratus	X	V	A			P
Petricola (P.) rugosa	X				A	
Protothaca (P.) thaca	X	V	V	P	A	A
Protothaca sp.	—				**P**	
Raeta (R.) undulata	—				?	P
Semele solida	X	P	P	V	V	P
Semimytilus algosus	X	P				P
Tagelus dombeii	X	A	P	P	A	P
Trachycardium* cf. *procerum	—				**V**	
Transennella pannosa	X	P	A	V	V	V
Venus antiqua	?	P			P	

V = Very abundant, A = Abundant, P = Present, X = extant, (X) = exceptionally present, — = not present in the area, ? = probably present, but not collected
Hol. = Holocene (Present). 5e, 7, 9, 11, >11 = Oxygen Isotope Stages

been mentioned previously in any other Pleistocene marine deposit of northern Chile. These species are: *Bulla punctulata* (A. Adams *in* Sowerby, 1850), *Cerithium stercusmuscarum* (Valenciennes, 1833), *Olivella* sp., *Prunum curtum* (Sowerby, 1832), *Turbo* cf. *fluctuosus* (Wood, 1828), *Anomia peruviana* (d'Orbigny, 1846), *Arcopsis solida* (Sowerby, 1833), *Argopecten circularis* (Sowerby, 1835), *Cyclocardia* cf. *spurca beebei* (Hertlein, 1958), *Donax peruvianus* (Deshayes, 1855), *Mactra velata* (Philippi, 1849), *Ostrea megodon* (Hanley, 1846), and *Trachycardium* cf. *procerum* (Sowerby, 1833; Fig. 5). These species are mostly Panamic species which nowadays live between the Gulf of California and northern Peru (Table 2). Their modern distribution range is generally limited to 6°S (or 14°S for *Trachycardium* cf. *procerum* and *Bulla punctulata*). Two species of the TAMA, however, pertain to the Peruvian province and range from Ecuador to southern Peru (*Prunum curtum* and *Donax peruvianus*).

The most common species found, often *in situ*, in the La Rinconada deposits, is *Trachycardium* cf. *procerum*. This species presently lives in the Panamic Province and the Paita Transition Zone (Olsson, 1961; 4–6°S). Episodically, though, it is observed along the northern half of the Peruvian coast (DeVries, 1986; Díaz and Ortlieb, 1993; Perrier *et al.*, 1992, 1994). Keen (1971) mentioned, erroneously, that the southernmost limit of its present distribution was northern Chile. *Trachycardium* cf. *procerum* was present, and locally abundant, in coastal lagoons of southern Peru during the last interglacial (Díaz

TABLE 2. Geographic distribution of the main warm-water molluscan species found in the Middle Pleistocene deposits of the La Rinconada area, with indications of the southernmost occurrences during the Pleistocene and Holocene along the coasts of Peru and Chile, according to varied sources and our own observations

Species	Present distribution range	Late Quaternary occurrence
GASTROPODS		
Bulla punctulata (A. Adams *in* Sowerby, 1850)	Baja California to N. Peru (Isla Lobos) (1,2,3). Exceptional at Antofagasta (a few beach drift samples collected in 1995 at La Rinconada)	One mention south of 6° S (possibly after an ENSO event) near Pisco (14°S) (4)
Cerithium stercusmuscarum (Valenciennes, 1833)	Baja California to N. Peru (Puerto Pizarro) (1,2)	Present in IS 5 deposits at Ilo (16°S) and in a Holocene palaeo-lagoon at Santa (9°S) (5, 6,7)
Olivella sp.	(extant ?)	(see text)
Prunum curtum (Sowerby, 1832)	Ecuador to N. Chile (Iquique) (1, 2, 3). Rare in southern Peru and northern Chile	
Turbo* cf. *fluctuosus (Wood, 1828)	Baja California, Nicaragua to N. Peru (Paita) (1,2)	Present in IS 5 deposits at Ilo (5, 6)
PELECYPODS		
Anomia peruviana (d'Orbigny, 1846)	California to N. Peru (Paita–Sechura) (1, 2, 8, 9)	Present in Holocene palaeo- lagoons (7) and in IS 5 deposits near San Juan Marcona (3); first mention for the Quaternary south of 16° S
Arcopsis solida (Sowerby, 1833)	Baja California to N. Peru (Paita) (1), or to central Peru (Chimbote) (2)	First mention for the Quaternary south of 9°S
Argopecten circularis (Sowerby, 1835)	Baja California to N. Peru (Paita) (1, 2, 3),	Present in a Holocene palaeo-lagoon at Santa (5, 6, 7, 12).
Cyclocardia* cf. *spurca beebei (Hertlein, 1958)	Gulf of California to Panama (1, 8)	(see text)
Donax peruvianus (Deshayes, 1855)=*Donax marincovichi* (Coan, 1983; 10), or = *Donax obesulus* (Reeve, 1854; 3, 7).	Ecuador to N. Chile (2, 3, 8, 10)	Modern distribution in N Chile linked to ENSO anomalies (6, 11).
Mactra velata (Philippi, 1849)	Gulf of California to N. Peru (Sechura) (3, 8) (or Chiclayo) (9)	First mention for the Quaternary south of 6°S.
Ostrea megodon (Hanley, 1846)	Baja California to N. Peru (Paita) (1, 8, 9) or central Peru (Chimbote) (2)	First mention for the Quaternary south of 9°S
Trachycardium* cf. *procerum (Sowerby, 1833)	Baja California to central Peru (Independencia Bay) (3) , or to Chile [doubtful!] (1, 2)	Present in IS 5 deposits at Ilo and also in a Holocene palaeo-lagoon at Santa (5, 6, 7, 12).

IS 5: Oxygen Isotope Stage 5 (last interglacial, 120 ka).

Sources: (1): Keen (1971); (2): Alamo and Valdivieso (1987); (3): DeVries (1986), (4) Paredes *et al.* (1988); (5): Ortlieb *et al.* (1990); (6): Díaz and Ortlieb (1993), (7): DeVries and Wells (1990), (8): Olsson (1961), (9): Peña (1971), (10): Coan (1983); (11) Tomicic (1985), (12): Perrier *et al* (1994).

and Ortlieb, 1993; Ortlieb *et al.*, *in press*), but has not been mentioned in any Late or Middle Pleistocene deposit in northern Chile. It was also relatively abundant in a mid-Holocene lagoon deposit near Santa in north-central Peru (9°S; Rollins *et al.*, 1986; DeVries and Wells, 1990; Perrier *et al.*, 1992, 1994).

Anomia peruviana is an epibenthic form strictly limited to the Panamic Province and the Paita Transition Zone (Olsson, 1961; Keen, 1971). Along the Peruvian coast, the species was only mentioned in late Pleistocene sediments at 15°30′S (DeVries, 1986) and in the Holocene TAMA of Santa (Rollins *et al.*, 1986; DeVries and Wells, 1990).

Arcopsis solida is a small pelecypod found in the intertidal area on sandy and rocky coastlines. Its range encompasses the Panamic Province and Paita Transition Zone, with a southernmost limit near Chimbote (Keen, 1971; Alamo and Valdivieso, 1987). To our knowledge, the species was not mentioned south of 6°S in any Holocene or Pleistocene deposits.

Argopecten circularis is the common scallop shell in the Panamic Province, with a wide bathymetric range (Keen, 1971). Its southern limit is presently at Sechura. The southernmost occurrence of the species is in the mid-Holocene paleo-lagoon deposit at Santa (Rollins *et al.*, 1986; DeVries and Wells, 1990).

Cyclocardia cf. *spurca beebei* is a poorly documented species. The samples of *Cyclocardia*, or *Cardita*, collected at La Rinconada could not be properly identified. They resemble *Cyclocardia velutinus* (Smith 1881) and/or *C. compressa* (Reeve 1843), that are cold-water species (extending southward to Magellan Straits; Soot-Ryan, 1959; Ramorino, 1966). *Cardita spurca beebei* lives nowadays in the warm-water between western Mexico and Panama (Olsson, 1961), while *Cardita (Cyclocardia) spurca* (Sowerby 1832) is a Chilean form extending northward to Lima (Olsson, 1961; Keen, 1971).

Donax peruvianus (which may correspond to *D. obesulus* [Reeve, 1854], according to Coan (1983) and/or to *Donax marincovichi* [Coan, 1983]) is generally found on exposed sandy coasts. In northern Chile it is reported as presently living (?) at Arica (18°30′S) and Iquique (20°S). Actually the only locality in northern Chile where we collected samples of *D. peruvianus* recently (in 1993–1995) is the sector of La Rinconada. The occurrence of the species is apparently limited to the months (and years?) that follow strong (or very strong) El Niño events, for example in 1982–1983 (Tomicic, 1985).

Mactra velata is a very large Panamic pelecypod that commonly lives on mud flats and ranges southward to northern Peru (7°S, according to Peña (1971)). To our knowledge, the species was not recorded south of 6°S in any Holocene or Pleistocene deposits.

Ostrea megodon has a wide ecological range occurring from shallow waters and about a 110 m depth (Keen, 1971). It is distributed between Baja California and northern Peru (6°S). According to Alamo and Valdivieso (1987), it may be found presently at Chimbote (9°S). It was locally very abundant in Early (?) and Middle Pleistocene 'tablazo' (marine terrace) deposits of northern Peru (Olsson, 1961; DeVries, 1986). It may be noted that the species was not present in the mid-Holocene TAMA of Santa.

Bulla punctulata is an opisthobranch gastropod which presently inhabits protected sandy or muddy environments north of Bayovar (6°S), although a small isolated population was described at Bahia Independencia (14°S; Paredes *et al.*, 1988). It was also found in the Holocene TAMA of Santa (DeVries and Wells, 1990). Its southernmost limit, presently, must be extended southward to Antofagasta, since we collected (in 1995) a few samples of live animals, on the beach at La Rinconada. To our knowledge, *Bulla* was not previously described in any Pleistocene deposit south of 6°S.

Cerithium stercusmuscarum normally lives in shallow embayments and coastal lagoons in the Panamic Province and the Paita Transition Zone. It was present in mid-Holocene lagoonal deposits near Santa and Chimbote (9°S). Some samples were also found in paleo-lagoon units assigned to the Oxygen Isotope Stage 5 in southern Peru (at Ilo, 18°S; Ortlieb *et al.*, 1990, *in press*).

Olivella sp., which abounds in some beds at La Rinconada, could not yet be identified. The species presents several significant morphological differences with *O. columellaris* (Sowerby, 1825), the most frequent species found in Holocene or Pleistocene deposits of northern Peru. To our knowledge, no other *Olivella* were described in Quaternary deposits from southern Peru or Chile.

Prunum curtum is a small and uncommon gastropod that lives on sandy or muddy substrates of the Peruvian coast. Its present distribution range may extend to northern Chile (DeVries, 1986; Alamo and Valdivieso, 1987), although it was not mentioned by authors that worked in Iquique (e.g. Marincovich, 1973).

Turbo cf. *fluctuosus* is a gastropod that lives on rocky substrate, below low tide level. It is rare in the southern end of its range, i.e. the Paita Transition Zone (Keen, 1971). Its southernmost occurrence during the Pleistocene was in southern Peru, at Ilo (Ortlieb *et al.*, 1990; Díaz and Ortlieb, 1993).

A few isolated individuals of other bivalves (*Protothaca* sp., *Panope* sp.) and gastropods (*Chorus* sp.) were found. Their identification is still pending. As they were encountered less frequently than all the others, cool or warm-water species, we consider that they were episodical forms, and of less significance than the rest of the TAMA species mentioned here.

Thus, the Middle Pleistocene TAMA of the La Rinconada block is composed mostly of elements which presently live north of 6°S, or 9°S. A few forms of the TAMA may be found episodically or in reduced number in particular localities of south-central Peru (Paracas embayment, Independencia Bay), particularly after occurrences of El Niño events (Paredes *et al.*, 1988). Many of the fossil species found at La Rinconada are presently living in the Bay of Bayovar, some 2000 km to the north (Fig. 1). In some way, present conditions in this bay within the Paita Transition Zone (SST annual range of 17–21°C) should help to reconstruct the paleoenviron-

ment of the La Rinconada area at 400 ka. On the other hand, one of the typical modern biotopes defined in the Paracas Bay area (14°S, SST annual range of 16–20°C), characterised by the assemblage *Donax peruvianus–Prunum curtum–Bulla punctulata–Mesodesma donacium* (Paredes *et al.*, 1988) from relatively protected sandy and silty environments may also represent a modern equivalent of one of the facies found at the La Rinconada site. Finally, there is a striking similarity between the fauna of the La Rinconada site and the mid-Holocene TAMA at Santa, north-central Peru (DeVries and Wells, 1990; Ortlieb *et al.*, 1990; Perrier *et al.*, 1992). In the paleolagoon of Santa the warm-water assemblage developed during more than 2000 years (6500–4300 BP), behind a large beach ridge, while a cool fauna co-existed in the nearshore area exposed to the effects of the Humboldt Current system (DeVries and Wells, 1990; Perrier *et al.*, 1994). A similar situation may have occurred at La Rinconada during Oxygen Isotope Stage 11, although probably during a much longer lapse. In both cases (Santa and the study area), it can be inferred that the shallow depth and warmer than present climatic conditions allowed for the survival and perpetuation of species which would not have lived in the cool, open, nearby ocean waters.

Paleogeographic and Paleoclimatic Interpretation

The Middle Pleistocene deposits of southern Pampa Mejillones, above +150 m, which also present a warm-water faunal assemblage, exhibit some of the same extralimital species (*Olivella* sp., *Cyclocardia* cf. *spurca beebei*, *Mactra velata*, *Ostrea megodon* and *Trachycardium* cf. *procerum)* of the La Rinconada TAMA. A few other species, also characteristic of the Panamic Province but not present at La Rinconada locality, like *Cyclinella subquadrata* (Hanley, 1845) and *Dosinia ponderosa* (Gray, 1838) are present in the oldest deposits of Pampa Mejillones. In both coastal plains, the TAMA indicate that during the presumed Oxygen Isotope Stage 11, the oceanographic conditions were such that numerous species that require warm water could live in protected environments both north and south of the Mejillones Peninsula. In the La Rinconada sector, like in southern Pampa Mejillones, permanent (or semi-permanent) coastal lagoons were formed behind the beach ridges. At La Rinconada, nowadays, without any lagoonal or closed environment (SST annual range 14–20°C), there is evidence that the morphological disposition of the coast is favourable to the episodical development of small communities of molluscs that are beyond their northern distributional range: *Bulla punctulata* and *Donax peruvianus* were found recently there, hundreds of kilometres south of their usual southernmost limit. In the case of Pampa Mejillones, it is interpreted that the Mejillones embayment was much more protected, in relation to the Present, from the cool water upwelled to the west and northwest of the peninsula, some 400,000 years ago. Before the 150–200 m slow uplift of the isthmus occurred, the coastline was much more profoundly indented than today, thus making possible the existence of protected biotopes.

Favourable palaeogeographic conditions for the formation of coastal environments with limited communication with the open oceans were possibly present in both cases, north and south of the peninsula. In these shallow lagoons, the solar radiation and the air temperature probably played a key role in maintaining warm-water conditions during most of the year. Also, winter air temperatures may have been significantly warmer than today (closer to the present-day summer temperatures). It is possible that a distinct seasonal range of air temperature variation could have been as important, or even more important in allowing the formation of the TAMA than a net increase of annual temperature.

A greater influence of atmospheric factors in relation to the oceanographic parametres is suggested. This is based on the strong evidence that coevally with the development of the TAMA, 'normal' cool water fauna was contemporaneously present on the exposed stretches of the coast, particularly on the northeastern shore of Antofagasta Bay. The cool-water component of the TAMA and the faunal content of the deposits in the eastern half of Pampa del Aeropuerto indicate clearly that the open sea temperature could not have been very different from the present-day conditions.

The mid-Holocene TAMA of Santa was here repeatedly referred to as a recent equivalent of the La Rinconada anomalous assemblage. Another equivalent situation was observed in Late Pleistocene lagoonal deposits of southern Peru (Ilo, 17°30′S), where warm-water forms (including: *Trachycardium* cf. *procerum* and *Cerithium stercusmuscarum)* were found with normal cool-water species (Ortlieb *et al.*, 1990; Díaz and Ortlieb, 1993). At Ilo, a complex story of coastal changes related to sea-level variations (within the last interglaciation) and tectonic deformations resulted in the formation of several lagoonal episodes, during which a relatively 'warm' fauna could develop (Ortlieb *et al.*, 1990, *in press*). There, also, it seems that the warm-water forms were closely linked to the existence of lagoonal environments. At Ilo, like at Santa, it was hypothesised that the introduction of the species in the lagoonal environment was possibly controlled by some coastal southbound currents, and/or by short-lived anomalies in the nearshore conditions like those accompagnying the El Niño occurrences (Díaz and Ortlieb, 1993). Larval transport of some species outside their normal distribution range has been one of the mechanisms invoked to explain the TAMA phenomenon (Zinsmeister, 1974). In any case, some relationship is demonstrated between the El Niño induced modifications on the coastal environment and the appearance of anomalous species in favourable sites (Tomicic, 1985; Paredes *et al.*, 1988; Díaz and Ortlieb, 1993).

CONCLUSION

Morphostratigraphic and geochronologic studies recently performed in the Mejillones Peninsula area provide

a new insight into the chronostratigraphic framework of the Middle Pleistocene coastal landforms and associated deposits in northern Chile. As a result, the identification of the remnants of the last three or four interglacial high seastands begins to be well assessed (Ortlieb *et al.*, 1995). The coastal features and sediments formed during Oxygen Isotope Stage 11 (ca. 400 ka) are not commonly preserved along the narrow coastal plain of northern Chile, between Antofagasta (24°S) and Iquique (21°S), but they are well developed in Mejillones Peninsula. It was discovered that the faunal composition of some of the deposits assigned to the 400 ka high seastand was exceptional, with respect to that of the other interglacial high seastand episodes. The most protected areas in two sectors of the peninsula are characterised by thermally anomalous molluscan assemblages (TAMA) which include a series of warm-water species that commonly live now in the Panamic Province and in the Paita Transition Zone (4–6°S). For most of these species, the 400 ka deposits at Mejillones Peninsula constitute the southernmost limit of occurrence during the Quaternary. Some of these species are found, at 23°S, about 2000 km further south than their modern end-limit.

The TAMA species at La Rinconada locality are generally lagoonal forms, or species that live in protected shallow water embayments. As evidenced in a few other cases of TAMA on the Peruvian coast (two modern ones in Paracas Bay and at Independencia Bay, one in the mid-Holocene at Santa, and another one in last interglacial deposits at Ilo), the anomalous assemblages of extralimital species are restricted to areas with limited circulation where the water temperature can be significantly higher than in the nearby open ocean. Besides, it may be noted that the modern occurrence of extralimital species is favoured during the months and years following strong El Niño events. Short-lived oceanographic and climatic anomalies may also have played a role in the southward transport of warm-water species along the Peruvian and Chilean coast in the past.

However, the fauna of the coastal deposits assigned to the Oxygen Isotope Stage 11 is not uniformly characteristic of warm water conditions. The exposed sectors of the coast were coevally inhabited by cool water species that do not differ significantly from those presently living in the area. Therefore, it may be inferred that the Humboldt Current and the coastal upwelling system were probably as active at that time as they are today. It was only in protected environments, physically separated by a sandy barrier from the cool nearshore waters, that Panamic molluscs could live. This suggests that ocean–atmosphere interactions were on a distinct mode than at present. The winter air temperature was probably higher by several degrees, and the solar radiation may also have been stronger than today. Atmospheric conditions which may be comparable to those prevailing at present in summer, may have lasted much longer in the yearly cycle.

The studied emerged coastal deposits assigned to Oxygen Isotope Stage 11 in Mejillones Peninsula are the only localities, among all the studied Quaternary marine units of northern Chile, that include a number of panamic species. It is stressed, for instance, that none of these warm-water species were found in any of the numerous Late Pleistocene (Oxygen Isotope Stage 5e) deposits. The warmer character of the ca. 400 ka interglaciation in relation with the subsequent Middle–Late Pleistocene interglacial episodes and the Holocene probably reflects a particular atmospheric circulation mode that may concern essentially the southern hemisphere, and not necessarily the whole globe.

ACKNOWLEDGEMENTS

The study was supported by ORSTOM, Dept TOA, UR 14 (Programme DESIRS) and UR 12 (Programme AIMPACT), in the framework of two scientific agreements with Universidad de Antofagasta, Facultad de Recursos del Mar and Universidad de Chile, Departamento de Geología. The authors thank Sheyla Saa for her help in the study of the fossil fauna. We are also grateful to V. Covacevich (Servicio Nacional de Geología y Minería, Santiago), D. Frassinetti (Museo Nacional de Historia Natural, Santiago) and J. Leal (Bailey-Matthews Shell Museum, Florida) who provided judicious advice to improve the manuscript. This is a contribution to IGCP project 367, to CLIP (Climates of the Past) and to the INQUA Subcommission on Quaternary Shorelines for the Americas.

REFERENCES

Aksu, A.E., Mudie, P.J., de Vernal, A. and Gillespie, H. (1992). Ocean-atmosphere responses to climatic change in the Labrador Sea: Pleistocene plankton and pollen records. *Palaeogeography, Palaeoclimatology, Palaeoecology*, **92,** 121–138.

Alamo, V.V. and Valdivieso, V. (1987). *Lista sistemática de moluscos marinos del Perú*. Instituto del Mar del Perú, Boletín extraordinario, 205 pp.

Armijo, R.and Thiele, R. (1990). Active faulting in northern Chile: ramp stacking and lateral decoupling along a subduction plate boundary? *Earth and Planetary Science Letters*, **98**, 40–61.

Burckle, L.H. (1993). Late Quaternary interglacial stages warmer than present. *Quaternary Science Reviews*, **12**, 825–831.

Charles, C.D., Froelich, P.N., Zibello, M.A., Mortlock, R.A. and Morley, J.J. (1991). Biogenic opal in Southern Ocean sediments over the last 450,000 years: Implications for Quaternary surface water chemistry. *Paleoceanography*, **6,** 697–728.

Coan, E. (1983). The Eastern Pacific Donacidae. *The Veliger*, **25,** 273–298.

DeVries, T.J. (1986). The geology and paleontology of the tablazos in northwest Peru. Ph.D. dissertation, Ohio State University, Columbus (Ohio), 964 pp.

DeVries, T.J. and Wells, L.E. (1990). Thermally-anomalous Holocene molluscan assemblages from coastal Peru: evidence for paleogeographic, not climatic change. *Palaeogeography, Palaeoclimatology, Palaeoecology*, **81,** 11–32.

Díaz, A. and Ortlieb, L. (1993). El Fenómeno 'El Niño' y los moluscos de la costa peruana. *Bulletin de l'Institut Francais d'Etudes Andines*, **22,** 159–177.

Ferraris, F. and Di Biase, F. (1978). Hoja Antofagasta, región de Antofagasta. *Carta Geológica de Chile* n°30, Instituto de Investigaciones Geológicas, Chile. 48 pp., 1 map 1:250.000.

Flint, S., Turner, P. and Jolley, E.J. (1991). Depositional architecture of Quaternary fan-delta deposits of the Andean fore-arc: relative sea-level changes as a response to aseismic ridge subduction. *International Association of Sedimentologists, Special Publication*, **12,** 91–103.

Hays, J.D., Imbrie, J. and Shackleton, N.J. (1976). Variations in the Earth's orbit: pacemaker of the ice ages. *Science,* **194,** 1121–1132.

Herm, D. (1969). Marines Pliozän und Pleistozän in Nord und Mittel- Chile unter besonderer Berucksichtigung der Entwicklung der Mollusken-Faunen. *Zitteliana (München),* **2,** 159 pp.

Hillaire-Marcel, C., Ghaleb, B., Cournoyer, L. and Ortlieb, L. (1996). Allo/isoleucine (A/I) and Th/U measurements in mollusk shells from Michilla and Mejillanes Bays, northern Chile. *II Annual Meeting of the International Geological Correlation Program,* Project 367 (Antofagasta, 19–28 Nov., 1995). Abstracts volume, p. 47. ORSTOM, Antofagasta, Chile.

Hodell, D.A. (1993). Late Pleistocene paleoceanography of the South Atlantic sector of the southern ocean: Ocean Drilling Program hole 704-A. *Paleoceanography,* **8,** 47–67.

Hopkins, D.M. (1967). Quaternary marine transgressions in Alaska. *In*: Hopkins, D.M. (ed.), *The Bering Land Bridge*, pp. 47–90. Stanford University Press, California.

Hopkins, D.M., Rowland, R.W., Echols, R.E. and Valentine, P.C. (1974). An Anvilian (early Pleistocene) marine fauna from western Seward Peninsula, Alaska. *Quaternary Research,* **4,** 441–471.

Howard, W.R. and Prell, W.L. (1992). Late Quaternary surface circulation of the southern Indian ocean and its relationship to orbital variability. *Paleoceanography,* **76,** 43–54.

Imbrie, J. and Imbrie, J.Z. (1980). Modeling the climate response to orbital variations. *Science,* **207,** 943–953.

Imbrie, J., Boyle, E.A., Clemens, S.C., Duffy, A., Howard, W., Kukla, G., Kutzbach, J., Martinson, D.G., McIntyre, A., Mix, A.C., Molfino, B., Morley, J.J., Peterson, L.C., Pisias, N.G., Prell, W.L., Raymo, M.E., Shackleton, N.J. and Toggweiler, J.R. (1992). On the structure and origin of major glaciation cycles, 1: Linear responses to Milankovitch forcing. *Paleoceanography,* **7,** 701–738.

Imbrie, J., Boyle, E.A., Clemens, S.C., Duffy, A., Howard, W., Kukla, G., Kutzbach, J., Martinson, D.G., McIntyre, A., Mix, A.C., Molfino, B., Morley, J.J., Peterson, L.C., Pisias, N.G., Prell, W.L., Raymo, M.E., Shackleton, N.J. and Toggweiler, J.R. (1993). On the structure and origin of major glaciation cycles, 2: The 100,000-year cycle. *Paleoceanography,* **8,** 699–735.

Jansen, J.H.F., Kuijpers, A. and Troelstra, S.R. (1986). A Mid-Brunhes climatic event: Long-term changes in global atmosphere and ocean circulation. *Science,* **232,** 619–622.

Kaufman, D.S., Walter, R.C., Brigham-Grette, D.M. and Hopkins, (1991). Middle Pleistocene age of the Nome River glaciation, northwestern Alaska. *Quaternary Research,* **36,** 277–293.

Kaufman, D.S. and Brigham-Grette, J. (1993). Aminostratigraphic correlations and paleotemperature implications, Pliocene-Pleistocene high-sea-level deposits, northwestern Alaska. *Quaternary Science Reviews,* **12,** 21–33

Keen, A.M. (1971). *Sea Shells of Tropical West America: Marine Mollusks from Baja California to Peru.* Stanford University Press, Stanford, 1064 pp.

Kellogg, T.B. (1977). Paleoclimatology and paleo-oceanography of the Norwegian and Greenland seas: The last 450,000 years. *Marine Micropaleontology,* **2,** 235–249.

Kennett, J. (1970). Pleistocene paleoclimates and foraminiferal biostratigraphy in subantarctic deep-sea cores. *Deep Sea Research,* **17,** 125–140.

Liu, H.S. (1992). Frequency variation of the Earth's obliquity and the 100-kyr ice-age cycles. *Nature,* **358,** 397–399.

Liu, H.S. (1995). A new view on the driving mechanism of Milankovitch glaciation cycles. *Earth and Planetary Science Letters,* **131,** 17–26.

MacNeil, F.S., Mertie, J.B. and Pilsbry, H.A. (1943). Marine invertebrate faunas of the buried beaches near Nome, Alaska *Journal of Paleontology,* **17,** 69–96.

Marincovich, L. (1973). Intertidal mollusks of Iquique, Chile. *National History Museum of Los Angeles County, Scientific Bulletin,* **16,** 1–49.

Morley, J.J. (1989). Variations in high-latitude oceanographic fronts in the southern Indian Ocean; An estimation based on faunal changes. *Paleoceanography,* **4,** 547–554.

Morris, P. (1966). *A Field Guide to Shells of the Pacific Coast and Hawai, Including Shells of the Gulf of California.* Houghton Miffin Co., Boston, 297 pp.

Okada, A. (1971). On the neotectonics of the Atacama fault zone region. Preliminary notes on late Cenozoic faulting and geomorphic development of the Coast Range of northern Chile. *Bulletin of the Department of Geography Kyoto University,* **3,** 47–65.

Olsson, A.A. (1961). *Mollusks of the tropical eastern Pacific, Panamic Pacific Pelecypoda.* Paleontological Research Institute, Ithaca, New York. 574 pp.

Oppo, D.W., Fairbanks, R.G. and Gordon, A.L. (1990). Late Pleistocene Southern Ocean $\delta^{13}C$ variability. *Paleoceanography,* **5,** 43–54.

Ortlieb, L. (1993). Vertical motions inferred from Pleistocene shoreline elevations in Mejillones Peninsula, northern Chile: Some reassessments. *II International Symposium on Andean Geodynamics* (Oxford, 1993), Extended Abstract volume, pp. 125–128.

Ortlieb, L., DeVries T. and Díaz, A. (1990). Ocurrencia de *Chione broggi* (Pilsbry and Olsson, 1943) (Pelecypoda) en depósitos litorales cuaternarios del sur del Perú: implicaciones paleoceanográficas. *Sociedad Geológica del Perú, Boletín,* **81,** 127–134.

Ortlieb, L. and Guzmán, N. (1994). La malacofauna pleistocena de la región de Antofagasta: variaciones en la distribución biogeográfica y potencial paleoceanográfico. Actas VII Congreso Geológico Chileno (Concepción, 1994), 1, pp. 498–502.

Ortlieb, L., Guzmán, N. and Candia, M. (1994). Moluscos litorales del Pleistoceno superior en el área de Antofagasta, Chile: Primeras determinaciones e indicaciones paleoceanográficas. *Estudios Oceanológicos,* **13,** 51–57.

Ortlieb, L., in coll. with J.L. Goy, C. Zazo, Cl. Hillaire-Marcel and G. Vargas (1995). *Late Quaternary Coastal Changes in Northern Chile.* Guidebook for a fieldtrip. *II annual meeting of the International Geological Correlation Program,* Project 367 (Antofagasta, 19–28 Nov. 1995), ORSTOM, Antofagasta, Chile. 175 pp.

Ortlieb, L., Zazo, C., Goy, J., Dabrio, C. and Macharé, J. (*in press*). Pampa del Palo: An anomalous composite marine terrace in the uprising coast of southern Peru. *Journal of South American Earth Sciences,* **9.**

Ortlieb, L., Zazo, C., Goy, J. L., Hillaire-Marcel, C., Ghaleb, B. and Cournoyer, L. (1966a). Coastal deformation and sea-level changes in the Northern Chile subduction area (23°S) during the last 330 ky. *Quaternary Science Reviews,* **15.**

Ortlieb, L., Goy, J.L., Zazo, C., Hillaire-Marcel, C., Ghaleb, B., Guzmán, N. and Thiele, R. (1996) *Quaternary morphostratigraphy and vertical deformation in Mejillones Peninsula, Northern Chile. 3rd International Symposium on Andean Geodynamics.* (St Malo, September 1996), Abstract volume, 211–214.

Paredes, C., Tarazona, J., Canahuire, E., Romero, L. and Cornejo, O. (1988). Invertebrados macro-bentónicos del área de Pisco, Perú. *In*: Salzwedel, H. and Landa, A. (eds), *Recursos y dinámica del ecosistema de afloramiento peruano,* Instituto del Mar del Perú, volumen extraordinario 1, pp. 121–132.

Peña, G.M. (1971). Zonas de distribución de los bivalvos marinos del Perú. *Anales Cientificos, Universidad Nacional Agraria La Molina,* **9,** 127–138.

Perrier, C., Ortlieb, L. and Hillaire-Marcel, C. (1992). Coastal evolution and El Niño impact in Santa area, NW Peru, based on isotopic composition of Holocene mollusk shells. *In*: Ortlieb, L. and Macharé J. (eds), *Paleo-ENSO records*

symposium, extended abstracts, International symposium on Former ENSO phenomena in western South America: Records of El Niño events (Lima, 4–7 march 1992), ORSTOM and CONCYTEC, Lima. pp. 237–243.

Perrier, Ch., Hillaire-Marcel, C. and Ortlieb, L. (1994). Paléogéographie littorale et enregistrement isotopique (^{13}C,^{18}O) d'événements de type El Niño par les mollusques holocènes et récents du nord-ouest péruvien *Géographie Physique et Quaternaire*, **48,** 23–38.

Radtke, U. (1987). Paleo sea levels and discrimination of the last and the penultimate interglacial fossiliferous deposits by absolute dating methods and geomorphological investigations, illustrated from marine terraces in Chile. *Berliner geographische Studien*, **25,** 313–342.

Radtke, U. (1989). Marine Terrassen und Korallenriffe. Das Probleem der Quartären Meeresspiegelschwankungen erläntert an Fallstudien aus Chile, Argentinien und Barbados. *Düsseldorfer geographische Schriften*, **27,** 245 pp.

Ramorino, L. (1966). Pelecypoda del fondo de la Bahía de Valparaíso. *Revista de Biología Marina (Chile)*, **13,** 175–285.

Ratusny, A. and Radtke, U. (1988). Jungere ergebnisse Küstenmorphologischer untersuchungen im "grossen Norden" Chiles. *Hamburger Geographische Studien*, **44,** 31–46.

Rollins, H.B., Richardson III, J.B. and Sandweiss, D.H. (1986). The birth of El Niño: geochronological evidence and implications. *Geoarcheology*, **1**, 3–15.

Roy, K., Jablonski, D. and Valentine, J.W. (1995). Thermally anomalous assemblages revisited: Patterns in the extraprovincial latitudinal range shifts of Pleistocene marine mollusks. *Geology*, **23,** 1071–1074.

Ruddiman, W.F. and McIntyre, A. (1976). Northeast Atlantic paleoclimatic changes over the past 600,000 years. *In*: Cline, R.M. and Hays, J.D. (eds), *Investigation of Late Quaternary Paleoceanography and Paleoclimatology*, Geological Society of America Memoir 145, pp. 111–146.

Ruddiman, W.F., McIntyre, A. and Raymo, M.E. (1986). Paleoenvironmental results from north Atlantic sites 607 and 609. *Ocean Drilling Program Scientific Results, Proceedings*, **94,** 855–878.

Ruddiman, W.F., Raymo, M.E., Martinson, D.G., Clement, B.M and Backman, J. (1989). Pleistocene evolution of northern hemisphere climate. *Paleoceanography*, **4,** 353–412.

Shackleton, N.J. (1987). Oxygen isotopes, ice volume and sea level. *Quaternary Science Reviews*, **6,** 183–190.

Shackleton, N.J. and Opdyke, N.D. (1973). Oxygen isotope and paleomagnetic stratigraphy of Equatorial Pacific core V28-238: Oxygen isotope temperatures and ice volume on a 10^5–10^6 year scale. *Quaternary Research*, **31,** 805–816.

Soot-Ryan, T. (1959). Pelecypoda. Reports of The Lund University, Chile Expedition 1948–1949, 35, 1–87.

Tomicic, J.J. (1985). Efectos del fenómeno El Niño 1982–83 en las comunidades de la Península de Mejillones. *Investigaciones Pesqueras (Chile)*, **32,** 209–213.

Valentine, J.W. (1955). Upwelling and thermally anomalous Pacific coast Pleistocene molluscan faunas. *American Journal of Science*, **253,** 462–474.

Zinsmeister, W.J. (1974). A new interpretation of thermally anomalous molluscan assemblages of the California Pleistocene. *Journal of Paleontology*, **48,** 84–94.

TIDES AND HUMAN INFLUENCES

Pergamon

Quaternary Science Reviews, Vol. 15, pp. 873–894, 1996.

PII: S0277–3791(96)00061–3
0277–3791/96 $32.00

TIDES IN THE NORTHEAST ATLANTIC: CONSIDERATIONS FOR MODELLING WATER DEPTH CHANGES

A.C. HINTON
School of Geography, Leeds University, Leeds LS2 9JT, U.K.

Abstract — A two-dimensional tidal model of the northeast Atlantic is used to simulate the M_2, S_2, μ_2, M_4, MS_4 and M_6 tides for present sea level and with mean water level lowered or raised by a uniform number of metres over the model area. M_2+S_2 tides predict the present spring tidal range, although the other constituents are needed to predict spring tides in shallow water areas. The accuracy of the assumptions made in modelling is assessed.

The relative amplitudes of the different tidal constituents vary, in a non-linear manner, depending on model water depth. Changes in the northeast Atlantic tides are relatively minor for tidal simulations with water depths 30 m below to 5 m above present levels. However, the situation is more complicated in the shallower waters of the northwest European shelf. Examples are given from a number of locations.

Results from the Northeast Atlantic model are used to run larger scale models of Morecambe Bay on the west coast of Britain and The Wash on the east coast. The tidal changes within these embayments highlight the local nature of the variations, in the amplitude of different tidal constituents and the importance of the scale at which modelling is carried out. Copyright © 1996 Elsevier Science Ltd

INTRODUCTION

Modelling of former tides on the northwest European continental shelf has largely involved the use of a model of the continental shelf area alone (e.g. Franken, 1987; Austin, 1988, 1991). Water depth reductions by a uniform number of metres across the model area have been employed to simulate former tides. Such bathymetric reductions of uniform amounts across the model area are increasingly unrealistic further back in time due to isostatic crustal movements on the shelf. However, these may be reasonably representative for the late Holocene when water depths were within a few metres of present levels. Uniform bathymetric reductions are employed in this paper for comparison with other published work and are used to indicate the manner in which changes to tides may occur.

Geological studies of former Holocene tidal range in the Netherlands (e.g. Roep and Beets, 1988; van de Plassche, 1995) contradict the results of palaeotidal modelling studies of the continental shelf (Franken, 1987; Austin, 1988, 1991). This raises questions as to whether the scale of modelling and use of specific tidal constituents is appropriate for the simulations carried out.

The main purpose of this paper is to compare results for different tidal constituents from a tidal model of the northeast Atlantic with results from more detailed models of local areas. This is carried out for water depths from 30 m below present to 5 m above. No attempt is made in this paper to assign 'ages' to the tidal simulations conducted.

METHODS

Two-dimensional finite difference tidal models, using a FORTRAN program only slightly modified from that developed by the Proudman Oceanographic Laboratory, Birkenhead, U.K. (POL) are employed. The Northeast Atlantic model, described in Flather (1981) and Andersen *et al.* (1995), is used to simulate broad changes to the tides at different water depths over the northwest European shelf. The Northeast Atlantic model has a latitude/longitude grid with a resolution of one third of a degree latitude and half a degree longitude. The grid extends from 71°40′N 30°W to 37°N 25°30′E, as shown in Fig. 1. The present day M_2 and S_2 tidal amplitude and phase values are used as input to the model on the open sea boundary. The model is started from still water and run for the time equivalent of one week before data are saved for analysis. The time equivalent of two weeks' data are used to analyse results for the M_2, S_2, μ_2, M_4, MS_4 and M_6 tidal constituents. Doodson and Warburg (1941) state that M_2 and S_2, together with their higher harmonics in shallow water areas, predict the spring tidal range on the northwest European shelf. Many sea-level indicators record the mean high water of spring tides altitude, so examination of changes to the relative

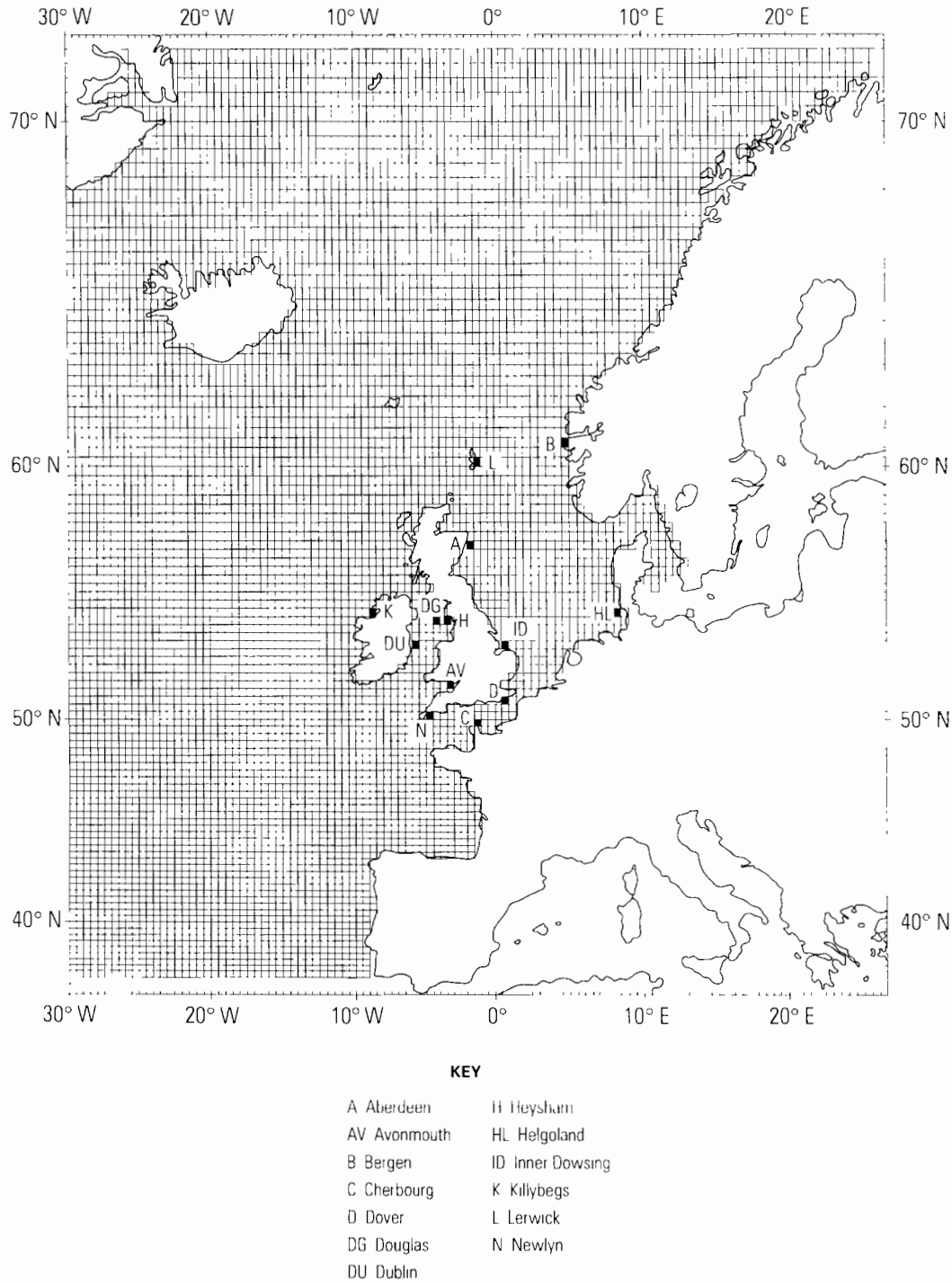

FIG. 1. Grid of the Northeast Atlantic model showing locations mentioned in the text (after Flather, 1981).

magnitude of these constituents is potentially of direct relevance for sea-level studies.

The Northeast Atlantic model results are presented for simulations with water depths 2, 5, 10, 15, 20, 25 and 30 m below present (comparable to Franken (1987) and Austin (1988, 1991) simulations for the continental shelf) and with water depths increased by 2 and 5 m above present levels. Sea levels are raised above present levels as a crude indication of what might occur with a warmer earth, neglecting sediment movement, crustal changes and the present day variability in magnitude and direction of sea-level change around northwest Europe, as illustrated by Woodworth *et al.* (1991).

In order to compare the Northeast Atlantic model results to tidal pattern changes within embayments, two further experiments were carried out. On the west coast of Britain, two models (POL's West Coast Model and Liverpool Bay Model) were run with reduced water depths of 2, 5, 10 and 15 m, employing open boundary tidal input from the next model up the scale in each case (Hinton, 1992a). The grid cell resolutions of the West Coast Model and Liverpool Bay Model, at 1/9 of a degree latitude and 1/6 of a degree longitude and 1/27 of a degree latitude and 1/18 of a degree longitude, respectively, were intermediate between those of the Northeast Atlantic model and the Morecambe Bay model. Thus information

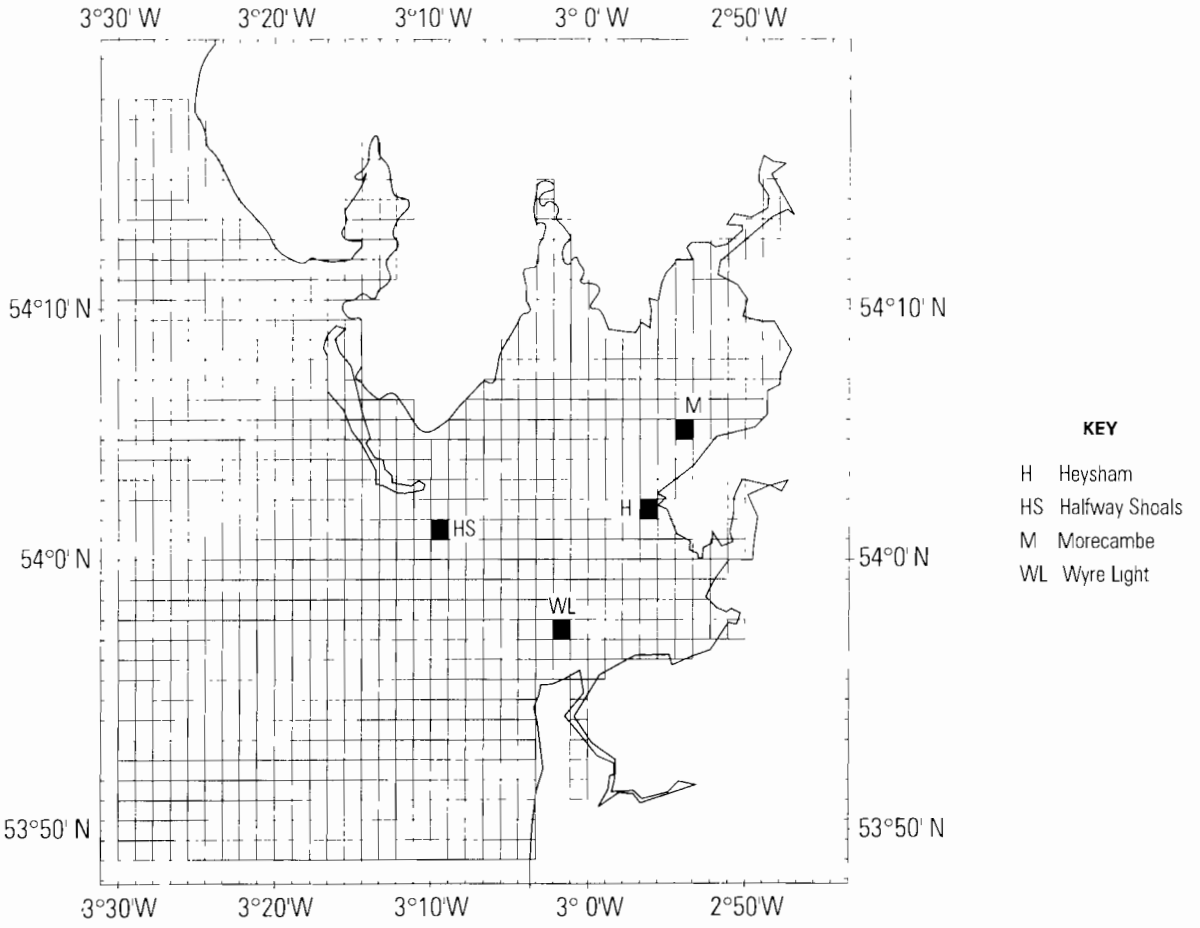

FIG. 2. Grid of the Morecambe Bay model showing locations mentioned in the text (after Flather and Hubbert, 1990).

on the six tidal constituents mentioned above was obtained along the open boundary of the Morecambe Bay Model (Flather and Heaps, 1975; Flather and Hubbert, 1990). The Morecambe Bay Model has a latitude/longitude grid resolution of 1/81 and 1/54 of a degree, respectively. The model grid extends from 54°17.78′N 3°30′W to 53°48.89′N 2°47.78′W, as shown in Fig. 2. It covers an area of approximately one grid cell of the Northeast Atlantic model and thus has the potential for direct comparison of tidal amplitudes with the Northeast Atlantic model results.

Another experiment with scale changes is made on the east coast of Britain. POL's East Coast Model (grid cell resolution 1/9 of a degree latitude and 1/6 of a degree longitude) is run as an intermediary between the Northeast Atlantic model and the EC3 model (Hinton, 1992a, b, 1995) to obtain open boundary tidal input with six constituents for 2, 5, 10 and 15 m water depth reductions for the EC3 model. The EC3 model has a latitude/longitude grid resolution of 1/27 and 1/18 of a degree, respectively. The grid covers the area from 53°57.78′N 0°13.3′W to 52°8.89′N 2°56.67′E, as shown in Fig. 3. The model area covers 25 grid cells of the Northeast Atlantic model.

All the models used have been shown to predict accurately (within 10% in amplitude and 10° in phase for the Northeast Atlantic model and better for the Morecambe Bay and EC3 models) present tidal amplitudes and phase values (Flather, 1981; Flather and Heaps, 1975; Flather and Hubbert, 1990; Hinton, 1992b). The reason for finishing simulations at 15 m below present water depths with the Morecambe Bay and EC3 models is that these are shallow embayments which are close to drying out when water depths are reduced by 15 m.

RESULTS

Northeast Atlantic Model

Figure 4(a–d) shows results for the Northeast Atlantic model with six tidal constituents for water depths increased by 5 m over present levels [+5], present sea level [0], and with water depths reduced by 15 and 30 m, hereafter referred to as simulations [−15] and [−30]. Amphidromic points of near zero tidal range are shown to move southward and eastward at lower sea levels. Locations with the highest tidal range (the Gulf of St Malo, just south of Cherbourg, the Severn Estuary/Bristol Channel, west of Avonmouth and the Dover Strait) undergo a number of alterations as water levels are raised and lowered. The contribution of shallow water constituents to these changes is greatest around the British Isles.

The highest tidal altitudes are recorded for present sea level (Fig. 4(b)). Water depths 5 m above those of present produce lower tides in the Severn Estuary and Gulf of St Malo than are found at the present day. With reductions

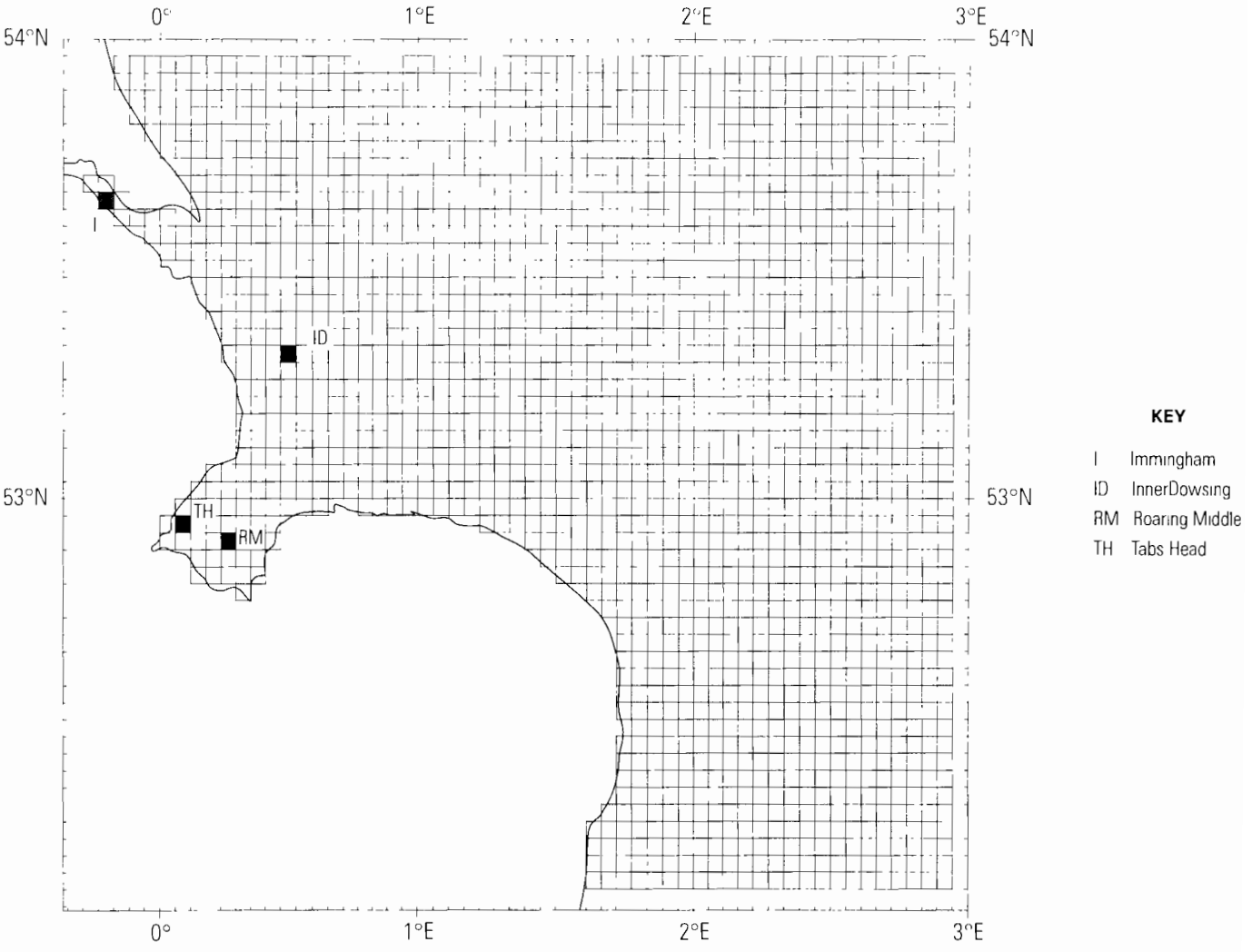

FIG. 3 Grid of the EC3 model showing locations mentioned in the text (after Hinton, 1992b).

of water depths, the area of high tides in the Dover Strait is found to move westwards down the English Channel. Broadly speaking, the highest tidal altitudes are found in the same locations as where the shallow water constituents reach maximum altitudes.

It has normally been assumed that the relationship of the various tidal constituents to each other (in terms of magnitude) does not vary. However, Table 1 illustrates that a number of changes do occur. The results in Table 1 are shown graphically in Fig. 5(a–m). The most dramatic changes are shown for the simulations with model water depths between 10 and 20 m below present levels. The Table 1 shows that there is an overall tendency for tidal amplitudes to decrease as water depths are reduced, but this is by no means a linear relationship. The relative contribution of different constituents to the overall tidal amplitudes recorded also shows a non-linear variation. The importance of the higher harmonic shallow water constituents increases relative to the other constituents as water depths are reduced, but this also occurs in a non-linear fashion. At Dublin, the movement of the amphidromic point nearby causes tidal amplitudes to fall initially as water depths are reduced and then to rise again with further reductions of water depths in the model. Heligoland gradually dries out with lower model water depths and the relative importance of the shallow water tidal constituents increases as water depths are reduced. Cherbourg, by contrast, has increasing tidal amplitudes as water depths are reduced. This is largely due to an increase of M_2 amplitudes disproportionately compared with the other constituents and the movement of the zone of highest tides in the English Channel away from the Dover Strait and out of the Gulf of St Malo.

Morecambe Bay Model

Results for the Morecambe Bay model for present sea level and with a water depth reduction of 10 m are shown in Fig. 6(a–f). The M_2 and S_2 results are presented separately from the results for all six constituents to highlight the major change to the tidal composition in this area when water depths are reduced by 10 m from present levels. The shallow water constituents are important in showing the variation in tidal amplitudes around Morecambe Bay, particularly over the extensive sand and mudflats surrounding the embayment. This variation is shown in the considerable differences in tidal amplitudes reached along the coastline. However, the main point illustrated by Fig. 6 is that S_2 becomes the dominant tidal

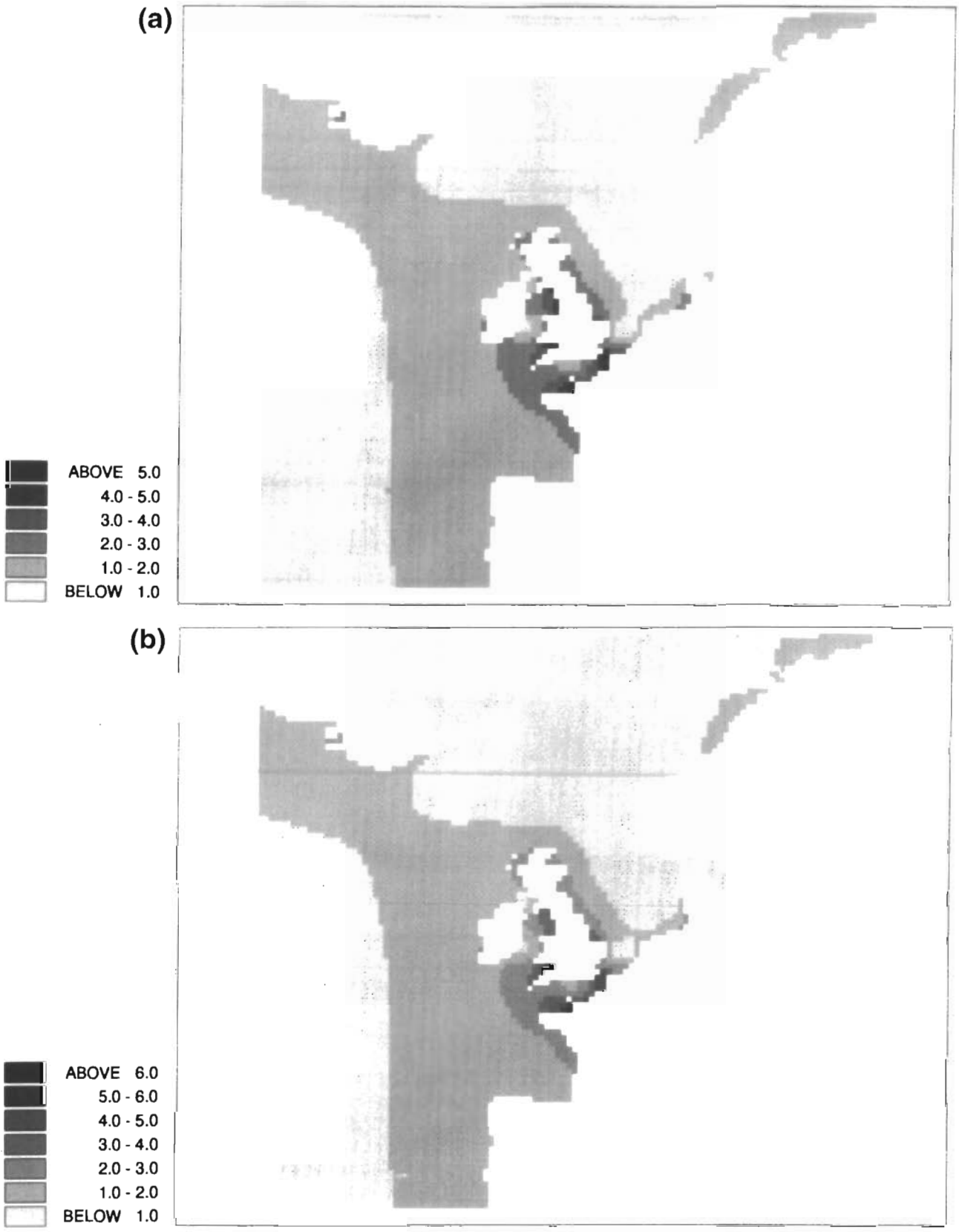

FIG. 4. Northeast Atlantic model tidal amplitude results for the maximum values of all six constituents combined (in metres). (a) Sea level increased by 5 m over present; (b) present sea level; (c) sea level reduced by 15 m from present; (d) sea level reduced by 30 m from present.

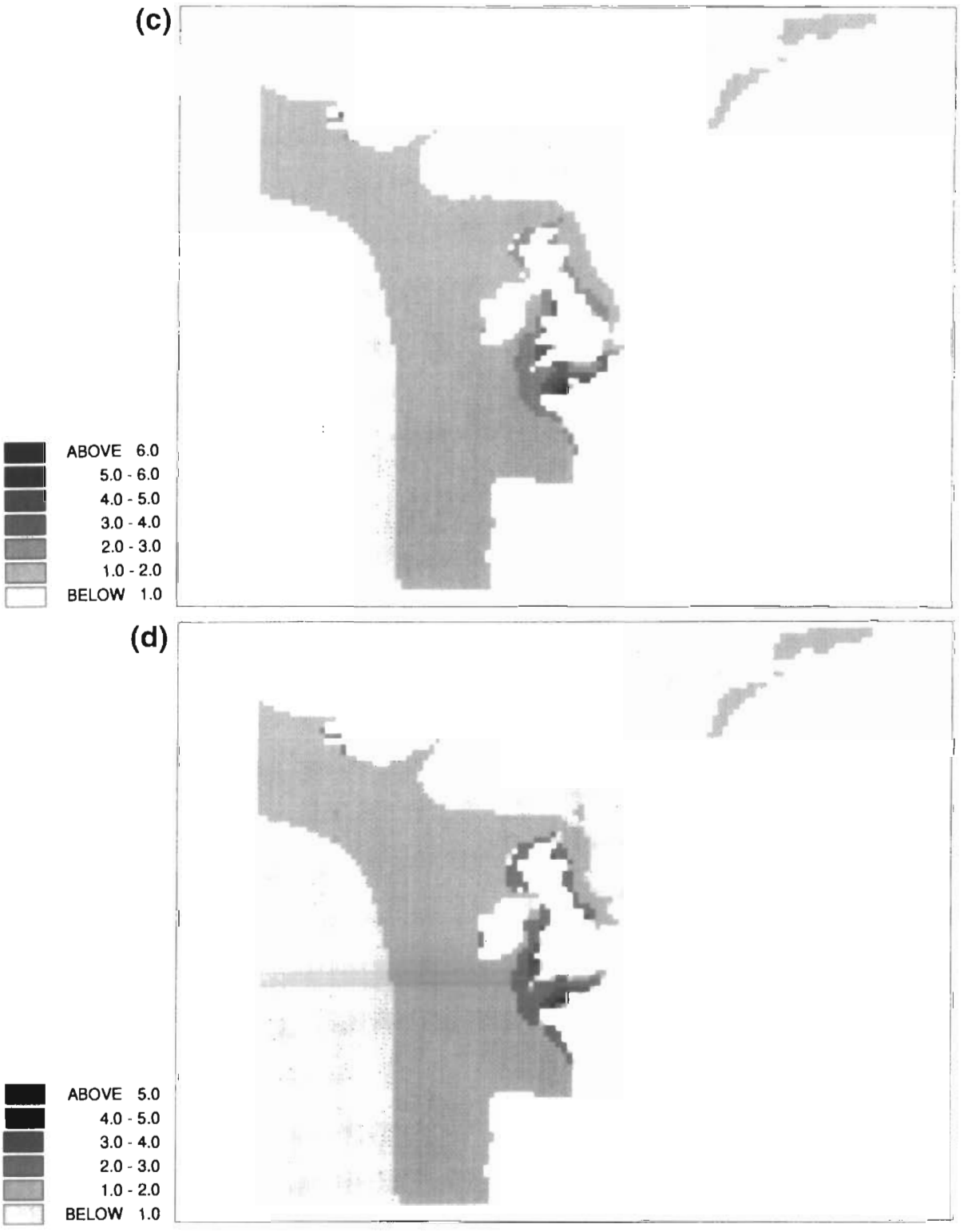

FIG. 4. c and d.

constituent when model water depths are reduced by 10 m. Its amplitude is around twice that of M_2 throughout Morecambe Bay with this simulation.

Fig. 7(a–d) and Table 2 give examples from around the Morecambe Bay model of the tidal amplitude alterations. Throughout the Bay as a whole, tidal amplitudes are reduced as model mean water levels are lowered. However, there is some local amplification of tidal altitudes as the area of the Bay is constricted due to drying out with water depth reductions, as shown for the deeper water areas of Wyre Light, Halfway Shoals and Heysham in Table 2. Fig. 7(a) incorporates the results for Heysham from the Northeast Atlantic model (which actually encompasses the whole of the Morecambe Bay model area) superimposed on the graph of the Morecambe Bay model results. It can clearly be seen that the scale of modelling has given very different figures at the same location. The Northeast

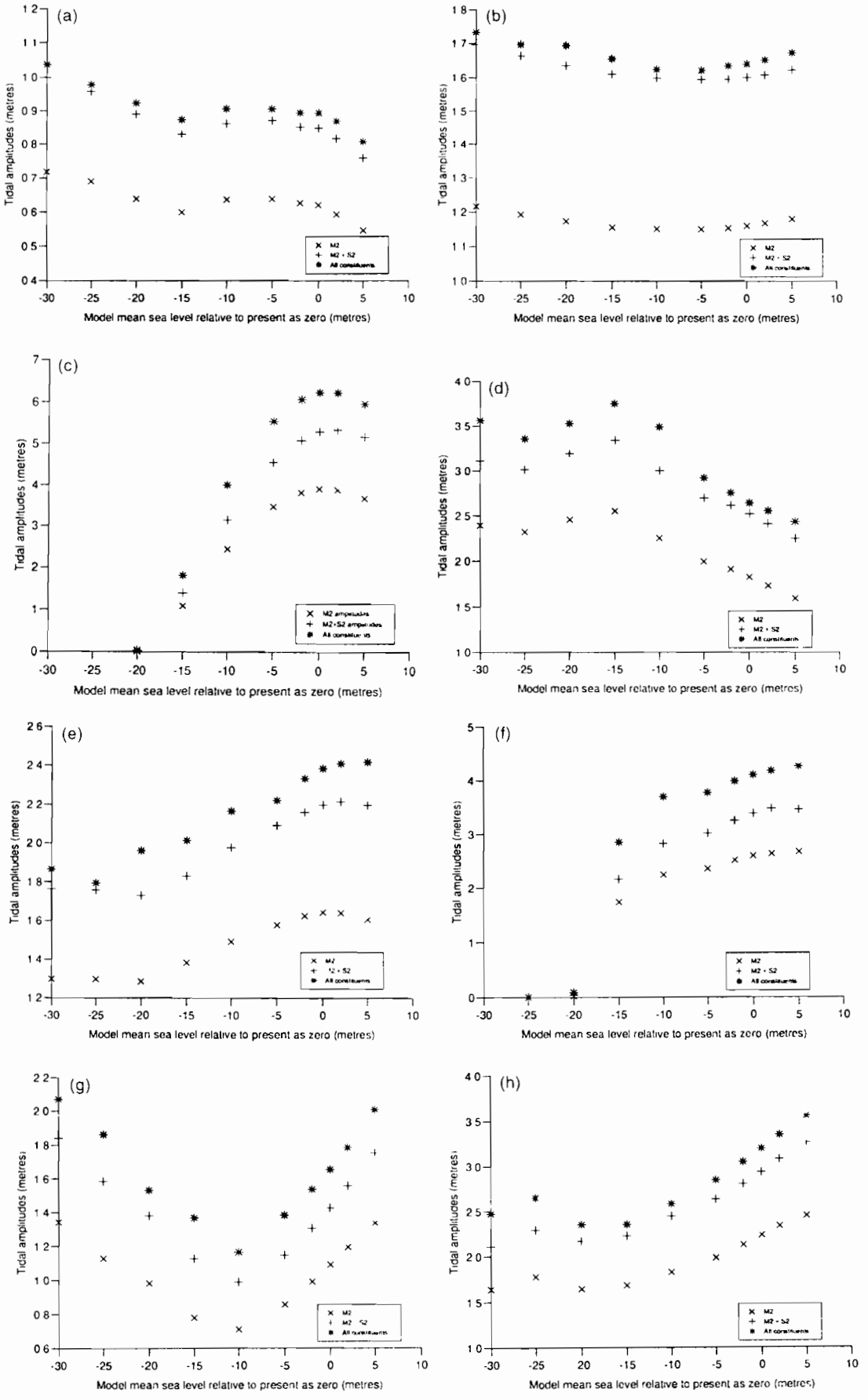

FIG. 5. Results of the maximum values of M_2, M_2+ S_2 and all six tidal constituents' amplitudes combined from the Northeast Atlantic model. Locations are shown on Fig. 1. (a) Lerwick; (b) Killybegs; (c) Avonmouth; (d) Cherbourg; (e) Newlyn; (f) Dover; (g) Dublin; (h) Douglas; (i) Inner Dowsing; (j) Helgoland; (k) Bergen; (l) Aberdeen; (m) Heysham.

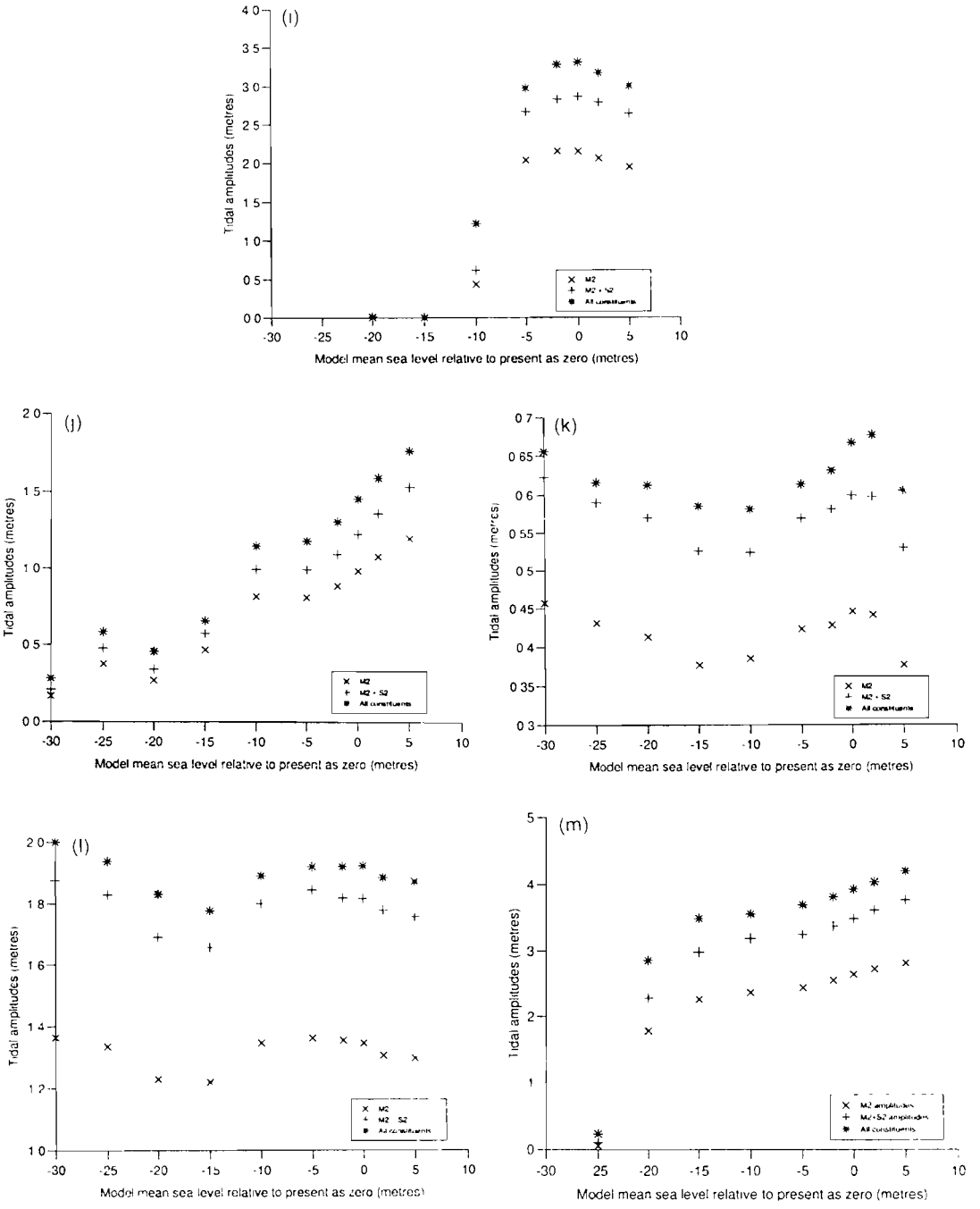

FIG. 5. i–m.

Atlantic model gives results for the area for water depth simulations 25 m below present levels. However, the same location is dry at 15 m below present sea level in the Morecambe Bay model. Tidal amplitudes incorporating results from all six constituents for the Morecambe Bay model are above those computed by the Northeast Atlantic model for present sea level and with water depth reductions of 2 and 5 m. However, when water depths are reduced by 10 m, the Morecambe Bay model results give tidal amplitudes below those of the Northeast Atlantic model. The Northeast Atlantic model does not record the major change to S_2 becoming the dominant tidal constituent with water depths reduced by 10 m.

EC3 Model

Results for the EC3 model for present sea level and with a reduction of 10 m are shown in Fig. 8(a–f). In all the present day simulation results, tidal amplitudes are shown to increase into the Wash embayment and up the Humber Estuary to Immingham to the north. When water depths are reduced by 10 m in the model, the highest S_2 amplitudes are off the Humberside coast in the northwest of the model. M_2 amplitudes are high in both the area of The Wash and off the Humberside coast. Shallow water constituent amplitudes are greatest off the Lincolnshire and north Norfolk coasts, surrounding The Wash. Hence, the highest amplitudes for all constituents combined are

TABLE 1. Tidal amplitudes for various locations on the northwest European continental shelf with different model water depths in the northeast Atlantic model. The locations are shown in Fig. 1
**** Indicates no result recorded as location was dry land for this simulation

Model mean sea level compared with present [0] as zero	Lerwick tidal amplitudes					Killybegs tidal amplitudes				
	M_2 (m)	S_2 (m)	Σ all six constituents (m)	S_2 % of M_2	Σ all six constituents % of [0]	M_2(m)	S_2(m)	Σ all six constituents(m)	S_2% of M_2	Σ all six constituents% of [0]
+5	0.546	0.213	0.808	39.0	90.5	1.180	0.443	1.673	37.5	102.0
+2	0.593	0.224	0.869	37.8	97.3	1.167	0.441	1.652	37.8	100.9
0	0.621	0.226	0.893	36.4	100.0	1.159	0.442	1.640	38.1	100.0
-2	0.626	0.226	0.894	36.1	100.1	1.153	0.443	1.635	38.4	99.8
-5	0.639	0.232	0.906	36.3	101.5	1.150	0.445	1.622	38.7	98.9
-10	0.637	0.226	0.907	35.5	101.5	1.181	0.448	1.624	38.9	99.0
-15	0.600	0.231	0.874	38.5	97.9	1.155	0.455	1.655	39.4	100.9
-20	0.639	0.251	0.923	39.3	103.4	1.173	0.462	1.693	39.4	103.2
−25	0.690	0.267	0.977	38.7	109.4	1.192	0.471	1.696	39.5	103.4
-30	0.718	0.281	1.037	39.1	116.1	1.216	0.480	1.733	39.5	105.8
Model mean sea level compared with present [0] as zero	Avonmouth tidal amplitudes					Cherbourg tidal amplitudes				
	M_2 (m)	S_2 (m)	Σ all six constituents (m)	S_2 % of M_2	Σ all six constituents % of [0]	M_2 (m)	S_2 (m)	Σ all six constituents (m)	S_2 % of M_2	Σ all six constituents % of [0]
+5	3.687	1.493	5.973	40.5	95.8	1.595	0.649	2.433	40.7	92.9
+2	3.888	1.454	6.237	37.3	100.0	1.730	0.681	2.552	39.4	96.7
0	3.911	1.374	6.237	35.1	100.0	1.825	0.695	2.639	38.1	100.0
−2	3.820	1.268	6.074	33.2	97.5	1.911	0.700	2.749	36.6	104.2
−5	3.476	1.078	5.554	31.0	89.0	1.955	0.698	2.917	35.0	110.5
−10	2.442	0.712	4.018	29.2	64.4	2.251	0.751	3.489	33.4	132.2
−15	1.092	0.305	1.819	27.9	29.2	2.551	0.788	3.755	30.9	138.5
−20	0.008	0.008	0.036	100.0	0.5	2.455	0.738	3.531	30.1	133.8
−25	****	****	****	****	****	2.315	0.697	3.353	30.1	127.1
−30	****	****	****	****	****	2.392	0.719	3.562	30.1	134.6

TABLE 1. Continued.

Model mean sea level compared with present [0] as zero	Newlyn tidal amplitudes					Dover tidal amplitudes				
	M_2 (m)	S_2 (m)	Σ all six constituents (m)	S_2 % of M_2	Σ all six constituents % of [0]	M_2 (m)	S_2 (m)	Σ all six constituents (m)	S_2 % of M_2	Σ all six constituents % of [0]
+5	1.607	0.591	2.416	36.8	101.3	2.663	0.884	4.257	33.2	137.5
+2	1.640	0.576	2.410	35.1	101.1	2.625	0.848	4.172	32.3	101.7
0	1.643	0.556	2.384	33.8	100.0	2.589	0.802	4.103	31.0	100.0
−2	1.625	0.536	2.332	33.0	97.8	2.508	0.746	3.982	29.7	97.3
−5	1.579	0.513	2.223	32.5	93.2	2.349	0.674	3.776	28.7	92.0
−10	1.492	0.484	2.166	32.4	90.9	2.237	0.579	3.703	25.9	90.3
−15	1.383	0.447	2.013	32.3	84.4	1.739	0.415	2.838	23.9	69.2
−20	1.285	0.445	1.960	34.6	82.2	0.025	0.055	0.088	60.0	21.4
−25	1.297	0.461	1.794	35.5	75.3	0.001	0.001	0.006	100.0	1.5
−30	1.298	0.466	1.865	35.9	78.2	****	****	****	****	****
Model mean sea level compared with present [0] as zero	Dublin tidal amplitudes					Douglas tidal amplitudes				
	M_2 (m)	S_2 (m)	Σ all six constituents (m)	S_2 % of M_2	Σ all six constituents % of [0]	M_2 (m)	S_2 (m)	Σ all six constituents (m)	S_2 % of M_2	Σ all six constituents % of [0]
+5	1.334	0.415	2.004	31.1	121.5	2.452	0.811	3.555	33.1	111.2
+2	1.192	0.363	1.782	30.5	108.0	2.334	0.744	3.349	31.4	104.8
0	1.090	0.335	1.650	30.7	100.0	2.234	0.703	3.197	31.5	100.0
−2	0.990	0.313	1.534	31.6	94.2	2.126	0.674	3.045	31.7	95.2
−5	0.857	0.289	1.382	33.7	83.8	1.982	0.649	2.845	32.7	89.0
−10	0.712	0.278	1.163	39.0	70.5	1.827	0.619	2.578	33.9	80.6
−15	0.780	0.347	1.366	44.5	82.8	1.684	0.543	2.353	32.2	73.6
−20	0.981	0.400	1.530	40.8	94.0	1.643	0.523	2.350	31.8	73.5
−25	1.128	0.456	1.861	40.4	112.8	1.777	0.513	2.648	28.9	82.8
−30	1.342	0.498	2.069	37.1	125.4	1.641	0.469	2.474	28.6	77.4

TABLE 1. Continued.

Model mean sea level compared with present [0] as zero	Inner dowsing tidal amplitudes					Helgoland tidal amplitudes				
	M_2 (m)	S_2 (m)	Σ all six constituents (m)	S_2 % of M_2	Σ all six constituents % of [0]	M_2 (m)	S_2 (m)	Σ all six constituents (m)	S_2 % of M_2	Σ all six constituents % of [0]
+5	1.947	0.693	3.006	35.6	90.8	1.201	0.333	1.762	27.7	121.0
+2	2.063	0.725	3.173	35.2	95.9	1.081	0.282	1.587	26.1	109.0
0	2.151	0.712	3.309	33.1	100.0	0.985	0.242	1.456	24.6	100.0
−2	2.156	0.672	3.282	31.2	99.2	0.888	0.207	1.308	23.3	89.8
−5	2.034	0.629	2.978	30.9	90.0	0.810	0.186	1.183	23.0	81.3
−10	0.435	0.185	1.217	42.5	36.9	0.818	0.177	1.148	21.6	72.0
−15	0.000	0.000	0.000	100.0	0.0	0.470	0.103	0.657	21.9	45.1
−20	0.003	0.003	0.013	100.0	39.3	0.271	0.070	0.458	25.8	31.5
−25	****	****	****	****	****	0.378	0.101	0.582	26.7	40.0
−30	****	****	****	****	****	0.168	0.042	0.282	25.0	19.4
Model mean sea level compared with present [0] as zero	Bergen tidal amplitudes					Aberdeen tidal amplitudes				
	M_2 (m)	S_2 (m)	Σ all six constituents (m)	S_2 % of M_2	Σ all six constituents % of [0]	M_2 (m)	S_2 (m)	Σ all six constituents (m)	S_2 % of M_2	Σ all six constituents % of [0]
+5	0.377	0.153	0.605	40.6	90.7	1.298	0.458	1.871	35.3	97.3
+2	0.441	0.156	0.677	35.4	101.5	1.307	0.471	1.883	36.0	98.0
0	0.446	0.153	0.667	34.3	100.0	1.346	0.470	1.922	34.9	100.0
−2	0.428	0.153	0.631	35.7	94.6	1.355	0.463	1.920	34.2	99.9
−5	0.423	0.146	0.614	34.5	92.1	1.362	0.481	1.920	35.3	99.9
−10	0.385	0.139	0.581	36.1	87.1	1.347	0.453	1.891	33.6	98.4
−15	0.377	0.149	0.585	39.5	87.7	1.220	0.437	1.777	35.8	92.5
−20	0.413	0.157	0.613	38.0	91.9	1.231	0.459	1.831	37.3	95.3
−25	0.431	0.159	0.616	36.9	92.4	1.336	0.493	1.938	36.9	100.8
−30	0.457	0.166	0.656	36.3	98.4	1.364	0.511	2.000	37.5	104.1
Model mean sea level compared with present [0] as zero	Heysham tidal amplitudes									
	M_2 (m)	S_2 (m)	Σ all six constituents (m)	S_2 % of M_2	Σ all six constituents % of [0]					
+5	2.821	0.945	4.203	33.5	107.0					
+2	2.730	0.883	4.043	32.3	102.9					
0	2.647	0.845	3.928	32.0	100.0					
−2	2.556	0.822	3.815	32.2	97.1					
−5	2.442	0.812	3.696	33.3	94.1					
−10	2.372	0.816	3.561	34.4	90.7					
−15	2.262	0.719	3.491	31.8	88.8					
−20	1.783	0.502	2.858	28.2	72.8					
−25	0.055	0.045	0.229	81.8	5.8					
−30	****	****	****	****	****					

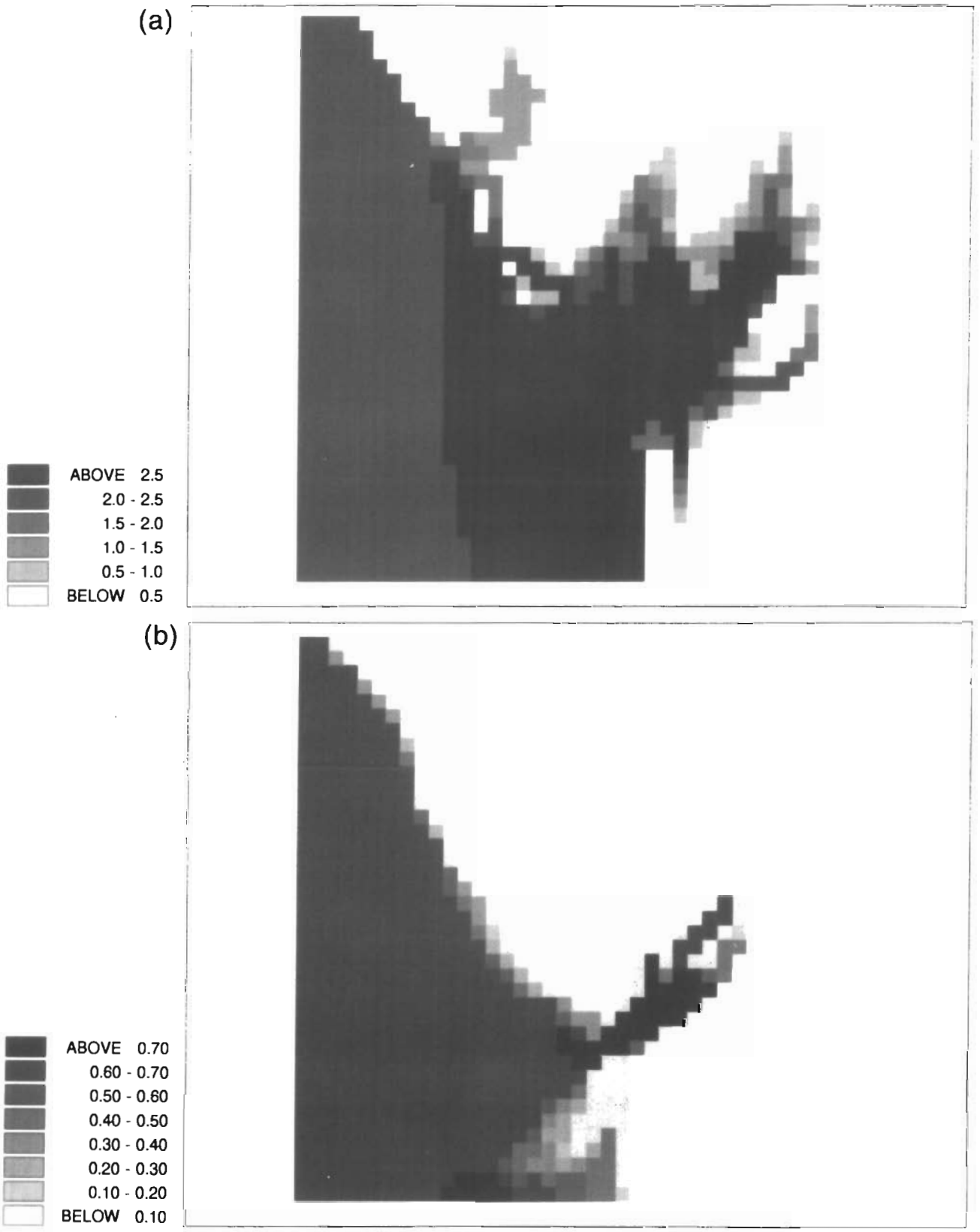

FIG. 6. Maximum values of tidal amplitudes from the Morecambe Bay model (in metres). (a) M_2 at present sea level; (b) M_2 with water depths reduced by 10 m; (c) S_2 at present sea level; (d) S_2 with water depths reduced by 10 m; (e) all six constituents at present sea level; (f) all six constituents with water depths reduced by 10 m.

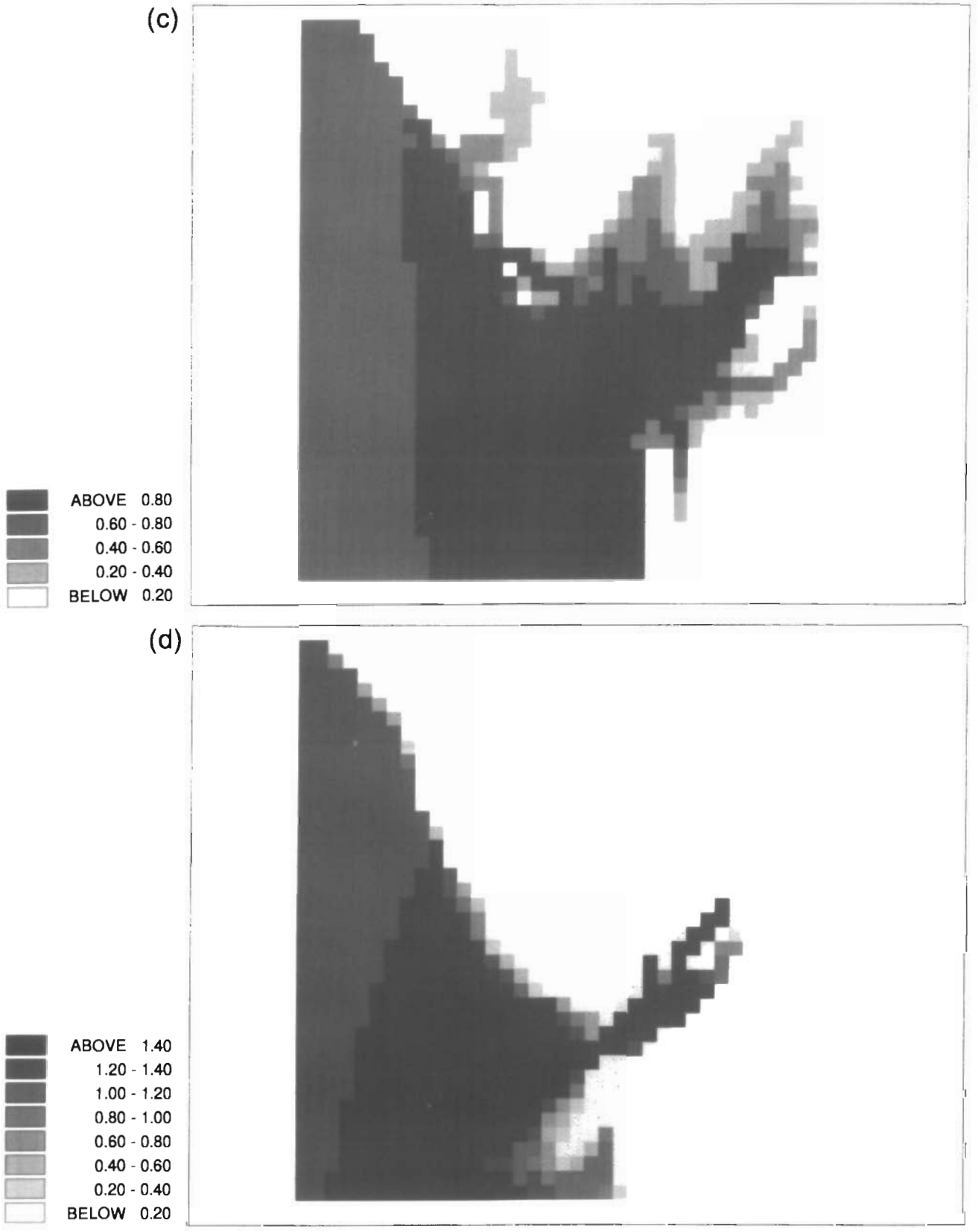
(c)
ABOVE 0.80
0.60 - 0.80
0.40 - 0.60
0.20 - 0.40
BELOW 0.20
(d)
ABOVE 1.40
1.20 - 1.40
1.00 - 1.20
0.80 - 1.00
0.60 - 0.80
0.40 - 0.60
0.20 - 0.40
BELOW 0.20

FIG. 6. c and d.

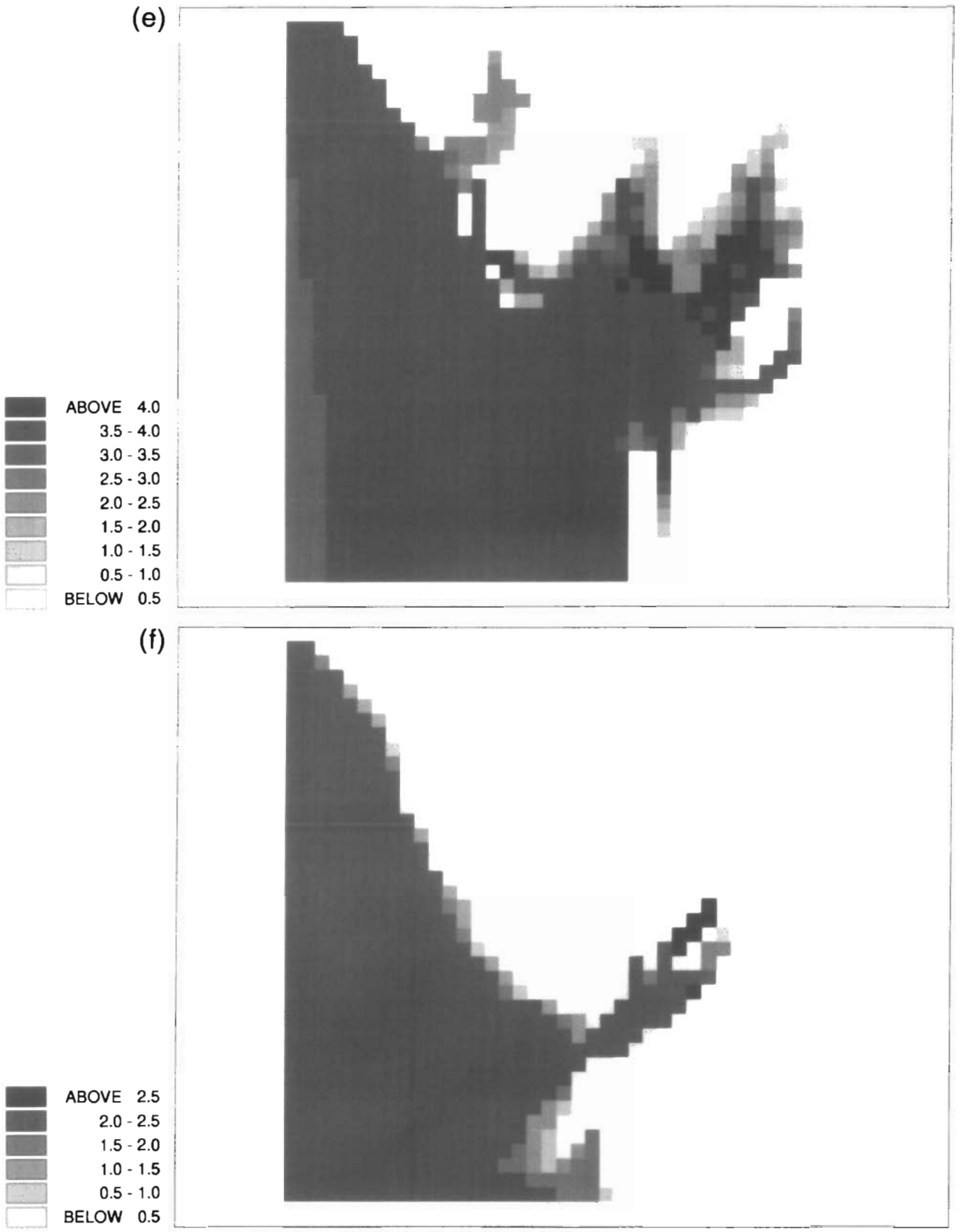
(e)
ABOVE 4.0
3.5 - 4.0
3.0 - 3.5
2.5 - 3.0
2.0 - 2.5
1.5 - 2.0
1.0 - 1.5
0.5 - 1.0
BELOW 0.5
(f)
ABOVE 2.5
2.0 - 2.5
1.5 - 2.0
1.0 - 1.5
0.5 - 1.0
BELOW 0.5

FIG. 6. e and f.

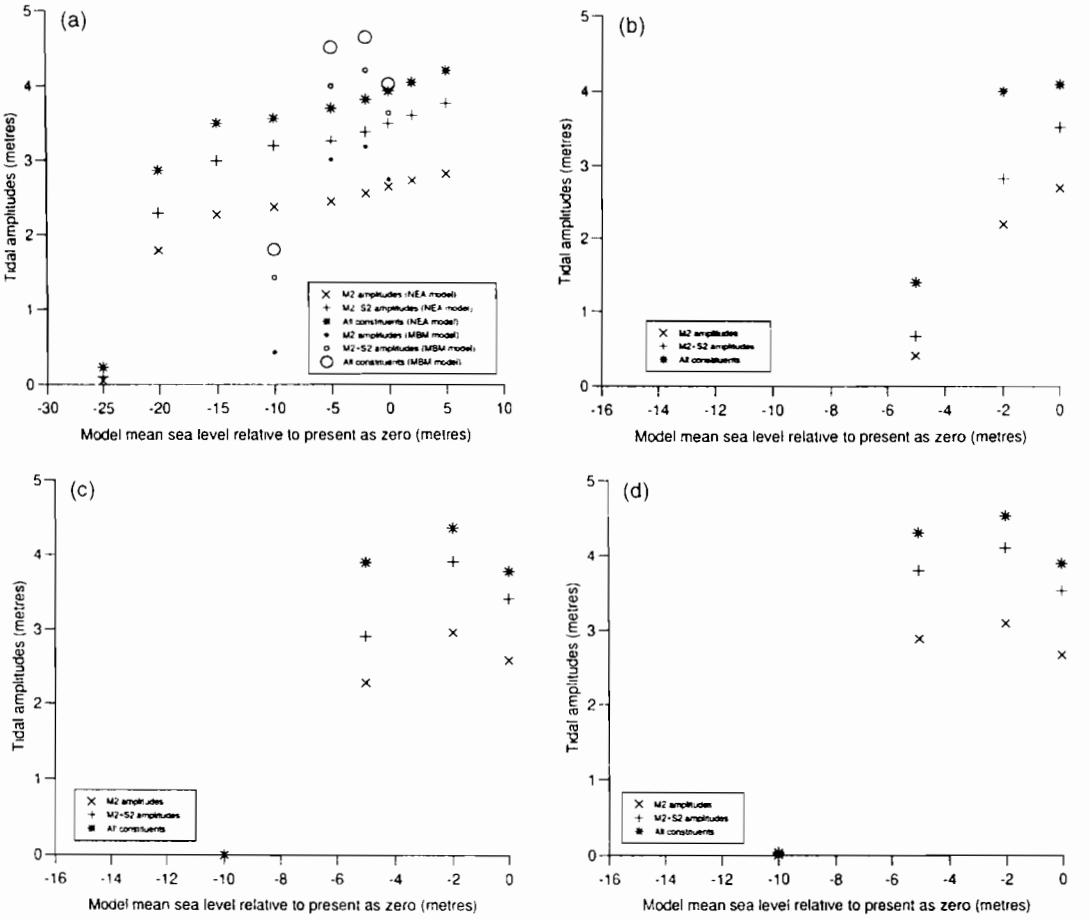

FIG. 7. Results of the maximum values of M_2, M_2+S_2 and all six tidal constituents' amplitudes combined from the Morecambe Bay model. Locations are shown in Fig. 2. (a) Heysham; (b) Morecambe; (c) Halfway Shoals; (d) Wyre Light.

in two areas, off Humberside and off The Wash, in the eastern part of the model.

Table 3 and Fig 9(a–d) illustrate examples from the coastal areas of the EC3 model of the alteration in tidal amplitudes as water depths are changed within the model. There is some local amplification of the M_2 tide when water depths are reduced by 2 m from present levels. However, in general, there is a fairly consistent decrease in tidal amplitudes with all tidal constituents as water depths are reduced. The major changes noted in Morecambe Bay are not found in the EC3 model. Fig. 9(a) shows results from the Northeast Atlantic model plotted over those of the EC3 model. The EC3 model results in this case give slightly higher tidal amplitudes than shown by the Northeast Atlantic model results.

DISCUSSION

Changes to the tidal patterns shown at the scale of the Northeast Atlantic model reflect the movement of amphidromic points and alterations in areas of amplification to the tidal wave at the present day due to resonance. Reductions of water depth result in increased amounts of friction within the model area. The amphidromic points in the models presented here are generally moved in an eastward direction as friction increases. Areas where tidal resonance is important in amplifying the altitudes attained may undergo changes to tidal amplitudes as a result of different geometric configurations as water levels are altered which compound the effect of differing tidal input to the area(s) concerned. Both these factors may be used to explain the various tidal patterns shown in Fig. 4.

Table 1 and Fig. 6 illustrate that the direction of change of tidal amplitudes is by no means constant as water depths are altered. The amplitude of the different tidal constituents varies considerably in relation to each other. These points should be borne in mind for palaeotidal studies. However, it should be stressed that uniform water depth reductions do not model past tides accurately at this scale. Furthermore, the tides in the northeast Atlantic may have changed as the ocean basin evolved to its present shape during the Holocene, requiring an alteration in the tidal boundary input to the Northeast Atlantic model. The contradiction of model results from this scale with geological evidence of tidal changes from coastal barriers and embayments (Roep and Beets, 1988; van de Plassche, 1995) suggests that this small scale of modelling may not be sufficient to highlight the local variations.

The scale changes between the Morecambe Bay model and the Northeast Atlantic model give very different results for the same area from two different models. The Morecambe Bay model highlights the considerable variation in tidal amplitudes within the model area. This is not shown by the Northeast Atlantic model, yet there are amplitude differences of over 4.5 m recorded

TABLE 2. Tidal amplitudes for various locations around Morecambe Bay computed with different water levels in the Morecambe Bay Model. The locations are shown in Fig. 2

Model mean sea level compared with present [0] as zero	Heysham tidal amplitudes					Morecambe tidal amplitudes				
	M_2 (m)	S_2 (m)	Σ all six constituents (m)	S_2 % of M_2	Σ all six constituents % of [0]	M_2 (m)	S_2 (m)	Σ all six constituents (m)	S_2 % of M_2	Σ all six constituents % of [0]
0	2.745	0.888	4 019	32.3	100.0	2.697	0.824	4.091	35.5	100.0
−2	3.180	1.025	4.644	32.2	115.6	2.189	0.632	3.997	28.9	97.7
−5	3.008	0.983	4.508	32.7	112.2	0.407	0.262	1.394	64.4	34.1
−10	0.426	0.993	1.794	231.7	44.6	****	****	****	****	****
−15	****	****	****	****	****	****	****	****	****	****
Model mean sea level compared with present [0] as zero	Halfway Shoals tidal amplitudes					Wyre Light tidal amplitudes				
	M_2 (m)	S_2 (m)	Σ all six constituents (m)	S_2 % of M_2	Σ all six constituents % of [0]	M_2 (m)	S_2 (m)	Σ all six constituents (m)	S_2 % of M_2	Σ all six constituents % of [0]
0	2.591	0.836	3.789	32.3	100.0	2.669	0.864	3.903	32.4	100.0
−2	2.972	0.950	4.369	32.0	115.3	3.102	1.000	4.537	32.2	116.2
−5	2.280	0.631	3.902	27.7	103.0	2.893	0.914	4.308	31.6	110.4
−10	0.000	0.000	0.000	100.0	0.0	0.007	0.007	0.036	100.0	0.9
−15	****	****	****	****	****	0.000	0.000	0.000	100.0	0.0

**** Indicates no result recorded as location was dry land for this simulation

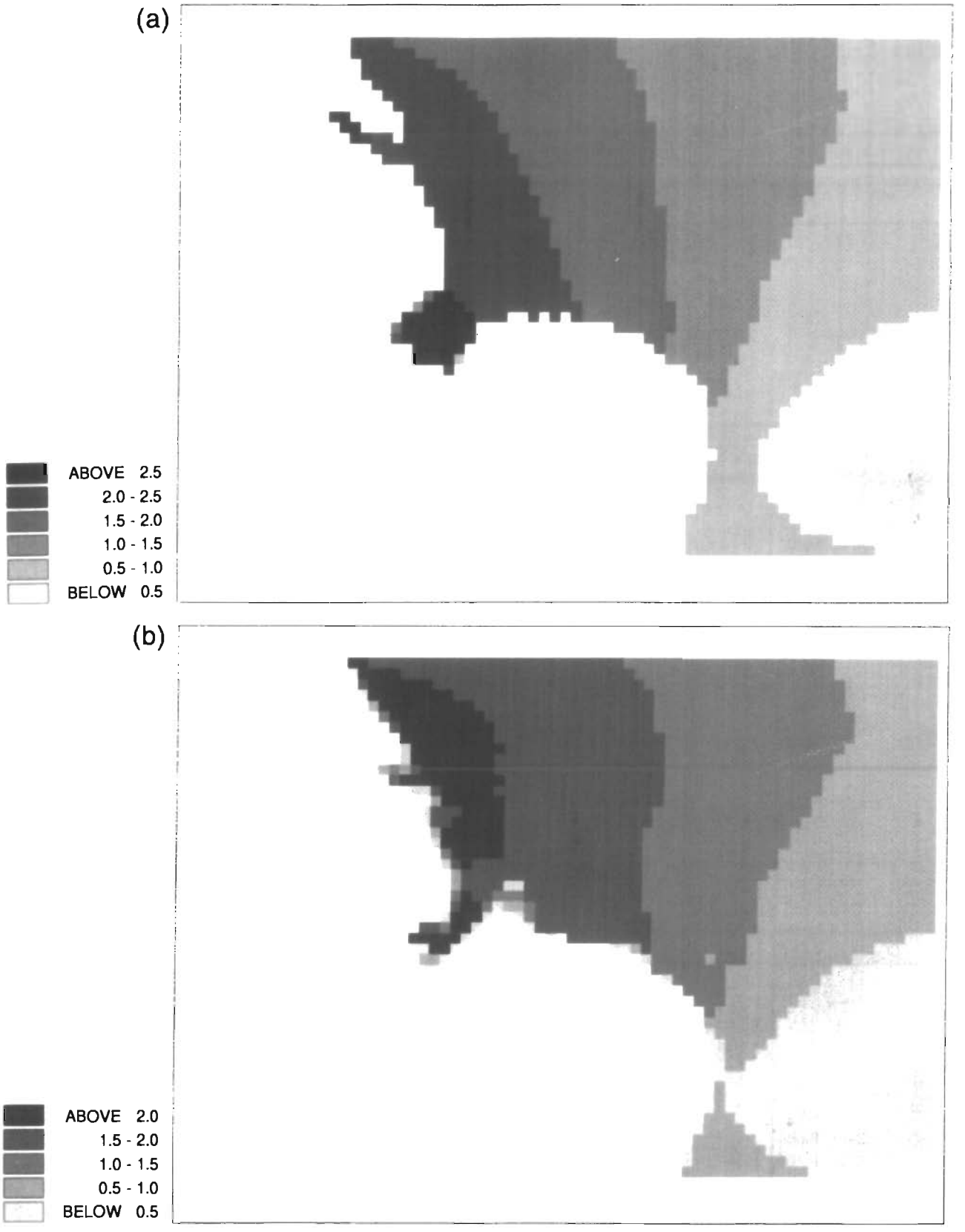

FIG. 8. Maximum values of tidal amplitudes from the EC3 model (in metres). (a) M_2 at present sea level; (b) M_2 with water depths reduced by 10 m; (c) S_2 at present sea level; (d) S_2 with water depths reduced by 10 m; (e) all six constituents at present sea level; (f) all six constituents with water depths reduced by 10 m.

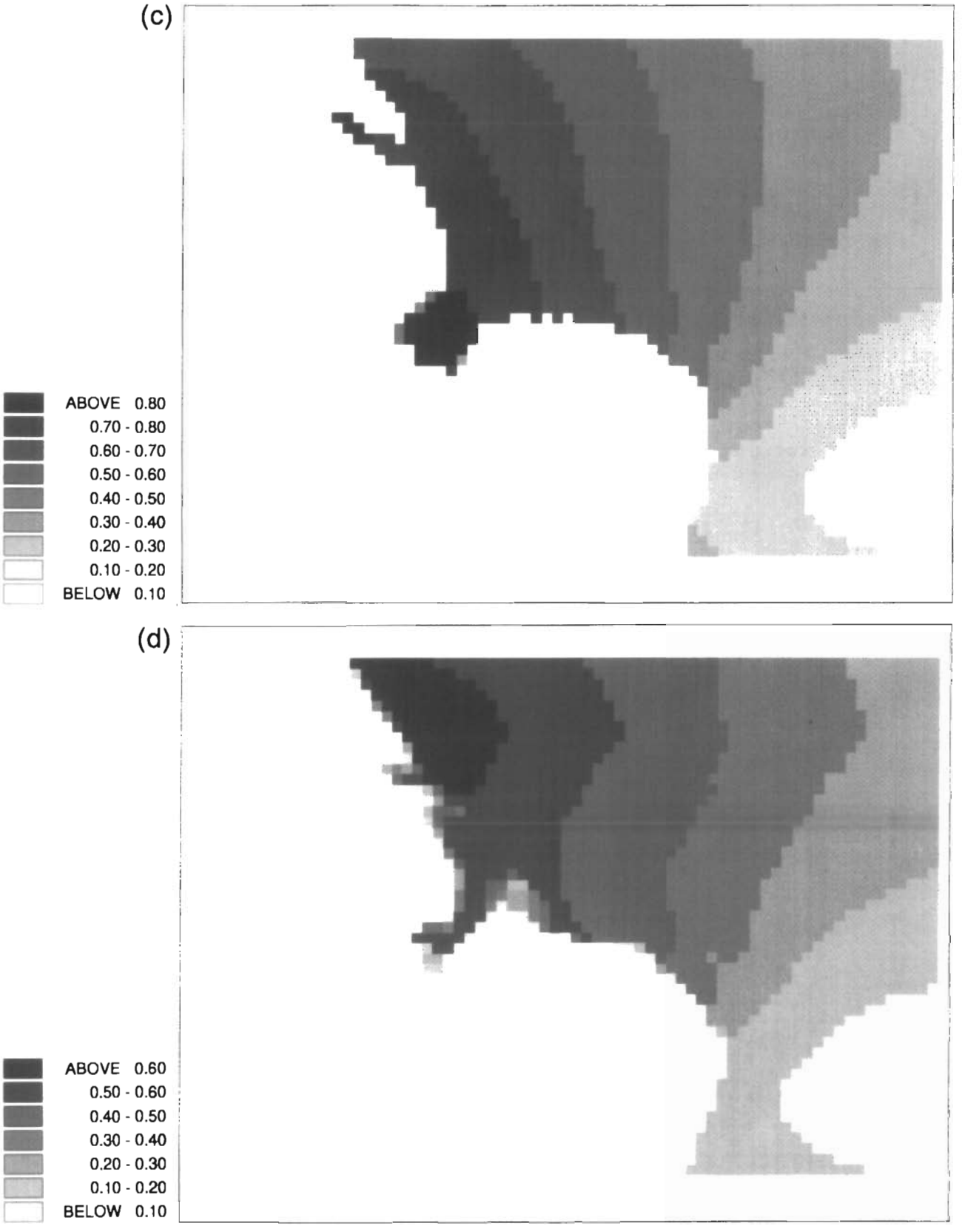
(c)
ABOVE 0.80
0.70 - 0.80
0.60 - 0.70
0.50 - 0.60
0.40 - 0.50
0.30 - 0.40
0.20 - 0.30
0.10 - 0.20
BELOW 0.10
(d)
ABOVE 0.60
0.50 - 0.60
0.40 - 0.50
0.30 - 0.40
0.20 - 0.30
0.10 - 0.20
BELOW 0.10

FIG. 8. c and d.

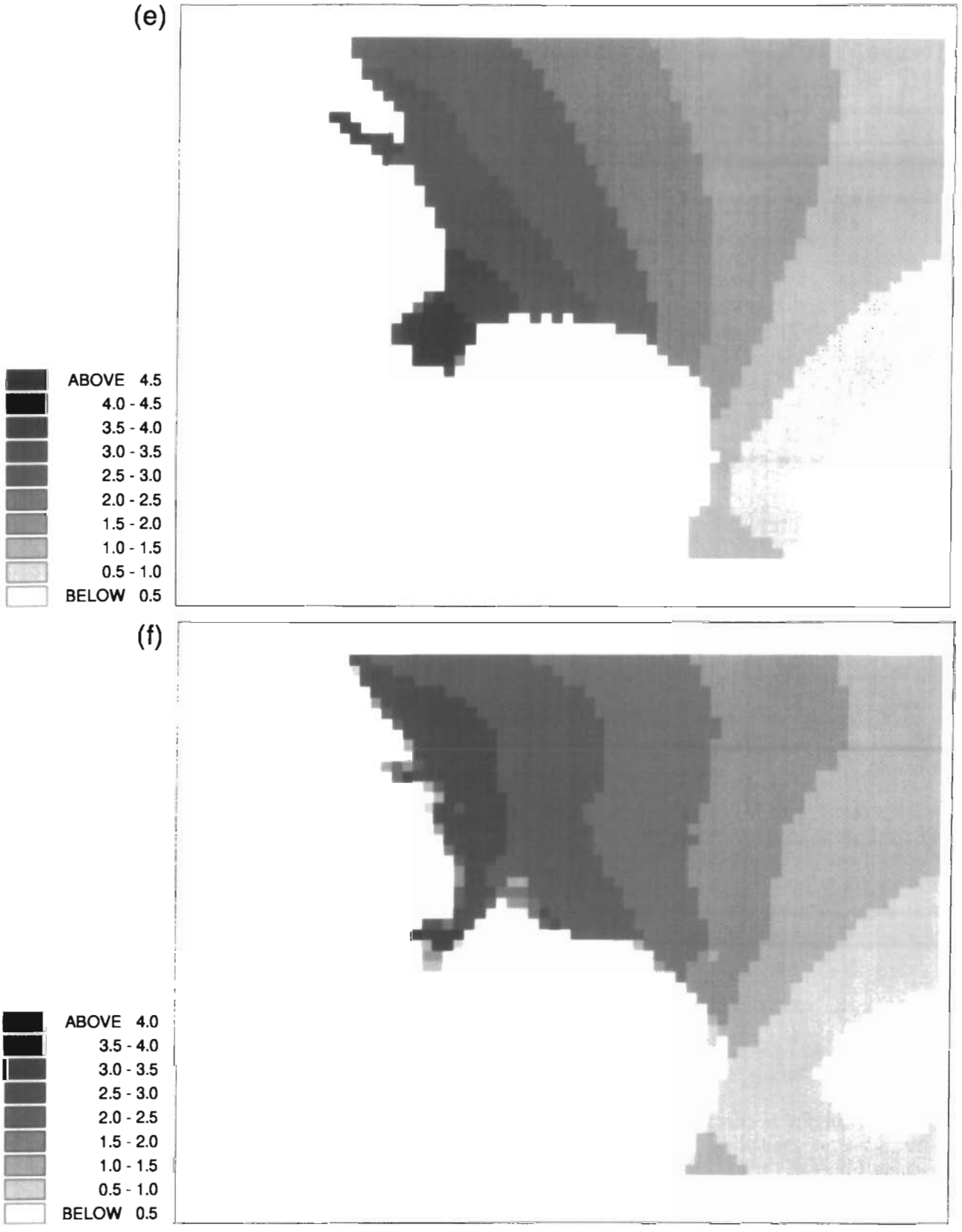
(e)
ABOVE 4.5
4.0 - 4.5
3.5 - 4.0
3.0 - 3.5
2.5 - 3.0
2.0 - 2.5
1.5 - 2.0
1.0 - 1.5
0.5 - 1.0
BELOW 0.5
(f)
ABOVE 4.0
3.5 - 4.0
3.0 - 3.5
2.5 - 3.0
2.0 - 2.5
1.5 - 2.0
1.0 - 1.5
0.5 - 1.0
BELOW 0.5

FIG. 9. e and f.

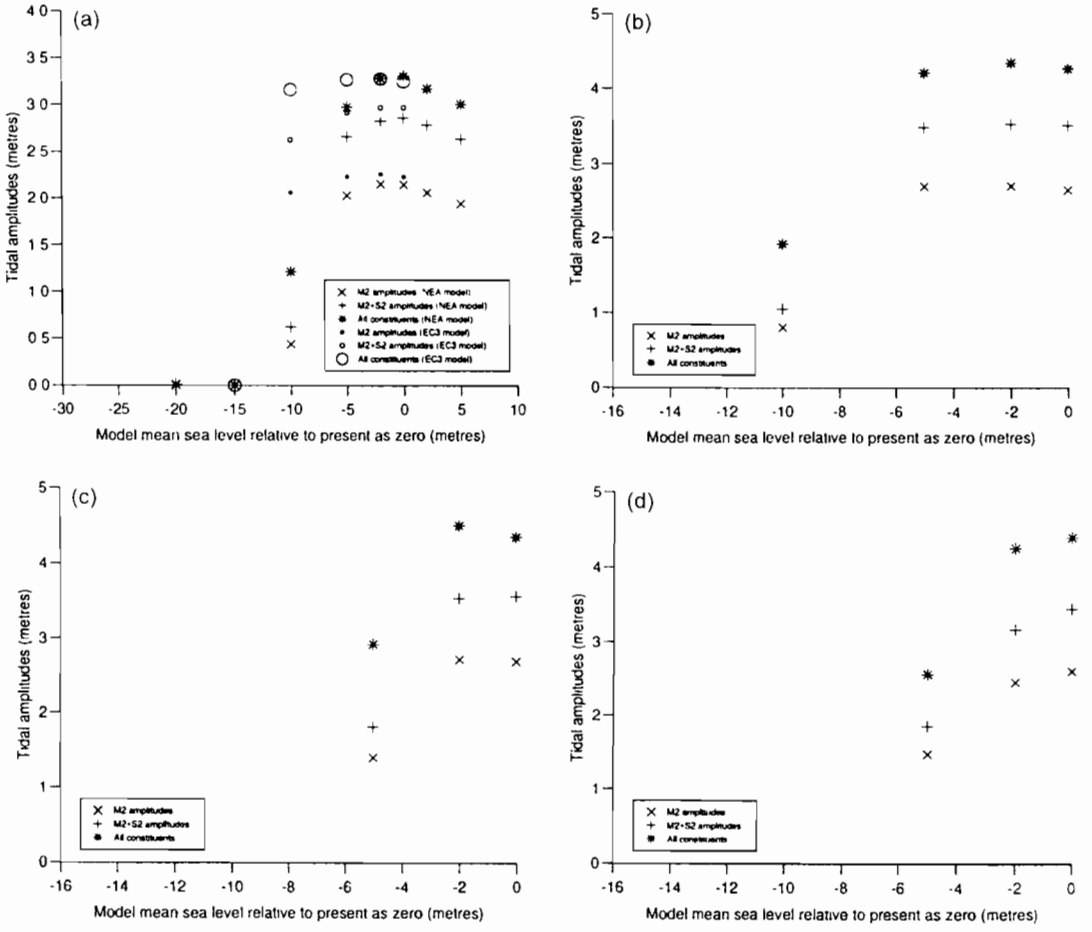

FIG. 9. Results of the maximum values of M_2, M_2+S_2 and all six tidal constituents' amplitudes combined from the EC3 model. Locations are shown in Fig. 3. (a) Inner Dowsing; (b) Roaring Middle; (c) Tabs Head; (d) Immingham.

(Fig. 6(e)). The complete change to S_2 dominance when water depths are reduced by 10 m emphasises, again, the considerable alterations of tidal constituents relative to one another.

The EC3 model again highlights the greater variation which a more local model shows for an area, compared with the Northeast Atlantic model. However, in this case, changes are not so great between the models of different scale as those found between the Morecambe Bay and Northeast Atlantic models.

CONCLUSIONS

Although the simulations carried out in this paper cannot be related directly to tidal conditions at any specific time, the manner in which tides vary with different water depths is illustrated. It has been shown that the scale of modelling is very important in determining the model results for any given location. More detailed models of local areas often have considerable variation of tidal amplitudes within the model than can be shown by a single result, averaged to one grid cell, from a smaller scale model. The differences extend to a considerable variation in results for different tidal constituents, as is most dramatically shown in the case of the Morecambe Bay model. Even at the scale of the Northeast Atlantic model, tidal constituents vary in their relationships to each other to a large degree. It is therefore inappropriate to use one tidal constituent, such as M_2, to deduce amplitudes of others at different water depths.

It cannot be assumed that the tidal constituents used in this study will be those most important for palaeotidal modelling. Each ocean basin amplifies a different set of tidal constituents, which interact in a non-linear fashion, and the relationships of these constituents may change over time as the boundary conditions and configuration of the basin shape itself change. This must be taken into account when carrying out a palaeotidal modelling exercise. The north Atlantic has undergone considerable width and depth changes as recently as the Holocene. This should be taken into account when determining the model ocean boundary tidal input for palaeotidal studies.

The way forward with tidal modelling studies is to include realistic estimates of the palaeobathymetry for an area in the model. This might be done by employing data from crustal rebound models in a formerly glaciated area. Modelling should be carried out at a scale appropriate to the results required. For detailed sea level studies within a coastal embayment, a final model grid resolution of 1 km might be reasonable. Models covering the area of the continental shelf are unlikely to produce realistic tidal amplitude results for such a study as changes to the tidal wave crossing the shelf edge are clearly important.

TABLE 3. Tidal amplitudes for various locations in the EC3 model computed with different water levels in the EC3 model. The locations are shown in Fig. 3

Model mean sea level compared with present [0] as zero	Immingham tidal amplitudes					Roaring Middle tidal amplitudes				
	M_2 (m)	S_2 (m)	Σ all six constituents (m)	S_2 % of M_2	Σ all six constituents % of [0]	M_2 (m)	S_2 (m)	Σ all six constituents (m)	S_2 % of M_2	Σ all six constituents % of [0]
0	2.609	0.848	4.403	32.5	100.0	2.646	0.863	4.263	32.6	100.0
−2	2.457	0.721	4.261	29.3	96.3	2.704	0.830	4.344	30.7	101.9
−5	1.473	0.386	2.567	26.7	58.3	2.694	0.791	4.207	29.4	98.7
−10	****	****	****	****	****	0.804	0.251	1.920	31.2	45.0
−15	****	****	****	****	****	****	****	****	****	****
Model mean sea level compared with present [0] as zero	Tabs Head tidal amplitudes					Inner Dowsing tidal amplitudes				
	M_2 (m)	S_2 (m)	Σ all six constituents (m)	S_2 % of M_2	Σ all six constituents % of [0]	M_2 (m)	S_2 (m)	Σ all six constituents (m)	S_2 % of M_2	Σ all six constituents % of [0]
0	2.696	0.880	4.363	32.6	100.0	2.236	0.736	3.250	32.9	100.0
−2	2.720	0.824	4.513	30.2	103.4	2.264	0.706	3.275	31.2	100.8
−5	1.401	0.408	2.917	29.1	66.9	2.238	0.678	3.268	30.3	100.5
−10	****	****	****	****	****	2.062	0.566	3.157	27.4	97.1
−15	****	****	****	****	****	0.000	0.000	0.001	100.0	0.0

**** Indicates no result recorded as location was dry land for this simulation.

Modelling should commence at the scale of the northeast Atlantic for detailed studies of coastal embayments on the northwest European shelf. This may explain the differences between geological studies of palaeotides (e.g. Roep and Beets, 1988; van de Plassche, 1995) and those found from numerical modelling work carried out on the northwest European shelf (e.g. Franken, 1987; Austin, 1988, 1991).

The real value of modelling former tides is that this can provide estimates of tidal altitudes to compare against geologically-derived sea-level curves or bands (van der Spek, 1994). Such modelling may provide a further key to the palaeoenvironment, leading to the re-interpretation of the geology of an area, as found by van der Spek (1994). On a local scale, palaeotidal modelling can help with relating a sea-level indicator to a former level of the tide (Devoy, 1987).

ACKNOWLEDGEMENTS

This work would not have been possible without the assistance of Roger Flather and colleagues of the Proudman Oceanographic Laboratory who supplied the tidal model program used in the study. Use of the Cray and Convex supercomputers at the University of London Computer Centre for producing the results is acknowledged with gratitude. Equally, the facilities of the University Computing Service and School of Geography at Leeds University proved invaluable in the production of this paper. David Appleyard, Graphics Unit, School of Geography, Leeds University, is thanked for preparing Figs 1, 2 and 3. The paper was completed during a visit to the Department of Earth and Atmospheric Sciences at the University of Alberta at Edmonton and Professor Nat Rutter's help with access to the necessary facilities is gratefully acknowledged. The reviewers are thanked for their constructive comments.

Work on the topic of palaeotidal modelling was commenced whilst the author was in receipt of a NERC research studentship at the University of Durham. This paper is a contribution to the IGCP project 367, Late Quaternary Records of Rapid Coastal Change international working group on Tidal Amplitude Changes, and the INQUA Subcommission on Shorelines of Northern and Western Europe.

REFERENCES

Andersen, O.B., Woodworth, P.L. and Flather, R.A. (1995). Inter-comparison of recent ocean tide models. *Journal of Geophysical Research*, **100, C12,** 25261–25282.

Austin, R.M. (1988). The Paleotidal Regime on the North-West European Continental Shelf. Unpublished M.Sc. thesis, University College of North Wales, Bangor, U.K.

Austin, R.M. (1991). Modelling Holocene tides on the north-west European continental shelf. *Terra Nova*, **3,** 276–288.

Devoy, R.J.N. (1987). Introduction and first principles. *In*: Devoy, R.J.N. (ed.) *Sea Surface Studies*. Croom Helm, Beckenham, Kent

Doodson, A.T. and Warburg, H.D. (1941). *Admiralty Manual of Tides*. HMSO, London.

Flather, R.A. (1981). Results from a model of the north-east Atlantic relating to the Norwegian coastal current. *In*: Sætre, R. and Mork, M. (eds) *The Norwegian Coastal Current*, **2**, pp. 427–458. Bergen, Norway.

Flather, R.A. and Heaps, N.S. (1975). Tidal computations for Morecambe Bay. *Geophysical Journal of the Royal Astronomical Society*, **42,** 489–517.

Flather, R.A. and Hubbert, K.P. (1990). Tide and surge models for shallow water — Morecambe Bay revisited. *In*: Davies, A.M. (ed.), *Modelling Marine Systems*, **1**. CRC Press, Boca Raton, Florida

Franken, A.F. (1987). Rekonstruktie van het paleo-getijklimaat in de Noordzee. Masters thesis, Delft Hydraulics Laboratory, The Netherlands.

Hinton, A.C. (1992a). Modelling Tidal Changes within The Wash and Morecambe Bay during the Holocene. Unpublished Ph.D. thesis, University of Durham, U.K.

Hinton, A.C. (1992b). Palaeotidal changes within the area of the Wash during the Holocene. *Proceedings of the Geologists' Association*, **103,** 259–272.

Hinton, A.C. (1995). Holocene tides of The Wash, U.K.: the influence of water-depth and coastline-shape changes on the record of sea-level change. *Marine Geology*, **124,** 87–111.

van de Plassche, O. (1995). Evolution of the intra-coastal tidal range in the Rhine-Meuse delta and Flevo Lagoon, 5700–3000 yrs cal B.C. *Marine Geology*, **124**, 113–128.

Roep, Th.B. and Beets, D.J. (1988). Sea level rise and paleotidal levels from sedimentary structures in the coastal barriers in the western Netherlands since 5600 BP. *Geologie en Mijnbouw*, **67,** 53–61.

van der Spek, A. (1994). Large-scale Evolution of Holocene Tidal Basins in The Netherlands. Doctoral thesis, University of Utrecht, The Netherlands

Woodworth, P.L., Shaw, S.M. and Blackman, D.L. (1991). Secular trends in mean tidal range around the British Isles and along the adjacent European coastline. *Geophysical Journal International*, **104,** 593–609.

Pergamon

Quaternary Science Reviews, Vol. 15, pp. 895–900, 1996.

0277–3791/96 $32.00

PII: S0277-3791(96)00060-1

COASTAL MODIFICATION DUE TO HUMAN INFLUENCE IN SOUTH-WESTERN TAIWAN

JIUN-CHUAN LIN

Department of Geography, National Taiwan University, Taipei, Taiwan

Abstract — The coastal zone of southwest Taiwan is characterised by muddy tidal flats, offshore bars, spits, lagoons and coastal sand dunes. These geomorphic features form an essential part of the natural defences against sea-level change and coastal erosion. Between 1955 and 1995 the area bounded by the Pei-Kang and Tseng-Wen rivers underwent considerable land use and topographic changes. Two examples were studied using time-series aerial photographs, remote sensing images and geomorphological field mapping. The result of this investigation demonstrates the influence of human activities and the importance of the natural coastal landscape in acting as a first-line of coastal defence and protection in Taiwan. Attention is drawn to: (1) inappropriately designed or misplaced coastal engineering structures which may destroy or reduce the effectiveness of neighbouring natural and engineered structures leading to storm damage, flooding and encroachment by the sea; (2) the need for a co-ordinated coastal management program to regulate on-shore activities, in particular the removal of ground water within the coastal zone. This research demonstrates that there is significant land subsidence and inland penetration of sea water into the ground water system in the coastal zone. Human activities also lead to considerable financial expenditure on the prevention of coastal erosion in Taiwan. Copyright © 1996 Elsevier Science Ltd

INTRODUCTION

The coastal zone of south-west Taiwan (Fig. 1) is characterised by muddy tidal flats, offshore bars, spits, lagoons and coastal sand dunes. According to Hsu (1962) the growth of the great coastal plain in south-western Taiwan is accelerated by the moderate uplifting of the region and deposition of sediments from rivers. However, this is also an environmentally sensitive area. Misplaced coastal engineering structures may destroy or reduce the effectiveness of neighbouring natural and engineered structures leading to storm damage, flooding and encroachment by the sea.

The recent increase in industrial and commercial activities within the coastal zone has resulted in modifications to the coastline due to coastal engineering works. These works have also modified the tidal regime. Degradation of the natural first-line of defence against the sea and significant changes to the coastal landscape have been the outcome.

Within the coastal zones, major longshore movements of sediments shape the coastal profile, producing erosional and depositional landforms (Viles and Spencer, 1995). The report of the Highland Regional Council (1991) on recent developments in ocean and coastal management makes some recommendations which are potentially useful in the Taiwanese context, especially for the tidal flat areas found in south-western Taiwan:

(1) Survey all potential and actual pressures on the coastal environment by comparing the present ecological state to historical data, and by using environmental indicators.
(2) Survey all potential and actual conflict between coastal users.
(3) Develop a continuous monitoring scheme for positive and negative changes in distribution and intensity of stresses on the environment.
(4) Formulate priority uses for the management strategy, weighing up the socio-economic and environmental factors locally.
(5) Establish a clear framework plan of specific development policies including coastal-use zoning and an implementation schedule in accordance with existing administrative and legislative constraints.

In this study two examples show environmental sensitivity and vulnerability in the coastal zone: human modifications in south-western Taiwan caused conflict in land use change, while coastal erosion problems became one of the main considerations for coastal management.

METHODOLOGY

In this research, land use change and the topographical change of coastal landforms is related to the dynamic coastal system, including its resources and management of the coastal zone, as well as sea-level change. There is an inherent conflict between the need to protect against

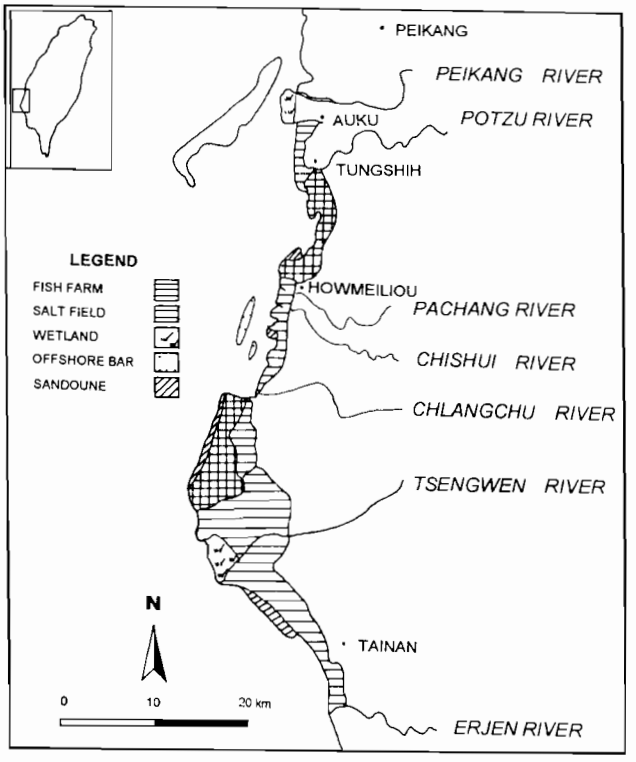

FIG. 1. A geomorphological map of the coastal zone of south-west Taiwan.

erosion and flooding and the need to allow coastal landforms to adjust to natural processes. Development on the coast may lead to significant changes elsewhere within a coastal system (Fig. 2). These changes can affect both the landforms, which provide natural coastal defences and the habitats which they support. The dynamic zone is directly affected by offshore and nearshore natural processes (e.g. storm surges, erosion, deposition, flooding, landslides). The mud flats and salt marshes in south-western Taiwan have developed where fine grained sediment is laid down in sheltered areas with high tidal ranges; coastal sand dunes have developed as a result of wind-blown sand transport.

Coastal systems are subjected to a range of disturbances, both human-induced and natural, and there are many approaches to understanding the response to such changes. Sensitivity and resilience are two concepts often employed to explain the response of environmental systems (Viles and Spencer, 1995). Many parts of the coast are subject to natural hazards.

The varied nature of the coastline also provides significant benefits of shelter and deep water for ports and harbours, breeding grounds for fish and shellfish and opportunities for recreation and tourism. The methodology for the integration of coastal planning and management should be based on:

(1) appreciation of the nature of the coastal environment;
(2) information needs for planning and management;
(3) appropriate responses to planning and management issues (DOE, 1993).

Along the south-western coast of Taiwan, the land reclamation schemes lead to increasing use of the coastal zone for agriculture, industry and settlement. Such human-induced activities enhance the coastal land use problem. However, a concurrent increase in wealth and changing public perception of the coastal resource may result in some coastal areas becoming 'preserved' and an increased desire to prevent widespread 'damage' to the coast in general.

There has been much debate in recent years concerning the global warming/rising sea level issue. It is clear that this rise may be defrayed by tectonic uplift in some parts of coastal Taiwan. However, the subsidence problem in the south-western coastal area is a rather sensitive issue. Regional subsidence, with its consequence of higher relative sea levels, is a threat to unprotected lowlands, some sand dunes, marshlands and mudflats. Sea level rise heightens coastal management problems in this area.

It is necessary to locate sites where human modifica-

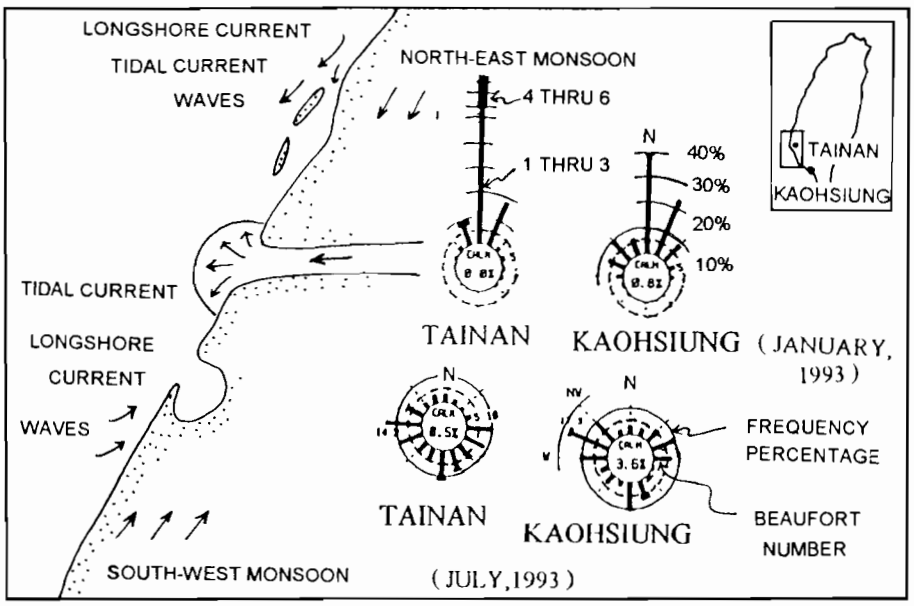

FIG. 2. A sketch map of the coastal environment of south-west Taiwan.

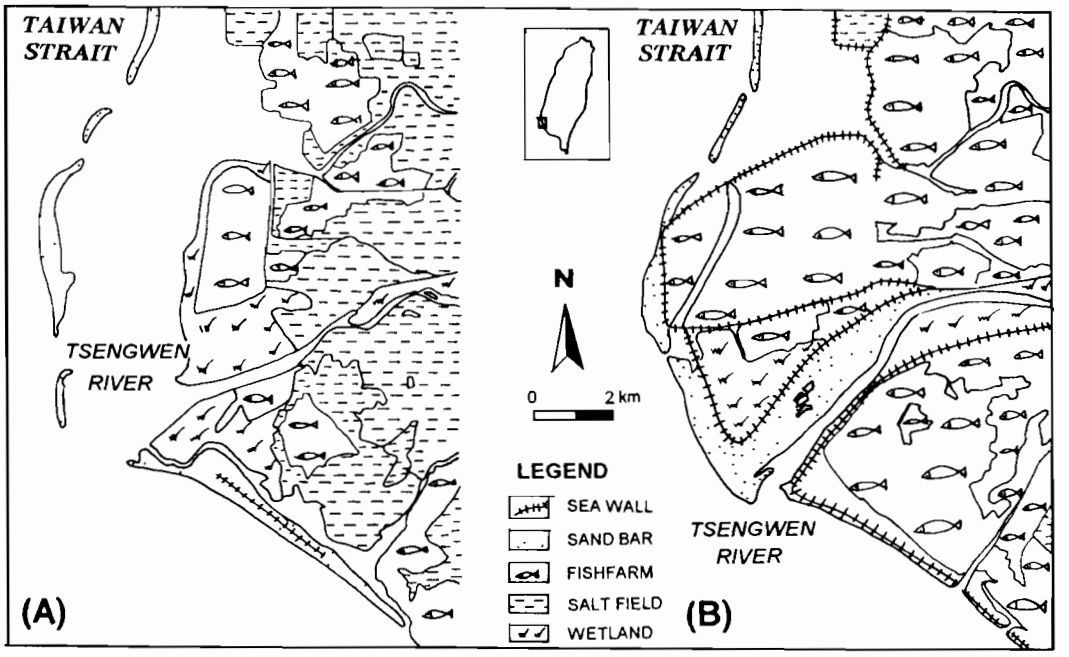

FIG. 3. Coastal change of the estuary of the Tsengwen river between 1955 and 1985. (A) Landuse map of 1955, there is not much human activity along the coastline; (B) landuse map of 1985 (after the construction of sea walls).

tion has occurred and collect data to demonstrate the adjustments of man–land interaction in this research.

The research method applied in this paper is divided into three stages: (1) map/aerial photo/image interpretation; (2) field survey assisted by GPS; (3) mapping and analysis of coastal evolution over a period of 40 years employing the results from stage (1) and (2) above. Map, aerial photo and remote sensing image interpretation help the classification of coastal landform evolution through time. It is necessary to monitor the changes regularly. Different versions of maps (at a scale of 1:5000) and aerial photos (at ca. 1:12,000) are used as references. Field survey helps in identifying and updating the land use. In mapping the evolution of the coastal landforms, ARC/INFO software is used.

RESULTS

The results of this research show that the south-west coast of Taiwan has undergone some significant changes due to human influence between 1955 and 1995. For example, a lagoon has been reclaimed and a thermal power plant has been built on this new land in Hsinda. The main results are listed below.

(1) Figure 3 shows that the estuary of Tsengwen river underwent considerable coastal change between 1955 and 1995. It was a tidal flat with a series of offshore bars (Fig. 3(A)), whereas now the land use type is mainly salt marshes with some fish farms. However, in this area a series of sea walls were built to assist the development of aquaculture. The offshore bars become a natural sea wall in front of the artificial sea walls.

(2) A series of lagoons, offshore bars, spits and coastal dunes has been rapidly submerged beneath the sea since 1955 (Figs 4 and 5). The sea-level change is mainly caused by removal of ground water for aquaculture. This abstraction of ground water results in serious relative land subsidence (5–10 mm/year). There is a need to maintain the sea walls at a reasonable height, such as 5 m above mean sea level for subsidence and storm surges and to ensure the

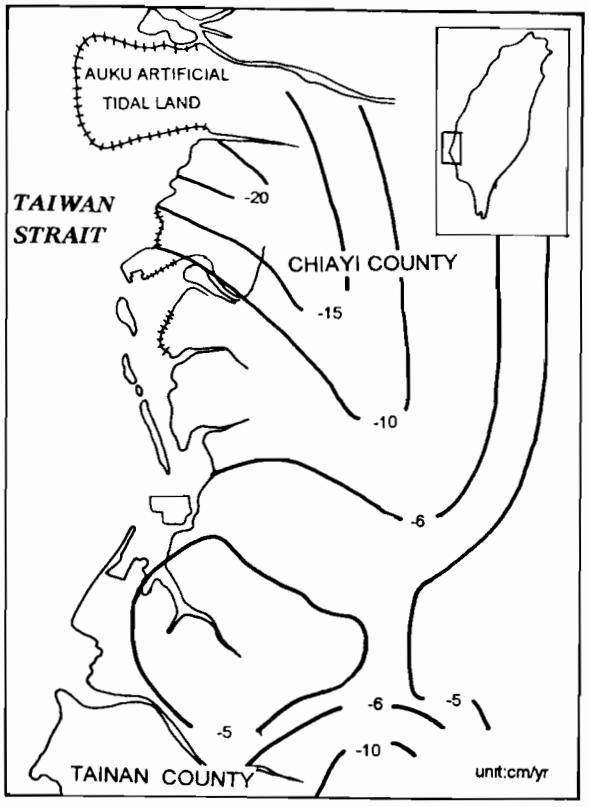

FIG. 4. A map of the subsidence in Chiayi county and Tainan county between 1991 and 1992.

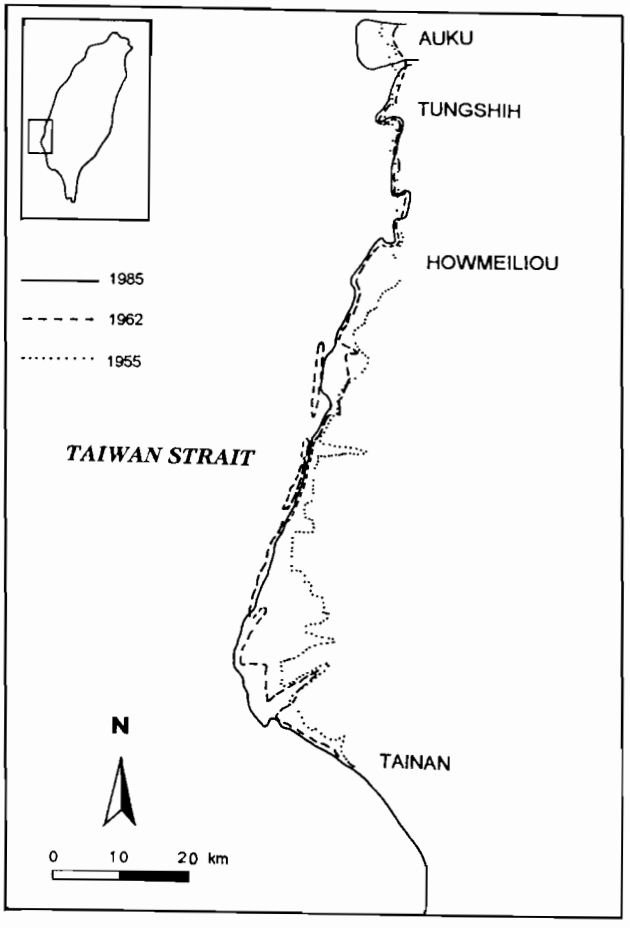

FIG. 5. Coastal change of the south-west coast from different version of maps.

safety of the fish farms. This land subsidence also affects the ongoing engineering projects along the coastline at a huge financial cost (Fig. 3(B)). The subsidence also results in more frequent marine flooding of this area.

(3) There are nine lagoons along the south-west coast. Some lagoons are now used as harbours and thermal power generating stations (Fig. 6) and this has changed the ecology of the lagoons and caused socio-economic concern. Fig. 6(A) shows that there was a lagoon with a long spit in the Hsin-Da area before 1980. The land use is mainly related to the marine industry. The building of the Hsin-Da thermal power station in this area changed the land use type from aquaculture to heavy industry (Fig. 6(B)). A series of sea walls were built to stabilise the coastline. However, due to subsidence, this area is once again under threat from the sea.

(4) The evolution of coastal landforms can be summarised as follows. (a) The fragile muddy tidal flat contains a large quantity of sediments deposited due to fluvial outflow along the coastline. Lagoons, sand bars and coastal plains are the main landforms. The landscape is composed of oyster farms, fish farms and salt fields (fields where salt is evaporated from the sea water). (b) There is significant coastal erosion in the research area resulting from land subsidence. According to the geodetic survey data, the maximum subsidence was more than 20 cm between Auku and Tung-Shih in 1992. The total erosion between Chiayi and Tainan between 1904 and 1987 was ca. 400–843 mm which works out at ca. 5–10 m/year. As a result of the subsidence, the building of sea walls became the most important engineering work along the coastline. These changes have led to coastal erosion of up to 10 m/year between 1976 and 1989 at Howmeiliou, Chiayi County. The erosion of offshore sand bars is serious due to the potential hazard of flooding and coastal

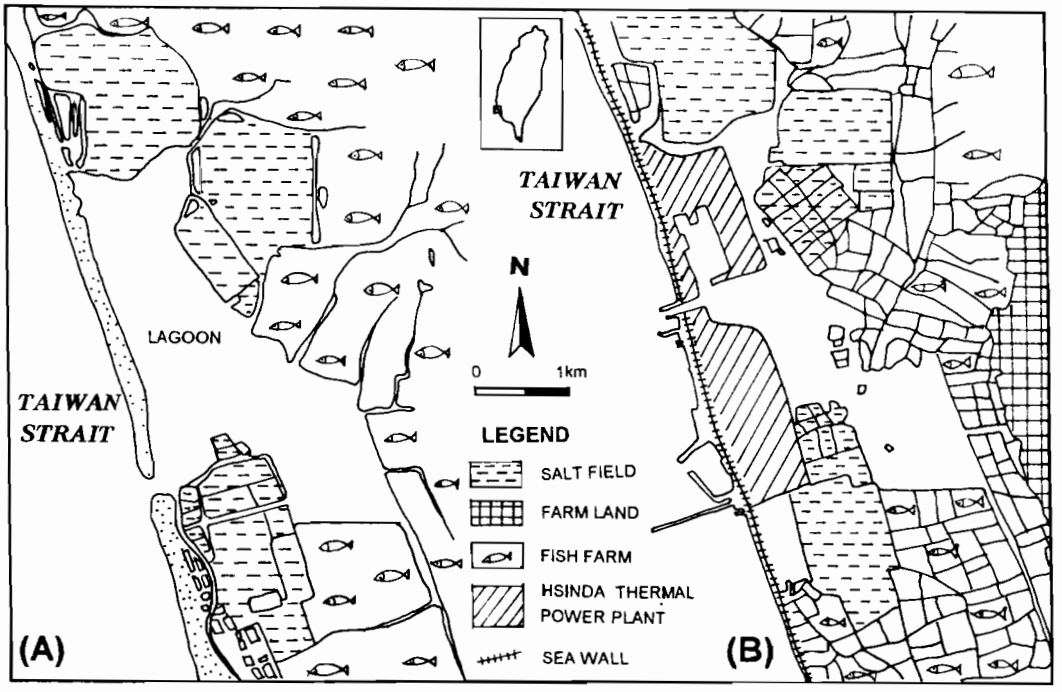

FIG. 6. The disappearing Hsinda lagoon. (A) Hsinda lagoon before the thermal power plant project; (B) after the launching of thermal power plant, the lagoon is disappearing.

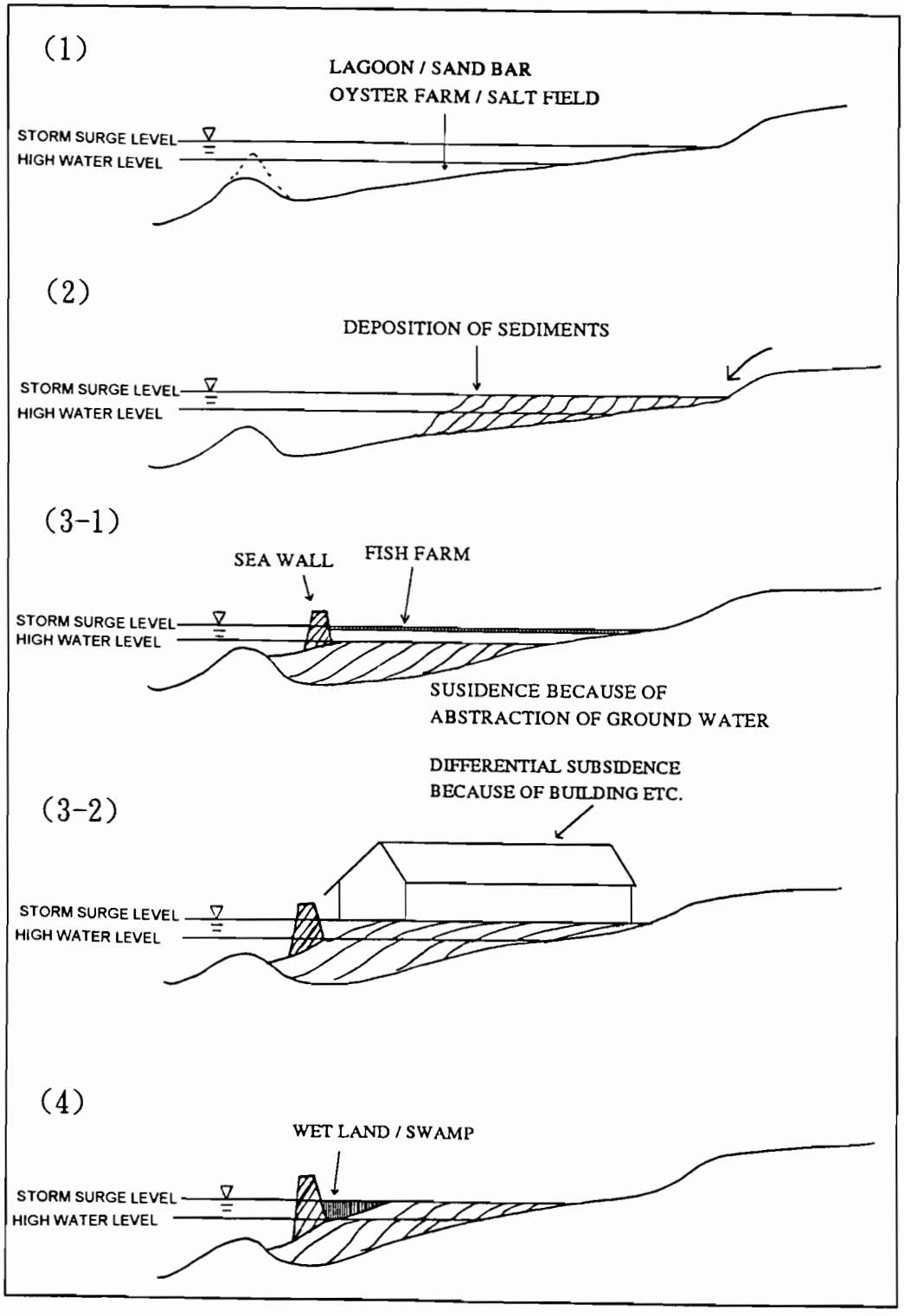

FIG. 7. Proposed coastal change model of south-west coast of Taiwan.

erosion as a result of relative sea level rise. (c) Differential subsidence because of different amounts of sediment compaction and liquefaction caused by earthquakes, also leading to ground subsidence, are other factors which make the coastline a potentially hazardous area (Fig. 7). (d) There are some proposals for an industrial park (Fig. 8) between Chiayi and Tainan. This area has now been protected by sea walls and tetrapods which form a unique landscape along the coastline of south-western Taiwan. The evolution of the coastline is highly dependent on the location of sea walls. In some places the sea walls have become the coastal boundary. (e) The dynamic nature of the coastal zone and the interdependence between beaches and nearshore sedimentation means that management of the coast cannot be considered in isolation. Human activities affecting coastal dunes include the alteration of beach processes and sediment budgets by the construction of sea walls, damage to vegetation, direct removal of dunes, graveyards built on the top of

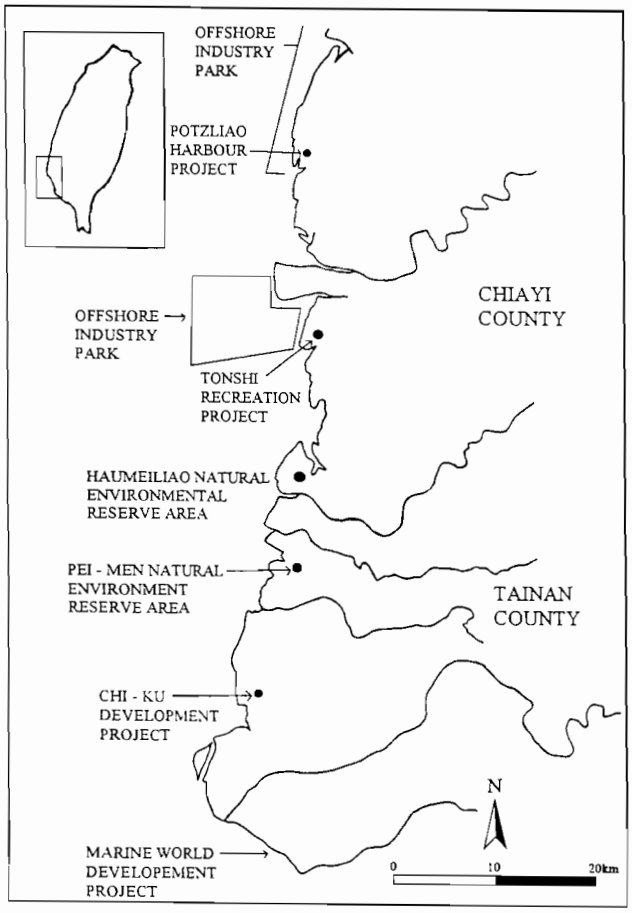

FIG. 8. Proposed coastal projects along the south-west coast of Taiwan.

coastal dunes, alterations to the groundwater table and pollution from oil spills and seeps. Most of the sand dunes along the coastal area of south-western Taiwan have been reclaimed and/or cultivated into paddy fields. The landward aeolian sand transport is mainly influenced by wind; sand is transported from the intertidal zone to the beach. Sand dunes become natural sea walls. The stabilisation of dunes is more important in the offshore bars because these form the first line of defence against sea level rise or coastal erosion. (f) The role of sea walls: many sea walls collapse due to coastal erosion. The reflected wave energy from the sea walls interacts with incoming wave energy, leading to sediment removal at the base of the sea walls, undermining of their foundations and their subsequent collapse. The building of sea walls has meant that the coastline has been turned into an artificial coast. The evolution of landforms is then limited to the littoral zone. The balance of the sediment budget is another factor affecting coastal change.

DISCUSSIONS

Coastal environments are dynamic, comprising continual fluxes of mass, energy and transportation of sediments. Coastal managers should be prepared to accept this dynamism and accommodate it within management structures (Carter, 1988) and south-western Taiwan is no exception. It is necessary to assess all the land units along the coastal zone.

The thermal power plant project has changed the coastal landforms from muddy tidal flats to artificial sea walls. Such changes have resulted in the disappearance of the Hsinda lagoon. Artificial sea walls have also changed the landuse type in that area. Many aquaculture activities were influenced by the project in the nearshore area too. Although the coastline has been stabilised by the artificial sea walls, the original land use and coastal landforms have been changed.

The development of wetland environments is controlled by the change in balance between tidal regime, wind–wave climate, sediment supply, relative sea level and wetland vegetation (Reed, 1990; Allen and Pye, 1992). In the coastal zone of south-western Taiwan there is another important factor, that of coastal engineering projects.

The result of this investigation demonstrates the importance of natural coastal structures in acting as a first line of coastal defence and protection in Taiwan. From the analysis of the coastal system (the dynamic zone, coastal resources and management aspects) the coastal zone of south-western Taiwan is shown to be both vulnerable and erodible. The subsidence of the coastal zone and the building of engineering projects have both changed the landscape along the coastline, increasing the difficulty of coastal management.

ACKNOWLEDGEMENTS

This paper is a contribution to IGCP 367 'Late Quaternary Records of Rapid Coastal Change: Application to Present and Future Conditions' The author would like to thank Dr Anne Hinton, School of Geography, University of Leeds, for her help in reviewing and correcting the draft.

REFERENCES

Allen, J.R.L. and Pye, K. (1992). Coastal salt marshes: their nature and importance. *In*: Allen, J.R.L. and Pye, K. (eds), *Salt Marshes: Morphodynamics, Conservation and Engineering Significance*, pp. 1–18. Cambridge University Press, Cambridge.

Carter, R.W.G. (1988). *Coastal Environments.* Academic Press, London, pp. 99–140.

DOE (1993). *Coastal Planning and Management: A Review.* HMSO, London, 178pp.

Highland Regional Council (1991). Recent developments in ocean and coastal management. *Ocean and Shoreline Management*, **16**, 79–85.

Hsu, T.L. (1962). A Study on the Coastal Geomorphology of Taiwan. *Proceedings of the Geological Society of China*, pp. 29–45.

Reed, D.J. (1990). The impact of sea level rise on coastal salt marshes. *Progress in Physical Geography*, **14**, 465–481.

Viles, H. and Spencer, T. (1995). *Coastal Problems.* Edward Arnold, London, 19–106.

SEISMIC EVENTS RECORDED IN COASTLINES

Pergamon

PII: S0277-3791(96)00059-5

Quaternary Science Reviews, Vol. 15, pp. 901–912, 1996

0277–3791/96 $32.00

COASTAL SEDIMENTATION ASSOCIATED WITH THE JUNE 2ND AND 3RD, 1994 TSUNAMI IN RAJEGWESI, JAVA

A.G. DAWSON,* S. SHI,† S. DAWSON,* T. TAKAHASHI‡ and N. SHUTO‡

**Centre for Quaternary Science, School of Natural and Environmental Sciences, Coventry University, Priory Street, Coventry CV1 5FB, U.K.*

†School of Applied Sciences, Inverness College, 3 Longman Road, Longman South, Inverness, U.K.

‡Disaster Control Research Centre, Tohoku University, Sendai 980, Japan

Abstract — This paper presents the second detailed study of sediments deposited by modern tsunamis, the first being that of the Flores (Indonesia) tsunami of December 1992 (Shi *et al.*, 1995). Sediment cores were collected from areas in which eyewitnesses reported sediment deposition. Grain size analysis shows pronounced vertical variations in grain size as well as changes in standard deviation, skewness and kurtosis that appear to be indicative of complex tsunami flooding. Vertical variations in grain size in individual cores are greater than spatial variations between cores taken along a transect completed perpendicular to the coastline. The Java tsunami-deposited sediments do not show unequivocal evidence of local erosion but instead evidence for sediment transport and deposition is clear and is characterised by dominantly unimodal sediments with fine-tailed distributions. Copyright © 1996 Elsevier Science Ltd

INTRODUCTION

Background

In recent years, a large number of studies have been undertaken on palaeotsunamis. For example, research on the Pacific coastline of North America in Cascadia (Atwater and Yamaguchi, 1991; Atwater and Moore, 1992), Hawaii (e.g. Moore and Moore, 1988), Chile (Paskoff, 1991), Japan (Minoura and Nakaya, 1991), Scotland (e.g. Dawson *et al.*, 1988) and Portugal (Andrade, 1992) have shown the significance of palaeotsunamis both in studies of seismic risk as well as coastal change.

In all these cases of prehistoric tsunamis, it has always been inferred that palaeotsunamis have taken place on the basis of a variety of geomorphological and sedimentary field evidence. This approach faces particular difficulties because in any investigation it is always necessary to distinguish those sediments and landforms attributable to tsunamis from similar features which may have resulted from long-term sea level changes and from storm surges.

Because of these difficulties, it was felt that there was a great urgency to investigate the sedimentary processes associated with modern tsunamis — for example, those which have taken place during the last three or four years, and that these would be of value as long as they were supported by eyewitness observations to confirm that tsunami sediment deposition had taken place in particular locations. An opportunity to make such a study was immediately after the earthquake and tsunami in June 1994 in Java, Indonesia.

THE 1994 JAVA TSUNAMI

On June 2nd and 3rd 1994, a magnitude 7.7 earthquake took place approximately 200 km south of the southern coastline of Java (Fig. 1). The earthquake caused a tsunami that flooded parts of Indonesia and Australia. In Rajegwesi, the flooding caused a tsunami that was observed by several eyewitnesses to have a maximum altitude of 10–12 m (Takahashi, *unpublished*). Numerical models of the tsunami made by Takahashi and Shuto (*unpublished*), show a pattern of complex flood runup at the coast but one which is generally in agreement with the eyewitness observations (Fig. 2). The investigation by the Survey Team indicated that three tsunami floodwaves had taken place in the Rajegwesi area and led to widespread destruction (Figs 3 and 4). Sediment observed by eyewitnesses to have been deposited by the tsunami were sampled by shallow coring along two profile lines (Fig. 1).

Methodology

In this study, the result of detailed granulometric investigations of sediment sheets is described for one site (Rajegwesi). Laboratory particle size analysis of these samples was completed using a laser granulometer

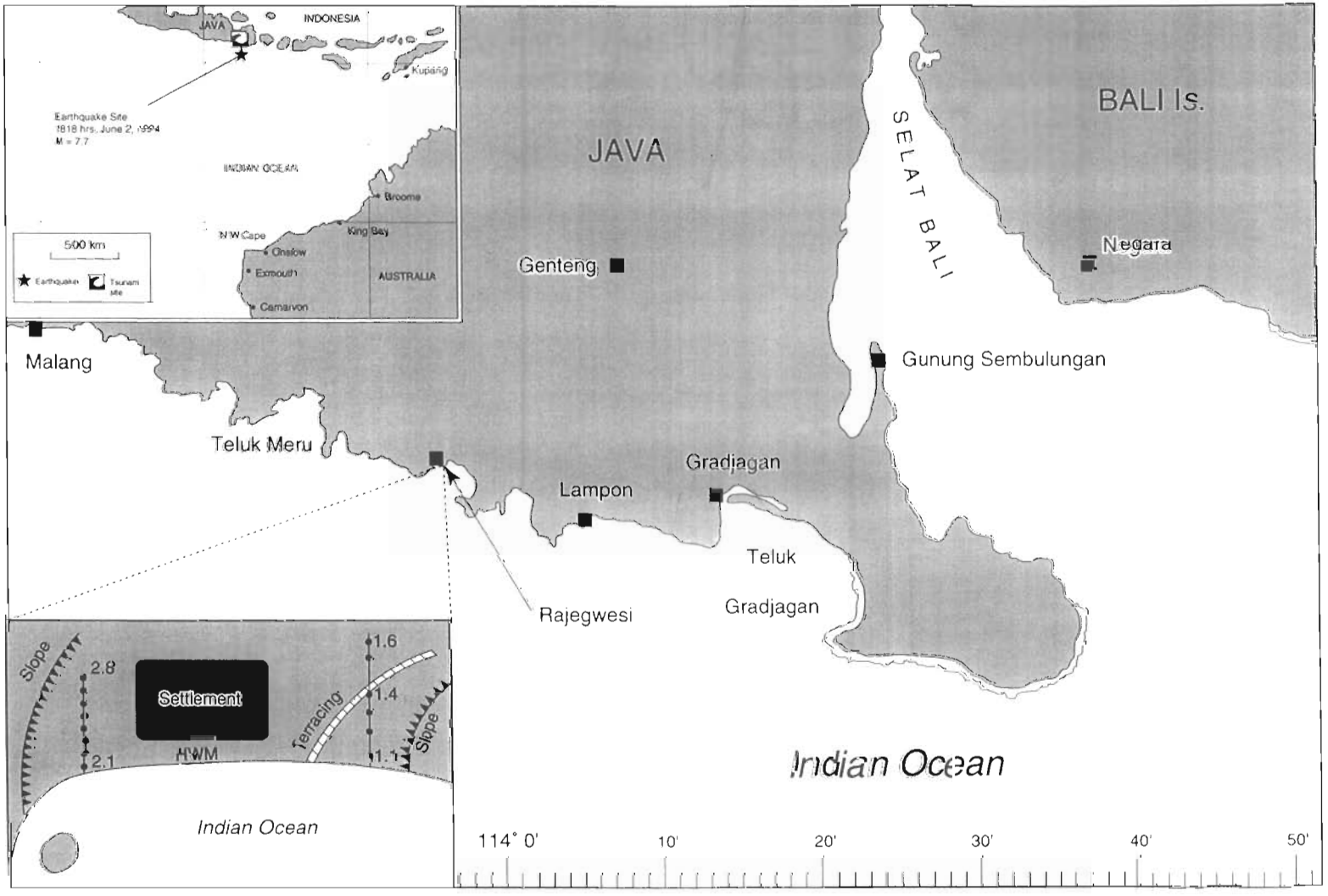

FIG. 1. Map showing earthquake location and Rajegwesi village. Inset shows position of borehole traverses.

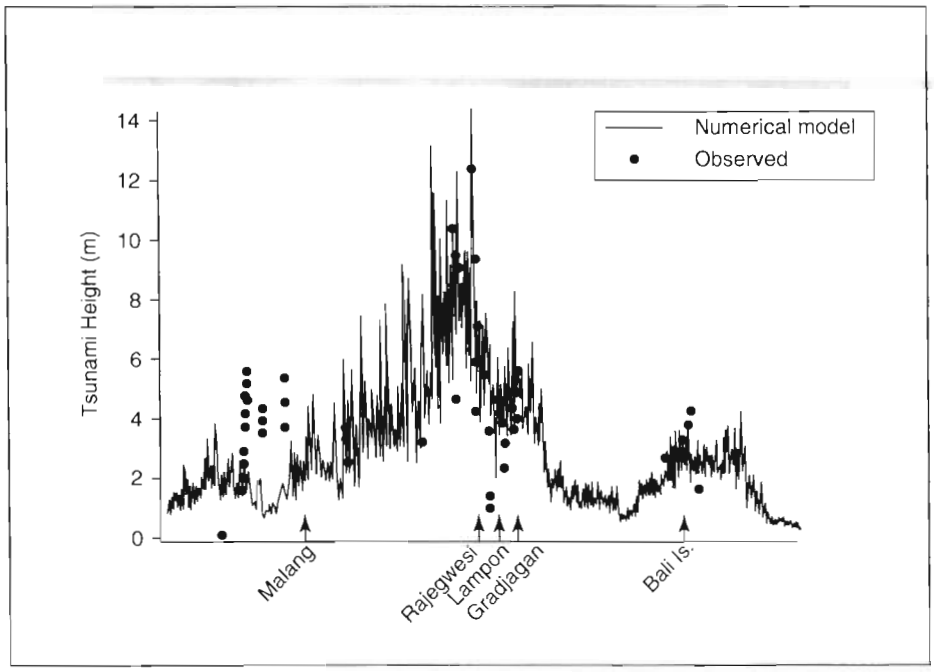

FIG. 2. Comparison of altitudes of tsunami runup as observed by eyewitnesses as well as the theoretical runup values as calculated from the numerical model of Takahashi and Shuto (*unpublished*).

(Malvern 2600 Series, Malvern Instruments, 1989). The statistical method used in this study adopts the formulae of moment statistics based on log–normal theory (McBride, 1971). The Malvern instrument provides analytical results in the form of percentage values of different size classes and the lower and upper limits of the classes are in dimensions of microns (μm). The calculations used involves conversion of values in micrometers into phi values. These conversions are based on:

$$\text{phi } (\phi) = -1 \times \log_2 X \tag{1}$$

where X = the size in mm.

Mean is the mean diameter of particles in a sample and is calculated with the following equation.

$$\text{Mean } (d) = \frac{\sum X_i d_i}{\sum X_i} \tag{2}$$

where d_i is the midpoint of class i, namely the arithmetic mean of the higher and lower limits of the class (in phi). X_i is the percentage of particles in the size band i.

Standard deviation is a measure of the spread from the mean diameter and is calculated from:

$$\delta = \left[\frac{\sum (d_i - d)^2 X_i}{\sum X_i}\right]^{1/2} \tag{3}$$

Skewness is a measure of the degree and direction to

FIG. 3. Coastal damage associated with Java tsunami of 1994. Note discontinuous tsunami sediment sheet in the foreground. Note also flattened vegetation caused by tsunami. (Photo courtesy of S. Tinti.)

FIG. 4. Destruction of settlements at Rajegwesi village. Note also discontinuous sediment sheet as well as transported concrete blocks and tree damage. (Photo courtesy of S. Tinti.)

which a frequency distribution leans (the deviation from normality). It is calculated from:

$$s = \frac{\sum (d_i - d)^3 X_i}{\sum \delta^3 X_i}. \quad (4)$$

Kurtosis is a measure of uniformity of a particle size distribution and is calculated from:

$$k = \frac{\sum X_i (d_i - d)^4}{100\delta^4}. \quad (5)$$

Sediment Sampling

Several days after the Java tsunami took place, one of the authors (TT) visited the area and obtained detailed information from eyewitnesses regarding the area around Rajegwesi that was flooded by the tsunami, as well as the number of individual tsunami waves that flooded this area. The eyewitness accounts made it clear that particular areas had been subject to sediment deposition and, accordingly, a brief survey was made of this area in order to obtain sediment samples confirmed by the eyewitnesses as having been deposited the tsunami. A series of cores were collected along two profile lines (Fig. 1) and these cores were returned to the laboratory for detailed analysis. In several areas near Rajegwesi, the tsunami was associated with the transport of coarse debris including concrete blocks and loose boulders. Tsunami flooding of Rajegwesi also led to the deposition of continuous and discontinuous sediment sheets up to 0.4 m in thickness (Figs 3 and 4). In the laboratory, each core was sliced at 1 cm (and on occasions 5–10 mm) intervals and these sediments were measured for mean (μm) standard deviation, skewness and kurtosis.

Particle Size Analysis: Downcore Variations

In general, the tsunami sediment grains present within each core largely occur within the size range between 100 and 400 microns. On rare occasions, the sand deposits contain shell material (e.g. core 2.8) (Fig. 5). It is clear that there are large variations in the composition of the particle size distributions as illustrated by the percentage frequency curves that range from very well-sorted to poorly-sorted sediments. The particle size distributions appear to have higher kurtosis values (better sorted) than that of the sediment described by Shi *et al.* (1995), and occur as three groups similar to the variations in particle size distribution described by Shi *et al.* for the Flores, Indonesia, tsunami of 1992 (Figs 6 and 7; Shi *et al.*, 1995).

1. Grain size distributions that are characterised by a dominant single mode and possessing an approximate log–normal grain size distribution that is indicative of well-sorted sediments. Generally, these sediments occur in the sand range and on many occasions also possess a distinctive sediment tail composed of silts and clays. The latter deposits generally constitute a small percentage of the total composition, whereas the dominant modal values range between 250 and 400 microns.
2. Multi-modal grain size distributions characterised by at least two dominant modes ranging between fine-grained sand and coarse sand (here defined in excess of 300 microns).
3. Poorly sorted distributions that do not exhibit a clear unimodal peak and which are composed of a mixture of sediments ranging from silts and clays to sands.

The tsunami sediments deposited at Rajegwesi are composed of three dominant sub-populations: (a) a major sub-population that ranges between 200 and 400 microns; (b) a component of fine-grain sediments that range between 100 and 150 microns; and (c) an infrequent coarse sub-population of sediments greater than approximately 350 microns. In general, the Java sediments are

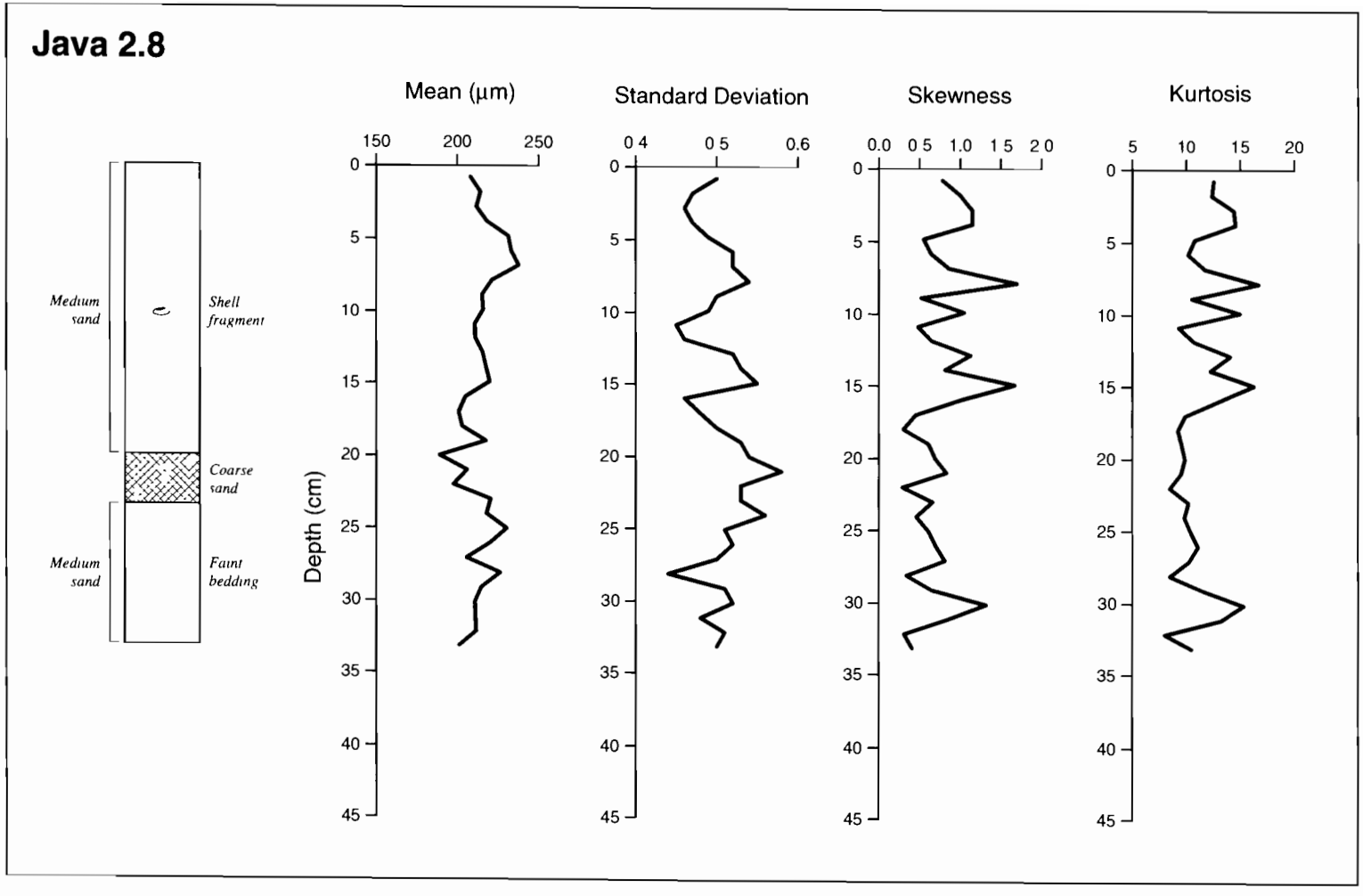

FIG. 5. Vertical variations of mean, standard deviation, skewness and kurtosis for core 2.8.

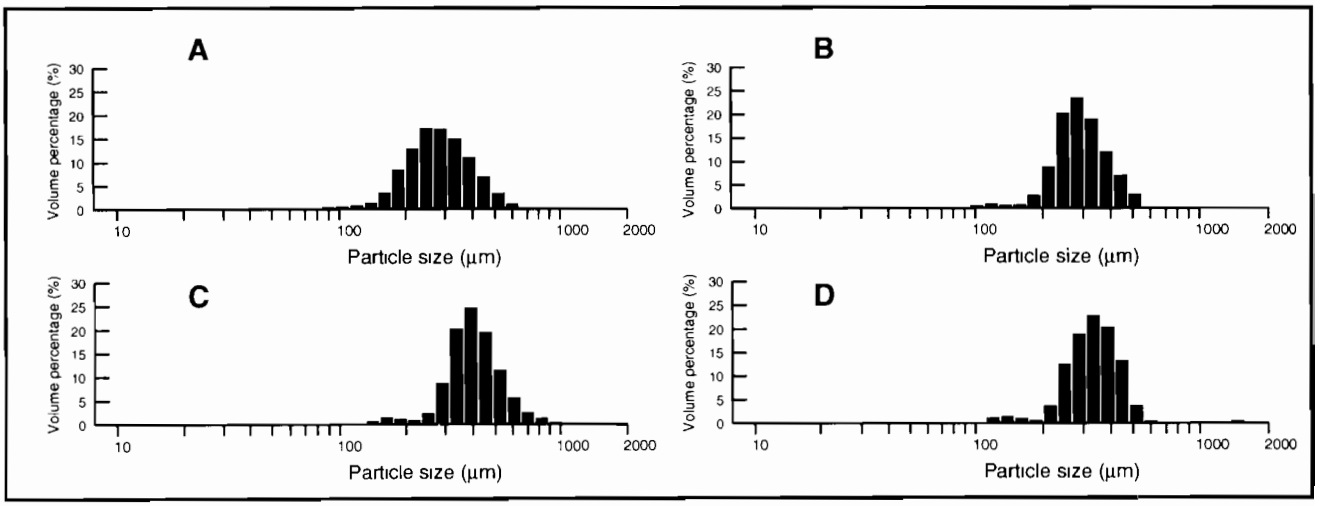

FIG. 6. Representative particle size distributions at core 1.2. Letters A–D are indicated on Fig. 9.

much more uniform than the Flores sediment in terms of particle size distributions.

The calculations of mean, standard deviation, skewness and kurtosis exhibit clear vertical variations in texture illustrated by sharp fluctuations in grain sizes. Many of cores exhibiting the above parameters are characterised by marked fluctuations downcore.

Vertical Variations in Mean Values

In some cases, the vertical changes are scarcely noticeable to the naked eye, yet they are indicated by high-resolution particle size analysis as representing changes in the mean value of no more than 50 μm from the base of individual cores to the top (e.g. core 2.4) (Fig. 8). In other instances, there are pronounced changes. For example, in core 1.2 there is a range in mean grain size over a core thickness of 31 cm of approximately 200 microns (range 210–380 μm) (Fig. 9). In other cores, there is clear evidence of an overall decrease in mean grain size with decreased depth upon which are superimposed episodic variations (e.g. core 2.7) (Fig. 10). In the latter core, the mean grain size decreases from a maximum value of 250 microns at the base of the core to mean values close to 210 μm near the top of the deposit. Throughout the length of this particular core, there are pronounced variations in mean grain size, short vertical intervals are characterised by changes in mean grain size in the order of approximately 50 microns. Similar trends are evident in core 2.7, where the vertical variation in mean grain size ranges between 200 and 250 microns and there are clear episodic variations in mean grain size superimposed upon an overall decrease in mean grain size from base to top (Fig. 10). In some cases, these changes in mean grain size are the most evident characteristic of the vertical grain size variations to such an extent that they mask any progressive variation in mean grain size downcore. In core 2.7, there are two distinctive graded sequences between the 24–30 cm and 14–18 cm depth where there are pronounced decreases in mean grain size with increasing altitude (Fig. 10).

The inspection of the data on mean grain size shows that there are only slight spatial variations in mean grain size and that there is no conspicuous decrease in mean grain size with increased distance inland.

Standard Deviation

In general, the values of standard deviation parallel the trends observed with the mean values, but the similarity in the two sets of data only corresponds in general terms but not in detail. For example, core 2.7 exhibits a progressive decrease in both mean grain size and standard deviation upcore, yet the plots of mean and standard deviation only correspond to each other broadly. In many instances there are mis-matches which appear to indicate that the shape of the grain size distribution varies, but that this variation does not correspond with a progressive change in mean grain size. In several cores there are abrupt vertical changes in standard deviation. For example, in core 2.4, the increase in mean grain size between 4 and 8 cm depth coincides with a sharp decrease in the values for standard deviation which is much higher for the rest of the core (i.e. between 8 and 33 cm) (Fig. 8). Since the measurement of standard deviation represents the spread of data around the mean, very sharp changes in standard deviation over relatively short time intervals indicate the incorporation together of different particle size subpopulations. However, the subpopulations themselves are rarely characterised by separate peaks.

Skewness

The values of skewness also show high magnitude change over relatively short vertical intervals. For example in core 2.7, the skewness values between 5 and 10 cm depth range between 0.3 and 2.9 (Fig. 10). The high values of skewness correspond to grain size distributions with a modal peak corresponding to

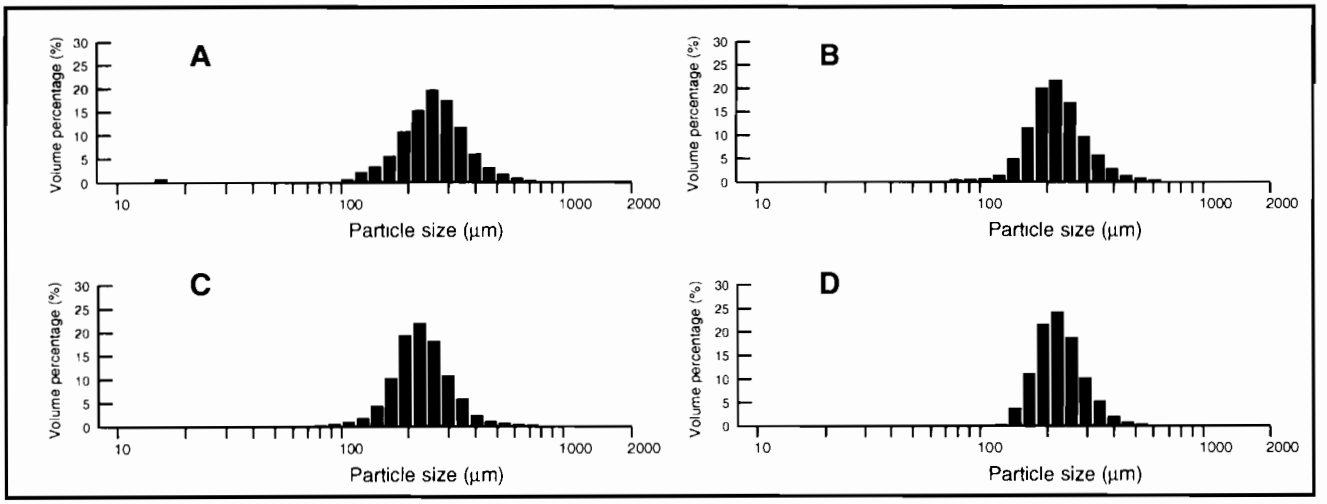

FIG. 7. Representative particle size distributions at core 2.7. Letters A–D are indicated on Fig. 10.

medium-grain sands and the corresponding tail to a distribution composed of finer-grain sediments. By contrast, low skewness values corresponds to grain size distributions in which there is a significant coarse-tail element. Such high magnitude changes in skewness occur in many other cores. For example in core 1.2 between 15 and 18 cm depth, the skewness values change from 0.0 to 1.5 over a vertical distance of 3 cm (Fig. 9). Inspection of the corresponding data for mean grain size show that these high magnitude changes in skewness are invariant with respect to changes in the mean, but appear to relate to variations in overall composition in grain sizes.

Kurtosis

The index of kurtosis generally refer to the degree in which the grain size distribution exhibits marked peakedness. High kurtosis values correspond to grain size distributions which are characteristically unimodal and which possess a peaked distribution. By contrast, low kurtosis values (e.g. 5–10) (McBride, 1971) correspond to much flatter grain size distributions. This appears to suggest that the reduction in kurtosis values corresponds to an increased presence of the coarse-tailed sediment component, although often this coarse-tailed fraction is not exhibited as a pronounced and separate population in the histograms (see paragraph above). Inspection of Figs 8–10 indicates that the changes in kurtosis generally mirror the vertical variations in skewness. Thus, grain size distributions that exhibit a coarse-tail are generally characterised by low kurtosis values indicative of flattened distributions (e.g. core 1.2) (Fig. 9). By contrast, the more common distributions observed for Rajegwesi that exhibit modal values in the medium-sand range, tend to have high skewness values associated with them as well as high kurtosis values indicative of relatively pronounced unimodal peaks in the grain size distributions. Yet, these two indices of the grain size distributions are not paralleled by corresponding increases or decreases of mean grain size of particular levels in the cores. Nor is there any clear correspondence with vertical changes in standard deviation in any of the cores. This would appear to indicate that sediment supply is abundant in the medium sand range and is characterised by a dominant and uniform grain size distribution. By contrast, the physical processes of transport and deposition appear to have been associated with more variable particle size distributions that are principally distinguished by slight changes in the slope of the curves.

DISCUSSION

Despite the existence of numerous publications concerned with the recognition of palaeotsunamis in coastal sediment sequences, there have been relatively few studies of sediments deposited by modern tsunamis. To the authors knowledge, the only modern tsunami which has been investigated to date in respect of sediment characteristics, was the December 12, 1992 tsunami in Flores, Indonesia (Shi *et al.*, 1993, 1995; Shi, 1995). The results of the present analysis for Java indicate a number of differences in the nature of sediments deposited by tsunamis. These differences are by the nature of the information available, only relevant to comparisons with the Flores tsunami.

Spatial Variations and Grain Size

Whereas Shi (1995) and Shi *et al.* (1995) indicated that there was a clear decrease in grain size from the coast inland associated with the Flores event, this is not the case with the Rajegwesi sediments. Indeed, the vertical variations in grain size in individual cores are perhaps greater than any spatial variation between cores. The reason for this difference is not clear. This is possibly related to the uniformity of sand grains in the source area (see above). It is suspected that at Rajegwesi, the three principal waves observed by the eyewitnesses to have been responsible for the deposition of the sediment, were

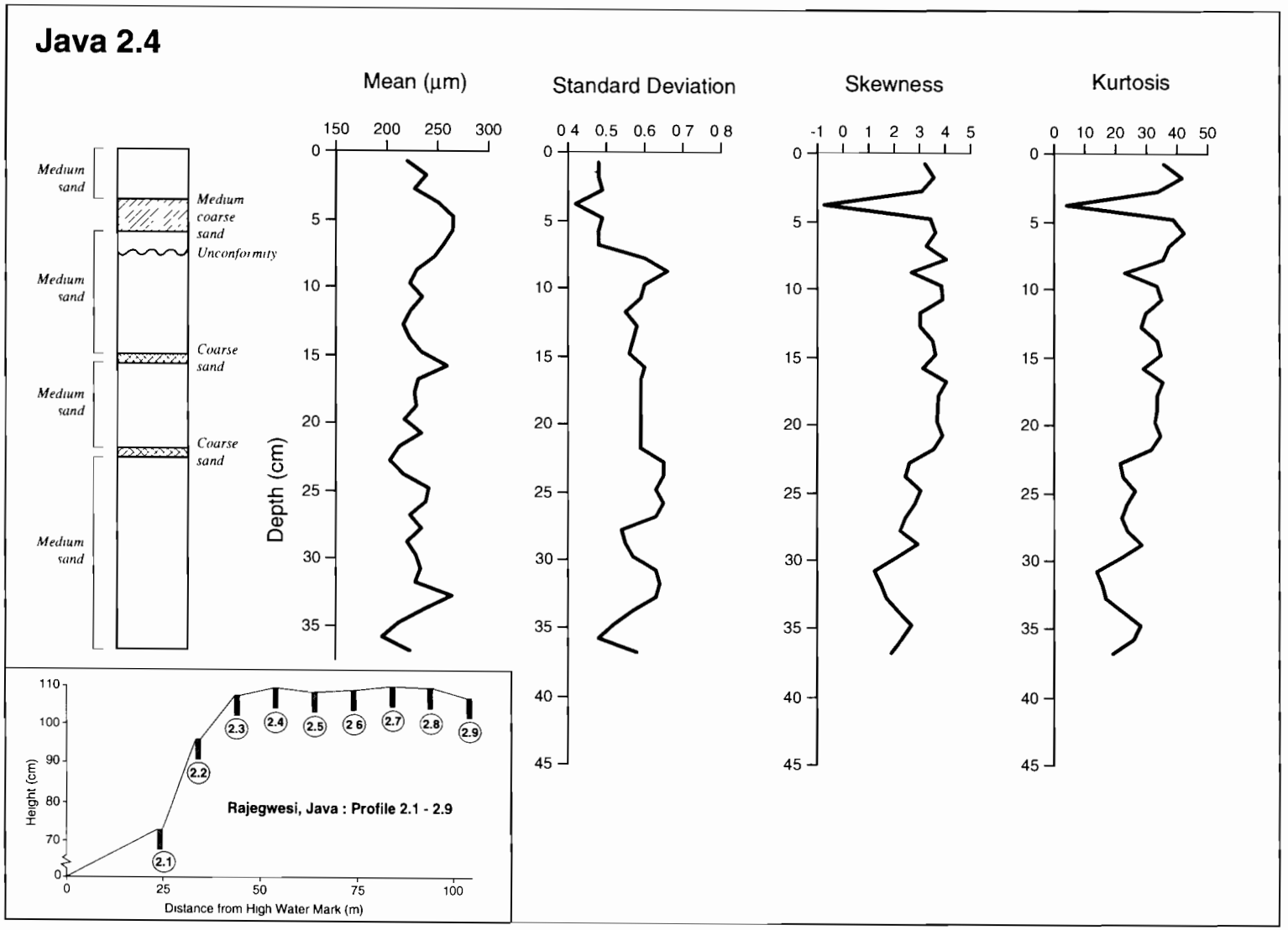

FIG. 8. Vertical variations of mean, standard deviation, skewness and kurtosis for core 2.4. Location of profile line and sampling locations are also shown.

associated with depositional processes which led to large short-term variations in the nature and style of sediment deposition and these changes were much greater than those associated with Flores.

The Rajegwesi grain size distributions on the whole are characterised by a dominant grain size mode and associated tail linked to the deposition of fine-grained sediment. The Rajegwesi grain size distributions do not possess many examples of distinctive multimodal sediment distributions as was observed in Flores. Again, the reasons for this difference are not clear although it is possible that the source sediment of the Java tsunami is much more uniform than in Flores (cf. Shi *et al.*, 1995).

Many of the grain size distributions at Rajegwesi have a distinctive yet inconspicuous tail of fine-grained sediment and some times a clear small-scale secondary grain size mode. In the case of the Flores tsunami, it was argued that much of the finer-grain sediments in the area inundated by the tsunami were removed offshore leaving a sediment mass dominated by medium- and coarse-sand deposits. Although it is not possible to demonstrate this similarity owing to the fact that no local sediments at Rajegwesi unaffected by tsunami were sampled, and therefore it is not possible to make comparisons. The presence of a secondary fine-grained sediment modal value may also indicate here that much of any fine-grain sediments in the local area were winnowed out by the movement of water during the tsunami.

Vertical Variations in Mean and Standard Deviation Values

Although there is a general correspondence between the vertical changes in mean grain size and standard deviation in several cores, there is a great deal of internal variability that in many cases masks the overall trends. The internal variability in both mean and standard deviations do not match each other, and many instances can be cited to demonstrate variations in standard deviation unconnected to progressive increases or decreases in mean grain size. The causes of these differences are not clear, but is possibly the result of controls on sedimentation by the characteristics of both the sediment sources and the processes of sedimentation.

Skewness and Kurtosis

In most cores, the skewness and kurtosis values parallel each other closely and show that coarse-tail distributions correspond with low values of kurtosis and associated flattened grain size distributions. By contrast, high values of skewness (the more common characteristic) are associated with high values of kurtosis and relatively peaked distributions. Yet these two parameters do not appear to correspond in any way with changes in standard deviation or the changes in the mean. Again it is not clear why this is the case, why there should be such changes in grain size distribution indicated by sudden changes in both skewness and kurtosis.

Tsunami Deposition and Sorting

As in the case of Flores, there appears to be sets of individual fining-upwards sequences represented by progressive vertical decreases in mean grain size in a series of cores. The separate sub-populations are readily identifiable as various fixed ranges and this would appear to indicate, together with the core data, that the coarsest material is deposited at the base of sediment accumulation and thereafter the tsunami sediment accumulation becomes finer and decreases in proportion upcore. These observation are in agreement with those noted at Flores and would appear to indicate a unique set of settling processes characterised by rapid rates of tsunami sedimentation arising from the simultaneous deposition of fine and coarse particles (Shi *et al.*, 1995). Also as in the case of Flores, the high-magnitude fluctuations with changing depth of the particle size parameters show that there is a positive correlation between a progressive upward-fining trend and an increase in the degree of sorting. It is concluded that these processes arise from a progressive decrease in the energy of the tsunami waves in the trend and the effects of short-time sorting of these sediments.

SUMMARY

The Rajegwesi, Java study is the second illustration (in addition to Flores, Indonesia) that sediments deposited by modern tsunamis exhibit distinctive grain size distributions and that these are linked to complex processes of tsunami sediment transport. Unlike Flores, the Java sediment accumulation is not associated with clear evidence of local erosion. Instead, it provides evidence for tsunami sediment transport and deposition that has resulted in the deposition of dominantly unimodal sediments with fine-tail distributions. Shi *et al.* (1995) have proposed that during periods when tsunamis inundate the coastal zone, that provided there is an adequate sediment supply, sedimentation rates are so high that tsunami sediment is frequently composed of several populations of particles in different size ranges. As a result, the interaction of turbulence, rapid sedimentation and the characteristics of the transported material play a large part in dictating the characteristics of the particular tsunami deposit. These conclusions also apply to Java and a comparison is also made that tsunamis are associated with rapid changes in the energy regime so that periods of high water turbulence (tsunami runup) are followed by still-water conditions (pre-backwash phase) and, in turn followed by increased turbulence (backwash). The complex hydrodynamics of tsunamis implies that particular coastal zones are unique insofar as it would appear great changes in the water state take place over the relatively short periods of time during which sediment may be deposited. In addition, the rapid changes in the direction of water flow across the coastal zone results in unique processes of coastal sediment transport and deposition. The complex patterns of the grain size distributions evident in the individual cores and the great

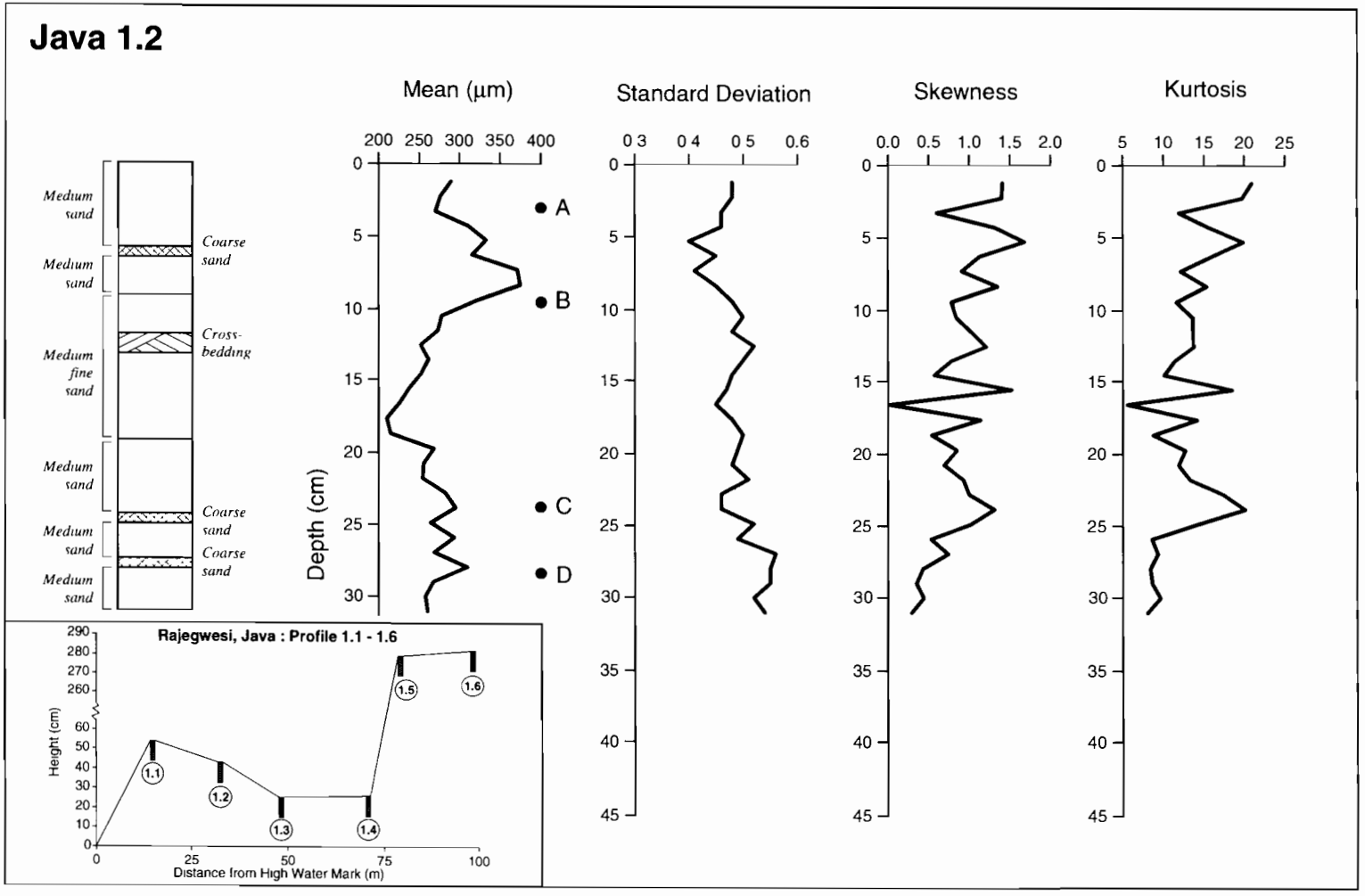

FIG. 9. Vertical variations of mean, standard deviation, skewness and kurtosis for core 1.2. Location of profile line and sampling locations are also shown.

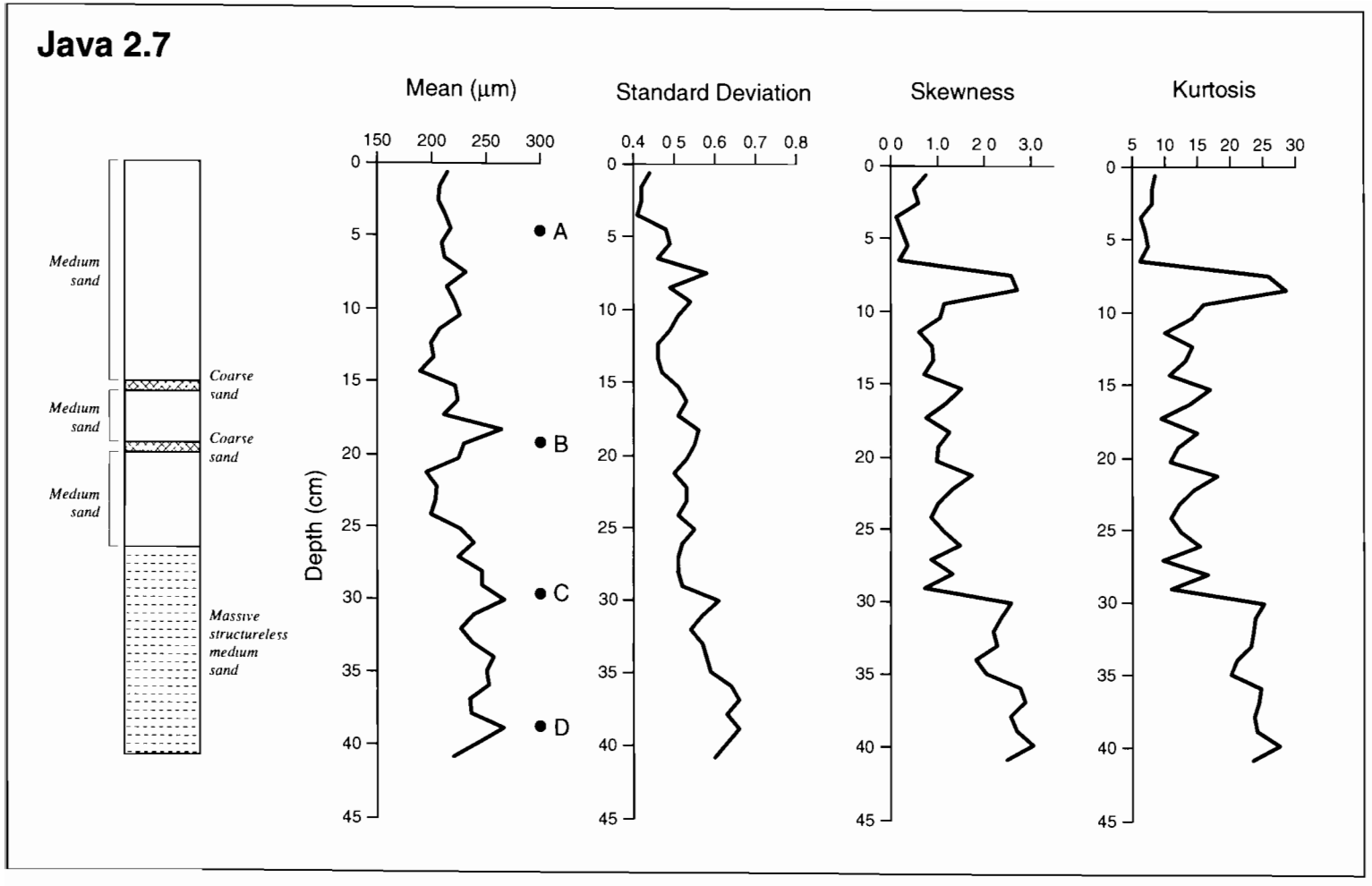

FIG. 10. Vertical variations of mean, standard deviation, skewness and kurtosis for core 2.7.

vertical variations in sediment properties within the individual cores demonstrates effectively the complexity of these processes. At present, however we can only speculate on the precise physical processes of sediment transport and deposition that produce these textural characteristics.

It is clear, however, that tsunami sedimentation patterns are complex insofar as modern events are concerned. On some occasions there are very clear fining-upwards sequences evident, but in other instances such trends are not so noticeable. It is not yet clear, if it is the case that most tsunami deposits are laid down during periods of flood runup or during some other phase of tsunami flooding. A great deal of consideration should be given to the hypothesis that tsunami sedimentation may take place during the turnround periods between phases of flood runup and backwash. This hypothesis, however, remains to be tested in a rigorous manner and this will require many more empirical studies of sedimentation processes associated with modern tsunamis.

ACKNOWLEDGEMENTS

The authors are grateful to Peter Taylor for the laboratory analysis. Cartographic assistance is gratefully acknowledged to Jason Jordan and Paul Bird. Financial support for the research was kindly provided by the Ogawa Commemorative Fund.

REFERENCES

Andrade, C. (1992). Tsunami generated forms in the Algarve barrier islands. *In*: Dawson, A.G. (ed.) *European Geophysical Society 1992 Tsunami Meeting Science Tsunami Hazards*, **10**, 21–34.

Atwater, B.F. and Moore, A.L. (1992). A tsunami about 1000 years ago in Puget Sound, Washington. *Science,* **258,** 1614–1617.

Atwater, B.F. and Yamaguchi, D.K. (1991). Sudden, probably coseismic submergence of Holocene trees and grass in coastal Washington State. *Geology,* **19,** 706–709.

Dawson, A.G., Long, D. and Smith, D.E. (1988). The Storegga Slides: evidence from eastern Scotland for a possible tsunami. *Marine Geology,* **82,** 271–276.

McBride, E.F. (1971). Mathematical treatment of size distribution data. *In*: Carver, H. (ed.), *Procedures in Sedimentary Petrology*. Wiley. New York.

Malvern Instruments (1989). Series 2600 — User Manual. Spring Lane South, Malvern, Worcs. WR14 1AQ, UK.

Minoura, K. and Nakaya, S. (1991). Traces of tsunami preserved in inter-tidal lacustrine and marsh deposits: some examples from northeast Japan. *Journal of Geology,* **99,** 265–287.

Moore, G.W. and Moore, J.G. (1988). Large-scale bedforms in boulder gravel produced by giant waves in Hawaii. *In*: Clifton, H.E. (ed.). *Sedimentologic Consequences of Convulsive Geologic Events, Geological Society of America Special Paper*, **229**, 101–110.

Paskoff, R. (1991). Likely occurrence of a mega-tsunami in the Middle Pleistocene near Coquimbo, Chile. *Revista Geologica de Chile,* **18,** 87–91.

Shi, S. (1995). Observational and theoretical aspects of tsunami sedimentation. Unpublished PhD Thesis, Coventry University, 282 pp.

Shi, S., Dawson, A.G. and Smith, D.E. (1993). Geomorphological impact of Flores tsunami of 12th December, 1992. *In*: *Tsunami '93, Proceedings of IUGG/IOC International Tsunami Symposium*, Wakayama, Japan, August 23–27, 1993, pp. 689–696.

Shi, S., Dawson, A.G. and Smith, D.E. (1995). Coastal sedimentation associated with the December 12th, 1992 tsunami in Flores, Indonesia. *Pure and Applied Geophysics,* **144,** 525–536.

Pergamon

Quaternary Science Reviews, Vol. 15, pp 913–937, 1996.

PII: S0277-3791(96)00058-3
0277-3791/96 $32.00

FORAMINIFERAL EVIDENCE FOR THE AMOUNT OF COSEISMIC SUBSIDENCE DURING A LATE HOLOCENE EARTHQUAKE ON VANCOUVER ISLAND, WEST COAST OF CANADA

JEAN-PIERRE GUILBAULT,* JOHN J. CLAGUE† and MARTINE LAPOINTE‡

**BRAQ-Stratigraphie, 10545 Meilleur, Montréal, Québec H3L 3K4, Canada*

†Geological Survey of Canada, Suite 101–605 Robson Street, Vancouver, British Columbia V6B 5J3, Canada

‡GEOTOP, Université du Québec à Montréal, C.P. 8888, Succursale Centre-Ville, Montréal, Québec H3C 3P8, Canada

Abstract — Foraminiferal data from two sites, 6 km apart, on the shores of an inlet near Tofino on the west coast of Vancouver Island, British Columbia, allow estimates to be made of the amount of coseismic subsidence during a large earthquake 100–400 years ago. The sampled sediment succession at the two sites is similar; peat representing a former marsh surface is abruptly overlain by intertidal mud grading upward into peat of the present marsh. At one of the sites, a layer of sand, interpreted to be a tsunami deposit, locally separates the buried peat from the overlying intertidal mud. The abrupt peat-mud contact records sudden crustal subsidence during the earthquake. The paleoelevation of each fossil sample was estimated by comparing its foraminiferal assemblage with modern assemblages of known elevation. The modern assemblages were obtained from surface samples collected along transects across the marsh near the fossil sample sites. Comparisons were made statistically using transfer functions. Estimates of coseismic subsidence, based on differences in paleoelevations just above and below the top of the buried peat, range from 20 cm to 1 m, with the most likely value in the 55–70 cm range. Post-seismic crustal rebound began soon after the earthquake and may have been largely complete a few decades later. Copyright © 1996 Published by Elsevier Science Ltd

INTRODUCTION

Foraminiferal data presented in this paper are used to estimate the amount of subsidence that accompanied a large earthquake on western Vancouver Island, British Columbia, less than 400 years ago. This study builds on, and refines, the previous study of Guilbault *et al.* (1995) in the same area. The work is founded on the principle that foraminiferal assemblages in tidal marshes vary with elevation and that a change in elevation of as little as 5–10 cm may produce a recognizable change in the foraminiferal assemblage at a given site. This is the essence of the conclusions of Scott and Medioli (1980), based on their investigation of Nova Scotia tidal marshes. This paper and others concerned more specifically with marsh foraminifera from the northwest coast of North America (Phleger, 1967; Williams, 1989; Patterson, 1990a; Jennings and Nelson, 1992; Jonasson and Patterson, 1992) and from Chile (Jennings *et al.*, 1995), provide a basis for discriminating upper marsh from lower marsh environments on the British Columbia coast. Broad limits can then be placed on paleoelevations of samples from intertidal sedimentary sequences using foraminiferal data (Jennings and Nelson, 1992), provided the vertical limits of the marsh zones are known and have not changed with time.

The originality of our method lies in the use of transfer functions to estimate paleoelevation (Imbrie and Kipp, 1971). This approach allows a more objective treatment of foraminiferal assemblages than is possible through visual inspection and can be applied to large, multivariate data sets. It also provides a paleoelevation for every sample in a sequence, thus improving the resolution.

In this paper, we compare fossil foraminiferal assemblages at two sites, 6 km apart, near Tofino, British Columbia, with modern assemblages from the adjacent marsh. At both sites, a peat layer representing a former marsh is abruptly overlain by mud that grades upward into peat of the present marsh. The abrupt change from peat to mud has been attributed to sudden subsidence during a large earthquake 100–400 years ago (Clague and Bobrowsky, 1994a). The earthquake may have resulted from the rupture of the boundary between the North America and Juan de Fuca plates along the Cascadia subduction zone (Fig. 1). Samples collected through the sediment sequence at each site were compared with samples taken from a nearby modern transect no more than 150 m away. This was done to minimize the

environmental differences between the fossil and modern sites, which could affect comparison of the data sets.

By assigning a paleoelevation to each fossil sample, we obtain an elevational history of the site, from which local submergence or emergence during an earthquake can be inferred. The instantaneous nature of earthquake subsidence or uplift eliminates complicating factors such as eustatic and isostatic sea level change, sediment accretion, slow tectonic movements, and long-term sediment compaction. The amount of sudden submergence or emergence determined from foraminiferal data, however, may differ from the amount of subsidence or uplift caused by the earthquake (Guilbault *et al.*, 1995). Possible sources of error include a change in tidal range due to a change in the shape of the basin during the earthquake, coseismic sediment compaction, the presence of an erosional hiatus in the succession of analyzed sediments, and early post-seismic rebound before sediment begins to accumulate on coseismically subsided surfaces. We will come back to these points in the discussion.

STUDY SITES

The two sampled sites are marshes adjacent to Browning Passage, an arm of the sea connecting the open ocean southwest of Tofino with fjords and channels farther inland (Fig. 1). Tidal marshes along Browning Passage are low-energy environments sheltered from the open Pacific Ocean by Esowista Peninsula and by numerous islands north and west of Tofino.

The 'cemetery' site (Guilbault *et al.*, 1995; site 4 of

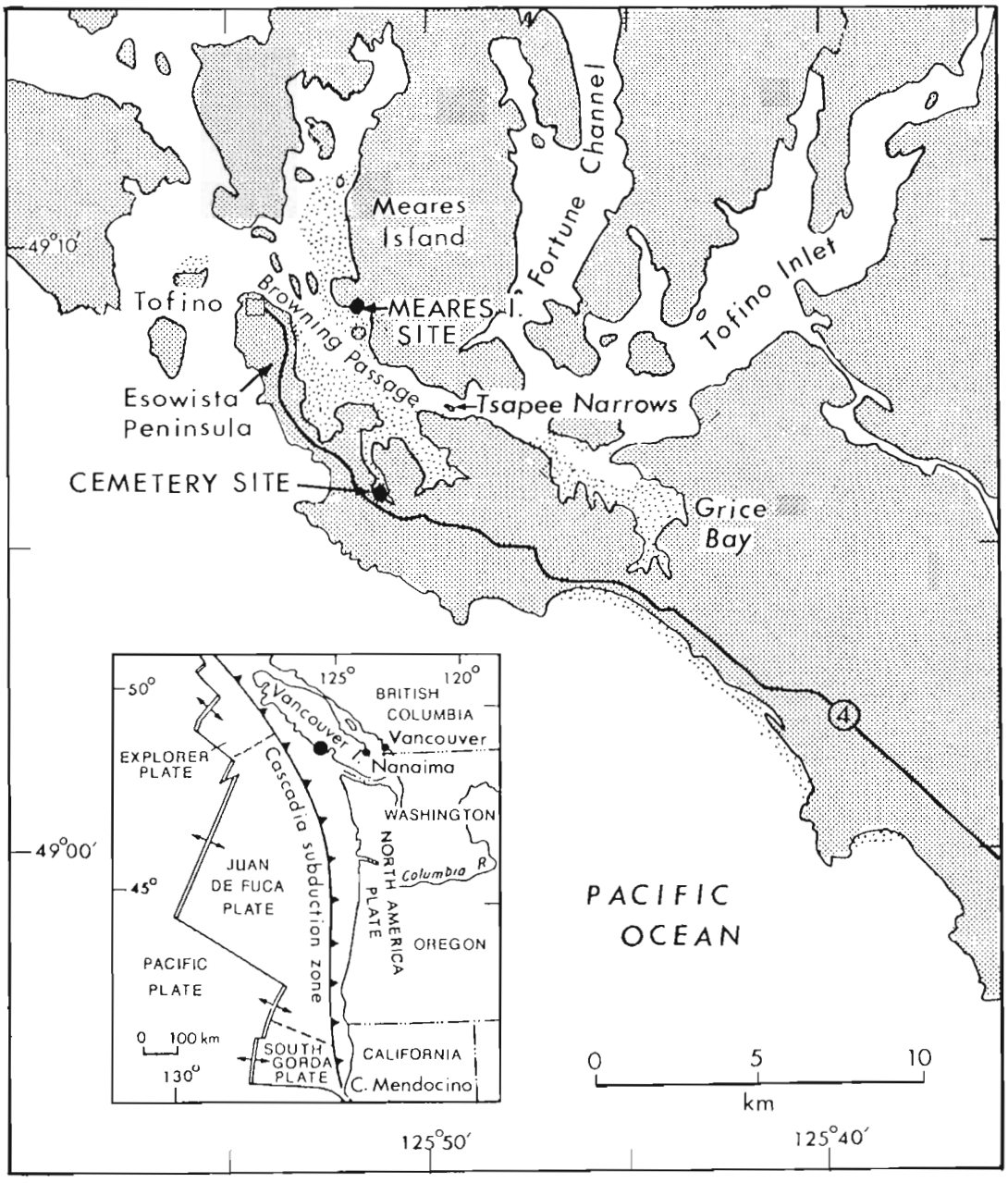

FIG. 1. Map of the Tofino area showing the locations of the cemetery and Meares Island sections. Stippled areas are intertidal. Inset map shows lithospheric plates; dot indicates the location of the detailed map.

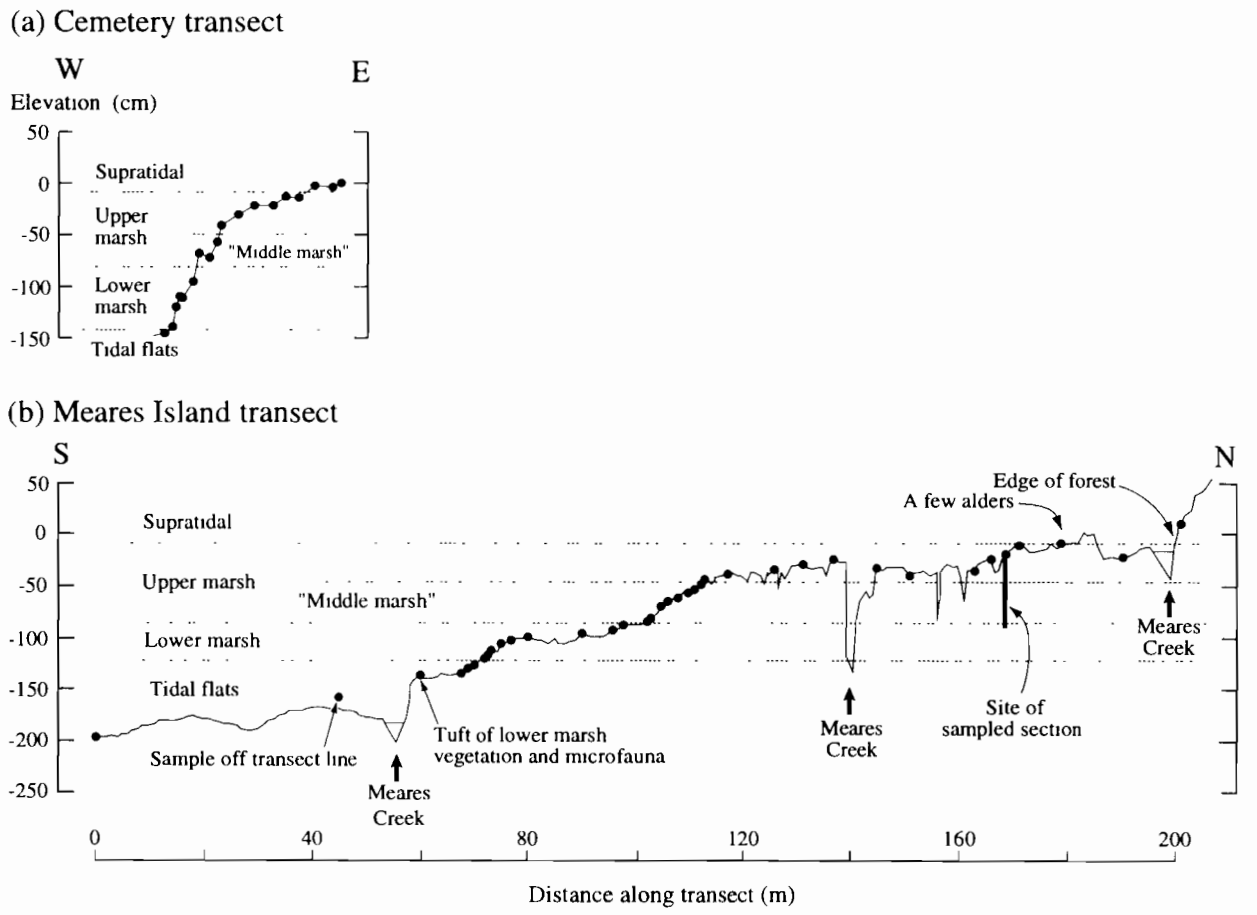

FIG. 2. Profiles of the two sampled marshes. Dots represent modern samples.

Clague and Bobrowsky, 1994a) is located 7 km south-southeast of Tofino, near the head of a long, narrow, shallow, winding arm of Browning Passage. This site is completely protected from wave action and is fringed by a narrow marsh. Samples of surface sediment for the modern data base were collected along a 32-m-long transect across the marsh (Fig. 2(a)). The site was chosen because it is close to the fossil section and because the marsh is broader here than elsewhere in the immediate vicinity; consequently, the different foraminiferal biofacies were expected to be better developed and more complete.

The succession of late Holocene sediments underlying the marsh was sampled in the wall of a tidal channel located approximately 100 m east-southeast of the modern transect. The following lithostratigraphic units are exposed in the section (Fig. 3):

Unit 5 (0–3 cm below the marsh surface): dark brown, rooty, muddy peat of the modern tidal marsh; grades downward into unit 4.

Unit 4 (3–27 cm): olive-gray, organic-rich mud, becoming lighter and less peaty downward; the contact between this unit and the underlying muddy peat (unit 3) is abrupt.

Unit 3 (27–31 cm): dusky brown, rooty, muddy peat (a former marsh surface) with a gradational lower contact.

Unit 2 (31–53 cm): olive-gray, organic-rich mud similar to unit 4; the uppermost several centimeters are darker and richer in plant material than the rest of the unit; grades downward into unit 1.

Unit 1 (53–75 cm): interstratified, olive-gray mud and sandy silt, becoming sandier downward; the uppermost 6 cm of the unit were sampled.

Unit 1 rests on late Pleistocene, glaciomarine, silty clay containing shells dated at about 16 000 years BP (calibrated age; Clague and Bobrowsky, 1994a). Large conifer stumps rooted in this clay or in the sediments that directly overlie it have been dated at about 7400 to 9000 years BP (Clague and Bobrowsky, 1994a). The five units described above overlie these fossil forest remains. Accelerator mass spectrometry (AMS) radiocarbon ages on *Triglochin* rhizomes from the cemetery section indicate that unit 2 is no more than 700 years old (Table 1).

The second study site (near site 1 of Clague and Bobrowsky, 1994a) is situated on Meares Island, 3 km east of Tofino and 6 km north of the cemetery site. It lies at the head of a broad bay that opens to the southwest onto Browning Passage. The tidal marsh is much broader here than at the cemetery site; the lower part is patchy and irregular, perhaps due to greater exposure to waves. Samples of surface sediment were collected along a 128-m-long transect from the forest edge to the unvegetated tidal flats (Fig. 2(b)). To maximize the comparability of the modern and fossil records, the fossil site was located along the transect; the uppermost sample at the fossil site is one of the modern samples of the transect. The transect crosses Meares Creek at three places (Fig. 2(b)); freshwater arcellacea are carried into the marsh at these points.

Fossil samples were collected from the wall of a pit that

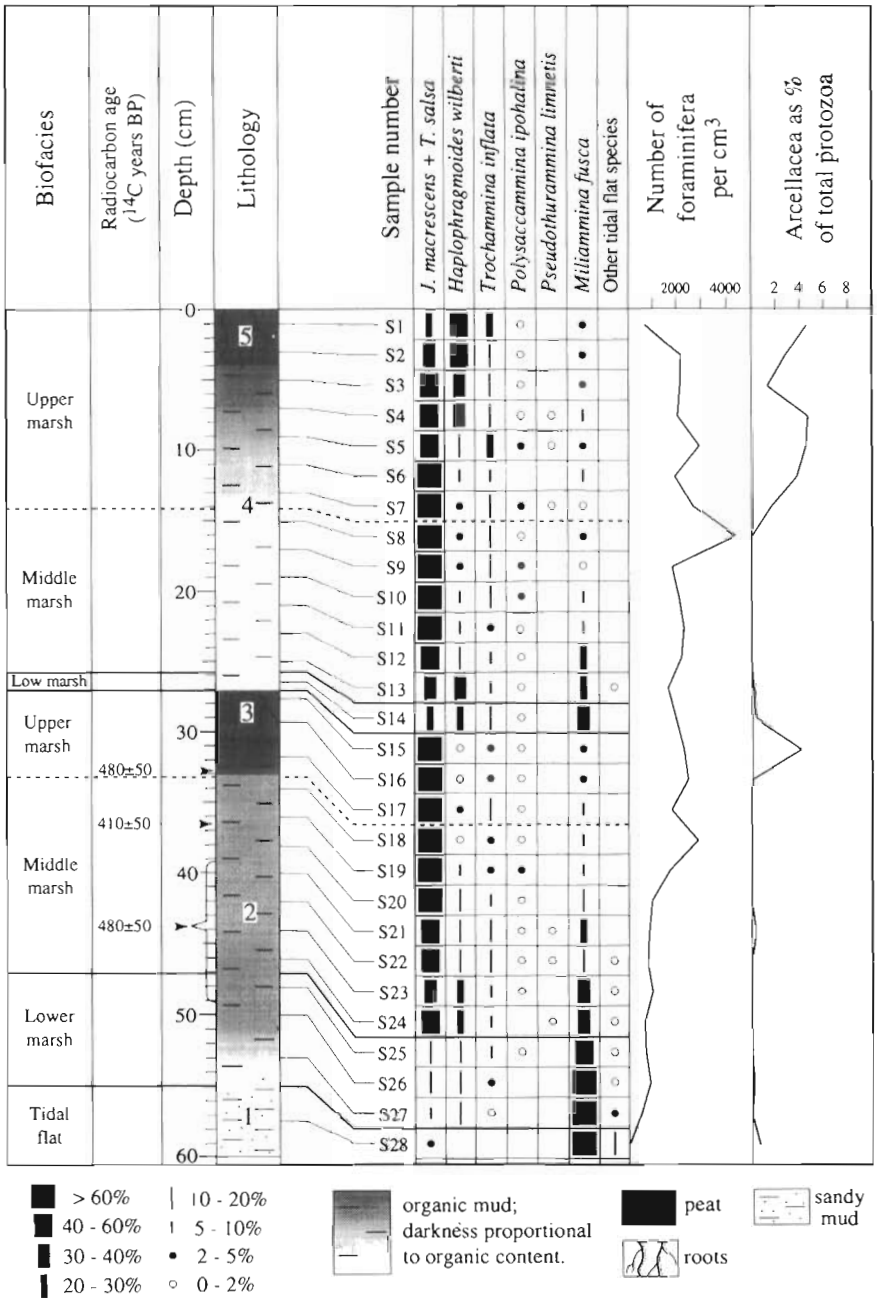

FIG. 3. Lithostratigraphy, radiocarbon ages and distribution of major foraminiferal taxa in the cemetery section. Percentages were computed on the sum of determined foraminifera only; percentages of arcellacea in the protozoa total are shown at the right. Numbered lithologic units are described in the text. Low marsh and tidal flat species other than *Miliammina fusca* (*Ammobaculites exiguus, Ammotium salsum* and *Polysaccammina hyperhalina*) have been grouped. *Miliammina fusca* percentages have been corrected for the '*M. fusca* factor' of Guilbault *et al.* (1995). The middle marsh is a subfacies of the upper marsh, hence the dashed boundary.

was dug in the upper part of the marsh. The following succession of stratigraphic units was recorded at this site (Fig. 4):

Unit 8 (0–4 cm below the marsh surface): dark brown, rooty, muddy peat of the present marsh; the contact with unit 7 is sharp.

Unit 7 (4–4.5 cm): silty mud (possibly a tsunami deposit; see Clague and Bobrowsky, 1994a, b); sharp lower contact.

Unit 6 (4.5–18 cm): brown muddy peat, upper part rooty, becoming muddier with depth; gradational lower contact.

Unit 5 (18–28 cm): olive gray, organic-rich mud; sharp lower contact.

Unit 4 (28–34 cm): fine sand (tsunami deposit; Clague and Bobrowsky, 1994a, b); sharp lower contact.

Unit 3 (34–39 cm): brown, rooty, muddy peat (former marsh surface); gradational lower contact.

Unit 2 (39–69 cm): olive gray, organic-rich mud similar to unit 5; sharp lower contact.

Unit 1 (69–83 cm): poorly sorted, gravelly sand grading downward into sandy gravel.

Unit 1 is a lag developed on late Pleistocene glaciomarine sediments (Clague and Bobrowsky,

TABLE 1. Radiocarbon ages from the two Tofino study sites

Radiocarbon age (^{14}C years BP)[a]	δ^{13}C (‰)	Calibrated age range (cal years before AD 1950)[b]	Laboratory number[c]	Stratigraphic unit[d]	Dated material
Cemetery site					
480±50		300–650	TO-4054	2	*Triglochin* rhizome[e]
410±50		0–630	TO-4055	2	*Triglochin* rhizome[e]
480±50		300–650	TO-3522	2	*Triglochin* rhizomes[e]
Meares Island					
180±50		0–470	TO-3518	3	Conifer needles, cedar scales
340±50		0–540	TO-3517	4	Branch
440±60		0–650	TO-3519	3	Rhizomes, leaves[e]
630±50		500–730	TO-3520	2	Conifer cone
680±50		510–780	TO-3521	2	Twig
700±60	−24.9	550–720	GSC-5522	2	Branch[f]
1140±50		800–1280	TO-3516	3	Conifer cone

[a]Laboratory-reported error terms are 2σ for GSC age and 1σ for all others. Ages corrected to δ^{13}C = −25.0‰ PDB.
[b]Determined from dendro-calibrated data of Stuiver and Pearson (1993). The range represents the 95% confidence interval based on the 2σ error limits of the radiocarbon age (error multiplier=2.0; note error multipliers expand laboratory-quoted errors to cover uncertainties in reproducibility and systematic bias; for a discussion, see Stuiver and Pearson, 1993).
[c]GSC=Geological Survey of Canada; TO=IsoTrace (University of Toronto).
[d]See text and and Figs 3 and 4
[e]In growth position.
[f]*Picea* sp. (identified by H. Jetté, GSC Wood Identification Report 93 10)

1994a). A branch lying at the top of unit 1 gave a calibrated radiocarbon age of 550–720 years BP (Table 1). Rhizomes in growth position just below unit 4 (tsunami sand) are less than 700 years old, and detrital wood and other plant material from within and just below this sand are no more than 600 years old. The sand has been optically dated at 325±25 years old (Huntley and Clague, 1996). The section as a whole is thus young, probably spanning no more than 1000 years.

The buried peat at the cemetery and Meares Island sites represents a former marsh that subsided suddenly during a large earthquake (Clague and Bobrowsky, 1994a). At Meares Island and at many other places along Browning Passage, the buried peat is overlain by sand that was deposited by the tsunami generated by the earthquake. The sand is not present, however, in the cemetery section. At some sites along Browning Passage, the tsunami apparently eroded the subsided marsh (Clague and Bobrowsky, 1994b), but this probably did not happen at the cemetery site, nor for that matter at Meares Island where delicate stems and leaves of herbaceous plants extend upward from the buried peat into the overlying sand.

Tides

The predicted level of the highest tide at the tidal gauge at Tofino harbour for the summer of 1994 (July, August, and September) is 3.7 m (Fisheries and Oceans, 1993). The recorded high tide at Tofino harbour on July 14, 1994, when we sampled the Meares Island transect, was 3.18 m. The recorded high tide on June 24, 1993, when we sampled the cemetery transect, was 3.21 m. We surveyed the level reached by high tide at the cemetery and Meares Island sites on these two days. We also estimated the height of the highest tide at the two sites during the summer of 1994 by assuming that the amplitude of tides are the same at the transects as at the Tofino gauge (Table 2). There is no proof, however, that tidal amplitude is the same at the three localities. Table 2 includes the height of an 'exceptional' tide; an exceptional tide is here defined as the level reached by the sea no more than 0.1% of the time. At Tofino harbour, this level is based on 18 years of tidal data collected from 1977 to 1994 inclusively (unpublished data from Fisheries and Oceans Canada).

METHODS

Modern samples (0–2 cm depth) were collected with a garden bulb planter. Eighteen samples (20 if the top of the section and one forest soil sample are included) were collected over a 1.45 m vertical range along the cemetery transect. Vertical intervals between these samples range

TABLE 2. Estimated maximum elevation (m) of high tides at Tofino cemetery and Meares Island

	Tide gauge, Tofino harbour	Cemetery	Meares Island
June 24, 1993	3.21	−0.64	—
July 14, 1994	3.18	—	−0.725
Maximum, summer 1994	3.7	−0.15	−0.205
Exceptional tide	4.1	0.25	0.195

Datum for tide gauge elevations is chart datum
Datum for cemetery and Meares Island elevations is edge of forest.

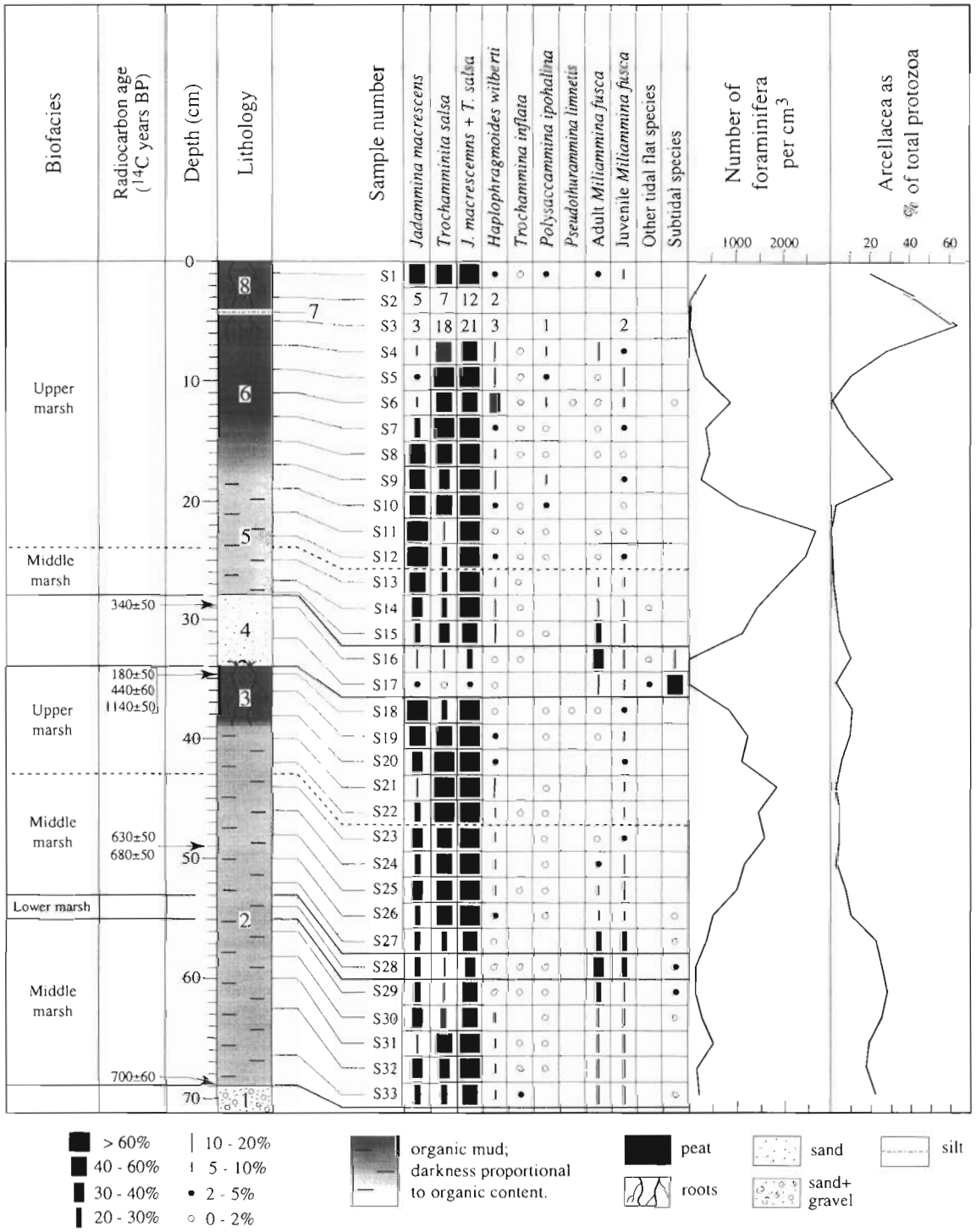

FIG. 4. Lithostratigraphy, radiocarbon ages and distribution of major foraminiferal taxa in the Meares Island section. There were small numbers of specimens in samples S2 and S3, therefore numbers of counted specimens are shown rather than percentages.

from 0 to 23 cm. At Meares Island, 37 modern samples were collected over a vertical range of 2.075 m. Over much of the transect, the samples are separated vertically by 4 to 6 cm; however, gaps of up to 12 cm exist. At both sites, an elevation of 0 m was arbitrarily assigned to the forest edge (=local datum).

The wall of the tidal channel at the cemetery site was cut back about 30 cm prior to sampling to preclude the possibility of contamination and destruction by oxidation of foraminiferal tests. As mentioned previously, the Meares Island samples were collected from a freshly dug pit. At both sites, most samples were 2 cm thick and there were no gaps between them. The sampling interval above and below the top of the buried peat was reduced to 0.5–1 cm to capture, as much as possible, conditions immediately before and after the earthquake.

Sample processing methods are detailed in Guilbault *et al.* (1995). The Meares Island samples were stored in

TABLE 3. Total counts of foraminifera and arcellacea (stained + unstained) from the modern marsh at the Meares Island site
Foraminifera/cm^3: identified + indeterminate foraminifera; this is the value shown on Fig. 3.
Biofacies: FW=freshwater; UM=upper marsh; MM=middle marsh; LM=lower marsh; TF=tidal flats

Sample number	1	2	3	4	S1	5	6	7	8	9	10	11	12	13	14	15	16	17	18
Elevation (cm)	10	−9.5	−11.5	−23	−19.5	−25.5	−25.5	−30.5	−32.5	−34.5	−35.5	−39.5	−40.5	−44.5	−48.5	−53.5	−57.5	−61.5	−65.5
Foraminifera/cm^3	1	2	186	62	369	40	158	1057	32	1918	106	1699	414	2922	1209	1762	2351	2580	2164
Biofacies	FW	FW	UM	UM	UM	UM	UM	UM	UM	UM	UM	UM	UM	UM	MM	MM	MM	MM	MM
Jadammina macrescens	—	—	79	39	109	30	35	15	38	23	119	164	29	104	128	155	59	89	145
Jadammina polystoma	—	—	1	—	2	—	—	1	—	1	—	16	—	24	17	16	5	9	13
Trochamminita salsa	—	1	79	3	98	5	55	72	1	111	5	309	48	90	176	143	91	93	145
Trochamminita irregularis	—	—	4	1	18	2	26	23	—	20	2	36	35	20	15	9	17	24	29
Haplophragmoides wilberti	—	—	3	32	7	6	9	78	1	29	5	77	52	113	71	97	50	70	143
H. wilberti 8+ chambers	—	—	1	—	—	1	—	31	—	12	2	21	14	10	12	16	8	16	24
Haplophragmoides manilaensis	—	—	—	—	—	—	—	1	—	—	—	—	—	1	—	—	—	2	—
Trochammina inflata	—	—	2	—	1	1	—	31	—	24	—	89	—	112	60	28	15	32	53
Siphotrochammina lobata	—	—	—	—	—	—	1	6	—	1	—	2	—	1	—	2	—	1	—
Trochammina ochracea	—	—	2	—	—	—	—	—	—	—	—	—	—	—	—	—	—	—	1
Trochammina cf. *nana*	—	—	1	—	—	—	—	—	—	—	—	—	—	—	—	—	—	—	—
Polysaccammina ipohalina	—	1	3	2	7	2	10	12	—	11	—	12	43	15	6	5	8	6	5
Pseudothurammina limnetis	—	—	—	—	—	—	6	6	—	—	—	2	3	—	1	—	—	—	—
Adult *Miliammina fusca*	—	—	4	5	7	2	1	3	—	8	—	22	2	22	19	24	17	36	53
Young *Miliammina fusca*	—	—	15	4	16	—	16	40	—	92	—	284	8	187	80	74	40	79	65
Ammotium salsum	—	—	—	—	—	—	—	—	—	—	—	—	—	—	—	—	—	—	—
Ammobaculites exiguus	—	—	—	—	—	—	—	—	—	—	—	—	—	—	—	—	—	—	—
Polysaccammina hyperhalina	—	—	—	—	—	—	—	—	—	—	—	—	—	—	—	—	—	—	—
Indeterminate miliolid	—	—	—	—	—	—	—	—	—	—	—	—	—	—	—	1	—	—	—
Epistominella vitrea	—	—	—	—	—	—	—	—	—	—	—	—	—	—	—	—	—	—	—
Glabratella luxuribulla	—	—	—	—	—	—	—	—	—	—	—	—	—	—	—	—	—	—	—
Glabratella sp.	—	—	—	—	—	—	—	—	—	—	—	—	—	—	—	—	—	—	—
Elphidium cf. *lene*	—	—	—	—	—	—	—	—	—	—	—	—	—	—	—	—	—	—	—
Elphidium cf. *frigidum*	—	—	—	—	—	—	—	—	—	—	—	—	—	—	—	—	—	—	—
Elphidium cf. *williamsoni*	—	—	—	—	—	—	—	—	—	—	—	—	—	—	—	—	—	—	—
Total identified foraminifera	0	2	194	86	265	49	159	319	40	332	133	1034	234	699	585	570	310	457	676
Indeterminate foraminifera	1	1	38	7	64	3	43	69	1	65	6	293	38	100	95	77	39	57	68
Centropyxis aculeata	—	17	9	41	23	25	70	29	81	6	67	11	42	1	2	1	—	—	15
Centropyxis constrictus	4	3	1	94	54	6	3	3	15	11	8	139	13	16	1	1	—	—	2
Plagiopyxis sp.	84	2	—	3	1	7	5	1	17	—	9	2	8	2	1	—	—	—	—
Cyclopyxis cf. *kahli*	—	2	—	3	2	3	3	1	14	1	13	—	1	—	—	—	—	—	—
Cyclopyxis cf. *puteus*	—	—	—	—		—	—	—	—	—	—	—	—	—	—	—	—	—	—
Trigonopyxis sp.	—	—	—	—		—	1	1	1	—	3	—	2	—	—	—	—	—	—

TABLE 3. Continued

Nebela cf. *collaris*	—	3	—	2	—	1	2	2	3	—	1	—	4	—	—	2	—	—	—
Nebela cf. *tubulosa*	—	1	1	—	—	1	—	—	1	—	—	—	1	—	—	1	—	—	—
Heleopera sphagni	1	1	—	—	—	1	—	1	6	—	2	—	—	—	—	—	—	—	1
Distomatopyxis couillardii	—	1	—	—	—	1	—	—	—	—	—	—	2	—	—	—	—	—	—
Difflugia globulus	—	—	—	—	—	—	—	—	—	—	—	—	—	—	—	—	—	—	—
Difflugia oblonga	—	1	—	2	—	10	7	2	21	1	6	2	5	—	—	—	—	—	—
Difflugia protaeiformis	—	—	—	—	—	—	—	—	—	—	—	—	1	—	—	—	—	—	—
Difflugia urceolata	—	—	—	—	—	—	1	—	—	—	2	—	2	—	—	—	—	—	—
Pontigulasia compressa	—	—	—	1	—	1	2	—	4	—	—	—	2	—	—	—	—	—	—
Phryganella sp.	—	—	—	2	—	5	2	—	5	2	—	—	4	—	—	—	—	—	1
Assulina sp.	—	—	—	—	—	—	—	—	1	—	—	—	—	—	—	—	—	—	—
Total identified arcellacea	89	31	11	148	80	61	96	40	169	21	111	154	87	19	4	5	0	0	19
Indeterminate arcellacea	2	0	0	0	0	0	3	1	3	0	1	0	2	0	0	0	0	0	0
Sample number	19	20	21	22	23	24	25	26	27	28	29	30	31	32	33	34	35	36	
Elevation (cm)	—70.5	—82.5	—85.5	—88.5	—92.5	—96.5	—99.5	—102.5	—106.5	—112.5	—117.5	—120.5	—126.5	—130.5	—135.5	—136.5	—157.5	—197.5	
Foraminifera/cm^3	2066	752	490	236	241	868	637	1415	1489	535	364	83	101	186	200	578	488	141	
Biofacies	MM	MM	MM	LM	LM	LM	LM	LM	LM	LM	LM	LM	TF	TF	TF	LM	TF	TF	
Jadammina macrescens	248	111	77	52	39	22	42	44	254	24	23	3	2	3	2	38	32	30	
Jadammina polystoma	27	18	10	10	13	4	6	11	54	2	7	1	—	2	1	9	5	8	
Trochamminita salsa	198	38	33	24	15	10	88	5	36	2	—	1	—	1	—	1	—	2	
Trochamminita irregularis	40	19	12	6	2	5	24	4	10	—	3	1	—	—	—	—	1	5	
Haplophragmoides wilberti	162	23	15	6	5	24	142	48	137	21	25	1	—	2	—	26	17	29	
H. wilberti 8+ chambers	9	3	—	—	—	1	11	1	8	4	1	—	—	—	—	3	—	—	
Haplophragmoides manilaensis	3	—	—	—	—	—	—	2	—	—	1	—	—	—	—	—	—	—	
Trochammina inflata	88	13	32	4	3	4	—	39	155	3	3	1	—	—	—	33	2	3	
Siphotrochammina lobata	3	—	4	—	—	—	—	—	1	—	—	—	—	—	—	—	—	1	
Trochammina ochracea	—	—	—	—	—	—	—	—	—	1	—	1	—	—	—	—	1	15	
Trochammina cf. *nana*	—	—	—	—	—	—	—	—	1	—	—	—	—	—	1	—	—	—	
Polysaccammina ipohalina	27	36	16	2	25	7	7	3	12	—	—	—	—	—	—	2	—	—	
Pseudothurammina limnetis	—	—	—	—	—	—	—	—	1	—	—	—	—	—	—	—	1	—	
Adult *Miliammina fusca*	152	84	67	111	128	181	109	179	285	239	155	153	102	166	152	141	362	483	
Young *Miliammina fusca*	78	40	24	79	66	43	51	55	102	87	61	57	21	18	23	51	94	126	
Ammotium salsum	—	—	—	1	—	—	—	—	—	2	—	2	6	4	5	—	—	2	
Ammobaculites exiguus	—	—	—	1	1	—	1	—	2	2	2	15	6	4	7	1	2	3	
Polysaccammina hyperhalina	—	—	—	1	—	—	1	1	2	3	3	6	21	29	25	8	11	4	
Indeterminate miliolid	—	—	—	—	—	—	—	—	2	—	—	—	—	—	—	—	—	—	
Epistominella vitrea	—	—	—	—	—	—	—	—	—	—	—	—	—	—	1	—	—	—	
Glabratella luxuribulla	—	—	—	—	—	—	1	2	—	2	1	1	—	—	—	—	—	—	

TABLE 3. Continued

Glabratella sp.	—	—	—	—	—	—	—	—	—	1	—	—	—	—	—	—	—	—
Elphidium cf. *lene*	—	—	—	—	—	—	—	—	—	—	—	2	—	2	1	—	2	1
Elphidium cf. *frigidum*	—	—	—	—	—	—	—	—	—	—	1	—	—	—	—	—	—	—
Elphidium cf. *williamsoni*	—	—	—	—	—	—	—	—	1	—	—	—	—	—	—	—	—	—
Total identified foraminifera	1035	385	290	297	297	301	483	394	1063	393	286	245	158	231	218	313	530	712
Indeterminate foraminifera	95	26	24	6	6	4	64	15	51	0	5	0	0	0	1	4	3	11
Centropyxis aculeata	—	—	—	—	—	—	—	—	—	2	1	—	—	—	—	1	12	29
Centropyxis constrictus	1	—	—	—	—	—	—	—	—	—	—	—	—	—	—	2	6	8
Plagiopyxis sp.	—	—	—	—	—	—	1	—	1	—	—	—	—	1	1	—	1	5
Cyclopyxis cf. *kahli*	—	—	—	—	—	—	—	—	—	—	—	—	—	—	—	1	2	4
Cyclopyxis cf. *puteus*	—	—	—	—	—	—	—	—	—	—	—	—	—	—	—	—	1	—
Trigonopyxis sp.	—	—	—	—	—	—	—	—	—	—	—	—	—	—	—	—	—	—
Nebela cf. *collaris*	—	—	—	—	—	—	—	—	—	—	—	—	—	—	—	1	—	1
Nebela cf. *tubulosa*	—	—	—	—	—	—	—	—	—	—	—	—	—	—	—	—	—	—
Heleopera sphagni	—	—	—	—	—	—	—	—	—	—	—	—	—	—	—	—	1	2
Distomatopyxis couillardii	—	—	—	—	—	—	—	—	—	—	—	—	—	—	—	1	1	1
Difflugia globulus	—	—	—	—	—	—	—	—	—	—	—	—	—	—	—	—	2	3
Difflugia oblonga	—	—	—	—	—	—	—	—	2	2	—	—	—	—	1	5	8	14
Difflugia protaeiformis	—	—	—	—	—	—	—	—	—	—	—	—	—	—	—	—	—	—
Difflugia urceolata	—	—	—	—	—	—	—	—	—	—	—	—	—	—	—	—	—	3
Pontigulasia compressa	—	—	—	—	—	—	—	—	—	—	—	—	—	—	—	2	—	9
Phryganella sp.	—	—	—	—	—	—	—	—	—	—	—	—	—	—	—	1	4	3
Assulina sp.	—	—	—	—	—	—	—	—	—	—	—	—	—	—	—	—	—	—
Total identified arcellacea	1	0	0	0	0	0	1	0	3	4	1	0	0	1	2	14	38	82
Indeterminate arcellacea	0	0	0	0	0	0	0	0	0	0	0	0	0	0	0	0	1	0

methanol instead of formaldehyde, as was done with the cemetery samples, because of the toxicity of formaldehyde. Methanol was added to the modern samples in the field and to the fossil samples one week later in the laboratory. After sieving, modern samples from both sites were fixed in formaldehyde and stained with Rose Bengal. Fixing and staining took at least two days for the cemetery samples and one week or more for the Meares Island samples. Excess stain was then washed away and the residues were placed in methanol for long-term storage. The stained specimens were counted separately, but the quantitative analysis of the modern data set that follows is based on sums of living and dead specimens. Counted fractions are stored at the senior author's laboratory in Montreal.

RESULTS

Modern Transects

Counts of foraminifera and arcellacea for samples collected along the modern transect at the cemetery site are reported in Guilbault *et al.* (1995); data for the Meares Island transect are presented in Table 3. Generalized percentage data for key taxa are displayed in Figs 5 and 6. There are three biofacies at both localities: (1) the unvegetated tidal flat and the lower marsh biofacies dominated by *Miliammina fusca*; (2) the upper marsh biofacies dominated by *Jadammina macrescens* and *Trochamminita salsa*; and (3) the supratidal biofacies dominated by arcellacea. The upper and lower marsh are defined on the basis of their foraminiferal biofacies and not vegetation.

The tidal flat at Meares Island can be distinguished from the low marsh by a greater number of tidal flat species other than *M. fusca* (*Ammobaculites exiguus*, *Ammotium salsum* and *Polysaccammina hyperhalina*) and by a very low *J. macrescens* and *T. salsa* content. However, total numbers of 'other tidal flat foraminifera' are rather small (maximum=22% of total; generally much less), and the definition of a separate biofacies does not seem justified, at least for the purpose of this paper. The single tidal flat sample at the cemetery section is faunally indistinguishable from the lower marsh.

The limit between the upper and lower marsh is set at the level where the sum of *J. macrescens* and *T. salsa* becomes greater than the sum of adult and juvenile *M. fusca*. Guilbault *et al.* (1995) counted many of the *T. salsa* in samples from the cemetery site as *J. macrescens* morphotype *polystoma* (see Remarks on Morphotypes in

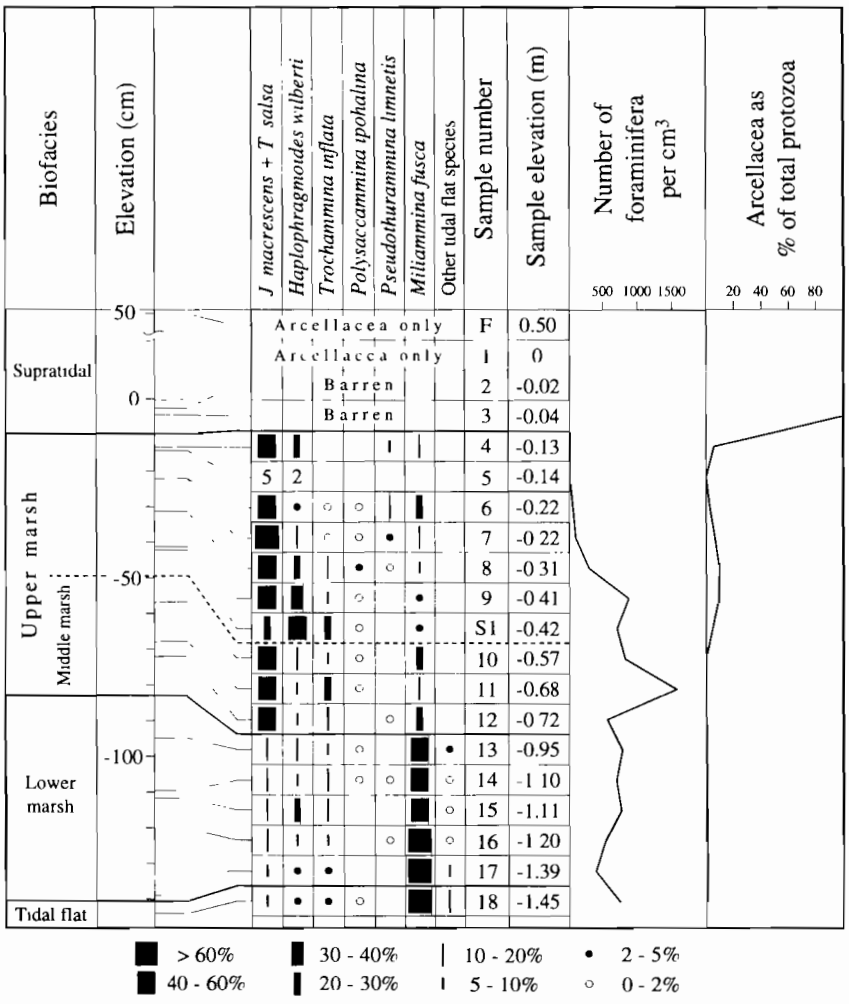

FIG. 5. Distribution of total foraminiferal microfauna (stained and unstained) along the modern transect at the cemetery site. *Miliammina fusca* percentages have been corrected using the '*M. fusca* factor' of Guilbault *et al.* (1995).

Appendix). Grouping *J. macrescens* and *T. salsa* allows data from the two study sites to be compared, while not changing the position of the high marsh-low marsh boundary at the cemetery site. There are two peaks of *J. macrescens* in the upper marsh at Meares Island, one from −11.5 to −35.5 cm elevation and the other from −48.5 to −85.5 cm (Fig. 6). *Trochamminita salsa* is generally high from −25.5 to −70.5 cm and is especially abundant at −11.5 and −19.5 cm. These trends vanish when the two species are combined; their sum gradually increases towards the top of the transect.

The *M. fusca* population at Meares Island is predominantly juvenile in the upper part of the upper marsh (Fig. 6; Remarks on Morphotypes in Appendix), as at the

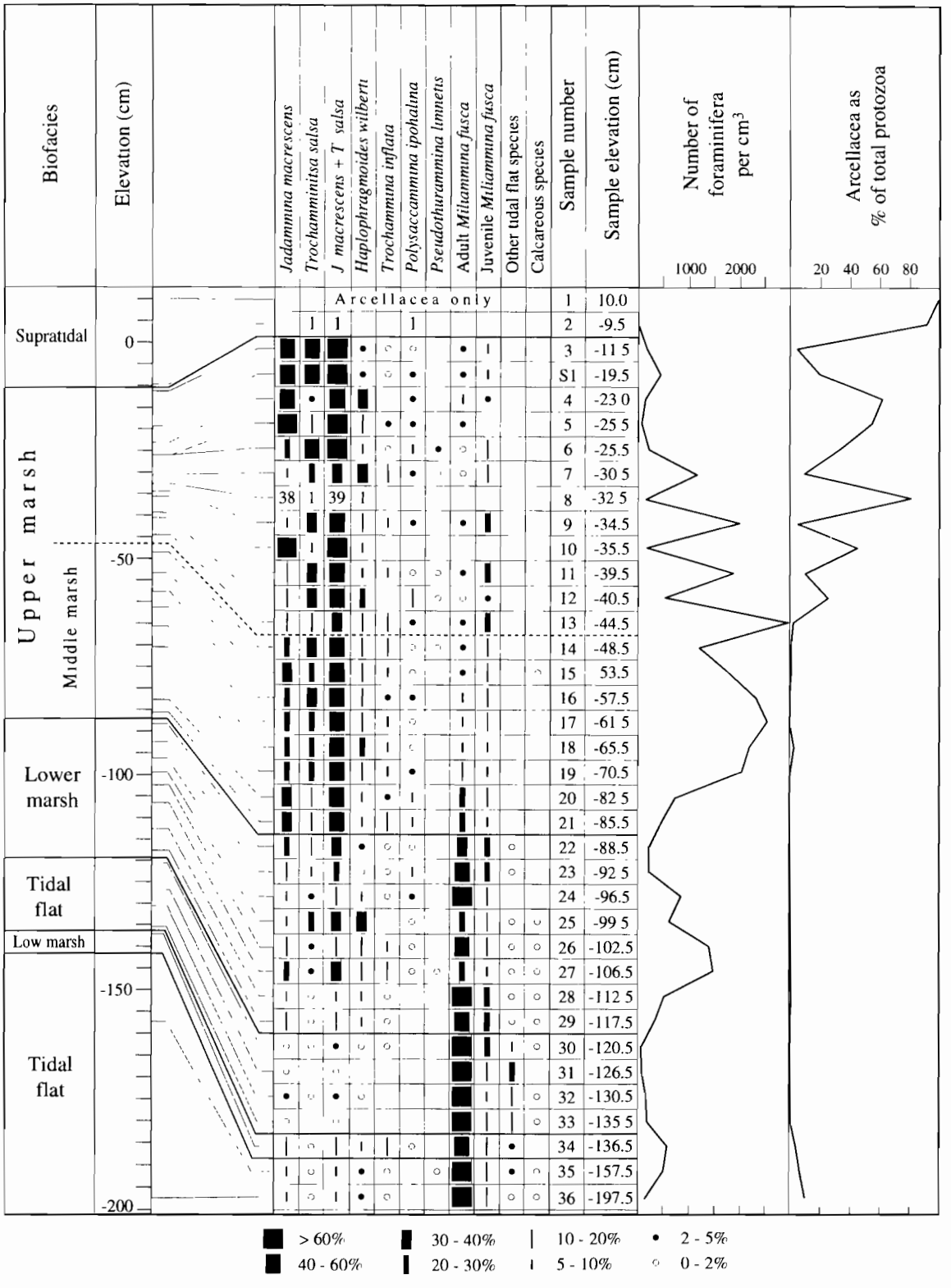

FIG. 6. Distribution of total foraminiferal microfauna (stained and unstained) along the modern transect at the Meares Island site.

cemetery site (Guilbault *et al.*, 1995). The interval between the top of the lower marsh and the point where the juvenile:adult ratio first reaches 8:1 or more constitutes a subfacies of the upper marsh called the 'middle marsh', which is recognized at both sites.

Haplophragmoides wilberti and *T. inflata* show little correlation with elevation. *H. wilberti* may be more closely controlled by salinity than elevation (Scott *et al.*, 1990). The closely related species *Haplophragmoides manilaensis* prefers brackish settings (Scott and Medioli, 1980; Scott *et al.*, 1991; de Rijk, 1995). Meares Creek, however, does not seem to have any effect on its numbers in the upper part of the Meares Island transect.

Almost all observed calcareous specimens were living (stained), and even those showed signs of dissolution. Most belong to the genera *Elphidium* and *Glabratella*. The total of calcareous specimens never exceeds 1.22% of any assemblage. Ostracodes are present in many samples, although in small numbers; most, like the calcareous foraminifera, were living and many were decalcified.

Samples above −22 cm at the cemetery site either have a limited fauna or are barren. This may be due to the relative dryness of the substrate. As a result, interpretation of paleoelevations above −22 cm at that site is difficult and reliability is poor (Guilbault *et al.*, 1995).

Samples 34, 35 and 36 from the Meares Island tidal flat contain up to 10% arcellacea (Table 3), presumably introduced by Meares Creek. Similarly, *J. macrescens* and *H. wilberti* in these samples may have been carried in by Meares Creek. The highest part of the Meares Island transect, near the forest edge (north of 140 m on Fig. 2(b)), is in a topographically irregular and somewhat depressed area that is strongly influenced by Meares Creek. This leads to assemblages that differ slightly from those observed below, with more than 60% *J. macrescens* + *T. salsa* and variable percentages of arcellacea (locally greater than the percentage of foraminifera).

The top of the Meares Island marsh is considered to lie between −9.5 and −11.5 cm elevation (Fig. 6). The unsampled interval between 0 and −9.5 cm may contain some foraminifera, but the presence of alders at −9.5 cm (Fig. 2(b)) indicates supratidal conditions at that elevation. The highest sample, at +10 cm, has a completely different arcellacea composition (*Plagiopyxis* sp.), which probably reflects the fact that this is not a marsh but a forest floor.

Correlation Between the Cemetery and Meares Transects

Figure 7 compares elevations of marsh zones along the cemetery and Meares Island transects. Despite a general similarity, there are uncertainties that limit an exact comparison of the two sites. The top of the marsh is 10 cm below the forest edge at both sites, but at the cemetery this value is approximate because it is interpolated between a foraminifer-bearing sample at −17 cm and a barren sample at −4 cm. The upper marsh-lower marsh boundary at Meares Island is precisely defined at −87±1.5 cm, whereas at the cemetery it occurs in an unsampled interval between −72 and −95 cm. The lowermost patch of the vegetation at Meares Island, at −136.5 cm, is within 1 cm of the elevation of the base of the marsh at the cemetery site. However, that patch of vegetation is, at best, a poor indicator of the level of the base of the marsh. The middle-upper marsh boundary at Meares Island is known to within a few centimeters (between −44.5 cm and −48.5 cm), whereas at the cemetery site it is poorly constrained within the broad interval between −42 cm and −57 cm.

Figure 7 also shows the highest level reached by tides on the respective days on which the two sites were sampled. By chance, on both days, the tide reached about the same level at the tidal gauge at Tofino (3.21 m and 3.18 m).

In summary, the marsh zones appear to be consistent in elevation along Browning Passage, but the uncertainties are such that we prefer to interpret each fossil section only on the basis of its associated modern transect.

Sections

Results of foraminiferal analysis of samples from the cemetery section can be found in Guilbault *et al.* (1995); the tallies for the Meares Island section are given in Table 4. Generalized results for the two sites are displayed in Figs 3 and 4. All foraminiferal species that occur along the transects are also found in the sections, with the exception of calcareous foraminifera which probably have undergone post-mortem dissolution. *Pseudothurammina limnetis* is rare in the sections, but also is known to be sensitive to post-mortem destruction (Scott *et al.*, 1981).

At the cemetery section (Fig. 3), the pre-earthquake succession begins with a tidal flat and lower marsh assemblage dominated by *M. fusca*. There is a gradual change upward into a clearly defined middle marsh interval dominated by *J. macrescens* and *T. salsa*, with abundant adult *M. fusca*, followed by upper marsh assemblages with high *J. macrescens–T. salsa* and juvenile : adult *M. fusca* ratios of 8:1 or more. The post-earthquake deposits show a similar regressive trend. At Meares Island (Fig. 4), the pre-earthquake succession begins abruptly in the middle marsh and, after a brief incursion in the lower marsh, returns to the middle marsh and finally reaches the upper marsh. Above the tsunami sand, there is a brief middle marsh interval which is succeeded by upper marsh assemblages that extend to the top of the section.

Differences between the two sections arise in part from their difference in elevation. The top of the cemetery section is 42 cm below the forest edge, whereas the top of the Meares Island section is 19.5 cm below this datum. This may explain why only one of the Meares Island samples records a lower marsh environment. Even the first marsh sample above the coseismically subsided marsh surface on Meares Island contains too few *M. fusca* to be called lower marsh. In contrast, the sample from the

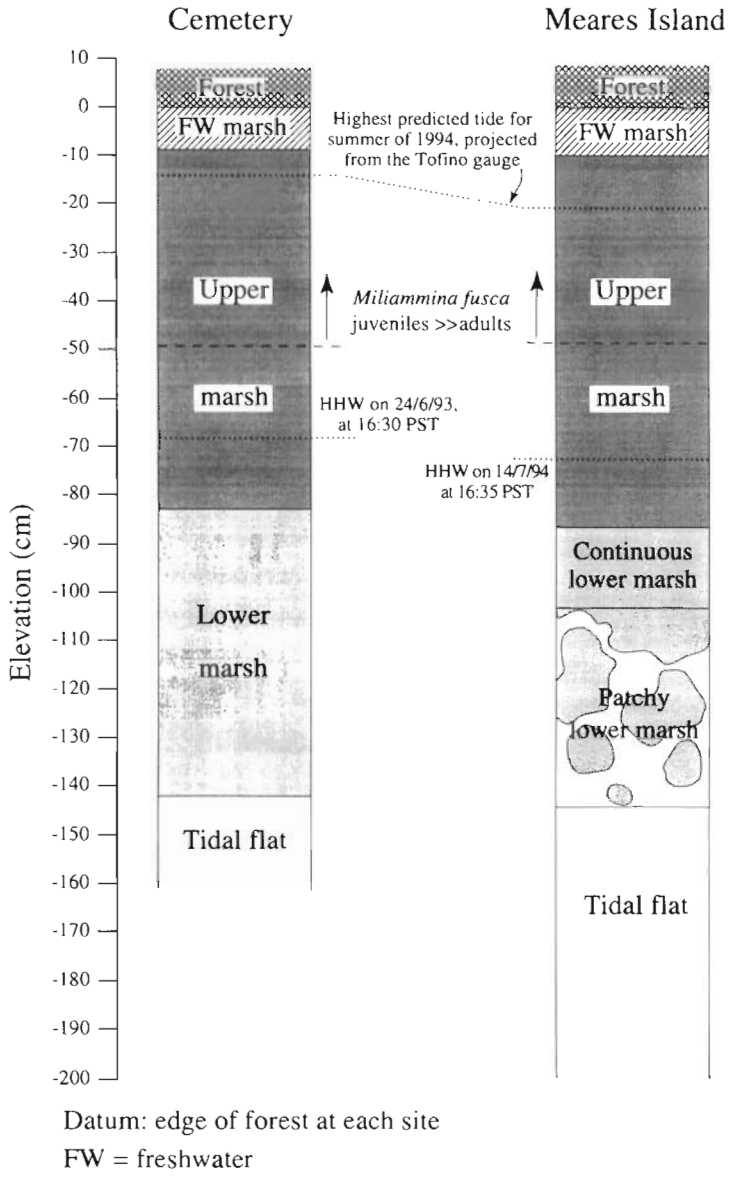

FIG. 7. Vertical distribution of modern biofacies at the cemetery and Meares Island sites. The horizontal dashed lines mark the upper limit of the 'middle marsh', above which the juvenile : adult ratio of *M. fusca* is greater than 8:1.

same stratigraphic level at the cemetery site is fully representative of a lower marsh environment.

Arcellacea are much better represented at the Meares Island site, both in terms of numbers and diversity, and their occurrence does not seem related to the foraminiferal biofacies. In contrast, in the cemetery section, arcellacea are more common in the upper marsh assemblages. This may reflect the influence of Meares Creek, since modern data show clearly that areas close to the creek contain abundant arcellacea, even as far down as the tidal flat. In general, arcellacea indicate the amount of freshwater input rather than elevation (Scott *et al.*, 1980).

Microfauna of Tsunami Sediments

The tsunami sand at Meares Island contains marsh foraminifera as well as species found in subtidal settings (Table 5). The presence of species that live only at elevations lower than the tidal marsh is strong evidence that the sand was transported landward and is not, for example, a fluvial deposit. *Trochammina nana* and *Eggerella advena* are common subtidal species that are extremely rare in tidal marshes, and we are unaware of any report of *Cribrostomoides jeffreysii* from marshes. *Trochammina ochracea* is common and may be locally dominant in Quaternary sediments off the British Columbia coast (J.-P. Guilbault and R.T. Patterson, *unpublished data*), but it is less indicative since it can be found in small numbers throughout tidal marshes (Table 3). All of these 'subtidal' specimens could as well have been transported from the lower part of the tidal flats, which we have not sampled, but they nevertheless constitute irrefutable evidence of landward transport.

The thin silt layer at 4–4.5 cm depth in the Meares Island section may have been deposited by the 1964 Alaska tsunami. This is the largest of the historical tsunamis on the British Columbia coast, reaching 2.47 m elevation at Tofino (Thomson, 1981, Table 9.1). The

TABLE 4. Total counts of foraminifera and arcellacea from the Meares Island section
Foraminifera/cm^3: determined + indeterminate foraminifera; this is the value shown on Fig. 4.
Biofacies: UM=upper marsh; MM=middle marsh; LM=lower marsh; TSU=tsunami deposit..

Sample number	S1	S2	S3	S4	S5	S6	S7	S8	S9	S10	S11	S12	S13	S14	S15	S16	S17
Depth (cm)	0-2	2-4	4-6	6-8	8-10	10-12	12-14	14-16	16-18	18-20	20-22	22-24	24-26	26-27.5	27.5-28	28-30	30-33
Foraminifera/cm^3	369	55	30	154	330	864	357	436	254	1036	2660	2446	1911	1411	1105	13	8
Biofacies	UM	UM	UM	UM	UM	UM	UM	UM	UM	UM	UM	UM	MM	MM	MM	TSU	TSU
Jadammina macrescens	110	5	3	3	2	23	54	94	61	174	492	283	190	194	68	9	3
Jadammina polystoma	2	—	—	—	—	—	—	—	1	—	—	1	5	24	3	—	1
Trochammmita salsa	98	5	10	24	41	110	101	80	50	144	49	83	72	146	89	7	2
Trochamminita irregularis	18	2	8	5	24	54	25	17	4	17	8	5	4	10	2	2	—
Haplophragmoides wilberti	7	2	2	7	11	120	7	19	15	11	7	9	18	62	35	1	1
H. wilberti 8+ chambers	—	—	1	2	4	18	1	2	1	1	—	—	—	—	1	—	—
Haplophragmoides manilaensis	—	—	—	—	—	—	—	1	—	—	—	—	—	—	—	—	—
Trochammina inflata	1	—	—	1	1	2	4	4	—	4	5	2	5	4	2	1	—
Siphotrochammina lobata	—	—	—	—	—	—	—	—	—	—	—	—	1	2	—	—	—
Trochammina ochracea	—	—	—	—	—	1	—	—	—	—	—	—	—	—	—	11	14
Remaneica helgolandica	—	—	—	—	—	—	—	—	—	—	—	—	—	—	—	—	2
Trochammina nana	—	—	—	—	—	—	—	—	—	—	—	—	—	—	—	11	62
Cribrostomoides jeffreysii	—	—	—	—	—	—	—	—	—	—	—	—	—	—	—	—	6
Eggerella advena	—	—	—	—	—	—	—	—	—	—	—	—	—	—	—	1	22
Polysaccammina ipohalina	7	—	1	3	2	22	4	2	8	17	1	1	—	—	2	—	—
Pseudothurammina limnetis	—	—	—	—	—	2	—	—	—	—	—	—	—	—	—	—	—
Adult *Miliammina fusca*	7	—	—	10	1	2	2	1	—	—	1	1	30	76	64	28	27
Juvenile *Miliammina fusca*	16	—	2	2	14	26	9	2	6	6	6	9	23	60	33	11	12
Ammobaculites exiguus	—	—	—	—	—	—	—	—	—	—	—	—	—	1	—	1	6
Total identified foraminifera	266	14	27	57	100	380	207	222	146	374	569	394	348	579	299	83	158
Indeterminate foraminifera	63	8	11	8	28	60	56	56	29	76	42	57	55	109	43	11	10
Arcella sp.	—	—	—	—	—	—	—	1	—	—	—	—	—	—	—	—	—
Centropyxis aculeata	23	8	17	12	7	—	10	37	13	4	—	—	1	7	8	5	—
Centropyxis constrictus	54	2	6	1	3	1	1	5	57	7	—	1	—	2	2	2	—
Plagiopyxis sp.	1	1	9	1	2	—	3	3	1	—	—	—	2	4	2	1	2
Cyclopyxis cf. *kahli*	2	—	1	—	—	—	1	1	—	—	—	—	—	1	1	1	—
Cyclopyxis cf. *puteus*	—	—	—	—	—	—	—	—	—	—	—	—	—	—	—	—	—
Trigonopyxis sp.	—	2	6	3	—	—	—	1	1	—	—	—	—	—	—	—	—
Hyalosphenia sp.	—	—	—	—	—	—	—	—	—	—	—	—	—	—	—	—	—
Nebela cf. *collaris*	—	—	6	—	—	1	1	1	—	—	—	—	—	—	—	—	—
Nebela cf. *tubulosa*	—	—	—	—	—	—	—	1	—	—	—	—	—	—	—	—	—
Heleopera sphagni	—	1	5	1	1	—	—	4	1	—	—	—	—	1	—	1	—
Distomatopyxis couillardii	—	—	3	1	—	1	1	—	1	—	—	—	—	—	—	—	—

TABLE 4. Continued.

Difflugia bacillariarum	—	—	—	—	—	—	—	—	—	—	—	—	—	—	—	—	—
Difflugia lithophila	—	—	1	—	—	—	—	—	—	—	—	—	—	—	—	—	—
Difflugia oblonga	—	2	5	1	1	—	5	4	2	—	—	1	1	—	—	—	2
Difflugia urceolata	—	—	—	—	—	—	—	—	—	—	—	—	—	—	—	—	—
Lagenodifflugia vas	—	—	—	1	—	—	—	—	—	—	—	—	—	—	—	—	—
Pontigulasia compressa	—	—	3	1	—	—	—	—	—	—	—	—	—	—	—	—	—
Phryganella sp.	—	—	—	2	—	—	1	4	1	—	—	—	—	4	1	—	—
Assulina sp.	—	—	—	1	—	—	—	—	—	—	—	—	—	—	—	—	—
Total identified arcellacea	80	16	62	25	14	3	23	62	77	11	0	2	4	19	14	10	4
Indeterminate arcellacea	0	1	3	0	0	0	0	1	0	0	0	0	0	0	0	0	0
Sample number	S18	S19	S20	S21	S22	S23	S24	S25	S26	S27	S28	S29	S30	S31	S32	S33	
Depth (cm)	34—35	35—37	37—39	39—41	41—43	43—45	45—47	47—49	49—51	51—53	53—55	55—57	57—59	59—61	61—64	64—69	
Foraminifera/cm^3	835	1218	1092	1826	1436	1567	1149	991	498	364	141	132	270	507	160	210	
Biofacies	UM	UM	UM	UM	UM	MM	MM	MM	MM	MM	LM	MM	MM	MM	MM	MM	
Jadammina macrescens	199	204	121	51	54	96	57	112	54	76	40	60	66	28	94	77	
Jadammina polystoma	—	—	—	—	—	—	—	—	—	—	—	2	1	—	1	—	
Trochamminita salsa	74	143	199	138	130	150	107	132	122	48	22	32	48	65	77	52	
Trochamminita irregularis	12	30	35	35	30	17	4	7	2	5	3	2	3	8	14	14	
Haplophragmoides wilberti	3	16	11	27	24	16	13	20	11	3	2	4	15	12	16	23	
H. wilberti 8+ chambers	—	—	1	2	1	—	—	3	—	1	—	—	—	—	—	—	
Haplophragmoides manilaensis	—	—	—	—	—	—	—	—	—	—	—	—	—	—	—	—	
Trochammina inflata	—	—	—	—	2	—	—	—	—	—	3	1	—	1	2	6	
Siphotrochammina lobata	—	—	—	—	—	—	—	1	—	—	—	—	—	—	—	—	
Trochammina ochracea	—	—	—	—	—	—	—	—	1	2	4	9	1	—	—	5	
Remaneica helgolandica	—	—	—	—	—	—	—	—	—	—	1	—	—	—	—	—	
Trochammina nana	—	—	—	—	—	—	—	—	—	—	—	1	—	—	—	—	
Cribrostomoides jeffreysii	—	—	—	—	—	—	—	—	—	—	—	—	—	—	—	—	
Eggerella advena	—	—	—	—	—	—	—	—	—	—	—	—	—	—	—	—	
Polysaccammina ipohalina	2	1	—	4	1	3	2	1	1	—	1	1	1	1	4	—	
Pseudothurammina limnetis	1	—	—	—	—	—	—	—	—	—	—	—	—	—	—	—	
Adult *Miliammina fusca*	1	5	—	—	—	2	10	20	21	69	71	57	41	21	45	44	
Juvenile *Miliammina fusca*	11	26	19	25	23	13	22	41	21	55	45	40	35	26	39	49	
Ammobaculites exiguus	—	—	—	—	—	—	—	—	—	—	—	—	—	—	—	—	
Total identified foraminifera	303	425	386	282	265	297	215	337	233	259	192	209	211	162	292	270	
Indeterminate foraminifera	44	24	44	29	38	31	22	47	39	16	14	22	25	33	35	37	
Arcella sp.	—	—	—	—	—	—	—	—	—	—	—	—	—	—	—	—	
Centropyxis aculeata	34	38	21	1	7	4	3	14	15	29	28	29	23	8	19	38	
Centropyxis constrictus	6	4	2	3	5	4	2	3	2	12	11	8	19	9	11	15	

TABLE 4. Continued.

Plagiopyxis sp.	—	1	—	2	1	4	1	2	4	10	12	16	5	6	12	3
Cyclopyxis cf. *kahli*	—	1	—	—	—	—	—	—	—	—	1	1	—	—	1	1
Cyclopyxis cf. *puteus*	—	—	—	—	—	—	—	1	—	1	—	1	—	—	—	—
Trigonopyxis sp.	—	—	—	—	—	1	—	3	—	—	1	2	3	2	5	1
Hyalosphenia sp.	—	—	—	—	—	—	—	—	—	—	—	—	—	—	1	1
Nebela cf. *collaris*	—	1	—	—	—	—	—	—	—	1	—	1	1	—	—	2
Nebela cf. *tubulosa*	—	—	—	—	—	—	—	—	—	—	—	—	—	—	—	—
Heleopera sphagni	—	—	—	—	—	—	—	—	—	2	1	2	2	1	5	—
Distomatopyxis couillardii	—	—	—	—	—	—	—	—	—	—	1	2	2	1	1	1
Difflugia bacillariarum	—	—	—	—	—	—	—	—	—	—	—	—	—	—	—	1
Difflugia lithophila	—	—	—	—	—	—	—	—	—	—	—	—	—	—	—	—
Difflugia oblonga	—	—	—	—	—	—	—	4	5	16	6	20	19	8	5	17
Difflugia urceolata	—	—	—	—	—	—	—	—	—	4	—	3	2	3	2	3
Lagenodifflugia vas	—	—	—	—	—	—	—	—	—	—	—	—	—	—	—	—
Pontigulasia compressa	—	—	—	—	—	—	—	—	—	—	—	—	—	2	2	1
Phryganella sp.	—	—	—	—	—	1	—	1	3	2	4	3	1	3	—	—
Assulina sp.	—	—	—	—	—	—	—	—	—	—	—	—	—	—	—	—
Total identified arcellacea	40	45	23	6	13	14	6	28	29	77	65	88	77	43	64	84
Indeterminate arcellacea	0	0	0	1	0	0	0	1	0	1	3	0	1	2	5	2

TABLE 5. Microfaunal content of the lower part of the tsunami sand at the Meares Island section (sample S17, Fig. 4)

Species	Number	%
Trochammina nana	62	38
Miliammina fusca (adult + juvenile)	39	24
Eggerella advena	22	14
Trochammina ochracea	14	9
Cribrostomoides jeffreysii	6	4
Ammobaculites exiguus	6	4
Jadammina macrescens	3	2
Remaneica helgolandica	2	1
Trochamminita salsa	2	1
Plagiopyxis sp.	2	1
Difflugia oblonga	2	1
Jadammina polystoma	1	1
Haplophragmoides wilberti	1	1
Indeterminates	10	—
Total	172	

%: Rounded values.

sample from 4–6 cm depth, which includes the silt layer, does not have an unusual faunal content that would support a tsunami origin, but the sample below it contains an anomalously high percentage of adult *M. fusca*. Statistical analysis assigns to this last sample a paleoelevation at least 25 cm lower than that of samples directly above and below it. Since there is no other evidence for a sudden change in relative sea level of this magnitude in recent time, we interpret these *M. fusca* as reworked from the lower marsh by the 1964 tsunami. They do occur 2 cm lower than expected, but it is possible that they were carried alive from the lower marsh and subsequently buried themselves in the sediment to escape the either too dry or too hyposaline conditions at the surface of the upper marsh. Bioturbation by other organisms is an unsatisfactory explanation because some adult *M. fusca* would be present in the 4–6 cm sample.

STATISTICAL ANALYSIS AND INTERPRETATION

We first estimated paleoelevations by visually comparing the distributions of the modern and fossil data in the same way as was done by Guilbault *et al.* (1995). The interpretation that follows is based mainly on statistical analysis, but the two approaches yielded similar results.

We began by performing Q-mode factor analysis

TABLE 6. B-Hat matrix and paleoelevations for samples from the cemetery section (modified from Guilbault *et al.*, 1995)

Sample no.	Sample depth (cm)	Communality	Factor 1 (*J. macrescens* + *T. salsa*)	Factor 2 (*M. fusca*)	Calculated paleoelevation (cm)
S1	0–2	0.9919	0.5376	0.1126	−49
S2	2–4	0.9977	0.7337	0.1169	−38
S3	4–6	0.9995	0.7902	0.0688	−32
S4	6–8	0.9985	0.7847	0.1953	−40
S5	8–10	0.8995	0.8796	0.0842	−28
S6	10–12	0.9864	0.9884	0.0941	−22
S7	12–14	0.9819	0.9908	0.0026	−16
S8	14–16	0.9783	0.9881	0.0431	−19
S9	16–18	0.9809	0.9902	0.0141	−17
S10	18–20	0.9860	0.9853	0.1058	−23
S11	20–22	0.9925	0.9874	0.1221	−24
S12	22–24	0.9967	0.8692	0.4451	−52
S13	24–26	0.9854	0.7601	0.3853	−54
S14	26–27	0.9988	0.5594	0.7037	−87
S15	27–28	0.9898	0.9927	0.0087	−16
S16	28–30.5	0.9896	0.9932	0.0244	−17
S17	30.5–33	0.9607	0.9755	0.0933	−23
S18	33–35	0.9899	0.9882	0.1002	−23
S19	35–37	0.9912	0.9899	0.1052	−23
S20	37–39	0.9935	0.9811	0.1599	−27
S21	39–41	0.9942	0.9152	0.3585	−44
S22	41–43	0.9855	0.9343	0.2624	−36
S23	43–45	0.9966	0.7103	0.6176	−73
S24	45–47	0.9941	0.7707	0.5624	−66
S25	47–49	0.9919	0.3203	0.9169	−114
S26	49–51	0.9895	0.2323	0.9624	−122
S27	51–55	0.9839	0.1257	0.9814	−130
S28	55–60	0.9888	0.0656	0.9899	−134

Regression equation: Paleoelevation= −66.337 (factor 1) + 56.495 (factor 2) −71.728.
Standard error of estimate, adjusted for degree of freedom: ±15.8 cm.

TABLE 7. B-Hat matrix and paleoelevations for samples from the Meares Island section

Sample no.	Sample depth (cm)	Communality	Factor 1 (*J. macrescens* + *T. salsa*	Factor 2 (*M. fusca*)	Factor 3 (*H. wilberti*)	Calculated paleoelevation (cm)
S1	0–2	0.9986	0.9927	0.1146	−0.0023	−29
S2	2–4	0.9794	0.9827	0.0660	0.0966	−24
S3	4–6	0.9965	0.9911	0.0939	0.0731	−28
S4	6–8	0.9704	0.9083	0.3575	0.1329	−61
S5	8–10	0.9913	0.9712	0.1412	0.1677	−36
S6	10–12	0.9571	0.8455	0.1112	0.4795	−33
S7	12–14	0.9981	0.9949	0.0906	0.0064	−26
S8	14–16	0.9900	0.9911	0.0738	0.0482	−25
S9	16–18	0.9932	0.9895	0.0824	0.0853	−27
S10	18–20	0.9966	0.9958	0.0702	−0.0095	−23
S11	20–22	0.9946	0.9944	0.0684	−0.0329	−22
S12	22–24	0.9952	0.9947	0.0735	−0.0197	−23
S13	24–26	0.9952	0.9782	0.1939	0.0254	−40
S14	26–27.5	0.9918	0.9436	0.2960	0.1178	−54
S15	27.5–28	0.9901	0.8776	0.4506	0.1298	−73
S18	34–35	0.9969	0.9950	0.0782	−0.0285	−24
S19	35–37	0.9963	0.9934	0.0974	0.0078	−27
S20	37–39	0.9962	0.9949	0.0798	−0.0051	−24
S21	39–41	0.9956	0.9889	0.0991	0.0886	−29
S22	41–43	0.9955	0.9892	0.0982	0.0858	−29
S23	43–45	0.9960	0.9943	0.0861	0.0083	−26
S24	45–47	0.9959	0.9837	0.1598	0.0518	−36
S25	47–49	0.9940	0.9772	0.1872	0.0624	−40
S26	49–51	0.9959	0.9754	0.2094	0.0261	−42
S27	51–53	0.9770	0.8003	0.5794	0.0284	−84
S28	53–55	0.9752	0.5731	0.8034	0.0374	−104
S29	55–57	0.9798	0.7789	0.6099	0.0334	−87
S30	57–59	0.9898	0.8866	0.4403	0.0994	−71
S31	59–61	0.9903	0.9351	0.3238	0.1054	−57
S32	61–64	0.9961	0.9358	0.3416	0.0604	−59
S33	64–69	0.9854	0.8870	0.4188	0.1528	−69

Regression equation: Paleoelevation= −45 319 (factor 1) −135.467 (factor 2) −23.461 (factor 3) + 31 333.
Standard error of estimate, adjusted for degrees of freedom: ±13.0 cm

(CABFAC program of Imbrie and Kipp, 1971) on the modern data. Two matrices were obtained: the varimax factor component matrix (factors vs. sites) and the varimax factor score matrix (factors vs. species). Then, we executed stepwise multiple regression analysis on the varimax factor component matrix and obtained a regression equation (the 'transfer function') which gives elevation as a function of species composition (REGRESS program of Imbrie and Kipp, 1971). Fossil foraminiferal assemblages were factored by applying the program THREAD (Imbrie and Kipp, 1971) to the varimax factor score matrix derived from the modern samples. This yielded a varimax factor component matrix (B-Hat matrix, Tables 6 and 7). The transfer function determined from REGRESS was then applied to the data in the B-Hat matrix to calculate paleoelevations of the fossil samples (Tables 6 and 7).

We initially used all of the taxonomic categories and all of the samples at each of the two sites. Then, we removed, one at a time, those taxa or samples that could bias the results. Supratidal samples weaken the linear correlation between *J. macrescens* and elevation because that species peaks in the upper marsh and disappears in the supratidal area. In addition, freshwater samples provide no information about elevations in the marsh. The removal of the single freshwater sample from the cemetery transect allowed a good correlation between *J. macrescens* and elevation, leading to the estimate of coseismic relative sea level change of 57 cm reported by Guilbault *et al.* (1995).

At Meares Island, the analysis was more complex because there is a larger number of taxonomic categories. The separation of *T. salsa* and *J. macrescens* left both species as poor elevation indicators (Table 8), even though they are known to concentrate in the upper marsh. We solved this problem by grouping *J. macrescens* and *T. salsa*. Both species have variable distributions, but their combined numbers correlate well with elevation (R=0.82, Table 8). Then, we removed the two supratidal samples at the top of the transect for the same reason as at the cemetery site. Also, we removed tidal flat samples 31 to 36 because, below a certain elevation, there is no more faunal variation except that resulting from material transported by Meares Creek. Finally, we removed the

TABLE 8. Correlation between elevation and species percentage at Meares Island

Species	Correlation coefficient (R): With freshwater samples and arcellacea	Freshwater samples removed with arcellacea	without arcellacea
Jadammina macrescens (+ *polystoma*)	+0.086	+0.333	+0.488
Trochamminita salsa (+ *irregularis*)	+0.336	+0.544	+0.634
J. macrescens + *T. salsa*	+0.279	+0.595	+0.816
Haplophragmoides wilberti	−0.033	+0 004	+0.202
Polysaccammina ipohalina	+0.018	+0.070	+0.168
Trochammina inflata (+ *S lobata*)	−0.167	−0.077	−0.041
Adult *Miliammina fusca*	−0.877	−0.896	−0.889
Juvenile *M. fusca*	−0.553	−0.473	−0.403
Total *M. fusca*	−0.874	−0.872	−0.858
Sum of arcellacea	+0.689	+0.596	—

All tidal flat samples except the highest one (no. 30, Fig. 6) have been removed from the data set.

arcellacea because their modern distribution shows they are mostly redeposited by Meares Creek.

CABFAC yielded 3 factors that explain 96.8% of the variance of the Meares Island data. Factor 1 is dominated by the sum of *J. macrescens* and *T. salsa* and accounts for 75.2% of the variance; it characterizes the upper marsh. Factor 2 (18.6% of the variance), dominated by adult *M. fusca*, is characteristic of the lower marsh. Factor 3 (3.0%) is dominated by *H. wilberti*; its significance is not known.

To harmonize the results from the two sites, we reran the cemetery data with *J. macrescens* and *T. salsa* grouped, and arcellacea removed. We also removed one modern cemetery sample that contained only seven specimens (sample 5) and was thus statistically invalid. The numbers of *M. fusca* were modified by the '*M. fusca* factor' as in Guilbault *et al.* (1995). CABFAC produced three factors that explain 98.5% of the variance. They are the same factors as at Meares Island and account for 70.7%, 23.1% and 4.7% of the variance, respectively. REGRESS considered only the first two factors (*J. macrescens-T. salsa* and adult *M. fusca*) in the regression equation, rejecting the third (*H. wilberti*).

Figure 8 shows paleoelevation curves for the two sections, along with standard errors calculated by the program REGRESS. The confidence intervals for statistically calculated modern elevations are compared to measured elevations in Fig. 9(a,b). The mean absolute value of residuals at the cemetery is about the same as reported by Guilbault *et al.* (1995) (11.2 cm vs. 11.9 cm), as are the correlation between calculated and measured elevations (Fig. 9(c); 0.949 vs. 0.941), and the correlation between measured elevations and residuals (Fig. 9(e); 0.315 vs. 0.337). At Meares Island, the mean absolute value of residuals is 10.7 cm, the correlation between calculated and measured elevations is 0.936, and the correlation between measured elevations and residuals is 0.352 (Fig. 9(d,f)). Correlation coefficients in the 0.3 to 0.4 range indicate that there is no systematic correlation between residuals and measured elevations (Fig. 9(e,f)).

Examination of Fig. 8 reveals that a sudden rise in relative sea level (i.e. submergence) terminated deposition of the buried peat. This submergence is a manifestation of subsidence during a large earthquake, probably the last great plate-boundary earthquake on the Cascadia subduction zone (Clague and Bobrowsky, 1994a). The magnitude of the submergence is similar at the two study sites. The mean value for the cemetery site is 71 cm (Table 9), whereas the mean value for the Meares Island site is 55 cm, which includes the difference in paleoelevation between the top and base of the tsunami sand (49 cm) plus the thickness of the sand itself (6 cm).

In the pre-earthquake part of the Meares Island section, there is an apparent submergence of about the same magnitude as the coseismic subsidence that is the focus of our work. The change from upper to lower marsh is too large to be explained by errors in paleoelevation estimates (Fig. 8), or by irregularities in the distribution of fauna in the lower marsh. The submergence is not likely due to compaction or mass movement, and probably is not the result of an earlier earthquake, as the change occurs over a few samples and thus is gradual. A seismic subsidence and rapid eustatic sea level rise are possible explanations.

DISCUSSION

The discussion of Guilbault *et al.* (1995) is worth reviewing in light of the new data from Meares Island. The limitations due to the small size of the previous paper's data base are much less of a problem now that a better sampled transect from another site that is more exposed to marine influence has given comparable results. We nevertheless maintain that it is preferable to interpret sections on the basis of close modern transects because of local site differences such as the presence or absence of streams. The vertical sampling interval that we used at Meares Island is sufficient to provide a good resolution of the vertical faunal changes. Problems are more likely to result from irregularities in distribution such as the low *M. fusca* contents of some lower marsh samples (nos 25 and 27, Fig. 6). However, the confidence interval for the calculated elevations (Fig. 9(b)) completely encloses the measured elevations along the

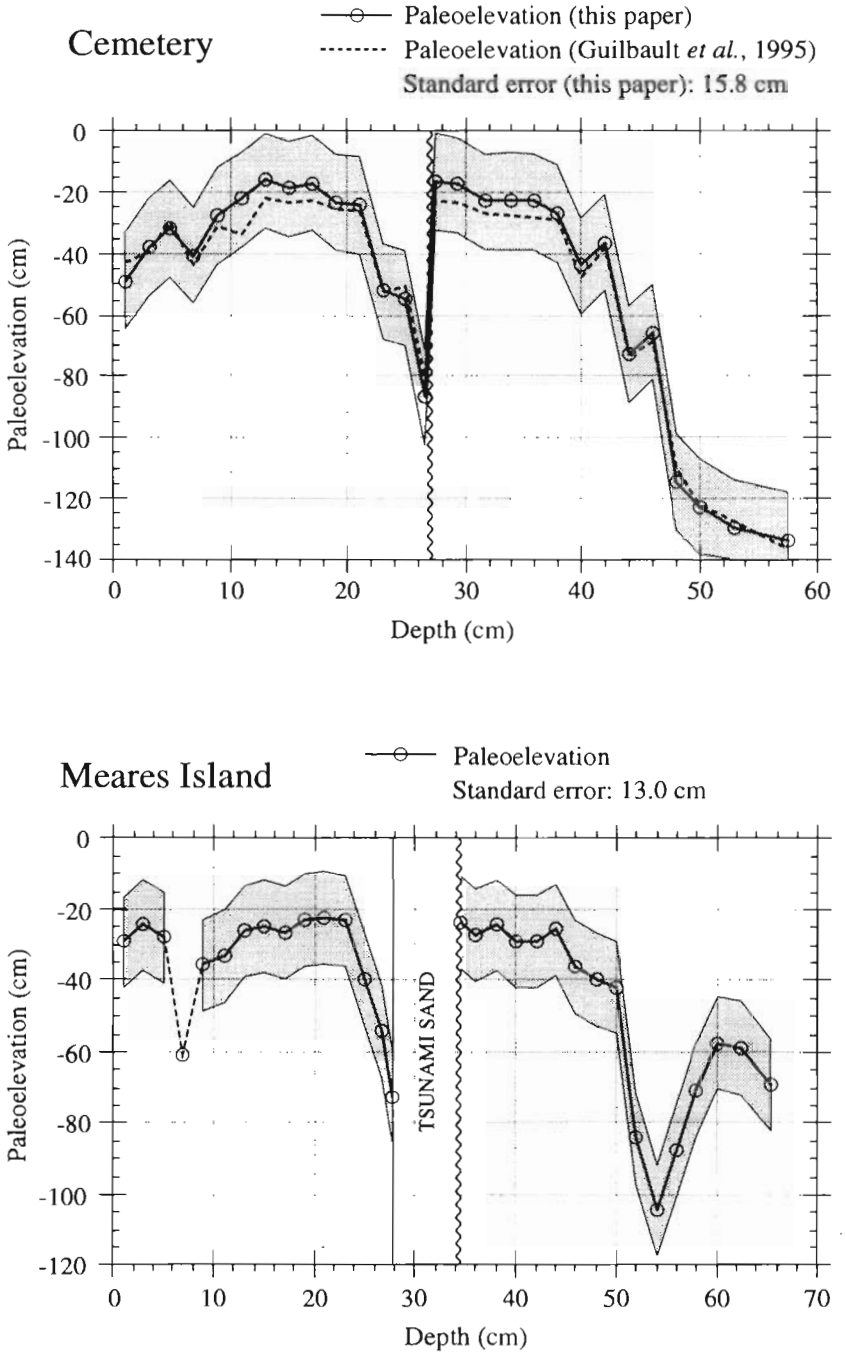

FIG. 8. Graphs of calculated paleoelevations for the cemetery and Meares Island sections determined by stepwise multiple regression analysis. The wavy vertical line marks the discontinuity at the top of the buried peat. The discontinuity coincides with a sharp decline in paleoelevation. The shaded envelope is the standard error of estimate calculated by the program REGRESS. The dashed segment in the Meares Island graph corresponds to sample S4, where faunal elements, probably reworked landward by the 1964 Alaska tsunami, skew the paleoelevation estimate.

transect. This means that all calculated elevations are reliable within the given margin of error.

Guilbault *et al.* (1995) wondered whether foraminiferal tests from the buried peat had been reworked and incorporated into the sediment immediately above, thus biasing the interpretation towards higher elevations. At Meares Island, a layer of tsunami sand blankets the peat over a large area around the section and constitutes evidence that no redeposition from the peat into the overlying mud has taken place. The sand itself contains too few foraminifera to be a source of error-causing redeposition.

Goldstein and Harben (1993) and Patterson *et al.* (1994) have shown that living foraminifera can occur to a depth of 30 cm beneath the tidal marsh surface and that there are variations in the composition of the living and total assemblages with depth. Patterson *et al.* (1994) further found that different zonal schemes could be proposed for cores from their study site at Nanaimo on Vancouver Island (Fig. 1), depending on whether the modern samples included only the uppermost centimeter of sediment, or the first 2 cm of sediment, or more, up to 10 cm. They observed little difference between zones obtained with 7-cm and 10-cm modern samples. We

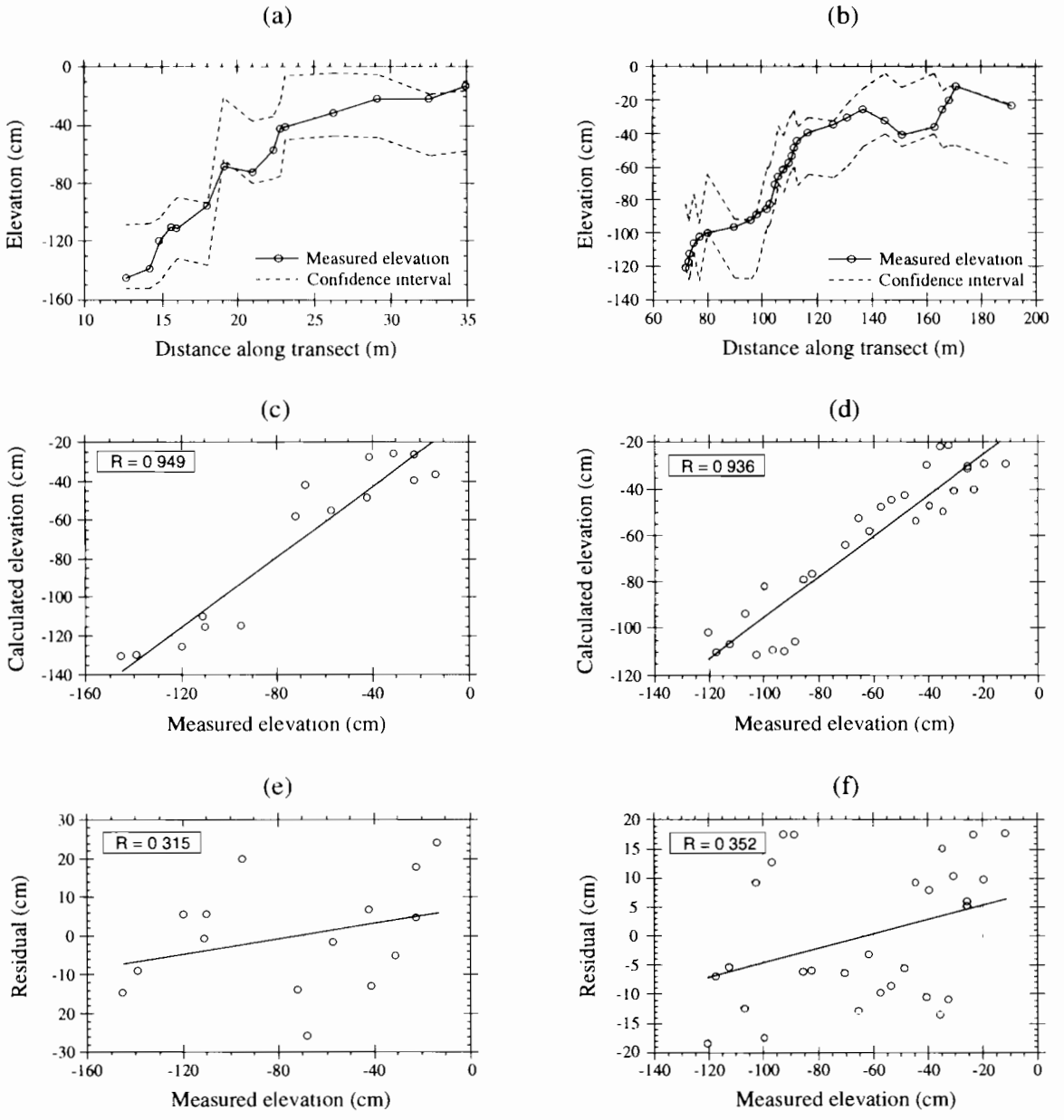

FIG. 9. Graphs showing some of the results of the statistical analysis of the modern data. (a) and (b) Measured sample elevations and envelope of elevations calculated by stepwise regression analysis (80% confidence interval). (c) and (d) Plots of measured vs. calculated elevations. (e) and (f) Plots of residuals (calculated elevations minus measured values) vs. measured elevations. R is the coefficient of correlation. (a), (c) and (e) Cemetery site; (b), (d) and (f) Meares Island site.

sampled only the uppermost 2 cm of sediment, which may introduce a bias. However, it is the opinion of R.T. Patterson (*pers. commun.*, 1995) that, because the greatest density of fauna is found just below the marsh surface, we have enough reliable information at our disposal with a 2-cm sampling depth to estimate paleoelevations, but that adding modern data from greater depths would increase accuracy. Work is now underway to investigate deep infaunal foraminifera at other sites on Vancouver Island where earthquake-induced subsidence has occurred.

Guilbault *et al.* (1995) argued that there has been no significant change in tidal range in the Tofino area in the last several hundred years. Any such change might alter faunal zonation in the marshes. Supporting evidence is the presence of living trees at least 250 years old near the edge of the marsh along the shores of Browning Passage and the absence of dead trees rooted in the marsh. The presence of old trees shows that upper limit of tides has not been noticeably higher than today since the trees started growing, because they cannot tolerate saltwater. Likewise, the absence of dead trees in the marsh tells us that the sea has not risen from a lower level in the recent past. The rather broad and deep connection between Browning Passage and the open ocean ensures that any increase in tidal prism, and hence salinity, due to coseismic subsidence would be minor. Furthermore, the fact that both sites have comparable foraminiferal distributions as a function of elevation despite the greater exposure of Meares Island to saltwater indicates that the zonation is not particularly sensitive to salinity.

Guilbault *et al.* (1995) concluded that any coseismic compaction would likely be small. The Holocene marsh

TABLE 9. Estimates of coseismic change in relative sea level

	Relative change in sea level (cm)		
	Minimum	Most likely	Maximum
Cemetery (Guilbault *et al.*, 1995 statistical)	20	57	94
Cemetery (Guilbault *et al.*, 1995 subjective)	50	68	95
Cemetery (this paper, statistical)	39	71	102
Meares Island (statistical)	29	55	80
Meares Island (subjective)	41	68	84

sequences investigated here are less than 1 m thick and overlie compact glaciomarine clay. In addition, sediment units above the buried marsh display no systematic differences in thickness between sites that are close to bedrock outcrops and those that are farther away (Clague and Bobrowsky, 1994a), which might be expected if the sediment pile compacted significantly during the earthquake.

Guilbault *et al.* (1995) were concerned that some of the coseismic subsidence they attempted to measure was not recorded due to elastic rebound of the Earth's crust soon after the earthquake, before sediment began to accumulate on the subsided marsh surface. To capture as much of the post-seismic rebound as possible, we collected a 1-cm-thick sample of sediment above the stratigraphic discontinuity (top of buried peat) at the cemetery site and a 0.5-cm-thick sample at the Meares Island site. At the cemetery site, it was not possible to prove that there was no hiatus in sedimentation following the earthquake, although such a hiatus is unlikely. At Meares Island, however, an early resumption of sedimentation is suggested by the presence of an undisturbed layer of tsunami sand on top of the buried peat. Stems and leaves of herbaceous plants rooted in the peat are covered by the sand, indicating that the subsided marsh was not eroded by the tsunami. In addition, a thin layer of sand probably could not remain exposed for long in the intertidal zone, more precisely in the middle marsh, without being washed away.

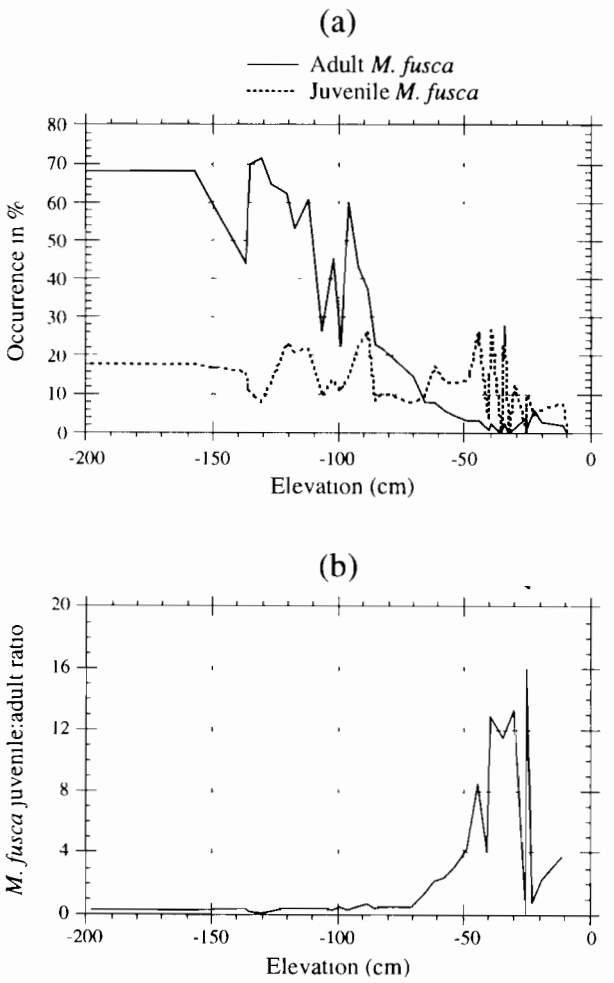

FIG. 10. (a) Vertical distribution of adult and juvenile *Miliammina fusca* (stained + unstained) along the Meares Island transect. (b) Juvenile : adult ratio for *M. fusca* along the Meares Island transect.

Both study sites yield comparable results for the amount of coseismic subsidence (Table 9) and for the period of postseismic rebound (i.e. rebound is largely complete within 6 cm of the top of the buried peat or tsunami sand; Fig. 8). This is strong evidence that the subsidence and post-earthquake recovery are well recorded at these sites.

CONCLUSIONS

Coseismic submergence at the Tofino cemetery site, determined by statistical analysis of foraminiferal data, is estimated to be 71 cm (possible range: 39 to 102 cm). This is comparable to the estimates of Guilbault *et al.* (1995) (most probable value: 57 cm; range: 20 to 94 cm). The estimate of submergence at Meares Island is 55 cm (range: 29 to 80 cm). The differences between the estimates for the two sites are not significant.

The presence of a well preserved layer of tsunami sand above the coseismically subsided marsh surface at the Meares Island site is an indication of good preservation and completeness of the record. Furthermore, the similarity of the post-seismic rebound at both sites (Fig. 8) strongly suggests that there is no hiatus in the sedimentary sequence and that much or all of the rebound is recorded in our samples. Each foraminiferal zone appears to have a similar composition and a similar vertical range over a large area along Browning Passage, and it is unlikely that the tidal prism in this area has changed in the last several hundred years, altering salinity and thus invalidating our paleoelevation estimates. These facts give us confidence that the estimated coseismic change in relative sea level is reasonable and approximates the amount of coseismic subsidence. The greatest uncertainty stems from the lack of information about deep infaunal foraminifera. We are encouraged by the fact that, at the cemetery section, no *Miliammina fusca* have burrowed from above the stratigraphic discontinuity into the underlying peat. Since *M. fusca* concentrates in the uppermost 2 to 3 cm of sediment in tidal marshes (Patterson *et al.*, 1994), the specimens of that species found just above the discontinuity must have lived there. Thus, the most critical samples for our interpretation would show only minimal bias.

ACKNOWLEDGEMENTS

We thank David B. Scott (Dalhousie University) and R Timothy Patterson (Carleton University) for advice on laboratory and field methods, interpretation, and species identification. We also thank Brian F. Atwater (U.S. Geological Survey), Richard Hebda (Royal British Columbia Museum), Anne E. Jennings (University of Colorado), and Alan R Nelson (U.S. Geological Survey) for helpful discussions. Richard E. Thomson (Fisheries and Oceans Canada) kindly supplied us with unpublished tidal data from the Tofino tidal station. Olav Lian assisted in the field Reviews by Thane Anderson (Geological Survey of Canada) and Roland Gehrels (University of Plymouth) improved the paper This is Geological Survey of Canada Contribution 30895.

REFERENCES

Andersen, H.V. (1953) Two new species of *Haplophragmoides* from the Louisiana coast. *Cushman Foundation for Foraminiferal Research, Contributions*, **4**, 20–22.

London, New SeriesBrady, H.B. (1881). Notes on some of the Reticularian Rhizopoda of the 'Challenger' Expedition, Part III. *Quarterly Journal of Microscopical Science*, **21,** 31–71.

Carter, H.J. (1864). On freshwater Rhizopoda of England and India. *Annals and Magazine of Natural History, Series 3*, **13,** 18–39.

Clague, J.J. and Bobrowsky, P.T. (1994a). Evidence for a large earthquake and tsunami 100–400 years ago on western Vancouver Island, British Columbia. *Quaternary Research*, **41**, 176–184

Clague, J.J. and Bobrowsky, P.T. (1994b). Tsunami deposits beneath tidal marshes on Vancouver Island, British Columbia. *Geological Society of America Bulletin*, **106**, 1293–1303

Cushman, J.A. (1933). New Arctic foraminifera collected by Capt. R.A. Bartlett from Fox Basin and off the northeast coast of Greenland. *Smithsonian Miscellaneous Collections*, **89,** 1–8.

Cushman, J.A. and McCulloch, I. (1940). Some Nonionidae in the collections of the Allan Hancock Foundation. *Publications of the Allan Hancock Pacific Expedition, University of Southern California*, **6,** 145–178.

de Rijk, S. (1995). Salinity control on the distribution of salt marsh foraminifera (Great Marshes, Massachusetts). *Journal of Foraminiferal Research*, **25,** 156–166.

Ehrenberg, G.C. (1832). Über die Entwicklung und Lebensdauer der Infusionsthieve, nebst ferneren Beitragen zu einer Vergleichung ihrer organischen Systemen. *Abhandlungen der königlichen Akademie der Wissenschaften, Berlin, 1831, Physikalische Abhandlungen*, 1–154, pls. 1–4.

Ehrenberg, G.C. (1848). Fortgesetzte Beobachtungen über jetzt herrschende atmosphärische mikroskopische Verhältnisse. *Bericht über die zur Bekanntmachung geeigneten Verhandlungen der königlichen Preussischen Akademie der Wissenschaften zu Berlin*, **13,** 370–381.

Fisheries and Oceans (1993). *Canadian Tide and Current Tables, 1994; Volume 6, Barkley Sound and Discovery Passage to Dixon Entrance. Canadian Department of Fisheries and Oceans, Ottawa, Ontario*, 93 pp.

Goldstein, S.T. and Harben, E.B. (1993). Taphofacies implications of infaunal foraminiferal assemblages in a Georgia salt marsh, Sapelo Island. *Micropaleontology*, **39,** 53–62.

Guilbault, J.-P., Clague, J.J. and Lapointe, M. (1995). Amount of subsidence during a late Holocene earthquake-evidence from fossil marsh foraminifera at Vancouver Island, west coast of Canada. *Palaeogeography, Palaeoclimatology, Palaeoecology*, **118,** 49–71.

Haynes, J.R. (1973). Cardigan Bay Recent foraminifera. *Bulletin of the British Museum (Natural History), Zoology, Supplement*, **4,** 245 pp.

Huntley, D.J. and Clague, J.J. (1996). Optical dating of tsunami-laid sands. *Quaternary Research*, **46**, in press

Imbrie, J. and Kipp, N.G. (1971). A new micropaleontological method for quantitative paleoclimatology; application to a late Pleistocene Caribbean core. *In*: Turekian, K.K. (ed.), *The Late Cenozoic Glacial Ages*, pp. 71–181. Yale University Press, New Haven, Connecticut.

Jennings, A.E. and Nelson, A.R. (1992). Foraminiferal assemblage zones in Oregon tidal marshes–relation to marsh floral zones and sea level. *Journal of Foraminiferal Research*, **22,** 13–29.

Jennings, A.E., Nelson, A.R., Scott, D.B. and Aravena, J.C. (1995). Marsh foraminiferal assemblages in the Valdivia estuary, south-central Chile, relative to vascular plants and sea level. *Journal of Coastal Research*, **11,** 107–123.

Jonasson, K.E. and Patterson, R.T. (1992). Preservation potential of marsh foraminifera from the Fraser River delta, British Columbia. *Micropaleontology*, **38,** 289–301.
Lamarck, J.-B. (1816). Histoire naturelle des animaux sans vertèbres. *Verdière (Paris)*, **2,** 568 pp.
Lankford, R.R. and Phleger, F.B. (1973). Foraminifera from the nearshore turbulent zone, western North America. *Journal of Foraminiferal Research*, **3,** 101–132.
Leidy, J. (1874). Notice on some rhizopods. *Academy of Natural Sciences of Philadelphia Proceedings, Series 3*, pp. 155–157.
Loeblich, A.R. and Tappan, H. (1953). Studies of Arctic Foraminifera. *Smithsonian Miscellaneous Collections*, **121,** 150 pp.
Medioli, F.S. and Scott, D.B. (1983). Holocene Arcellacea (Thecamoebians) from eastern Canada. *Cushman Foundation for Foraminiferal Research, Special Publication*, **21,** 63 pp.
Murray, J.W. (1971). *An Atlas of British Recent Foraminiferids*. Heinemann Educational Books, London, 244 pp.
Ogden, C.G. and Hedley, R.H. (1980). *An Atlas of Freshwater Testate Amoebae*. British Museum (Natural History), London, 222 pp.
Parker, F., Phleger, F.B. and Peirson, J.F. (1953). Ecology of foraminifera from San Antonio Bay and environs, southwest Texas. *Cushman Foundation for Foraminiferal Research, Special Publication*, **2,** 75 pp.
Patterson, R.T. (1990a). Intertidal benthic foraminiferal biofacies on the Fraser River Delta, British Columbia: modern distribution and paleoecological importance. *Micropaleontology*, **36,** 229–244.
Patterson, R.T. (1990b). New and renamed species of benthic foraminifera from the Pleistocene Santa Barbara Formation of California. *Journal of Paleontology*, **64,** 681–691.
Patterson, R.T., Ozarko, D.L., Guilbault, J.-P. and Clague, J.J. (1994). Distribution and preservation potential of marsh foraminiferal biofacies from the Lower Mainland & Vancouver Island, British Columbia. *Geological Society of America, Abstracts with Programs*, **267,** A–530.
Phleger, F.B. (1967). Marsh foraminiferal patterns, Pacific coast of North America, *Universidad Nacional Autónoma de México, Instituto de Biologia Anales* 38, *ser. Ciencia del Mar y Limnologia*, **1**, 11–38.
Rhumbler, L. (1938). Foraminiferen aus dem Meeressand von Helgoland, gesammelt von A. Remane (Kiel). *Kieler Meeresforschungen*, **2,** 157–222.
Scott, D.B. and Medioli, F.S. (1980). Quantitative studies of marsh foraminiferal distributions in Nova Scotia: implications for sea level studies. *Cushman Foundation for Foraminiferal Research, Special Publication*, **17,** 58 pp.
Scott, D.B., Schafer, C.T. and Medioli, F.S. (1980). Eastern Canadian estuarine foraminifera: a framework for comparison. *Journal of Foraminiferal Research*, **10,** 205–234.
Scott, D.B., Williamson, M.A. and Duffett, T.E. (1981). Marsh foraminifera at Prince Edward Island: their recent distribution and application for former sea level studies. *Maritime Sediments and Atlantic Geology*, **17,** 98–129.
Scott, D.B., Schnack, E.J., Ferrero, L., Espinosa, M. and Barbosa, C.F. (1990). Recent marsh foraminifera from the east coast of South America–comparison to the Northern Hemisphere. *In*: Hemleben, C., Scott, D.B., Kaminski, M.A. and Kuhnt, W. (eds), *Paleoecology, Biostratigraphy, Paleoceanography, and Taxonomy of Agglutinated Foraminifera*, pp. 717–738. Kluwer, Dordrecht, Proceedings of NATO ASI/ Series C, Vol. **327**.
Scott, D.B., Suter, J.R. and Kosters, E.C. (1991). Marsh foraminifera and arcellaceans of the lower Mississippi Delta: controls on spatial distributions. *Micropaleontology*, **37,** 373–392.
Stuiver, M. and Pearson, G.W. (1993). High-precision bidecadal calibration of the radiocarbon time scale, AD 1950–500 BC and 2500–6000 BC. *Radiocarbon*, **35,** 1–23.
Thomson, R.E. (1981). Oceanography of the British Columbia coast. *Canadian Special Publication of Fisheries and Aquatic Sciences*, **56,** 291 pp.
Williams, H.F.L. (1989). Foraminiferal zonation on the Fraser River delta and their application to paleoenvironmental interpretations. *Palaeogeography, Palaeoclimatology, Palaeoecology*, **73,** 39–50.
Williamson, W.C. (1858). *On the Recent Foraminifera of Great Britain. Ray Society Publications*, 107 pp.

APPENDIX: TAXONOMIC NOTES

Complementary faunal reference list

Guilbault *et al.* (1995) provided a synonym list for the species they observed at the cemetery site. Most of the species reported in the present paper are the same; the following list includes only species that were not reported by Guilbault *et al.* (1995).

Cribrostomoides jeffreysii (Williamson)

Nonionina jeffreysii Williamson, 1858, p. 34, pl. 3, Figs 72–73.

Alveolophragmium jeffreysii (Williamson). Loeblich and Tappan, 1953, p. 31, pl. 3, Figs 4–7.

Cribrostomoides jeffreysii (Williamson). Murray, 1971, p. 23, pl. 4, Figs 1–5.

Difflugia globulus (Ehrenberg)

Arcella ? globulus Ehrenberg, 1848, p. 379.

Difflugia globulus Medioli and Scott, 1983, p. 24, pl. 5, Figs 1–15.

Difflugia lithophila Penard

Difflugia lithophila Penard. Ogden and Hedley, 1980, p. 142, pl. 60.

Difflugia oblonga (Ehrenberg)

Difflugia oblonga Ehrenberg, 1832, p. 90.

Difflugia protaeiformis Lamarck

Difflugia protaeiformis Lamarck, 1816, p. 95.

Difflugia urceolata Carter

Difflugia urceolata Carter, 1864, p. 27, pl. 1, Fig. 7.

Elphidium frigidum Cushman

Elphidium frigidum Cushman, 1933, p. 5, pl. 1, Fig. 8.

Elphidium lene (Cushman and McCulloch)

Elphidium incertum (Williamson) var. *lene* Cushman and McCulloch, 1940, p. 170, pl. 19, Figs 2, 4.

Cribrononion lene (Cushman and McCulloch). Lankford and Phleger, 1973, p. 118, pl. 3, Fig. 18.

Remark: Our specimens belong to a morphotype of *Elphidium excavatum* (Terquem) which differs from the published morphotypes *clavata, excavata, selseyensis*, and *lidoensis*. They resemble *Elphidium lene*, which probably also is a morphotype of *Elphidium excavatum*.

Elphidium williamsoni Haynes

Elphidium williamsoni Haynes, 1973, p. 207, pl. 24 Fig. 7, pl. 25 Figs 6, 9, pl. 27 Figs 1–3.

Epistominella vitrea Parker

Epistominella vitrea Parker *in* Parker *et al.*, 1953, p. 9, pl. 4, Figs 34–36, 40, 41.

Glabratella luxuribulla Patterson

Glabratella luxuribulla Patterson, 1990b, p. 689, Figs 6.6–6.9, 7.1, 7.2.

Haplophragmoides manilaensis Andersen

Haplophragmoides manilaensis Andersen, 1953, p. 21, pl. 4, Fig. 8.
Haplophragmoides bonplandi Todd and Brönniman. Scott and Medioli, 1980, p. 40, pl. 2, Figs 4, 5.
Remarks: Scott *et al.* (1991) suggest that *H. manilaensis* may be synonymous with *Haplophragmoides wilberti*, but we prefer to separate the two until more data are available. Our material resembles the *Haplophragmoides bonplandi* illustrated by Scott and Medioli (1980).
Lagenodifflugia vas (Leidy)
Difflugia vas Leidy, 1874, p. 155.
Lagenodifflugia vas (Leidy). Medioli and Scott, 1983, p. 33, pl. 2, Figs 18–23, 27, 28.
Nebela tubulosa Penard
Nebela tubulosa Penard. Ogden and Hedley, 1980, p. 112, pl. 45.
Pontigulasia compressa (Carter)
Difflugia compressa Carter, 1864, p. 22, pl. 1, Figs 5, 6.
Pontigulasia compressa (Carter). Medioli and Scott, 1983, p. 35, pl. 6, Figs 5–14.
Remaneica helgolandica Rhumbler
Remaneica helgolandica Rhumbler, 1938, p. 194.
Trochammina nana (Brady)
Haplophragmium nana Brady, 1881, p. 50.
Trochammina nana (Brady). Loeblich and Tappan, 1953, p. 50, pl. 8, Fig. 5.0

Remarks on morphotypes

Morphotypes of some of the foraminiferal species were counted separately in the hope that they might have paleoenvironmental significance. *Jadammina macrescens* was counted separately from *Jadammina macrescens* morphotype *polystoma* because the latter seems to prefer more saline settings (Scott and Medioli, 1980; de Rijk, 1995). Large *Haplophragmoides wilberti* with eight or more fully developed chambers in the last whorl were abundant in one sample near the top of the cemetery transect and thus were counted separately from specimens with fewer chambers. *Siphotrochammina lobata* may be a morphotype of *Trochammina inflata*, but until the two are proven to be synonyms, we will keep them separate. *Trochamninita irregularis*, a variant of *Trochamminita salsa* (Jennings *et al.*, 1995), was also counted separately from the typical morphotype, but only at the Meares Island site. Many, maybe most, of the specimens of *T. salsa* observed by Guilbault *et al.* (1995) at the cemetery site were mistakenly counted as *Jadammina macrescens* morphotype *polystoma*. This is probably one of the reasons for the higher recorded number of *T. salsa* at Meares Island.

Guilbault *et al.* (1995) observed that the upper part of the upper marsh at the cemetery site contained abundant juvenile *Miliammina fusca* and almost no adults, whereas adults were more abundant than juveniles elsewhere in the marsh. This suggests marginal living conditions for that species in the uppermost marsh. Guilbault *et al.* (1995) introduced a '*M. fusca* index' to take into account the variations in the juvenile : adult ratio at the cemetery site. The distinction between juvenile and adult was made on the basis of the length of the test, the boundary being set arbitrarily at 183 µm. At Meares Island, adult and juvenile *M. fusca* were counted separately; adults dominate at lower elevations and decrease rapidly upward, whereas juveniles have a much more regular distribution except near the top of the transect (Fig. 10).

Of these various attempts at separating morphotypes, the only one to give useful results for the paleoenvironmental interpretation was the discrimination between adult and juvenile *Miliammina fusca*. However, all morphotypes that are not specified in the text as having been grouped were kept separate in the statistical analysis.

Pergamon

PII: S0277-3791(96)00057-1

Quaternary Science Reviews, Vol. 15, pp. 939–948, 1996

0277-3791/96 $32.00

LIQUEFACTION AND VARVE DEFORMATION AS EVIDENCE OF PALEOSEISMIC EVENTS AND TSUNAMIS. THE AUTUMN 10,430 BP CASE IN SWEDEN

NILS-AXEL MÖRNER

Paleogeophysics & Geodynamics, Stockholm University, S-10691 Stockholm, Sweden

Abstract — Coastal seismic events generate instantaneous changes in relative sea level (i.e. land level vs sea level). Tsunamis may cause disastrous damage to coasts and coastal habitation. Liquefaction and deformations of annually varved sediments provide information on paleoseismic events. The evidence for a major earthquake and associated tsunami waves in Sweden are explored. Thanks to the varve chronology, liquefaction structures and varve deformations caused by this event can be dated at the autumn 10,430 varve years BP. The magnitude is estimated at 8 (or more) on the Richter scale. The tsunami washed the previously blocked outlet of the Baltic free of icebergs and pack-ice so that marine water could suddenly invade the entire Baltic, forming the *Yoldia* Sea.

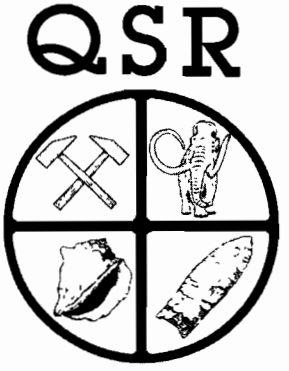

INTRODUCTION

The changes in relative sea level are the combined function of all changes in the level of the sea surface and the level of the land surface (e.g. Mörner, 1987). These variables include parameters of quite different application with respect to time and amplitude (Fig. 1). We are dealing with different spectra of sea and land level changes, respectively (Mörner, 1996a).

We may argue about what part of these spectra (Figs 1A and B) that can be classified as generating 'rapid changes in sea level'. This paper will deal with 'instantaneous' changes in land and sea level by means of seismo-tectonics and tsunamis as exemplified by the sedimentological criteria of a major paleoseismic event in Sweden dated at the autumn of varve 10,430 BP.

Paleoseimicity

It is well known that present day earthquakes primarily are concentrated along plate boundaries and spreading centres (i.e. the so-called high-seismic zones). In these areas, seismicity usually exhibits some sort of recurrences-time and lateral segmentation activity. Present day seismic recurrence is measured in time/magnitude relations. The recurrence time of paleoseismic events is measured in time/fault-offset relations or simply in time/seismic repetition. Some linear or semi-linear relation can often be established (Fig. 2A). This is a fairly powerful tool for semi-quantitative predictions of near-future events. Sometimes, however, a long unidirectional trend may become suddenly broken and even reversed. This is, for example, the case of the Greece record studied by Pirazzoli *et al.* (1981) where 10 events of moderate subsidence suddenly were followed by a 2.8 m uplift followed by 1500 years of quiescence (Fig. 3).

In intra-plate and cratonal regions, the situation is quite different. These regions are often termed 'stable' or seismically 'quiet'. This is misleading and incorrect. We have now understood that even a seemingly low-activity area may suddenly experience quite drastic events. Whether these represent singular stochastic events or long-term strain and stress build-up/release, is not known.

In formerly glaciated areas like Fennoscandia, we have understood that the seismic situation, at the time of deglaciation and peak-rates of glacial isostatic uplift, was quite different from that of today (e.g. Mörner, 1991). This is illustrated by a time/magnitude relation superimposed on a parabolic (glacial isostatic) function instead of a linear function (Fig. 2B).

Paleo-Tsunamis

Coastal and submarine vertical fault movements and huge submarine slides may set up special ocean waves of extraordinary wave lengths, known as tsunamis (e.g. Bretschneider, 1982). When these waves break against a coast they may rise to immense sizes of several tens of meters height (even up to 100 m) which usually causes disastrous coastal damage. The Lisbon 1755 event is

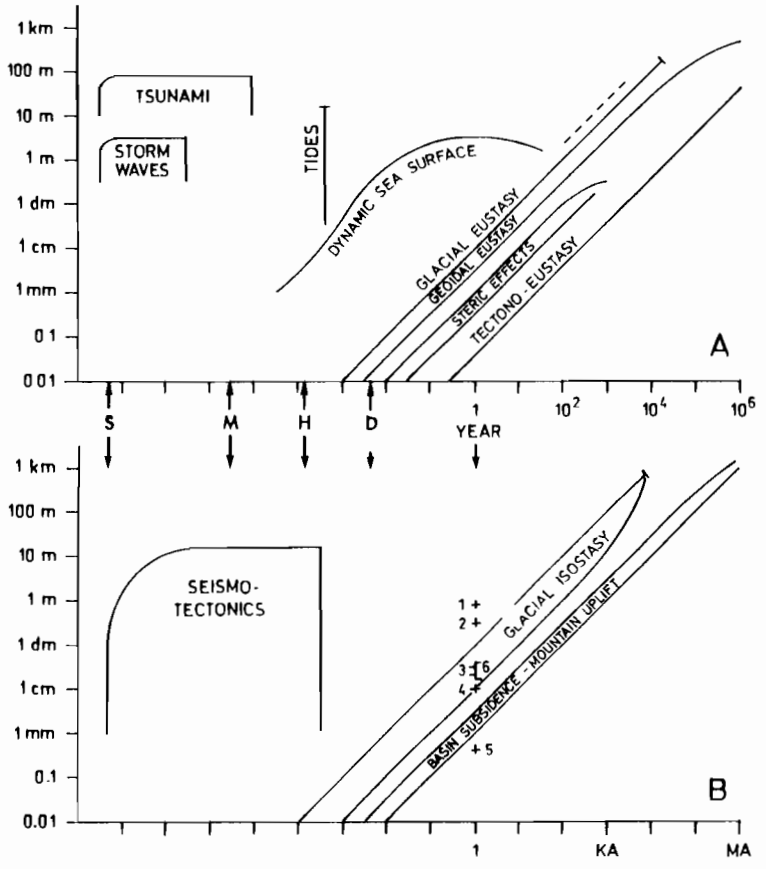

FIG. 1. Relations between time and amplitude (rates) of different variables controlling the ocean level (A) and the land level (B). Scales in 10 potency; D=1 day, H=1 hour, M=1 minute, S=1 second (from Mörner, 1996a).

classic (e.g. Dawson *et al.*, 1994). A few examples are given in Table 1.

We have quite recently started to appreciate that such tsunami events also occurred in the past (i.e. paleo-tsunamis). Even in regions like the North Sea, such events have been reported (Dawson *et al.*, 1988). In this paper I will discuss a very large event which occurred in the Baltic 10,430 BP.

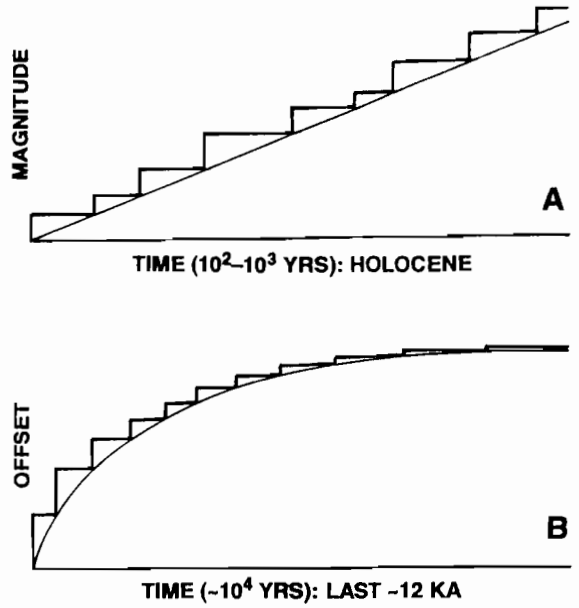

FIG. 2. Schematic illustrations of the time/magnitude relation of instrumental and historical earthquakes in high-seismic zones (A) and the time/offset relation of paleoseismic events in cratonal Fennoscandia superposed on a parabolic trend of the glacial isostatic uplift (B).

MATERIAL AND METHODS

At the peak-rate of glacial isostatic uplift around 10,000 BP, the Swedish bedrock rose by 10 cm (in the south) to 50 cm (in the center of uplift) per year (Morner, 1979). This is an enormous rate and by far exceeds the horizontal rates recorded in the high-seismic zones of the globe today. Hence, it is by no means surprising to find — rather what one would expect — that this period of uplift was characterized by a very high seismic activity (both in amplitude and frequency). Besides the vertical uplift, there were horizontal extensional forces in the tangential and radial directions of uplift. The strain rates were 2 orders of magnitude larger than those of today, and differently directed with respect to the long-term forces from the opening of the Atlantic (Mörner, 1991).

Our observational records of Fennoscandian paleoseismicity include morphological elements such as fault-scarps, fractures, 'blown-up' rock surfaces and hills turned into block/bedrock cave systems, sediment deformations and liquefactions (see review in Mörner and Tröften, 1993). The length/height of the fault-scarps give some information on the magnitudes involved (e.g. Slemmons, 1982). So do the different types and shapes of bedrock deformation (Nikonov, 1996). Liquefaction is known from Italy to commence at MCS-magnitude 6.8

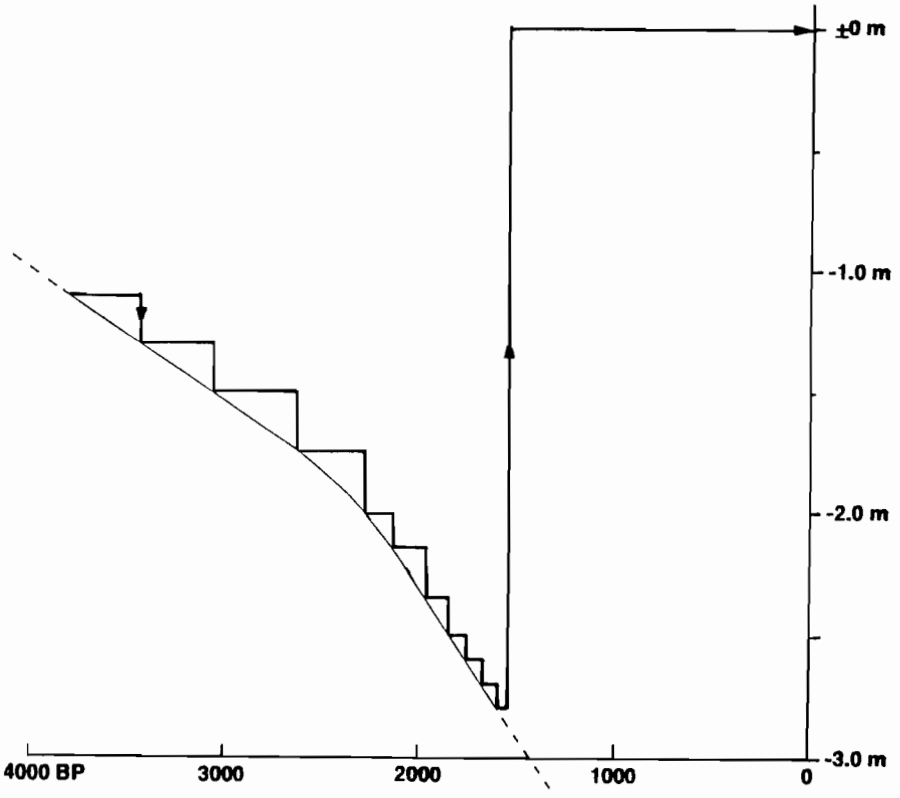

FIG. 3. Time/offset relations of the island of Antikythira for the last 4000 years (based on data from Pirazzoli *et al.*, 1981). After 10 events of subsidence, the picture suddenly reversed to a 2.8 m uplift followed by a long period of quiescence.

with a linearly increasing relation between magnitude and distance from the epicenter (Galli and Meloni, 1993; Galli and Ferreli, 1995).

The dating of paleoseismic events is usually a difficult problem. In Sweden, the situation is different, however. Thanks to the Swedish Varve Chronology (De Geer, 1940; Strömberg, 1989; Brunnberg, 1995), we are often able to date a past event with an accuracy of 1 year (in the case here discussed, even to the season of a year). Table 2 lists some major paleoseismic events in Sweden together with three large historical events.

In a few cases, we can establish the recurrence time on a yearly basis; so, for example, are we able to define three (probably, at least, five) events with a time spacing of only about 20 years in the Stockholm region (Table 2; e.g. Mörner and Tröften, 1993).

The occurrence of certain 'seismites' in the varve records, allows us to define — with an annual time resolution — the areas of deformation of one single event. So, for example, are sediment deformations recorded over 120×120 km for the Sundsvall 9287 BP event, over 220×30 km for the Iggesund 9663 BP event and over 320×60 km for the Mariefred-Stockholm 10,430 BP event (Table 2).

TABLE 1. Some historical tsunamis (for further information, see e.g. Dawson *et al.*, 1994) and two paleo-tsunamis (Dawson *et al.*, 1988; Mörner, this paper)

Time	Place	Comments
1995	Chile	erosion, sand deposition, lake ingression
1992	Indonesia	erosion, sand deposition (1 m sand in a house)
1992	Nicaragua	extensive erosion/resedimentation
1964	Alaska	sand and silt deposited up 67 m a.s.l.
1960	Chile	sand deposition some 4 km inlands
1952	Hawaii	sand deposition of the airport ramp
1946	Hawaii	roads and parkinglots covered by sand
1869	Hawaii	an old church covered by sand and coral blocks
1868	Hawaii	trees covered by 2 m sand
1771	Japan	pieces of coral thrown up 85 m a.s.l.
1755	Portugal	severe destruction of Lisbon, sand and fish thrown up on land
7200 BP	Norway	the big Storegga Slide with significant effects along the coasts of Norway and Scotland
10,430 BP	Sweden	free-washing of the Närke Strait allowing marine water suddenly to invade the Baltic (Yoldia Sea)

TABLE 2. Some very large paleoseismic events in Sweden (age in years BP) and three historical earthquakes (age in years AD) of moderate magnitude

Age	Magnitude	Name/location	Ref.
~12,000	6–7	Äspö (subglacial)	1
11,700	>7	Kinnarumma	2,3
10,469	6–7	Stockholm-1	3
10,447	6–7	Stockholm-2	3
aut. 10,430	>8	Mariefred-1/Stockholm-3	3,4,5
~10,400	6–7	Billingen	5,3,2
9663	7–8	Iggesund	6,2
9287	6–7	Sundsvall	2
~9150	>8	Lansjarv	7
~9000	>8	Parve	8(3,5)
~8500	7?	Sturuman (to be confirmed)	2
~3500	6–7	Mariefred-2	2,9
~1000	6–7	Torekov (to be confirmed)	2,3
AD 1497	>4.8	Vanern	10
AD 1759	>5.3	Skagerack-Bohuslan	10
AD 1904	>5.4	Bohuslän-Skagerack	10

References (1) Morner, 1993, (2) unpublished material, (3) e.g. Morner and Trotten, 1993, (4) Morner, 1996b, (5) Morner, 1985, (6) Sjoberg, 1994, (7) e.g. Lagerback, 1990, (8) e.g. Lundqvist and Lagerback, 1976; (9) Morner, 1995 & 1996, (10) historical data (e.g. Kijko *et al.*, 1992)

DISCUSSION: THE 10,430 BP EVENT

When the ice receded over southern Sweden, a huge ice dammed lake (the Baltic Ice Lake) was formed in the Baltic depression. When the ice halted during the Younger Dryas Stadial, building up extensive terminal moraines all around Fennoscandia, the Baltic Ice Lake was dammed some 26 m a.s.l. When the ice later receded from the northern slope of the damming mountain (Mt Billingen), the entire ice lake drained to the level of the sea. This occurred at 10,740 varve years BP (Fig. 4). Yet no saltwater entered into the Baltic. The outlet changed from the Strait of Öresund in the south to the Narke Strait in south-central Sweden. In the Baltic, fully lacustrine conditions prevailed with an *Ancylus*-fauna living along the shores of the islands of Öland and Gotland (Mörner, 1995) and a lacustrine diatom flora recorded both in the Närke Strait area (Florin, 1944) and in the Öland region (Thomasson, 1927).

At varve 10,430 BP (De Geer's varve-1073), there was a sudden ingression of saltwater changing the character of the varves both in Sweden and Finland. By definition (e.g. De Geer, 1940), this marks the onset of the *Yoldia* Sea stage in the Baltic (Fig. 4). Originally, it was correlated with the drainage of the Baltic Ice Lake at Billingen (De Geer, 1940; Caldenius, 1944). This was fully logical as the sudden, 1-year, ingression of saltwater called for a very drastic causation event. We now know (Mörner, 1995; Brunnberg, 1995) that there is, in fact, a period of 310 years of fully freshwater conditions (Fig. 4) between the drainage (10,740 BP) and the ingression (10,430 BP). This calls for a significant reinterpretation (Mörner, 1995).

It implies that the classical drainage of the Baltic Ice Lake (e.g. Caldenius, 1944; Björck and Diegerfeldt, 1984; Björck, 1995; Glückert, 1995) occurred much earlier and in no way affected the sudden ingression of saltwater to the Baltic. The ingression of marine water to the Baltic — though it had been on a level with the sea for 310 years — calls for another mechanism that can explain both the rapidity (within less than 1 year) and the extension (the entire Baltic) of the change in environmental conditions at varve 10,430 BP.

I have previously called attention to the fact that the sudden ingression of saltwater is linked to a varve characterized by strong turbidite transport with unusual deposition (sand-beds within the clay) at many places and erosion in other places in this very varve (known as varve -1073). I, therefore, proposed that this varve represents a major paleoseismic event (Morner, 1980, 1985). Not until later, however, was the additional 310 years between the end of the Baltic Ice Lake and the onset of the true *Yoldia* Sea (*sensu stricto*) understood (Mörner, 1995). This means that the seismic event of varve-1073 (=10,430 BP) has to represent a major earthquake that caused the Närke outlet area suddenly to become open — free of pack-ice and icebergs — so that the marine water could enter into the Baltic. The area is traversed by an extensive E–W fault. Because relative sea level was some 150–200 m higher in the Stockholm-Närke area at that time, a seismo-tectonic fault displacement is likely to have set up a considerable tsunami wave. It was therefore proposed (Mörner, 1995) that (1) the Baltic Ice Lake drained at 10,740 BP, that (2) it was followed by totally freshwater stage of 310 years' duration, and that (3) in the year 10,430 BP a major earthquake occurred that set up a tsunami wave which washed the Narke Strait free of icebergs and pack-ice so that the marine water could suddenly invade the Baltic basin forming the *Yoldia* Sea stage (*sensu stricto*).

In 1995, a number of remarkable stratigraphic

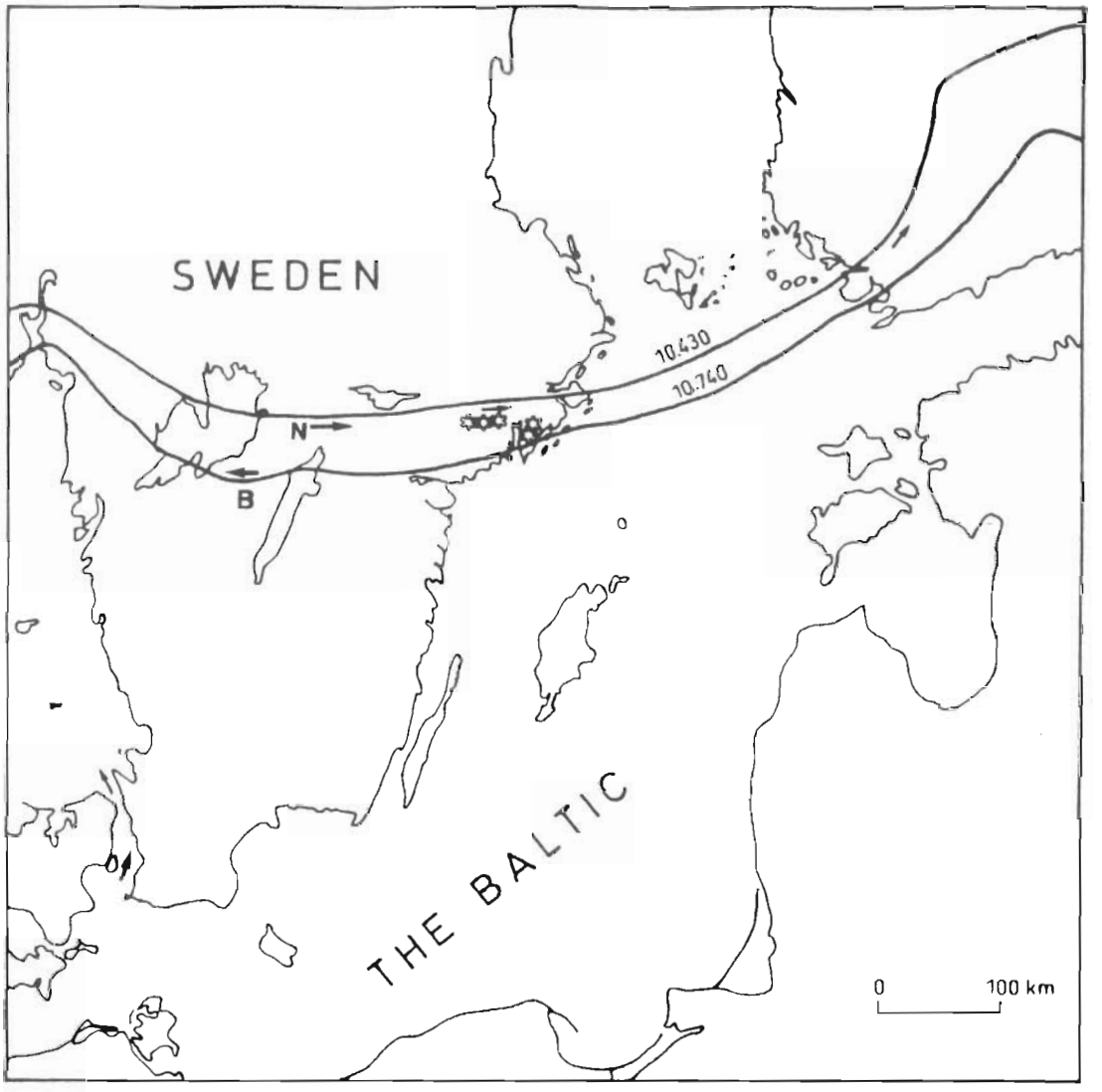

FIG. 4. Positions of the ice margin at the time of the drainage of the Baltic Ice Lake at 10,740 varves BP and at the time of the sudden ingression of marine water at 10,430 varves BP in association with a huge earthquake and tsunami in the autumn of that year. Stars give the location of the section west (Figs 8–12) and south (Figs 5–7) of Stockholm here discussed. B=Mt Billingen, N=the Närke Strait.

FIG. 5. Contorted and liquefied varves pre-dating the seismic deformation event (road cut south of Stockholm).

FIG. 6. Differential deformation of varves (road cut south of Stockholm). An undeformed fine laminated layer separates a lower part of contorted varves from an upper unit of pop-up-like deformation.

FIG. 7. Multiple liquefaction phenomena occur in this gravel pit (Olivelund, south of Stockholm). In this picture, we see an upper, large-scale, liquefaction structure of finer deposits pushing/rising upwards through coarser sand and a lower, pocket-like, slide, faulted downwards (to the right of the 1 m scale).

FIG. 8. The glacially well-polished and striated bedrock surface to the right was down-faulted in latest glacial to early postglacial time by some 6–8 m. This N–S directed fault represents a secondary fault to the main E–W fault (rail road cut west of Läggesta).

FIG. 9. The wavy layers give evidence of a significant ground acceleration that shaked and swung the sediment surface into this pattern. Below follows a unit of contorted and liquefied sand and silt, and further down a liquefied and faulted sand unit (rail road cut at Ryssjöbrink, west of Stockholm).

sequences were made available in connection with the construction of a new railroad and motorway west of Stockholm (between Mariefred and Södertälje) and a new road south of Stockholm (between Stockholm and Nynäshamn). These records give evidence of extensive liquefaction and varve deformation (Figs. 5–12), the details and character of which indicate that they can only have been generated by a very large earthquake (cf. Cakmak and Herrera, 1989; Lucchi, 1995; Galli and Ferreli, 1995). Judging from the size of the area of deformation and the magnitude/distance from epicenter graph of Galli and Meloni (1993) for liquefaction structures, the earthquake should be in the order of 8 (or more) on the Richter scale. This is also the area of a major, pre-existing, E–W fault which seems to have been reactivated at about the time of deglaciation (Mörner, 1985). A displacement along this fault, at that time below

FIG. 10. Detail of a long road cut (at Turinge west of Stockholm) showing strongly liquefied silty-sandy beds that penetrate up through the lacustrine varve unit where it stops just where the environment changes to brackish-marine varved clay.

FIG. 11. The change from freshwater varves to brackish-marine varves is very well expressed in this section (marked by the pen). The area was deglaciated 35 varves before this environmental change took place. Some 60–70 varves were counted and measured in details (road tunnel section at Turinge west of Stockholm).

FIG. 12. The erosive contact between the two clay units some 10 m north of the concordant section shown in Fig. 11. The depression on the left side of the picture began to fill up again (restored quiet condition after an event of deformation) in the autumn of varve 10,430 BP indicating that the paleoseismic event occurred in the autumn this very year. The sudden varve environmental change, refers to the sudden ingression of marine water at this very moment (due to the tsunami flushing of the Närke Strait).

some 150–200 m of water, is almost bound to set up a considerable tsunami wave. The actual occurrence of a tsunami seems indicated by the sudden free-washing of the Närke Strait and ingression of saltwater, and the occurrence of sand layers in small lake-basins. Some old diatomological records (Florin, 1944) show that these sand layers are associated with a sudden onset of marine conditions (further studies are now in progress).

The new sedimentary sequences merit special attention (Mörner *et al.*, 1996; Mörner, 1996b).

Along an 8-km new road south of Stockholm, there are numerous sites of remarkable deformations of the varves (Figs 5 and 6); including faulting, contortion, folding, liquefaction, pop-up like features, thick beds tilted in vertical position, turbidides and erosion. Multiple liquefaction structures are recorded in a gravel pit (Fig. 7). The ground acceleration must have been considerable.

West of Stockholm, there are a number of sections that provide exceptionally clear evidence of high-amplitude ground shaking with generation of liquefactions and other types of deformations. Figure 8 shows a fault of 6–8 m that may have moved just at the time in question. The fault surface contains melted silica, foliated rock, carbonate precipitation and unconsolidated fracture-fill. The road section in Fig. 9 shows a lower sand unit including liquefied and faulted structures, a completely contorded middle unit and an upper unit of shaken, stratified sand layers. Figure 10 represents a large section with numerous different types of deformation and liquefaction phenomena. As the liquefied sand penetrates up into the covering clay unit, the causation event must have occurred some time after the deglaciation when the deposition of glacial clay was going on. In a near-by varved clay sequence, we were able to date the event not only to the year but also to the season of the year; the autumn 10,430 BP.

In this section, there is a beautiful sequence of glacial varves. Some 60–70 individual varves were measured and counted. The change from freshwater to saltwater environment is very clear (Fig. 11). It occurred 35 varves after the deglaciation (i.e. at a time when the ice margin was some 7 km farther to the north). The main part of the section exhibits a concordant change from the lower lacustrine varves to the upper brackish-marine varves (Fig. 11). Laterally, however, there were significant disturbances in the lower varve unit and at the contact between the two units, here erosive (Fig. 12). The first sediments to be deposited in a small erosional trough — i.e. the deposits that represented the restoration of quiet conditions after the deformation event — were the autumn and winter parts of the first saltwater varve. The summer part of this varve was missing. We therefore concluded that the major paleoseismic event responsible for all the deformation recorded in the area, must have occurred in the autumn of the year when marine water suddenly flushed into the Baltic basin. We know that the first full varve to denote this ingression dates at the year 10,429 BP (the old varve -1073 = -1191 in the revised chronology of Strömberg, 1989). Hence, we can date the big earthquake and the related tsunami at the autumn of the year before; i.e. 10,430 BP.

ANALOGUES

The relationship between liquefaction structures and earthquakes is well established (e.g. Galli and Meloni, 1993; Galli and Ferreli, 1995). The sedimentological characteristics are usually well defined (e.g. Cakmak and Herrera, 1989; Lucchi, 1995; Galli and Ferreli, 1995).

Liquefaction in sandy-silty deposits have been reported in association with the post-glacial earthquake along the Lansjärv Fault in northern Sweden (Lagerbäck, 1991). In Southern Sweden, only a few limited examples were

FIG. 13. Section from Mejillones Peninsula north of Antofagasta, Chile. 'Concretions' in off-shore silt and sand represent small-scale diapiric mounds of silt intruded into the covering sandy beds. With time, the silt mounds have become cemented, whilst the sandy deposits have remained easily eroded allowing wind to expose the cemented structures. No doubt, we are here seeing fossil liquefaction structures from marine deposits of Late Pliocene or Early Pleistocene age (photo: Mörner, 1995).

previously known (e.g. Mörner, 1985; Mörner and Tröften, 1993).

Deformations and liquefaction structures in glacial lacustrine sediments have been reported from Scotland (Ringrose, 1989).

Because Chile represents a high-seismic area, it is significant that similar, not to say identical, liquefaction structures were recorded in uplifted marine beds of Pliocene–Pleistocene age north of Antofagasta (Fig. 13). Differential erosion has here exposed the cemented liquefied silt in three dimensions so that the upwards injection and mushroom-pattern are easily seen.

CONCLUSIONS

In the autumn 10,430 BP, a major earthquake occurred along the E-W fault south and west of Stockholm. The ground acceleration caused extensive deformations and liquefactions. Judging from the area of deformation, the corresponding magnitude is likely to be in the order of 8 (or more) on the Richter scale. This sub-aqueous event set up a tsunami wave that washed the Närke Strait free of icebergs and pack-ice so that marine water could suddenly invade the entire Baltic basin within 1 year.

The identification of the areal distribution of single liquefaction events by means of a firm varve chronology with an annual time resolution provides a new method of estimating the intensity (magnitude) of paleoseismic events.

ACKNOWLEDGEMENTS

This project was financed by grants from the Swedish National Research Council. It is a contribution to the IGCP-367 project. I acknowledge with thanks useful comments and critical reading by David Scott, Alistair Dawson and John Clague.

REFERENCES

Björck, S. (1995). A review of the history of the Baltic Sea, 13.0–8.0 ka BP. *Quaternary International*, **27**, 19–40.

Björck, S. and Diegerfeldt, G. (1984). Climatic changes at the Pleistocene/Holocene boundary in the Middle Swedish End-moraine zone, mainly inferred from stratigraphic indications. *In*: Mörner, N.-A. and Karlén, W. (eds), *Climatic Changes on a Yearly to Millennial Basis*, pp. 37–56. Reidel, Dordrecht.

Bretschneider, C.L. (1982). Tsunamis. *In*: Schwartz, M.L. (ed.), *The Encyclopedia of Beaches and Coastal Environments*, pp. 843–846. Encyclopedia of Earth Science Series, Hutchinson & Ross, **15**.

Brunnberg, L. (1995). Clay-varve chronology and deglaciation during the Younger Dryas and Preboreal in the easternmost part of the Middle Swedish ice marginal zone. Ph.D.-thesis, Quaternary Geology, Stockholm University.

Caldenius, C. (1944). Baltiska issjöns sänkning till Västerhavet, En geokronologisk studie. *Geologiska Föreningen i Stockholm Forhandlingar*, **66**, 366–382.

Cakmak, A.S. and Herrera, I. (1989). *Soil Dynamics and Liquefaction*. Comput. Mechan. Publ.

Dawson, A.G., Hindson, H., Andrade, C., Freitas, C., Parish, R. and Bateman, M. (1994). Tsunami sedimentation associated with the Lisbon earthquake of 1 November AD 1755: Boca do Rio, Algarve, Portugal. *Holocene*, **5**, 209–215.

Dawson, A.G., Long, D. and Smith, D.E. (1988). The Storegga slides: evidence from eastern Scotland for a possible tsunami. *Marine Geology*, **82**, 271–276.

De Geer, G. (1940). Geochronologia suecia principles. *Kungliga Svenska Vetenskaps Akademins Handlingar, Series 3*, **18**, 1–367.

Florin, M.B. (1944). En sensubarktisk transgression i trakten av södra Kilsbergen enligt diatomacésuccessionen i områdets högre liggande fornsjölagerföljder. *Geologiska Föreningen i Stockholm Förhandlingar*, **66**, 417–448.

Galli, P. and Ferreli, L. (1995). A methodological approach for historical liquefaction research. *In*: Serva, L. and Slemmons, D.B. (eds), *Perspectives in Paleoseismology*, pp. 35–48. AEG Spec. Publ., **6**.

Galli, P. and Meloni, F. (1993). New national catalogue of liquefaction phenomena during historical earthquakes in Italy. *Il Quaternaria*, **6**, 105–126. (Also, *Bull. INQUA Neotectonics Comm.*, **17**, 45).

Glückert, G. (1995). The Baltic Ice Lake in South Finland and its outlets. *Quaternary International,* **27,** 47–51.

Kıjko, A., Skordas, E., Wahlström, R. and Mantyniemi, P. (1992). Maximum likelihood estimation of seismic hazard for Sweden. *In:* Skordas, E. (ed.), Some aspects of cause and effects of the seismicity in Fennoscandia with emphasis to Sweden. Ph.D. thesis, Uppsala University, Acta Universitatis Upsaliensis, **390**, part V.

Lagerbäck, R. (1990). Late Quaternary faulting and paleoseismicity in northern Sweden, with particular reference to the Lansjärv area, northern Sweden. *Geologiska Föreningen i Stockholm Forhandlingar,* **112,** 333–354.

Lagerbäck, R. (1991). Seismically deformed sediments in the Lansjärv area, northern Sweden. *SKB,* **TR91-17,** 58–.

Lucchi, F.R. (1995). Sedimentological indicators of paleoseismicity. *In*: Serva, L. and Slemmons, D.B. (eds), *Perspectives in Paleoseismology*. AEG Spec. Publ., **6**, pp. 7–17.

Lundqvist, J. and Lagerbäck, R. (1976). The Pärve Fault: A late-glacial fault in the Precambrian of Swedish Lapland. *Geologiska Föreningen i Stockholm Förhandlingar,* **98,** 51–54.

Mörner, N.-A. (1979). The Fennoscandian uplift and Late Cenozoic geodynamics: geological evidence. *GeoJournal,* **3,** 287–318.

Mörner, N.-A. (1980). A 10,700 years' paleotemperature record from Gotland and Pleistocene/Holocene boundary events in Sweden. *Boreas,* **9,** 283–287.

Mörner, N.-A. (1985). Paleoseismicity and geodynamics in Sweden. *Tectonophysics,* **117,** 139–153.

Mörner, N.-A. (1987). Models of global sea-level changes. *In*: Tooley, M.J. and Shennan, I. (eds), *Sea-level Changes*, pp. 332–355. Blackwell.

Mörner, N.-A. (1991). Intense earthquakes and seismotectonics as a function of glacial isostasy. *Tectonophysics,* **188,** 407–410.

Mörner, N.-A. (1993). Boulder trail from subglacial earthquake, Äspö, Sweden. *Supp. -Bd, Zeitschrift für. Geomorphologie. N.F.,* **94,** 159–166.

Mörner, N.-A. (1995). The Baltic Ice Lake-Yoldia Sea transition. *Quaternary International,* **27**, 95–98. (Also, *Bull. INQUA Neotectonics Comm.*, **18**, 32–33.)

Mörner, N.-A. (1995 & 1996). *Tvärvetenskaplig Natur och Kultur Kunskap*. Internal course compendium. Paleogeophysics & Geodynamics, Stockholm University, 1995 & 1996, **32**.

Mörner, N.-A. (1996a). Rapid changes in coastal sea level. *Journal of Coastal Research*, **12**. (Also, *Bull. INQUA Neotectonics Comm.*, **18**, 1995, 35–37.)

Mörner, N.-A. (1996). Geologisk sensation! Jättejordbävning skakade Mälardalen för 10476 år sedan. *Forskning och Framsteg,* **5/96,** 30–33.

Mörner, N.-A. and Tröften, P.E. (1993). Palaeoseismotectonics in glaciated cratonal Sweden. *Supp. -Bd., Zeitschrift für.Geomorphologie. N.F.,* **94,** 107–117.

Mörner, N.-A., Tröften, P.E., Sjöberg, R. and Wigren, H. (1996). Paleoseismicity and Neotectonics. The Sodertörn Excursion: Part II, *NKS, SKI, SKB*, pp. 8.

Nikonov, A.A. (1996). Seismogeologic effects on the Earth's surface. *Bulletin of the INQUA Neotectonics Commission*, **19**, (in press).

Pirazzoli, P.A., Thommeret, J., Thommeret, Y., Laborel, J and Montaggioni, L.F. (1981). Les rivages émergés d'Antikythira/Cerigotto): corrélations avec la Crète occidentale et implications cinématiques et géodynamiques. *In: Actes Coll. Niveaux Marines et Tectonique Quaternaires Dans l'aire Médeterranéenne, CNRS*, vol. 1, pp. 49–65.

Ringrose, P.S. (1989). Palaeoseismic (?) liquefaction event in late Quaternary lake sediments at Glen Roy, Scotland. *Terra nova,* **1,** 57–62.

Sjöberg, R. (1994). Bedrock caves and fractured rock surfaces in Sweden, Occurrence and origin. Ph.D. thesis, Paleogeophysics & Geodynamics, Stockholm University.

Slemmons, D.B. (1982). Determination of design earthquake magnitudes for microzonation, *Proceedings 3rd International Conference on Earthquake Microzonation*, **1**, 119–130.

Strömberg, B. (1989). Late Weichselian deglaciation and clay-varve chronology in east-central Sweden. *Sveriges Geol. Undersökning,* **Ca-73,** 1–70.

Thomasson, H. (1927). Baltiska tidsbestämmelser och baltisk tidsindelning vid Kalmarsund. *Geologiska Föreningen i Stockholm Förhandlingar,* **49,** 21–76.

Pergamon

Quaternary Science Reviews, Vol 15, pp 949–960, 1996

PII: S0277-3791(96)00056-X
0277-3791/96 $32.00

COSEISMIC COASTAL UPLIFT AND CORALLINE ALGAE RECORD IN NORTHERN CHILE: THE 1995 ANTOFAGASTA EARTHQUAKE CASE

LUC ORTLIEB,*‡ SERGIO BARRIENTOS† and NURY GUZMAN‡

*ORSTOM (Institut Français de Recherche Scientifique pour le Développement en Coopération), Casilla 1190, Antofagasta, Chile

†Departamento de Geofísica, Universidad de Chile, Blanco Encalada 2085, Santiago, Chile

‡Facultad de Recursos del Mar, Universidad de Antofagasta, Casilla 170, Antofagasta, Chile

Abstract — Coralline algae that may be predominant in the upper part of the infralittoral zone along rocky shorelines proved to be a useful indicator of rapid coastal uplift. As these encrusting algae cannot survive desiccation, even for short periods at low tide, they can provide estimates of positive vertical motions like those which may accompany seismic events. The desiccation of a fringe of the algal encrustment, at the base of the intertidal area (=infralittoral fringe), combined with effects of solar radiation rapidly kills the organisms. This mortality results in a conspicuous alteration of the pigmentation from pink/beige/reddish to white. After the July 30, 1995 Antofagasta earthquake (M_w 8.1), in northern Chile, such a white fringe appeared in some parts of the bay of Antofagasta and surroundings. The width of the dead algae fringe varied from 0 to more than 1.8 m. The widest observed widths are related to local parametres (exposition to wave splash, geometric disposition) that account for an amplification of the width of the dead algae fringe, and must be identified. Thus, a careful study of each locality led us to determine the extent of the coastal areas that had been uplifted, and to reconstruct, with a precision of the order of 2 cm, the amount of the vertical deformation along the Antofagasta Bay and southern Mejillones Peninsula.

It was thus shown that the coastline bordering the town of Antofagasta suffered practically no coseismic uplift, while areas to the south and to the west of Antofagasta Bay proved to have been uplifted by as much as 25 and 40 cm, respectively. The maximum uplift (80 cm) was seen at the southwestern tip of the peninsula of Mejillones. These precise reconstructions are of great help for the calibration of geodetic studies performed independently and for the modelling of the coseismic deformation at a regional scale. Copyright © 1996 Elsevier Science Ltd

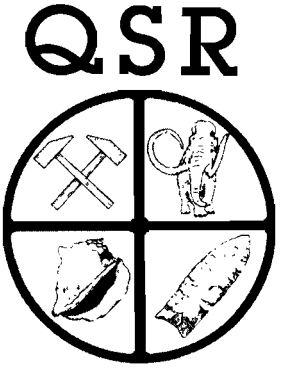

CORALLINE ALGAE AND COASTAL INSTABILITY

For almost one and a half centuries (Darwin, 1846), intertidal organisms and upper subtidal algae have been used, although not systematically, to document coastal uplift, particularly in the case of coseismic motions (Plafker, 1964; Johansen, 1971; Lebednik, 1973; Bodin and Klinger, 1986). In Chile, studies performed in relation to the 3 March 1985, M_s 7.8 earthquake focused on the post-seismic displacement of cirripeds, molluscs and kelp algae (*Lessonia nigrescens*), giving major importance to the subsequent reorganisation of the vertical zonation in the intertidal area (Castilla, 1988; Castilla and Oliva, 1990). In these papers there was only a brief mention of the death and bleaching of 'lithothamnioid algae' that preceded the downward shift of the lower level of kelp beds (*L. nigrescens*). It must be noted that for the March 1985 Chilean earthquake, unlike the cases of the Alaskan (Plafker, 1964; Johansen, 1971) and Mexican (Bodin and Klinger, 1986) earthquakes, coralline algae were not actually used to evaluate the amount of coseismic uplift.

The group of coralline algae pertain to the **Corallinacaea family (Rhodophyta,** Cryptonemiales). This family is characterised by the presence of calcium carbonate in the cell walls that confers to most of the genus the possibility to encrust bedrock, hence their other name of 'crustose algae'. Their latitudinal distribution is very wide, from polar seas to the Equator (Littler, 1972). The tropical species associated with coral reefs are probably the best known, but the group is represented by many genus and species in temperate and cold oceanic environments as well. As algae, they depend on light for their photosynthetic activity, and thus are commonly found between the intertidal zone downward to a depth of the order of 100 m or so. In terms of vertical zonation, in many coastal areas the most common genus found in the uppermost subtidal area are *Porolithon* and *Neogoniolithon*, while the genus *Lithothamnium*, *Mesophyllum* and *Archaeolithothamnium* are dominant at greater depths (50–80 m; Adey, 1986).

Coralline algae are known under a variety of names: Corallinacea, Melobesioids, crustose algae, lithothamnium s.l. (or 'lithothamnion'). Not many authors are able to differentiate the distinct subfamilies, genus and species within this family (e.g. *Lithophyllum* spp., *Pseudolithophyllum* spp., *Mesophyllum* spp., *Porolithon* spp., etc.). The determination of specimens, even at the generic

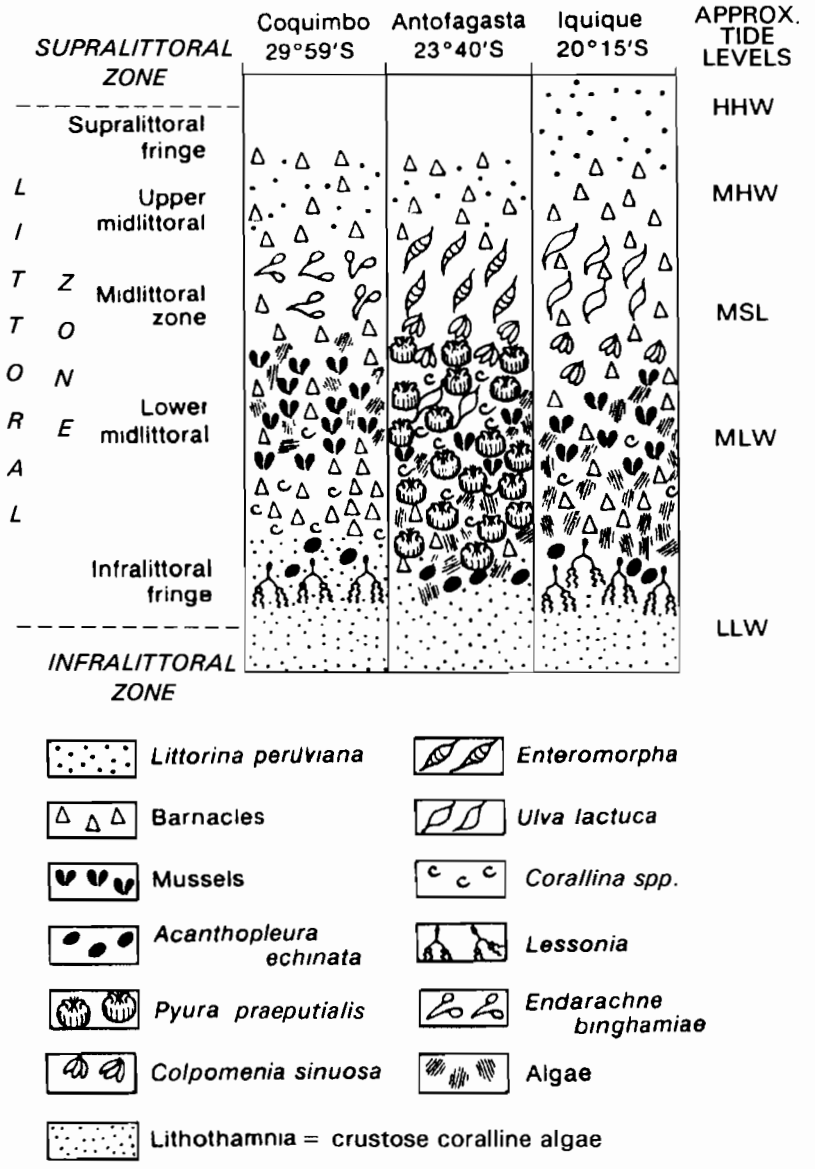

FIG 1 Sketch of the biological vertical zonation of the littoral area in northern Chile (including Antofagasta), modified from Guiler (1959) and Stephenson and Stephenson (1972) with indication of the tidal levels (only valid in quiet and protected areas)

level, cannot be made in the field and normally requires ground sections and scanning electron microscope analysis. The taxonomic identification is based on the cell size, location of heterocysts, type of hypothallium, presence and diameter of multispored conceptacles and/or sporangial sori size (Johansen, 1971; Adey and Johansen, 1972; Adey, 1986; Meneses, 1986).

In a review on the studies concerning this group, Meneses (1986) emphasised that, in spite of their wide representation along the Chilean coasts, practically no taxonomic studies had been conducted (except in the Magellan region, to the south, at the beginning of the century) and that much work was still needed to understand the ecology, distribution and characteristics of each species along the Pacific coast of South America. This implies that nowadays it is practically impossible to identify the distinct species of coralline algae in Chile.

In central and northern Chile, the coralline algae are abundant and may form a belt at the limit of the intertidal and subtidal zones (Guiler, 1959; Stephenson and Stephenson, 1972; Meneses, 1986). In the area of Iquique (20°S), Guiler (1959) distinguished, without identifying them, 'three obvious species of *Lithothamnia*, a purple-red coloured species, a deep red and a pink, the latter being the most common'. In the area of Antofagasta, where rocky shorelines are predominant, coralline algae are abundant in the subtidal zone and in the lowermost ponds and hollows of the intertidal area (Fig. 1). Their presence is apparently weakly controlled by the lithology of the rocky substrate, since they grow without visible differences on volcanic rocks (La Negra Formation), granite (Bolfin Formation) or conglomerates (Caleta Coloso Formation). Much more important is the exposition to the wave action, as indicated by most authors (e.g. Adey and Vassar, 1975; Raffaelli, 1979; Johansen, 1971). The water motion plays a role in the calcification process, and also in the protection from some grazers and/or in limiting the competition with other organisms. The upper limit of the coralline algae belt is strictly determined as the area which never desiccates completely. Because of

splash action, this level may be several cm, or dm, above the lowest tide mark. Furthermore, the survival of the algae does not require submergence, but (at least) permanent wetness. Well-exposed areas that are almost permanently subjected to strong waves (all year long), and where the biological zonation is displaced upward, may thus exhibit an upper limit of the algal belt that stands significantly higher than the mean low water mark. In general though, along most of the protected sectors of the coastline, this upper limit is found near, or slightly above, the mean low water line. At Antofagasta, the tides are of the mixed semi-diurnal type, the mean tidal range is about 0.8 m, with extremes of 0.6 and 1.6 m.

The well defined upper limit of the coralline algae belt in the Antofagasta area often coincides with the lower limit of extension of the *Pyura praeputialis*, an endemic species of ascidians (Chordata) only found in the bay of Antofagasta (Guiler, 1959; Gutierrez and Lay, 1965; in both ref., *P. praeputialis* is erroneously identified as *P. chilensis*, an infralittoral species). In the areas most exposed to the ocean swell, particularly on the southern and western coast of Mejillones Peninsula, kelp algae are abundant, and a near coincidence is observed in the respective upper limits of the coralline algae belt and that of *L. nigrescens*. Both algae can be used to define the limit between the sublittoral zone and the infralittoral fringe (Fig. 1).

The line which is defined by the top of the coralline algae belt in the infralittoral fringe provides one of the most precise bioindicators related to sea level in that region. Actually this line, perfectly horizontal in the open protected environments, is so well defined that it can be used to evaluate the amplitude of exceptional low tide stands and of sudden uplift motions produced by seismic activity. As the algae is extremely sensitive to desiccation, it may die rapidly if subjected to sudden desiccation, even of short duration (i.e. an hour or so, during the low tide hemicycle). The death of the algae is commonly accompanied by a whitening of the dead material. The decolouration of the algal material is most probably due to solar radiation effects (bleaching) on the strong pigmentation of the coralline algae. Thus, the desiccation of a few centimetres of the upper part of the coralline algae belt produces a white fringe (of the corresponding width) that contrasts sharply with the reddish or pink encrustment of living algae immediately below.

The conspicuous white belt of dead coralline algae that can be formed immediately after an uplift episode, appears in the few days following the seismic event, and may be visible for weeks, or a few months. We used this bio-indicator to quantify uplift motions related to the 30 July, 1995 Antofagasta earthquake. Moreover, we address some of the problems in reconstructing the amplitude of the vertical motions.

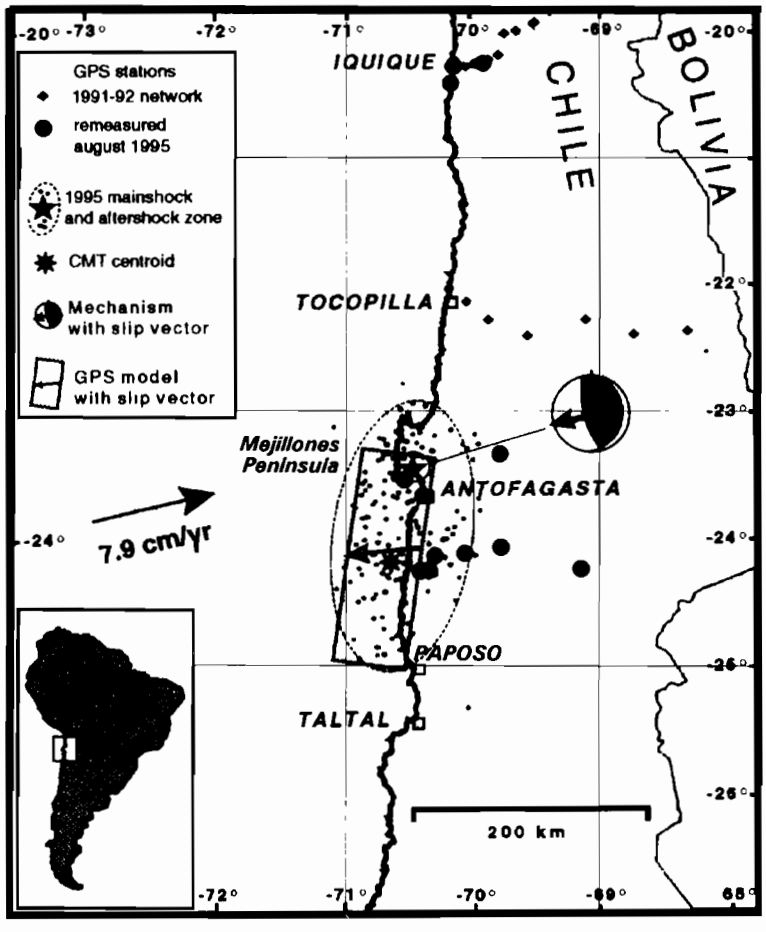

FIG. 2. The 30 July, 1995 Antofagasta earthquake: extension of the rupture, focal mechanism and distribution map of the aftershocks, simplified from Ruegg *et al.* (1996). The rectangle represents the best uniform slip model satisfying observed deformation field based on GPS measurements (see Fig. 3).

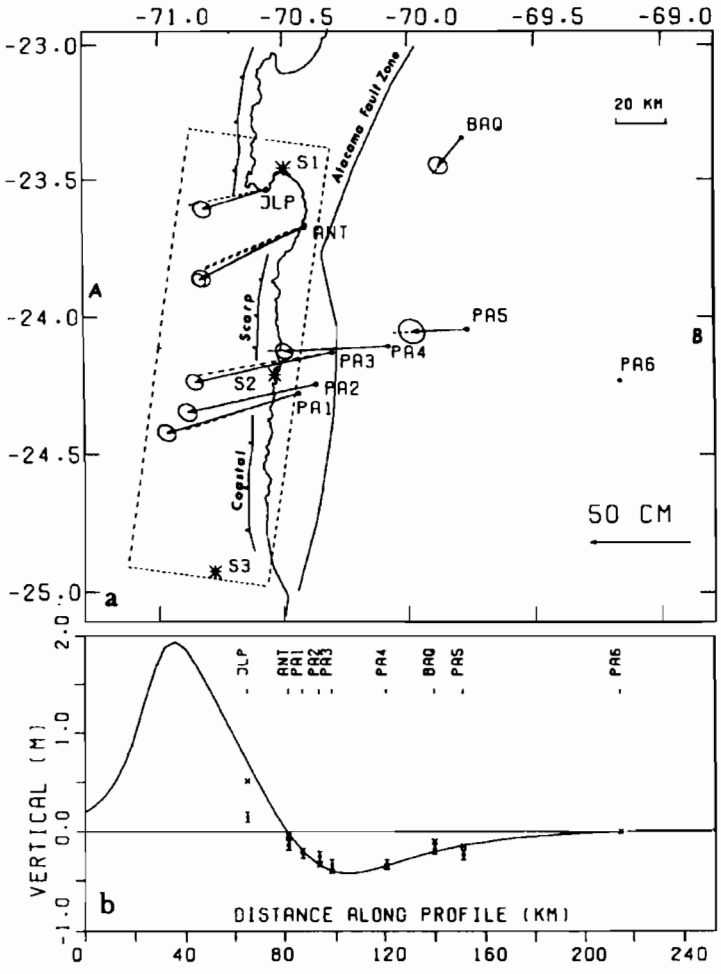

FIG. 3. Uniform slip model of deformation of the 1995 Antofagasta earthquake, calculated from GPS measurements, from Ruegg *et al.* (1996). The model suggests that the town of Antofagasta was precisely, and fortunately, located in the nodal area which separates the coseismically uplifted western area from the subsident inland region. This interpretation was assessed by the coralline algae record of deformation of the coastal area.

THE ANTOFAGASTA EARTHQUAKE

The M_s 7.3 Antofagasta earthquake which occurred on July 30, 1995 is the largest event of the last century in northern Chile. A local permanent seismological network (ORSTOM/EOPG-Strasbourg/Universidad de Chile) located the hypocentre at 23°26.7′S, 70°28.5′W and at a depth of 36 km below the Cerro Moreno airport of the city of Antofagasta (Fig. 2). According to the calculated moment magnitude (M_w 8.1) and the distribution of the aftershocks (Monfret *et al.*, 1995; Delouis *et al.*, in press), the rupture zone extended over an area of about 180 km by 70 km, from the northern half of Mejillones Peninsula (23°10′S) southward to Paposo (25°S; Ruegg *et al.*, 1996; Delouis *et al.*, in press). The earthquake ruptured an area located in the southernmost portion of an 800 km-long seismic gap. In the gap, two large earthquakes had occurred in 1868 and 1877, and produced heavy damage. Considering its large moment magnitude, the Antofagasta earthquake was surprisingly harmless, causing three deaths and little visible damage to the buildings of the city.

Surface deformation in the surroundings of Antofagasta and along the coast southward to Paposo was extremely reduced. In particular, no clear evidence for reactivation of faulting activity along the numerous recent fault scarps known in the area, including Mejillones Peninsula, the Atacama Fault Zone, and the coastal strip between El Cobre and Paposo was found (Ortlieb *et al.*, 1995a). The most conspicuous manifestations of co-seismic deformation were limited to gravity slides which occurred along the unstable coastal cliffs of the northern end of Antofagasta Bay, and some caving-in of loose ground (road embankment, in-fills in the quays of Antofagasta harbour). Near Blanco Encalada (24°20′S) some circular structures, with a diameter of several tens of metres, appeared in stabilised coastal dunes, and suggest some settling phenomena.

As the recurrence for strong earthquakes (M_w>8) in Northern Chile was evaluated to about 100 years (Comte and Pardo, 1991), and because the last major earthquake occurred in 1877, the whole area has been subjected, for the last few years, to a series of geological and geophysical studies to detect any possible precursor manifestation of a large earthquake. Thus, for instance, a geodetic (GPS) survey that encompasses the northern territory of Chile between 18° and 25°S and includes about 50 benchmarks, was initiated in 1991 and

remeasured in 1992. Two weeks after the earthquake, the southernmost portion of the geodetic network, near Antofagasta, was remeasured. Between 1992 and August 1995, a relative westwards horizontal displacement of about 0.70 m and a subsidence of several decimetres of the pampa area (east of the Cordillera de la Costa range) were thus determined with respect to a reference benchmark located about 100 km east of the coastline (Ruegg *et al.*, 1996). The southern tip of Mejillones Peninsula, where only one benchmark was set, seemed to have been uplifted by an amount of at least 15 cm. Combined teleseismic (from very broad band digital records) and geodetic data were analysed and produced a deformation model reproduced in Fig. 3 (Ruegg *et al.*, 1996).

As only three geodetic stations had been previously (1992) set up in the Antofagasta coastal area (more were established after the 1995 earthquake), the vertical component of the modelled deformation was only weakly constrained (Fig. 2). Fortunately, the dead coralline algae belt provided independent quantitative data in a series of coastal localities that contributed to assess the solution proposed in Fig. 3 (Ruegg *et al.*, 1996). The presence, or lack, of a white fringe of coralline algae, and the variation in width of this feature, along the coast were used, for the first in Chile, to determine the extension of the uplifted area and the net amount of coseismic vertical motion (Ortlieb *et al.*, 1995a, b).

THE CORALLINE ALGAE RECORD OF THE COSEISMIC DEFORMATION IN THE ANTOFAGASTA AREA

The Study Area

During the survey for evidence of the coseismic, and/or post-seismic, ground deformation performed in the third week following the Antofagasta earthquake, we discovered at low tide a white fringe that had recently developed. We were rapidly convinced that the white belt was produced by local uplift motions, and not by some regional oceanographic phenomenon, like a particularly low tide, because there was a strong variation of the width of the belt along the Antofagasta embayment. The fact that along the coastline the belt width was progressively decreasing, or increasing, in some parts of the bay, and that it was practically nil in other parts, strongly suggested that irregular land/sea relative motions had recently occurred. The attribution of these motions to localised coastal uplift was the most logical interpretation. Interestingly, the gradients of increasing and decreasing values of the belt width along the coast varied from one area to the other within Antofagasta Bay and along the southern tip of Mejillones Peninsula. This pattern seemed to be compatible with tectonic motions related, in some cases, to block faulting and tilting.

The survey of the white belt that corresponded to the area of dead crustose coralline algae, located in the sublittoral fringe, needed to be performed precisely during the low tide maximum. Thus, the study and measurement of the dead algal belt was possible only during short spans every day. The total coastal area that was surveyed measured more than 250 km, between Mejillones (23°S) and Paposo (25°S; Fig. 2). A more detailed study concerned the area limited by Punta Coloso, at the southern extremity of the Antofagasta Bay, and Herradura de Mejillones Bay, on the northwestern coast of Mejillones Peninsula. Within this area, some coastal sectors which could not be reached by land were not visited. Most of the area studied with detail is rocky and thus was potentially interesting. Actually, it was confirmed that the coralline algae are well represented, albeit in varying abundance, all along the rocky coastlines, with only one major exception: within about 3 km north and south of the mining installation of El Cobre (24°15′S). Another stretch of the coast without coralline algae coatings is the northern Antofagasta Bay because the rocky shores are replaced there by sandy beaches. Finally, the area for which precise information was gathered covered a total of 70 km within the embayment and in the western coast of Mejillones Peninsula. Between El Cobre and Paposo, the survey of the coastline was negative (coralline algae were present but did not suffer any whitening) except for one single locality, on the southern side of Punta Tragagente (24°28′S). At that locality, a 10 cm wide belt of dead algae was measured along a very small sector (a few hundred metres long), while the maximum uplift recorded at about 1.5 km to the north and to the south of Punta Tragagente was less than 2 cm.

Measurement Methodology

The goal of the survey was to determine the amount of uplift indicated by the dead coralline algae a short time after the earthquake. No precise previous study had been dedicated to the position of the uppermost limit of the algae in distinct localities of the area. Thus, no absolute measurement, with respect to some reference datum (e.g. mean sea level) could be done, and that the approach was necessarily empirical. It was assumed that the difference in vertical height between the top of the living coralline algae encrustment and the top of the former upper limit (a few weeks before) of the encrustment, on the same transect, represented the amount of the coseismic uplift.

In many localities, the determination of the height, or width, of the white belt was straightforward and yielded a value which was relatively constant for hundreds of metres, or kilometres. Alternatively, in other stretches of the coastline, the values might increase (decrease), more or less continuously, laterally along the shoreline. But in some spots of the localities visited, the fringe exceeded 30% of the width measured in the close vicinity. These variations within a few metres, or a few tens of metres, along the coastline, were mostly due to the degree of exposure to strong waves, and to the effect of splash within the locality. They were commonly related to differences in the orientation of the coast and to variations in the microtopography of the area. These variations of belt width raised more important problems in terms of the accuracy of the evaluation of uplift amount than the precision of the measurements itself.

The width of the dead algae belt was measured with a tape disposed vertically. In most localities, the precision of the measurement was of the order of 1 cm (Fig. 4A and 4B). The cases in which the accuracy of the measurements posed some problems were those concerning the areas of smallest uplift (less than a few cm) and where the dead algal belt was thin and discontinuous. In a few cases (notably at Antofagasta, or immediately to the south of the town) the only evidence of uplift consisted in an alignment of small white patches. In these cases, the upper limit of the coralline algae was not well defined by an horizontal level, and ended upward by a series of isolated small patches, that eventually whitened after the earthquake.

To resolve the problems posed by differences within short distances of the width of the dead algae belt, we tried to establish a series of criteria, that would provide the most representative and accurate evaluation of the local uplift of the land.

One of these criteria was the parallelism of the upper and lower limits of the white belt of dead algae. The inclination of the lower and/or upper limits of the belt, with respect to the horizontal plane, indicated that wave motions were strong enough to displace upward the extension of the coralline algae belt, within the intertidal zone (Fig. 1). In these cases, the width of the white belt provided an amplified evaluation of the relative vertical motion. The parallelism of the white belt limits was normally observed in areas of agitated waters (for an optimal development of the algae) but with limited wave splash (at low tide). Such conditions were usually met in protected small re-entrants, or micro-coves, that remained linked with the open ocean even at the lowest tide level. An extreme opposite situation is that of vertical cliffs beaten by permanently strong waves (even on calm days), in which the upper limit of living coralline algae may be observed at up to 1 or 2 m above the mean low tide line (Fig. 5).

Another useful criteria for the representativity of the measurements was the coincidence between values determined on vertical microcliffs (Fig. 4A) and upon 'dormant' boulders commonly found in the infralittoral fringe (that had not been moved by the waves since the earthquake occurrence).

When, in a given locality, variation of the belt-width was large it appeared that the best estimate of uplift was near the lowest values obtained. The highest values corresponded to areas of relatively stronger waves, and thus were discarded. The lowest measured values were sometimes due to the fact that some threshold separated the open ocean from the measured spot, in such a way that the measured belt width underestimated the amplitude of the reconstructed vertical motion. In every locality, it was necessary to locate the areas least affected by non-tectonic local effects that were susceptible to either amplify or diminish the evaluation of the coseismic uplift. This could not be determined on the basis of a mean value of several measurements of the height of the white belt, unless the measured values (within a few metres, or tens of metres of coastline) were differing by less than about 5%.

Results and Interpretation

The measured width of the dead coralline algal belt that was formed in a series of visited localities is indicated in Fig. 6. Two categories of measured values are distinguished: those satisfying the above mentioned quality criteria, and those which although of lower quality are the only evaluations possible of the amplitude of the belt. The latter category includes localities where the observations could not be completed satisfactorily due to difficulty of access, areas exposed to strong waves, measurements made before or after the low tide maximum, or those where the (former, and/or new) upper limit of the coralline algae zone was not neatly defined.

The survey of the distribution and width of the white fringe of coralline algae showed that the vertical motions caused by the 1995 Antofagasta earthquake were limited to an area between the northern Mejillones Peninsula and the southern extremity of the Bay of Antofagasta. The impossibility of accessing the coastline south of Punta Coloso left some doubts regarding the extension toward the south of the uplifted area. A coastal road could be used between Caleta El Cobre (24 10′S) and Paposo (25°S). At Caleta El Cobre, copper mining activities seem to have eliminated the coralline algae in the infralittoral zone, so that no record was possible. But at a few kilometres south of Caleta El Cobre, when the crustose algae are present in the infralittoral fringe, no white belt was observed. It is concluded that the area was not uplifted coseismically. The same situation (living coralline algae without white fringe) was observed southward, all along the coast, with the exception of one locality, Punta Tragagente, where a belt measuring up to 10 cm was observed. This area might have experienced a localised tectonic motion, unlike the coast to the north and south. At Paposo, coralline algae are common but no indication of desiccation of the upper limit of the algal crust was noticed.

Near Punta Coloso, a relatively 'steep' gradient of uplift motions was documented. In a short distance, the dead algal belt increased from less than 5 cm to about 25 cm (El Lenguado). It could not be determined whether the indicated deformation reflected a local tectonic effect linked, for instance, to a triggered slip on a small fault. Alternatively, it may reflect the fact that the coastline is locally trending ENE–WSW, instead of roughly N–S like further north, along the city of Antofagasta, and that the ENE–WSW direction would be that of the steeper gradient of the deformation pattern in that area.

Along the eastern shore of Antofagasta Bay, the coralline algae are as abundant in the infralittoral fringe than elsewhere, but no continuous, well-defined, white belt of desiccated algae was observed. Only a rather discontinuous narrow fringe or isolated small patches of white dead algae were visible along the shoreline, between the mouth of Quebrada El Way and La Chimba. These data suggest that the uplift motions in the area were less than 5 cm, and locally less than 2 cm, along a 35 km long stretch of coastline.

At the north-westernmost end of Antofagasta Bay, at La Rinconada, an irregular belt and aligned white patches

FIG. 4. Typical aspects of the white, dead fringe of coralline algae after the 1995 Antofagasta earthquake in a series of localities. (A) Conspicuous fringe of dead coralline algae, at Punta Jorge (southern tip of Mejillones Peninsula). At that relatively protected locality, the width of the white fringe measured 31 cm. (B) Close up of the limit between the white fringe of dead algae and the unaltered pink encrustment of the same algae, on a 'dormant' boulder. Note that the precision of the measurement may be better than 1 cm. (C) Small pond in the lower intertidal zone which is permanently submerged and where the coralline algae remained alive (pink colour), while the surroundings are coated with white dead algae (hammer for scale at left in the foreground). (D) Example of the white fringe on the western side of Mejillones Peninsula, close to Caleta Bandurria del Sur. Measured width was 28 cm. (E) The white fringe at El Lenguado, near the southern end of Antofagasta Bay. Note the coincidence between the top of the white fringe and the base of the colonies of *Pyura praeputialis* (ascidians). It is expected that, unless the coast registers a subsequent subsidence, the ascidians will colonise the area abandoned by the coralline algae. (F) About 10 weeks after the earthquake, the (formerly white) fringe of dead crustose algae get covered with green algae: observe evolution with respect to photo 4E. Monitoring the position of the upper limit of the living coralline algae encrustment should provide information regarding the evolution of the vertical motions (including an eventual compensatory subsidence).

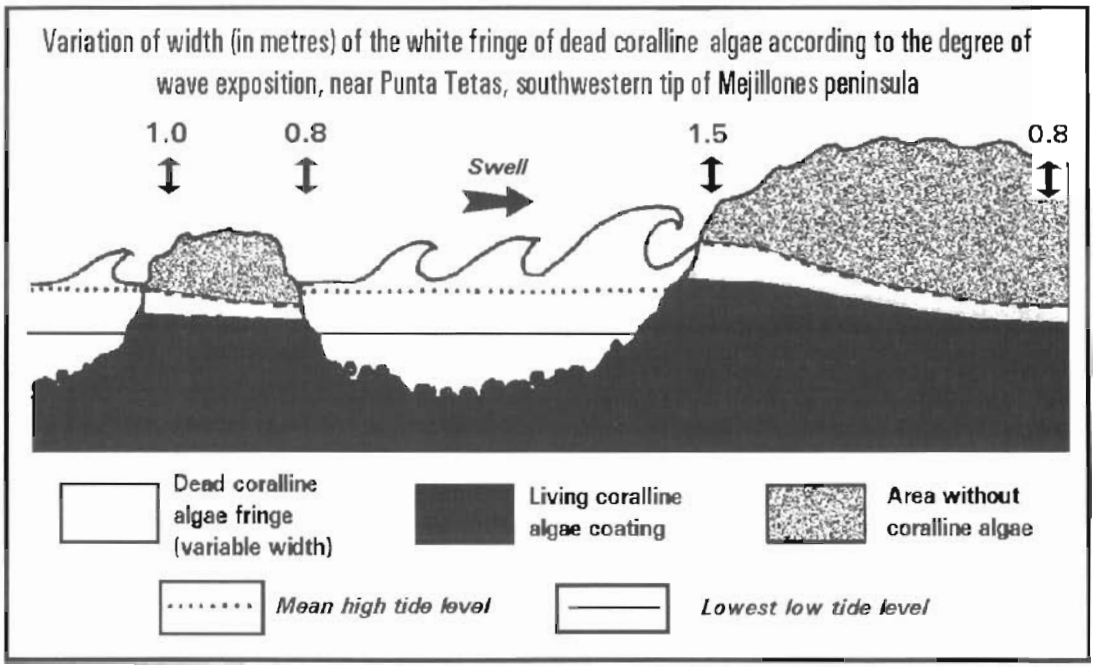

FIG. 5. Sketch of the vertical zonation of the dead and living coralline algae at the south-westernmost end of Mejillones Peninsula (near Punta Tetas), in the locality where wave activity is very strong. Note the variation in height of the upper limit of the crustose algae coating which may even reach the mean high tide level. In this locality (see also Figs 6 and 7A) was measured in the protected part of the coastline, not the 1.0 or 1.5 m values observed in the more exposed areas.

of desiccated coralline algae appeared in the infralittoral fringe. At most, the width of the irregular white belt measured between 5 and 8 cm. In that locality the uplift motion was probably less than 5 cm. Southward from La Rinconada, several localities were visited and showed increasing values of a much better defined belt. At Playa Los Metales, the village of Juan Lopez, and Punta Jorge (the southernmost point of Mejillones Peninsula, Fig. 6), the belt measured, respectively, 20, 25 and 31 cm (Fig. 4A). The reconstructed deformation pattern along this NNE–SSW oriented coastal stretch clearly indicates an increasing differential uplift toward the southern tip of Mejillones Peninsula. This coastal stretch is partly controlled by a major, left-lateral normal, fault that has been active during the Quaternary (Okada, 1971; Armijo and Thiele, 1990; Ortlieb *et al.*, 1995b, 1996a, b), but no indication of any triggered slip was observed, neither along the coast nor inland, to the north of La Rinconada. Furthermore, the vertical distribution of the Middle and Late Pleistocene marine terraces of the area indicates that, at least on the long term, greater uplift of the western faulted block occurred north of La Rinconada, and that the southern tip of the peninsula had been uplifted less. We conclude that the recorded deformation of the northwestern shores of Antofagasta Bay was not caused by slip on the La Rinconada fault, but, rather, is due entirely to coseismic slip of the main thrust plain.

The southern extremity of Mejillones Peninsula, between Punta Jorge and Punta Tetas, is of difficult access, and could be visited only briefly in the weeks

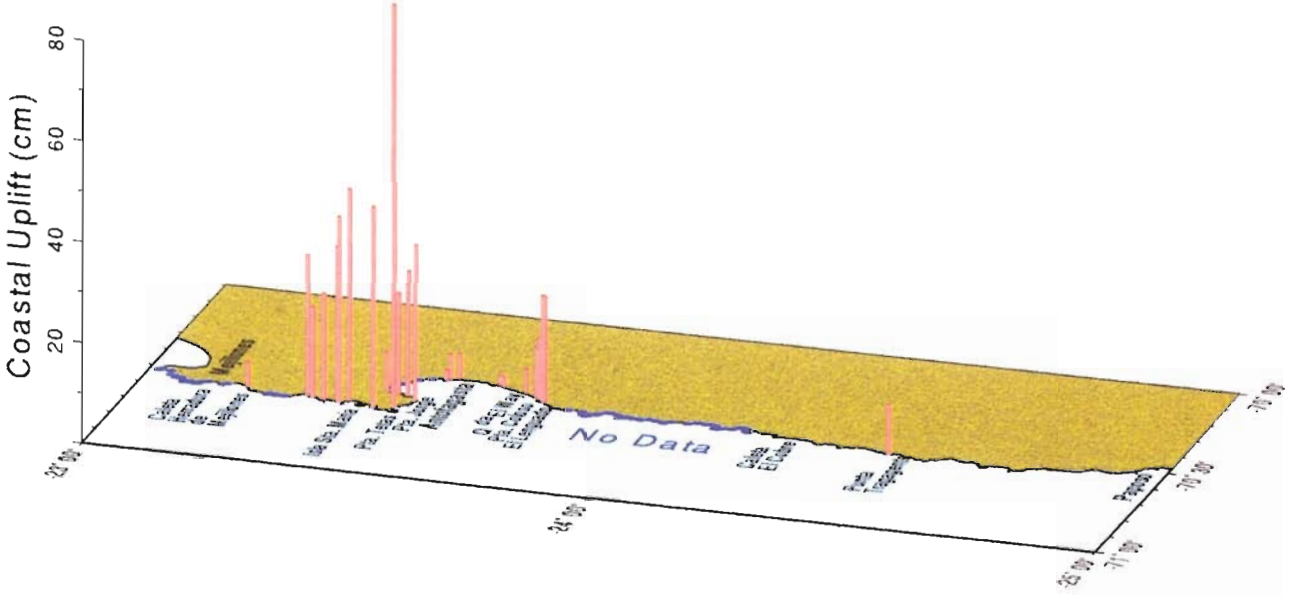

FIG. 6. Reconstruction of the coseismic uplift motion associated with the July 30, 1995 Antofagasta earthquake as recorded in the intertidal zone, between 23° and 25°S, through the width of the dead coralline algae fringe. Regions without data are indicated in blue. Maximum uplift was recorded at the south-easternmost extremity of Mejillones Peninsula.

following the 1995 earthquake. To the northwest of Punta Tetas, a wide fringe of dead algae was observed, and a rough evaluation of about 40 cm was made (from the distance). Only in the last week of December 1995, was it possible to make more thorough observations in the area, specifically in the northern part of the large bay to the east of Punta Tetas. Remnants of the white fringe produced by the 30 July, 1995 earthquake were still visible, and measured 80 cm (Fig. 7). This *in situ* measurement is 50–100% higher than the preliminary data previously reported (Ortlieb *et al.*, 1995a, b). The location of the bay at the southwestern tip of the peninsula, and its orientation toward the south, enhance its exposure to high waves and thus explains the vertical zonation of the intertidal area is greatly expanded upward (Fig. 5). The infralittoral fringe and coralline algae encrustment there, are wider than in the rest of the Antofagasta area. These considerations cast some doubt upon the precision of the estimated amplitude of the uplift indicated by the (formerly) white fringe of dead algae. However, the 80 cm value may not be exaggerated, for it is supported by the observation of former belts of dead ascidian *P. praeputialis* now located 1 m above the top of the infralittoral fringe (i.e. the top of the encrusted living coralline algae; Fig 7A). This is the only locality where the ascidians did not survive the consequences of the coseismic uplift, probably because there was substantially larger uplift in that area. It must be mentioned that during the December 1995 survey, another, much more recent, white belt of dead algae was present in the infralittoral fringe (Fig. 7). That newly formed white belt, which measured some 10–12 cm, is tentatively assigned to a small uplift episode that would have occurred shortly(?) before the third week of December. At the end of December, no other locality showed any newly developed white fringe, so that it is inferred that no regional oceanographic phenomenon was involved in the process. However, as the permanent siesmological network did not register any significant event in November or December (T. Montfret, *pers. commun.*, 1996), the formation of the new small white fringe in the Punta Tetas area cannot be correlated to any precise aftershock, and is perhaps the slow response of movement on a local independent block.

In western Mejillones Peninsula, well exposed to oceanic swell, the infralittoral fringe is often covered with large kelp (*L. nigrescens*) but coralline algae are also present. The southern half of this coastal stretch manifested a practically continuous belt of dead coralline algae, with a width varying between 20 and 45 cm. From Caleta Bandurrias del Sur (23°20′S) northward, there is no access to the coast (high, heavily beaten, seacliffs which cannot be reached easily by sea or from inland), until the Bay of Herradura de Mejillones. In the last locality, on the western side of the bay, the only evidence of a recent vertical motion were discontinuous remnants of a narrow light pink (not quite white) fringe of about 5 cm width. We suggest that the bay was located at the northern limit of the coseismically deformed region. Near Mejillones (El Rincon), and further to the north (Chacaya, Hornitos), no evidence of uplifted coralline algae were found.

Figure 6 synthesises the distribution of uplift estimated from the dead coralline algae belt. We emphasise that the plotted values do not simply correspond to the measured width of the white belt in all the localities, but are restricted to the data that may best represent the vertical changes. In many localities wider bands of dead crustose algae were observed but they corresponded to areas struck by the waves that could not provide useful data (Fig. 5).

Dislocation theory offers useful models to explain surface deformation. Uniform slip faults embedded in an elastic halfspace, such as that proposed by Ruegg *et al.* (1995), or variable slip models, being preliminary examined, can reproduce the observed vertical changes (as well as horizontal GPS data) fairly well. Because we are mainly concerned with the coastal changes, and not on the modelling aspects of the data, we shall only briefly discuss the fault characteristics. Figure 8 shows the expected elevation change due to a fault that extends nearly 150 km long (north–south) by 80 km wide with maximum fault displacement of about 7 m (offshore Caleta El Cobre), where the largest moment release has been detected by teleseismic waveform modelling (Ruegg *et al.*, 1995). The dip of the fault is 19°E, corresponding to the dip of the Wadati-Benioff zone, defined by the aftershocks located by the local network (Monfret *et al.*, 1995). Slip direction on the fault is assumed to be the same as the convergence direction between the Nazca and South American plates.

The maximum vertical displacement (1.8 m) occurring offshore, Caleta El Cobre, is responsible for the small tsunami observed along the coast. (1.6 m of upward movement recorded by the mareograph located in the port of Antofagasta.) Along the coast, the model predicts almost no uplift except in the southern portion of Mejillones Peninsula, reaching more than half a meter of uplift in its southwestern end. The total moment of this model reaches 2×10^{21} Nm, equivalent to a magnitude M_w 8.2, one tenth higher than previous estimates from long period seismic waves and geodetic observations (Ruegg *et al.*, 1995), and almost 1° higher than the magnitude estimated with surface waves at shorter periods. This discrepancy is reflecting large fault displacements with low frequencies or, in other words, a significant behavior as a slow earthquake.

CONCLUSIONS

Common pink-coloured coralline algae cover the infralittoral fringe and the infralittoral zone along the rocky shorelines of northern Chile, and of Antofagasta area in particular. The upper limit of extension of these algae may be defined as the line below which no drying-up occurs ever, even during the lowest tides. Desiccation and exposure to natural UV radiation, produce immediately the death and subsequent whitening of these algae.

The 30 July, 1995 the Antofagasta earthquake was accompanied by coastal uplift motions that could be

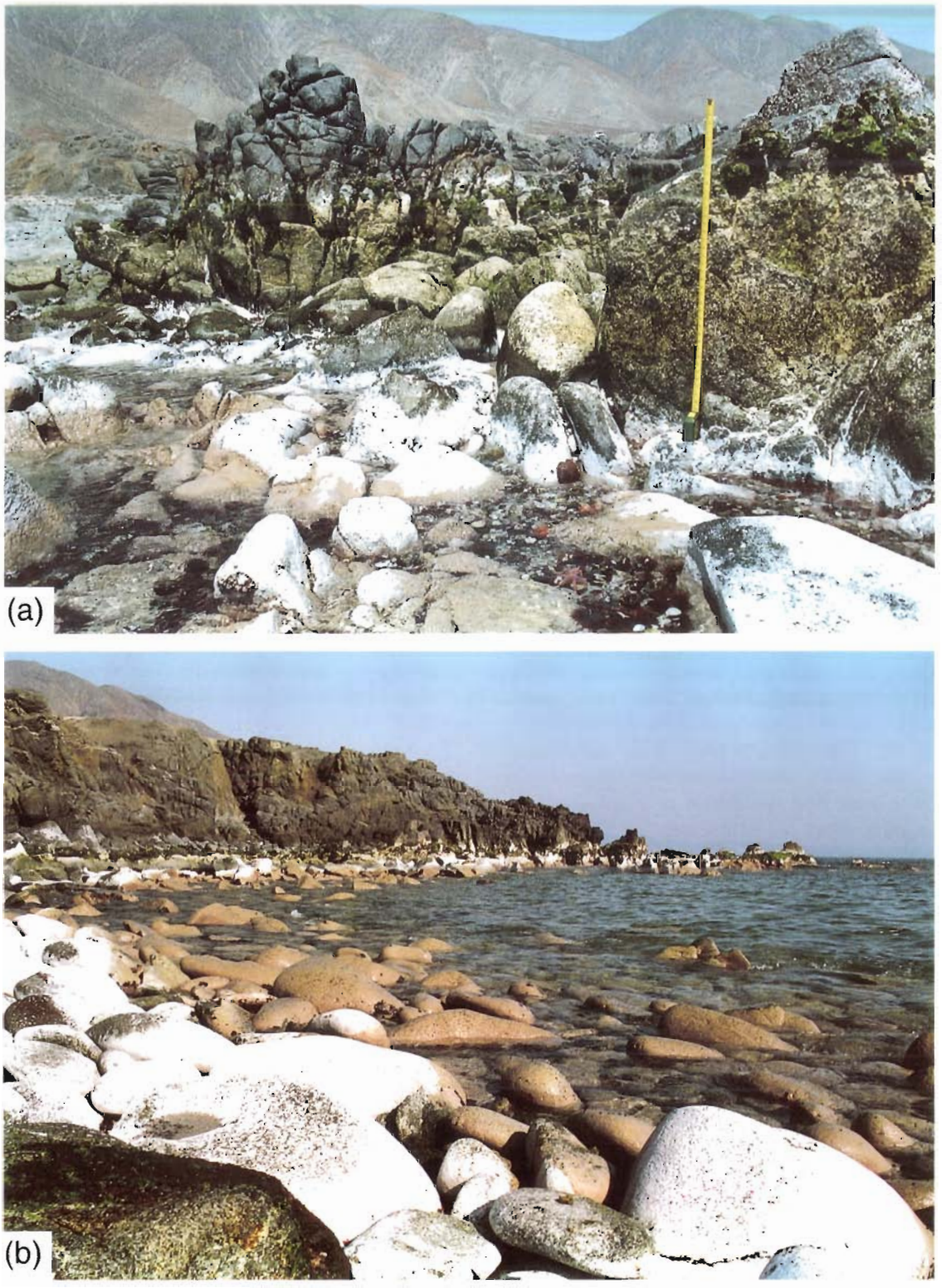

FIG. 7. Near the southwesternmost extremity of the Mejillones Peninsula, was observed the highest width of the dead algal fringe (80 cm) produced by the 30 July earthquake, and also evidence for a second small (10 cm) local uplift motion that occurred before mid(?) December 1995. (A) Remnants of the post-July 1995 fringe of dead algae are visible from the base of the 1 m scale up to 20 cm below the top of scale. The top of the former upper limit of the crustose algae coating is figured by a 20 cm high fringe of ascidians (*Pyura praeputialis*), like in Fig. 4E and 4F. Below the scale, a conspicuous, more recently formed white fringe of 10–12 cm width was observed at the end of December 1995. This secondary feature depicts a new uplift episode of minor amplitude. (B) 2 km SW from the locality of 7A, in south-westernmost Mejillones Peninsula, boulders in the infralittoral fringe (photograph taken at low tide) also registered the secondary 10 cm uplift in December 1995.

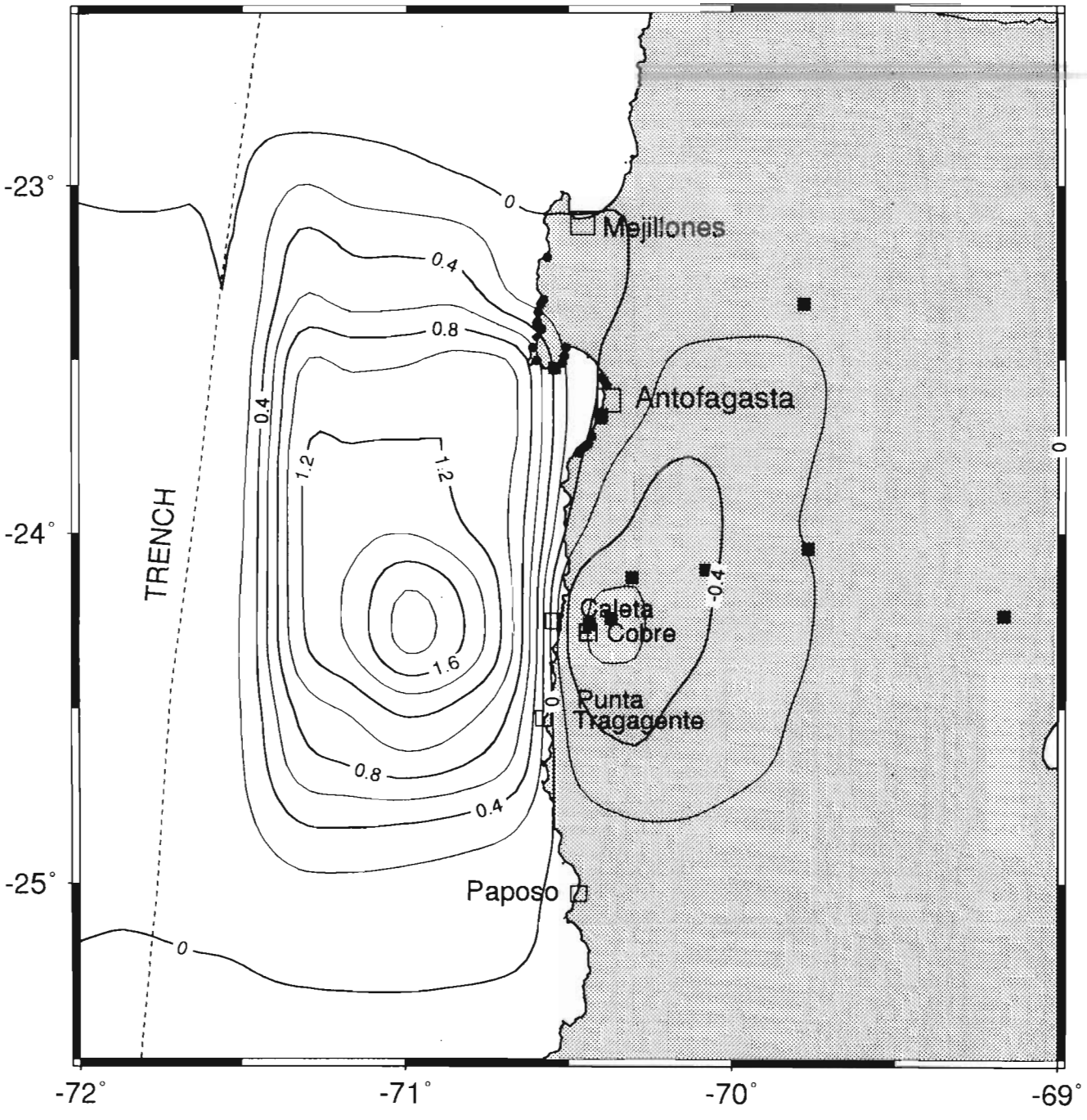

FIG. 8. Expected elevation change (contours in m) associated with the July 30, 1995 Antofagasta earthquake. These values are based on a variable fault slip model derived from the study of the coralline algae fringe and geodetic (GPS) observations. The nil elevation change runs parallel to the coast south of Antofagasta. The deformation is limited to the area between Mejillones and Paposo.

recorded by these algae. A white belt formed by the rapid death of the algae appeared at low tide in the study area, and was visible during the following weeks and months. This belt of varying width along Antofagasta Bay and around Mejillones Peninsula was assumed to depict the area of the infralittoral fringe that had been uplifted. Through a cautious study of a series of localities, it was shown that this was true in relatively protected areas, but that in the more exposed coastal stretches some particular requisites were necessary to determine the amplitude of the coseismic uplift.

Providing that in every locality, the most representative value of the belt width was selected (and not the mean, or the largest or smallest measured value), the dead coralline algae fringe effectively provided the best available evaluation of the positive vertical motion suffered by the coastal area during the Antofagasta earthquake.

Through a monitoring of the vertical position of the base of the dead algal belt (i.e. the upper limit of the presently living coralline algae) in a number of studied localities, we expect to determine in the future whether some areas will subside or, on the contrary, be more uplifted. In some localities, like the area of Punta Coloso, marine terrace data strongly suggest that no significant

long term vertical uplift motion occurred in the course of the last 125,000 years (Ortlieb *et al.*, 1993, 1995b), so that it would be possible that some compensatory subsidence happened after the 1995 earthquake. Though, one year after the Antofagasta earthquake, no subsequent vertical motion, in either direction, was registered in the Coloso area (Fig. 4E and 4F). In another locality, at the southern tip of Mejillones Peninsula, a 10 cm secondary uplift that probably occurred in early December 1995 that was observed, but could not be related to any single seismic event. Finally in the case that no further vertical motions occur, the periodic photographic control set up in some localities should be useful to study the biological colonisation and reorganisation of the sublittoral zone, immediately above the new infralittoral fringe.

ACKNOWLEDGEMENTS

The study was supported by ORSTOM, Dept TOA, UR 14 (Progr. DESIRS) and UR 12 (Progr. AIMPACT), in the framework of two scientific agreements with Universidad de Antofagasta (Facultad de Recursos del Mar) and with Universidad de Chile (Departamento de Geologia y Depto de Geofísica). The authors thank A Lavenu and T. Monfret (ORSTOM-Chile), J Cl. Ruegg (IPG, Paris), J. Laborel (Univ. Aix-Marseille), G Cabioch (ORSTOM-Villefranche) for their collaboration and/or useful discussions. The authors acknowledge the useful help of P. Bodin and T. Monfret who reviewed a previous version of the paper. This is a contribution to IGCP project 367, the INQUA Subcommission on Quaternary Shorelines for the Americas, and the INQUA Neotectonics Commission.

REFERENCES

Adey, W.H. (1986). Coralline algae as indicator of sea-level. *In*: Van de Plassche (ed.), *Sea-Level Research: A Manual for the Collection and Evaluation of Data*, pp. 229–280. GeoBooks, Norwich.

Adey, W H and Johansen, H W (1972). Morphology of Corallinaceae with special reference to *Clathromorphum*, *Mesophyllum* and *Neopolyporolithon*, gen. nov. (Rhodophyceae Cryptonemiales). *Phycologia*, **13**, 329–344.

Adey, W.H. and Vassar, M. (1975). Colonization, succession and growth rates of tropical crustose coralline algae (Rhodophyta, Cryptonemiales). *Phycologia*, **14**, 55–69.

Armijo, R. and Thiele, R. (1990). Active faulting in northern Chile: ramp stacking and lateral decoupling along a subduction plate boundary? *Earth and Planetary Science Letters*, **98**, 40–61

Bodin, P. and Klinger, T. (1986). Coastal uplift and mortality of intertidal organisms caused by the September 1985 Mexico earthquakes. *Science*, **233**, 1071–1073.

Castilla, J.C. (1988). Earthquake-caused coastal uplift and its effects on rocky intertidal kelp communities. *Science*, **242**, 440–443.

Castilla, J.C. and Oliva, D. (1990). Ecological consequences of coseismic uplift on the intertidal kelp belts of *Lessonia nigrescens* in central Chile. *Estuarine, Coastal and Shelf Science*, **31**, 45–56.

Darwin, C. (1846). *Geological Observations on South America*. Smith, Elder & Co.

Delouis, B., Monfret, T., Dorbath, L., Pardo, M., Rivera, L., Comte, D., Haessler, H., Caminade, J.P., Ponce, L., Kausel, E. and Cisternas, A. (*in press*). Forecasting the end of a gap: the large Antofagasta (Northern Chile) earthquake of July 30, 1995 and tectonic implications. *Bulletin of the Seismological Society of America*.

Guiler, E.R. (1959). Intertidal belt-forming species on the rocky coasts of Northern Chile. *Papers and Proceedings of the Royal Society of Tasmania*, **93**, 33–57.

Gutierrez, J.E. and Lay, J.E. (1965). Observaciones biológicas en la población de *Pyura chilensis* Molina. 1782, en Antofagasta (Urochordata Ascidiacea, Pyuridae). *Estudios Oceanológicos (Chile)*, **1**, 1–32.

Johansen, H.W. (1971). Effects of elevation changes in benthic algae in Prince Willian Sound. *In*: *The Great Alaska Earthquake of 1964*, pp. 35–68. National Academy of Sciences, Washington, D.C.

Lebednik, P.A. (1973). Ecological effects of intertidal uplifting from nuclear testing. *Marine Biology*, **20**, 197–207.

Littler, M.M. (1972). The crustose Corallinaceae. *Oceanography and Marine Biology*, **10**, 103–120.

Meneses, I. (1986). Estado actual del conocimiento de las algas coralináceas crustosas. *Gayana Botánica (Chile)*, **43**, 19–46.

Monfret, T., Dorbath, L., Caminade, J.P., Pardo, M., Comte, D., Ponce, L., Cisternas, A., Delouis, B. and Rivera, L. (1995). The July 30, 1995 Antofagasta earthquake: an 'hypocritical' seismic event. American Geophysical Union Fall Meet. (San Francisco, 1995), Suppl. *Eos*, **76**,(46), F427 (abstr.).

Okada, A. (1971). On the neotectonics of the Atacama fault zone region. Preliminary notes on late Cenozoic faulting and geomorphic development of the coast range of northern Chile. *Bulletin of the Department of Geography Kyoto University*, **3**, 47–65.

Ortlieb, L., Ghaleb, B., Hillaire-Marcel, Cl. and Pichet, P. (1993). Deformación de la línea de costa del último interglacial en la región de Antofagasta, Norte de Chile. *International Workshop on The Quaternary of Chile (Santiago, 1993)*, abstr. vol., p.25.

Ortlieb, L., Barrientos, S., Lavenu, A. and Monfret, T. (1995a). Coseismic uplift motions near Antofagasta, N Chile, related to the July 30, 1995, Ms 7.3 event: First field evidence from the intertidal area. American Geophysical Union, Fall Meeting (San Francisco, 1995), Suppl. *Eos*, **76**, F375–F376 (abstr.).

Ortlieb, L., Goy, J.L., Zazo, C., Hillaire-Marcel, Cl. and Vargas, G. (1995b). *Late Quaternary Coastal Changes in Northern Chile*. Guidebook for a fieldtrip, II annual meeting of the International Geological Correlation Program, Project 367 (Antofagasta, 19–28 Nov. 1995), ORSTOM, Antofagasta, Chile. 175 pp.

Ortlieb, L., Goy, J.L., Zazo, C., Hillaire-Marcel, C., Ghaleb, B., Guzmán, N. and Thiele, R. (1996). Quaternary morphostratigraphy and vertical deformation in Mejillones Peninsula, Northern Chile. *3rd International Symposium on Andean Geodynamics. (St. Malo, Sept. 1996)*, 4 pp. (*in press*).

Ortlieb, L., Díaz, A. and Guzman, N. (1996). A warm interglacial episode during isotope stage 11 in Northern Chile. *Quaternary Science Reviews*, **15**, (*this issue*).

Plafker, G. (1964). Tectonic deformation associated with the 1964 Alaskan earthquake. *Science*, **148**, 1675pp.

Raffaelli, D. (1979). The grazer-algae interaction in the intertidal zone of New Zealand rocky shores. *Journal of Experimental Marine Biology and Ecology*, **38**, 81–100.

Ruegg, J.C., Campos, J., Armijo, R., Barrientos, S., Briole, P., Thiele, R., Arancibia, M., Cañuta, J., Duquesnoy, T., Chang, M., Lazo, D., Lyon-Caen, H., Ortlieb, L., Rossignol, J.C. and Serrurier, L. (1966). The Mw=8.1 Antofagasta (North Chile) earthquake of July 30,1995: First results from teleseismic and geodetic data. *Geophysical Research Letters*, **23**, 917–920.

Stephenson, T.A. and Stephenson, A. (1972). *Life Between Tide Marks on Rocky Shores*. Freeman, W.H. and Company, San Francisco.

CURRENT LITERATURE SURVEY

THE QUATERNARY

General and chronology

Fundamental problems in radiometric dating - How can we define the meaning of a radiometric age? (in Japanese)
I. Kaneoka, *Quaternary Research (Tokyo)*, 34(3), 1995, pp 261-264.

Recent progress in accuracy and precision of radiometric dating for Quaternary samples and understanding of their dates (in Japanese)
T. Fukuoka, *Quaternary Research (Tokyo)*, 34(3), 1995, pp 265-270.

Resolution and reliability of the α-spectrometric $^{230}Th/^{234}U$ method for age determination (in Japanese)
A. Omura, A. Ise, K. Sasaki, T. Shinsaka & Y. Hasebe, *Quaternary Research (Tokyo)*, 34(3), 1995, pp 195-207.

Present status and problems of electron spin resonance (ESR) dating (in Japanese)
S. Tsukamoto, *Quaternary Research (Tokyo)*, 34(3), 1995, pp 239-248.

Past, present and future of the K-Ar method for Quaternary research (in Japanese)
T. Itaya & T. Okada, *Quaternary Research (Tokyo)*, 34(3), 1995, pp 249-259.

Thermoluminescence dating: with special reference to accuracy and reliability of age determination using quartz of volcanic rocks (in Japanese)
I. Takashima, *Quaternary Research (Tokyo)*, 34(3), 1995, pp 209-220.

Towards precise measurement of zircon and glass fission-track geochronology for Quaternary tephras (in Japanese)
T. Danhara, *Quaternary Research (Tokyo)*, 34(3), 1995, pp 221-237.

An investigation of high-precision and high-accuracy ^{14}C dating using accelerator mass spectrometry (in Japanese)
T. Nakamura, *Quaternary Research (Tokyo)*, 34(3), 1995, pp 171-183.

Optical dating studies of Quaternary organic-rich sediments from southwestern British Columbia and northwestern Washington State
O. B. Lian, J. Hu, D. J. Huntley & S. R. Hicock, *Canadian Journal of Earth Sciences*, 32(8), 1995, pp 1194-1207.

Refinement of radiocarbon dates for higher precision and accuracy (in Japanese)
K. Okumura, *Quaternary Research (Tokyo)*, 34(3), 1995, pp 191-194.

Extension of radiocarbon calibration curve (in Japanese)
H. Kitagawa, *Quaternary Research (Tokyo)*, 34(3), 1995, pp 185-190.

Averaging of multiple assays and wiggle-matching: some techniques for accurate age determinations (in Japanese)
Y. Kojo, *Quaternary Research (Toyko)*, 34(3), 1995, pp 129-134.

Radiocarbon dating of palaeosols in aeolian sands
J. M. Van Mourik, P. E. Wartenbergh, W. J. Mook & H. J. Streurman, *Mededelingen - Rijks Geologische Dienst*, 52, 1995, pp 425-439.

A research tool for integrated palaeo- and actuoecological studies: the Amsterdam Information Management System (AIMS)
H. J. L. Witte & T. A. Wijmstra, *Mededelingen - Rijks Geologische Dienst*, 52, 1995, pp 497-510.

The problem of Atlantis investigation (in Russian)
E. V. Glushko, *Vestnik - Moskovskogo Universiteta, Seriya Geografiya*, 6, 1995, pp 79-85.

Timescales, climate and river development
J. Vandenberghe, *Quaternary Science Reviews*, 14(6), 1995, pp 631-638.

Megaherbivores and southern Appalachian grass balds
P. D. Weigl & T. W. Knowles, *Growth & Change*, 26(3), 1995, pp 365-382.

Ground temperature observations at Mt. Gassan in northern Japan: a comparison between a wind-swept slope and a snowpatch hollow
Y. Kariya, *Geographical Review of Japan, Series B*, 68(1), 1995, pp 75-85.

On the principles of the U-trend method for dating Quaternary sediments, I: model, experimental procedures and data
A. G. Latham, *Quaternary Science Reviews*, 14(4), 1995, pp 409-420.

On the principles of the U-trend method for dating Quaternary sediments, II: alternative U-trend type models
A. G. Latham, *Quaternary Science Reviews*, 14(4), 1995, pp 421-430.

A Bayesian approach to wiggle-matching
J. A. Christen & C. D. Litton, *Journal of Archaeological Science*, 22(6), 1995, pp 719-725.

Explicit treatment of inheritance in dating depositional surfaces using in situ ^{10}Be and ^{26}Al
R. S. Anderson, J. L. Repka & G. S. Dick, *Geology*, 24(1), 1996, pp 47-51.

Between Diluvium and Deluge: the origin of the Younger Dryas concept
J. H. J. Joosten, *Geologie en Mijnbouw*, 74(3), 1995, pp 237-240.

Lichens: lichenometric dating of diachronous surfaces
D. McCarroll, *Earth Surface Processes & Landforms*, 20(9), 1995, pp 829-831, diskette.

The ^{210}Pb chronology of late Holocene deposition in an eastern Australian lake basin
S. J. Gale, R. J. Haworth & P. C. Pisanu, *Quaternary Science Reviews*, 14(4), 1995, pp 395-408.

ESR dating of aeolian sand near Tennant Creek, Northern Territory, Australia
K. Tanaka, M. N. Machette, A. J. Crone & J. R. Bowman, *Quaternary Science Reviews*, 14(4), 1995, pp 385-393.

Archaeologically-relevant dating techniques for the next century: small, hot and identified by acronyms
A. G. Wintle, *Journal of Archaeological Science*, 23(1), 1996, pp 123-138.

Blood from stones? Some methodological and interpretive problems in blood residue analysis
S. J. Fiedel, *Journal of Archaeological Science*, 23(1), 1996, pp 139-147.

Cold plasma ashing preparation of plant phytoliths and their examination with scanning electron microscopy and energy dispersive analysis of X-rays
K. A. Jakes & J. C. Mitchell, *Journal of Archaeological Science*, 23(1), 1996, pp 149-156.

Improving *in situ* cosmogenic chronometers
D. H. Clark, P. R. Bierman & P. Larsen, *Quaternary Research*, 44(3), 1995, pp 367-377.

Precision of terrestrial exposure ages and erosion rates estimated from analysis of cosmogenic isotopes produced in situ
A. R. Gillespie & P. R. Bierman, *Journal of Geophysical Research*, 100(B12), 1995, pp 24,637-24,649.

Radioactivity measurements applied to glaciers and lake sediments
J. F. Pinglot & M. Pourchet, *Science of the Total Environment*, 173-174, 1995, pp 211-223.

Calibration of radiocarbon ages and the interpretation of paleoenvironmental records
P. J. Bartlein, M. E. Edwards, S. L. Shafer & E. D. Barker Jr, *Quaternary Research*, 44(3), 1995, pp 417-424.

Benzene synthesis for radiocarbon dating at Shizuoka University (in Japanese)
T. Fukuhara, H. Inomata & H. Wada, *Geoscience Reports - Shizuoka University*, 22, 1995, pp 47-58.

Lichenometric method of Holocene deposits dating (Russian Literature Review) (in Russian)
O. S. Savoskyl, *Izvestiya - Akademiya Nauk, Seriya Geograficheskaya*, 5, 1995, pp 94-101.

Palaeoclimatology

Aspects of Quaternary cold stage palaeoecology
R. G. West, *Mededelingen - Rijks Geologische Dienst*, 52, 1995, pp 213-219.

Multivariate analysis of the middle and late Pleistocene Funza pollen records of Colombia
R. Van't Veer, E. T. H. Ran, H. J. P. M. Mommersteeg & H. Hooghiemstra, *Mededelingen - Rijks Geologische Dienst*, 52, 1995, pp 195-212.

The indicator value of fossil fungal remains, illustrated by the palaeoecological record of a late Eemian/early Weichselian deposit in the Netherlands
B. Van Geel, J. P. Pals, G. B. A. Van Reenen & J. Van Huissteden, *Mededelingen - Rijks Geologische Dienst*, 52, 1995, pp 297-315.

Palynological evidence of younger middle Pleistocene interglacials (Holsteinian, Reinsdorf and Schoningen) in the Schoningen open cast lignite mine (eastern Lower Saxony, Germany)
B. Urban, *Mededelingen - Rijks Geologische Dienst*, 52, 1995, pp 175-185.

The Asian monsoon during the late Quaternary: a test of orbital forcing and palaeoanalogue forecasting
R. J. Wasson, *Memoirs - Geological Society of India*, 32, 1995, pp 22-35.

Loess-palaeosol sequences as witnesses of palaeoclimatic records? The Kashmir Valley as an example
A. Bronger & T. Heinkele, *Memoirs - Geological Society of India*, 32, 1995, pp 109-123.

Climate during the past 250 years over the western Himalayas: a dendroclimatic reconstruction
G. B. Pant, H. P. Borgaonkar & K. R. Kumar, *Memoirs - Geological Society of India*, 32, 1995, pp 78-97.

Climatic change in Asia and the Western Pacific: its significance for greenhouse scenarios
J. M. Bowler, R. Jones & An Zhisheng, *Memoirs - Geological Society of India*, 32, 1995, pp 1-21.

Non-glacial varved lake sediment as a natural timekeeper and detector on environmental changes (in Japanese)
H. Fukusawa, *Quaternary Research (Tokyo)*, 34(3), 1995, pp 135-149.

New mechanism proposed for glacial cycles
A. Newman, *Eos*, 76(48), 1995, pp 489-490.

Reconstruction of the climate of the smaller glaciation epoch and its modelling (in Russian)
A. V. Kislov & V. V. Popova, *Vestnik - Moskovskogo Universiteta, Seriya Geografiya*, 5, 1995, pp 9-15.

Inferring past climatic changes in Canada using paleolimnological techniques
J. P. Smol, B. F. Cumming, M. S. V. Douglas & R. Pienitz, *Geoscience Canada*, 21(3), 1995, pp 113-118.

Paleoenvironments of the Canadian High Arctic derived from pollen and plant macrofossils: problems and potentials
K. Gajewski, M. Garneau & J. C. Bourgeois, *Quaternary Science Reviews*, 14(6), 1995, pp 609-629.

Greenland palaeotemperatures derived from GRIP bore hole temperature and ice core isotope profiles
S. J. Johnsen, D. Dahl-Jensen, W. Dansgaard & N. Gundestrup, *Tellus, Series B*, 47B(5), 1995, pp 624-629.

Complexity of Holocene climate as reconstructed from a Greenland ice core
S. R. O'Brien, P. A. Mayewski, L. D. Meeker, D. A. Meese, M. S. Twickler & S. I. Whitlow, *Science*, 270, 1995, pp 1962-1964.

Changes in continental and sea-salt atmospheric loadings in central Greenland during the most recent deglaciation: model-based estimates
R. B. Alley & 7 others, *Journal of Glaciology*, 41(139), 1995, pp 503-514.

Lake-level fluctuations at Ljustjarnen, central Sweden and their implications for the Holocene climate of Scandinavia
H. Almquist-Jacobson, *Palaeogeography, Palaeoclimatology, Palaeoecology*, 118(3-4), 1995, pp 269-290.

Continental climate response to orbital forcing from biogenic silica records in Lake Baikal
S. M. Colman & 6 others, *Nature*, 378(6559), 1995, pp 769-771.

Glaciers and climate of the mountains of the former USSR during the Neoglacial (in Russian)
L. R. Serebryanny & O. N. Solomina, *Izvestiya - Akademiya Nauk, Seriya Geograficheskaya*, 5, 1995, pp 38-49.

Carbon and oxygen isotope variations among lacustrine ostracods: implications for palaeoclimatic studies
T. H. E. Heaton, J. A. Holmes & N. D. Bridgwater, *Holocene*, 5(4), 1995, pp 428-434.

Interpreting natural climate signals in ice cores
R. C. Bales & E. W. Wolff, *Eos*, 76(47), 1995, pp 477,482-483.

Applications of freshwater diatoms to geographical research
K. A. Moser, G. M. MacDonald & J. P. Smol, *Progress in Physical Geography*, 20(1), 1996, pp 21-52.

Hydrogen isotope fractionation in wood-producing avocado seedlings: biological constraints to paleoclimatic interpretations of δD values in tree ring cellulose nitrate
V. J. Terwilliger & M. J. DeNiro, *Geochimica et Cosmochimica Acta*, 59(24), 1995, pp 5199-5207.

Stable carbon isotope composition of tree rings of a Japanese cypress from the Old-Fuji mudflow, of the last glacial period (in Japanese)
H. Aoki, H. Wada & N. Niitsuma, *Geoscience Reports - Shizuoka University*, 22, 1995, pp 37-46.

Spatial variability of late-Quaternary paleoclimates in the western United States
C. J. Mock & P. J. Bartlein, *Quaternary Research*, 44(3), 1995, pp 425-433.

Records of climate change in the Canadian Arctic: towards calibrating oxygen isotope data with geothermal data
H. Beltrami & A. E. Taylor, *Global & Planetary Change*, 11(3), 1995, pp 127-138.

Biostratigraphic evidence of the Allerod-Younger Dryas-preboreal oscillation in northern Iceland
M. Rundgren, *Quaternary Research*, 44(3), 1995, pp 405-416.

The GISP2 $\delta^{18}O$ climate record of the past 16 500 years and the role of the Sun, ocean, and volcanoes
M. Stuiver, P. M. Grootes & T. F. Braziunas, *Quaternary Research*, 44(3), 1995, pp 341-354.

Regional differences in the lateglacial climate of northern Europe based on coleopteran analysis
G. R. Coope & G. Lemdahl, *Journal of Quaternary Science*, 10(4), 1995, pp 391-395.

Rapid late-glacial atmospheric CO_2 changes reconstructed from the stomatal density record of fossil leaves
D. J. Beerling, H. H. Birks & F. I. Woodward, *Journal of Quaternary Science*, 10(4), 1995, pp 379-384.

Analiza $\delta^{13}C$ i $\delta^{34}S$ w profilach torfowych a zmiany glbalne ($\delta^{13}C$ and $\delta^{34}S$ analysis in peat profiles and global changes)
M. O. Jedrysek & 7 others, *Przeglad Geologiczny*, 43(12), 1995, pop 1004-1010.

Climate changes of the last millennium inferred from borehole temperatures: Results from the Czech Republic - Part I
L. Bodri & V. Cermak, *Global & Planetary Change*, 11(3), 1995, pp 111-125.

The climate of north Eurasia in the Allerod period of late Glacial (in Russian)
V. A. Klimanov, *Izvestiya - Akademiya Nauk, Seriya Geograficheskaya*, 5, 1995, pp 81-93.

Paleorainfall reconstructions from pedogenic magnetic susceptibility variations in the Chinese loess and paleosols
B. A. Maher & R. Thompson, *Quaternary Research*, 44(3), 1995, pp 383-391.

Oceans

Quaternary coccolith biostratigraphy and the age of the Pliocene/Pleistocene boundary (in Japanese)
T. Takayama, T. Sato, K. Kameo & T. Goto, *Quaternary Research (Tokyo)*, 34(3), 1995, pp 157-170.

Pleistocene terrestrial mammal faunas from the North Sea
T. Van Kolfschoten & C. Laban, *Mededelingen - Rijks Geologische Dienst*, 52, 1995, pp 135-151.

Coupled response of the late glacial climatic shifts of northwest Europe reflected in Greenland ice cores: evidence from the northern North Sea
H. Haflidason, H. P. Sejrup, D. K. Kristensen & S. Johnsen, *Geology*, 23(12), 1995, pp 1059-1062.

A deep-sea channel in the northwestern Mediterranean Sea: morphology and seismic structure of the Valencia Channel and its surroundings
B. Alonso, M. Canals, A. Palanques & J.-P. Rehault, *Marine Geophysical Researches*, 17(5), 1995, pp 469-484.

Marine sediments and palaeoclimatic variations since the late Pleistocene: an overview for the Arabian Sea
R. Nigam & N. H. Hashimi, *Memoirs - Geological Society of India*, 32, 1995, pp 380-390.

Geochemical record of the Panama Basin during the Last Glacial Maximum carbon event shows that the glacial ocean was not suboxic
Yong-Liang Yang, H. Elderfield, T. F. Pedersen & M. Ivanovich, *Geology*, 23(12), 1995, pp 1115-1118.

Thermally anomalous assemblages revisited: patterns in the extraprovincial latitudinal range shifts of Pleistocene marine molluscs
K. Roy, D. Jablonski & J. W. Valentine, *Geology*, 23(12), 1995, pp 1071-1074.

Increased biological productivity and export production in the glacial Southern Ocean
N. Kumar & 6 others, *Nature*, 378(6558), 1995, pp 675-680.

A 100-kyr periodicity in the flux of extraterrestrial ^3He to the sea floor
K. A. Farley & D. B. Patterson, *Nature*, 378(6557), 1995, pp 600-603.

Mapping Holocene upwelling in the eastern equatorial Pacific using Radiolaria
S. K. Haslett, *Holocene*, 5(4), 1995, pp 470-478.

Brief interstadial events in the Santa Barbara Basin, NE Pacific, during the past 60 kyr
R. J. Behl & J. P. Kennett, *Nature*, 379(6562), 1996, pp 243-246.

North Atlantic deepwater temperature change during late Pliocene and late Quaternary climatic cycles
G. S. Dwyer, T. M. Cronin, P. A. Baker, M. E. Raymo, J. S. Buzas & T. Correge, *Science*, 270(5240), 1995, pp 1347-1351.

Late Quaternary paleoceanography of the mid- to outer continental shelf, east Greenland
K. M. Williams, J. T. Andrews, N. J. Weiner & P. J. Mudie, *Arctic & Alpine Research*, 27(4), 1995, pp 352-363.

Last interglacial and Holocene climatic development in the Norwegian Sea region: ocean front movements and ice-core data
H. P. Sejrup, H. Haflidason, D. K. Kristensen & S. J. Johnsen, *Journal of Quaternary Science*, 10(4), 1995, pp 385-390.

Late Weichselian to early Holocene litho- and biostratigraphy in the Devil's Hole area, central North Sea, and its relation to glacial isostasy
S. S. R. Ekman, *Journal of Quaternary Science*, 10(4), 1995, pp 343-352.

Tropics and sub-tropics

Understanding India's Rivers: late Quaternary palaeofloods, hazard assessment and global change
V. R. Baker, L. L. Ely, Y. Enzel & V. S. Kale, *Memoirs - Geological Society of India*, 32, 1995, pp 61-77.

Geomorphology of arid western India
A. Kar, *Memoirs - Geological Society of India*, 32, 1995, pp 168-190.

The Quaternary formations of Gujarat
L. S. Chamyal & S. S. Merh, *Memoirs - Geological Society of India*, 32, 1995, pp 246-257.

Red dunes and Quaternary palaeoenvironment in India and Sri Lanka
R. A. M. Gardner, *Memoirs - Geological Society of India*, 32, 1995, pp 391-404.

Insect fossil evidence of late glacial and Holocene environments in the Bolson de Mapimi, Chihuahuan Desert, Mexico: comparisons with the paleobotanical record
S. A. Elias, T. R. Van Devender & R. De Baca, *Palaios*, 10(5), 1995, pp 454-464.

The Younger Dryas climatic event in the Cordillera de Talamanca, Costa Rica
G. A. Islebe, K. Van der Borg & H. Hooghiemstra, *Geologie en Mijnbouw*, 74(3), 1995, pp 281-283.

A short review of the Younger Dryas in the eastern Mediterranean area
S. Bottema, *Geologie en Mijnbouw*, 74(3), 1995, pp 271-273.

The Younger Dryas-sapropel S1 connection in the Mediterranean Sea
S. R. Troelstra & J. E. Van Hinte, *Geologie en Mijnbouw*, 74(3), 1995, pp 275-280.

Solar and ENSO signatures in laminated deposits from Lake Magadi (Kenya) during the Pleistocene/Holocene transition
B. Damnati & M. Taieb, *Journal of African Earth Sciences*, 21(3), 1995, pp 373-382.

Potential of opal phytoliths for use in paleoecological reconstruction in the humid tropics of Africa
F. Runge, *Zeitschrift fur Geomorphologie, Supplementband*, 99, 1995, pp 53-64.

New results on late Quaternary landscape and vegetation dynamics in eastern Zaire (Central Africa)
J. Runge, *Zeitschrift fur Geomorphologie, Supplementband*, 99, 1995, pp 65-74.

Foraminiferal evidences for 77-year cycles of droughts in India and its possible modulation by the Gleissberg solar cycle
R. Nigam, N. Khare & R. R. Nair, *Journal of Coastal Research*, 11(4), 1995, pp 1099-1107.

Palaeoarctic elements in mountain forest ecosystems of northern Vietnam (in Russian)
D. A. Krivolutsky, G. N. Ogureeva & Huin Kim Hoy, *Vestnik - Moskovskogo Universiteta, Seriya Geografiya*, 6, 1995, pp 53-59.

Loess mounds on the Laizhou Bay plain south of Bohai Sea and their paleogeographic implication (in Chinese)
Zhang Zulu, *Acta Geographica Sinica*, 50(5), 1995, pp 464-470.

Preliminary palynological results on the Pleistocene-Holocene transition, Seram Trench, offshore Irian Jaya, Indonesia
S. Van der Kaars, *Geologie en Mijnbouw*, 74(3), 1995, pp 285-286.

Thermoluminescence dating of dune podzols at Cape Arnhem, northern Australia
B. G. Lees, J. Stanner, D. M. Price & Lu Yanchou, *Marine Geology*, 129(1-2), 1995, pp 63-75.

Holocene evolution of coastal wetlands in wet-tropical northeastern Australia
G. M. Crowley & M. K. Gagan, *Holocene*, 5(4), 1995, pp 385-399.

The evolution of the continental and coastal environments during the last climatic cycle in Brazil (120 ky BP to present)
K. Suguio & 8 others, *Boletim IG - Universidade de Sao Paulo, Instituto de Geociencias: Serie Cientifica*, 24, 1993(1995), pp 27-41.

Quaternary wadi and floodplain sequences of Tripolitania, northwest Libya: a synthesis of their stratigraphic relationships, and their implications in landscape evolution
J. M. Anketell, S. M. Ghellali, D. D. Gilbertson & C. O. Hunt, in: *Mediterranean Quaternary river environments*, ed J. Lewin & others, (Balkema), 1995, pp 231-244.

Alluvial Holocene terraces in eastern Maghreb: climate and anthropogenic controls
J.-L. Ballais, in: *Mediterranean Quaternary river environments*, ed J. Lewin & others, (Balkema), 1995, pp 183-194.

Palaeosols in late Quaternary colluvium, northern KwaZulu-Natal, South Africa
G. A. Botha & N. Fedoroff, *Journal of African Earth Sciences*, 21(2), 1995, pp 291-311.

Imja glacier dead-ice melt rates and changes in a supra-glacial lake, 1989-1994, Khumbu Himal, Nepal: danger of lake drainage
T. Watanabe, S. Kameyama & T. Sato, *Mountain Research & Development*, 15(4), 1995, pp 293-300.

Radiocarbon dating and sedimentation rates in the Holocene alluvial sediments of the northern Bihar plains, India
R. Sinha, P. F. Friend & V. R. Switsur, *Geological Magazine*, 133(1), 1996, pp 85-90.

Lithostratigraphy and alluviation history of Quaternary deposits of southern part of Gangetic plain, Uttar Pradesh
S. P. Bhartiya, S. Narayan & A. C. Nigam, *Journal - Geological Society of India*, 46(4), 1995, pp 393-399.

Quaternary facies and palaeoenvironment in north and east of Sambhar Lake, Rajasthan
R. M. Sundaram & S. Pareek, *Journal - Geological Society of India*, 46(4), 1995, pp 385-392.

Sedimentology of Quaternary alluvial deposits of the Gandak-Kosi interfan, North Bihar plains
R. Sinha, *Journal - Geological Society of India*, 46(5), 1995, pp 521-532.

Quaternary stratigraphy and sedimentation of the Indo-Gangetic plains, Haryana
J. L. Thussu, *Journal - Geological Society of India*, 46(5), 1995, pp 533-544.

A sea-running Changjiang River during the last glaciation? (in Chinese)
Li Congxian & Zhang Guijia, *Acta Geographica Sinica*, 50(5), 1995, pp 459-463.

Mid-latitude and extra-glacial

Vegetation and climate of the last glacial-interglacial cycle in southern Illinois (USA)
Hong Zhu & R. G. Baker, *Journal of Paleolimnology*, 14(3), 1995, pp 337-354.

Ostracode $\delta^{18}O$ and $\delta^{13}C$ evidence of Holocene environmental changes in the sediments of two Minnesota lakes
A. Schwalb, S. M. Locke & W. E. Dean, *Journal of Paleolimnology*, 14(3), 1995, pp 281-296.

Modelling of icecap glaciation of the northern Rocky Mountains of Montana
W. W. Locke, *Geomorphology*, 14(2), 1995, pp 123-130.

Post-glacial vegetation history of the Mission Mountains, Montana
L. M. Gerloff, L. V. Hills & G. D. Osborn, *Journal of Paleoliminology*, 14(3), 1995, pp 269-279.

Late-glacial and early Holocene lake sediments, groundwater formation and climate in the Atacama Altiplano 22-24°S
M. Grosjean, M. A. Geyh, B. Messerli & U. Schotterer, *Journal of Paleolimnology*, 14(3), 1995, pp 241-252.

Middle Pleistocene Hoxnian Stage interglacial deposits at Hitchin, Hertfordshire, England
S. Boreham & P. L. Gibbard, *Proceedings - Geologists' Association*, 106(4), 1995, pp 259-270.

Notice of raised beach deposits at Llanddona, Anglesey, North Wales
S. Campbell, M. Wood, K. Addison, J. D. Scourse & R. E. Jones, *Quaternary Newsletter*, 77, 1995, pp 1-5.

Pollen records from the Velay craters: a review and correlation of the Holsteinian interglacial with isotopic stage 11
J.-L. De Beaulieu & M. Reille, *Mededelingen - Rijks Geologische Dienst*, 52, 1995, pp 59-70.

The expression of the tripartition of the Allerod chronozone in the lithofacies of Late Glacial polycyclic profiles in Belgium and the Netherlands
J. M. Van Mourik & R. T. Slotboom, *Mededelingen - Rijks Geologische Dienst*, 52, 1995, pp 441-450.

The Dinkel valley revisted: Pleniglacial stratigraphy of the eastern Netherlands and global climatic change
T. Van der Hammen, *Mededelingen - Rijks Geologische Dienst*, 52, 1995, pp 343-355.

Some palaeobotanical data on the fluviatile Rhine/Meuse Kreftenheye Formation in the Netherlands (Weichselian)
J. De Jong, *Mededelingen - Rijks Geologische Dienst*, 52, 1995, pp 369-385.

Late Glacial and Holocene pollen records from the Aisne and Vesle valleys, northern France: the pollen diagrams Maizy-Cuiry and Bazoches
C. Bakels, *Mededelingen - Rijks Geologische Dienst*, 52, 1995, pp 223-234.

Correlation of Middle-European late-Pleistocene pollen sequences of the Pfefferbichl and Zeifen types
E. Gruger, *Mededelingen - Rijks Geologische Dienst*, 52, 1995, pp 97-104.

Early Pleistocene depositional environments and stratigraphy at Obel (Burggen), Nordrhein-Westfalen, Germany
P. L. Gibbard, L. Krook & J. Vandenberghe, *Mededelingen - Rijks Geologische Dienst*, 52, 1995, pp 83-96.

Terrassenstratigraphie des Mittelpleistozan am Niederrhein und Mittelrhein (Middle Pleistocene terrace stratigraphy of the lower and middle Rhine)
W. Boenigk, *Mededelingen - Rijks Geologische Dienst*, 52, 1995, pp 71-87.

A paleohidrologiai kutatasok ujabb eredmenyei (New results of the paleohydrological investigations in Hungary)
G. Gabris, *Foldrajzi Ertesito*, 44(1-2), 1995, pp 101-109.

Le premier stratotype continental de quatre stades isotopiques successifs du Pleistocene moyen pour le basin mediterraneen septentrional: le Vallo di Diano (Campanie, Italie) (The first continental stratotype for four successive isotope stages of the Middle Pleistocene for the northern Mediterranean Basin: the Vallo di Diano, Campania, Italy)(French with abridged English)
E. R. Ermolli & 7 others, *Comptes Rendus - Academie des Sciences, Serie II: Sciences de la Terre et des Planetes*, 321(10), 1995, pp 877-884.

Macrofossils and pollen representing forest of the pre-Taupo volcanic eruption (c. 1850 yr BP) era at Pureora and Benneydale, central North Island, New Zealand
B. R. Clarkson, M. S. McGlone, D. J. Lowe & B. D. Clarkson, *Journal - Royal Society of New Zealand*, 25(2), 1995, pp 263-281.

Stratigraphy and chronology of late Quaternary andesitic tephra deposits, Tongariro Volcanic Centre, New Zealand
S. L. Donoghue, V. E. Neall & A. S. Palmer, *Journal - Royal Society of New Zealand*, 25(2), 1995, pp 115-206.

Pleistocene palynology of the Petone and Seaview drillholes, Petone, Lower Hutt Valley, North Island, New Zealand
D. C. Mildenhall, *Journal - Royal Society of New Zealand*, 25(2), 1995, pp 207-262.

Vertical tectonic movement in northeastern Marlborough: stratigraphic, radiocarbon, and paleoecological data from Holocene estuaries
Y. Ota, L. J. Brown, K. R. Berryman, T. Fujimori & T. Miyauchi, *New Zealand Journal of Geology & Geophysics*, 38(3), 1995, pp 269-282.

Thermoluminescence dating of late Pleistocene loess and tephra from eastern Washington and southern Oregon and implications for the eruptive history of Mount St. Helens
G. W. Berger & A. J. Busacca, *Journal of Geophysical Research*, 100(B11), 1995, pp 22,361-22,374.

A 12 000 year radiocarbon date of deglaciation from the Continental Divide of northwestern Montana
P. E. Carrara, *Canadian Journal of Earth Sciences*, 32(9), 1995, pp 1303-1307.

Textural, geochemical and mineralogical evidence for the origin of Peoria loess in central and southern Nebraska, USA
N. R. Winspear & K. Pye, *Earth Surface Processes & Landforms*, 20(8), 1995, pp 735-745.

Opal phytoliths as an indicator of the floristics of prehistoric grasslands
R. F. Fisher, C. N. Bourn & W. F. Fisher, *Geoderma*, 68(4), 1995, pp 243-255.

Geochronology of Quaternary coastal plain deposits, southeastern Virginia, USA
J. E. Mirecki, J. F. Wehmiller & A. F. Skinner, *Journal of Coastal Research*, 11(4), 1995, pp 1135-1144.

Isotopic evidence for shifts in atmospheric circulation pattern during the late Quaternary in mid-North America
R. Amundson, O. Chadwick, C. Kendall, Yang Wang & M. DeNiro, *Geology*, 24(1), 1996, pp 23-26.

Evolucion comparada de bahias de la peninsula Mitre, Tierra del Fuego (Comparative evolution of bays of Mitre Peninsula, Tierra del Fuego)
F. I. Isla, *Revista - Asociacion Geologica Argentina*, 49(3-4), 1994, pp 197-205.

Palaeoecology of a *Donatia-Astelia* cushion bog, Magellanic moorland-subantarctic evergreen forest transition, southern Tierra del Fuego, Argentina
C. J. Heusser, *Review of Palaeobotany & Palynology*, 89(3-4), 1995, pp 429-440.

Edad y genesis del Rio de la Plata (Age and origin of the Rio de la Plata)
G. Parker, C. M. Paterlini & R. A. Violante, *Revista - Asociacion Geologica Argentina*, 49(1-2), 1994, pp 11-18.

Environmental change and tephra deposition: the Strath of Kildonan, northern Scotland
D. J. Charman, S. West, A. Kelly & J. Grattan, *Journal of Archaeological Science*, 22(6), 1995, pp 799-809.

Late Quaternary vegetation history of the Western Isles of Scotland
J. A. Fossitt, *New Phytologist*, 132(1), 1996, pp 171-196.

The climate of the Younger Dryas in the Netherlands
J. Vandenberghe, *Geologie en Mijnbouw*, 74(3), 1995, pp 245-249.

Valley bottoms in the late Quaternary
W. Schirmer, *Zeitschrift fur Geomorphologie, Supplementband*, 100, 1995, pp 27-51.

Palynological investigations of Younger Dryas sediments in the northern Netherlands
E. Mook-Kamps, *Geologie en Mijnbouw*, 74(3), 1995, pp 261-264.

Younger Dryas deposits of the Tjonger Valley fill in the NE Netherlands
S. Van der Meulen, *Geologie en Mijnbouw*, 74(3), 1995, pp 257-260.

Younger Dryas cooling and fluvial response (Maas River, the Netherlands)
C. Kasse, *Geologie en Mijnbouw*, 74(3), 1995, pp 251-256.

Late Weichselian and Holocene fluvial palaeogeography of the southern Rhine-Meuse delta (the Netherlands)
H. J. T. Weerts & H. J. A. Berendsen, *Geologie en Mijnbouw*, 74(3), 1995, pp 199-212.

Le Gour de Tazenat et l'evolution de l'environnement du Tardiglaciaire au Boreal dans la Chaine des Puys septentrionale (Massif Central, France) (The 'Gour de Tazenat' and the late glacial to Boreal environmental changes in the northern Chaine des Puys)(French with abridged English)
E. Juvigne & B. Bastin, *Comptes Rendus - Academie des Sciences, Serie II: Sciences de la Terre et des Planetes*, 321(11), 1995, pp 993-999.

La Tephra des Roches, marqueur du volcanisme contemporain de la fin du Magdalenien dans le Massif Central francais (The Les Roches Tephra: a marker of volcanism contemporary with the late Magdalenian in the Massif Central, France)(French with abridged English)
G. Vernet & J.-P. Raynal, *Competes Rendus - Academie des Sciences, Serie II: Sciences de la Terre et des Planetes*, 321(8), 1995, pp 713-720.

Les diatomees des depots lacustres du maar de Ribains (Haute-Loire), durant le dernier interglaciaire et les periodes qui l'encadrent (Diatoms of the lacustrine infilling from Ribains maar (Haute-Loire), during the last interglacial)(-French with abridged English)
P. Rioual, *Comptes Rendus - Academie des Sciences, Serie II: Sciences de la Terre et des Planetes*, 321(8), 1995, pp 705-712.

Les travertins de la vallee du Lez (Montpellier, Sud de la France). Datations $^{230}Th/^{234}U$ et environnements pleistocenes (The Lez Valley travertines (Montpellier, south of France). $^{230}Th/^{234}U$ dating and Pleistocene environments)(-French with abridged English)
P. Ambert, Y. Quinif, P. Roiron & R. Arthuis, *Comptes Rendus - Academie des Sciences, Serie II: Sciences de la Terre et des Planetes*, 321(8), 1995, pp 667-674.

De l'histoire du genre *Betula* dans les Alpes francaises du nord (Notes on the late Quaternary history of the genus *Betula* in the northern French Alps)
F. David & M. Barbero, *Review of Palaeobotany & Palynology*, 89(3-4), 1995, pp 455-467.

Microfabrics, grain-size-distributions and grain surface textures in late Pleistocene basin sediments of Brandenburg (northern Barnim)
L. Schirrmeister, *Zeitschrift fur Geomorphologie, Supplementband*, 99, 1995, pp 75-89.

Quartarmorphologisches Nord-Sudprofil durch Brandenburg (Quaternary morphological north-south profile through Brandenburg)
P. Gartner, L. Behrendt, S. Bussemer, J. Marcinek, G. Markuse & N. Schlaak, *Berichte zur Deutschen Landeskunde*, 69(2), 1995, pp 229-262.

Fluvial geomorphodynamics in the Danube River valley and tributary river systems near Regensburg during the Upper Quaternary - theses, questions and conclusions
M. W. Buch & K. Heine, *Zeitschrift fur Geomorphologie, Supplementband*, 100, 1995, pp 53-64.

The middle Neckar as an example of fluvio-morphological processes during the middle and late Quaternary period
E. Bibus & J. Wesler, *Zeitschrift fur Geomorphologie, Supplementband*, 100, 1995, pp 15-26.

The development of the middle and lower course of the Weser river during the late Pleistocene
K. Meinke, *Zeitschrift fur Geomorphologie, Supplementband*, 100, 1995, pp 1-13.

The Wutach Gorge in SW Germany: late Wurmian (periglacial) downcutting versus Holocene processes
G. Einsele & W. Ricken, *Zeitschrift fur Geomorphologie, Supplementband*, 100, 1995, pp 65-87.

Geomorphological evidence for anti-Apennine faults in the Umbro-Marchean Apennines and in the peri-Adriatic Basin, Italy
M. Coltorti, P. Farabollini, B. Gentili & G. Pambianchi, *Geomorphology*, 15(1), 1996, pp 33-45.

The Holocenic evolution of a stretch of an eastern Italian Alpine valley
C. Friz, V. Villi & M. C. Turrini, *Earth Surface Processes & Landforms*, 20(8), 1995, pp 747-757.

Did a late Wurm broad-leaved flora exist in the Altay range?
A. P. Derevyanko, S. A. Laukhin, E. M. Malayeva, M. V. Shun'kov, L. A. Orlova & A. V. Postnov, *Transactions Doklady - Russian Academy of Sciences: Earth Science Sections*, 331(5), 1993(1995), pp 128-133; translated from: *Doklady Rossiyskoy Akademii Nauk*, 330(6),. 1993, pp 736-739

Holocene evolution of peatland and paleoenvironmental changes in the Sarobetsu Lowland, Hokkaido, northern Japan (in Japanese)
A. Ohira, *Geograpical Review of Japan, Series A*, 68A(10), 1995, pp 695-712.

Palynological characteristics of near-shore shell-bearing Pliocene through Holocene sediments of Florida, Georgia, and South Carolina
F. J. Rich, *Tulane Studies in Geology & Paleontology*, 28(3-4), 1995, pp 97-112.

Paleoecological aspects of a late Wisconsinan aquatic mollusk assemblage associated with mastodon bone recovered from the north fork of Ward Creek, Baton Rouge, Louisiana
B. Lewis, *Tulane Studies in Geology & Paleontology*, 28(3-4), 1995, pp 57-81.

Documentation and evaluation of radiocarbon dates from the 'Cape Fear coquina' (late Pleistocene) of Snows Cut, New Hanover County, North Carolina
J. A. Dockal, *Southeastern Geology*, 35(4), 1995, pp 169-186.

Diverse nonmarine biota from the Whidbey Formation (Sangamonian) at Point Wilson, Washington
P. F. Karrow, A. Ceska, R. J Hebda, B. B. Miller, K. L. Seymour & A. J. Smith, *Quaternary Research*, 44(3), 1995, pp 434-437.

Holocene glacial chronology in Patagonia: Tyndall and Upsala glaciers
M. Aniya, *Arctic & Alpine Research*, 27(4), 1995, pp 311-322.

Late Pleistocene interglacial deposits at Pennington Marshes, Lymington, Hampshire, southern England
L. G. Allen, P. L. Gibbard, M. E. Pettit, R. C. Preece & J. E. Robinson, *Proceedings - Geologists' Association*, 107(1), 1996, pp 39-50.

An abrupt mid-Holocene decline of *Pinus sylvestris* in Glen Torridon, north west Scotland: implications for palaeoclimate change
D. Anderson, *Research Paper - University of Oxford, School of Geography*, 52, 1995, 29 pp.

Palaeoecology of a late Weichselian vertebrate fauna from Norre Lyngby, Denmark
K. Aaris-Sorensen, *Boreas*, 24(4), 1995, pp 355-365.

Holocene sedimentary sequences in the Arc River delta and the Etang de Berre in Provence, southern France
M. Provansal, in: *Mediterranean Quaternary river environments*, ed J. Lewin & others, (Balkema), 1995, pp 159-165.

La formation de Montfleury pres de Geneve: etude palynologique et sedimentologique d'une sequence du Pleistocene moyen (The Montfleury Formation near Geneva: palynology and sedimentology of a mid-Pleistocene sequence)
S. Wegmuller, G. Amberger & J.-P. Vernet, *Eclogae Geologicae Helvetiae*, 88(3), 1995, pp 595-614.

Stratigraphic and paleogeographic interpretation of analysis results of magnetic susceptibility of loesses at Bojanice (NW Ukraine)
A. Bogucki, H. Maruszczak & J. Nawrocki, *Annales - Universitatis Mariae Curie-Sklodowska, Sectio B*, 50, 1995, pp 51-64.

Development stages of loessial and glacial formations in Ukraine: (Stratigraphy of loesses in Ukraine)
P. Gozhik, V. Shelkoplyas & T. Khristoforova, *Annales - Universitatis Mariae Curie-Sklodowska, Sectio B*, 50, 1995, pp 65-74.

The profile of loesses at Korshov (NW Ukraine) in the light of heavy minerals analyses
R. Racinowski & A. Bogucki, *Annales - Universitatis Mariae Curie-Sklodowska, Sectio B*, 50, 1995, pp 191-205.

Loesses and their bedrock in the southeastern part of the Miechow Upland (S Poland)
L. Lindner & A. E. Siennicka-Chmielewska, *Annales - Universitatis Mariae Curie-Sklodowska, Sectio B*, 50, 1995, pp 75-90.

Glacial cycles of loess accumulation in Poland during the last 400 ka and global rhythms of paleogeographic events
H. Maruszczak, *Annales - Universitatis Mariae Curie-Sklodowska, Sectio B*, 50, 1995, pp 127-156.

Accumulation conditions and the upper limit of Neopleistocene loesses in the central Roztocze region (SE Poland)
H. Maruszczak, *Annales - Universitatis Mariae Curie-Sklodowska, Sectio B*, 50, 1995, pp 157-171.

Stratigraphical and paleogeographical interpretation of the results of heavy minerals analyses in loesses of Voivodina
H. Maruszczak & M. Wilgat, *Annales - Universitatis Mariae Curie-Sklodowska, Sectio B*, 50, 1995, pp 173-190.

***Viviparus diluvianus* (Kunth) w osadach interglacjalu mazowieckiego w Grabanowie na Podlasui (*Viviparus diluvianus* (Kunth) in the sediments of Mazovian Interglacial from Grabanow in Podlasie, E Poland)**
K. M. Krupinski & S. Skompski, *Przeglad Geologiczny*, 43(12), 1995, pp 1045-1048.

Malacofauna of the Vistulian loess in the Cracow region (S Poland)
S. W. Alexandrowicz, *Annales - Universitatis Mariae Curie-Sklodowska, Sectio B*, 50, 1995, pp 1-28.

Loess and alluvia in the Krzeczkowski Stream valley in Przemysl environs (SE Poland)
S. W. Alexandrowicz & M. Lanczont, *Annales - Universitatis Mariae Curie-Sklodowska, Sectio B*, 50, 1995, pp 29-50.

Stratigraphy and paleogeography of loess on the Przemysl Foothills (SE Poland)
M. Lanszont, *Annales - Universitatis Mariae Curie-Sklodowska, Sectio B*, 50, 1995, pp 91-126.

Soils of Quaternary river sediments in the Algarve
P. A. James & D. K. Chester, in: *Mediterranean Quaternary river environments*, ed J. Lewin & others, (Balkema), 1995, pp 245-262.

The influence of Quaternary tectonics on river capture and drainage patterns in the Huercal-Overa Basin, southeastern Spain
E. Wenzens & G. Wenzens, in: *Mediterranean Quaternary river environments*, ed J. Lewin & others, (Balkema), 1995, pp 55-63.

Controls on drainage evolution in the Sorbas basin, southeast Spain
A. E. Mather & A. M. Harvey, in: *Mediterranean Quaternary river environment*, ed J. Lewin & others, (Balkema), 1995, pp 65-76.

Tectonics versus climate: an example from late Quaternary aggradational and dissectional sequences of the Mula Basin, southeast Spain
A. E. Mather, P. G. Silva, J. L. Goy, A. M. Harvey & C. Zazo, in: *Mediterranean Quaternary river environments*, ed J. Lewin & others, (Balkema), 1995, pp 77-87.

Pleistocene environmental change in the Guadalope Basin, northeast Spain; fluvial and archaeological records
M. G. Macklin & D. G. Passmore, in: *Mediterranean Quaternary river environments*, ed J. Lewin & others, (Balkema), 1995, pp 103-113.

Quaternary soil and river terrace sequences in the Aguas/Feos river systems: Sorbas Basin, southeast Spain
A. M. Harvey, S. Y. Miller & S. G. Wells, in: *Mediterranean Quaternary river environments*, ed J. Lewin & others, (Balkema), 1995, pp 263-281.

Quaternary valley floor erosion and alluviation in the Biferno Valley, Molise, Italy: the role of tectonics, climate, sea level change, and human activity
G. W. Barker & C. O. Hunt, in: *Mediterranean Quaternary river environments*, ed J. Lewin & others, (Balkema), 1995, pp 145-157.

Facies sequences and sedimentation influences in late Quaternary alluvial deposits, southwast Cyprus
R. L. Stevens & P. O. Wedel, in: *Mediterranean Quaternary river environments*, ed J. Lewin & others, (Balkema), 1995, pp 219-229.

Quaternary drainage development, sediment fluxes and extensional tectonics in Greece
R. E. L. Collier, M. R. Leeder & J. A. Jackson, in: *Mediterranean Quaternary river environments*, ed J. Lewin & others, (Balkema), 1995, pp 31-44.

River response to Quaternary tectonics with examples from northwestern Anatolia, Turkey
C. Kuzucuoglu, in: *Mediterranean Quaternary river environments*, ed J. Lewin & others, (Balkema), 1995, pp 45-53.

Climatic forcing of alluvial fan regimes during the late Quaternary in the Konya Basin, south central Turkey
N. Roberts, in: *Mediterranean Quaternary river environments*, ed J. Lewin & others, (Balkema), 1995, pp 207-217.

A study on the Holocene buried tidal sand bodies in the south Yellow Sea coastal land
Chen Baozhang, Li Congxian & Ye Zhizheng, *Acta Geographica Sinica*, 50(5), 1995, pp 447-457.

Late Quaternary displacement rate, paleoseismicity, and geomorphic evolution of the Alpine Fault: evidence from Hokuri Creek, South Westland, New Zealand
R. Sutherland & R. J. Norris, *New Zealand Journal of Geology & Geophysics*, 38(4), 1995, pp 419-430.

Glacial landforms and sediments

Insights into alpine moraine development from cosmogenic ^{36}Cl buildup dating
M. G. Zreda & F. M. Phillips, *Geomorphology*, 14(2), 1995, pp 149-156.

Diversion of the upper Bear River: glacial diffluence and Quaternary erosion, Sierra Nevada, California
L. A. James, *Geomorphology*, 14(2), 1995, pp 131-148.

Hypsometric forcing of stagnant ice margins: Pleistocene valley glaciers, San Juan Mountains, Colorado
E. E. Small, *Geomorphology*, 14(2), 1995, pp 109-121.

Late-glacial paleoenvironment of Lake Algonquin sediments near Clarksburg, Ontario
P. F. Karrow, T. W. Anderson, L. D. Delorme, B. B. Miller & L. J. Chapman, *Journal of Paleoliminology*, 14(3), 1995, pp 297-309.

Landforms and structures of the waterlain west end of St. Thomas moraine, SW Ontario, Canada
A. Dreimanis, *Geomorphology*, 14(2), 1995, pp 185-196.

Ice wedges on hillslopes and landform evolution in the late Quaternary, western Arctic coast, Canada
J. R. Mackay, *Canadian Journal of Earth Sciences*, 32(8), 1995, pp 1093-1105.

A subglacial valley system of Saalian age in the eastern Netherlands and neighbouring Germany
E. A. Van de Meene, *Mededelingen - Rijks Geologische Dienst*, 52, 1995, pp 153-165.

Notes on the Alpine Rhine glacier and the chronostratigraphy of the Upper Wurm
L. W. S. De Graaff & M. G. G. De Jong, *Mededelingen - Rijks Geologische Dienst*, 52, 1995, pp 317-330.

New micromorphological knowledge of the last Pleistocene glacial cycle in the loess profile at Praha-Sedlec
J. Hradilova, *Journal - Czech Geological Society*, 39(4), 1994, pp 319-329.

Sea ice scouring on the inner shelf of the southeastern Canadian Beaufort Sea
A. Hequette, M. Desrosiers & P. W. Barnes, *Marine Geology*, 128(3-4), 1995, pp 201-219.

Accumulation rates of coarse-grained terrigenous sediment in the Norwegian-Greenland Sea: signals of continental glaciation
P. M. Goldschmidt, *Marine Geology*, 128(3-4), 1995, pp 137-151.

Recent drumlins, flutes and lineations at Vestari-Hagafellsjokull, Iceland
J. K. Hart, *Journal of Glaciology*, 41(139), 1995, pp 596-606.

Origin, chronology and climatological significance of annual-moraine ridges at Myrdalsjokull, Iceland
J. Kruger, *Holocene*, 5(4), 1995, pp 420-427.

The Monington esker, near Cardigan, Dyfed
H. G. Owen, *Swansea Geographer*, 32, 1995, pp 79-87.

Glacial flow systems in the zone of confluence between the Scandinavian and Novaya Zemlya Ice Sheets
M. Punkari, *Quaternary Science Reviews*, 14(6), 1995, pp 589-603.

Geomorphic effect and hydraulics of the late Pleistocene jokulhlaups of ice-dammed lakes in the Altai (in Russian)
A. N. Rudoi, *Geomorfologiya*, 4, 1995, pp 61-76.

Characteristics and genesis of moraine-derived flowtill varieties
T. Zielinski & A. J. Van Loon, *Sedimentary Geology*, 101(1-2), 1996, pp 119-143.

Tunnel valley genesis
C. O. Cofaigh, *Progress in Physical Geography*, 20(1), 1996, pp 1-19.

A shear-diffusion model of till genesis based on the dispersal pattern of indicator rocks in the Grand-Volume Till of central Gaspesie, Quebec, Canada
R. Charbonneau & P. P. David, *Boreas*, 24(4), 1995, pp 281-292.

Mineral magnetic analysis of a 'weathering' surface within glacigenic sediments at Glanllynnau, North Wales
J. Walden & K. Addison, *Journal of Quaternary Science*, 10(4), 1995, pp 367-378.

The growth and decay of the late Weichselian Ice Sheet in western Svalbard and adjacent areas based on provenance studies of marine sediments
A. Elverhoi & 9 others, *Quaternary Research*, 44(3), 1995, pp 303-316.

Deposition of organic matter in the Norwegian-Greenland Sea during the past 2.7 million years
T. Wagner & J. A. Holemann, *Quaternary Research*, 44(3), 1995, pp 355-366.

Englacial and proglacial glaciotectonic processes at the snout of a thermally complex glacier in Svalbard
M. J. Hambrey & D. Huddart, *Journal of Quaternary Science*, 10(4), 1995, pp 313-326.

The margin of the last Barents-Kara ice sheet at Markhida, Northern Russia
J. Tveranger, V. Astakhov & J. Mangerud, *Quaternary Research*, 44(3), 1995, pp 328-340.

Analiza litofacjalna i litostratygrafia osadow lessowych w strefie kontaktu z osadami glacjalnymi fazy pomorskiej ostatniego zlodowacenia w Starym Objezierzu, Pomorze Zachodnie (Lithofacies analysis and loess sequences in the contact zone with glacial deposits of the last glaciation Pomeranian phase at Stare Objezierze, west Pomerania)
K. Issmer, *Badania Fizjograficzne nad Polska Zachodnia, Seria A, Geografia Fizyczna*, 46, 1995, pp 63-84.

Lodowce gruzowe (Rock glaciers)
W. Dobinski, *Czasopismo Geograficzne*, 65(2), 1994, pp 109-123.

Wlasciwosci i cechy diagnostyczne bazalnych glin morenowych vistulianu, jako wyraz dynamiki srodowiska depozycyjnego ostatniego ladolodu na Nizinie Wielkopolskiej (Characteristics and diagnostic features of Vistulian basal lodgement till as indicators of dynamics of depositional environment of the last glaciation in the great Poland lowland)
ANON, *Badania Fizjograficzne nad Polska Zachodnia, Seria A, Geografia Fizyczna*, 46, 1995, pp 29-62.

Pliocene-Quaternary sedimentation and Alpine Fault related tectonics in the lower Cascade Valley, South Westland, New Zealand
R. Sutherland, S. Nathan, I. M. Turnbull & A. G. Beu, *New Zealand Journal of Geology & Geophysics*, 38(4), 1995, pp 431-450.

The Holocene

Archaeometry: a source of buried information
A. Kshirsagar, B. Deotare & V. Gogte, *Memoirs - Geological Society of India*, 32, 1995, pp 466-472.

The results of education: natural formation research and scalar analysis of archaeological deposits
L. Wandsnider, *Memoirs - Geological Society of India*, 32, 1995, pp 435-445.

Refutation of stylistic constructs in Palaeolithic rock art
R. G. Bednarik, *Comptes Rendus - Academie des Sciences, Serie II: Sciences de la Terre et des Planetes*, 321(9), 1995, pp 817-821.

A high resolution Holocene pollen record from Lago do Pires, SE Brazil: vegetation, climate and fire history
H. Behling, *Journal of Paleolimnology*, 14(3), 1995, pp 253-268.

Contemporary changes of Baltic Sea ice
J. P. Girjatowicz & K. M. Kozuchowshi, *Geographia Polonica*, 65, 1995, pp 43-50.

La Grotte de La Martina (Dinant, Belgique) et sa sepulture mesolithique (Mesolithic burial place in La Martina Cave, Dinant, Belgium)
M. Dewez, J.-M. Cordy, E. Gilot & M.-C. Grossens-Van Dyck, *Comptes Rendus - Academie des Sciences, Serie II: Sciences de la Terre et des Planetes*, 321(7), 1995, pp 639-641.

Pollen analysis of two plaggen soils in the province of North Brabant, the Netherlands
W. Groenman-van Waateringe & H. Luijten, *Mededelingen - Rijks Geologische Dienst*, 52, 1995, pp 331-342.

Landscape development and vegetation history of the state nature reserve 'Haterts-Overasseltse Vennen' near Nijmegen, the Netherlands
D. Teunissen, *Mededelingen - Rijks Geologische Dienst*, 52, 1995, pp 481-493.

Palynology of young acid forest soils in the Netherlands
E. F. Dijkstra & J. M. Van Mourik, *Mededelingen - Rijks Geologische Dienst*, 52, 1995, pp 283-295.

Palaeoecological investigations of a Late Bronze Age watering-place at Bovenkarspel, the Netherlands
J. Buurman, B. Van Geel & G. B. A. Van Reenen, *Mededelingen - Rijks Geologische Dienst*, 52, 1995, pp 249-270.

Bergumermeer-De Leyen (Friesland, the Netherlands): a mesolithic wetland in a dry setting
W. A. Casparie & J. H. A. Bosch, *Mededelingen - Rijks Geologische Dienst*, 52, 1995, pp 271-282.

Fluvial activity and vegetation development 4000-2000 BP in southwestern Utrecht, the Netherlands
C. R. Janssen, H. J. A. Berendsen & A. J. D. Van Broekhuizen, *Mededelingen - Rijks Geologische Dienst*, 52, 1995, pp 357-367.

The Saalian Complex and the first traces of human activity in the Netherlands in a stratigraphic and ecologic context
J. Vandenberghe, *Mededelingen - Rijks Geologische Dienst*, 52, 1995, pp 187-194.

Etude de la dynamique vegetale Tardiglaciaire et Holocene en Italie centrale: le marais de Colfiorito (Ombrie) (Lateglacial and Holocene vegetation dynamics in central Italy: swamp of Colfiorito, Umbria)(French with abridged English)
E. Brugiapaglia & J.-L. De Beaulieu, *Comptes Rendus - Academie des Sciences, Serie II: Sciences de la Terre et des Planetes*, 321(7), 1995, pp 617-622.

Landscape dynamics of Karelian isthmus, Priladozhie and Izhora land during last 500 years: main factors and stages (in Russian)
G. A. Isachenko, *Izvestiya - Russkogo Geografischeskogo Obshchestva*, 127(5), 1995, pp 17-24.

Late Quaternary stratigraphy and an Upper Acheulian occupation site in the Kalubhar Valley, Saurashtra
S. Chakrabarti, *Memoirs - Geological Society of India*, 32, 1995, pp 277-281.

The contribution of the Earth sciences to the development of Indian archaeology
R. S. Pappu, *Memoirs - Geological Society of India*, 32, 1995, pp 414-434.

Natural and cultural formation processes of the Acheulian sites of the Hunsgi and Baichbal valleys, Karnataka
K. Paddayya & M. D. Petraglia, *Memoirs - Geological Society of India*, 32, 1995, pp 333-351.

Quaternary stratigraphy and prehistory of the upper Indus Valley, Ladakh
K. K. Sharma, *Memoirs - Geological Society of India*, 32, 1995, pp 98-108.

Prehistoric and Quaternary studies at Nevasa: the last forty years
S. Mishra, *Memoirs - Geological Society of India*, 32, 1995, pp 324-332.

Quaternary geology and prehistoric environments in the Son and Belan valleys, north central India
M. A. J. Williams & M. F. Clarke, *Memoirs - Geological Society of India*, 32, 1995, pp 282-308.

An early Soan assemblage from the Siwaliks: a comparison of processing sequences between this assemblage and of an Acheulian assemblage from Rajasthan
C. Gaillard, *Memoirs - Geological Society of India*, 32, 1995, pp 231-245.

Geoarchaeology of the Thar Desert, northwest India
V. N. Misra, *Memoirs - Geological Society of India*, 32, 1995, pp 210-230.

Quaternary stratigraphy of the intermontane Dun valleys of Dang-Deokhuri and associated prehistoric settlements in western Nepal
G. Corvinus, *Memoirs - Geological Society of India*, 32, 1995, pp 124-149.

Early human cultures and environments in the northern Punjab, Pakistan: an overview of the Potwar Project of the British Archaeological Mission to Pakistan (1981-1991)
B. Allchin, *Memoirs - Geological Society of India*, 32, 1995, pp 150-167.

Late Holocene palynology and palaeovegetation of tephra-bearing mires at Papamoa and Waihi Beach, western Bay of Plenty, North Island, New Zealand
R. M. Newnham, D. J. Lowe & G. N. A. Wigley, *Journal - Royal Society of New Zealand*, 25(2), 1995, pp 283-300.

Late Pleistocene and Holocene vegetation history, Central Otago, South Island, New Zealand
M. S. McGlone, A. F. Mark & D. Bell, *Journal - Royal Society of New Zealand*, 25(1), 1995, pp 1-22.

High-resolution stable isotope analysis of tree rings: implications of 'microdendroclimatology' for palaeoenvironmental research
N. J. Loader, V. R. Switsur & E. M. Field, *Holocene*, 5(4), 1995, pp 457-460.

Reconstructing the climate of Mexico from historical records
S. L. O'Hara & S. E. Metcalfe, *Holocene*, 5(4), 1995, pp 485-490.

Late Flandrian coastal change and tidal palaeochannel development at Hills Flats, Severn Estuary (SW Britain)
J. R. L. Allen & M. G. Fulford, *Journal - Geological Society (London)*, 153(1), 1996, pp 151-162.

Human occupation of the southern Netherlands during the Younger Dryas
J. Deeben, *Geologie en Mijnbouw*, 74(3), 1995, pp 265-269.

Late Younger Dryas to Holocene palaeoenvironments of the southern Kattegat, Scandinavia
K. Conradsen, *Holocene*, 5(4), 1995, pp 447-456.

'Blooms' of the toxic dinoflagellate *Gymnodinium catenatum* as evidence of climatic fluctuations in the late Holocene of southwestern Scandinavia
T. A. Thorsen, B. Dale & K. Nordberg, *Holocene*, 5(4), 1995, pp 435-446.

Holocene tree-limit and climate history from the Scandes Mountains, Sweden
L. Kullman, *Ecology*, 76(8), 1995, pp 2490-2502.

Toward an integrated model for raised-bog development: theory and field evidence
H. Almquist-Jacobson & D. R. Foster, *Ecology*, 76(8), 1995, pp 2503-2516.

Holocene river and slope dynamics in the Black Forest and Upper Rhine Lowlands under the impact of man
R. Mackel & G. Zollinger, *Zeitschrift fur Geomorphologie, Supplementband*, 100, 1995, pp 89-100.

Sedimentary behavior of the alpine Ruetz River (Stubai Valley, Tyrol, Austria) in historical times
R. Blattler, H. Hagedorn, D. Busche & R. Baumhauer, *Zeitschrift fur Geomorphologie, Supplementband*, 100, 1995, pp 101-113.

Holocene vegetation succession and degradation as responses to climatic change and human activity in the Serra da Estrela, Portugal
W. O. Van der Knaap & J. F. N. Van Leeuwen, *Review of Palaeobotany & Palynology*, 89(3-4), 1995, pp 153-211.

Charcoal analysis and the history of *Pinus pinaster* (cluster pine) in Portugal
I. Figueiral, *Review of Palaeobotany & Palynology*, 89(3-4), 1995, pp 441-454.

Palaeoclimatological reconstruction using stable isotope data on continental molluscs from Valle di Castiglione, Roma, Italy
F. Bonadonna & G. Leone, *Holocene*, 5(4), 1995, pp 461-469.

Methodological premises of pollenological studies in arid zone (in Russian)
T. A. Abramova, *Vestnik - Moskovskogo Universiteta, Seriya Geografiya*, 6, 1995, pp 18-26.

Human impact on environment in the Neolithic-Bronze Age in southern Primorye (far eastern Russia)
Y. V. Kuzmin & A. V. Chernuk, *Holocene*, 5(4), 1995, pp 479-484.

Mammoth extinction: two continents and Wrangel Island
P. S. Martin & A. J. Stuart, *Radiocarbon*, 37(1), 1995, pp 7-10.

Vegetation response to Holocene climatic change: pollen and palaeolimnological data from the Middle Atlas, Morocco
H. F. Lamb & S. Van der Kaars, *Holocene*, 5(4), 1995, pp 400-408.

Radiocarbon dating of Ohalo II: archaeological and methodological implications
D. Nadel, I. Carmi & D. Segal, *Journal of Archaeological Science*, 22(6), 1995, pp 811-822.

Evolution and geological significance of Holocene emerged shell beds on the southern coastal zone of Sri Lanka
J. Katupotha, *Journal of Coastal Research*, 11(4), 1995, pp 1042-1061.

Archaeobotanical evidence for Zoku-Jomon subsistence at the Mochiyazawa Site, Hokkaido, Japan
A. C. D'Andrea, *Journal of Archaeological Science*, 22(5), 1995, pp 583-595.

Late Quaternary change in the mountains of New Guinea
G. Hope & J. Golson, *Antiquity*, 69(265), 1995, pp 818-830.

The Australian transition: real and perceived boundaries
D. Frankel, *Antiquity*, 69(265), 1995, pp 649-655.

Environmental change in greater Australia
A. P. Kershaw, *Antiquity*, 69(265), 1995, pp 656-675.

The transition on the coastal fringe of Greater Australia
J. M. Beaton, *Antiquity*, 69(265), 1995, pp 798-806.

Infilling rates of a steepland catchment estuary, Whangamata, New Zealand
A. T. Sheffield, T. R. Healy & M. S. McGlone, *Journal of Coastal Research*, 11(4), 1995, pp 1294-1308.

Holocene *Astrangia* (Scleractinia) in foreshore shell accumulations, Bogue Banks, North Carolina
W. Miller III, *Tulane Studies in Geolgoy & Paleontology*, 28(3-4), 1995, pp 91-96.

Improved age estimates for the White River and Bridge River tephras, western Canada
J. J. Clague, S. G. Evans, V. N. Rampton & G. J. Woodsworth, *Canadian Journal of Earth Sciences*, 32(8), 1995, pp 1172-1179.

The formation of inertinite-rich peats in the mid-Cretaceous Gates Formation: implications for the interpretation of mid-Albian history of paleowildfire
M. N. Lamberson, R. M. Bustin, W. D. Kalkreuth & K. C. Pratt, *Palaeogeography, Palaeoclimatology, Palaeoecology*, 120(3-4), 1996, pp 235-260.

Dynamics of a Holocene cliff-top dune along Mountain River, Northwest Territories, Canada
C. Begin, Y. Michaud & L. Filion, *Quaternary Research*, 44(3), 1995, pp 392-404.

Climate in southwestern Ontario, Canada, between AD 1610 and 1885 inferred from oxygen and hydrogen isotopic measurements of wood cellulose from trees in different hydrologic settings
W. M. Buhay & T. W. D. Edwards, *Quaternary Research*, 44(3), 1995, pp 438-446.

Microwave archaeointensities from Peruvian ceramics
J. Shaw, D. Walton, S. Yang, T. C. Rolph & J. A. Share, *Geophysical Journal International*, 124(1), 1996, pp 241-244.

Palynology and sediment slumping in a high arctic Greenland lake
B. Fredskild, *Boreas*, 24(4), 1995, pp 345-354.

Holocene landscape evolution in the Mellemfjord area, Disko Island, central West Greenland: area presentation and preliminary results
O. Humlum & 6 others, *Geografisk Tidsskrift*, 95, 1995, pp 28-41.

Early Holocene pollen and molluscan records from Enfield Lock, Middlesex, UK
F. M. Chambers, T. M. Mighall & D. H. Keen, *Proceedings - Geologists' Association*, 107(1), 1996, pp 1-14.

Patterned fen development in northern Scotland, hypothesis testing and comparison with ombrotrophic blanket peats
D. J. Charman, *Journal of Quaternary Science*, 10(4), 1995, pp 327-342.

Morphogenese-Pedogenese: Les heritages du dernier cycle glaciaire en foret de Fougeres (Ille et Vilaine, France) (Landform development and pedogenesis: the effects of the Last Glacial cycle in the forest of Fougeres, Ille et Vilaine, Brittany, France)
B. Van Vliet-Lanoe, J. Pellerin & M. Helluin, *Zeitschrift fur Geomorphologie*, 39(4), 1995, pp 489-510.

L'hypothese du determinisme climatique des premieres traces polliniques de neolithisation sur le massif jurassien (France) (The hypothesis of the climatic control of the first pollen evidence of the early Neolithic in the Jura, France) (French with abridged English)
H. Richard & P. Ruffaldi, *Comptes Rendus - Acadamie des Sciences, Serie II: Sciences de la Terre et des Planetes*, 322(1), 1996, pp 77-83.

Late-glacial and Holocene malacofaunas from archaeological sites in the Somme Valley (North France)
N. Limondin, *Journal of Archaeological Science*, 22(5), 1995, pp 683-698.

Comparative morphometric study of a human phalanx from the Lower Pleistocene site at Cueva Victoria, (Murcia, Spain), by means of Fourier analysis, shape coordinates of landmarks, principal and relative warps
P. Palmqvist, J. A. Perez-Claros, J. Gibert & J. L. Santamaria, *Journal of Archaeological Science*, 23(1), 1996, pp 95-107.

Summary report on the mummified glacier corpse found at Hauslabjoch in the Otztal Alps
K. Spindler, *Eclogae Geologicae Helvetiae*, 88(3), 1995, pp 699-709.

Human activity, landscape change and valley alluviation in the Feccia Valley, Tuscany, Italy
C. O. Hunt & D. D. Gilbertson, in: *Mediterranean Quaternary river environments*, ed J. Lewin & others, (Balkema), 1995, pp 167-176.

The Holocene alluvial records of the chorai of Metapontum, Basilicata, and Croton, Calabria, Italy
J. T. Abbott & S. Valastro Jr, in: *Mediterranean Quaternary river environments*, ed J. Lewin & others, (Balkema), 1995, pp 195-205.

Early Neolithic farming in the Thessalian river landscape, Greece
T. H. Van Andel, K. Gallis & G. Toufexis, in: *Mediterranean Quaternary river environments*, ed J. Lewin & others, (Balkema), 1995, pp 131-143.

Glaciation, river behaviour and Palaeolithic settlement in upland northwest Greece
J. C. Woodward, J. Lewin & M. G. Macklin, in: *Mediterranean Quaternary river environments*, ed J. Lewin & others, (Balkema), 1995, pp 115-129.

Mammalian remains from the Upper Palaeolithic site of Kamenka, Buryatia (Siberia)
M. Germonpre & L. Lbova, *Journal of Archaeological Science*, 23(1), 1996, pp 35-57.

Mollsucan fauna from site 4 of Tell Jenin (northern West Bank - Palestine)
M. Al-Zawahra, H. Salem & A. Ezzughayyar, *Journal of Archaeological Science*, 23(1), 1996, pp 1-6.

Paleoenvironment and archaeology of Drotsky's Cave: western Kalahari Desert, Botswana
L. H. Robbins & 10 others, *Journal of Archaeological Science*, 23(1), 1996, pp 7-22.

Stable isotope analysis of ten individuals from Afetna, Saipan, northern Mariana Islands
R. McGovern-Wilson & C. Quinn, *Journal of Archaeological Science*, 23(1), 1996, pp 59-65.

A chronostratigraphic analysis of landbird extinction on Tahuata, Marquesas Islands
D. W. Steadman & B. Rolett, *Journal of Archaeological Science*, 23(1), 1996, pp 81-94.

Sea-level and river terraces

An heuristic model for sea level rise due to the melting of small glaciers
T. M. L. Wigley & S. C. B. Raper, *Geophysical Research Letters*, 22(20), 1995, pp 2749-2752.

Coastal Massachusetts pond development: edaphic, climatic, and sea level impacts since deglaciation
M. G. Winkler & P. R. Sanford, *Journal of Paleolimnology*, 14(3), 1995, pp 311-336.

Optical dating of aeolian sediments from the Sefton coast, northwest England
K. Pye, S. Stokes & A. Neal, *Proceedings - Geologists' Association*, 106(4), 1995, pp 281-292.

Documentary sources of the sea surges in Venice from AD 787 to 1867
S. Enzi & D. Camuffo, *Natural Hazards*, 12(3), 1995, pp 225-287.

Prehistory and Quaternary sea level changes along the west coast of India: a summary
A. Marathe, *Memoirs - Geological Society of India*, 32, 1995, pp 405-413.

Radiometric dating of late Quaternary sea levels of the Saurashtra coast, western India: an experiment with oyster and clam shells
N. Juyal, R. K. Pant, R. Bhushan & B. L. K. Somayajulu, *Memoirs - Geological Society of India*, 32, 1995, pp 372-379.

Multiple Pliocene-Quaternary marine highstands, northeast Gulf coastal plain - fallacies and facts
E. G. Otvos, *Journal of Coastal Research*, 11(4), 1995, pp 984-1002.

Coastal areas at risk from storm surges and sea-level rise in northeastern Italy
M. Bondesan & 6 others, *Journal of Coastal Research*, 11(4), 1995, pp 1354-1379, map.

On the lowest sea level during the culmination of the latest glacial period in South China (in Chinese)
Huang Zhenguo, Zhang Weigiang, Chai Fuxiang & Xu Qihao, *Acta Geographica Sinica*, 50(5), 1995, pp 385-393.

Glacial isostatic adjustment and the anomalous tide gauge record of eastern North America
J. L. Davis & J. X. Mitrovica, *Nature*, 379(6563), 1996, pp 331-333.

The postglacial relative sea-level lowstand in Newfoundland
J. Shaw & D. L. Forbes, *Canadian Journal of Earth Sciences*, 32(9), 1995, pp 1308-1330.

Salt-marsh growth and fluctuating sea level: implications of a simulation model for Flandrian coastal stratigraphy and peat-based sea-level curves
J. R. L. Allen, *Sedimentary Geology*, 100(1-4), 1995, pp 21-45.

Late Weichselian shore displacement in Halland, southwestern Sweden: relative sea-level changes and their glacio-isostatic implications
M. Berglund, *Boreas*, 24(4), 1995, pp 324-344.

Periglacial

Permafrost terminology
R. J. E. Brown & W. O. Kupsch, *Biuletyn Peryglacjalny*, 32, 1992(1995), 176 pp.

Steppe-tundra transition: a herbivore-driven biome shift at the end of the Pleistocene
S. A. Zimov, V. I. Chuprynin, A. P. Oreshko, F. S. Chapin III, J. F. Reynolds & M. C. Chapin, *American Naturalist*, 146(5), 1995, pp 765-794.

The Kesgrave and Bytham sands and gravels of eastern Suffolk
R. J. O. Hamblin & B. S. P. Moorlock, *Quaternary Newsletter*, 77, 1995, pp 17-31.

A reassessment of the relict Pleistocene 'pingos' of west Wales: hydraulic pingos or mineral palsas?
S. D. Gurney, *Quaternary Newsletter*, 77, 1995, pp 6-16.

Fluvial periglacial environments, climate and vegetation during the middle Weichselian in the northern Netherlands, with special reference to the Hengelo Interstadial
C. Kasse, S. J. P. Bohncke & J. Vandenberghe, *Mededelingen - Rijks Geologische Dienst*, 52, 1995, pp 387-413.

The foundations of geocrioecology (in Russian)
V. I. Solomatin, *Vestnik - Moskovskogo Universiteta, Seriya Geografiya*, 6, 1995, pp 26-33.

Microbial life in permafrost: a historical review
D. Gilichinsky & S. Wagener, *Permafrost & Periglacial Processes*, 6(3), 1995, pp 243-250.

Recent climatic trend and thermal response of permafrost in Salluit, northern Quebec, Canada
Baolai Wang & M. Allard, *Permafrost & Periglacial Processes*, 6(3), 1995, pp 221-233.

The Holocene development of a debris slope in subarctic Quebec, Canada
J. Marion, L. Filion & B. Hetu, *Holocene*, 5(4), 1995, pp 409-419.

Forms of unusual patterned ground: examples from the Falkland Islands, South Atlantic
P. Wilson, *Geografiska Annaler, Series A*, 77A(3), 1995, pp 159-165.

Archaeological and environmental evidence for the Roman impact on vegetation near Carlisle, Cumbria
M. R. McCarthy, *Holocene*, 5(4), 1995, pp 491-495.

Ventifacts as palaeo-wind indicators in southern Scandinavia
P. Schlyter, *Permafrost & Periglacial Processes*, 6(3), 1995, pp 207-219.

Zeitliche und raumliche Variabilitat solifluidaler Prozesse und ihre Ursachen. Eine Zwischenbilanz nach acht Jahren Solifluktionsmessungen (1985-1993) an der Messstation 'Glorer Hutte', Hohe Tauern, Osterreich (Temporal and spatial variability solifluction processes and their causes. A provisional appraisal after eight years of solifluction measurements (1985-1993) at Glorer Hutte measuring station, Hohe Tauern, Austria)
H. Veit, H. Stingl, K.-H. Emmerich & B. John, *Zeitschrift fur Geomorphologie, Supplementband*, 99, 1995, pp 107-122.

The chronology of Upper Pleistocene stratified slope-waste deposits in central Italy
M. Coltorti & F. Dramis, *Permafrost & Periglacial Processes*, 6(3), 1995, pp 235-242.

A note on rock glaciers in the Albanian Alps
G. Palmentola, K. Baboci, G. Gruda & G. Zito, *Permafrost & Periglacial Processes*, 6(3), 1995, pp 251-257.

Cryogenic landslides on the Yamal Peninsula, Russia: preliminary observations
M. O. Leibman, *Permafrost & Periglacial Processes*, 6(3), 1995, pp 259-264.

Ice-wedge formation in northern Asia during the Holocene
Y. K. Vasil'chuk & A. C. Vasil'chuk, *Permafrost & Periglacial Processes*, 6(3), 1995, pp 273-279.

Gelifluction in the alpine periglacial environment of the Tianshan Mountains, China
Liu Gengnian, Xiong Heigang & Cui Zhijiu, *Permafrost & Periglacial Processes*, 6(3), 1995, pp 265-271.

Active layer changes (1968-1993) following the forest-tundra fire near Inuvik, NWT Canada
J. R. Mackay, *Arctic & Alpine Research*, 27(4), 1995, pp 323-336.

Observations of open system pingos in a marsh environment, Mellemfjord, Disko, central West Greenland
H. H. Christiansen, *Geografisk Tiddskrift*, 95, 1995, pp 42-48.

Nunataks of the last ice sheet in northwest Scotland
D. McCarroll, C. K. Ballantyne, A. Nesje & S.-O. Dahl, *Boreas*, 24(4), 1995, pp 305-323.

Eologliptolity i struktury po klinach zmarzlinowych w strefie przedpola fazy poznanskiej ostatniego zlodowacenia na Wysoczyznie Poznanskiej (Ventifacts and frost fissures in the foreland of the Poznan phase of the last glaciation - the Poznan Till Plain)
Z. Tresci, *Badania Fizjograficzne nad Polska Zachodnia, Seria A Geografia Fizyczna*, 46, 1995, pp 7-17.

Plejstocenskie lodowce gruzowe w Karkonoszach (Pleistocene rock glaciers in the Karkonosze Mts)
H. Chmal & A. Traczyk, *Czasopismo Geograficzne*, 64(3-4), 1993, pp 253-263.

Implications of frost heave for patterned ground, Tibet Plateau, China
Baolai Wang & H. M. French, *Arctic & Alpine Research*, 27(4), 1995, pp 337-344.

Secondary precipitates in Pleistocene and present cryogenic environments (Mendoza Precordillera, Argentina, Transbaikalia, Siberia, and Seymour Islands, Antarctica)
T. Vogt & A. E. Corte, *Sedimentology*, 43(1), 1996, pp 53-64.

QUATERNARY SCIENCE REVIEWS

The International Multidisciplinary Research and Review Journal

Volume 15 Numbers 8–9 **1996**

Contents

This Journal is abstracted in: *Res Alert, Chem Abstr Serv, Geo Abstr, Geo Bib & Indx, INSPEC Data, Curr Cont Sci Cit Ind* and *Curr Cont SCISEARCH Data*


0277-3791(1996)15:8-9;1-6